# EROSION OF CLAY-SAND-SILT-GRAVEL MIXTURES

*Submitted to*

**INDIAN NATIONAL COMMITTEE ON SURFACE WATER**
**(MINISTRY OF WATER RESOURCES)**

*by*


**Prof. Z. AHMAD**
*(Principle Investigator)*

**Mr. U. K. SINGH**
*(Research Scholar)*

DEPARTMENT OF CIVIL ENGINEERING
INDIAN INSTITUTE OF TECHNOLOGY ROORKEE
ROORKEE- 247667


JULY 2017

# ABSTRACT

Alluvial channel are closely linked with the development of civilization from the ancient time. Constructions of hydraulic structures like dam, barrage, canals, bridges, etc, on the rivers; serve many purposes like storage of water, irrigation water supply, electricity generation, etc; that needed in day to day life. However, failure of these structures resulted in enormous loss of life and money. One main reason for the failure of hydraulic structures in alluvial channel is cited as sediment transport. For an example, Garde and Ranga Raju (2000) cited the failure of Islam weir on the Sutlej River due to degraded river bed. In Yellow river, bed level was lowered by an average of 4.5 m in a 50 km reach due to less heavily sediment-laden water (Garde and Ragga Raju, 2000). The sediment transport in alluvial channel significantly affects the life of hydraulic structures founded on alluvial channels. Sediment deposition in the reservoir reduces it's water storage capacity or shorten the design life of reservoir. For an example, Srirama Sagar reservoir in Andra Pradesh found to have lost 25 % of its capacity during the first 14 years of impounding (Kothyari, 1996). Owens et al. (2005) reported that 10% of lakes, rivers and bays of the USA have sediment contaminated with toxic chemicals. Human activity accelerated the changes occurring in the channel bed morphology that causes the various problems like reservoir sedimentation, hydraulic structures failures, aggradation and degeadation, flood problems, water quality issues, navigation problems, etc. Hence, the study on detachment and transportation of sediment in an alluvial channel becomes important for addressing the problems associated with it.

Understanding of incipient motion of sediment particles is needed in estimation of sediment transport. The incipient motion is characterized as the beginning of the movement of bed particles when the flow induced shear stress over the bed exceeds to a certain critical value. Shields (1936) has been the pioneer for introducing the incipient motion curve widely known as Shields curve for the computation of critical shear stress of uniform cohesionless sediment. The unequal mobility concept has been considered for the incipient motion of individual particles present in sediment mixture (Egiazaroff 1965, Ashida and Michiue 1971, Hayashi et al. 1980, Parker et al. 1982, Bridge and Bennett 1992, Kuhnle 1993, Patel and Ranga Raju 1999, Wu et al.

2000, Wilcock et al. 2001, etc). Most of the study, conducted for incipient motion of non-uniform sediment, is of mixture sand and gravel. However, the critical shear stress still under investigation for non-uniform cohesionless sediment especially in presence of silt. River bed material consists of mixture of cohesive as well as cohesionless materials. Singh et al. (2007) reported that the Ganga river bed is consisted of sediment having clay, silt, sand, and gravel. Jain (2008) reported the presence of clay, sand, and gravel mixture on the bank of the river Ganga at Rishikesh. The erosion characteristic of cohesive sediment is significantly different from the cohesionless sediment due to dominancy of physio-chemical properties of the cohesive sediment (Kothyari & Jain 2010a). Several experimental studies have been reported on incipient motion for different cohesive sediment mixtures like clay-sand, clay-silt-sand, clay-gravel, clay-sand-gravel, etc. (Kamphuis & Hall 1983, Mitchener & Torfs 1996, Torfs et al. 2000, Ansari et al. 2007, Kothyari & Jain 2008, Ahmad et al. 2011, Wang et al. 2012). The computation of critical shear stress in case of cohesive sediment mixture is still under investigation and needed to be explored more especially in presence of silt and gravel together. Aberle *et al.* (2004) noticed an exponential decay of erosion rate with time and concluded the erosion rate depends on bed material properties, such as dry bulk density, water content, organic content and sand content. Empirical formulations have been derived for the computation of erosion rate of cohesionless as well as cohesive sediment by various researchers (Meyer-Peter and Müller, 1948; Parker, 1979; Misri et al., 1984; Samaga et al., 1986; Parker, 1990; Mitchener and Torfs, 1996; Sanford and Maa, 2001; Aberle, 2004; Jain and Kothyari, 2009; Xu et al., 2014). Most of the study in the past has been conducted for cohesive mixture of mud-sand, clay-sand, clay-gravel, clay-sand-gravel, etc. However, the study on the transport rate of sediments in the cohesive mixture of clay consisting of silt and gravel together has not yet performed. Garde and Ranga Raju (2000) defined the equilibrium condition as "a certain length of an alluvial stream is said to be in equilibrium if the amount of sediment coming into this reach is equal to the sediment going out from the same". Stream equilibrium is significantly important in the study of sediment transport as it responses to degradation and aggradation in the channel bed. Julian (2002) reported occurrence of degradation in response to carrying capacity of stream till a stable bed condition reached and further there is no transport of sediment due to development of an armor layer corresponds to equilibrium condition. The rate of degradation of channel bed decreases with time as the erosion rate decreases with time (Vogel et al., 1992; Jain, 2008). The channel bed

degradation is affected by the variation of clay percentage in the sediment mixture. Formulation for the computation of transient bed profile in case of cohesive sediment mixture needs to be investigated yet. The study of turbulence flow characteristics is useful in future references for linking it with sediment transport study. Dey et al. (2011) conducted experimental study for turbulence characteristics near the bed of non-cohesive sediment corresponding to entrainment threshold. Köse (2011) observed vertical distribution of turbulence quantities on rough bed of trapezoidal open channel. Carollo et al. (2005) presented results of an experimental study of turbulence intensity in the gravel bed. Guo and Julien (2001) investigated the theoretical and experimental results of suspended sediment on turbulence parameters and reported that vertical distribution of turbulence intensity decreases in the sediment-laden flow. Nikora and Goring (2000) reported different behavior for the vertical distributions of local mean velocities, turbulence intensities, and shear stresses over weakly and fixed gravel bed. Most of the above study has been conducted on channel bed made of cohesionless sediment. Hence, turbulence characteristics of flow over degraded cohesive bed need to be investigated.

The present study aims on the following objectives:

I. Identification of correct parameters that influence initiation of detachment condition and erosion rates of clay-sand-silt-gravel mixtures having cohesive properties.
II. Development of rational methods for computation of the condition for initiation of detachment and erosion rate of cohesive non-uniform sediments.
III. Validation of the developed methods using laboratory data.
IV. To study the bed degradation profile of the cohesive bed consisting of clay-silt-sand-gravel, clay-silt-gravel and clay-silt-sand mixtures.
V. To study the turbulence flow characteristics on degraded cohesive bed of non-uniform mixture.

The experiments were conducted in a tilting flume having 16 m length, 0.75 m width and 0.50 m depth in Hydraulic Engineering Laboratory, Civil Engineering Department, Indian Institute of Technology Roorkee, Roorkee, India. The channel had a test section of 6.0 m length, 0.75 m width and 0.18 m depth starting at a distance of 7.0 m from the channel entrance. Three types of cohesive sediment mixtures i.e. clay-silt-gravel, clay-silt-sand-gravel and clay-silt-sand were used in the present study. In all three cohesive sediment mixtures, the percentage of clay was

varied from 10% to 50% on weight basis while the other sediments (i.e. cohesionless sediments) were taken in equal proportions. The test section of the channel bed was prepared using dynamic compaction method. Incipient motion was examined for the coarsest particle present in the mixture i.e. critical shear stress was measured for gravel particles in case of clay-silt-gravel mixture and clay-silt-sand-gravel mixture; however, in case of clay-silt-sand mixture the incipient motion was observed for sand particles. The transported sediment was collected in terms of bed load using rectangular trap for sand and gravel particles while suspended load collected using integrated depth sampler for silt and clay particles. The transient bed profile, water surface profile along with the bed load and suspended load were measured simultaneously at regular time intervals. The flow in the channel was continued till the bed profile comes in static state and collection of bed load becomes very less compared to initial bed load collected. The degraded channel bed was established after the equilibrium stage reached for the transport of sediment from the channel bed. Then, the Vectrino+ ADV was installed over the flume in the working section part of the channel bed for collecting the three dimensional velocity data. The 3D-velocity data were collected corresponding to 0%, 30%, and 50% clay content in all the degraded channel bed of clay-silt-gravel, clay-silt-sand-gravel, and clay-silt-sand mixtures. The data were collected in both directions i.e. longitudinally and vertically. A four transducer beam probe (down-looking) of ADV was used to capture the instantaneous velocity components. The data were measured at a sampling rate of 100 Hz for duration of 2400 s to achieve a statistically time-independent averaged quantity.

The critical shear stress for the gravel particles was found to be lower in presence of silt. The physical appearance of top surface of bed was dominating with gravel particles for lower clay content after the incipient motion run. A new equation is developed for predicting the critical shear stress of gravel particle in cohesionless sediment mixture which shows a good agreement between observed and computed values. High clay percentage significantly increases the critical shear stress. Clay content and bulk density along with sediment size are identified as the main parameters governing the incipient motion in case of cohesive sediment mixture. A relationship has been developed for the computation of critical shear stress of gravel particles that suited to cohesive sediment mixture of clay-gravel, clay-sand-gravel, clay-silt-gravel, and clay-silt-sand-gravel. A relationship has also been developed for the computation of critical shear stress of sand particles in cohesive sediment mixture of clay-silt-sand. Clay content and excess shear stress

along with time was found to be governing factors for the computation of the transport rate of sediment. The model has been developed based on identified parameters for the computation of bed load transport rate and suspended load transport rate respectively for clay-silt-gravel mixture, clay-silt-sand-gravel mixture, and clay-silt-sand mixture. Degradation of channel bed decreases with the increase of clay percentage. Increase in excess shear stress accelerates the degradation, and the bed degradation found decreases with the increases of time. The maximum degradation was found to occur at 50 cm from the entrance of upstream working section for all the three cohesive sediment mixture in the present study. A relationship has been proposed for the computation of bed profile for cohesive mixture of clay-silt-gravel, clay-silt-sand-gravel, and clay-silt-sand. The fluctuation for vertical distribution of velocity is higher in upstream sections than that of downstream sections over the degraded bed. The fluctuation in vertical distribution of velocity was found reduced with increase of clay percentage. The maximum degradation section in the channel bed was noticed around the section where the resultant flow velocity appeared to be reversal. The position of maximum value of normalized turbulence intensity, turbulence kinetic energy, and Reyonlds shear stress has been found around the initial bed level for cohesive mixture; however, this position of maximum value occurs below the initial bed level in case of absence of clay in the mixture.

# LIST OF SYMBOLS

| Symbol | Description of symbol |
|---|---|
| $A$ | Cross sectional area of flow |
| $A_c$ | Movability number corresponding to incipient motion |
| $a_m$ | Mobility factor |
| $A_x^\eta$ | Derivative of A with respect to x when $\eta$ is held constant |
| $B$ | Water surface width |
| $B_p$ | Bimodality parameter |
| $B_r$ | Minimum value of $B$ |
| $b_2$ | Exponent |
| $C$ | Chezy friction coefficient |
| $C_{ae}$ | Flux-averaged total-load volumetric concentration |
| $C_i$ | Size-specific sediment concentration |
| $C_D$ | Drag coefficient |
| $C_L$ | Lift coefficient |
| $C_1$ and $C_2$ | Constants related to the mud cohesion |
| $Clay(U.S.)$ | Mass fraction finer than 0.005 mm in percent |
| $C_*$ | Dimensionless Cohesion for cohesive sediment mixture |
| $d_a$ | Arithmetic mean size of the sediment mixture |

| | |
|---|---|
| $D_c$ | Grain size of coarse mode in bimodal sediments |
| $D_f$ | Grain size of fine mode in bimodal sediments |
| $d_g$ | Geometric mean size of the sediment mixture |
| $d_j$ | Particles staying in front of particle size $d_i$ |
| $D_k$ | Size-specific sediment deposition fluxes |
| $d_{scw}$ | Depth of scour in the wake zone of pier |
| $d_{sdo}$ | Median size of the silt particle |
| $d_{sm}$ | Maximum scour depth in cohesive sediment |
| $d_{smc}$ | Maximum scour depth in cohesionless sediment |
| $d_{ss}$ | Depth of scour in cohesionless sediment at the end of run |
| $D_T$ | Total sediment deposition fluxes |
| $d_*$ | Scaling grain size |
| $d_{50}$ | Median size of the sediment |
| $d_{50}$ | Median diameter of sediment in transport |
| $d_*$ | Non-dimensional particle diameter; |
| $E$ | Erosion rate |
| $E_k$ | Size-specific sediment entrainment fluxes |
| $e_r$ | Void ratio |
| $E_T$ | Total sediment entrainment fluxes |
| $f_{ak}$ | Fraction of the k$^{th}$ size sediment in active layer |

| | |
|---|---|
| $F_d$ | Dimensionless particle Froude number |
| $f_i$ | Proportion of fraction i in the bed sediment |
| $Fines$ | Fines content (<0.075 mm) of the soil in percent |
| $f_{ik}$ | Fraction of the $k^{th}$ size sediment |
| $f_{xai}$ | Transport capacity distribution function for size fraction $i$ |
| $F_{w1}$ | Parameter for clay-gravel mixture bed |
| $F_{w2}$ | Parameter for clay-sand-gravel mixture bed |
| $g$ | Acceleration due to gravity |
| $G_s(x,t)$ | Solid transport intensity |
| $h$ | Flow depth |
| $\tilde{h}$ | Non-dimensional flow depth |
| $i_B$ | Percentage of sediment size by weight in the bed load |
| $i_b$ | Percentage of sediment size by weight in the bed material |
| $\tilde{I}_{HET}$ | Predicted erosion rate index for the hole erosion test |
| $I_p$ | Plasticity index |
| $I_w$ | Lower plastic limit |
| $k_c$ | Characteristic dimension of supporting particles |
| $K_d$ | Size gradation correction factor |
| $k_u$ | Coefficient dependent on Kramer's uniformity coefficient |
| $K'$ | Bed dependent characteristic coefficient |

| | |
|---|---|
| $k_1$ | Proportionality constant for particle volume |
| $k_2$ | Proportionality constant for particle weight lever arm |
| $k_3$ | Proportionality constant for drag force lever arm |
| $k_4$ | Proportionality constant for lift force lever arm |
| $k_5$ | Proportion of normally projected area exposed |
| $k_6$ | Proportionality constant for normally projected area |
| $k_7$ | Proportion of parallel projected area exposed |
| $k_8$ | Proportionality constant for parallel projected area |
| $k_9$ | Proportionality constant for velocity position |
| $k_{10}$ | Multiple of bed particle size for grain roughness |
| $LL$ | Liquid limit in percent |
| $M$ | Kramer's uniformity coefficient |
| $m_v$ | Empirical parameter |
| $M_n$ | Total number of fractional particle in the sediment mixtures |
| $m_p$ | Constant in power law |
| $n_f$ | Factor multiple of $u_{cw}^{'}$ |
| $N_d$ | Number of granulometric classes |
| $OWC$ | Optimum water content in percent |
| $P'$ | Percentage of the individual sediment in sediment mixture |
| $P$ | Wetted perimeter |
| $P_m$ | Fraction of bed material by dry weight |

| | |
|---|---|
| $P_c$ | Clay percentage (in fraction) by weight |
| $P_{ej}$ | Total exposed probability for particle size $d_j$ |
| $P_{hj}$ | Total hidden probabilities for particle size $d_j$ |
| $PI$ | Plasticity index of the soil |
| $Pinhole$ | Pinhole test classification expressed as an ordinal number |
| $P_j$ | Percentage of particles corresponding to $d_j$ particles |
| $P_m$ | Proportion in mode in bimodal sediments |
| $P_s$ | Sand percentage in fraction |
| $P_{silt}$ | Percentage of silt content in sand-silt mixture |
| $P_{*c}$ | Dimensionless clay content |
| $Q$ | Flow discharge |
| $q$ | Flow discharge per unit width |
| $Q_b^v$ | Volumetric bed load discharge |
| $q_{bv}^v$ | Volumetric transport rate per unit width for $d_j$ |
| $q_l$ | Lateral inflow rate into the stream |
| $q_{Bl}$ | Bed load transport rate in weight per unit width |
| $q_{sl}$ | Suspended load transport rate |
| $q_{sl}$ | Sediment input rate entering the stream laterally |
| $Q_s^v$ | Volumetric suspended load discharge |
| $Q_{st}^v$ | Volumetric sediment transport rate |

| | |
|---|---|
| $q_{st}^{v}$ | Unit total volumetric sediment discharge |
| $R$ | Hydraulic radius |
| $R_{ca}$ | Calcium-sodium ratio |
| $R_m$ | Gravity based particle Reynolds number for size $d_a$ |
| $R_s$ | Gravity based particle Reynolds number for size $d_s$ |
| $R_v$ | Sediment volume on the bed per unit volume of bed layer |
| $R_e$ | Particle Reynolds number |
| $S$ | Degree of saturation in percent |
| $SC\%$ | Silt-clay percentage |
| $S_f$ | Energy slope |
| $S_v$ | Vane shear strength |
| $S_0$ | Slope of the bed in flow direction |
| $t$ | Time |
| $t_*$ | Dimensionless time |
| $\tau$ | Total shear stress |
| $\tau_{bx}$ | Shear stresses at the channel bottom in the x-direction |
| $\tau_{by}$ | Shear stresses at the channel bottom in the y-direction |
| $\tau_{cr}$ | Critical shear stress for cohesive sediment |
| $\tau_{ci}$ | Critical shear stress for $d_i$ particle size |
| $\tau_{cr}$ | Critical shear stress for cohesive river bank |

| | |
|---|---|
| $\tau_{cri}$ | Shields critical shear stress |
| $\tau_{cri,i}$ | Shields shear stress for individual size grain |
| $\tau_{cr}$ | Critical shear stress for sand |
| $\tau_{cr,f}$ | Critical shear stress for sand fraction in sand-silt mixture |
| $\tau_e$ | Excess shear stress for the arithmetic mean size |
| $\tau_{exx}$ | Depth-averaged effective stress in x-x plane |
| $\tau_{exy}$ | Depth-averaged effective stress in x-y plane |
| $\tau_{eyy}$ | Depth-averaged effective stress in y-y plane |
| $\tau_{c,m}$ | Critical shear stress for erosion of pure mud |
| $\tau_{c,s}$ | Critical shear stress for erosion of pure sand |
| $\tau_{mud}$ | Critical shear stress for mud |
| $\tau_{ri}$ | Reference critical shear stress of individual sediment size |
| $\tau_{sm}$ | Critical erosion shear stress for sand-mud mixture |
| $\tau_{*ci}$ | Dimensionless critical shear stress for cohesive mixture |
| $\tau_{*ci}$ | Dimensionless critical shear stress for size fraction $d_i$ |
| $\tau_{*cri}$ | Dimensionless critical shear stress as per Shields criteria |
| $\tau_{*cri}$ | Dimensionless critical shear stress of $d_{50}$ size |
| $\tau_m^*$ | Non-dimensional erosion resistance for mass erosion |
| $\tau_p^*$ | Non-dimensional erosion resistance for particle erosion |
| $\tau_{*ri}$ | Dimensionless reference critical shear stress for $d_i$ |
| $u$ | Flow velocity |

| | |
|---|---|
| $u_k$ | Time-averaged velocity at a grain |
| $UCS$ | Unconfined compressive strength of cohesive mixture |
| $u'_{rms}$ | Standard deviation |
| $-\overline{u'v'}$ | Reynolds stress |
| $u_*$ | Flow shear velocity |
| $u_{*c}$ | Shear velocity corresponding to incipient motion |
| $UCS^*$ | Dimensionless unconfined compressive strength |
| $v_{cf}$ | Velocity profile correction factor |
| $W$ | Antecedent moisture content of cohesive sediment |
| $W_s^*$ | Dimensionless bed load parameter |
| $w_s$ | Settling velocity of the particle |
| $W_s$ | Moisture content at saturation |
| $x$ | Horizontal distance |
| $y_0(x,t)$ | Free surface level |
| $z$ | Bed elevation |
| $z_0$ | Vertical distance |
| $\upsilon$ | Kinematic viscosity of fluid |
| $\rho$ | Fluid density |
| $\rho_b$ | Bulk density |
| $\rho_b(z)$ | Bulk density at sediment depth $z$ |

| | |
|---|---|
| $\rho_d$ | Dry density of the soil |
| $\left(\rho_d / \rho_{d\max}\right)$ | Percentage compaction in percent |
| $\rho_{d\max}$ | Maximum dry density |
| $\rho_m$ | Mud density |
| $\rho_{mix}$ | Density of water–sediment mixture |
| $\rho_r$ | Relative density |
| $\rho_s$ | Particle density |
| $\rho_b$ | Density of saturated bed material |
| $\sigma_g$ | Geometric standard deviation of the sediment mixture |
| $\phi$ | Angle of internal friction |
| $\phi_B$ | Dimensionless bed load transport rate |
| $\phi_{Bi}$ | Dimensionless bed load transport parameter for $d_i$ |
| $\phi_{cg}$ | Angle of repose for coarse grain |
| $\phi_S$ | Suspended-load transport-rate parameter |
| $\phi_t$ | Threshold value |
| $\phi_{vc}$ | Fine solids weight fraction |
| $\phi'$ | Pivot angle |
| $\phi_*$ | Dimensionless angle of internal friction |
| $\phi_{*c}$ | Dimensionless angle of repose for cohesive mixture |

| | |
|---|---|
| $\alpha_{1sg}$ | Area shape factor |
| $\alpha_{3sg}$ | Volume shape factor |
| $\alpha_s$ and $\beta_s$ | Coefficients that vary with mixture grain size distribution |
| $\beta_c$ | Empirical coefficients |
| $\beta_i$ | Concentration of the $i^{th}$ granulometric size class |
| $\beta_k$ | Velocity discrepancy coefficient |
| $\beta_l$ | Local parameter |
| $\alpha_{\beta s}, \beta_{\beta s}$, and $\zeta_{\beta s}$ | Coefficients related to flow and sediment properties |
| $\gamma_s$ | Specific weight of sediment |
| $\zeta_n$ and $\xi_n$ | Coefficients |
| $\xi_s$ i | Elevation of the bottom surface of active layer |
| $\xi_{\theta i}$ | Exposure-sheltering coefficient for sediment size $d_i$ |
| $\varepsilon_{hi}$ | Hiding function |
| $\xi_s$ | Coefficient accounted for sheltering effect |
| $\varepsilon_{ei}$ | Exposure correction |
| $\xi_{s,i}$ | Sheltering-exposure and interference parameter |
| $\theta$ | Dimensionless Shields number |
| $\theta_{ic}$ | Vertical gradient of the critical bed shear stress |
| $\eta_w$ | Water level |
| $\lambda$ | Porosity of the bed layer |

| | |
|---|---|
| $\delta$ | Thickness of active layer |
| $\Gamma$ | Total sediment feeding rates per unit channel length |
| $\Gamma_i$ | Size-specific sediment feeding rates per unit channel length |
| $\Delta w_r$ | Water content ratio in percent |
| $\chi$ | Non-dimensional soil parameter |

# LIST OF ABBREVIATIONS

| | |
|---|---|
| ADV | Acoustic Doppler velocimeter |
| ADVP | Acoustic Doppler velocity Profiler |
| ASSET | Adjustable shear stress erosion and transport |
| COR | Correlation |
| DCM | Decoupled model |
| FCM | Fully coupled model |
| GSC | Clay-silt-gravel |
| GSSC | Clay-silt-sand-gravel |
| HOLE | Hole erosion test |
| LDA | Laser Doppler anemometer |
| LGM | Largest grain method |
| MOC | Method of characteristics |
| NIWA | National Institute of Water and Atmospheric Research |
| PCM | Partially coupled model |
| PIV | Particle image velocimetry |
| RTM | Reference transport method |
| SET | Slot erosion test |
| SGM | Surface gradient method |
| SLIC | Slope Limiter Centred |

| | |
|---|---|
| SNR | Signal to noise ratio |
| SSC | Clay-silt-sand |
| TKE | Turbulent kinetic energy |

# LIST OF FIGURES


| Figure No. | Description | Page No. |
|---|---|---|
| 1.1 | Ash River bed degradation in South Africa (Beck and Basson, 2003) | 2 |
| 1.2 | Excessive scouring around footing of bridge on river Chakki, Punjab (Ramesh, 2012) | 2 |
| 1.3 | Failure of Bridge on River Gola at Haldwani, Uttrarakhand in 2008 (Ramesh, 2012) | 3 |
| 1.4 | Bed material composition of Ganga river at Rishikesh, India (Jain, 2008) | 6 |
| 3.1 | Size distribution for sediments used in experiments | 68 |
| 3.2 | A schematic view of experimental set-up of flume | 70 |
| 3.3 | Cylindrical container connected with pipe used for the measurement of bed slope | 71 |
| 3.4 | Rectangular trap used for the bed load collection | 72 |
| 3.5 | Depth integrated suspended load sampler for the collection of suspended load | 73 |
| 3.6 | 2D bed profiler | 74 |
| 3.7 | Vectrino plus down-looking probe | 75 |
| 3.8(a-b) | Preparation of sediment mixture and cohesive channel bed | 76 |
| 3.9 | Patches from the test section after incipient motion run for (a) gravel-silt mixture, and (b) gravel-sand-silt mixture | 79 |
| 3.10(a-d) | Visual observations for incipient motion at clay-silt-sand-gravel and clay-silt-gravel mixture bed | 82 |

| | | |
|---|---|---|
| 3.11 | Visual observations for incipient motion at clay-silt-sand mixture bed | 83 |
| 3.12(a-b) | Physical appearance of the top surface of the channel bed | 86 |
| 3.12(c-d) | Physical appearance of the top surface of the channel bed | 87 |
| 3.12(e-f) | Physical appearance of the top surface of the channel bed | 88 |
| 3.13 | ADV set-up over the flume | 91 |
| 3.14 | Schematic diagram of experimental flume for ADV measurements | 92 |
| 4.1 | Variation of dimensionless critical shear stress with particle Reynolds number | 97 |
| 4.2 | Observed and computed critical shear stress as per (a) Egiazaroff (1965); (b) Hayashi et al. (1980); (c) Wu *et al.* (2000); (d) present study Eq. (4.8) | 99 |
| 4.3. | Variation of dimensionless critical shear stress with particle Reynolds number for cohesive sediment mixture and cohesionless sediment | 106 |
| 4.4 | Variation of $(\tau_{cc}/\tau_{cm})$ with $P_c$ | 108 |
| 4.5 | Variation of $(\tau_{cc}/\tau_{cm})$ with $\sigma_{cc}$ it | 109 |
| 4.6 | Variation of $(\tau_{cc}/\tau_{cm})$ with $(\gamma_b/\gamma_w)$ it | 110 |
| 4.7 | Comparison of observed and computed value of $(\tau_{cc}/\tau_{cm})$ using Eq. (4.15) | 112 |
| 4.8 | Comparison of observed and computed value of $(\tau_{cc}/\tau_{cm})$ using Eq. (4.16) | 113 |
| 4.9 | Bed level variations for clay-silt-gravel mixture having 10% clay content | 117 |
| 4.10 | Variation of sediment transport rate for clay-silt-gravel mixture having 50% clay content | 118 |
| 4.11 | Equilibrium time plot w.r.t. clay % for clay-silt-sand-gravel mixture | 118 |
| 4.12 | Variation of clay fraction with dimensionless equilibrium time | 120 |

| | | |
|---|---|---|
| 4.13a | Variation of $t_e^*$ with $\tau_c^*$ for different % of clay in clay-silt-gravel mixture | 120 |
| 4.13b | Variation of $t_e^*$ with $\tau_c^*$ for different % of clay in clay-silt-sand-gravel mixture | 121 |
| 4.13c | Variation of $t_e^*$ with $\tau_c^*$ for different % of clay in clay-silt-sand mixture | 121 |
| 4.14 | Comparison between computed and observed dimensionless equilibrium time | 122 |
| 4.15 | Variation of initial bed load transport rate with clay percentage | 124 |
| 4.16 | Variation of initial bed load transport rate with dimensionless excess shear stress for clay-silt-gravel mixture | 125 |
| 4.17 | Variation of initial bed load transport rate with dimensionless excess shear stress for clay-silt-sand-gravel mixture | 125 |
| 4.18 | Variation of initial bed load transport rate with dimensionless excess shear stress for clay-silt-sand mixture | 126 |
| 4.19 | Comparison between computed and observed value of $q_{BT}^*$ | 128 |
| 4.20 | Variation of $M_{BT,e}^*$ with $P_c$ | 130 |
| 4.21 | Variation of $M_{BT,e}^*$ with $\tau_c^*$ | 131 |
| 4.22 | Variation of $M_{BT,e}^*$ with $h^*$ | 132 |
| 4.23 | Comparison of observed and computed value of $M_{BT,e}^*$ using Eq. (4.39) | 134 |
| 4.24 | Comparison of observed and computed value of $M_{BT,e}^*$ using Eq. (4.40) | 137 |
| 4.25 | Comparison of observed and computed value of $M_{BT,e}^*$ using Eq. (4.41) | 138 |
| 4.26 | Variation of bed load transport rate with clay fraction for the | 139 |

present study

| | | |
|---|---|---|
| 4.27 | Variation of bed load transport rate with time | 140 |
| 4.28 | Variation of bed load transport rate with excess shear stress | 141 |
| 4.29 | Fitted curve for clay-silt-gravel mixture in the present study | 142 |
| 4.30 | Fitted curve for clay-silt-sand-gravel mixture in the present study | 143 |
| 4.31 | Fitted curve for clay-silt-sand mixture in the present study | 143 |
| 4.32 | Comparison between computed and observed value of $q_{BT}^*$ | 144 |
| 4.33 | Variation of initial suspended load transport rate with clay fraction in dimensionless form | 145 |
| 4.34 | Variation of initial suspended load transport rate with excess shear stress in dimensionless form for clay-silt-gravel mixture | 146 |
| 4.35 | Variation of initial suspended load transport rate with excess shear stress in dimensionless form for clay-silt-sand-gravel mixture | 146 |
| 4.36 | Variation of initial suspended load transport rate with excess shear stress in dimensionless form for clay-silt-sand mixture | 147 |
| 4.37 | Comparison between computed and observed value of $q_{sf}^{i*}$ | 148 |
| 4.38 | Variation of suspended load transport rate with clay fraction for the present study | 149 |
| 4.39 | Variation of suspended load transport rate with time for the present study | 150 |
| 4.40 | Variation of suspended load transport rate with excess shear stress for the present study | 150 |
| 4.41 | Fitted curve for clay-silt-gravel mixture in the present study | 152 |
| 4.42 | Fitted curve for clay-silt-sand-gravel mixture in the present study | 153 |
| 4.43 | Fitted curve for clay-silt-sand mixture in the present study | 153 |
| 4.44 | Comparison between computed and observed value of $q_{sf}^*$ | 154 |

| | | |
|---|---|---|
| 4.45 | Variation of degradation with clay fraction for present study | 155 |
| 4.46 | Variation of degradation with excess shear stress for present study | 156 |
| 4.47 | Variation of degradation with time for 10% clay in mixtures | 157 |
| 4.48 | Variation of degradation along the channel bed for present study | 158 |
| 4.49 | Variation of maximum degradation with clay fraction for present study | 159 |
| 4.50 | Variation of maximum degradation with excess shear stress for present study | 160 |
| 4.51 | Comparison between computed and observed $z_{max}$ | 161 |
| 4.52 | Variation of $\frac{z}{z_{max}}$ with $\frac{t}{t_e}$ for 10% clay in the mixtures | 162 |
| 4.53 | Variation of $\frac{z}{z_{max}}$ of with $\frac{X}{L_{min}}$ | 163 |
| 4.54a | Comparison between computed and observed $\frac{z}{z_{max}}$ | 164 |
| 4.54b | Comparison between computed and observed $\frac{z}{z_{max}}$ | 165 |
| 4.54c | Comparison between computed and observed $\frac{z}{z_{max}}$ | 165 |
| 4.55 | Comparison between computed and observed bed profile for 10% clay in clay-silt-gravel mixture | 166 |
| 4.56 | Comparison between computed and observed bed profile for 20% clay in clay-silt-gravel mixture | 167 |
| 4.57 | Comparison between computed and observed bed profile for 30% clay in clay-silt-gravel mixture | 168 |
| 4.58 | Comparison between computed and observed bed profile for 40% clay in clay-silt-gravel mixture | 169 |

| | | |
|---|---|---|
| 4.59 | Comparison between computed and observed bed profile for 50% clay in clay-silt-gravel mixture | 170 |
| 4.60 | Comparison between computed and observed bed profile for 10% clay in clay-silt-sand-gravel mixture | 171 |
| 4.61 | Comparison between computed and observed bed profile for 20% clay in clay-silt-sand-gravel mixture | 172 |
| 4.62 | Comparison between computed and observed bed profile for 30% clay in clay-silt-sand-gravel mixture | 173 |
| 4.63 | Comparison between computed and observed bed profile for 40% clay in clay-silt-sand-gravel mixture | 174 |
| 4.64 | Comparison between computed and observed bed profile for 50% clay in clay-silt-sand-gravel mixture | 175 |
| 4.65 | Comparison between computed and observed bed profile for 10% clay in clay-silt-sand mixture | 176 |
| 4.66 | Comparison between computed and observed bed profile for 20% clay in clay-silt-sand mixture | 177 |
| 4.67 | Comparison between computed and observed bed profile for 30% clay in clay-silt-sand mixture | 178 |
| 4.68 | Comparison between computed and observed bed profile for 40% clay in clay-silt-sand mixture | 179 |
| 4.69 | Comparison between computed and observed bed profile for 50% clay in clay-silt-sand mixture | 180 |
| 5.1 | Velocity profile over degraded bed of clay-silt-sand mixture for run no. SSC 9 | 185 |
| 5.2 | Velocity profile over degraded bed of clay-silt-sand mixture for run no. SSC 12 | 185 |
| 5.3 | Velocity profile over degraded bed of clay-silt-sand mixture for run no. SSC 20 | 186 |
| 5.4 | Velocity profile over degraded bed of clay-silt-sand mixture for run no. SSC 19 | 186 |
| 5.5 | Velocity profile over degraded bed of clay-silt-sand mixture for run no. SSC 21 | 187 |

| | | |
|---|---|---|
| 5.6 | Velocity profile over degraded bed of clay-silt-sand mixture for run no. SSC 22 | 187 |
| 5.7 | Velocity profile over degraded bed of clay-silt-sand-gravel mixture for run no. GSSC 7 | 188 |
| 5.8 | Velocity profile over degraded bed of clay-silt-gravel mixture for run no. GSC 15 | 188 |
| 5.9 | Distribution of resultant velocity for clay-silt-sand mixture for run no. SSC 9 | 190 |
| 5.10 | Distribution of resultant velocity for clay-silt-sand mixture for run no. SSC 12 | 190 |
| 5.11 | Distribution of resultant velocity for clay-silt-sand mixture for run no. SSC 20 | 191 |
| 5.12 | Distribution of resultant velocity for clay-silt-sand mixture for run no. SSC 19 | 191 |
| 5.13 | Distribution of resultant velocity for clay-silt-sand mixture for run no. SSC 21 | 192 |
| 5.14 | Distribution of resultant velocity for clay-silt-sand mixture for run no. SSC 22 | 192 |
| 5.15 | Distribution of resultant velocity for clay-silt-sand-gravel mixture for run no. GSSC 7 | 193 |
| 5.16 | Distribution of resultant velocity for clay-silt-gravel mixture for run no. GSC 15 | 193 |
| 5.17(a-d) | Distribution of turbulence parameters over degraded bed of clay-silt-sand mixture for run no. SSC 9 | 198 |
| 5.17(e-h) | Distribution of turbulence parameters over degraded bed of clay-silt-sand mixture for run no. SSC 9 | 199 |
| 5.18(a-d). | Distribution of turbulence parameters over degraded bed of clay-silt-sand mixture for run no. SSC 12 | 200 |
| 5.18(e-h). | Distribution of turbulence parameters over degraded bed of clay-silt-sand mixture for run no. SSC 12 | 201 |
| 5.19(a-d). | Distribution of turbulence parameters over degraded bed of clay-silt-sand mixture for run no. SSC 20 | 202 |

| | | |
|---|---|---|
| 5.19(e-h). | Distribution of turbulence parameters over degraded bed of clay-silt-sand mixture for run no. SSC 20 | 203 |
| 5.20(a-d) | Distribution of turbulence parameters over degraded bed of clay-silt-sand mixture for run no. SSC 19 | 204 |
| 5.20(e-h) | Distribution of turbulence parameters over degraded bed of clay-silt-sand mixture for run no. SSC 19 | 205 |
| 5.21(a-d) | Distribution of turbulence parameters over degraded bed of clay-silt-sand mixture for run no. SSC 21 | 206 |
| 5.21(e-h) | Distribution of turbulence parameters over degraded bed of clay-silt-sand mixture for run no. SSC 21 | 207 |
| 5.22(a-d) | Distribution of turbulence parameters over degraded bed of clay-silt-sand mixture for run no. SSC 22 | 208 |
| 5.22(e-h) | Distribution of turbulence parameters over degraded bed of clay-silt-sand mixture for run no. SSC 22 | 209 |
| 5.23(a-d) | Distribution of turbulence parameters over degraded bed of clay-silt-sand-gravel mixture for run no. GSSC 7 | 210 |
| 5.23(e-h) | Distribution of turbulence parameters over degraded bed of clay-silt-sand-gravel mixture for run no. GSSC 7 | 211 |
| 5.24(a-d) | Distribution of turbulence parameters over degraded bed of clay-silt-gravel mixture for run no. GSC 15 | 212 |
| 5.24(e-h) | Distribution of turbulence parameters over degraded bed of clay-silt-gravel mixture for run no. GSC 15 | 213 |

# LIST OF TABLES


| Table No. | Description | Page No. |
|---|---|---|
| 3.1 | Clay properties | 68 |
| 3.2 | Proportion of sediments in their mixture | 69 |
| 3.3 | Range of measured parameters for incipient motion of cohesive sediment mixture in the present study | 78 |
| 3.4 | Range of data on erosion and transport for cohesionless mixture | 89 |
| 3.5 | Range of data on erosion and transport for cohesive mixture | 89 |
| 4.1 | Range of parameters for incipient motion | 96 |
| 4.2 | Statistical analysis for computed and observed value of $\tau_{cw,g}$ | 102 |
| 4.3 | Range of measured parameters for incipient motion of cohesive sediment mixture in the present study | 104 |
| 4.4 | Range of *UCS* (KN/m$^2$) for compaction level used in the present study | 111 |
| 4.5 | Statistical analysis of computed and observed $(\tau_{cr}/\tau_{cw})$ as per Eqs. (4.17) - (4.19) | 115 |
| 4.6 | Statistical analysis of computed and observed value of $M_{BL,r}^{c*}$ | 135 |

# CONTENTS


| *Chapter* | *Title* | *Page No.* |
|---|---|---|
| | Abstract | i |
| | List of Symbols | vii |
| | List of Abbreviations | xix |
| | List of Figures | xxi |
| | List of Tables | xxix |
| | Contents | xxxi |
| 1 | **INTRODUCTION** | |
| | 1.1 INTRODUCTION | 1 |
| | 1.2 BRIEF REVIEW OF LITERATURE | 4 |
| | 1.2.1 Incipient Motion for Cohesionless Sediment Mixture | 4 |
| | 1.2.2 Incipient Motion for Cohesive Sediment Mixture | 5 |
| | 1.2.3 Detachment and Transport of Sediment | 7 |
| | 1.2.4 Equilibrium and Channel Bed Degradation | 8 |
| | 1.2.5 Turbulence Characteristics | 9 |
| | 1.3 THE PROBLEM IDENTIFICATION | 10 |
| | 1.4 OBJECTIVES | 10 |
| | 1.5 METHODOLOGY | 11 |
| | 1.6 LIMITATIONS | 11 |

1.7 STRUCTURE OF THE REPORT 12

2 **REVIEW OF LITERATURE**

2.1 GENERAL 13

2.2 CRITICAL SHEAR STRESS FOR NON-UNIFORM SEDIMENT 13

2.2.1 Critical Shear Stress of Non-uniform Cohesionless Sediment 13

2.2.2 Critical Shear Stress of Cohesive Sediment 24

2.3 TRANSPORT RATE OF SEDIMENT 32

2.4 COMPUTATION FOR THE DEGRADED BED PROFILE 46

2.5 TURBULENCE CHARACTERISTICS OF FLOW OVER CHANNEL BED 55

2.6 CONCLUDING REMARKS 65

3 **MATERIALS AND METHODS**

3.1 GENERAL 67

3.2 SEDIMENT AND ITS MIXTURE 67

3.2.1 Sediment Properties 67

3.2.2 Sediment Mixture 69

3.3 EXPERIMENTAL SET-UP & MEASUREMENTS 69

3.3.1 Channel Slope Measurement 70

3.3.2 Discharge Measurement 71

3.3.3 Bed Load Measurement 71

3.3.4 Suspended Load Measurement 72

3.3.5 Bed and Water Surface Profile Measurements 73

3.3.6 Velocity Measurements for Turbulence Parameter 74

3.4 COHESIVE BED PREPARATION 75

3.5 EXPERIMENTAL PROCEDURE AND OBSERVATIONS 76

3.5.1 Incipient Motion Process 76

3.5.2 Visual Observations for Incipient Motion 78

3.5.2.1 Visual observations for cohesionless sediment mixture 78

3.5.2.2 Visual observations for cohesive sediment mixture 80

3.5.3 Transport of Sediments and bed degradation 84

3.5.3.1 Transport of sediments and bed degradation for cohesionless mixture 84

3.5.3.2 Transport of sediments and bed degradation for cohesive mixture 84

3.5.4 Turbulence Characteristic of flow 90

3.6 CONCLUDING REMARKS 92

4 **RESULTS AND DISCUSSIONS**

4.1 INTRODUCTION 95

4.2 INCIPIENT MOTION FOR COHESIONLESS SEDIMENT MIXTURE 95

4.2.1 Development of a New Formulation 98

4.2.2 Goodness of Fit Test 101

4.3 INCIPIENT MOTION FOR COHESIVE SEDIMENT 102

4.3.1 Development of Relationships for Critical Shear Stress 105

4.3.2 Goodness of Fit Test 113

4.4 TRANSPORT OF SEDIMENT FROM COHESIVE CHANNEL BED 116

4.4.1 Equilibrium Time 116

4.4.2 Bed Load Transport 123

4.4.2.1 Initial bed load transport rate 123

4.4.2.2 Cumulative bed load 128

4.4.2.3 Bed load transport rate 138

4.4.3 Suspended Load Transport 144

4.4.3.1 Initial suspended load transport rate 144

4.4.3.2 Suspended load transport rate 149

4.5 TRANSIENT BED SURFACE PROFILES 154

4.6 CONCLUDING REMARKS 181

5 **TURBULENCE CHARACTERISTICS OF FLOW**

5.1 INTRODUCTION 183

5.2 FLOW VELOCITY 183

5.2.1 Longitudinal Velocity Profile 184

5.2.2 Vector Plot for Resultant Velocity 189

5.2.3 Turbulence Characteristics 194

5.3 CONCLUDING REMARKS 214

| | | |
|---|---|---|
| 6 | CONCLUSIONS | 215 |
| | REFERENCES | 219 |
| | APPENDIX – A | 229 |
| | APPENDIX – B | 233 |
| | APPENDIX – C | 277 |

# CHAPTER - I

# INTRODUCTION

## 1.1 INTRODUCTION

Weathering is the first step in the transforming of solid rocks into sediments. In the process of formation of sediment, the weathered product is eroded from their original location by erosion process that may be taken place due to action of gravity or running water or wind action or by moving ice. However, fluvial hydraulics deals with the process of erosion, transportation, and deposition of sediment in channels by the action of running water. Development of human life is significantly linked with the progress in the knowledge of river engineering as most of the early civilizations developed near river valley. The progress in the knowledge of hydraulic structures resulted in the construction of structures across the rivers which instrumental in the development of civilization. For example, constructions of dam across the river serve the purpose of storage of water, irrigation supply, electricity generation, etc. The construction of bridges connects the pathway across the river. However, failure of these structures resulted in enormous loss of life and money which becomes the indicator of need to focus the study on the behavior of alluvial channels in respect of sediment transport. The sediment transport in alluvial channel significantly affected the life of hydraulic structures made under alluvial channels. Alluvial rivers are generally in a process of natural adjustment through changes in cross-sectional geometry, bed elevation, slope, etc in response to the variations in runoff and sediment inflow. However, human activity accelerated the changes occurring in the rivers. Deposition of sediments upstream of dams, degradation of channel bed below dams, local scour around hydraulic structures, etc. are some examples of changes in river morphology due to human activity. The quantity of sediment coming with flow in alluvial channel plays a significant role in the erosion of channel bed in alluvial river. Little or no sediment in the incoming flow in channel may result in hungry water or sediment-starved water that leads to channel incision and may cause the undermining of bridges and other structures. Garde and Ranga Raju (2000) cited the failure of Islam weir on the Sutlej River due to degradation. In Yellow river, bed level was lowered by an average of 4.5 m in a 50 km reach due to less heavily sediment-laden water (Garde and Ragga Raju, 2000). Few examples in the physical form for degradation have been illustrated below through Fig. 1.1 to 1.3

which shows the bed degradation in alluvial channel, scour around footing of bridge and failure of bridge.

Fig. 1.1 Ash River bed degradation in South Africa (Beck and Basson, 2003)

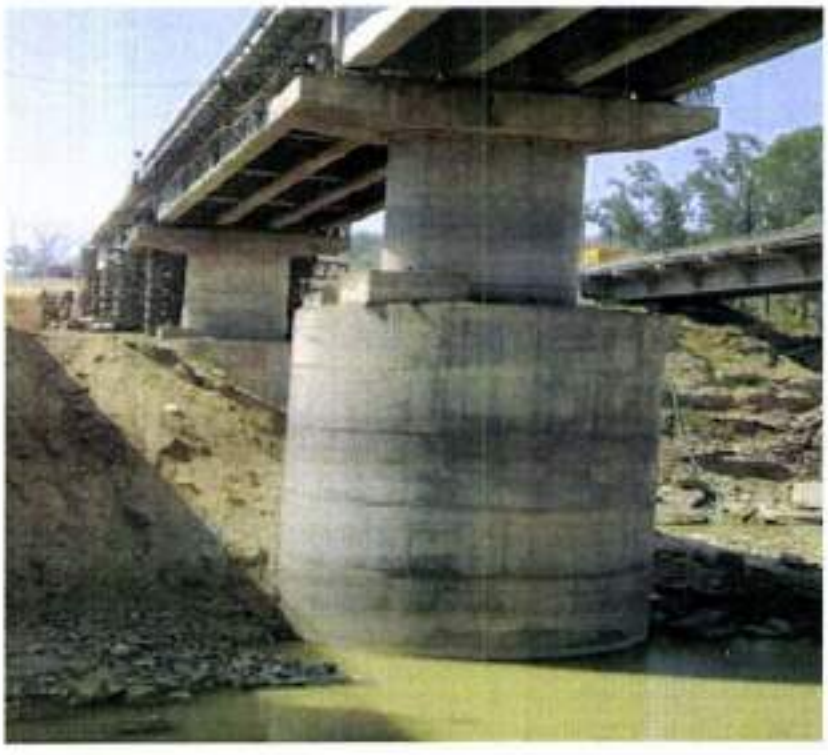

Fig. 1.2 Excessive scouring around footing of bridge on river Chakki, Punjab (Ramesh, 2012)

Fig. 1.3 Failure of Bridge on River Gola at Haldwani, Uttrarakhand in 2008 (Ramesh, 2012)

The erosion of sediment from the bed in an alluvial channel starts when the hydrodynamic forces that cause erosion exceeds the forces within the sediment that resists it. However, eroded particles from the channel bed may need not result in the equal quantity of yield as that erosion. The part of eroded sediments may deposit in between the reach before downstream end due to insufficient carrying capacity of sediment by flow or may be due to obstacles of hydraulic structure like dam. The deposition of sediment in between the reach may have detrimental effects, for example, Kothyari (1996) reported a bridge constructed in 1919 over a torrent crossing the Dehradun-Mussoorie road had a clearance of 16.7 m below its soffit, however, due to deposition of sediment particles or aggradation leads to reduction in clearance up to 12.2 m in 1941. Sediment deposition in the reservoir reduces it's the water storage capacity or shorten the design life of reservoir. For ex., Srirama Sagar reservoir in Andra Pradesh found to have lost 25 % of its capacity during the first 14 years of impounding (Kothyari, 1996). Durgunoğlu and Singh (1993) reported the storage in Loiza Reservoir in Puerto Rico was reduced from $25.3 \times 10^6$ $m^3$ to $14.4 \times 10^6$ $m^3$ in 39 years as a result of sedimentation. Erosion and transport of sediment in a river channel may cause the issue of water quality that may have the harmful impact on the aquatic environment, wild life, and human life. Owens et al. (2005) reported that 10% of lakes, rivers and bays of the USA have sediment contaminated with toxic chemicals. Sedimentation or silting in river channels and aggradation of bed may causes endangering navigation and also

impacted on the economic aspect, so, to maintain the utility of the reservoir, dam, navigation channel, etc deposited sediments have to be removed periodically that costs enormously. Durgunoğlu and Singh (1993) reported a four year dredging project in Illinois cost approximately $10 million for the removal of about 2.7 x $10^6$ $m^3$ sediments from the upstream delta portion of Lake Springfield. So the change in river bed morphology causes the various problems like reservoir sedimentation, hydraulic structures failures, aggradation, flood problems, water quality issues, siltation, navigation problems, etc. Hence, the study on detachment and transportation of sediment in an alluvial channel becomes important for sustainable development and use of river waters as its understanding assists in controlling the various issues reported above.

## 1.2 BRIEF REVIEW OF LITERATURE

### 1.2.1 Incipient Motion for Cohesionless Sediment Mixture

Sediment transport is the movement of solid particles i.e. sediment, typically due to a combination of gravity acting on the sediment, and/or the movement of the fluid/water in which the sediment is entrained. The mechanism of detachment and transport of sediment in alluvial channel is an important aspect in the channel behavior. The beginning of the movement of sediment particles, from the channel bed, is characterized by the incipient motion condition in an open channel flow. The incipient motion condition occurs when the flow induced shear stress over the bed exceeds to a certain critical value known as critical shear stress. The study of incipient motion is significantly important as it is instrumental in solving various problems like soil erosion, reservoir sedimentation, design of stable channel, river morphological predictions and effect of deposition of fine sediment on aquatic life etc. Shields (1936) have been the pioneer for introducing the incipient motion curve widely known as Shields curve for determining the critical shear stress of uniform cohesionless sediment. Later on incipient motion for uniform cohesionless sediments was studied by Iwagaki (1956), Yang (1973), Yalin and Karahan (1979), and others. Several investigations on incipient motion of non-uniform cohesionless sediment were also reported in the literature (Egiazaroff 1965, Ashida and Michiue 1971, Parker *et al.* 1982, Bridge and Bennett 1992, Patel and Ranga Raju 1999, Dey and Debnath 2000, Wu *et al.* 2000). The incipient motion criterion is well established for the computation of critical shear stress in case of uniform cohesionless sediment (Garde and Ranga Raju 2000). However, the

critical shear stress still under investigation for non-uniform cohesionless sediment especially in presence of silt. The movement of individual particles in sediment mixture comes under the concept of unequal mobility and reported in the literature by several investigations (Egiazaroff 1965, Ashida and Michiue 1971, Hayashi et al. 1980, Parker et al. 1982, Bridge and Bennett 1992, Kuhnle 1993, Patel and Ranga Raju 1999, Wu et al. 2000, Wilcock et al. 2001, etc). Most of the study, conducted for incipient motion of non-uniform sediment, is of mixture sand and gravel. Many of the formulation for incipient motion of non-uniform cohesionless sediment are similar to the existing formulation of uniform sediment with additional correction factors. For example, Bridge and Bennett (1992) used the correction factor as a function of individual particle size and arithmetic mean of non-uniform sediment while Patel and RangaRaju (1996) used a correction factor in terms of Kramer's uniformity coefficient which is a function of particle size and its percentage. Wu et al. (2000) used a correction factor responsible for the hiding-exposure effect in non-uniform sediment transport and developed equation for the computation of critical shear stress of non-uniform sediment based on that correction factor. Based on the correction factors, a number of equations were developed for the computation of critical shear stress of non-uniform sediment (Egiazaroff 1965, Hayashi et al. 1980, Bridge and Bennett 1992, Patel and RangaRaju 1999, Wu et al. 2000, etc). However, most of the study conducted for incipient motion of non-uniform cohesionless sediment is for mixture of sand and gravel.

### 1.2.2 Incipient Motion for Cohesive Sediment Mixture

In nature the river bed material consists of mixture of cohesive as well as cohesionless materials. Singh et al. (2007) reported that the Ganga river bed is consisted of sediment having clay, silt, sand, and gravel. Jain (2008) reported the presence of clay, sand, and gravel mixture on the bank of the river Ganga at Rishikesh in Himalyan Shiwaliks. Figure 1.4 shows the bed material composition in river Ganga at Rishikesh, India.

Fig. 1.4 Bed material composition of Ganga river at Rishikesh, India (Jain, 2008)

The surface physico-chemical forces are dominating in case of cohesive sediment as the cohesive sediments are composed of small particles having large specific area. Theses physico-chemical forces includes the Van der Waals forces and other bonding forces such as hydrogen bond, cat-ion bond, chemical cementation between particles by various compounds, the double layer and particle interaction force etc. in the clay-water medium (Jain 2008). These forces vary with degree of saturation, type of shear application, drainage condition, clay percentage, and type of clay etc., therefore, the resistance of cohesive sediment to the shearing action of the stream flow is yet under investigation.

The erosion characteristic of cohesive sediment is significantly different from the cohesionless sediment due to dominancy of physio-chemical properties of the cohesive sediment (Kothyari & Jain 2010a). On mixing the cohesionless sediment with cohesive sediment, the resulting mixture possesses certain amount of cohesive property (Mitchener & Torfs 1996, Kothyari & Jain 2010a); therefore, it is treated as cohesive sediment mixture. In past, several experimental studies have been conducted on incipient motion for different cohesive sediment mixtures like clay-sand, clay-silt-sand, clay-gravel, clay-sand-gravel, etc. (Dunn 1959, Kamphuis & Hall 1983, Mitchener & Torfs 1996, Panagiotopoulos et al. 1997, Torfs et al. 2000, Julian & Torres 2006, Ansari et al. 2007, Kothyari & Jain 2008, Ahmad et al. 2011, Wang et al. 2012).

However, studies have not been found on incipient motion for the sediment mixture which includes the clay along with the silt and gravel particles. And also a few studies were found which conducted for incipient motion for the cohesive mixture of clay-silt-sand (e.g. Kamphuis and Hall 1983).

### 1.2.3 Detachment and Transport of Sediment

The resistance against the erosion is due to the submerged weight of particles in case of cohesionless sediment; however, surface physico-chemical forces are dominating factors against the erosion for cohesive sediment. When the shear stress due to stream flow exceeds the resistance force of the cohesive bed then detachment of sediment starts from the cohesive bed. And further increase in shear stress due to flow causes the transport of sediment along with the flow. The understanding of transport phenomena is important as it may result in harmful consequences. The transport of sediment in the channel may reduce the expected design life of hydraulic structures by damaging it. Deposition of sediment may block the navigation channel which may result in flooding. The deposition of fine sediment into gravel interstices acts to impede inter-gravel water flow (Owens et al. 2005) which causes reduction in oxygen levels, vital to benthic organisms.

Empirical formulations have been derived for the computation of erosion rate of cohesionless as well as cohesive sediment by various researchers (Meyer-Peter and Müller, 1948; Einstein, 1950; Ashida and Michiue, 1972; Engelund and Fredsoe, 1976; Parker, 1979; Misri et al., 1984; Parchure and Mehta, 1985; Samaga et al., 1986; Mehta et al., 1989; Parker, 1990; Mitchener and Torfs, 1996; Jepsen et al., 1997; Sanford and Maa, 2001; Aberle, 2004; Wong and Parker 2006; Jain and Kothyari, 2009; Van Prooijen and Winterwerp, 2010; Winterwerp et al. 2012; Xu et al., 2014)

Mitchenner and Torfs (1996) reported the presence of mud in the range of 3% to 15% changes the erosion mode from cohesionless to cohesive behavior. Aberle *et al.* (2004) noticed an exponential decay of erosion rate with time and concluded the erosion rate depends on bed material properties, such as dry bulk density, water content, organic content and sand content. They also reported that the erosion rate of cohesive sediment in salt environment were five times lesser than those of the fresh water environment. Jain (2008) conducted the experiment on the transport of cohesive sediment mixture (clay-gravel and clay-sand-gravel) and proposed the rate

of bed load transport in which there is no feeding of sediment in the channel and transport of sediment occurred due to excess shear stress developed on the channel bed by the clear water incoming flow. Jepsen et al. (2010) measured cohesive sediment erosion rate directly using adjustable shear stress erosion and transport (ASSET) flume and reported the fine particles moved in suspension while the coarse material (sand) transported as bed load. They concluded that fine sediments with little or no sand eroded as aggregates and maintained their integrity in the flume channel while moving as bed load while the natural sediments that have high % of sand also eroded as aggregates, however, quickly disaggregated. Most of the study in the past has been conducted for cohesive mixture of mud-sand, clay-sand, clay-gravel, clay-sand-gravel, etc. However, the study on the transport rate of sediments in the cohesive mixture of clay consisting of silt and gravel together has not yet performed.

### 1.2.4 Equilibrium and Channel Bed Degradation

A stream in equilibrium is defined as the one in which channel dimensions and slope are so adjusted over a period of time that it carries incoming sediment load and water without appreciable erosion or deposition (Mackin, 1948). Garde and Ranga Raju (2000) also defined the equilibrium condition as "a certain length of an alluvial stream is said to be in equilibrium if the amount of sediment coming into this reach is equal to the sediment going out from the same". Stream equilibrium is significantly important in the study of sediment transport as it responses to degradation and aggradation in the channel bed. When equilibrium condition in stream deviates then a change occurs in alluvial channel geometry which may causes the lowering of channel bed till the equilibrium condition of flow reached so that it balances between inflowing and outflowing water and sediment discharges. Julian (2002) reported a formation of armor layer as a representative of stable bed conditions in cohesionless channel bed when the incoming flow in the channel is clear water (i.e. no feeding of sediment in the channel) and degradation occurred in response to carrying capacity of stream till a stable bed condition reached (in case of sufficient bed depth) further which there is no transport of sediment due to development of an armor layer which corresponds to equilibrium condition as there is no incoming sediment and no outgoing sediment. The rate of degradation of channel bed decreases with time as the erosion rate decrease with time (Vogel et al., 1992; Jain, 2008) i.e. the total load increases with time in a slower manner. The channel bed degradation also affected by the variation of clay percentage in the

sediment mixture. Formulation for the computation of total bed load may serve as one of the important tools in the modeling of sediment transport study.

### 1.2.5 Turbulence Characteristics

Turbulence characteristics of flow in an open channel are very important in river hydraulics as it deals with the sediment transport, contaminant transport, and river bed degradation. Turbulence studies has been investigated in an open channel flow over the past decades on various aspects like turbulence characteristics of flow for uniform flow, steady flow, unsteady flow, effect of varying discharge, roughness of bed, sediment-laden flow, fixed channel bed, weakly mobile bed, vegetative channel bed, effect of bed forms, effect on sediment threshold, over block ramps, and around obstructions (ex. pier, abutment) made in the channel bed, etc by various researchers (Nezu 1977; Tominaga et al. 1989; Lyn 1993; Song and Graf 1996; Ahmad and Rajaratnam 1998; Nikora and Goring 2000; Song and Chiew 2001; Muzzamil and Gangadhariah 2003; Cellino and Lemmin 2004; Carollo et al. 2005; Dey and Barbhuiya 2006; Mazumdar and ojha 2007; Rodriguez and Garcia 2008; Kirkil and Constantinescu 2010; Köse 2011; Kumar and Kothyari 2012; Ahmad et al. 2013; Guan et al. 2014).

Nikora and Goring (2000) compared vertical distribution of local mean velocities, turbulence intensities, and shear stresses over weakly and fixed gravel bed. Guo and Julien (2001) investigated the theoretical and experimental results of suspended sediment on turbulence parameters and reported vertical distribution of turbulence intensity decreases in the sediment-laden flow. Carollo et al. (2005) presented results of an experimental study of turbulence intensity in the gravel bed channel using acoustic Doppler velocimeter (ADV) and reported the maximum value of turbulence intensity reduces as the roughness height increases. Dey et al. (2011) conducted experimental study for turbulence characteristics at near the bed of non-cohesive sediment corresponding to entrainment threshold. Kumar and Kothyari (2012) measured turbulence characteristics of flow around circular uniform pier and circular compound pier in the transient stage of scour hole. Ahmad et al. (2013) studied turbulence analysis over the block ramp using ADV. They found vertical turbulence intensity, Reynolds stresses and turbulent kinetic energy increases along the block ramp length.

Most of the above study has been conducted on channel bed made of cohesionless sediment. However in nature the channel bed is composed of mixture of cohesive and non-

cohesive sediment. Very few studies have been found on degraded channel bed that made of cohesive sediment mixture. Jain et al. (2015) conducted experimental study for turbulence characteristics of flow on degraded channel bed of sand-gravel mixture. However, study yet needed to be explored on degraded bed for cohesive mixture of clay-silt-gravel, clay-silt-sand-gravel, and clay-silt-sand mixture.

## 1.3 THE PROBLEM IDENTIFICATION

The brief and significant review presented above revealed that incipient motion for non-uniform sediment still under investigation. It is illustrated that, in nature, river bed material may consist mixture of cohesive and cohesionless sediment i.e. mixture of clay, silt, sand, and gravel. It has been reported that few studies conducted for the computation of critical shear stress of cohesive mixture of clay-sand, clay-sand-gravel, clay-gravel, and clay-silt-sand. However, no investigation yet carried out for cohesive mixture that contains silt and gravel together along with the clay. Turbulence characteristics of flow are an important part in the study of sediment transport. Very few studies has been available on turbulence characteristics of flow over degraded cohesive bed; however, study has not been reported so far on turbulence characteristics of flow over degraded bed composed of clay-silt-gravel, clay-silt-sand-gravel, and clay-silt-sand. It is also reported that erosion characteristics for cohesive sediment is significantly different from the cohesionless sediment. Therefore, study is needed for sediment transport under influence of clay. The present study is intended to study the sediment transport under the influence of cohesion along with presence of sand, silt, and gravel which has not been taken up so far.

## 1.4 OBJECTIVES

The present study aims on the following objectives:

I. To study the influence of cohesion on the process of incipient motion for three cohesive bed consisting of clay-silt-sand-gravel, clay-silt-gravel, and clay-silt-sand mixtures.
II. Identification of parameters influencing the initiation of detachment condition and erosion rates for all the three cohesive bed.
III. Development of rational methods for computation of incipient motion for all the three cohesive bed.

IV. Development of rational methods for computation of erosion rate for all the three cohesive bed.

V. Development of a rational method for the quantification of bed degradation profile of the cohesive bed consisting of clay-silt-sand-gravel, clay-silt-gravel and clay-silt-sand mixtures.

VI. To study the turbulence flow characteristics over degraded cohesive bed of clay-silt-sand-gravel, clay-silt-gravel, and clay-silt-sand mixtures.

## 1.5 METHODOLOGY

The present study intended to study the incipient motion, transport of sediment, and bed degradation quantification under the influence of clay along with the turbulence characteristics of flow over degraded bed. These studies have been done by carried out an extensive experiment in Hydraulic Engineering Laboratory, Civil Engineering Department, Indian Institute of Technology Roorkee, Roorkee, India. Data have been collected through conducting the experiments and then these data has been analyzed rigorously and finally analyzed data has been putted in the form of a model for the computation of incipient motion, sediment transport rate, and bed degradation profile. The other researchers' data in the past has been used in the analysis part as per the availability along with the present study data in order to make the present study proposed outcomes verified and have wider applicability. The velocity data for turbulence characteristics of flow over the stabilized degraded bed has been collected using ADV (Accoustic Doppler Velocimeter). The collected raw data of velocity has been filtered using WinADV and computations have been made for turbulence characteristics of flow i.e. for turbulence intensity, turbulence kinetic energy, and Reynolds Shear stresses.

## 1.6 LIMITATIONS

The cohesive mixture used in the present study consisted of silt, sand and gravel mixed with varying percentage of clay. The variation of clay percentage limited as 10-50%. Also the clay mineral composition used in the experiments is of single type. Experiments were conducted with uniform sediment of gravel of median size 5.5 mm, sand of median size 0.60 mm, and silt of median size 0.062 mm. The percentage of weight for cohesionless sediment was kept equal in

ratio for all the mixture. Flume used in the experiment is of rectangular shape and having constant width with side glasses.

## 1.7 STRUCTURE OF THE REPORT

For the purpose of lucid presentation, this thesis is divided into six chapters. Chapter 1 provides the basics problems in respect of sediment transport in an alluvial channel along with the objectives, methodology, and limitations of the present study. Chapter 2 describes the state-of-the art literature review for incipient motion, transport rate of sediment, bed degradation studies, and turbulence characteristics of flow. Chapter 3 describes the experimental setup and procedure adopted for the experimental investigations in the present study. Chapter 4 describes the results and discussions which involve the analysis of the collected data and the model development based on the data analysed for the computation of incipient motion, transport rate of sediment, and bed degradation profile. Chapter 5 describes the velocity profile over the degraded bed along with the turbulence characteristics of flow i.e. turbulence intensity, turbulence kinetic energy, and Reynolds Shear stress. Chapter 6 presents the outcomes of the present study.

CHAPTER – II

# REVIEW OF LITERATURE

## 2.1 GENERAL

The sediment existed in the nature may be broadly categorized as cohesionless and cohesive sediment. Further, mixing of two or more different size of sediment resulted in non-uniform sediment. The formulation for the computation of critical shear stress of uniform cohesionless sediment has been well established (Garde and Ranga Raju, 2000). There are various literature exist on the study of incipient motion for non-uniform cohesionless and cohesive sediment. The objective of the present study deals with the cohesive sediment. However, it is observed that the critical shear stress for cohesive sediment converges into cohesionless sediment under a specific condition. Hence, it is necessary to go through the literature for non-uniform cohesionless sediment before attempting on cohesive sediment. Initial sections of this chapter present the literature review on the incipient motion of cohesionless and cohesive sediments. Then the literature review has been presented on the detachment and transport rate of non-uniform sediment that includes cohesive as well as cohesionless sediment. Then in the next section, literature review regarding the study conducted for the computation of degradation bed profile has been presented. As one of the objective in the present study deals with the velocity and turbulence characteristics distribution of flow over the degraded channel bed, hence in this respect the literature review presented on the study of velocity and turbulence characteristics distribution of flow over channel bed in various conditions.

## 2.2 CRITICAL SHEAR STRESS FOR NON-UNIFORM SEDIMENT

As the non-uniform sediment classified into the cohesionless and cohesive sediment, hence this section deals with the literature review based on the study for incipient motion for cohesionless and cohesive sediment.

### 2.2.1 Critical Shear Stress of Non-uniform Cohesionless Sediment

This section mainly focused on the literature review of non-uniform cohesionless sediment. However, a widely used formula for the computation of critical shear stress of uniform cohesionless sediment as per Shields (1936) and Brownlie (1981) has been presented here.

**Shields (1936)** has been the pioneer for introducing a curve, known as Shields curve, for computing the critical shear stress of uniform cohesionless sediment. Shields curve (1936), plotted between Sheilds parameter (i.e. dimensionless critical shear stress) and particles Reynolds number, represented in the following form as

$$\theta = \frac{\tau_{cw}}{(\rho_s - \rho) g d_{50}} = f(R_*) = f\left(\frac{u_* d_{50}}{\upsilon}\right) \quad (2.1)$$

Where, $\theta$ is the dimensionless Shields number; $\tau_{cw}$ is the Shields critical shear stress ($N/m^2$); $g$ is the acceleration due to gravity ($m/s^2$); $\rho_s$ and $\rho$ are the particle and fluid density ($kg/m^3$) respectively; $d_{50}$ is the median size of the sediment (m); $R_*$ is the particle Reynolds number; $u_*$ is the flow shear velocity (m/s); and $\upsilon$ is the kinematic viscosity of fluid ($m^2/s$).

**Egiazaroff (1965)** developed the formula for the incipient motion criteria of non-uniform sediment based on the assumption that the particle is entrained when the reference velocity equals the fall velocity of the particles and this reference velocity for a particle of size $d_i$ was taken at a distance 0.63 $d_i$ from the bed. He proposed the following expression for the computation of critical shear stress of non-uniform sediment

$$\frac{\tau_{*ci}}{\tau_{*cm}} = \left[\frac{\log(19)}{\log(19\frac{d_i}{d_a})}\right]^2 \quad (2.2)$$

Where $\tau_{*ci}$ is the dimensionless critical shear stress for particle size corresponding to $d_i$ in sediment mixture; $\tau_{*cm}$ is dimensionless critical shear stress as per Shields criteria for mean size of sediment mixture; $d_a$ is arithmetic mean size of the sediment mixture (m).

**Hayashi *et al.* (1980)** modified the proposed equation of Egiazaroff (1965) for the entrainment of individual fractions in the sediment mixture. They assumed the reference velocity to act at a distance of 0.27 $d_i$ from the bed instead of 0.63 $d_i$ as per Egiazaroff (1965) and they also considered lift force responsible for entrainment of particles from the channel bed which is not with the case of Egiazaroff (1965). They expressed the following relationship for the computation of critical shear stress of individual fractions in the sediment mixture.

$$\frac{\tau_{*ci}}{\tau_{*cm}} = \left[\frac{d_i}{d_a}\right]^2, \text{ for } \frac{d_i}{d_a} < 1.0 \qquad (2.3)$$

$$\frac{\tau_{*ci}}{\tau_{*cm}} = \left[\frac{\log(8)}{\log(8\frac{d_i}{d_a})}\right]^2, \text{ for } \frac{d_i}{d_a} > 1.0 \qquad (2.4)$$

**Brownlie (1981)** has given an expression for Shields curve such that the dimensionless critical shear stress of uniform cohesionless sediment could be computed through expression instead of using Shields curve. The following equation has been expressed by him as:

$$\tau_{*cm} = 0.22Y + 0.06(10)^{-7.7Y} \qquad (2.5)$$

Where, $Y = (\sqrt{(\rho_s - \rho)g(d_{50})^3/\rho\nu^2})^{-0.6}$

**Parker et al. (1982)** used the measurable but low value of sediment transport rate for identification of incipient motion of sediment. They suggested the following incipient motion

criteria based on the dimensionless bed load transport rate for non-uniform cohesionless sediment as:

$$W_i^* = \frac{\left(\frac{\rho_s}{\rho} - 1\right) g q_{bi}^*}{f_i u_*^3}$$

(2.6)

Where $W_i^*$ is the dimensionless bed load parameter; $q_{bi}^*$ is the volumetric transport rate per unit width for the $i^{th}$ fraction of bed load ($m^2/s$); and $f_i$ is the proportion of fraction i in the bed sediment.

The value of $W_i^*$ was suggested as 0.002 for the incipient motion criteria. They also proposed the following relationship for the computation of critical shear stress for sediment fraction in non-uniform cohesionless sediment as:

$$\frac{\tau_{*ri}}{\tau_{*rm}} = \left(\frac{d_i}{d_{50}}\right)^{-0.982}$$

(2.7)

Where, $\tau_{*ri}$ is the dimensionless reference critical shear stress of individual sediment that produces a small reference transport rate (< 0.002).

**Wiberg and Smith (1987)** derived an expression, based on the balance of forces acting on individual particles at the surface of a bed, for the computation of critical shear stress for both uniform and heterogeneous sediment. They found that the critical shear stress for uniform sediment or well sorted sediment differs significantly when compared with poorly sorted or heterogeneous sediment and this difference is primarily due to the relative protrusion of the particle into the flow, the particle angle of repose, or bed pocket geometry results from sediment mixture on the bed. Their derived expression for uniform sediment depends on the near-bed drag force, lift force to drag force ratio, and particle angle of repose for a given particle size and density while for mixed or heterogeneous sediment the critical shear stress additionally depends on the relative protrusion of the grains into the flow.

**Wilcocok and Southard (1988)** conducted an experimental study and found the sorting of the sediment mixture had little effect on the critical shear stress of individual fraction in the sediment mixture. They used the Reference Transport Method as per Parker *et al.* (1982) for incipient motion of fractions corresponding to a very low, but measurable, dimensionless bed load transport rate. Their results were apparently true for the recirculating system and the feed system i.e. the system where the transport rates of individual fractions solely determined by the flow and bed sediment (recirculating system) and the systems where the fractional transport rates are imposed on the system (feed system).

**James (1990)** presented a model based on the moments of forces acting on a particle for predicting entrainment conditions for non-uniform cohesionless sediments. The method adopted is an extension of the pivoting analysis concept. The model was based on the assumption (a) initial movement of particles will take place by rolling, rather than sliding; (b) entrained particles are spherical; (c) entrained particle will roll between two adjacent supporting particles; and (d) the distance between the particle centroid and the pivot axis is assumed to be proportional to the characteristic dimension of the particle. The critical condition was analyzed in terms of the equilibrium of the moments of all forces acting on a particle about the pivot axis. The following expression was developed for the computation of critical shear stress as:

$$\frac{u_{*c}^2}{gd_{50}(\rho_r - 1)} = \frac{k_1 k_2 \sin(\phi' - S_0)}{16.531 \log_{10}^2(30.2 k_9 d_{50} v_{\sigma'} / k_{10} k_c)(C_D k_5 k_6 (k_2 \cos\phi' + k_3) + C_L k_7 k_8 (k_2 \sin\phi' + k_4))} \quad (2.8)$$

Where, $u_{*c}$ is the shear velocity corresponding to incipient motion (m/s); $\rho_r$ is the relative density; $\phi'$ is the pivot angle; $S_0$ is the slope of the bed in flow direction; $v_{\sigma'}$ is the velocity profile correction factor; $k_c$ is the characteristic dimension of supporting particles (m); $C_D$ is the drag coefficient; $C_L$ is the lift coefficient; $k_1$ is proportionality constant for particle volume; $k_2$ is proportionality constant for particle weight lever arm; $k_3$ is proportionality constant for drag force lever arm; $k_4$ is proportionality constant for lift force lever arm; $k_5$ is proportion of normally projected area exposed; $k_6$ is proportionality constant

for normally projected area; $k_y$ is proportion of parallel projected area exposed; $k_s$ is proportionality constant for parallel projected area; $k_0$ is proportionality constant for velocity position; and $k_{10}$ is multiple of bed particle size for grain roughness.

**Wilcock (1993)** identified the degree of bimodality for the computation of critical shear stress of individual sediment in the mixed size sediment. He proposed the following equation for the computation of the critical shear stress which depends upon mean grain size of mixture, size of each fraction, and the degree of bimodality of the mixture size distribution.

$$\frac{\tau_{ri}}{\tau_{csm}} = \alpha_s \left( \frac{\tau_{csi}}{\tau_{csm}} \right)^{\beta_s} \tag{2.9}$$

Where, $\tau_{ri}$ is the reference critical shear stress of individual sediment that produces a small reference transport rate (< 0.002) (N/m$^2$); $\tau_{csi}$ is the Shields shear stress for individual size grain; $\alpha_s$ and $\beta_s$ are the coefficients that vary with the mixture grain size distribution.

He reported the value of $\alpha_s$ as 0.6 for strong bimodal sediment. The value of $\beta_s$ could be computed based on the degree of bimodality of the mixture which is defined as

$$B_p = \left( \frac{D_c}{D_f} \right)^{1/2} \sum P_m \tag{2.10}$$

$$\beta_s = 0, \qquad \text{for } B_p < B_r \tag{2.11}$$

$$\beta_s = 1 - \frac{B_r}{B_p}, \quad \text{for } B_p > B_r \tag{2.12}$$

Where, $B_p$ is the Bimodality parameter; $B_r$ is the minimum value of $B$; $D_c$ and $D_f$ are grain size of coarse mode and fine mode respectively in bimodal sediments; and $P_m$ is the proportion in mode in bimodal sediments.

**Kuhnle (1993)** conducted an experimental study in a laboratory flume for incipient motion of gravel-sand mixture in proportion of gravel:sand as 0:100, 10:90, 45:55, and 100:0. He found that the critical shear stress for gravel particles in sand-gravel mixture deviated when

compared with 100% gravel. He reported the higher value of critical bed shear stress with increasing percentage of gravel sediment in the sediment mixture which may be due to the inhabitation of the formation of a coarse bed surface layer caused by presence of the large amount of sand in the mixtures.

**Patel and Ranga Raju (1999)** proposed a formulation for the computation of critical shear stress of non-uniform fractions in the sediment mixture that depends upon the size of the sediment fraction, the geometric mean size and the geometric standard deviation of the mixture. They carried experimental work in a tilting, recirculating flume having a width of 0.40 m, a depth of 0.52 m and a working length of 12.0 m. Five type of sediment mixture was used in their experiment in which the median size of sediment range from 2.0 mm to 4.0 mm. They maintained the recirculation of sediment by manually feeding back the sediment collected in the trap and care was taken to ensure that the flow was uniform and equilibrium conditions had been attained. Equilibrium conditions have been attained when three successive samples collected in the trap was practically invariant with time in terms of transport rate. The incipient motion was considered corresponding to low discharge of sediment transport by visual observations. They estimated the critical shear stress of the median-sized sediment by three methods i.e. visual observation, largest grain method (LGM), and reference transport method (RTM). It was found that RTM was well matched with the experimental data results, however, they noticed the limitation of data plots needed in RTM methods. The following relationship was proposed by them for incipient motion of non-uniform cohesionless sediment as:

$$\frac{\tau_{*ci}}{\tau_{*c\sigma}} = \left[\frac{d_i}{d_\sigma}\right]^{-0.36} \tag{2.13}$$

$$d_\sigma = d_g \sigma_g \tag{2.14}$$

Where, $\tau_{*c\sigma}$ is the dimensionless critical shear stress of $d_\sigma$ size; $\sigma_g$ is the geometric standard deviation of the sediment mixture; and $d_g$ is geometric mean size of the mixture (m).

**Wu *et al.* (2000)** proposed a formulation for the computation of critical shear stress of non-uniform sediment in the sediment mixture of channel bed. They modified the Shields (1936)

criteria by introducing a correction factor which stochastically related to sediment size and the bed material. The formulation based on correction factor was given as

$$\tau_{*ci} = \frac{\tau_{ci}}{(\rho_s - \rho)gd_i} = \tau_{*cm}\left(\frac{P_{ei}}{P_{hi}}\right)^{m_i} \tag{2.15}$$

Where, $\tau_{ci}$ is the critical shear stress for particle size corresponding to $d_i$ in the sediment mixture (N/m$^2$); $m_i$ is an empirical parameter; $\frac{P_{ei}}{P_{hi}}$ is the correction factor; $P_{ei}$ and $P_{hi}$ are the total exposed and hidden probabilities, respectively, for particle size $d_i$ and defined as

$$P_{hi} = \sum_{j=1}^{M_n} P_j \frac{d_i}{d_i + d_j} \tag{2.16}$$

$$P_{ei} = \sum_{j=1}^{M_n} P_j \frac{d_i}{d_i + d_j} \tag{2.17}$$

Where, $M_n$ is the total number of fractional particle in the sediment mixtures; $d_j$ is the particles staying in front of particle size $d_i$ ; and $P_j$ is the percentage of particles corresponding to $d_j$ particles. They reported the value of $\tau_{*cm}$ and $m_i$ as 0.03 and -0.6 respectively by using laboratory and field data.

**Shvidchenko *et al.* (2001)** presented the results of an experimental study for incipient motion of individual size fraction in sand-gravel composed stream bed. They concluded the parameters governing the incipient motion were ratio of the sediment size to median size of mixture, mixture standard deviation, absolute value of median size of mixture, and the bed slope. They proposed a formulation for the computation of critical shear stress of individual sediment size in unimodal/weakly bimodal sediment mixture as:

$$\tau_{*ci} = \varepsilon_{ii} \frac{0.60}{a_m} S_0^{0.278} \tag{2.18}$$

Where, $\varepsilon_{ki}$ is the hiding function which depends upon relative size with respect to median size and mixture standard deviation; and $a_m$ is the mobility factor which depends upon absolute value of median size of mixture.

**Dey and Raju (2002)** conducted an experimental study for computation of critical shear stress of gravel and coal beds under unidirectional steady-uniform flow. They identified the parameters affected the incipient motion were the Shields parameter, particle Froude number, non-dimensional particle diameter and non-dimensional flow depth. The incipient motion was considered when all fractions of bed particles (on the surface) had movement over a period of time and collecting the removed particles in a wire-net downstream. They found the experimental results for gravel and coal bed was in disagreement with the standard curves proposed by Shields (1936). The following expressions have been proposed by them for the computation of critical shear stress of gravel and coal bed as:

$$\tau_{*ci} = 0.085 F_d^{1.01} d_*^{1.52} \hat{h}^{1.27} \quad \text{(For both gravel and coal bed)} \tag{2.19}$$

$$\tau_{*ci} = 0.013 F_d^{2} d_*^{0.48} \hat{h}^{0.49} \quad \text{(For gravel bed)} \tag{2.20}$$

$$\tau_{*ci} = 0.058 F_d^{2} d_*^{0.62} \hat{h}^{0.63} \quad \text{(For coal bed)} \tag{2.21}$$

Where, $F_d$ , $d_*$ , and $\hat{h}$ are the dimensionless particle Froude number, non-dimensional particle diameter and non-dimensional flow depth respectively.

**Zanke (2003)** focused on the work of influence of turbulence on the initiation of motion of sediment particles. In case of non-turbulent flow the critical shear stress is solely defined by the angle of internal friction or the angle of repose of single grains. In turbulent flow, fluctuations in the shear stress as well as lift forces produced by these fluctuations affecting the initiation of motion of sediment particles. He derived a relationship for computation of critical shear stress under the influence of lift force and the turbulence induced fluctuations as:

$$\tau_{*ci} = \frac{0.7 \tan\phi}{\left(1 + n_f \frac{u'_{rms,b}}{u_b}\right)^2 \left(1 + \frac{1}{2.5}\left(n_f \frac{u_{rms,b}}{u_*}\right)^2 \tan\phi\right)} \tag{2.22}$$

Where, $\phi$ is the angle of internal friction; $n_f$ is a factor which is multiple of $u'_{rms}$ ; $u'_{rms}$ is standard deviation; and $u_s$ is time-averaged velocity at a grain.

**Dong (2007)** presented a formulation for determining the relative critical shear stress of sand fraction in a non-cohesive sand-silt mixture. He found that the computed relative critical shear stress increases with the silt content. The predicted critical shear stress for the sand fraction also found to increase with finer silt size for given silt content in sand-silt mixture. He proposed the following expressions for the computation of critical shear stress for sand fraction in sand-silt mixture:

$$\frac{\tau_{csf}}{\tau_{cs}} = \frac{f(R_m)}{f(R_s)} \tag{2.23}$$

$$f(R_m) = 0.22R_m^{-0.6} + 0.06\times 10^{\left(-7.7R_m^{-0.5}\right)} \tag{2.24}$$

$$f(R_s) = 0.22R_s^{-0.6} + 0.06\times 10^{\left(-7.7R_s^{-0.5}\right)} \tag{2.25}$$

$$R_m = \frac{\sqrt{Rgd_o}\,d_m}{\upsilon} \tag{2.26}$$

$$R_s = \frac{\sqrt{Rgd_o}\,d_s}{\upsilon} \tag{2.27}$$

$$d_o = d_s(1-P_{silt}) + d_{silt}P_{silt} \tag{2.28}$$

Where, $\tau_{csf}$ is the critical shear stress for sand fraction in sand-silt mixture ($N/m^2$); $\tau_{cs}$ is the critical shear stress for sand ($N/m^2$); $R_m$ and $R_s$ are gravity based particle Reynolds number corresponding to size $d_m$ and $d_s$ respectively; $d_s$ and $d_{silt}$ are the median size of the sand and silt particles respectively; and $P_{silt}$ is the percentage of silt content in sand-silt mixture.

**Beheshti and Ataie-Ashtiani (2008)** compared the incipient motion criteria among the different methods that based on the Shields curve, the concept of probability of sediment movement, and an empirical method based on movability number and concluded that the method based on the movability number predict better incipient motion criteria than the other

methods. He also proposed a formulation for the computation of critical shear velocity based on the movability number as following:

$$\frac{u_{*c}}{w_s} = 9.6674 \times d_*^{-1.37} \qquad \text{for } D_* \leq 10 \tag{2.29}$$

$$\frac{u_{*c}}{w_s} = 0.4738 \times d_*^{-0.226} \qquad \text{for } D_* > 10 \tag{2.30}$$

$$d_* = \left[\frac{(\rho_s - \rho)g}{\rho \upsilon^2}\right]^{1/3} d_{50} \tag{2.31}$$

Where, $w_s$ is the settling velocity of the particle (m/s).

**Patel *et al.* (2009)** modified the formulation proposed by Patel and Ranga Raju (1999). Modified formulation was applicable for both unimodel and bimodal sediments for the computation of critical shear stress of non-uniform fractions in the sediment mixture that depends upon the size of the sediment fraction, the geometric mean size, and the geometric standard deviation of the mixture and the modified relationship was proposed as:

$$\frac{\tau_{*ci}}{\tau_{*cm}} = 1.0541\left[\frac{d_i}{d_m}\right]^{-0.7458} \tag{2.32}$$

$$\tau_{*cm} = 0.0329(\sigma_g)^{-0.5691} \tag{2.33}$$

**Gaucher *et al.* (2010)** investigated the effects of compaction on the erodibility of cohesionless soil (i.e. mixture of sand and gravel) through laboratory experimental study. They carried the experiment in a horizontal, rectangular flume of 0.5 m wide, 0.7 m deep, and approximately 6 m with glass walls and the test section was located at 3.4 m from the flume entrance. They determined the optimum dry density as a function of soil moisture for each soil using Proctor's Standard method and identified the maximum and minimum dry densities of soil using a vibrating table procedure applicable to cohesionless soils. They found the soil compacted at the Proctor optimum dry density have a higher resistance against the erosion than those compacted at lower and higher densities. Further they tested the experimental data with two commonly used incipient motion criteria of Yang's (1973) and Shields-Yalin (Yalin and Karahan 1979) criterion and found that the data trends exhibit a stronger correlation with

Yang's incipient motion criterion than Shields-Yalin's criterion. They performed additional validation tests on non-compacted poorly graded sands and conclude that Yang's criterion is less sensitive, with a nearly perfect agreement between computed and measured critical values. They used the method of extrapolating the transport rates as a function of shear stress to a zero reference value for finding the incipient motion condition.

**Simões (2014)** developed empirical criteria for incipient motion of particles which was based on the movability number. Movability number is defined as the ratio of the shear velocity to the particle's settling velocity and settling velocity was calculated as per Dietrich (1982). The incipient motion criterion was developed based on the experimental data collected independently by many researchers. The following equations were used for the computation of critical velocity based on the movability number as:

$$A_c = \frac{u_{*c}}{w_s} \tag{2.34}$$

$$A_c = 0.215 + \frac{6.79}{d_*^{1.7}} - 0.075e^{-2.62\times10^{-3}d_*} \tag{2.35}$$

$$d_* = \left[\frac{(s-1)g}{\upsilon^2}\right]^{\frac{1}{3}} d_{50} \tag{2.36}$$

Where, $A_c$ is the movability number corresponding to incipient motion.

### 2.2.2 Critical Shear Stress of Cohesive Sediment

**Dunn (1959)** experimentally determined the critical shear stress required to initiate the movement of soil particles by applying a vertical jet impinging upon submerged soil samples. The magnitude of the shear was measured by replacing the sample with a shear plate coated with soil particles. He identified the parameters like clay content, vane shear strength, particle size distribution of cohesive sediments and plasticity index controlling the critical shear stress. Dunn presented a formulation for the computation of critical shear stress using statistical analysis techniques as:

$$\tau_{cr} = 0.2 + \frac{S_v + 180}{1000}\tan(30 + 1.73PI) \tag{2.37}$$

$$\tau_{cr} = 0.2 + \frac{S_v + 180}{1000} \tan(0.06(100P_c)) \quad (2.38)$$

Where $\tau_{cr}$ is the critical shear stress for cohesive sediment (N/m$^2$); $S_v$ is the vane shear strength in (N/m$^2$); $P_c$ is the clay percentage (in fraction) by weight; and $PI$ is the plasticity index of the soil.

**Smerdon and Beasley (1961)** conducted the laboratory experiment to study the behavior of incipient motion of cohesive sediment (clay-sand) mixture by applying the tractive force theory under various factors like plasticity index, dispersing ratio, mean particle size of clay and percentage of clay. They defined the point of bed failure arbitrarily as general movement of the bed material. They derived the following relationships (Zhu *et al.* 2008) for computation of critical shear stress as

$$\tau_{cr} = 0.493[10^{0.0182(100P_c)}] \quad (2.39)$$

$$\tau_{cr} = 0.163(PI)^{0.84} \quad (2.40)$$

**Lyle and Smerdon (1965)** conducted experimental study for incipient motion of cohesive sediment mixture and correlated the critical shear stress with soil bed properties. The experiment were carried out in a laboratory flume having 72 ft length, 2.5 ft wide and 1.33 ft deep with clear plexiglass sides and at constant bed slope of 0.2 %. They used seven Texas soils in their experiment namely Amarillo fine sandy loam, Houston black clay, Reagan silty clay loam, Lufkin fine sandy loam, San Saba clay, Lufkin clay (B-horizon) and Lake Charles clay. The incipient motion condition of cohesive sediment mixture was visually observed by increasing the flow rate by small increments until the soil began to erode and the shear stress was determined as the tractive force acting on the soil by the product of the slope of the energy gradient and the unit weight of water. The test were conducted under the three degrees of compaction, i.e., at three values of the void ratio. They found the range of void ratio varied from 0.65 to 1.86 in the tests. They reported linear variation of shear stress with compaction in terms of void ratio and the critical shear stress were found to be increases with compaction. They reported the determined critical shear stress was best correlated to the soil properties in the following order: plasticity index, dispersion ratio, percent organic matter, vane shear strength, cation exchange capacity, mean particle size, calcium-sodium ratio, and percent clay

and expressed the critical shear stress with the calcium-sodium ratio, the mean particle size, and the lower plastic limit as bleow:

$$\tau_{cr} = 000771 + b_1(1.2 - e_r) + 0.000796 I_w \quad (2.41)$$

$$b_1 = -0.0438 R_{ca}^{-0.39} \quad (2.42)$$

Where $e_r$ is the void ratio; $I_w$ is the lower plastic limit; and $R_{ca}$ is the calcium-sodium ratio.

**Murray (1976)** investigated the erosion characteristics of cohesive sediment mixture composed of sand and clayey silt. He conducted the experiment in a laboratory flume constructed of plexiglass, 152 cm long, 11cm wide, and 11cm deep with a headbox and tailbox for the purpose of uniform flow distribution and trapping of sediments respectively. Uniform sand (median size 0.80mm) was mixed with clayey silt in various proportions and the clayey silt had the composition of 5% fine sand (>62 $\mu m$), 85% silt, and 10% clay (<2 $\mu m$). The X-ray diffraction test revealed the composition of minerals of clayey silt as 52% montmorillonite, 40% illite, and 8% kaolinite. The properties of cohesive channel bed was determined as liquid limit =33, plastic limit =26, and plasticity index =7. He found the bed shear stress required to move a given rate of sediment increases with the percentage of fine materials in the sediment bed as reported by Dunn (1959) and Smerdon and Beasley (1961). However, he noticed the critical shear stress doesn't increase as rapidly with the percentage fines as previously reported by Dunn (1959) and Smerdon and Beasley (1961).

**Kamphuis and Hall (1983)** conducted experimental study for the incipient motion of consolidated cohesive sediment mixture of clay-sand under a unidirectional flow of clear water. They used the cohesive sediment from the bottom of the Mackenzie River at Norman Wells, Canada as well as from a land-based location within the same formation. The composition of sediment mixture was as 50-60% quartz, 15-20% iron rich chlorite, 20-25% illite, and 1-10% montmorillonite. The fine material i.e. silty clay has median size of 0.0036 mm and coarser particle has 0.105 mm. The cohesive bed was consolidation in the range of 48 kPa-350 kPa. They reported the linear variation of critical shear stress with unconfined compressive strength and vane shear strength. The resistance of cohesive bed against erosion was found to be increases with clay content and plasticity index. They noticed the progressive

rate of erosion after the initiation of erosion and attributed this to the increase in hydrodynamic roughness at the soil surface.

**Mitchener and Torfs (1996)** investigated the erosion behavior of mud-sand mixture by using both laboratory and field experimental data. Mud (passed through a sieve of size 62.5 $\mu$m) was mixed with two type of sand having median size of 150 $\mu$m and 230 $\mu$m in various proportions. They worked on two types of mixture i.e. artificial mud-sand mixture and undisturbed natural mixtures. In case of artificial mud-sand mixture, they found the light increment in critical shear stress when the sand content was in the range of 0% to 50% in the sediment mixture; however, the optimal value i.e. maximum critical shear stress was observed when sand content lied in the range of 50% to 70% by weight. They noticed the mode of erosion from cohesionless to cohesive behavior when mud content was in the range of 3% to 15%. In case of undisturbed natural mixtures, they reported the increase in critical shear stress with the bulk density of the sediment and proposed an equation for the computation of critical shear stress based on bulk density which is of the form as:

$$\tau_{sm} = E1(\rho_b - 1000)^{E2} \qquad (2.43)$$

Where, $\tau_{sm}$ is the critical erosion shear stress for sand-mud mixture (N/m$^2$); $\rho_b$ is the bulk density (kg/rn$^3$); and E1 = 0.015, E2 = 0.73.

**Panagiotopulos *et al.* (1997)** investigated the influence of clay on incipient motion for sand-estuarine mud mixture under steady and oscillatory flow conditions. The experiments were conducted in a recirculating (Armfield) flume of 5.00 m long, 0.30 m wide, and 0.45 m deep with an open top and glass-sided wall. Two type of sand (median size of 152.50 mm and 215.00 mm) was mixed with mud (median size less than 50 $\mu$m) and the mud content was varying from 5 to 50 % by dry weight. They reported the critical shear stress increases with the increase of clay content in the mud. They found the critical velocity linearly increases with the mud content under oscillatory flow conditions when clay fraction was in excess of 11% and this attributed to increase in mud content which surrounds the sand particles and control the erosion behavior. They found no trend for erosion threshold when clay fraction was less than 11% in mud and this attributed to increase in the angle of internal friction.

**De Sutter *et al.* (2000)** presented the incipient motion characteristics for the artificial mixtures of non-cohesive and cohesive sediments under steady flow condition. The

experimental study were carried out in an 11 m long tilting flume with semicircular cross-section (internal diameter of 0.39 m) and fixed bed slope of 0.3%. The flume wall was covered with abrasive paper. The measurements were made in central section of the flume which has the length of 4 m. The cohesive sediment used in the study was Kaolinite clay (median size 7 $\mu$m) and two type of sand (median size 230 mm and 320 mm). They visually observed the sediment entrainment from cohesive bed in which clay is varying from 10 to 40%. They found a positive relationship between clay content and critical bed shear stress up to 20% clay.

**Torfs *et al.* (2001)** investigated the incipient motion condition for cohesive sediment mixture under steady flow in a 9 m long and 40 cm wide recirculating flume. They have used three type of sediment mixture in the experiment consisted of Kaolinite (2 $\mu$m)+sand (0.23 mm), clay-silt mud(25 $\mu$m)+sand(0.23 mm), and montmorillonite (8 $\mu$m)+sand(0.23 mm). They observed a lower critical shear stress when a small quantity of fines is added to sand and attributed it to a reduction in the inter-granular friction between sand particles due to partial filling of pore spaces by fines. They reported that the critical shear stress was varying non-monotonically with fine grained weight fraction and concluded that the filling of fines in the pore matrix of sand play an important role in controlling the incipient motion. They concluded that the interactive nature of the fine sediments by space filling within the pores of the sandy bed matrix plays an important role in controlling the erosion. They have proposed the formulation for the computation of critical shear stress for cohesive sediment mixture, however, application of it confined to the original data on which they are based. The formulation was given as below:

$$\tau_{cc} = \left[ \frac{\alpha_{1cg} \tan \phi_{cg}}{\alpha_{1cg} + \alpha_{2cg} \tan \phi_{cg}} + \frac{K' \zeta_b (\phi_c - \phi_{cc})^{\xi_b}}{g(\rho_s - \rho) d_{ss}} \right] g(\rho_s - \rho) d_{ss} \qquad (2.44)$$

Where, $\phi_{cc}$ is the fine solids weight fraction, $\phi_c$ is the threshold value of $\phi_{cc}$ below which the bed matrix is not fully particle-supported; $\zeta_b$ and $\xi_b$ are coefficients which depend on bed composition and the degree of consolidation; $K'$ is the bed dependent characteristic coefficient ( $K' = 0$ implies the absence of fine material); $\alpha_{1cg}$ is an area shape factor; $\alpha_{3cg}$ is

a volume shape factor; $\alpha_{Lag} = \alpha_{lag}(C_L/C_D)$ in which $C_L$ and $C_D$ are the lift and drag coefficients respectively; and $\phi_{cg}$ is the angle of repose for coarse grain.

**Julian and Torres (2006)** investigated the hydraulic erosion of cohesive river bank on a 600 m reach of an urban ephemeral stream with active bank erosion in the Hitchcock Woods. They estimated the critical shear stress using silt-clay percentage based on the assumption that critical shear stress would be maximum and minimum at 100% and 0% silt–clay content respectively. They proposed a third degree polynomial for the estimation of critical shear stress which passes through shear stress of 0.1 N/m$^2$ which is the lower limit of the Shields curve. The formulation was expressed as:

$$\tau_{cr} = 0.1 + 0.1779(SC\%) + 0.0028(SC\%) - 2.34E-5(SC\%)^3 \quad (2.45)$$

Where, $\tau_{cr}$ is the critical shear stress for cohesive river bank (N/m$^2$); and $SC\%$ is the silt-clay percentage.

**Ansari *et al.* (2007)** conducted experimental study in a tilting flume of 30.0 m long, 1.0 m wide and 0.60 m deep for cohesive sediment mixture of clay-sand. The cohesive sediment mixture was prepared by mixing clay (median size 0.0053 mm) with sand (median size 0.27 mm) in which clay varied from 5% to 20%. They reported the composition of clay minerals as Kaolinite (10%), Illite (75%), and Montmorillonite (15%) using X-ray diffraction test. They conducted 25 experimental run for incipient motion and in each run the working section of channel bed was compacted either by dynamic compaction method or kneading method as per antecedent moisture content in the bed. They visually identified the incipient motion and reported the appearance of a series of very fine parallel lines on the cohesive bed surface, however, these parallel lines disappeared as the critical velocity was approached and then the erosion became apparent by the removal of lumps or chunks from the bed surface. They reported the factors affecting the incipient motion of clay-sand mixture were antecedent moisture content, clay content, plasticity index and void ratio. They proposed a functional relationship for the computation of critical shear stress for clay-sand mixture, however, reported ± 50% error for that relationship for their most of the data. The proposed relationship was given below as:

$$\tau_{*cr} = 0.001(1+PI)^{2.89}(W/W_s)^{3.1}10^{[-0.64c_c+2.3]} \quad (2.46)$$

$$\tau_{*cr} = \tau_{cr}/(\rho_s - \rho)gd_a \tag{2.47}$$

$$d_a = \frac{\sum(d_{50}.P')}{\sum P'} \tag{2.48}$$

Where, $\tau_{*cr}$ is the dimensionless critical shear stress of cohesive sediment mixture; $W$ is the antecedent moisture content of cohesive sediment; $W_s$ is the moisture content at saturation; and $P'$ is the percentage of the individual sediment in the sediment mixture.

**Kothyari and Jain (2008)** studied the influence of cohesion on the incipient motion of cohesive sediment mixture of clay-gravel and clay-sand-gravel. Clay was varied from 10% to 50% in each sediment mixture. They visually identified the incipient motion condition and noticed it was changed with the clay percentage, antecedent moisture characteristics, and the applied shear stress. They reported three modes of erosion as per clay content namely pothole erosion, line erosion, and mass erosion. They reported the main parameters controlling the incipient motion condition of the cohesive sediment mixture were clay percentage, void ratio, and unconfined compressive strength of the sediment bed. A relationship was also proposed for the computation of critical shear stress of clay-gravel and clay-sand-gravel mixture as below:

$$(\tau_{cr}/\tau_{cm}) = 0.94(1+P_c)^{3/2} e_r^{-3/4}(1+0.00UCS^*)^{9/20} \tag{2.49}$$

$$UCS^* = UCS/(\rho_S - \rho)gd_a \tag{2.50}$$

Here, $UCS^*$ is the dimensionless unconfined compressive strength of cohesive sediment mixture; and $UCS$ is the unconfined compressive strength of cohesive sediment mixture ($N/m^2$).

**Ahmad *et al.* (2011)** developed a formulation to compute the critical shear stress for sand and mud mixture which is based on the critical shear for pure sand and pure mud together with fraction contents. The sediment used for the formulation was mud (mean size 50 $\mu$m) and three type of sand having median size of 0.1525 mm, 0.2150 mm, and 0.230 mm. The formulation was calibrated with the experimental data from Panagiotopoulos *et al.* (1997) and then validated using experimental data cited in Mitchener and Torfs (1996). The reported that the new formulation has advantages over the existing formulation as it has only one tuning

coefficient which can be easily determined using site-specific data and applicable for the whole range of relative sand and mud contents. The formulation was made under the various assumptions (i) Only the physical factors were considered and not the chemical and biological factors; (ii) The sediment fraction and cohesion assumed to be the major contributing parameters for the incipient motion; and (iii) The layer of sediment mixture is assumed homogeneous with depth and in the horizontal plane. The proposed formulation by them was given as:

$$\tau_{cm} = e^{\beta_s\left(1-\frac{1}{P_s}\right)}\tau_{c,s} + (1-P_s)\tau_{c,m} \qquad (2.51)$$

Where, $P_s$ is sand percentage in fraction; $\tau_{c,s}$ is the critical shear stress for erosion of pure sand; $\tau_{c,m}$ critical shear stress for erosion of pure mud; and $\beta_s$ is an empirical coefficients.

**Wang *et al.* (2012)** studied the influence of dry unit weight and particle size on incipient motion of consolidated cohesive fine sediment in a rectangle piping flume. The sediments used in the test having the median diameters of 0.03, 0.05, 0.08 and 0.1 mm. The consolidation time for cohesive bed was varied from 1 to 60 days and accordingly critical shear stress was measured and related to the dry unit weight of the sediment. They observed the incipient motion for cohesive bed occurred only at a few isolated spots. They reported the influence to incipient motion was not significant when dry unit weight increases quickly; however, incipient motion was strongly affected when dry unit weight increases slowly. The influence of dry unit weight on incipient motion of cohesive sediment was greater with finer mean particle size. They observed incipient motion was more difficult when consolidation of cohesive bed last longer.

**Xu et al. (2015)** studied the influence of density of cohesive mud, on incipient motion of cohesive coastal mud taken from Huangmaohai Estuary, South China Sea; by conducting experimental study in a laboratory flume of dimensions of 22.0 m×0.5 m×0.6 m which have test section 2.0 m long and 0.1 m deep. They found the critical shear stress ranges from 0.029 to 4.191 N/m$^2$ corresponding to the density of cohesive mud ranges from 1100 to 1550 kg/m$^3$. They identified four types of erosion pattern namely fluid muds, strips, pieces, and blocks corresponding to mud density ($\rho_m$)<1250 kg/m$^3$, 1250 kg/m$^3$ ≤ $\rho_m$ <1310 kg/m$^3$, 1300 kg/m$^3$

$\leq \rho_m < 1400$ kg/m$^3$, and $\rho_m \geq 1400$ kg/m$^3$, respectively. They concluded critical shear stress increases with the increase of density of mud and proposed a relationship between them as:

$$\tau_{mcd} = C_1(\rho_m - \rho)^{C_2} \tag{2.52}$$

Where $\tau_{mcd}$ is the critical shear stress for mud (N/m$^2$); $C_1$ and $C_2$ are constants related to the mud cohesion to be determined by the experiment; $\rho_m$ is the mud density. They found value of $C_1$ and $C_2$ in their experiment as $1.59 \times 10^{-8}$ (Nm/kg) and 3.06 respectively.

## 2.3 TRANSPORT RATE OF SEDIMENT

Transport rate of sediment includes the bed load as well as suspended load of sediment present in the sediment mixture. Sediments were detached from the channel bed and then transported over it as bed load and suspended load. This channel bed may be made of cohesionless or cohesive sediment. Hence, this section presents the literature review for the study of transport rate for both cohesionless and cohesive channel bed.

**Proffitt and Sutherland (1983)** modified the existing transport rate formulae of Ackers and White (1973) and Paintal (1971) for the computation of transport rates and size distributions of transported material by knowing the hydraulic conditions and the bed-material grain size distribution. They introduced an exposure correction in the formulae of Ackers and White (1973) and Paintal (1971) for the bed load transport prediction for cohesionless non-uniform sediments. The Ackers and White and the Paintal transport formulae were modified by introducing exposure correction as given below:

For Paintal (1971) formula

$$0.6 < \frac{d_i}{d_s} < 10 \qquad \varepsilon_{si} = 1.0\left(\frac{d_i}{d_s}\right)^{0.51} \tag{2.53}$$

$$\frac{d_i}{d_s} < 0.6 \qquad \varepsilon_{si} = 1.16\left(\frac{d_i}{d_s}\right)^{0.81} \tag{2.54}$$

For Ackers and White (1973) formula

$$3.7 < \frac{d_i}{d_a} \qquad \varepsilon_{ei} = 1.30 \qquad (2.55)$$

$$0.075 < \frac{d_i}{d_a} < 3.7 \qquad \varepsilon_{ei} = 0.53\log\left(\frac{d_i}{d_a}\right) + 1.0 \qquad (2.56)$$

$$\frac{d_i}{d_a} < 0.075 \qquad \varepsilon_{ei} = 0.40 \qquad (2.57)$$

Where, $d_a$ is the scaling grain size; and $\varepsilon_{ei}$ is the exposure correction.

**Misri *et al.* (1984)** proposed methods for the computation of the bed load transport rates of different fractions in a mixture. They carried the experimental work in a in a tilting flume of length of 16.0 m, width of 0.75 m, and a depth of 0.48 m with four coarse uniform materials and nine sediment mixtures as the bed material. The eroded sediment form the channel bed were collected in a trap at the downstream end of the flume and then fed back manually at the upstream end of the flume at a constant rate to maintain sediment equilibrium. They also assessed the accuracy of existing methods for the computation of bed load transport rate and concluded bed load transport of uniform sediment satisfactorily determined, however, Einstein's method hasn't predicted satisfactorily the bed load transport rates of individual fractions in a mixture. The following equations were proposed by them for the computation of bed load transport rate of individual fractions in a mixture as below:

$$\xi_e = \frac{0.0386_a\left(\frac{\tau}{\tau_{cm}}\right)^{0.75}}{\left(\frac{\tau}{\Delta\gamma_s d_i}\right)^{1.2}\left[1+0.0031\left(\frac{\tau}{\Delta\gamma_s d_i}\right)^{-2.1}\right]^{0.33}} \qquad (2.58)$$

$$\phi_B = \frac{i_B q_{BT}}{\gamma_s d_i i_b}\sqrt{\frac{\gamma_f}{\Delta\gamma_s g d_i}} \qquad (2.59)$$

Where $\xi_e$ is the coefficient accounted for sheltering effect; $k_a$ is the coefficient dependent on Kramer's uniformity coefficient; $\tau$ is the total shear stress for the arithmetic mean size of sediment mixture ($N/m^2$); $\phi_B$ is the dimensionless bed load transport rate; $i_B$ percentage of

any size present by weight in the bed load; $q_{BT}$ is the bed load transport rate in weight per unit width (N/m/s); and $f_b$ percentage of any size present by weight in the bed material.

**Samaga *et al.* (1986a)** modified the work of Misri *et al.* (1984) for the computation of bed load transport for individual fraction in a cohesionless sediment mixture. The experiments were conducted in a recirculating tilting flume 30.0 m long, 0.20 m wide and 0.50 m deep with four mixtures having different arithmetic mean diameters ranges from 0.256 mm to 0.578 mm and different Kramer's uniformity coefficient ranges from 0.230 to 0.465. The thickness of channel bed was reported as 0.15 m. The discharge was measured with the help of a calibrated orifice-meter and the total load concentration with the help of a width-integrating sampler. They checked the existing methods of Proffitt and Sutherland (1983) and Misri et al. (1984) for the computation of the bed load transport of individual fractions in the sediment mixtures and reported their limitations as the inadequacies of the correction factor proposed by Proffitt and Sutherland (1983), non-applicability of Misri et al. (1984) method over wide range of shear stresses. They reported the ratio of shear stress to critical shear stress ranges from 0.50-1.50 for Misri et al. (1984) method; however, it was from 3.50-9.80 for their experimental study. They proposed modifications in existing relationship between the dimensionless grain shear stress and the dimensionless bed load transport rate of Misri et al. (1984) so that it will applicable to a wider range of shear stresses.

**Samaga *et al.* (1986b)** conducted the laboratory experiment in which suspended load transport rates were measured and compared with both Einstein's (1950) and Holtorff's (1983) methods of calculation of suspended load for individual fractions. The experiments were conducted in a recirculating tilting flume 30.0 m long, 0.20 m wide and 0.50 m deep with four mixtures having different arithmetic mean diameters ranges from 0.256 mm to 0.578 mm and different Kramer's uniformity coefficient ranges from 0.230 to 0.465. The thickness of channel bed was reported as 0.15 m. They found the method of Einstein (1950) and Holtroff (1983) for suspended loaded transport of individual fractions in a mixture has not well supported by the flume data collected during the study. They made the modification in the existing relationship between the dimensionless shear stress and the suspended transport rate for uniform sediment to make it applicable to non-uniform sediment. They introduced the correction factor to existing equation of uniform sediment in order to predict the transport rate

of individual fractions in a mixture. the correction factor has been the function of dimensionless shear stress, ratio of shear stress to critical shear stress, and Kramer's coefficient. They found a fair agreement with the data of the Snake river suspended transport rate of individual particles.

**Woo *et al.* (1987)** tested the applicability of the existing Einstein's (1950) sediment transport formula and Colby's (1964) graphical method for predicting the total bed sediment discharge in flows of clay suspensions. They used the flume data collected by Simons *et al.* (1963) with high concentrations of both fine sediments and sands to test the applicability of these two methods. They reported that the large concentrations of fine sediments increase the viscosity and density of the suspension. They found that the sediment discharge as per Einstein's method remains practically unchanged in presence of fine sediments and that Colby's graphical relations yield results quite similar to those of Einstein without correction and concluded Colby's graphical method do not provide better prediction of the total bed sediment discharge than Einstein's formula.

**Swamee and Ojha (1991)** developed the empirical equations for the computation of transport rate of bed load and suspended load of non-uniform sediments. They assumed bed load to materials that transported within a height of two grain diameters from the bed and the rest is suspended load. They used the previous existing data of Samaga *et al.* (1986), Einstein (1950), and Misri (1981) and proposed the following empirical equations:

For bed load transport rate

$$\phi_B = \left[\left\{\left(\frac{0.8}{M}\right)^{4.75} + M\right\}^{1.75}\left(\frac{0.0871}{\tau_{*_c}^{M^{0.27}}}\right)^{9} + \left\{\left(\frac{0.01}{M}\right)^{0.6} + M^{3.35}\right\}^{1.2}\left(\frac{0.339}{\tau_{*_c}^{9M/\left(8M^{3}+1\right)}}\right)^{1.6}\right]^{-1} \quad (2.60)$$

For suspended load transport rate

$$\phi_S = \left[\left\{\left(\frac{0.073}{M}\right)^{8} + M^{3.8}\right\}\left(\frac{0.567}{\tau_{*_c}^{M^{0.63}}}\right)^{6} + \left\{\left(\frac{0.177}{M}\right)^{2} + M^{1.45}\right\}^{2}\left(\frac{0.538}{\tau_{*_c}^{18M/\left(7M^{1.425}+1\right)}}\right)^{3}\right] \quad (2.61)$$

Where, $\phi_s$ is the dimensionless suspended load transport rate parameter for non-uniform sediment; and $M$ is Kramer's uniformity coefficient.

**Roberts *et al.* (1998)** investigated the effect of particle size and bulk density on the erosion of quartz particles which size ranged from 5 to 1,350 $\mu m$ and bulk densities ranged from approximately 1.65 to 1.95 g/cm$^3$. They measured the erosion rate using Sedflume at shear stress ranged from 0.2 to 6.4 N/m$^2$. They found the sediments behaved in a non-cohesive manner for larger particles while in cohesive manner for smaller particles. They observed that the erosion rate decreases rapidly as the bulk density increases for smaller particles and attributed it to the increasing cohesive forces relative to the lift and drag forces. They concluded that the erosion rates as a strong decreasing function of density for the finer particles and essentially independent of density for the larger particles.

**Ansari *et al.* (2003)** investigated the temporal variation of scour depth around circular bridge piers founded in cohesionless and cohesive sediments separately. They carried the experimental study in laboratory under steady and clear water flow condition. They noticed the significant difference for the geometry, location and extent of the scour hole around bridge piers in cohesive sediments when compared to cohesionless sediments. They found horse shoe vortex as the prime agent causing scour in cohesive sediments. They developed the following empirical relationships for the computation of temporal variation of scour depth around bridge piers in cohesive sediments.

$$\frac{d_{sme}}{d_{sme}} = 1.51\left(\frac{W}{W_*}\right)^{0.55}\left(\frac{C_*}{\phi_*}\right)^{0.2} \qquad \text{for } PI = 0 \qquad (2.62)$$

$$\frac{d_{sme}}{d_{sme}} = \frac{6.02 - 10.82\left(\frac{W}{W_*}\right) + 5.41\left(\frac{W}{W_*}\right)^2}{\left(\frac{C_*}{\phi_*}\right)^{0.2}} \qquad \text{for } PI \geq 4 \qquad (2.63)$$

Where, $d_{sme}$ is the maximum scour depth below the bed level in cohesive sediment (m); $d_{sme}$ is the maximum scour depth below the bed level in cohesionless sediment (m); $C_*$

and $\phi_{s_f}$ represents the cohesion and the angle of repose in dimensionless form for cohesive sediment mixture respectively.

**Wu *et al.* (2003)** proposed the methods for the computation of transport rates for non-uniform sediment in sand-bed channels based on the Transport Capacity Fraction concept. They reported that this method has the advantage of avoiding discrepancies due to the distribution and number of class intervals in computing bed-material load, and it limits the errors in computing concentrations for individual size fractions. Their approach incorporated the sheltering and exposure effects exist in the sediment mixtures which represented by $d_i/d_m$ ratio. The following expression was given by them for the computation of transport rates of non-uniform sediment.

$$f_{tcak} = \frac{P_{bi}\left[\left(\frac{d_i}{d_m}\right)^{\alpha_{fi}} + \zeta_{fi}\left(\frac{d_i}{d_m}\right)^{\beta_{fi}}\right]}{\sum_{i=1}^{N} P_{bi}\left[\left(\frac{d_i}{d_m}\right)^{\alpha_{fi}} + \zeta_{fi}\left(\frac{d_i}{d_m}\right)^{\beta_{fi}}\right]} \qquad (2.64)$$

Where, $f_{tcak}$ transport capacity distribution function for size fraction $i$; $P_{bi}$ fraction of bed material by dry weight; $\alpha_{fi}, \beta_{fi}$, and $\zeta_{fi}$ are the coefficients related to flow and sediment properties.

**Aberle *et al.* (2004)** collected cohesive sediments from several aquatic environments near Church and Hamilton, New Zealand and measure the erosion rate of cohesive sediment by the National Institute of Water and Atmospheric Research (NIWA) in situ flume in fresh water and salt environment. The cohesive sediment had the combination of clay-silt-sand in which sediment size ranges from 6 $\mu$ m to 108 $\mu$ m. They analyzed the erosion rate for the collected data from the NIWA in situ flume in several different aquatic environments by using formulation proposed by Sanford and Maa (2001) given as below:

$$E = \rho_b(z)\beta'(\tau_0 - \tau_{cr})e^{-\alpha_w\beta(\tau-\tau_c)} \qquad (2.65)$$

Where, $E$ is the erosion rate (kg/m$^2$/s); $\rho_s(z)$ is the bulk density at sediment depth z (kg/m$^3$), $\beta_1$ is a local parameter (m/s/Pa), $\tau_0$ is total bed shear stress applied at $t = t_0$ (N/m$^2$), $t$ is time (s), and $\theta_{cr}$ is the vertical gradient of the critical bed shear stress (N/m$^3$).

They used two methods, namely bulk and last step method, for the evaluation of the parameters in Sanford and Maa (2001) formula and reported both methods leads to similar results. They noticed an exponential decay of erosion rate with time an indicative of depth limited erosion. The erosion rate depends on bed material properties, such as dry bulk density, water content, organic content and sand content. They reported that the erosion rate in salt environment were five times lesser than those of the fresh water environment.

**Wan and Fell (2004)** developed slot erosion test (SET) and hole erosion test (HET) to study the erosion characteristics of soil in the cracks of embankment dams. They tested 13 types of cohesive soil (median size for clay 5 $\mu$m and median size for silt 75 $\mu$m) ranging from non-plastic to high plasticity (60%) in which clay content was varying from 9% to 80%. They proposed the erosion rate index which measures the rate of erosion for coarse grained and fine grained soils as given below:

For coarse-grained soil:

$$\hat{I}_{HET} = 6.62 - 0.016\rho_d - 0.10\rho_d/\rho_{d\max} - 0.044W - 0.074\Delta w_c + 0.11S + 0.061Clay(U.S.) \quad (2.66)$$

Where $\hat{I}_{HET}$ is predicted erosion rate index for the hole erosion test; $\rho_d$ is dry density of the soil (kg/m$^3$); $\left(\rho_d/\rho_{d\max}\right)$ is the percentage compaction in percent; $\rho_{d\max}$ is the maximum dry density; $\Delta w_c\left(=\frac{W-OWC}{OWC}\times 100\%\right)$ is the water content ratio in percent; $OWC$ is the optimum water content in percent; $S$ is the degree of saturation in percent; and $Clay(U.S.)$ is the mass fraction finer than 0.005 mm in percent.

For fine-grained soil:

$$\hat{I}_{HET} = -10.20 + 9.57\rho_d - 0.042{}^{\rho_d}\!/_{\rho_{max}} + 0.10W + 0.0097\Delta w_c - 0.0056Fines + 0.042Clay(U.S.) - 0.090LL + 0.11I_p + 0.44Pinhole \quad (2.67)$$

Where, *Fines* is the fines content (<0.075 mm) of the soil in percent; *LL* is liquid limit in percent; $I_p$ is the plasticity index; and *Pinhole* is the pinhole test classification expressed as an ordinal number.

The values of the erosion rate index ranges from 0 to 6 which indicating that soils can differ in their rates of erosion by up to 106 times. They noticed that the rate of erosion of cohesive soil to be dependent on its clay content, plasticity index, degree of saturation, density, clay mineralogy and presence of cementing materials such as iron oxides. They reported the coarse-grained soil (non-cohesive) erode more rapidly than fine-grained soils. They found a specimen compacted to a higher dry density, and the optimum water content has a higher erosion rate index i.e. higher erosion resistance.

**Wu *et al.* (2004)** introduced a size gradation correction factor in the formulation of bed load computation of single particle of uniform sediment so that it improves accuracy of calculations for sediment mixture. They testes their method using laboratory and field data in the median size range from 0.091–0.715 mm and concluded the proposed correction factor is expected to be applicable to laboratory flumes and natural rivers with median diameter that ranges for sand size bed material. They noticed that the improvement on transport rate by correction factor is significant for data with standard deviation of bed material greater than 2, while the correction is negligible for data with standard deviation less than 1.5. The size gradation correction factor expressed as a function of the geometric standard deviation of bed material as below:

$$K_d = e^{0.5(b_2 \ln \sigma_g)^2} \quad (2.68)$$

They observed the median diameter of sediment in transport is generally finer than the median diameter of bed material and developed a relationship between them with standard deviation of sediment. The relationship was given as:

$$\frac{d_{50t}}{d_{50}} = \sigma_g^{-b_2 \ln \sigma_g} \qquad (2.69)$$

Where, $K_d$ is the size gradation correction factor; $b_2$ is the exponent; and $d_{50t}$ median diameter of sediment in transport (m).

**Ravisangar *et al.* (2005)** investigated the erosional stability of cohesive bed, settled from concentrated suspensions, in terms of the sediment pore-water chemistry that include pH, ionic strength, and natural organic matter. They conducted the experimental study in a closed recirculating flume with 6 m length, 38 cm wide and 38 cm deep. The slope of the flume was adjusted by a motorized screw jack located at the tail end of the flume. The test section located at a distance of 4.3 m downstream from the inlet section of the flume. They observed different structures of settled beds with changes in chemical parameters and reported that for low pH and low organic content conditions, the initial suspension before settling is flocculated and for high pH or high organic content conditions at low ionic strength, the initial suspension is dispersed. They reported the possible particle associations in a clay suspension were edge-to-face, edge-to-edge, and face-to-face and noticed the particle interactions in beds settled from flocculated suspensions have predominantly edge-to-face associations, whereas beds settled from stable suspensions has face-to-face associations.

**Debnath *et al.* (2007)** measured the erosion data for cohesive sediment mixture of clay-silt-sand in several fresh and salt water environments in New Zealand using in situ flume of the National Institute of Water and Atmospheric Research, New Zealand. They portioned the total erosion into resuspension and bed load. The erosion rate was estimated from direct measurements of bed surface elevations by acoustic sensors, whereas resuspension rate was obtained using data on sediment concentrations measured by optical backscatter sensors. The bed load contribution to the total erosion rate is evaluated from the conservation equation for sediments. They reported that a commonly used assumption that the erosion rate is equal to the resuspension rate is not always valid as bed load plays a significant role in cohesive sediment erosion. The ration of erosion rate to resuspension rate gradually increased with increasing bed-shear stress; however, it remained unchanged for shear stress greater equal to 0.5 Pa. They found that the resuspension component of the total erosion decreased with

increase in clay content and attributed it to changes in sediment structure due to formation of larger-sized sediment aggregates. The maximum value of ration of erosion rate to resuspension rate obtained at around 35% sand content and then decreases with increasing sand content. They reported the cohesion within the clay-silt-sand matrix decreases with increase in sand content and it results in smaller sized sediment aggregates leading to increased suspension load and decreased bed load. They concluded that the variability of the erosion rate parameters were attributed to spatial and temporal variation of the vertical structure of bed material properties, rather than flume characteristics.

**Mostafa *et al.* (2008)** investigated the surface erodibility of undisturbed and remolded samples of cohesive soils collected from different bridge sites in the form of large undisturbed chunks. They conducted the experimental work in a laboratory flume of 14.5 m long, 1.2 m deep, and 0.75 m wide with a constant bottom slope of 0.0033. In their experiment, the percentage of the coarse particles ranged from 6% to 29%, the percentage of fine particles of size less than 6 $\mu$ m ranged from 20% to 46%, the percentage of particles size less than 4 $\mu$ m ranged from 14% to 32% and the percentage of particles size less than 2 $\mu$ m ranged from 9% to 23% as per by weight. They observed the particle erosion and mass erosion for both field samples and remolded samples. They found the ratio of mass erosion to particle erosion resistance ranged from 3.7 to 5.4 for the undisturbed samples. The erosion resistance increased with increase of moist bulk density and decreases with mean sediment size. They noticed the erosion resistance increased with an increase of water content to a certain level. They introduced a non-dimensional soil parameter $\chi$ that incorporates water content, plasticity and the specific gravity of the soil and found $\chi$ and the non-dimensional erosion resistances follow linear relationship. They formulated a relationship for the estimation of the particle and mass erosion resistance from the measured water content, plasticity index, and the moist bulk density of a cohesive soil sample that represented by $\chi$ as below:

$$\tau_p^* = -23.67\chi + 17.28 \tag{2.70}$$

$$\tau_m^* = -107.56\chi + 79.59 \tag{2.71}$$

Where, $\tau_p^*$ and $\tau_m^*$ are non-dimensional erosion resistance for particle erosion and mass erosion respectively; and $\chi$ is the non-dimensional soil parameter that includes water content, plasticity index, and moist bulk density of a soil sample.

**Jain and Kothyari (2009)** investigated the influence of cohesion on bed load transport of fractions in cohesive sediment mixture. They used two cohesive sediment mixtures, clay-gravel and clay-sand-gravel, in their experimental study. The proportion of clay (median size 0.0039 mm) in both the sediment mixture varied from 10% to 50% by weight. The median size for sand and gravel were reported as 0.23 mm and 3.1 mm. They reported the significant reduction in the bed load transport rate of cohesionless material in the presence of clay in the sediment mixture. They found the clay percentage and unconfined compressive strength of the sediment bed were the main factors controlling bed load transport rate of in cohesive sediment mixtures.

The following expressions were proposed by them for the computation of bed load transport of gravel and sand for the cohesive sediment mixture of clay-sand-gravel and clay-gravel.

For $0.02 < (\xi_{B_j} \tau_{*_{cr}}) < 0.062$

$$\phi_{B_j} = 10^8 (\xi_{B_j} \tau_{*_{cr}})^{8.345} \left(1 + \frac{P_{*_c}}{\phi_*}\right)^{(-8/25)} (1 + UCS^*)^{(-1/3)} \tag{2.72}$$

For $0.062 < (\xi_{B_j} \tau_{*_{cr}}) < 0.175$

$$\phi_{B_j} = \left[\begin{matrix} -2545.5(\xi_{B_j} \tau_{*_{cr}})^3 - 412.23(\xi_{B_j} \tau_{*_{cr}})^2 \\ +518.81(\xi_{B_j} \tau_{*_{cr}})^3 - 81.01(\xi_{B_j} \tau_{*_{cr}})^2 + 6.19(\xi_{B_j} \tau_{*_{cr}}) - 0.178 \end{matrix}\right] \left(1 + \frac{P_{*_c}}{\phi_*}\right)^{(-8/25)} (1 + UCS^*)^{(-1/3)} \tag{2.73}$$

For $0.175 < (\xi_{B_j} \tau_{*_{cr}}) < 1.83$

$$\phi_{B,i} = 13.895\left(\xi_{B,i}\tau_{*ci}\right)^{1.9556}\left(1+\frac{P_c}{\phi_*}\right)^{\left(-\frac{3}{2.5}\right)}\left(1+UCS^*\right)^{\left(-\frac{1}{3}\right)} \quad (2.74)$$

Where $\phi_{B,i}$ is the dimensionless bed load transport parameter for sediment size $d_i$; $\xi_{B,i}$ is the exposure-sheltering coefficient for sediment size $d_i$; $P_c$ dimensionless clay content; and $\phi_*$ is the dimensionless angle of internal friction.

**Jepsen *et al.* (2010)** measured cohesive sediment erosion rate directly using adjustable shear stress erosion and transport (ASSET) flume. They also investigated the transport processes of bed load and suspended load. Natural fine sediment was used taken from the mid channel of Boston Harbor, Massachusetts, Canaveral, Florida, and Savannah River Entrance Channel, Georgia. The fine sediments had the median size of 19 $\mu$m and coarser had 1250 $\mu$m size. They reported the fine particles moved in suspension while the coarse material (sand) transported as bed load and was caught in the bed load traps. They analyzed three natural mixed sediments with different sand fractions in which one was predominately fine with 16% sand fraction and the other two mixed cohesive sediments had 63% and 86% sand content. They concluded that fine sediments with little or no sand eroded as aggregates and maintained their integrity in the flume channel while moving as bed load into traps located downstream end of flume. The natural sediments that have high % of sand also eroded as aggregates, however, these aggregates quickly disaggregated and then sand moved as bed load while fine particles moved predominantly in suspension.

**Khullar *et al.* (2010)** studied the transport of suspended wash load through a coarse-bed stream. The experimental work conducted in a laboratory having recirculating tilting flume of length 30 m, width 0.204 m and depth 0.5 m. The flume had a steel bottom, a glass wall on one side, and a painted mild steel plate wall on the other side. Sand and gravel were used as sediment for flume bed in the experiment. Silt was used as the suspended sediment having uniform size of median diameter 0.064 mm. They carried the experiments under different concentrations of suspended sediment as wash load with three different coarse-bed sediments: two having uniform sizes and one with non-uniform size distribution. They noticed no difference between wash load and suspended load transport rate and applied the relationship given by Samaga *et al.* (1986) for the computation of suspended load transport rate which

didn't predict well the results for their data range. They modified the relationship of Samaga *et al.* (1986) and a new relationship was proposed for the computation of suspended load transport rate as below:

$$\log_{10}\left[\xi_{s,i}\left(\frac{\tau}{\tau_{cw}}\right)^{0.62}\right] = 0.703 + 0.54\log_{10}\left(\frac{d_i}{d_a}\right) + 0.03\left[\log_{10}\left(\frac{d_i}{d_a}\right)\right]^2 + 0.0308\left[\log_{10}\left(\frac{d_i}{d_a}\right)\right]^3 \quad (2.75)$$

Where, $\xi_{s,i}$ is the sheltering-exposure and interference parameter; and $\tau$ is the total shear stress.

**Houssais and Lajeunesse (2012)** extended the work of Lajeunesse *et al.* (2010) from uniform sediment to non-uniform or bimodal sediment to see the effects of non-uniformity on bed load transport rate. Mixture of small (median diameter $0.7 \pm 0.1$ mm) and large (median diameter $2.2 \pm 0.4$ mm) quartz grains were used for the composition of bed. They carried the experimental work in a tilting flume of 240 cm length, 9.6 cm width, and 10 cm bed thickness with side glass walls under steady and spatially uniform turbulent flow. They measured the surface density of moving particles and of their average velocity for each size fraction. They captured the motion of the particles using a high speed camera (250 images/s, $1024 \times 1024$ pixels) positioned vertically above the bed. They measured manually the surface densities of small and large moving particles by counting the numbers of particles of each size moving downstream. The control parameters in their experiment were bed slope, water discharge, and flow depth which ranged from $5 \times 10^{-3}$ to $7 \times 10^{-2}$, 20 to 62 liter/min., and 1 to 3 cm respectively. They observed that the critical Shields numbers for both small and large grains decreases linearly with the fraction of the bed surface covered with small grains. They found the surface density of moving particles increases linearly with the Shields number and the average velocity increases linearly with the square root of the Shields number. They concluded that when the particle comes in motion then the average velocity and the surface density of moving particles followed the same law irrespective of uniform or non-uniform sediment. However, they found a difference regarding critical Shields number for non-uniform sediment when compared with uniform sediment case. In case of bimodal bed the critical Shields number for a given grain size depends on the grain-size distribution at the bed

surface and particle Reynolds number while in case of uniform sediment the critical Shields number uniquely determined from the particle Reynolds number.

**Kothyari *et al.* (2014)** investigated the development of scour hole in the wake region of pier placed over cohesive sediment bed under clear water condition. They used two types of channel bed in which working section made of clay-gravel and clay-sand-gravel mixture with clay varied from 20% to 60%. They conducted the experimental study in a tilting flume of 16 m long, 0.75 m wide, and 0.5 m deep and having the working section of dimension 6.0 m length, 0.75 m wide, and 0.50 m depth starting at a distance of 7.5 m from the channel entrance. They found the shape, geometry, and depth of scour hole developed in the cohesive sediment case was significantly different from that of cohesionless sediments. They reported the main factors controlling the scour hole development in the wake region of pier were clay fraction and unconfined compressive strength of cohesive sediment mixture. They proposed the equation for the computation of scour depth in the wake region of piers for both cohesive sediment mixtures as below:

For clay-gravel mixture

$$\frac{d_{scw}}{d_{sc}} = \frac{1}{F_{sc1}} \tag{2.76}$$

$$F_{sc1} = \left(1+P_c\right)^{5.04}\left(1+UCS^*\right)^{0.42}\left(t_*\right)^{-0.24} \tag{2.77}$$

For clay-sand-gravel mixture

$$\frac{d_{scw}}{d_{sc}} = \frac{1}{F_{sc2}} \tag{2.78}$$

$$F_{sc2} = \left(1+P_c\right)^{5.91}\left(1+UCS^*\right)^{0.69}\left(t_*\right)^{-0.42} \tag{2.79}$$

Where, $d_{scw}$ is the depth of scour in the wake zone of pier in cohesive sediment (m); $d_{sc}$ is the depth of scour in cohesionless sediment at the end of run (m); $F_{sc1}$ is parameter representing the cohesion of sediment bed for clay-gravel mixture; $F_{sc2}$ is parameter

representing the cohesion of sediment bed for clay-sand-gravel mixture; and $t_*$ is the dimensionless time.

## 2.4 COMPUTATION FOR THE DEGRADED BED PROFILE

**Chollet and Cunge (1980)** developed the model to simulate the variations of longitudinal river bed profile during long periods of unsteady flow. The developed mathematical model was the form of extension of existing models and it differentiated from other models by considering the variable flow resistance resulting from the sand dunes. They used Engelund and Hansen (1967) and Einstein (1950) methods for the computation of energy dissipation and solid transport intensity. Their set of equation for the model development based on the hypothesis followed as: (i) the flow is assumed to be unidimensional; (ii) liquid discharge disturbances propagate at a much faster rate than solid transport; (iii) the liquid discharge is assumed to be constant; and (iv) time-dependent liquid discharge variations were introduced in the form of constant value steps. Based on the hypothesis they used following equations:

$$\frac{\partial}{\partial x}\left(\frac{Q^2}{2A^2}+gy_s\right)+gS_f=0 \tag{2.80}$$

$$(1-\lambda)B\frac{\partial z}{\partial t}+\frac{\partial G_s}{\partial x}=0 \tag{2.81}$$

Here, $y_s(x,t)$ and $z(x,t)$ are the free surface level and the bed level respectively (m); $S_f$ is the energy slope; $B$ is the water surface width (m); $A$ is cross sectional area of flow ($m^2$), $Q$ is discharge ($m^3s^{-1}$), and $G_s(x,t)$ is the solid transport intensity. The system of equations was solved numerically by using finite difference method described by Cunge and Perdreau (1973).

**Krishnappan, B. G. (1985)** developed a numerical model that predicts the long-term change in the riverbed slope and estimates the change in river regime. They used Ackers and White (1973) developed relationship for the estimation of sediment transport rate. Einstein (1950) method was used for the computation of average concentration. They treated the unsteady flow as quasi-steady. The governing equations used in the model were:

$$\frac{\partial Q}{\partial x} + B\frac{\partial h}{\partial t} + P\frac{\partial z}{\partial t} - q_l = 0 \tag{2.82}$$

$$\frac{\partial Q}{\partial t} + \frac{2Q}{A}\frac{\partial Q}{\partial x} + gA\frac{\partial h}{\partial x} - B\frac{Q^2}{A^2}\frac{\partial h}{\partial x} = gA(S_o - S_f) + \frac{Q^2}{A^2}A_x^{\eta} \tag{2.83}$$

$$\frac{\partial Q_w^*}{\partial x} + PR_* \frac{\partial z}{\partial t} + BC_{w*}\frac{\partial h}{\partial t} + A\frac{\partial C_{w*}}{\partial t} - q_{s1} = 0 \tag{2.84}$$

Here, $Q_w^*$ is volumetric sediment transport rate ($m^3/s$); $P$ is wetted perimeter (m); $q_{s1}$ is the sediment input rate entering the stream laterally due to overland flow ($m^2/s$), etc.; $q_l$ is the lateral inflow rate into the stream ($m^2/s$); $A_x^{\eta}$ is the derivative of A with respect to x when $\eta$ is held constant (m); $C_{w*}$ is the flux-averaged total-load volumetric concentration; and $R_*$ is the volume of sediment on the bed per unit volume of bed layer.

First and second equation represented the flow continuity and momentum equations respectively, whereas the third equation was the mass balance equation for sediment transported by the flow. The set of governing equations were solved numerically using an implicit finite-difference scheme. They tested the model using laboratory and field conditions and reported good agreement with measured data. The laboratory verification was carried out for degradation and aggradation of sand beds resulting from the variation of sediment feed rate at the upstream section of the channel. The field verification was done with the data collected in the South Saskatchewan River reach below Gardiner Dam, in Saskatchewan, Canada.

**Lyn, D. A. (1987)** examined one-dimensional equations of unsteady sediment transport in alluvial river. He studied two physical cases (i) Where no change in upstream sediment or water discharge is imposed; and (ii) where only a change in upstream sediment discharge is considered. The governing equation was represented as below:

$$\frac{\partial h}{\partial t} + \frac{\partial}{\partial x}(uh) = 0 \tag{2.85}$$

$$\frac{\partial u}{\partial t}+\frac{\partial}{\partial x}\left[\frac{1}{2}u^2+gh+gz\right]=-\frac{u_*^2}{h} \tag{2.86}$$

$$\frac{\partial z}{\partial t}+\frac{1}{1-\lambda}\frac{\partial q_{st}^{v}}{\partial x}=0 \tag{2.87}$$

Where, $h$ is the flow depth (m); $z$ is the bed elevation (m); $\lambda$ represent the porosity of the bed layer; $q_{st}^{v}$ is unit total volumetric sediment discharge ($m^2/s$); $x$ is the horizontal distance; and $u$ is the velocity.

He examined the governing equations of unsteady sediment transport in their dimensionless form and identified two disparate time or length scales. He used a formal perturbation approach to the movable bed problem that allowed a complete treatment of the characteristic equation associated with the hyperbolic system. The numerical results were shown with the illustration of the problem of sediment-deposition upstream of a dam.

**Bhallamudi and Chaudhry (1991)** presented a one-dimensional, unsteady, coupled model for studying aggradation and degradation in alluvial channels. They solved the Saint-Venant equations for water flow and the sediment continuity equation using second order MacCormac explicit finite difference scheme. The governing equations were given as

$$\frac{\partial h}{\partial t}+\frac{\partial q}{\partial x}=0 \tag{2.88}$$

$$\frac{\partial q}{\partial t}+\frac{\partial}{\partial x}\left(\frac{q^2}{h}+\frac{gh^2}{2}\right)+gh\frac{\partial z}{\partial x}+ghS_f=0 \tag{2.89}$$

$$\frac{\partial}{\partial t}\left[(1-\lambda)z+\frac{q_s^{v}h}{q}\right]+\frac{\partial q_{st}^{v}}{\partial x}=0 \tag{2.90}$$

Where, $q$ is the discharge per unit width ($m^2/s$).

The numerical coupled model was applied to simulate aggradation due to sediment overloading; base level lowering; and bed-level changes associated with the knick-point migration. They used the data from Soni et al. (1980) and Bagin et al. (1981) found the

satisfactory agreement between computed and the experimental data which validates the model.

**Cui *et al.* (1996)** developed a numerical decoupled model for bed aggradation of heterogeneous sediment and the downstream fining of gravel in rivers. They used one-dimensional St. Venant equations, a Keulegan resistance relation, the gravel transport relation of Parker (1990), and the formulation of the Exner equation for sediment continuity of mixtures. The model explicitly includes the operative mechanisms and relies minimally on the fitting of coefficients. The governing equations used were as:

$$\frac{\partial h}{\partial t}+\frac{\partial}{\partial x}(uh)=0 \tag{2.91}$$

$$\frac{\partial u}{\partial t}+\frac{\partial}{\partial x}\left[\frac{1}{2}u^2+gh+gz\right]=-\frac{u_*^2}{h} \tag{2.92}$$

$$\frac{\partial z}{\partial t}+\frac{1}{1-\lambda}\frac{\partial q_m^v}{\partial x}=0 \tag{2.93}$$

The model was tested for three large scale experiments on downstream fining and they found a good agreement between model results and observations for aggradation, propagating front and downstream fining processes. They used an empirical formulation in the model to predict interfacial exchange fractions of material transferred to the substrate during the process of aggradation. With the premise that a decoupled model might fail when applied to the rapidly varying boundary conditions, they developed a fully coupled numerical model for uniform sediment, and then a comparison was made between the decoupled and coupled model as applied to uniform material. The model was also compared for strongly variation in water discharge, sediment feed rate and downstream water surface elevation. They reported the identical results for the both two models even when Froude numbers near to unity.

**Kassem and Chaudhry (1998)** developed two-dimensional coupled and semi-coupled numerical models for bed variations in alluvial channels. They solved vertically averaged Navier-Stokes equations in transformed coordinates in conjunction with the sediment

transport equation for the bed load. The governing equations for flow and sediment in 2-D was given as:

$$\frac{\partial h}{\partial t}+\frac{\partial (hu)}{\partial x}+\frac{\partial (hv)}{\partial y}=0 \tag{2.94}$$

$$\frac{\partial}{\partial t}(hu)+\frac{\partial}{\partial x}\left(hu^2+\frac{gh^2}{2}\right)+\frac{\partial}{\partial y}(huv)=-gh\frac{\partial z}{\partial x}-\frac{1}{\rho}\tau_{bx}+\frac{1}{\rho}\frac{\partial}{\partial x}(h\tau_{exx})+\frac{1}{\rho}\frac{\partial}{\partial y}(h\tau_{exy}) \tag{2.95}$$

$$\frac{\partial}{\partial t}(hv)+\frac{\partial}{\partial y}\left(hv^2+\frac{gh^2}{2}\right)+\frac{\partial}{\partial x}(huv)=-gh\frac{\partial z}{\partial y}-\frac{1}{\rho}\tau_{by}+\frac{1}{\rho}\frac{\partial}{\partial y}(h\tau_{eyy})+\frac{1}{\rho}\frac{\partial}{\partial x}(h\tau_{exy}) \tag{2.96}$$

Where, $\tau_{bx}$ and $\tau_{by}$ are the shear stresses at the channel bottom in the x- and y-direction respectively (N/m$^2$); $\tau_{exx}$, $\tau_{exy}$, and $\tau_{eyy}$ represents the depth-averaged effective stresses (N/m$^2$).

They simulated the transient bed and water surface profiles for aggradation and degradation of channel bed and using Beam and Warming alternating direction implicit scheme to solve the governing equations. They used data of Soni *et al.* (1980) in both coupled and semi-coupled models for the testing purpose and found negligible difference between the results obtained from semi-coupled model and fully coupled model which contradicted the conclusions of Lyn (1987). They reported that the semi-coupled model can be used to simulate the rapid changes of sediment transport at the boundaries without introducing significant errors. They concluded semi-coupled model has more suitable applicability compared to the fully coupled model for a wide range of applications, however, their conclusions restricted to applications of bed loads with uniform sediment.

**Cao *et al.* (2002)** tested the performance of three models for aggradation and degradation processes in alluvial river, namely, (i) A fully coupled model (*FCM*) that employs the complete equations and synchronous solution procedure (ii) A partially coupled model (*PCM*) that uses the simplified equations compared to *FCM* but solved simultaneously (iii) the commonly used concept decoupled model (*DCM*) which is characterized by an asynchronous solution procedure. The governing equations used were as:

$$\frac{\partial h}{\partial t}+u\frac{\partial h}{\partial x}+h\frac{\partial u}{\partial x}+\frac{\partial z}{\partial t}=0 \tag{2.97}$$

$$\frac{\partial u}{\partial t}+g\frac{\partial h}{\partial x}+u\frac{\partial u}{\partial x}+g\frac{\partial z}{\partial x}=-gS_f \tag{2.98}$$

$$(1-\lambda)\frac{\partial z}{\partial t}+\frac{\partial}{\partial t}(C_m h)+\frac{\partial q_m^v}{\partial x}0 \tag{2.99}$$

They used three-node fourth-order interpolation scheme for testing the performance of the models for the aggradation due to overloading and for the degradation due to sediment diminution. The method of characteristics (MOC) was used by them to solve the governing equations. They used the data of Soni *et al.* (1980) for testing of the models. They noticed negligible effects on degradation when the continuity equations were simplified by neglecting sediment storage in water column for the water-sediment mixture and bed material; however, inaccuracy was noticed in the case of aggradation. They found the asynchronous solution procedure worsen the physical problem mathematically due to need of extra upstream boundary condition in the case of supercritical flow regime in upstream. They concluded that the coupled system of complete governing equations needs to be synchronously solved for refined modeling of alluvial rivers.

**Singh *et al.* (2004)** developed a one dimensional fully coupled model that simulates the sharp hydraulic and bed transients in alluvial rivers. The following equations have been used as the governing equations:

$$B\frac{\partial h}{\partial t}+\frac{\partial Q}{\partial x}+P\frac{\partial z}{\partial t}=0 \tag{2.100}$$

$$\frac{\partial Q}{\partial t}+\frac{2Q}{A}\frac{\partial Q}{\partial x}-B\frac{Q^2}{A^2}\frac{\partial h}{\partial x}+gA\frac{\partial h}{\partial x}+gA\frac{\partial z}{\partial x}+gAS_f=0 \tag{2.101}$$

$$P(1-\lambda)\frac{\partial z}{\partial t}+\frac{\partial Q_b^v}{\partial x}+\frac{\partial Q_s^v}{\partial x}+BC_m\frac{\partial h}{\partial t}+A\frac{\partial C_m}{\partial t}=0 \tag{2.102}$$

Here, $Q_b^v$ is volumetric bed load discharge ($m^3/s$), and $Q_s^v$ is volumetric suspended load discharge ($m^3/s$).

The above equations have been discretized with the generalized Preissmann implicit finite difference scheme and the resulting set of non-linear partial difference equations was solved by using Newton–Raphson iterative procedure. The features of mixed super critical and sub-critical regime, non-equilibrium sediment transport for bed load and suspended load, criterion for limiting concentration of wash load were incorporated in the model. The model was validated by simulating the Quail Creek Dike failure, USA. They extended the model to simulate the processes of grain sorting, wash load transport and non-equilibrium sediment transport.

**Arico and Tucciarelli (2008)** simulated the sediment transport problem in unsteady flow conditions for artificial channels like sewer systems. They used the various assumptions in model development: (i) transport equilibrium holds for both the suspended and the bed load; (ii) the solid load concentration does not affect the water density; (iii) the Manning resistance law, originally found for uniform flow conditions, holds in the momentum equation; and (iv) local energy dissipation and erosion were neglected.

They used the following governing equations

$$\frac{\partial A}{\partial t}+\frac{\partial Q}{\partial x}=0 \tag{2.103}$$

$$\frac{\partial Q}{\partial t}+\frac{\partial\left(\frac{Q^2}{A}\right)}{\partial x}+gA\left(\frac{\partial h}{\partial x}+\frac{\partial z}{\partial x}\right)=-gA\frac{u^2}{C^2R} \tag{2.104}$$

$$(1-\lambda)\frac{\partial(\beta_i z)}{\partial t}+\frac{\partial q_{si}^{v}}{\partial x}=0 \qquad i=0,1,2,\ldots,N_d \tag{2.105}$$

$$\sum_{i=1}^{N_d}\beta_i=1 \tag{2.106}$$

Here, $C$ is Chezy friction coefficient ($m^{1/2}/s$); $R$ is hydraulic radius (m); $\beta_i$ concentration of the $i^{th}$ granulometric size class; and $N_d$ number of granulometric classes.

The double order approximation time and space marching scheme were used for the solution of the governing equations. They reported the advantage of the model as (i) required less computational effort, and (ii) only information needed of size distribution, porosity, relative density, and friction coefficient as the bed material properties.

**Kothyari and Jain (2010b)** developed one dimensional coupled numerical model to simulate the bed degradation profile in cohesive sediment mixture. They used two types of cohesive sediment mixture clay-gravel mixture and clay-sand-gravel mixture; and in both mixtures clay proportion was varied 10–50% by weight. They used the following governing equations in coupled form for one-dimensional, unsteady flow in rectangular prismatic channel with no lateral discharge of water and sediment.

$$\frac{\partial h}{\partial t}+\frac{\partial q}{\partial x}+\frac{P}{B}\frac{\partial z}{\partial t}=0 \tag{2.107}$$

$$\frac{\partial q}{\partial t}+\frac{\partial}{\partial x}\left(\frac{q^2}{h}+\frac{1}{2}gh^2\right)+gh\frac{\partial z}{\partial x}+ghS_f=0 \tag{2.108}$$

$$\frac{P}{B}(1-\lambda)\frac{\partial z}{\partial t}+\frac{1}{\gamma_s}\frac{\partial q_{BT}}{\partial x}+\frac{1}{\gamma_s}\frac{\partial q_{sf}}{\partial x}+\frac{\partial(C_{av}h)}{\partial t}=0 \tag{2.109}$$

Here, $q_{BT}$ is the bed load transport rate of given size fraction present in cohesive sediment bed (N/m/s); $q_{sf}$ is the suspended load transport rate (N/m/s); and $\gamma_s$ is the specific weight of sediment (N/m$^3$).

They used their developed relationship (Jain and Kothyari, 2009; 2010b) for bed and suspended load transport of cohesive sediment mixtures as the auxiliary equations in the numerical model. The system of governing equations mentioned along with the relationships for resistance to flow and sediment transport were solved using the second-order explicit essentially non oscillatory finite difference scheme proposed by Nujic (1995) and Singh and Bhallamudi (1997). They tested the developed model for bed and water surface profile using their experimental data and reported good agreement between observed and computed data. They also reported that model predicts good results for transient bed and water surface

profiles in case of cohesionless sediment (for sand-gravel mixture and gravel only) in which clay percentage was given as zero.

**Qian *et al.* (2015)** presented non-capacity one dimensional fully coupled well-balanced model to simulate flows and non-uniform sediment transport as both bed load and suspended load in alluvial rivers. They used the following governing equations:

$$\frac{\partial \eta_w}{\partial t}+\frac{\partial hu}{\partial x}=\frac{\Gamma}{B} \tag{2.110}$$

$$\frac{\partial hu}{\partial t}+\frac{\partial}{\partial x}\left[hu^2+\frac{1}{2}g\left(\eta_w^{\,2}-2\eta_w z\right)\right]=-g\eta_w\frac{\partial z}{\partial x}-ghS_f+\frac{u(\rho_0-\rho_{mix})\Gamma}{\rho_{mix}B(1-\lambda)}-\frac{(\rho_s-\rho)gh^2}{2\rho_{mix}}\frac{\partial C_{sv}}{\partial x}$$
$$+u\frac{\rho_s-\rho}{\rho_{mix}}\sum\frac{\partial hu(\beta_k-1)C_k}{\partial x}+\frac{u(\rho_0-\rho_{mix})}{\rho_{mix}}\frac{E_T-D_T}{1-\lambda} \tag{2.111}$$

$$\frac{\partial hC_k}{\partial t}+\frac{\partial \beta_k huC_k}{\partial x}=\frac{\Gamma_k}{B}+\left(E_k-D_k\right) \tag{2.112}$$

$$\frac{\partial z}{\partial t}=\frac{D_T-E_T}{1-P} \tag{2.113}$$

$$\frac{\partial \delta f_{ak}}{\partial t}+f_{bk}\frac{\partial \xi_a}{\partial t}=\frac{D_k-E_k}{1-P} \tag{2.114}$$

Here, $\eta_w$ is water level (m); $\Gamma,\Gamma_k$ are the total and size-specific sediment feeding rates per unit channel length ($m^2/s$) respectively; $\rho_{mix}$ is density of water–sediment mixture ($kg/m^3$); $\rho_0$ is density of saturated bed material ($kg/m^3$); $\beta_k$ is the velocity discrepancy coefficient; $C_k$ is the size-specific sediment concentration; $E_T, D_T$ are the total sediment entrainment and deposition fluxes respectively (m/s); $E_k, D_k$ are the size-specific sediment entrainment and deposition fluxes respectively (m/s); $\delta$ is the thickness of active layer (m); $f_{ak}$ is the fraction of the $k^{th}$ size sediment in active layer; $f_{bk}$ is the fraction of the $k^{th}$ size

sediment in the interface between the active layer and substrate layer; and $\xi_a$ is the elevation of the bottom surface of active layer (m).

They incorporated active layer formulation to resolve the change of bed sediment composition. The governing equations were solved by the surface gradient method (SGM) along with the finite volume Slope LImiter Centred (SLIC) scheme. They tested the model with cases of irregular topography, including the refilling of dredged trenches, aggradation due to sediment overloading and flood flow due to land slide dam failure and found well matched agreement between the computed results and measured data.

## 2.5. TURBULENCE CHARACTERISTICS OF FLOW OVER CHANNEL BED

This section deals with the literature review on velocity and turbulence characteristics distribution of flow over channel bed under various aspects of flow and channel bed. For ex. over fixed channel bed, mobile bed, under bed forms, oscillatory flow, etc.

**Tominaga *et al.* (1989)** investigated the secondary currents and 3D flow structure in an open channel (rectangular and trapezoidal) flows using a carefully calibrated hot-film anemometer. They carried the experimental study in a tilting flume with 12.5 m length and 40 cm x 40 cm cross-section. The test section was located at 7.5 m downstream from the entrance of channel where a fully developed, uniform flow was established by adjusting the bed slope and the movable weir at the channel end. Their aim of study was to see the effects of the free surface, the channel shape and the boundary roughness on secondary current structures and three-dimensional turbulent structures. For this, they classified the experiments into three groups (i) smooth rectangular open channels in which channel width was fixed, the flow depth was changed in order to examine the effect of aspect ratio on secondary currents. (ii) trapezoidal open channels in which the side walls were inclined at an angle of 60°, 44° and 32° to horizontal plane (iii) rectangular rough open channels having roughness elements of glass beads with 12 mm diameter and they were densely attached to the wall. The velocities were measured in a half cross-section at about 100 points with sampling frequency 50 Hz and sampling time of 50 seconds. They found the difference in secondary current structure existed between the trapezoidal and rectangular open channel flow and this was attributed to the generation of revered vortex in the region between the side wall and the free surface in case of

trapezoidal open channel. When the boundary roughness condition was varied then the span-wise vortex scale increases as the ratio of the side-wall shear to the bottom wall shear becomes larger. They reported that for each case the three-dimensional structure of the primary mean velocity, the turbulence intensities and the Reynolds stresses, and the span-wise distribution of boundary shear stress affected considerably by the secondary currents.

**Lyn (1993)** conducted an experimental study for the turbulence characteristics of flow using laser Doppler velocimetry over the fixed channel bed having different bed forms. The first type of artificial bed form taken as unrealistic dune type while the second type of bed form approximates close to the geometry of real dunes. Both bed forms differing only in the upstream geometry. The bed forms were made of treated wood, and a layer of 0.25 mm sand was epoxied onto the bed forms as grain roughness. He found the Reynolds shear stress distribution was generally well approximated by the flat-bed profiles for regions of flow far from the bed. He noticed that the turbulence characteristics have not follow the flat-bed behavior in the lower part of the flow, however, matches fairly well over most of the flow depth.

**Song and Graf (1996)** studied the mean flow and turbulence parameters over a gravel bed in an unsteady open channel flow using acoustic Doppler velocity profiler (ADVP). The discharge was measured with an electromagnetic flow meter connected with the flume and the mean flow depth was measured at six different locations with the help of ultrasonic limnimeters having an accuracy of 1 mm. They studied 33 hydrographs for horizontal velocity, vertical velocity and turbulence profiles. They concluded that the mean horizontal velocity profiles little affected by the unsteadiness of the hydrograph and the rising branch of hydrograph having the larger horizontal velocity then that of falling branch. Also, the horizontal, vertical turbulence intensity and the Reynolds shear were reported higher in the rising branch.

**Wijetunge and Sleath (1998)** investigated the effect of the sediment transport on the fluid velocities and turbulence in oscillatory flow using a laser Doppler anemometer (LDA). They used the sediment consisted of nylon granules cylindrical in shape with length equal to diameter (median diameter of 4.0 mm) and a specific gravity of 1.137. The purpose of using this type of sediment was to ensure that the bed remained as nearly plane as possible

throughout the tests and also to remove the need for sediment concentration measurements. A single layer of sediment granules was glued to stainless steel plates fixed rigidly to the bottom of the tunnel. Then after removing the excess sediment the fluid velocity were measured first with the rigid bed and no moving sediment and then measurements were made over flat beds in an oscillatory flow with known gradually increasing quantities of sediment. LDA was operated in two modes i.e. one in forward-scatter mode corresponding to low sediment concentrations and second in back-scatter mode for relatively high sediment concentration. The signal was passed to a microcomputer where it was sampled 100 times per cycle for 50 cycles with the help of a phase marker. They found that the turbulence intensity at any given height above the initial bed level was less in flows with sediment motion when compared to fixed bed provided the bed remained flat.

**Nikora and Goring (2000)** presented experimental results for turbulence structure over irrigation canal with static and weakly mobile gravel beds. They measured instantaneous velocity using acoustic Doppler velocimeter in three set of experiments. One set of experiments corresponds to high flow rate with a weakly mobile bed and other two sets for lower flow rates with fixed bed. They conducted experiment at sampling frequency of 25 Hz and time duration of point measurements was from 2 to 4 min. They found the results from static and weakly mobile beds have a number of common features, like the existence of the roughness sub-layer and the adjacent logarithmic layer in both cases, however; they noticed the appreciable differences like wake region exist for fixed bed and not for weakly bed flow, reduction in the von Kármán constant for weakly mobile bed flow, the thickness of the roughness sub-layer was found larger for weakly mobile bed, the correlation coefficient was lower for weakly mobile bed, and the variation in turbulent intensity noticed to lower for weakly mobile bed. They concluded the difference between the two results (i.e. weakly and fixed bed) due to differences in span-wise spacing between eddies.

**Song and Chiew (2001)** investigated turbulence profiles in non-uniform open channel flows i.e. under both accelerating and decelerating flows using a 3D acoustic Doppler velocimeter. They conducted experimental study in an 18 m long, 60 cm wide, and 80 cm high recirculating flume tilted to a longitudinal bed slope in the range of -0.2% to 1%. The flume has glass walls and the flume bed covered with a rough aluminum plate on which sand

particles of 2.6 mm diameter were glued. They obtained 10 profiles for accelerating flow and 15 profiles for decelerating flow under the sampling data frequency of 25 Hz for 2 minutes. Measurements were taken at five sections located at x = 5, 7, 9, 11, and 13 m along the flume and the number of measuring points at each section varied from 25 to 55 depending on the water flow depth. They found both the turbulence intensities and the Reynolds stress were decreased and increased in accelerating flow decelerating flow respectively, when compared with those in uniform flow. The data revealed that the Reynolds stress distribution is not linear in either an accelerating or a decelerating flow. In an accelerating flow, it has a concave form and the maximum value occurs close to the bed. For a decelerating flow, it has convex form and its minimum value occurs at the water surface. They developed theoretical expressions for the distribution of vertical velocity and the Reynolds stress based on the Reynolds equation and the continuity equation of 2D open-channel flow. The following equation was proposed by them for computation of the distribution of the Reynolds stress at a given section under known parameters of bed slope, bed roughness, water flow depth, variation of water flow depth along stream-wise direction, and cross-sectional velocity.

$$-\overline{u'v'} = g(h-z_v)\left(S_0-\frac{dh}{dx}\right)+u^2\frac{dh}{dx}\left[\frac{(1+m_p)^2}{m_p(m_p+2)}\right]\left(1-\left(\frac{z_v}{h}\right)^{(1-m_p)/m_p}\right)^{(m_p+2)/m_p} \qquad (2.115)$$

Where, $-\overline{u'v'}$ is the Reynolds stress ($m^2/s^2$); $dh/dx$ is the spatial variation of flow depth; $z_v$ is the vertical distance (m); and $m_p$ is the constant in power law.

**Ferro (2003)** conducted experimental study for velocity measurement by an acoustic Doppler velocimeter over gravel bed in a rectangular flume having 30 m long, 0·77 m wide, and 0·935 m deep and horizontal bed slope. The water discharge was measured by a concentric orifice plate installed in the feeding pipe. He conducted experiment under five different bed arrangements (c0, c1 c2, c3, and c4) characterized by different concentrations of coarser elements, and for the two hydraulic conditions of small- and large-scale roughness. The experiments were carried out over a fixed bed (i.e. motion of particles not permitted) with high roughness characteristics. The measuring reach was divided using a reference area 0·77 × 0·77 $m^2$, and in each area having a fixed number of coarser elements. The boulders were placed on top of the base layer and were completely protruding from the bed. He found that

the measurements of velocity profile vary with the concentration of boulder elements and the depth/sediment ratio. For all bed arrangements when the values of the depth sediment ratio are greater than 5·5 the velocity profile showed the dip and the logarithmic profile fits well with the measurements; for depth sediment ratio less than 5·5 but greater than 2 the velocity profile for the bed shape of c0, c1 and c3 is logarithmic while for the bed shapes c2 and c4 it is S-shaped. When the depth sediment ratio between 1 and 2 then the velocity profile for the bed shapes c2, c3 and c4 is always S-shaped.

**Carollo *et al.* (2005)** investigated the turbulence intensity profile over a rough gravel bed in a rectangular flume of dimension 30 m long, 0.77 m wide, and 0.65 m deep. The measurements of velocity were made using acoustic Doppler velocimeter under steady flow. The test section was located at 22.39 m from the inlet section of the flume. The test section was divided into references areas of 0.77X0.77 $m^2$ and in each area a fixed number pebbles (median diameter 5.43 cm) was randomly arranged on the base layer of quarry rubble bed (median diameter 2.04 cm). The experiments were conducted under four different arrangements c0, c1, c2, c3 of the pebbles placed over the base layer and under no motion condition of particles. They carried six runs for each arrangement of bed by varying discharge and flow depth. They reported the existence of two layers below and above the tops of coarse elements where the turbulence intensity profile shows a different trend. They reported that the turbulence damping efficiency increases when the roughness elements protrude inside the flow. They found the turbulence intensity showed an increasing trend with distance from the bed, reaching a peak value then followed by a decreasing trend.

**Bigillon *et al.* (2006)** used the particle image velocimetry (PIV) technique to investigate characteristics of a turbulent flow over a transitionally-rough fixed bed in an open-channel flow. The distributions of velocities, turbulence intensities, Reynolds stress were measured in a region above $z^+\left(=\frac{z_i u_*}{\nu}\right)=10$ due to the lack of quality image data in the near wall region of the transitionally rough flows. They conducted the experimental study under uniform flow conditions in which the flow depth range from about 0.025 m to about 0.045 m; Reynolds number in the range from about 4,500 to 12,000; and the Froude number was in the subcritical range of 0.4 to 0.5. They kept the width to depth ratio in the range from about 7 to 12 to avoid

side-wall effects. The roughness height of the bed was taken as equal to the mean size of sand grain (0.00053 m). They used double-averaging procedure for the vertical distribution of the mean stream-wise velocity i.e. first time averaging of the velocity fields computed then followed by a spatially longitudinal averaging of the vertical velocity profiles computed over the time-averaged field. They found their results are very similar to those obtained for smooth walls and show a good agreement with models previously derived for smooth walls, however, they noticed some quantitative differences which accounts for the bed roughness effects and limited to the wall-region.

**Rodriguez and Garcia (2008)** measured 3D flow velocities and turbulence characteristics using a micro acoustic Doppler velocimeter (ADV) over fixed rough bed in an open channel flow. They carried the experiment in a tilting flume 12.20 m long, 0.91 m wide, and 0.6 m high and used crushed stone chips of mean size 0.57 cm for fixed hydraulic rough bed. The ADV was operated at a sampling rate of 25 Hz and velocity point was sampled for at least 120 s. The test section was located at a distance of 6 m downstream from the channel entrance where the flow was uniform and the boundary layer was fully developed. The secondary circulation and flow variability over a rough bed were analyzed under two flow conditions (i) aspect ratios (width over depth) of 8.5 and (ii) aspect ratios of 6.3. The aspect ratios were chosen such that secondary flows exhibited in the whole cross section. They found that the bed shear stresses and turbulence patterns were consistent with the secondary flow cellular circulations which contradict the general perception that secondary circulation cells die out at an aspect ratio > 2.5 from the walls and they attributed this behavior to the bed roughness and to the difference in roughness between bed and walls.

**Ojha and Mazumder (2010)** investigate the effect of the superposition of surface waves of different frequencies on the mean fluid flow and turbulence over artificial bed forms. They carried the experiments in a recirculating flume having dimension of 10 m long, 50 cm wide, and 50 cm deep. The velocity data were measured with the aid of 3-D micro acoustic Doppler velocimeter (ADV) having down-looking probe at a rate of 40 Hz for 5 min with the lowest point measured at 0.40 cm above the bed surface and the highest point at about 24 cm for each profile. The filtering of measured data were satisfied the value of the signal to noise ratio (SNR) >15 and Correlation >70%. Before the fixing of bed forms the experimental run over

the flat surface were performed for two Reynolds numbers. The combined wave-current experiments were performed with a combination of two different flows Reynolds numbers and three different waves Reynolds numbers. They found that the superposition of surface waves with increasing frequency leads to an increase in the apparent bottom roughness due to a vortex in the lee. They noticed that the effect of surface waves increases the flow stability, consequently reducing flow separation and enhanced mixing in the lee side of the bed form. Reynolds shear stress was found to increase with superposition of waves.

**Dey *et al.* (2011)** conducted an experimental study for the quantification of the near-bed turbulence characteristics in an open trapezoidal channel flow over immobile and entrainment-threshold beds for non-cohesive sediments. They used a four-beam down-looking vectrino probe to capture the instantaneous velocity components at a sampling rate of 100 Hz over duration of 300 s to achieve a statistically time-independent averaged quantities. The closest measuring location was taken at 3 mm above the bed and the sampling length used was 1 mm in lower flow zone (i.e. $z_r/h < 0.2$) while in the upper flow zone (i.e. $z_r/h > 0.2$) the sampling length was taken as 4 mm. They filter the data using signal-to-noise ratio as 17 or above and the correlations between transmitted and received pair of pulses were greater than in the range of $70 \pm 5\%$. They found, near the bed, the departure in the distributions of the observed time-averaged stream-wise velocity from the logarithmic law was more in immobile beds when it compared with the entrainment threshold beds while the damping was higher near the bed for the sediment entrainment than that for immobile beds in case of the Reynolds shear stress distributions. Dimensionless Reynolds shear stress distributions strongly deviated from the linear law for both immobile bed and entrainment-threshold near the bed, however, in upper flow zone the distributions were reasonably consistence with the linear law.

**Köse (2011)** investigated the distribution of turbulence intensity, Reynolds stresses for three velocity components, and turbulence kinetic energies along water depth in an experimental study using acoustic Doppler velocimeter (ADV) over the rigid rough bed in a rectangular open channel. He used 100 Hz frequency for sampling the data and 1 min as the sampling time for each measurement points. The data filtering criteria for signal-to-noise-ratio (SNR) were taken as 15 and correlation (COR) criteria as 70% or above. He found the distribution of

turbulent kinetic energy (TKE) suddenly increases very close to the bed and it reaches its maximum at relative depth (ratio of vertical distance to flow depth) 0.02, then decrease by following a fluctuating trend. The distribution of primary Reynolds stress component reaches its maximum at relative depth 0.10.

**Kumar and Kothyari (2012)** compared the experimental results for flow patterns and turbulence characteristics within the developing scour hole around circular uniform and compound piers. They conducted the experiment in a 30.0 m long, 1.0 m wide rectangular channel using an acoustic Doppler velocimeter for the measurement of flow velocity. The test section was located 12.0 m downstream of the flume entrance and filled with uniform cohesionless material i.e. sand of median size 0.40 mm. They conducted four series of experiment in which one for uniform circular pier of diameter 114 mm and the other three series for circular compound pier of diameter 114 mm and footing diameter 210 mm. In case of circular compound pier, the top surface of the footing was placed at three different elevations with respect to the general level of the channel bed, i.e., above the bed level, at the bed level, and below the level of the channel bed. The turbulence characteristics were made around the piers in radial planes at 0°, 30°, 60°, 90°, 120°, 150°, and 180° from flow axis. They found that the velocity, turbulence intensities, and Reynolds shear stress around each of the pier models at different vertical planes exhibit almost similar profiles along the flow depth. However, the measurements close to the pier have significant change in the vertical profile of the flow parameters when position of the top surface of the footing varied with respect to general bed level of the channel. They reported the diameter of the principal vortex upstream of the compound pier was 1.11 times as large as that for the circular uniform pier when top surface of the footing is above the general level of the channel bed. And the size of the principal vortex is 0.85 times its size for the uniform pier when the top surface of the footing was below the channel bed level. They observed the bed shear stress within the scoured region was much smaller compared with the bed shear stress of the approach flow.

**Ahmad *et al.* (2013)** conducted an experimental study for turbulence characteristics of flow over a block ramp using acoustic Doppler velocimeter (ADV). They measured the data in a rectangular channel having 7.5 m length, 1.5 m width, 1.0 m depth, and bed slope of 3.5% under the maximum discharge of the system 0.462 $m^3s^{-1}$. The crushed boulders of varying

size 7-25 cm were placed on the channel bed. This channel bed has the thickness of 27 cm. The longitudinal turbulence intensity increases along the ramp length, while the vertical turbulence intensity decreases due to breaking of larger eddies by the protrusions on the bed and transverse turbulent intensity initially decreases and then attains an equilibrium value. Reynolds stresses and turbulent kinetic energy increase along the block ramp as a result of development of boundary layer. Skewness coefficients of the longitudinal and transverse velocity components were observed to be uncorrelated with the block ramp length whereas skewness coefficient of vertical velocity component was observed to vary linearly with the length of block ramp.

**Guan *et al.* (2014)** carried experimental study in a tilting flume of dimension 12 m long, 0.38 m deep, and 0.44 m wide for the distributions of flow patterns, bed shear stresses, and turbulence structures in the approach flow and the equilibrium scour hole downstream of a submerged weir under clear water scour condition. The weir has 10 mm thick rectangular plastic plate and having the same width as flume and was located 4.5 m from the outlet of the flume. The flow velocities were measured using acoustic Doppler velocimeter with a sampling rate of 200 Hz and data sampling time was taken as 2 minutes. The measured data were filtered by maintaining the signal-to-noise (SNR) ratio above 15 and correlation above 70. They reported the significant change in the flow structures by the presence of the weir. A recirculation zone and a flow reattachment region were found along the flume centerline longitudinal direction. The maximum turbulence intensities, TKE, and Reynolds shear stresses were observed on the upstream slope of the scour hole and the maximum scour depth was found at the rear of the flow reattachment region close to the left flume glass wall. They observed the higher Reynolds shear stress near the bed when compared to the absolute values of critical bed shear stresses immediately downstream of the weir. The secondary flows were observed in the scour hole in the transverse direction.

**Jain *et al.* (2015)** focused on turbulence characteristics measurement over degraded bed of cohesionless sediment mixture of sand-gravel. They conducted experimental study in a rectangular tilting flume of 16 m long, 0.75 m wide, and 0.5 m deep. The channel had a test section of 6.0 m length, 0.75 m wide and 0.13 m depth starting at a distance of 8.0 m from channel entrance. The measurements of the instantaneous velocity, turbulence intensity and

the Reynolds stress were made using acoustic Doppler velocimeter at three locations on the degraded channel bed (i) 0.2 m from the start of test section (referred as section-I), (ii) at distance 0.5 m downstream of section-I and (iii) at distatnce1.5 m downstream of section-I. The turbulence intensity found to be increases and reaches the maximum value at near relative depth of zero i.e. at the level of channel bed surface before the start of detachment and then decreases towards top surface. The maximum value of the Reynolds stress also occurred at the start of the degradation profile i.e. at the level of channel bed surface before the start of detachment. They observed that the magnitude of turbulence intensities and the Reynolds stresses were reduced towards the downstream along the degraded bed profile.

**Singh *et al.* (2016)** investigated the effect of the superposition of surface waves of different frequencies on the turbulent flow structure over the bed-mounted artificial cubic obstacle. The 3D velocity was measured using an acoustic Doppler velocimeter (ADV) in test section starting 11 m downstream from the entrance in an open channel flume with 18.3 m long, 0.90 m wide, 0.90 m deep, and a constant slope of 0.00025. An artificial cube was made of wooden cube (0.025 m width, 0.025 m length, and 0.025 m height). They performed three different tests in their study: (i) current only over a flat bottom surface, (ii) current only around the cubic obstacle mounted on the flat surface, and (iii) superimposition of surface waves of different frequencies on the current flow over the cubic obstacle. The results highlight the changes induced in the mean velocity profile, turbulent intensity, and Reynolds shear stress in a plane of symmetry from the superposition of surface waves of different frequencies. Modifications in the mean velocities, turbulence intensities, and Reynolds shear stresses with respect to the flat surface case, in the vicinity of the cube, have been explored. The measurements were taken at seven different measuring locations along the centerline of the flume from upstream to downstream of the cube at the dimensionless distances (longitudinal distance to cube height) of −2.5, −1.5, 0, 1.5, 2.5, 4.5, and 6.5. The data sampling rate was taken as 40 Hz for 5 min duration. The lowest and highest measurement point was taken as 0.42 cm and 14 cm above the flat surface respectively and the mean flow depth was constant at 20 cm for all tests. The ADV data were filtered as per signal-to-noise ratio data >15 and the correlation >70%. They compared the turbulence parameters characteristics between the velocity profiles over the flat surface and those measured over the bed-mounted cube and found that there was a shift of the position where the velocity profile met the flat-surface

profile from the superposition of surface wave. Near the bed, as the frequency of the surface wave increased, there was a shift in the locations of the positive bottom-normal velocities behind the cube, which would likely affect the local sediment mobility. The stream-wise turbulent intensities found to be increased towards the free surface. They reported the maximum Reynolds shear stress immediately behind the cube.

## 2.6 CONCLUDING REMARKS

This chapter discusses the literature review on incipient motion, transport of sediment, bed degradation, and turbulence characteristics of flow.

- Literature review reveals that most of the study has been reported on the incipient motion of the non-uniform cohesionless sediment for sand-gravel mixture. However, presence of silt in the mixture affected the critical shear stress and it is still under investigation.
- On mixing the cohesionless sediment with cohesive sediment, the resulting mixture possesses certain amount of cohesive property and treated as cohesive sediment mixture. The erosion characteristic of cohesive sediment is significantly different from the cohesionless sediment due to dominancy of physio-chemical properties of the cohesive sediment.
- Several experimental studies have been reported on incipient motion for different cohesive sediment mixtures like clay-sand, clay-silt-sand, clay-gravel, clay-sand-gravel. However, the presence of silt with gravel particles in cohesive mixture has still the topic needed to be investigated.
- Identification of parameters is an important task in the development of equations for the computation of transport rate of sediment in the presence of clay in sediment mixture. Those parameters needed to be explored more in case of cohesive sediment mixture.
- Most of the mathematical models have been developed for the computation of degradation in a channel bed made of cohesionless sediment. Very few studies have been reported on cohesive sediment mixture of clay-gravel and clay-sand-gravel. Model development for computation of degradation needed to be extended for cohesive sediment in presence of silt.

- Literature review indicates that turbulence characteristics of flow has been investigated on various aspects like roughness of bed, sediment-laden flow, fixed channel bed, weakly mobile bed, vegetative channel bed, over block ramps, and around pier, etc. Most of the above study has been conducted on channel bed made of cohesionless sediment. And the further investigation is needed to study the turbulence characteristics of flow over degraded cohesive bed.

CHAPTER – III

# MATERIALS AND METHODS

## 3.1 GENERAL

This chapter deals with the properties of sediment and its mixture, experimental set-up & measurements, channel bed preparation, experimental procedure for incipient motion and transport of sediment, bed level variations, and visual observations of the channel bed after the end of the run. It also describes the experimental set-up and procedure for the collection of data for the study of turbulence parameters. Keeping above points in mind, an extensive experimental work was planned and conducted in Hydraulic Engineering Laboratory, Civil Engineering Department, Indian Institute of Technology Roorkee, Roorkee, India to study the sediment transport for the cohesive mixture of clay-silt-gravel, clay-silt-sand-gravel, and clay-silt-sand under varying percentage of clay.

## 3.2. SEDIMENT AND ITS MIXTURE

### 3.2.1. Sediment Properties

Cohesive as well as cohesionless sediment were used in the present study. Clay was used as the cohesive sediment while silt, sand, and gravel were used as cohesionless sediment. Laboratory tests were conducted for the determination of clay properties as per Indian Standard Code of Practice IS-1498 (IS 1970). Size of clay particle was determined through laser particle size analyzer while sieve analysis was used for the size distribution of silt, sand, and gravel sediments. Clay, silt, sand, and gravel had the median size ($d_{50}$) of 0.014 mm, 0.062 mm, 0.60 mm, and 5.50 mm respectively. The size distribution for each sediment, used in the present study, was shown in Fig. 3.1. The geometric standard deviation for sediment ($\sigma_g$) of clay, silt, sand and gravel were 2.06, 1.18, 0.73, and 1.31 respectively. The $\sigma_g$ was computed as $\frac{1}{2}[(d_{84}/d_{50})+(d_{50}/d_{16})]$ (Garde and Ranga Raju 2000) where $d_{84}$, $d_{50}$ and $d_{16}$ are the sediment size such that 84%, 50% and 16% of material is finer than that size by weight respectively. The relative density of silt, sand, and gravel was 2.65. The engineering properties of clay like liquid limit, plastic limit, maximum dry density, optimum moisture content, cohesion, clay mineralogy were summarized in the Table 3.1.

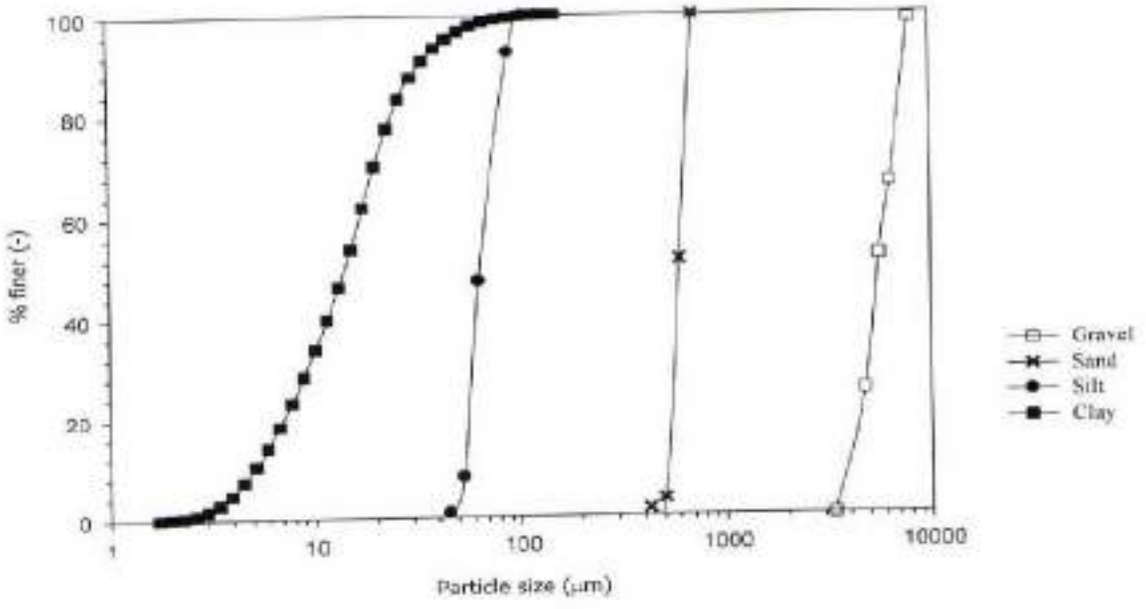


Fig. 3.1 Size distribution for sediments used in experiments

**Table 3.1** Clay properties

| **Clay properties** | **Value** | **Method used** |
|---|---|---|
| Liquid limit | 38.90 % | Casagrande apparatus |
| Plastic limit | 19.90 % | By making threads of 3.00 mm dia. |
| Plasticity index | 19.00 % | Liquid limit - Plastic limit |
| Maximum dry density | 1.70 g/cc | Standard proctor compaction test |
| Optimum moisture content | 18.00 % | |
| Cohesion | 28.59 kN/m$^2$ | Triaxial shear test |
| Angle of internal friction | 31.8° | |
| Relative density | 2.60 | Pycnometer |
| Clay mineralogy | Kaolinite – 78%<br>Illite – 17 %<br>Montmorillonite – 5 % | X-ray diffraction (XRD) test |

### 3.2.2. Sediment Mixture

Three type of sediment mixture were used in the present study namely; clay-silt-gravel, clay-silt-sand-gravel, and clay-silt-sand mixture. For preparation of sediment mixture, cohesive and cohesionless sediment were mixed together in different proportions. Clay was mixed with silt and gravel in various proportions to obtain clay-silt-gravel mixture. Similarly, clay-silt-sand-gravel mixture and clay-silt-sand mixture were obtained by mixing their corresponding sediments. In all three sediment mixture, clay was varied from 0% to 50% while cohesionless sediments were varied in equal proportions in the rest amount. Table 3.2 shows the variation of all sediment proportions in their mixture.

**Table 3.2** Proportion of sediments in their mixture

| Clay-silt-gravel mixture | | | Clay-silt-sand-gravel mixture | | | | Clay-silt-sand mixture | | |
|---|---|---|---|---|---|---|---|---|---|
| Clay % | Silt % | Gravel % | Clay % | Silt % | Sand % | Gravel % | Clay % | Silt % | Sand % |
| 0 | 50 | 50 | 0 | 33.3 | 33.3 | 33.3 | 0 | 50 | 50 |
| 10 | 45 | 45 | 10 | 30 | 30 | 30 | 10 | 45 | 45 |
| 20 | 40 | 40 | 20 | 26.7 | 26.7 | 26.7 | 20 | 40 | 40 |
| 30 | 35 | 35 | 30 | 23.3 | 23.3 | 23.3 | 30 | 35 | 35 |
| 40 | 30 | 30 | 40 | 20 | 20 | 20 | 40 | 30 | 30 |
| 50 | 25 | 25 | 50 | 16.7 | 16.7 | 16.7 | 50 | 25 | 25 |

## 3.3 EXPERIMENTAL SET-UP & MEASUREMENTS

The experiments were conducted on a tilting flume having 16 m length, 0.75 m width, and 0.50 m depth in Hydraulic Engineering Laboratory, Civil Engineering Department, Indian Institute of Technology Roorkee, Roorkee, India. The channel had a test section of 6.0 m length, 0.75 m width and 0.18 m depth starting at a distance of 7.0 m from the channel entrance. The depth of the test section in the channel for sediment filling was 0.18 m which considered here as general level of the flume bed. In order to simulate the roughness of the test section on rest of the flume bed; a thin layer of sediment was uniformly pasted. The water flow in the flume was regulated with the help of a valve provided in the inlet pipe coming from the overhead tank. A rectangular

tank is provided at the end of flume after the flow deflector for discharge measurement. A tail gate is located at downstream end of flume for maintaining the flow depth. A depth integrated sampler is installed just before the tail gate for the purpose of suspended load measurement. The side wall of the channel is made of glass. The two-dimensional bed profiler is mounted on the railing of flume for the bed level measurement. A schematic view of experimental set-up is shown in Fig. 3.2.

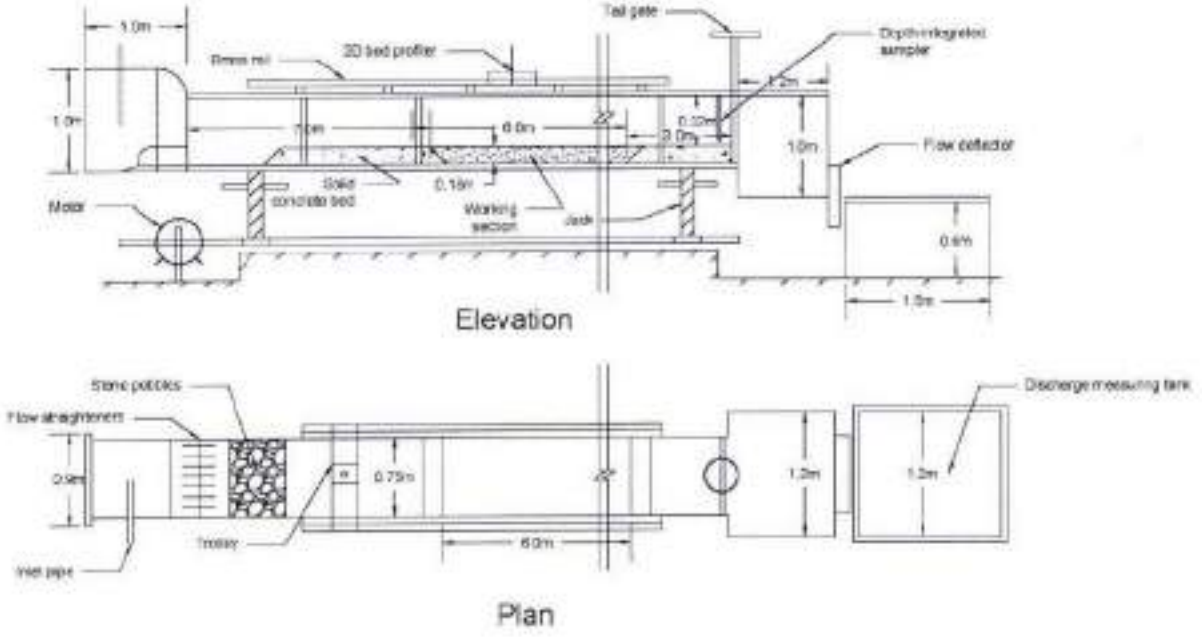


Fig. 3.2 A schematic view of experimental set-up of flume

### 3.3.1. Channel Slope Measurement

The channel bed slope was measured with the aid of two containers connected at their bottom through a long plastic tube as shown in Fig. 3.3. These containers were placed on the bed of the flume one at upstream and one at downstream end along the length of flume. The distance between two containers was noted down. After filling of water in upstream container; both containers were left for sufficient time for equalization of water levels. After the equalization of water level in containers; the vertical drop in the water level was computed by subtracting the water level of two containers that was measured by a pointer gauge mounted on the flume rails. The channel bed slope was computed through vertical drop in water level over the length

between containers. The measured slope has also been cross checked with surveyor's level and results in both methods were found close to each other.

Fig. 3.3 Cylindrical container connected with pipe used for the measurement of bed slope

### 3.3.2. Discharge Measurement

The measurement of discharge was carried out volumetrically with the help of a tank (dimension 1.50 m x 1.20 m x 0.60 m) provided just after the flow deflector at the end of the flume (Jain 2008). Flow deflector diverted the flow into tank and time was noted down for filling the tank with water flow into the tank. Then the discharge was computed by dividing the volume of water filled in the tank to time taken in filling the tank.

### 3.3.3. Bed Load Measurement

The sediment was detached and transported through the channel bed by the action of flowing water. The coarse sediment gravel and sand were transported as bed load and collected in a trap placed at the end of the flume just after the tail gate as shown in Fig. 3.4. The trap was rectangular in shape and it was made of wire-mess supported on the iron rod. It was covered with

a net cloth such that bed load sediments were retained on the trap. The collected sediment in the trap was dried and weighted.

Fig. 3.4 Rectangular trap used for the bed load collection

### 3.3.4. Suspended Load Measurement

The suspended load was collected through a depth integrated sampler installed at the end of the flume just before the tail gate location as shown in Fig. 3.5. The fine particles, clay and silt, were detached from the channel bed and transported as suspended load. The suspended sediments in the form of sediment-laden water were collected in a 15 liters capacity bucket by traversing the depth integrated sampler over the entire width of flow. The collected sediment-laden water in the bucket was weighted and left for over 24 hours so that the suspended sediment was settled down at the bottom of the bucket. After settlement of fine sediments the water was removed from the bucket and the wetted sediment at the bottom of the bucket was transferred to the pan and putted in oven for drying. The dried suspended sediment was weighted and concentration of suspended load was computed by dividing the weight of dry sediment to the measured weight of sediment-laden water.

Fig. 3.5 Depth integrated suspended load sampler for the collection of suspended load

### 3.3.5. Bed and Water Surface Profile Measurements

Two-dimensional (2D) bed level profiler was used to measure the profile of the channel bed. The profiler consists of a support beam, a profiler carriage, a probe, a power supply unit and a computer as shown in Fig. 3.6. The support beam was mounted over the bed where the bed profile has to be measured. The profiler carriage drives on the support beam along the length of the flume. The probe was fitted to the front of the profiler carriage which moves vertically up-down. As per the command instructed, the probe drives down at that location and takes a reading by touching the bed. The surface profile was also measured using flat gauge having a least count of 0.1 mm. The water surface profile was measured with the help of a pointer gauge having a least count of 0.1 mm. Bed and water surface profiles were taken at longitudinal spacing of 0.5 m along the center line of the flume. Both profiles were measured at an time interval of about 15 minutes for initial durations of the run when the bed level degradation was rapid and then the interval was keeping high as 30, 60, and 120 minutes when the bed transients becomes gradual.

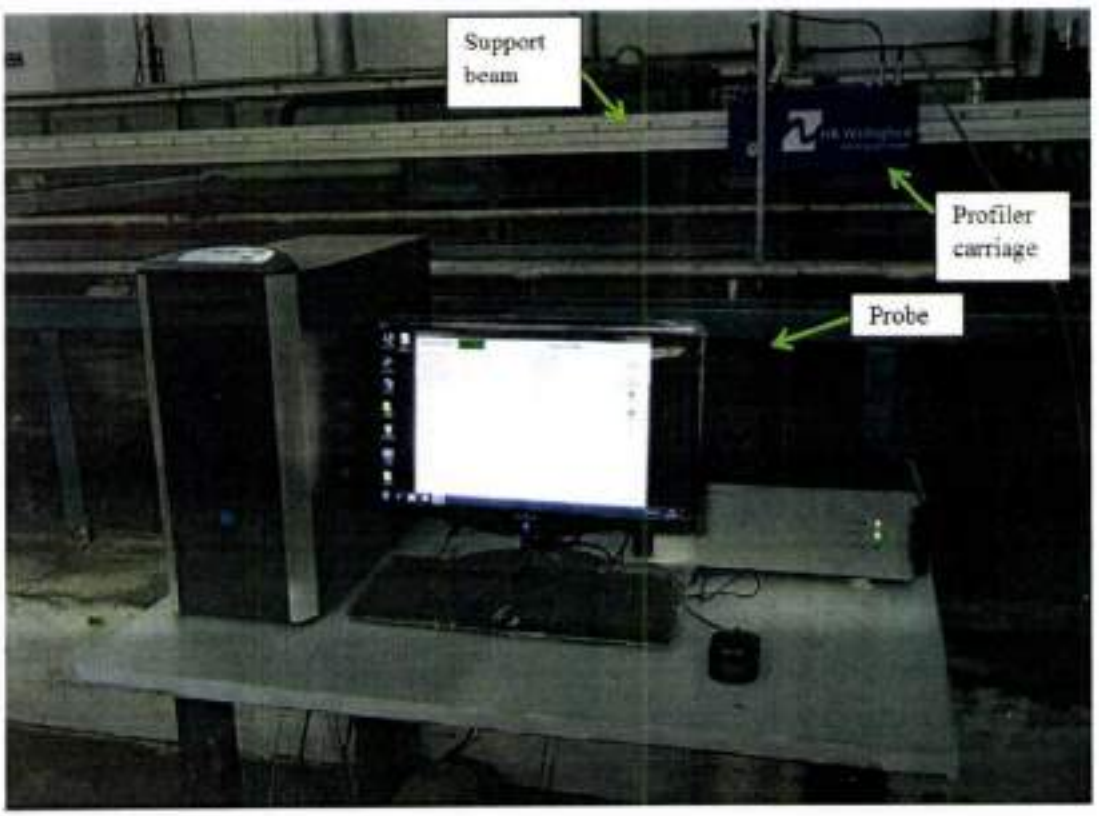


Fig. 3.6 2D bed profiler

### 3.3.6. Velocity Measurements for Turbulence Parameter

The turbulence parameters were computed using 3D-velocity which was measured with the help of Vectrino ADV (Accoustic Doppler Velocimeter). The 3D-velocity data were collected using a four transducer beam down-looking probe as shown in Fig. 3.7. The down-looking probe consist one sound emitter transducer and three sound receiver transducer. The sound emitter transducer generates an acoustic signal which is reflected back by sound scattering particles present in the water, and, then the scattered sound is received by the three receivers and flow velocity is measured in three directions. The ADV was mounted over the railing of the flume after the stabilization of the degraded bed. The ADV measures the velocity in a sampling volume which is located at 5 cm away from the sensing elements. The data were measured at a sampling rate of 100 Hz and for the longer duration of 2400 s to ensure the observations become stationary. The data were collected in both directions i.e. longitudinally (along the flow) as well as vertically (towards the free surface).

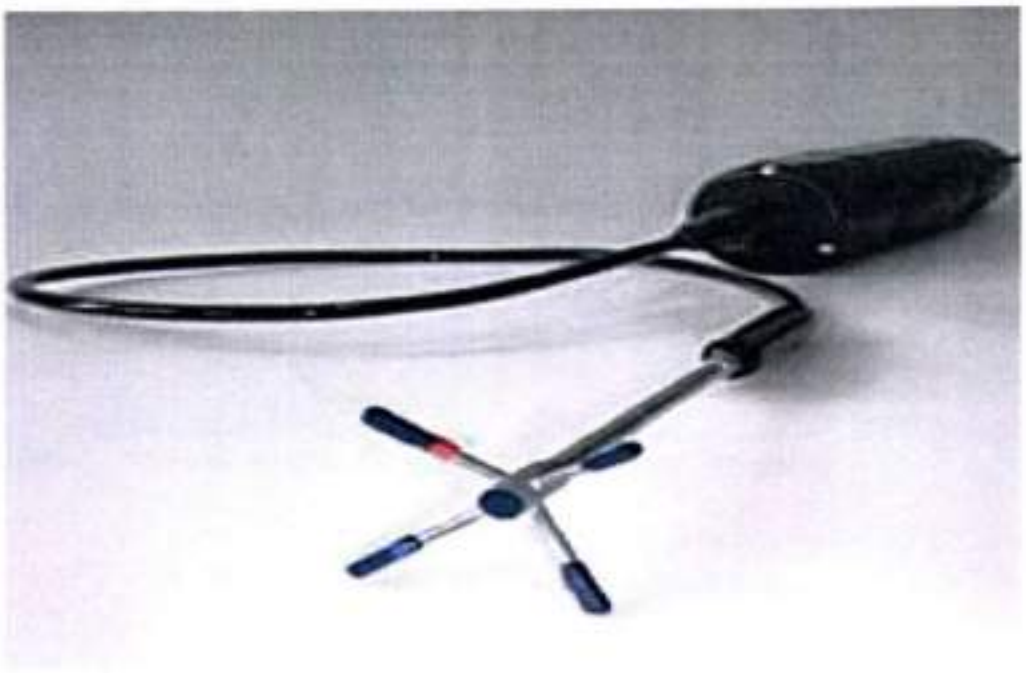

Fig. 3.7 Vectrino plus down-looking probe

### 3.4. COHESIVE BED PREPARATION

Three types of cohesive sediment mixtures i.e. clay-silt-gravel, clay-silt-sand-gravel and clay-silt-sand were used in the present study. In all three cohesive sediment mixtures, the percentage of clay was varied from 0% to 50% on weight basis while the other sediments (i.e. cohesionless sediments) were taken in equal proportions. For preparation of the channel bed, initially the required sediments were dried and weighted as per proportion and then manually mixed together. Water was added to sediment mixture and mixed them thoroughly well. The mixed sediments were covered with polythene and left for around 24 hours for uniform moisture distribution. The sediments were mixed thoroughly again before placing it into the test section. The sediments were filled in the test section and compacted in three layers for preparing a cohesive bed. The dynamic compaction method was used for compacting the channel bed. In this, each layer was compacted with a cylindrical roller having weight equal to 400 N and the sides of channel were compacted by hand rammer having rectangular bottom as shown in Fig. 3.8. To ensure bonding among different layers, the top surface was roughened by trowel before laying the next layer over it. After compacting all the three layers, extra sediments were chiseled off using sharp edge large knife. The finally prepared cohesive bed was left for around 16 hours in order to achieve

the cohesive bonding between the cohesive and non-cohesive matrix (Debnath *et al.* 2007b). Samples were taken out from the downstream section of cohesive bed for the determination of their bulk density, unconfined compressive strength, and moisture content. The bulk unit weight of sediment mixture was determined using standard core cutter method as per IS-2720 Part XXIX (IS 1975). Unconfined compressive strength (UCS) was determined in laboratory as per IS-2720 Part X (IS 1991) taking cylindrical specimen samples from the compacted bed. Water content was determined as per dry oven method for the compacted cohesive bed corresponding to all runs. Dry density of the channel bed was computed through the measured value of bulk density and water content of the bed. The void ratio of the channel bed was determined using the computed value of dry density. Before the beginning of experimental run, bed was saturated for 24 hours in order to achieve the field's condition (Jain 2008). For all the experimental runs, the sediment beds were prepared afresh.


Fig. 3.8(a-b) Preparation of sediment mixture and cohesive channel bed

## 3.5. EXPERIMENTAL PROCEDURE AND OBSERVATIONS

### 3.5.1 Incipient Motion Process

For each run, a low discharge was initially allowed in the flume and uniform flow was maintained by operating the tail gate. During the process of establishing the uniform flow, the

sediment bed was inspected visually in order to examine the detachment of the sediment particles. Here, the incipient motion was detected for the coarsest particle present in the mixture i.e. critical shear stress was measured for gravel particles in case of clay-silt-gravel mixture and clay-silt-sand-gravel mixture; and, in case of clay-silt-sand mixture the incipient motion was observed for sand particles. If there was no detachment of the coarsest particles from the channel bed then a small increment in the discharge was made and allowed in the flume and the bed condition was again inspected carefully. This operation i.e. small increment in discharge and maintaining the uniform flow was repeated till the beginning of the movement of coarsest particle occurs. Visual observation method to identify incipient motion condition have been earlier adopted by Kothyari and Jain (2008), however, in the present study quantitative measurement of sediment transport rate also has been included for reliability in the visual observations as reported in Table 3.3. The measurement of discharge, water surface profile, and bed surface profile were taken corresponding to the flow condition at which incipient motion occurs. Both water and bed surface profile was measured at an interval of 0.50 m on the center line of the test section along the longitudinal direction of flow. The mean velocity was computed using the measured data of discharge and flow depth. Flow depth was computed as average of difference between the measured bed and water surface profile at middle of each section on 50 cm interval from upstream working section along the flow direction. Generally the sidewall correction was needed in laboratory flumes to account for the differences in surface roughness between channel bed and sidewalls (made of glass in present study). For the computation of critical shear stress the concept of effective shear stress on the channel bed were applied instead of total shear stress by using Manning-Strickler roughness coefficient as per Einstein (1942) for accounting the sidewall correction which was earlier applied by Meyer-Peter and Müller (1948), Misri et al. (1984), and Jain (2008). The above process corresponding to incipient motion was done for each run. The total number of run conducted for incipient motion were 76 in which 12 runs corresponding to cohesionless sediment and 64 runs for cohesive sediment and in cohesive sediment mixture 22 runs on clay-silt-gravel mixture, 20 runs on clay-silt-sand-gravel mixture and 22 runs on clay-silt-sand mixture were conducted.

**Table 3.3** Range of measured parameters for incipient motion of cohesive sediment mixture in the present study

| Sediment mixture | Number of runs | $P_c$ | $d_a$ | $\gamma_b$ | $\sigma_{ag}$ | $W$ | $UCS$ | $h$ | $U$ | $S_f$ | $R_o$ | $q_{Ci}$ | $\tau_{ac}$ |
|---|---|---|---|---|---|---|---|---|---|---|---|---|---|
| | | % | (mm) | (kN/m$^3$) | (-) | % | (kN/m$^2$) | (m) | (m/s) | (-) | (-) | (N/m/s) | (N/m$^2$) |
| Clay-silt-gravel | 22 | 10-50 | 1.3975-2.5043 | 16.39-20.60 | 2.92-5.23 | 7.72-16.45 | 0.0-42.17 | 0.023-0.059 | 0.306-0.502 | 0.0045-0.0123 | 10.21-11.11 | 0.0010-0.0038 | 1.301-4.031 |
| Clay-silt-sand-gravel | 20 | 10-50 | 1.034-1.850 | 16.96-21.06 | 4.19-7.49 | 7.88-18.25 | 0.0-43.25 | 0.030-0.066 | 0.275-0.726 | 0.0060-0.0165 | 09.38-10.95 | 0.0002-0.0013 | 0.853-2.812 |
| Clay-silt-sand | 32 | 10-50 | 0.1725-0.2993 | 17.30-20.20 | 1.804-3.130 | 12.20-19.38 | 5.95-34.06 | 0.026-0.052 | 0.214-0.501 | 0.0027-0.0122 | 07.66-09.81 | 0.0009-0.0017 | 0.488-1.035 |

Here, $P_c$ is clay percentage, $d_a$ is arithmetic mean diameter of the cohesive sediment mixture, $\gamma_b$ is the bulk unit weight of the cohesive sediment mixture, $\sigma_{ag}$ is weighted geometric standard deviation of the cohesive sediment mixture, $W$ is antecedent moisture content of cohesive sediment mixture, $UCS$ is unconfined compressive strength of cohesive sediment mixture, $h$ is average flow depth, $U$ is mean flow velocity, $S_f$ is energy slope, $q_{Ci}$ is the transport rate for coarser particles present in the cohesive sediment mixture, $\tau_{ac}$ is critical shear stress for the cohesive sediment mixture and Rouse number = $R_o = w_s/(ku_*)$; where is $k$ (von Kármán constant) = 0.41, $u_*$ (shear velocity) = $\sqrt{\tau_{ac}/\rho}$, $\rho$ is the density of water = 1000 Kg/m$^3$, $w_s$ (sediment settling velocity) = $[(Rgd_a^2)/(C_1\upsilon + (0.75C_2Rgd_a^3)^{0.5})]$ is determined as per Ferguson and Church (2004) for sieve diameters for natural grains for which $C_1$ = 18.0 and $C_2$ = 1.0, $R = (\rho_s - \rho)/\rho$, $g$ = 9.81 m/s$^2$, $\rho_s$ (sediment density) = 2650 kg/m$^3$, $\upsilon$ = kinematic viscosity = $10^{-6}$ m$^2$/s.

### 3.5.2 Visual Observations for Incipient Motion

#### 3.5.2.1 Visual observations for cohesionless sediment mixture

Incipient motion condition in case of cohesionless sediment mixture was visually identified and the channel bed was also visually observed after the end of incipient motion run. In case of gravel-silt mixture and gravel-sand-silt mixture, it was observed that before the beginning of the movement of gravel particle, the fine particle silt was lifted up in the flow and washed away along with the flow as no silt particles were observed at the top surface of the channel bed after the end of incipient motion run. Figure 3.9(a-b) shows the patches from the test section of the

channel bed for gravel-silt and gravel-sand-silt mixture respectively which depict the dominancy of gravel particles on the top surface of the channel bed. In case of sand-silt mixture, sand particles were observed to be dominated on the channel bed after the end of incipient motion run.

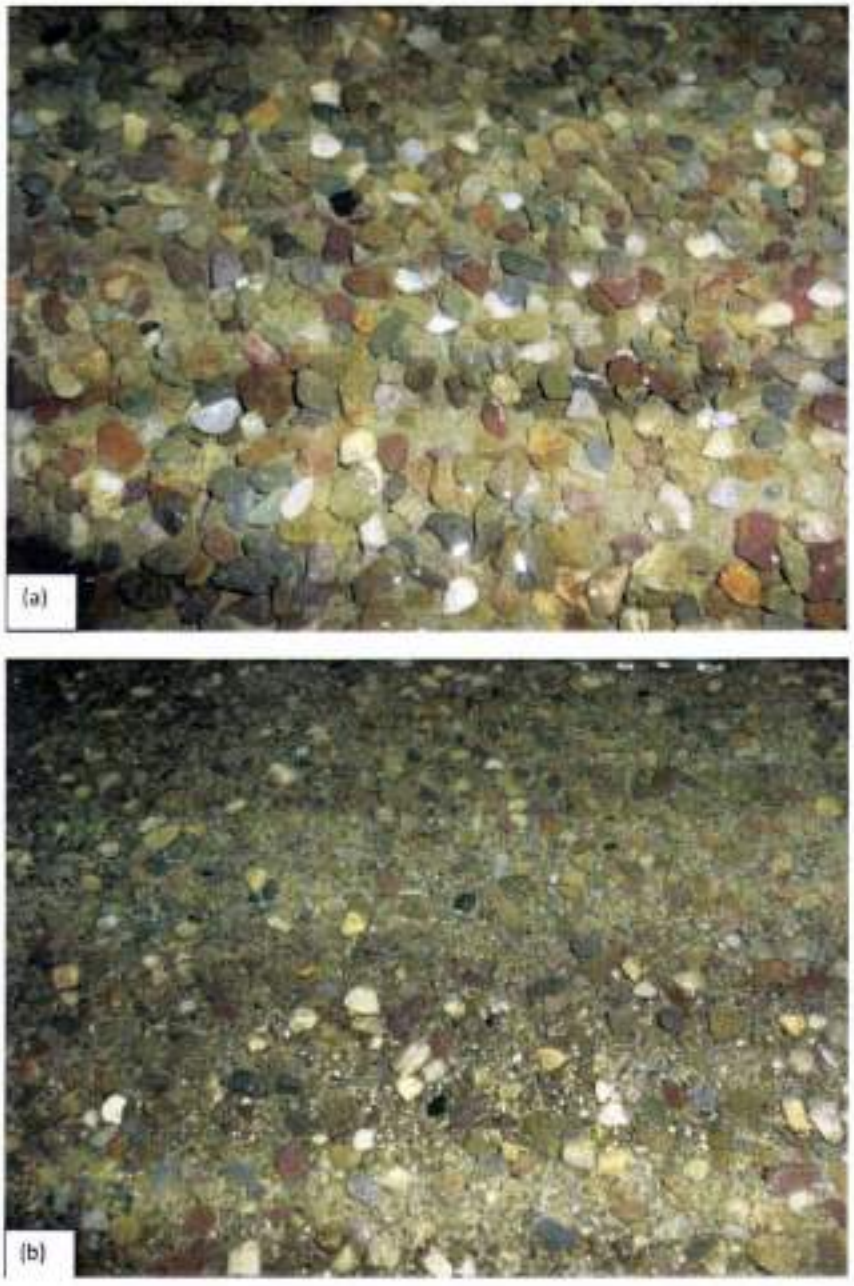


Fig. 3.9 Patches from the test section after incipient motion run for (a) gravel-silt mixture, and (b) gravel-sand-silt mixture

### 3.5.2.2 Visual observations for cohesive sediment mixture

The present study focused on the incipient motion process for cohesive sediment mixture. Incipient motion condition for the coarsest particles present in the cohesive sediment mixture was visually as well as quantitatively identified. In the process of incipient motion it was observed that before the beginning of the movement of coarsest particles the fine particles (clay and silt) were started to leave the bed in the form of suspension and the movement of coarsest particles started later on. The bed load sediment was collected in a rectangular trap installed at the end of flume just after the tail gate for the quantitative measurements. The flow condition at which entrainment of coarsest particle occurs was taken as incipient motion condition and measurements were made corresponding to this flow condition. Three types of cohesive sediment mixtures i.e. clay-silt-gravel, clay-silt-sand-gravel and clay-silt-sand were used in the present study. In all three cohesive sediment mixtures, the percentage of clay was varied from 10% to 50% on weight basis while the other sediments (i.e. cohesionless sediments) were taken in equal proportions. It was observed that cohesive bed profiles corresponding to incipient motion varied with the change in the percentages of clay from 10% to 50% for all the three cohesive sediment mixture. During incipient motion, the coarsest particles from the cohesive bed was observed to move in the form of bed load as a single particle or in the form of chunks depending upon the bonding between the particles which depends on the clay percentage and water content present in the sediment mixture.

In case of clay-silt-gravel mixture, as the clay percentage varied from 10% to 30% the fine particles (i.e. clay and silt) present in the cohesive sediment mixture rapidly came into the suspension thus leaving the gravel particles on the top surface of the bed. Finally at the end of run the cohesive bed was appeared in the form of sheet and line erosion with the presence of gravel particles on the top surface of the bed. For the clay percentage between 40% - 50%, it was observed that particles were eroded in the form of bunch or chunks as the bonding between the particles were much better due to the cohesive nature of the clay particles. At the end of run the cohesive bed appears like the mass eroded mainly towards the upstream of working section. Mass erosion was also found in few runs corresponding to 30% of clay content, however, pattern of line erosion was dominating in most of the runs for 30% clay content in the mixture.

In case of clay-silt-sand-gravel mixture, the visual appearance of the bed profile (i.e. line, sheet and mass erosion) seems similar to as that of clay-silt-gravel mixture. For the clay

percentage of 10% - 30%, sheet and line erosions were observed with the appearance of gravel particles mixed with sand on the top surface of channel bed, however, the appearance of gravel particles were dominating over sand particles. Mass erosion was observed mainly towards the upstream working section when the clay percentage was varied from 40 - 50% and at the end of run, it seems gravel and sand particles were tightly held with the cohesive channel bed.

Figure 3.10 shows the visual observations in the form of erosion pattern on top surface of the channel bed corresponding to incipient motion for different percentage of clay in the cohesive mixtures of clay-silt-gravel and clay-silt-sand-gravel. For 10% clay content in clay-silt-sand-gravel mixture, the cohesive bed appears like the gravel particles were on the top surface of the bed while the fine sediments (clay and silt) washed away along with the flow of water. Sheet erosion pattern was observed corresponding to 20% clay content in the cohesive sediment mixture of clay-silt-sand-gravel as illustrated in Fig. 3.10(a). In this, at the end of the run, the bed appeared like sheet erosion after a thin layer of fine sediments were removed from the top surface of the bed. Line was appeared on the top surface of the bed for 30% clay content in cohesive sediment mixture of clay-silt-sand-gravel mixture as illustrated in Fig. 3.10(b). Figures 3.10(c) and 3.10(d) show the mass erosion noticed for the 40% and 50% of clay content in the mixture of clay-silt-gravel.

In clay-silt-sand mixture, the appearance of the working section of the channel bed was observed in two parts which differ significantly from each other. First part covers the initial section of 3.0 m in the working section while the remaining section was covered by the 2$^{nd}$ part. For the 10 - 20% of clay content, the lines were appeared in the 1$^{st}$ part of working section while these lines were weakened towards the 2$^{nd}$ part of the working section. When clay content in mixture increases to 30% then deeper line were appeared with lumps on the 1$^{st}$ part of working section while these lines and lumps were significantly weakened towards the 2$^{nd}$ part. For the 40 - 50% of clay content, mass erosion with lumps was appeared in the 1$^{st}$ part while mass erosion weakened towards the 2$^{nd}$ part. The transition phase from line to mass erosion was seemed at 30% of clay content. Figure 3.11 shows the erosion pattern for incipient motion on the working section of clay-silt-sand mixture bed corresponding to the 30% and 40% of clay content.

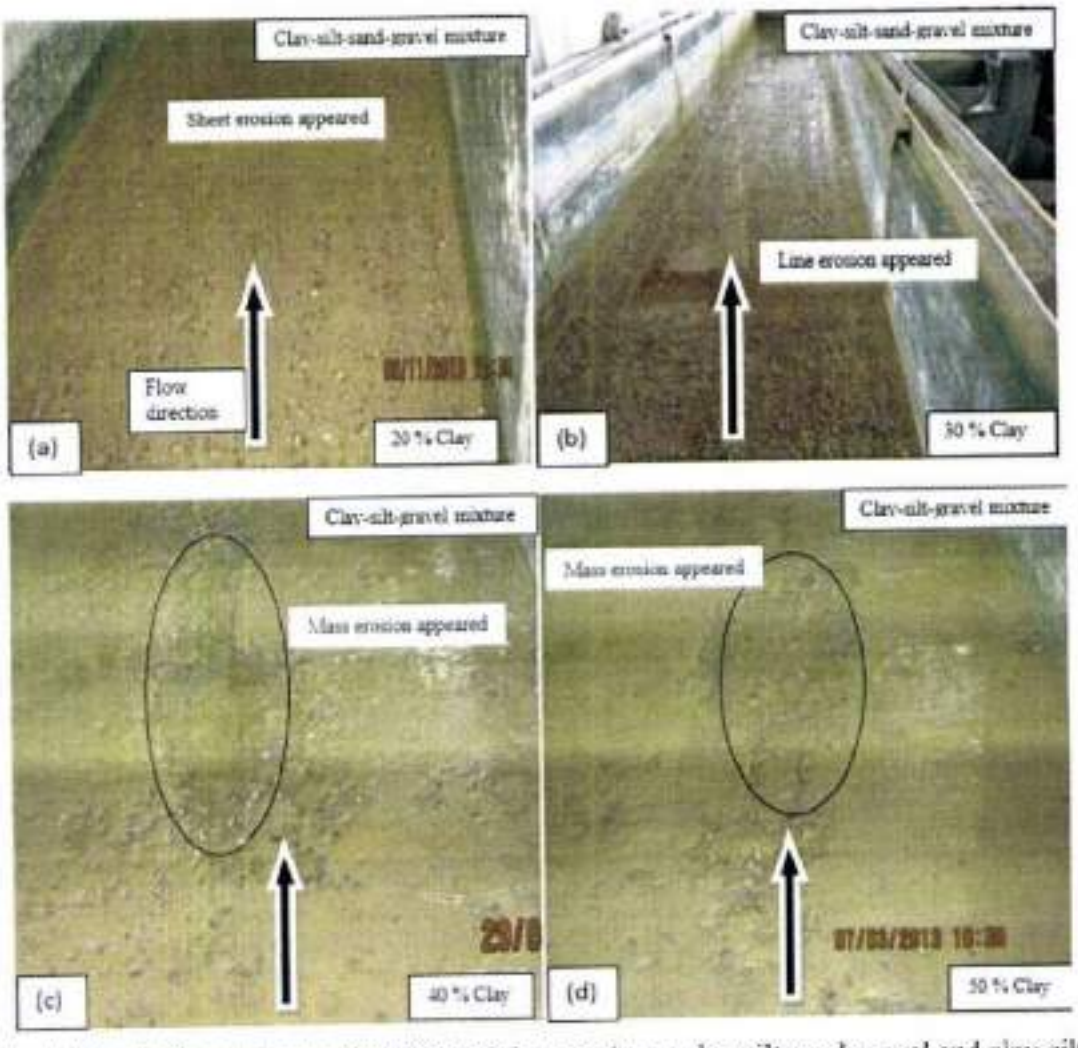


Fig. 3.10(a-d) Visual observations for incipient motion at clay-silt-sand-gravel and clay-silt-gravel mixture bed

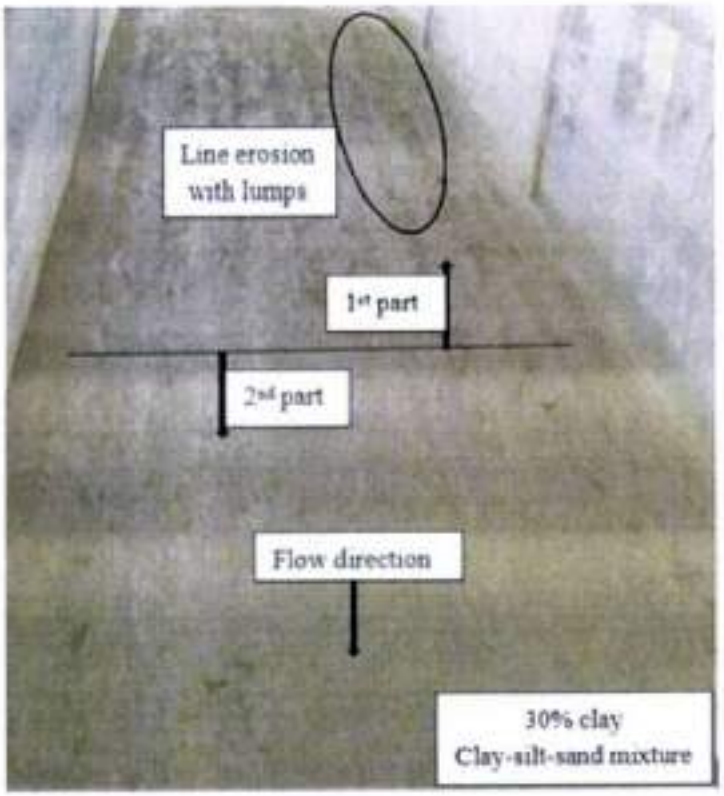


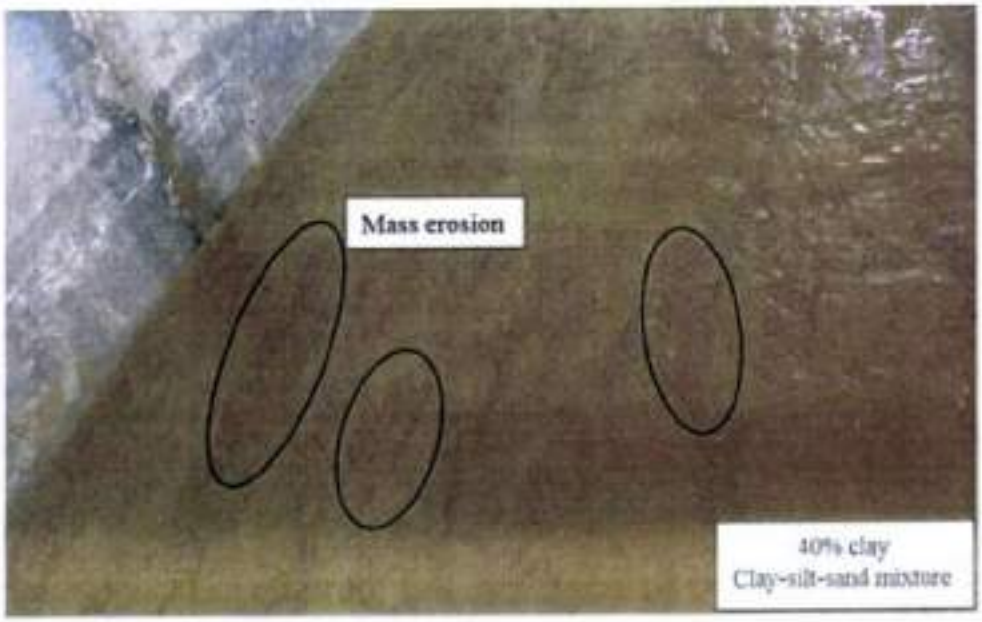


Fig. 3.11 Visual observations for incipient motion at clay-silt-sand mixture bed

### 3.5.3 Transport of Sediments and bed degradation

#### 3.5.3.1 Transport of sediments and bed degradation for cohesionless mixture

Three types of cohesionless sediment mixture were used in the present study, namely, gravel-silt, gravel-sand-silt, and sand-silt mixture. The flume was set at pre-determined slope and flow discharge after preparing the channel bed for cohesionless sediment mixture. The erosion of sediment from the channel bed was initiated as the shear stress developed by the flow on the channel bed exceeds the critical shear stress. The transported sediment was collected in terms of bed load for sand and gravel particles while suspended load for silt particles. The transient bed profile, water surface profile along with the bed load and suspended load were measured simultaneously at regular time intervals. Initially the time interval for measurements were kept as 15 minutes as the transport rate of sediment was observed to be faster while later on this time interval was increased to 30, 45, 60, 120 minutes as transport rate decrease with passes of time. The duration of each run was counted till the bed profile seems to be in static condition i.e. very less or no sediment transpoet occurring. The channel bed was visually observed after the end of the run and found that more degradation on the bed was occurred towards the upstream side compared to downstream of the working section. The top surface of the channel bed was dominated with gravel and sand after the end of run for gravel-silt mixture and sand-silt mixture respectively. The gravel particles mixed with sand were observed on the top surface of the channel bed in case of gravel-sand-silt mixture. The range of parameters on transport of sediment in case of cohesionless mixture used in the present study has been shown in Table 3.4.

#### 3.5.3.2 Transport of sediments and bed degradation for cohesive mixture

The present study deals with the cohesive sediment mixture of clay-silt-gravel, clay-silt-sand-gravel, and clay-silt-sand in which clay percentage varied from 10% to 50%. Similarly as in the case of cohesionless sediment mixture the same procedure has been adopted for cohesive sediment transport. After the preparation of cohesive channel bed the flume was set to a predetermined slope and discharge. It was observed that gravel and sand particles transported as bed load, hence, the collection of bed load was measured for sand and gravel particles while suspended load for clay and silt particles. Measurement of transient bed profile, water surface profile, bed load, and suspended load was measured simultaneously at different time intervals.

The flow in the channel was continued till the bed profile comes in static state or collection of bed load becomes very less compared to initial bed load collected.

It was observed that bed load collection and duration of run was affected by the clay percentage present in the sediment mixture. The duration of run increases with the clay percentage as it varied from 10% to 50% while collection of bed load per unit time decreases with the increase of clay percentage.

The appearance of the top surface of the channel bed after the end of the run was observed and found that the layer of fine particles (clay and silt) disappeared at the end of run and gravel particles dominated on the top surface in case of clay-silt-gravel mixture for 10 - 20% clay content in the mixture, and, more degradation was observed in upstream working section than that of downstream working section as shown in Fig. 3.12(a-b). The dominancy of gravel particles were reducing as clay content increases from 10% to 50% for clay-silt-gravel mixture and clay-silt-sand-gravel mixture as illustrated in Fig. 3.12(a-d). It was observed that gravel and sand particles detached as single particles in case of 10% and 20% clay content in the mixture while detached in the form of flakes or chunks for 40% and 50% clay content in the mixture. It seems like phase changing of detachment from single particle to bunch form occurred at 30% clay content, however, dominancy of chunks detachment occurred at 40% and 50% clay content in the mixture. The channel bed was eroded like mass erosion along the channel length in the central part of the channel bed in case of 40% and 50% clay content as shown in Fig. 3.12(d, f). Figure 3.12(e, f) illustrated the physical appearance of channel bed before and after the run for 50% of clay content in the mixture of clay-silt-sand. The range of parameters on transport of sediment in case of cohesive mixture used in the present study has been shown in Table 3.5.


Fig. 3.12(a-b) Physical appearance of the top surface of the channel bed


Fig. 3.12(c-d) Physical appearance of the top surface of the channel bed


Fig. 3.12(e-f) Physical appearance of the top surface of the channel bed

**Table 3.4** Range of data on erosion and transport for cohesionless mixture

| Mixture | Silt (%) | Sand (%) | Gravel (%) | $d_a$ (m) | $Q$ ($m^3/s$) | $S_{ti}$ (-) | $q^*_{BT}$ (N/m/s) | $q^*_{sf}$ (N/m/s) | $q_{BT}$ (N/m/s) | $q_{sf}$ (N/m/s) | Maximum degradation (cm) |
|---|---|---|---|---|---|---|---|---|---|---|---|
| Gravel-silt | 50.0 | - | 50.0 | 0.002781 | 0.05003 - 0.07026 | 0.00721 – 0.00946 | 0.15236 - 0.19608 | 0.10664 - 0.16052 | 0.00143 - 0.19608 | 0.00028 - 0.16052 | 12.5 - 14.6 |
| Gravel-sand-silt | 33.3 | 33.3 | 33.3 | 0.002054 | 0.05088 - 0.06976 | 0.00721 – 0.00946 | 0.25706 - 0.46530 | 0.09616 - 0.14118 | 0.00143 - 0.19608 | 0.00028 - 0.16052 | 12.9 - 14.7 |
| Sand-silt | 50.0 | 50.0 | - | 0.000331 | 0.03031 - 0.04388 | 0.00272 – 0.00465 | 0.12215 - 0.19601 | 0.10576 - 0.17358 | 0.00191 - 0.19601 | 0.00017 - 0.17358 | 10.7 - 11.8 |

**Table 3.5** Range of data on erosion and transport for cohesive mixture

| Mixture | $P_c$ (%) | $d_a$ (m) | $W$ (%) | $\gamma_b$ ($kN/m^3$) | $UCS$ ($kN/m^2$) | $Q$ ($m^3/s$) | $S_{ti}$ (-) | $t_e$ (min) | $q^*_{BT}$ (N/m/s) | $q^*_{sf}$ (N/m/s) | $q_{BT}$ (N/m/s) | $q_{sf}$ (N/m/s) | Maximum degradation (cm) |
|---|---|---|---|---|---|---|---|---|---|---|---|---|---|
| Clay-silt-gravel | 10-50 | 0.0013975 - 0.0025043 | 07.7167 - 16.4516 | 16.38931 - 20.60045 | 0.00000 - 42.17261 | 0.05010 - 0.07122 | 0.00721 – 0.00946 | 695 - 960 | 0.03457 - 0.16345 | 0.06502 - 0.14376 | 0.000233 - 0.163456 | 0.000262 - 0.143767 | 07.7 - 15.3 |
| Clay-silt-sand-gravel | 10-50 | 0.001034 - 0.00185 | 07.8791 - 18.2486 | 16.95838 - 21.05571 | 0.00000 - 43.25396 | 0.04973 - 0.06973 | 0.00721 – 0.00946 | 595 - 800 | 0.09208 - 0.25918 | 0.06046 - 0.13084 | 0.000486 - 0.259180 | 0.000231 - 0.130844 | 05.8 - 15.1 |
| Clay-silt-sand | 10-50 | 0.0001725 - 0.0002993 | 0.12195 - 0.18705 | 17.29983 - 20.20210 | 5.947420 - 34.06250 | 0.02917 - 0.04524 | 0.00272 – 0.00465 | 625 - 745 | 0.05587 - 0.18342 | 0.07288 - 0.15299 | 0.000612 - 0.183425 | 0.000146 - 0.152992 | 05.9 - 12.8 |

### 3.5.4 Turbulence Characteristic of flow

The degraded channel bed was established after the equilibrium stage reached for transport of sediment from the channel bed. Then, the Vectrino$^+$ ADV was installed over the flume in the working section part of the channel bed for collecting the three dimensional velocity data as shown in Fig. 3.13. The 3D-velocity data were collected corresponding to 0%, 30%, and 50% clay content in all the degraded channel bed of clay-silt-gravel, clay-silt-sand-gravel, and clay-silt-sand mixtures. The data were collected in both directions i.e. longitudinally (along the central part of the channel bed) and vertically (towards to free water surface from the channel bed bottom). The horizontal interval for velocity measurement was chosen as 20 cm from start of the upstream working section and measured up to 200 cm. The vertical measurements were taken at 3 mm, 5 mm, 7 mm, 10 mm, 20 mm, 30 mm, and so on from the bottom of degraded channel bed towards the free water surface. The velocity measurements were not taken in top 5 cm of flow depth as per limitation of the instrument. A schematic diagram (Fig. 3.14) of the experimental set-up was illustrating in the Cartesian coordinate system for describing the measurement points in the working section of the channel bed. The origin of the coordinate system is set at the junction of solid and mobile bed with the intersection of the centerline of the flume along the flow. The velocity components in the Cartesian coordinate system x, y, and z are represented by u, v, and w respectively. A four transducer beam probe (down-looking) was used to capture the instantaneous velocity components. The data were measured at a sampling rate of 100 Hz. The data samplings were made over duration of 2400 s to achieve a statistically time-independent averaged quantity. Measurements obtained using an ADV was used to investigate the time averaged velocity components, turbulence intensity components, turbulent kinetic energy, and Reynolds stresses.

Fig. 3.13 ADV set-up over the flume

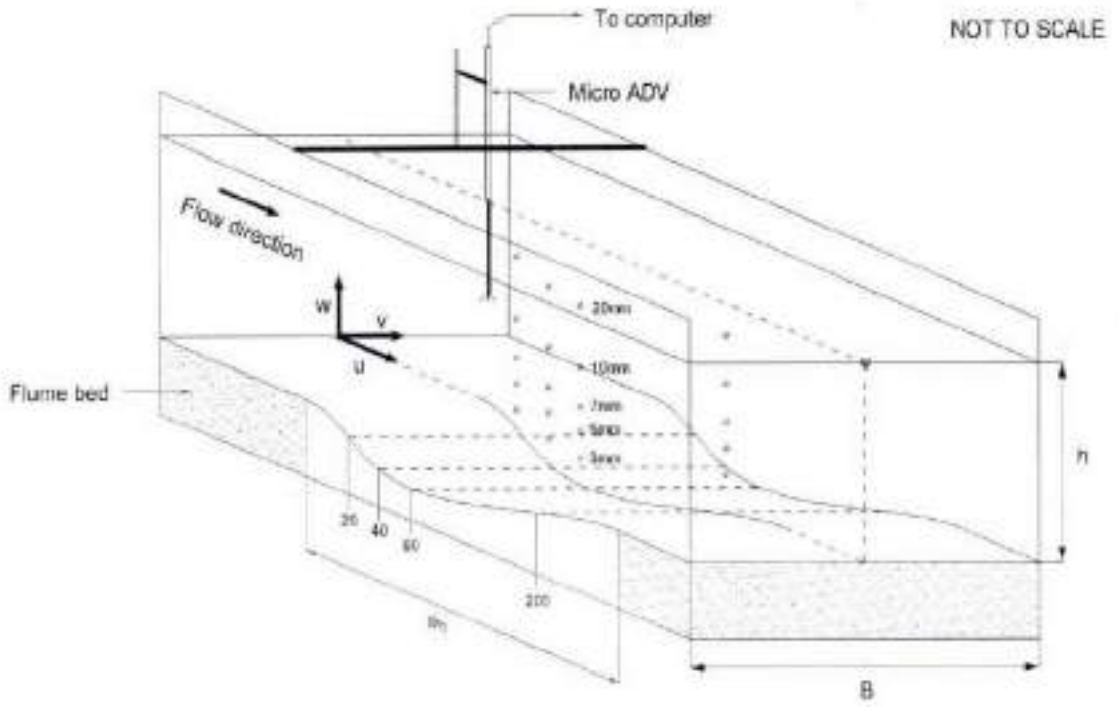


Fig. 3.14 Schematic diagram of experimental flume for ADV measurements

## 3.6 CONCLUDING REMARKS

This chapter focused on the experimental set-up and its procedure.

- The experiments were conducted on a tilting flume had a test section of 6.0 m length, 0.75 m width and 0.18 m depth starting at a distance of 7.0 m from the channel entrance.
- The channel bed slope was measured with the aid of two containers connected at their bottom through a long plastic tube. The measurement of discharge was carried out volumetrically with the help of a tank provided at the end of the flume.
- A rectangular trap, placed at the end of the flume just after the tail gate, is used for the collection of bed load. The suspended load was collected through a depth integrated sampler installed at the end of the flume just before the tail gate.
- A two-dimensional bed level profiler is used to measure the profile of the channel bed. The channel bed profile was also measured by flat gauge of least count 0.10 mm. The water surface profile was measured with the help of a pointer gauge having a least count of 0.10 mm.

- Three type of sediment mixture were used in the present study namely; clay-silt-gravel, clay-silt-sand-gravel, and clay-silt-sand mixture. The dynamic compaction method has been used for the preparation of cohesive bed.
- The properties of cohesive bed i.e. bulk density, unconfined compressive strength, and moisture content has been determined through laboratory experiments.
- The flow condition at which entrainment of gravel particles occurs was taken as incipient motion condition and measurements of corresponding discharge, water surface profile, and bed surface profile were taken.
- The physical appearance of the top surface of cohesive bed was observed visually after the end of each run and found varied with the clay content in the mixture. The dominancy of gravel particles were reducing as clay content increases from 10% to 50% for clay-silt-gravel mixture and clay-silt-sand-gravel mixture.
- The turbulence parameters were computed using 3D-velocity which was measured with the help of Vectrino+ ADV. The data were measured at a sampling rate of 100 Hz and for the longer duration of 2400 s to ensure the observations become stationary. The data were collected in both directions i.e. longitudinally as well as vertically.

# CHAPTER – IV

# RESULTS AND DISCUSSIONS

## 4.1 INTRODUCTION

The data collected from the present experimental study are analyzed along with the previous data reported by the other investigators. The analysis involves the development of new formulations based on the dimensional analysis for the computation of critical shear stress, bed load transport rate, suspended load transport rate, and bed degradation profile for cohesive mixture of clay-silt-gravel, clay-silt-sand-gravel, and clay-silt-sand.

## 4.2 INCIPIENT MOTION FOR COHESIONLESS SEDIMENT MIXTURE

Mixing of two or more cohesionless sediment of different sizes resulted in cohesionless sediment mixture or non-uniform cohesionless sediment. The incipient motion condition for uniform cohesionless sediment can be determined by Shield (1936) method using the known parameters of sediment properties (density and size) and fluid properties. However, presence of other size of particles in the channel bed significantly affects the incipient motion condition (Dong 2007). In case of non-uniform sediment, the incipient motion condition may be defined for each sediment size present in the mixture. Most of the study, in case of non-uniform sediment, has been conducted for the mixture of gravel-sand as reported in section 2.2.1. However, incipient motion for gravel particles in the presence of silt has not been studied yet. The present study focuses on the determination of critical shear stress for gravel particles in the two sediment mixture i.e. gravel-silt and gravel-sand-silt. To quantify the effect of non-uniformity, the critical shear stress determined experimentally for the channel bed having gravel particles only and compared it with the critical shear stress of gravel particles in sediment mixture.

The observed dimensionless critical shear stress for gravel particles in the mixture of gravel-silt and gravel-sand-silt has been plotted on the Shields parameters for the present study data as illustrated in Fig. 4.1. A shields curve is superimposed on the plot which shows critical shear stress for uniform sediment. The data of other investigators (Wilcock et al. 2001; Patel and Ranga Raju 1999; Kuhnle 1993; and Misri 1981) also used in the plot to compare the results among different sediment mixtures. The range of various hydraulic parameters for their study for

the incipient motion is shown in Table 4.1.The critical shear stress for sediment present in the sediment mixture is generally expressed in terms of exposure and hides effect of the particle. It can be seen that, from Fig. 4.1, the data of present study for both mixtures (gravel-silt and gravel-sand-silt) lie below the Shields curve. The silt particles in the sediment mixtures were lifted up in the flow from the channel bed before the commencement of gravel particles movement. The relatively less weight of silt particles and weak bonding nature with the other particles resulted easily suspension of silt particles in the flow. The removal of silt particles from the channel bed disturbed the position of gravel particles in the channel bed and as a consequence of it, the movement of gravel particles started at low critical shear stress. As per Fig. 4.1, Kuhnle's (1993) data reveals that more critical shear stress is required for the gravel particles in sand-gravel mixture. This is due to fact that the presence of the large amount of sand in the bed mixtures inhibited the formation of a coarse bed surface layer due to filling of sand in interstices of the gravel particles. Data of Patel and Ranga Raju (1999) also lies slightly above the Shields curve as they studied for the critical shear stress of sediment having size equal to mean size of sediment mixture.

**Table 4.1** Range of parameters for incipient motion

| Study | Sediment mixture | Number of run | $d_s$ | $h$ | $S_f$ | $\tau_{cw,c}$ | Transport Rate |
|---|---|---|---|---|---|---|---|
| | | | (m) | (m) | (-) | (N/m$^2$) | (N/m/s) |
| Present study | Gravel | 4 | 0.0055 | 0.070-0.097 | 0.0051-0.0085 | 4.545-4.616 | 0.000174-0.001467 |
| | Gravel-silt | 4 | 0.002781 | 0.024-0.025 | 0.0077-0.0105 | 1.254-1.546 | |
| | Gravel-sand--silt | 4 | 0.002054 | 0.025-0.026 | 0.0067-0.0092 | 1.178-1.253 | |
| Wilcock et al. (2001) | Gravel-sand | 5 | 0.0084-0.0122 | 0.099-0.108 | 0.0032-0.0056 | 2.820-5.420 | 0.000002-0.00018 |
| Kuhnle (1993) | Gravel-sand | 9 | 0.00048-0.00097 | 0.1024-0.1079 | 0.00038-0.0016 | 0.250-1.038 | 0.00004-0.023 |
| Misri (1981) | Gravel | 9 | 0.00237-0.00436 | 0.0222-0.0793 | 0.00317-0.01067 | 1.525-3.044 | 0.000244-0.002062 |
| | Gravel-sand | 7 | 0.00221-0.00382 | 0.0559-0.1573 | 0.00201-0.00329 | 1.534-2.185 | |

Since the mean size of mixture is smaller than that of gravel particles so the lesser exposure available for their movement and resulted in higher critical shear sand-gravel mixture.

Wilcock's et al. (2001) data indicates low critical shear stress for gravel particles in sand-gravel mixture in which percentage of gravel is higher than that of sand. Lower percentage of sand in the mixture leads to higher exposure of gravel particles with flow due to inadequate filling of it in interstices of gravel particles and resulted in lower critical shear stress. It can be concluded from Fig. 4.1 that the critical shear stress, in case of non-uniform sediment; deviates from that of uniform sediment (represented as Shields curve). In view of this, equations have been developed in literature for the prediction of critical shear stress of individual particles in the sediment mixture.

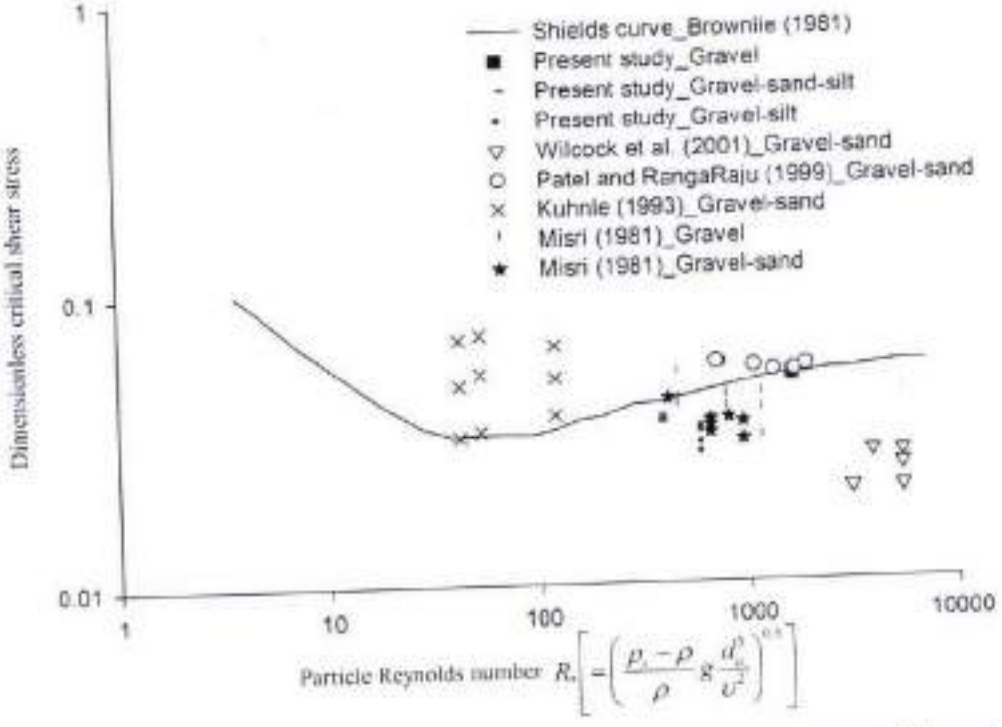


Fig. 4.1 Variation of dimensionless critical shear stress with particle Reynolds number

In the present study, the existing equations of Egiazaroff (1965), Hayashi *et al.* (1980), and Wu *et al.* (2000) i.e., Eqs. (2.2), (2.4), and (2.15) respectively; has been used for computing critical shear stress of gravel particles in non-uniform sediment. The applicability of these equations have been checked using the data of present study along with the data of Wilcock *et al.* (2001), Kuhnle (1993), and Misri (1981). For this, a plot has been made between observed and computed

value as illustrated in Fig. 4.1. Figures 4.2(a), 4.2(b), and 4.2(c) show the comparison between observed and computed value of critical shear stress for gravel particle by Eqs. (2.2), (2.4), and (2.15) respectively. Energy slope method was used to compute the observed critical shear stress for the data of present study. Figures 4.2(a), 4.2(b), and 4.2(c) depict that the critical shear stress for gravel particle is not well predicted by the existing Eqs. (2.2), (2.4), and (2.15). Therefore, a new equation is required to develop for predicting the critical shear stress of gravel particle in cohesionless sediment mixture.

### 4.2.1 Development of a New Formulation

Analysis of data revealed that critical shear stress ( $\tau_{cm,g}$ ) of gravel particles in the sediment mixtures is the function of following variables

$$\tau_{cm,g} = f(\tau_{cm}, \rho_s, \rho, g, P_f, d_{50,g}, d_a) \tag{4.1}$$

Using dimensional analysis, Eq. (4.1) can be rearranged into the following dimensionless form:

$$\tau_{*cm,g} = f(\tau_{*cm}, \frac{P_{c,g}}{P_{b,g}}, \frac{d_{50,g}}{d_a}) \tag{4.2}$$

$$\tau_{*cm,g} = \frac{\tau_{cm,g}}{(\rho_s - \rho)gd_a} \tag{4.3}$$

$$\tau_{*cm} = \frac{\tau_{cm}}{(\rho_s - \rho)gd_a} \tag{4.4}$$

$$d_a = \frac{\sum_{j=1}^{M}[(d_{50})_j P_j]}{\sum_{j=1}^{M} P_j} \tag{4.5}$$

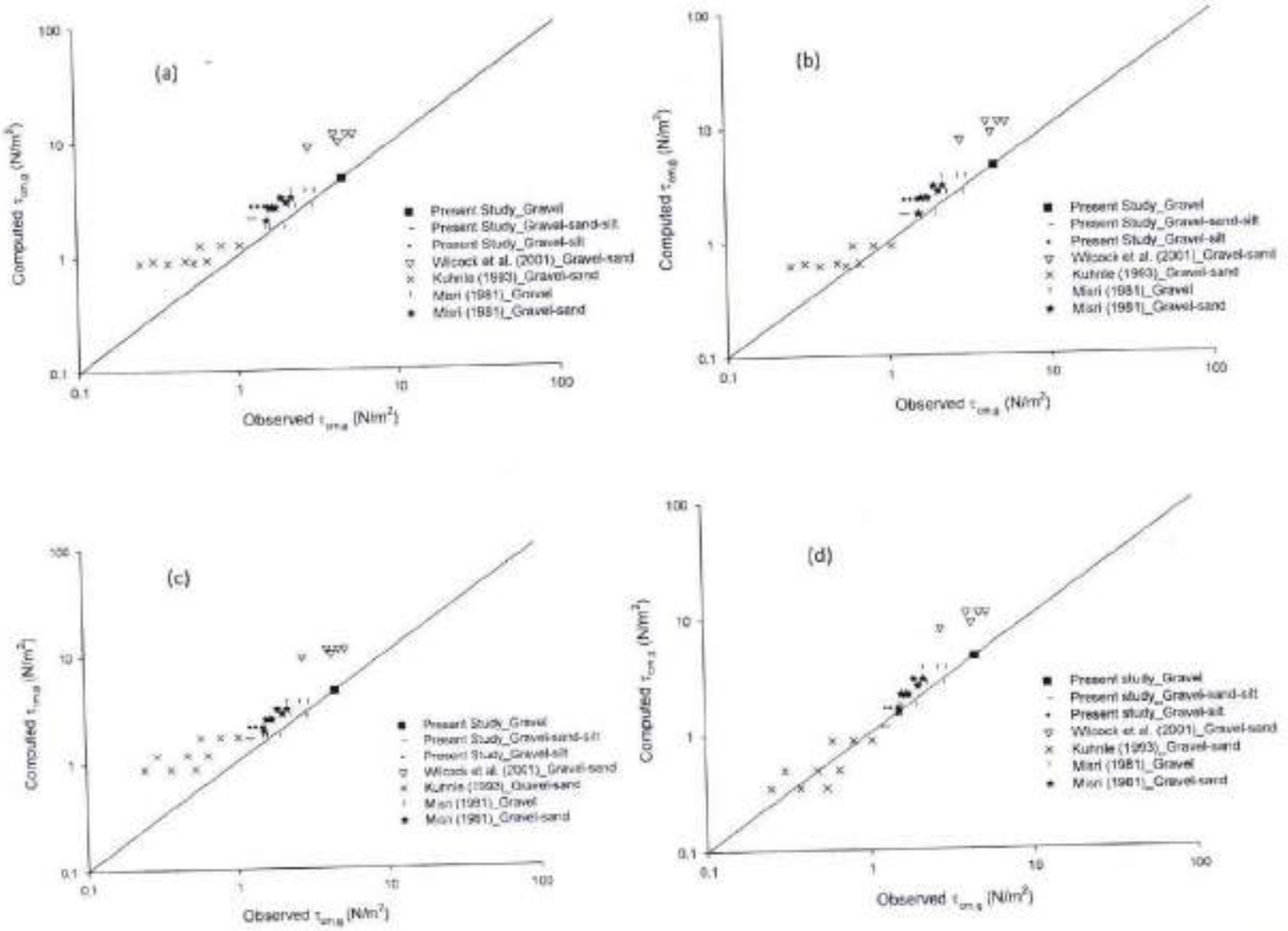


Fig. 4.2 Observed and computed critical shear stress as per (a) Egiazaroff (1965); (b) Hayashi et al. (1980); (c) Wu *et al.* (2000); (d) present study Eq. (4.8)

$$P_{h,g} = \sum_{j=1}^{M} P_j \frac{d_j}{d_{50,g} + d_j} \tag{4.6}$$

$$P_{e,g} = \sum_{j=1}^{M} P_j \frac{d_{50,g}}{d_{50,g} + d_j} \tag{4.7}$$

Here, $\tau_{*cm,g}$ is the dimensionless critical shear stress (-) for gravel particles in the sediment mixture of present study; $\tau_{cm}$ is the critical shear stress (N/m$^2$) as per Brownlie (1981) for arithmetic mean size of non-uniform sediment; $P_j$ is the percentage of particles present in the sediment mixture as per $j$ particles; $d_{50,g}$ is the mean size (m) of gravel particles; $d_a$ is the arithmetic mean size (m) of non-uniform sediment which converted into mean size of individual particle in case of uniform sediment; $P_{e,g}$ and $P_{h,g}$ are the exposing and hiding probability, respectively, of gravel particles by the particles $d_j$ present in the sediment mixture.

The data of present study were used for development of equation for the computation of critical shear stress. A large number of trials with the variables given in Eq. (4.2) led the following relationships for the computation of critical shear stress of gravel particle:

$$\tau_{*cm,g} = \tau_{*cm} \left( \frac{P_{e,g}}{P_{h,g}} \right)^{-0.6} \left( \frac{d_{50,g}}{d_a} \right)^{0.62} \tag{4.8}$$

The factor $(P_{e,g}/P_{h,g})$ in the formulation (14) governs the exposing and hiding effects for gravel particles with the particles present in the sediment mixture. Relative size of gravel particles with mean size of the sediment mixture is also instrumental in entrainment of gravel particle, and is presented in Eq. (4.8) by factor $(d_{50,g}/d_a)$. The value of the factors $(P_{e,g}/P_{h,g})$ and $(d_{50,g}/d_a)$ become equal to unity for uniform sediment and the formulation (14) converges into the equation for computation of critical shear stress for the uniform sediment as per Brownlie (1981). The critical shear stress computed from the proposed Eq. (4.8) is plotted against the observed one in Fig. 4.2(d) for the data of present study along with the data of Wilcock *et al.* (2001), Kuhnle (1993), and Misri (1981). Figure 4.2(d) shows a good agreement between observed and computed values compared to Figs. 4.2(a), 4.2(b), and 4.2(c). The critical shear stress is over-predicted for the data of Wilcock *et al.* (2001). This is attributed to lower observed shear stress as they reported lower transport rate. This critical shear stress is expected to be higher in order to

have uniform criteria in terms of quantitative measurement of bed load for incipient motion with the other investigators. And this expected higher shear stress might be better governed by the proposed Eq. (4.8). Hence, the proposed Eq. (4.8) well predicts the critical shear stress of gravel particles in sediment mixture of gravel-sand, gravel-silt, and gravel-sand-silt.

### 4.2.2 Goodness of Fit Test

The equation proposed in the present study along with the existing equations proposed by Egiazaroff (1965), Hayashi *et al.* (1980), and Wu *et al.* (2000) for the computation of critical shear stress of gravel particles in the sediment mixture were tested against the goodness of fit test by using statistical methods adopted by Yang *et al.* (1996) *i.e.* using Eqs. (4.9) - (4.10).

$$\text{Discrepancy ratio, } R_k = \frac{(\tau_{*cw,g})_{c,k}}{(\tau_{*cw,g})_{o,k}} \tag{4.9}$$

$$\text{Mean discrepancy ratio, } \overline{R} = \frac{\sum_{k=1}^{N} R_k}{N} \tag{4.10}$$

$$\text{Standard deviation, } \sigma_{\overline{R}} = \sqrt{\frac{\sum_{k=1}^{N} (R_k - \overline{R})^2}{N-1}} \tag{4.11}$$

Here, $(\tau_{*cw,g})_{c,k}$ and $(\tau_{*cw,g})_{o,k}$ are the computed and observed value of $\tau_{*cm,g}$ respectively, $N$ is the total number of observations and $\sigma_{\overline{R}}$ is the standard deviation for the discrepancy ratio.

Table 4.2 shows the results of statistical performance as per the goodness of fit test for the proposed Eq. (4.8) and existing equations of Egiazaroff (1965) Eq. (2.2), Hayashi *et al.* (1980) Eq. (2.4), and Wu *et al.* (2000) Eq. (2.15) for the data of present study along with the data of Wilcock *et al.* (2001), Kuhnle (1993), and Misri (1981). The better statistical results were found the proposed Eq. (4.8) as more than 85% data lies within the range of description ratio of 0.50 – 1.50 and also other statistics having better value for Eq. (4.8) compared to Eq. (2.2), (2.4), and (2.15) for all the data shown in Table 4.1.

**Table 4.2** Statistical analysis for computed and observed value of $\tau_{cw,c}$

| Equation | Data | Sediment mixture | N | Discrepancy ratio | | | |
|---|---|---|---|---|---|---|---|
| | | | | $\bar{R}$ | % of data in range | | $\sigma_{rc}$ |
| | | | | | 0.75 – 1.25 | 0.50 – 1.50 | |
| Proposed Eq. (4.8) | Present study | Gravel-silt | 4 | 1.024 | 100 | 100 | 0.098 |
| | | Gravel-sand-silt | 4 | 1.021 | 100 | 100 | 0.027 |
| | Wilcock et al. (2001) | Gravel-sand | 5 | 2.347 | 0 | 0 | 0.357 |
| | Kuhnle (1993) | Gravel-sand | 9 | 1.072 | 44.44 | 88.89 | 0.337 |
| | Misri (1981) | Gravel-sand | 7 | 1.283 | 42.86 | 85.71 | 0.167 |
| Wu *et al.* (2000) Eq. (2.15) | Present study | Gravel-silt | 4 | 1.521 | 0 | 50 | 0.145 |
| | | Gravel-sand-silt | 4 | 1.373 | 0 | 100 | 0.037 |
| | Wilcock et al. (2001) | Gravel-sand | 5 | 2.557 | 0 | 0 | 0.499 |
| | Kuhnle (1993) | Gravel-sand | 9 | 2.445 | 0 | 0 | 0.800 |
| | Misri (1981) | Gravel-sand | 7 | 1.446 | 0 | 71.43 | 0.118 |
| Hayashi et al. (1980) Eq. (2.4) | Present study | Gravel-silt | 4 | 1.638 | 0 | 25 | 0.156 |
| | | Gravel-sand-silt | 4 | 1.435 | 0 | 100 | 0.038 |
| | Wilcock et al. (2001) | Gravel-sand | 5 | 2.353 | 0 | 0 | 0.349 |
| | Kuhnle (1993) | Gravel-sand | 9 | 1.480 | 44.44 | 55.56 | 0.536 |
| | Misri (1981) | Gravel-sand | 7 | 1.379 | 14.29 | 85.71 | 0.142 |
| Egiazaroff (1965) Eq. (2.2) | Present study | Gravel-silt | 4 | 1.904 | 0 | 25 | 0.182 |
| | | Gravel-sand-silt | 4 | 1.750 | 0 | 0 | 0.047 |
| | Wilcock et al. (2001) | Gravel-sand | 5 | 2.487 | 0 | 0 | 0.418 |
| | Kuhnle (1993) | Gravel-sand | 9 | 2.053 | 11.11 | 22.22 | 0.771 |
| | Misri (1981) | Gravel-sand | 7 | 1.490 | 0 | 57.14 | 0.119 |

## 4.3 INCIPIENT MOTION FOR COHESIVE SEDIMENT

The critical shear stress for the uniform cohesionless sediment is well represented by the Shields curve, which has also been used in the form of Brownlie (1981) equation for the computation of dimensionless critical shear stress of the cohesionless sediment (Dong, 2007). The incipient motion of non-uniform cohesionless sediment mainly had the function of individual sediment

size, arithmetic mean size of non-uniform sediment, percentage of sediment, and critical shear stress of uniform cohesionless sediment. However in case of cohesive sediment, in addition of the above parameters; clay percentage and strength of cohesive bed plays a significant role in entrainment of sediment. Hence, to incorporate the above all factors the present study focuses on the parameters which govern the clay percentage, strength of the bed, and hiding-exposure effect. The strength of the bed depends on the compaction applied on the bed and is measured in terms of UCS (unconfined compressive strength) and reflected by the easily measurable parameters such as porosity and bulk density. To incorporate hiding-exposure effect, different form of correction factors had been used and correlated it as function of individual sediment size, arithmetic mean of non-uniform sediment and percentage of sediment. In the present study hiding-exposure effect has been taken into account in the form of weighted standard deviation of sediment mixture. It is a function of individual sediment size, arithmetic mean size of non-uniform sediment, and percentage of sediment. Although the different form of correction factors has been tried in trials, however, form of weighted standard deviation provides the best results and hence used in present study.

The present study deals with the three cohesive sediment mixture namely; clay-silt-gravel, clay-silt-sand-gravel, and clay-silt-sand. The visual observations has been adopted for identifying the incipient motion condition, however, quantitative measurement of sediment transport rate also has been included for reliability in the visual observations as reported in Table 4.3. The range of various parameters related to different experimental runs for clay-silt-gravel, clay-silt-sand-gravel and clay-silt-sand mixture in the present study were shown in Table 4.3.

**Table 4.3** Range of measured parameters for incipient motion of cohesive sediment mixture in the present study

| Sediment mixture | Number of runs | $P_c$ | $d_a$ | $\gamma_s$ | $\sigma_{ag}$ | $W$ | $UCS$ | $h$ | $U$ | $S_f$ | $R_*$ | $q_{cf}$ | $\tau_{cr}$ |
|---|---|---|---|---|---|---|---|---|---|---|---|---|---|
| | | % | (mm) | (kN/m$^3$) | (-) | % | (kN/m$^2$) | (m) | (m/s) | (-) | (-) | (N/m/s) | (N/m$^2$) |
| Clay-silt-gravel | 22 | 10-50 | 1.3975-2.5043 | 16.39-20.60 | 2.92-5.23 | 7.72-16.45 | 0.0-42.17 | 0.023-0.059 | 0.306-0.902 | 0.0045-0.0123 | 10.21-11.11 | 0.0016-0.0038 | 1.301-4.031 |
| Clay-silt-sand-gravel | 20 | 10-50 | 1.034-1.850 | 16.96-21.06 | 4.19-7.49 | 7.88-18.25 | 0.0-43.25 | 0.030-0.066 | 0.275-0.726 | 0.0060-0.0165 | 09.38-10.95 | 0.0002-0.0013 | 0.853-2.812 |
| Clay-silt-sand | 22 | 10-50 | 0.1725-0.2993 | 17.30-20.20 | 1.804-3.130 | 12.20-19.38 | 5.95-34.06 | 0.026-0.052 | 0.314-0.501 | 0.0022-0.0122 | 07.66-09.81 | 0.0009-0.0017 | 0.488-1.035 |

Where, $P_c$ is clay percentage, $d_a$ is arithmetic mean diameter of the cohesive sediment mixture, $\gamma_s$ is bulk unit weight of the cohesive sediment mixture, $\sigma_{ag}$ is weighted geometric standard deviation of the cohesive sediment mixture, $W$ is antecedent moisture content of cohesive sediment mixture, $UCS$ is unconfined compressive strength of cohesive sediment mixture, $h$ is average flow depth, $U$ is mean flow velocity, $S_f$ is energy slope, $q_{cf}$ is the transport rate for coarser particles present in the cohesive sediment mixture, $\tau_{cr}$ is critical shear stress for the cohesive sediment mixture and Rouse number = $R_* = w_s/(ku_*)$; where is $k$ (von Kármán constant) = 0.41, $u_*$ (shear velocity) = $\sqrt{\tau_{cr}/\rho}$, $\rho$ is the density of water = 1000 kg/m$^3$, $w_s$ (sediment settling velocity) = $[(Rgd_a^2)/(C_1\upsilon+(0.75C_2Rgd_a^3)^{0.5})]$ is determined as per Ferguson and Church (2004) for sieve diameters for natural grains for which $C_1$= 18.0 and $C_2$= 1.0, $R=(\rho_s-\rho)/\rho$, $g$= 9.81 m/s$^2$, $\rho_s$ (sediment density) = 2650 kg/m$^3$, $\upsilon$ = kinematic viscosity = $10^{-6}$ m$^2$/s.

The behavior of cohesive sediment significantly differs from the cohesionless sediment because of the presence of clay in the cohesive sediment mixture (Kothyari and Jain 2010a). To quantify the effect of cohesion i.e. presence of clay; the dimensionless critical shear stress of cohesive sediment mixture ($\tau_{*c}$) is compared with that of cohesionless sediment having the same arithmetic mean size as that of the cohesive sediment mixture on the plot of Shields parameters as shown in Fig. 4.3 in which abscissa $R_*[=((\rho_s-\rho/\rho)gd_a^3/\upsilon^2)^{0.5}]$ is the dimensionless particle Reynolds number. Shields curve drawn on this plot corresponds to the critical shear stress for the cohesionless sediment. The data for the plotting of Shields curve is

taken from Brownlie (1981). Figure 4.3 depicts that the value of $\tau_{*_{cr}}$ for cohesive sediment is higher and much above the line of Shields curve compared to that of cohesioness sediment for most of the data of present study as well for the data of other investigators. However few value of $\tau_{*_{cr}}$ in the present study (cohesive sediment mixtures having gravel) is lying below the line of Shields curve for the 10 - 20% of clay content in the mixture. This may be attributed to the presence of higher percentage of silt in the mixture with clay content in the range of 10 - 20% and also the size of the gravel particles which is much larger than the fine particles present in the mixture. Large amount of fine particles covers the top surface of bed and cohesion may not be sufficient high (as low clay content) to bind the particles together on the top surface which resulted in the exposure of gravel particles at low shear stresses. Ansari (1999) also reported that few value of dimensionless critical shear stress were below the Shields curve for the cohesive sediment (clay-sand) mixture. It indicates the presence of clay and silt significantly affects the incipient motion condition. The present study made an attempt to develop a relationship for the computation of critical shear stress of gravel particles for cohesive mixture of clay-silt-gravel, clay-silt-sand-gravel, and clay-silt-sand.

### 4.3.1 Development of Relationships for Critical Shear Stress

The experimental study has been done due to the lack of governing equation for the incipient motion of cohesive sediment mixture because of the complex interaction between the flow and cohesive sediment. The resistance against the erosion of cohesionless sediment is well controlled by the sediment size and their density, however, the erosion of cohesive sediment is affected by the several parameters due to complex physico-chemical properties of the clay (Kothyari and Jain 2010a). As such various parameters have been considered in the present study to develop relationship for the critical shear stress of coarser particles present in the cohesive sediment mixture. However, only the parameters which yielded in better results were represented in the analysis below. The coarser particle here represented by gravel for cohesive mixture clay-silt-gravel and clay-silt-sand-gravel; while sand represents the coarser particle for the mixture of clay-silt-sand. Following variables has been considered which affect the critical shear stress of coarser particles present in the cohesive sediment mixtures as

$$\tau_{cr} = f(\tau_{cm}, P, P_c, d_{50}, d_{gs}, \sigma_g, \gamma_b, \gamma_w) \tag{4.12}$$

Here, $\gamma_b$ is the bulk unit weight (N/m$^3$) of the cohesive sediment mixture and $\gamma_w$ is the unit weight of water (N/m$^3$).

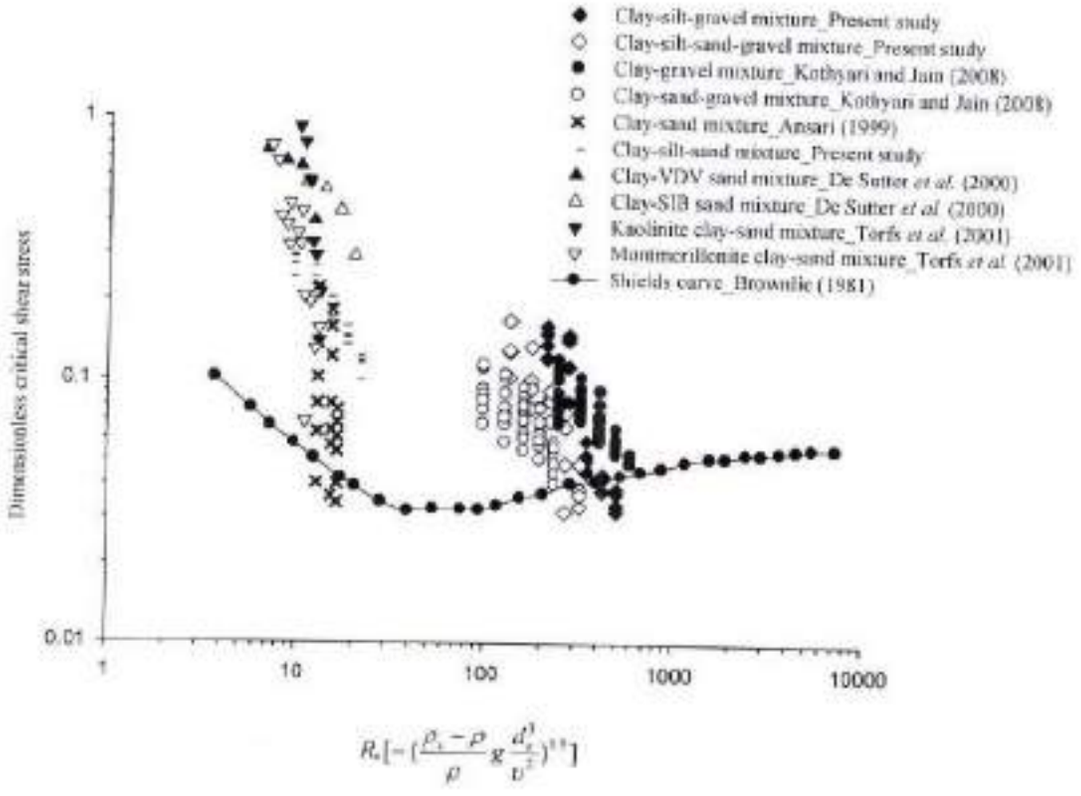


Fig. 4.3 Variation of dimensionless critical shear stress with particle Reynolds number for cohesive sediment mixture and cohesionless sediment

Using dimensional analysis, Eq. (4.12) can be converted into dimensionless form as

$$\frac{\tau_{cc}}{\tau_{cm}} = f(P_c, \sigma_{cc}, \frac{\gamma_b}{\gamma_w}) \tag{4.13}$$

Where, $$\sigma_{cc} = \frac{\Sigma(d_{50}.\sigma_g)}{d_a} \tag{4.14}$$

Here, $\sigma_{cc}$ is the weighted geometric standard deviation of the cohesive sediment mixture.

Equation (4.13) represents the functional relationship corresponding to incipient motion for coarser particles in the cohesive sediment mixtures. Here parameter $P_c$ accounts for the presence of clay content in the sediment mixture and to consider the variability of compactness of cohesive bed the parameter $\gamma_b/\gamma_w$ has been taken. As the mean size of cohesive sediment mixture ($d_g$) is significantly different from the median size ($d_{50}$) of individual sediment present in the mixture and this variability in sediment sizes creates the hiding-exposure phenomena; hence to account this variability the parameter $\sigma_{cc}$ has been incorporated for developing the relationship for critical shear stress. The variation of these parameters i.e. parameters presented in Eq. (4.13) with $\tau_{cc}/\tau_{cm}$ has been illustrated through Figs. 4.4 – 4.6. Figure 4.4 depicts the variation of $P_c$ with $\tau_{cc}/\tau_{cm}$ while the variation of $\sigma_{cc}$ and $\gamma_b/\gamma_w$ against the value of $\tau_{cc}/\tau_{cm}$ were shown in Figs. 4.5 and 4.6 respectively. The value of $\tau_{cc}/\tau_{cm}$ increases with the increase of clay percentage as illustrated in Fig. 4.4 for the data of present study along with the data of Kothyari and Jain (2008), Torfs *et al.* (2001), De Sutter *et al.* (2000), Ansari (1999), and Panagiotopoulos *et al.* (1997). Similar result on the variation of clay percentage with the critical shear stress has also been reported by Kamphuis and Hall (1983). The value of $\tau_{cc}/\tau_{cm}$ has been found higher for clay-silt-sand mixture compared to sediment mixture having gravel.

This is because of the greater bonding for clay-silt-sand mixture compared to cohesive sediment mixture having presence of gravel in the sediment mixture as gravel has large median size compared to the other sediment which affects the bonding nature between the particles in the mixture. The value of $\tau_{cc}/\tau_{cm}$ for the data of Torfs *et al.* (2001) and De Sutter *et al.* (2000) has been found much higher as they used clay-sand mixture while the mud-sand mixture has the lower value of $\tau_{cc}/\tau_{cm}$ as shown in Fig 4.4. The effect of $\sigma_{cc}$ on $\tau_{cc}/\tau_{cm}$ has been shown in the Fig. 4.5, which depicts that, the value of $\tau_{cc}/\tau_{cm}$ increases with the increase of $\sigma_{cc}$ for the data of present study as well as other investigators data. In the earlier studies, the variation of $\sigma_{cc}$ was not reported, therefore, the value of $\sigma_{cc}$ for the data of other investigators has been computed using the Eq. (4.14). Figure 4.6 indicates that value of $\tau_{cc}/\tau_{cm}$ increases with the increase in $\gamma_b/\gamma_w$. Similar trend, also, noticed for the data of Kothyari and Jain (2008), Ansari (1999), and

De Sutter *et al.* (2000). Mitchener and Torfs (1996) also reported similar result for the variation of bulk density against the critical shear stress.

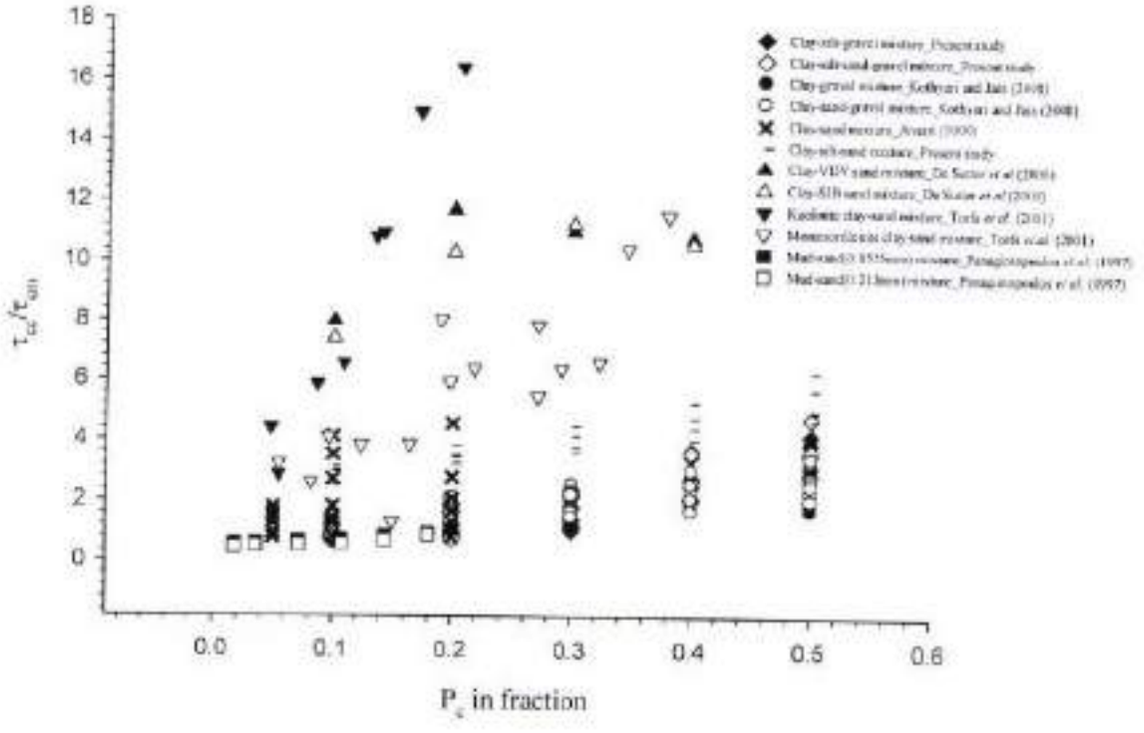


Fig. 4.4 Variation of $(\tau_{cr}/\tau_{cm})$ with $P_c$

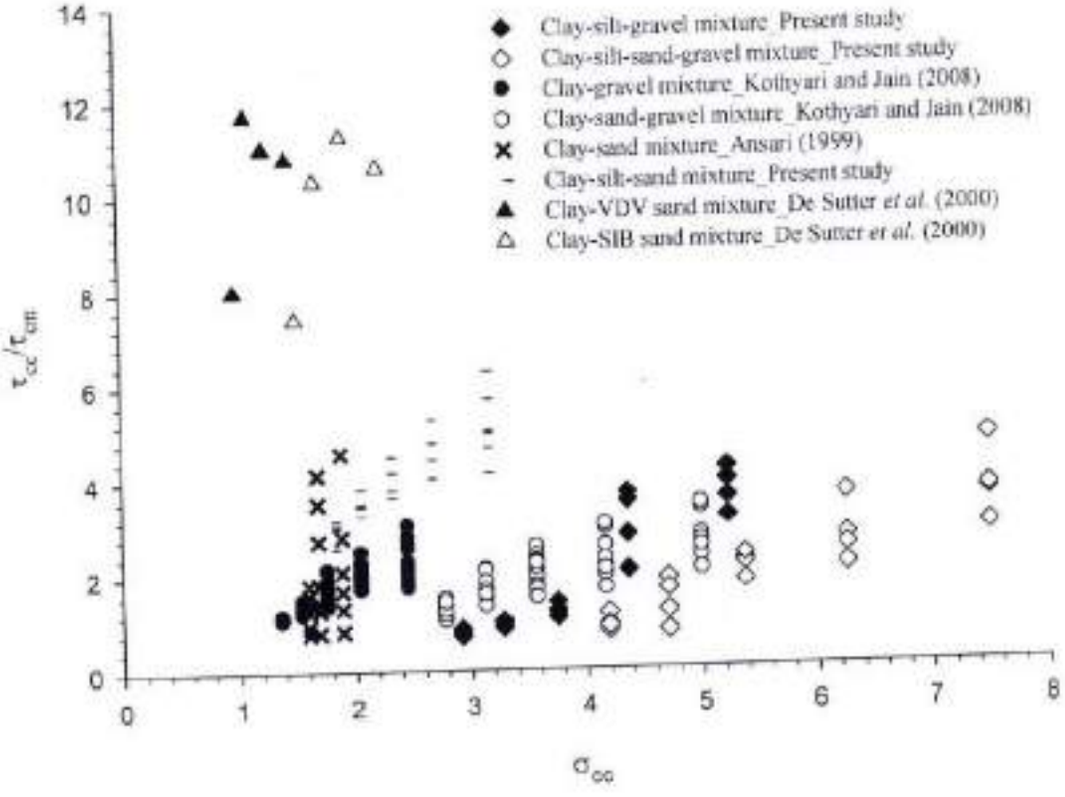


Fig. 4.5 Variation of $(\tau_{cc}/\tau_{cm})$ with $\sigma_{cc}$

In the above discussions, the value of $\tau_{cc}/\tau_{cm}$ has been found significantly varied for the cohesive sediment mixture with gravel from that of without gravel. Hence, for the computation of critical shear stress of coarser particles in the cohesive sediment mixture two formulations have been developed i.e. one for the clay-silt-gravel with clay-silt-sand-gravel mixture and other for the clay-silt-sand mixture.

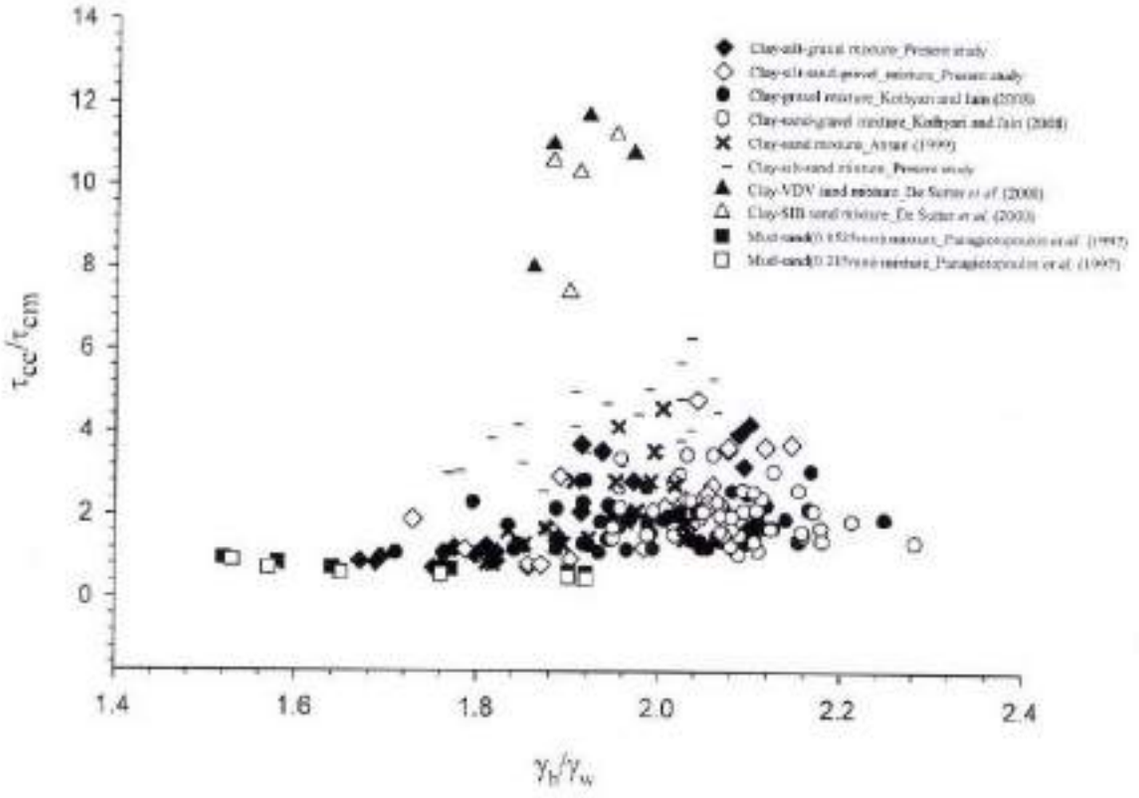


Fig. 4.6 Variation of $(\tau_{cc}/\tau_{cm})$ with $(\gamma_b/\gamma_w)$

A large number of trials with the parameters given in Eq. (4.13) led the following relationships as Eq. (4.15) & (4.16) for computation of critical shear stress for clay-silt-gravel with clay-silt-sand-gravel mixture and clay-silt-sand mixture respectively:

$$\frac{\tau_{cc}}{\tau_{cm}} = 1 + 0.1428 P_c^{1.294} \sigma_{cc}^{1.553} \left(\frac{\gamma_b}{\gamma_w}\right)^{3.814} \tag{4.15}$$

$$\frac{\tau_{cc}}{\tau_{cm}} = 1 + 0.092 P_c^{0.591} \sigma_{cc}^{0.842} \left(\frac{\gamma_b}{\gamma_w}\right)^{4.625} \tag{4.16}$$

The proposed Eq. (4.15) developed using the data of the present study (clay-silt-gravel and clay-silt-sand-gravel mixture) as well as data of Kothyari and Jain (2008). The proposed Eq. (4.16) developed using data of present study (clay-silt-sand mixture) and Ansari (1999) data. The compaction level used in preparation of cohesive channel bed may play a significant role in the

entrainment of sediment particles; hence, this compaction level may serve as limitation for the formulations (12) and (13) developed in the present study which has been reported in Table 4.4. The computed value of $\tau_{cr}/\tau_{cm}$ from Eq. (4.15) were plotted against the observed value as shown in Fig. 4.7 for the experimental data of present study (for cohesive sediment mixture having gravel) as well as for the data of Kothyari and Jain (2008). The data of other investigators have not been utilized in this figure due to unavailability of the study on the incipient motion of cohesive sediment mixture having presence of gravel in the mixture. From the Fig. 4.7, it is clear that the Eq. (4.15) predicts well the value of $\tau_{cr}/\tau_{cm}$ for the data of present study and as well as for the data of Kothyari and Jain (2008). The proposed Eq. (4.15) also has a good value of regression coefficient ($R^2 = 0.78$) for the data used in developing the equation as shown in Fig. 4.7. Also a good value of regression coefficient is found for the individual data set of present study (clay-silt-gravel and clay-silt-sand-gravel) and Kothyari and Jain (2008) data (clay-gravel and clay-sand-gravel) as reported in Fig. 4.7.

**Table 4.4** Range of *UCS* (kN/m$^2$) for compaction level used in the present study

| Sediment mixture | Clay percentage | | | | |
|---|---|---|---|---|---|
| | 10% | 20% | 30% | 40% | 50% |
| Clay-silt-gravel | 0 | 05.41-07.57 | 10.27-18.38 | 18.92-22.17 | 30.28-42.17 |
| Clay-silt-sand-gravel | 0 | 06.49-09.73 | 17.84-20.00 | 16.76-29.74 | 19.46-43.25 |
| Clay-silt-sand | 05.95-07.03 | 07.57-11.89 | 17.84-30.28 | 23.25-34.06 | 19.46-32.98 |

Similarly to check the suitability of Eq. (4.16), the computed value of $\tau_{cr}/\tau_{cm}$ is plotted against the observed value in Fig. 4.8 for the data of present study (for clay-silt-sand mixture) and Ansari (1999) data. The data of other investigators on the study of clay-silt-sand could not be utilized in this figure due to lack of availability of data corresponding to the parameters involved in Eq. (4.16). Figure 4.8 shows a good value of regression coefficient ($R^2 = 0.71$) for the data used in developing the Eq. (4.16). Data of present study has reasonably good value of regression coefficient ($R^2 = 0.82$) which indicates that predicted data are in good agreement with the observed data. However, Ansari (1999) data are not in good agreement (as $R^2 = 0.42$) with the

proposed equation. This may be due to the absence of the silt particles in the sediment mixture as clay-sand mixture was used by Ansari (1999) and limitation of clay percentage which varied from 5% to 20%. Also, Ansari (1999) reported ±50% error line in his proposed equation for the determination of dimensionless critical shear stress.

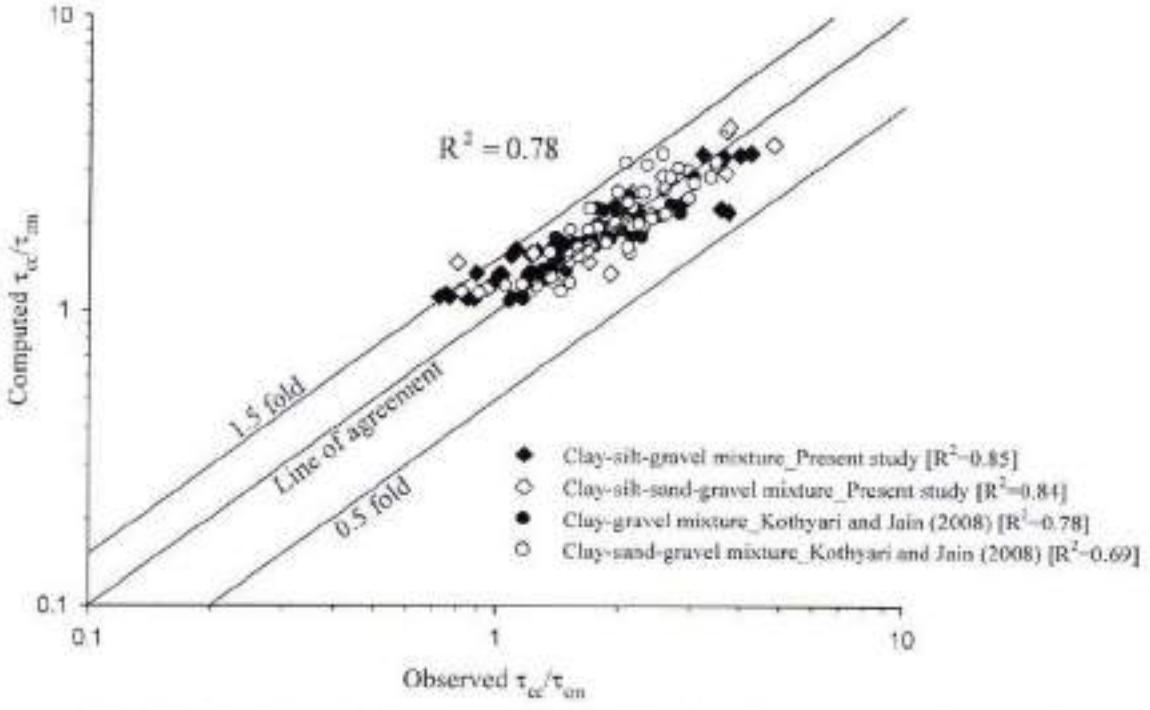


Fig. 4.7 Comparison of observed and computed value of $(\tau_{cc}/\tau_{cm})$ using Eq. (4.15)

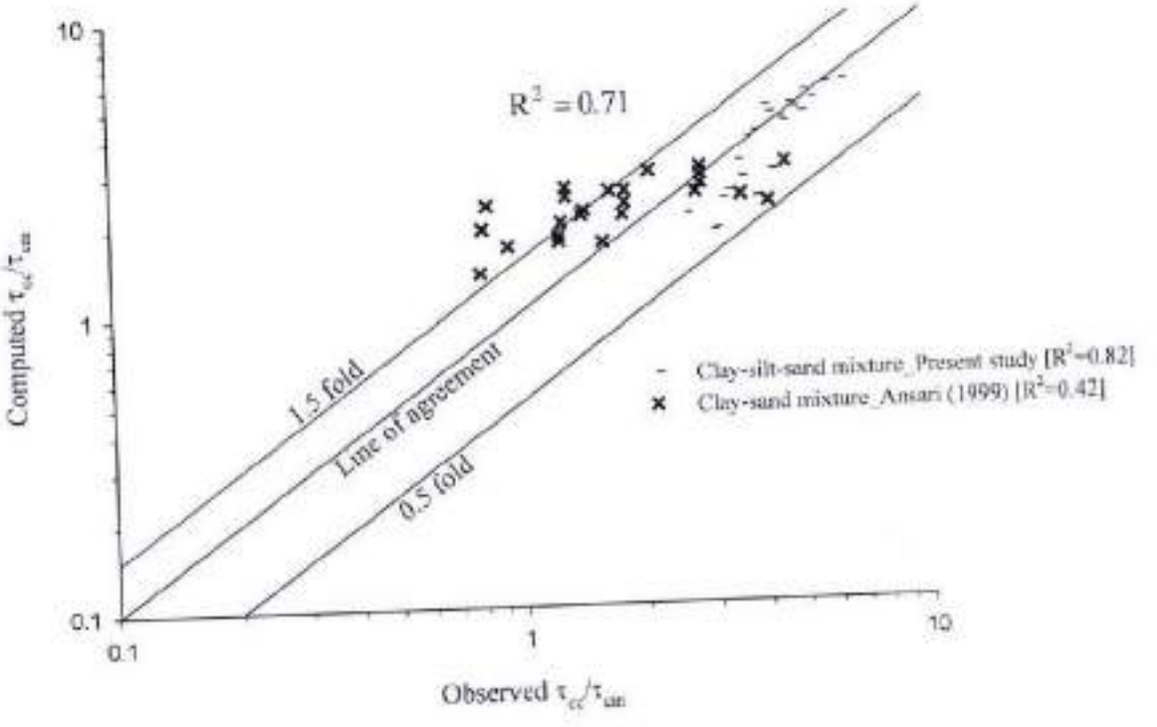


Fig. 4.8 Comparison of observed and computed value of $(\tau_{cc}/\tau_{cw})$ using Eq. (4.16)

### 4.3.2 Goodness of Fit Test

The mean discrepancy ratio and standard deviation are computed to test the goodness of fit between observed and computed value corresponding to the proposed Eqs. (4.15) and (4.16). Following Eqs. (4.17) - (4.19) are used for the computation of the discrepancy ratio, mean discrepancy ratio, and standard deviation, respectively (Yang *et al.* 1996).

$$\text{Discrepancy ratio, } R_i = \frac{(\tau_{cc}/\tau_{cw})_{c,i}}{(\tau_{cc}/\tau_{cw})_{o,i}} \tag{4.17}$$

Here, $(\tau_{cc}/\tau_{cw})_{c,i}$ and $(\tau_{cc}/\tau_{cw})_{o,i}$ are the computed and observed value of $\tau_{cc}/\tau_{cw}$ respectively.

$$\text{Mean discrepancy ratio, } \overline{R} = \frac{\sum_{i}^{N} R_i}{N} \tag{4.18}$$

Here, $N$ is the total number of observations.

$$\text{Standard deviation, } \sigma_{R_i} = \sqrt{\frac{\sum_{1}^{N}(R_i - \overline{R})^2}{N-1}} \tag{4.19}$$

Here, $\sigma_{R_i}$ is the standard deviation for the discrepancy ratio.

The equations proposed in the present study for the computation of critical shear stress of coarse particles in the cohesive mixtures are tested against the goodness of fit test by using statistical methods adopted by Yang *et al.* (1996) i.e. using Eqs. (4.17) - (4.19). The present study data and other investigators data (Kothyari and Jain 2008, Torfs *et al.* 2001, De Sutter *et al.* 2000, Ansari 1999) were utilized to check the applicability of proposed equations on the basis of statistical analysis to the various cohesive sediment mixtures. The proposed equations also compared with the existing equations. For this purpose, equation of Kothyari and Jain (2008) and Smerdon and Beasley (1961) were taken as per availability of data required.

Table 4.5 depicts that more than 80% data of the present study having gravel in the sediment mixture as well as Kothyari and Jain (2008) data lie in the range of 0.75 to 1.50 of discrepancy ratio which indicates that the proposed Eq. (4.15) is applicable to Kothyari and Jain (2008) study i.e. cohesive sediment mixture of clay-gravel and clay-sand-gravel. In case of Ansari (1999) study, 44% data of his study lies in the range of 0.75 to 1.50 of discrepancy ratio ($R_i$) while no data lies in that range when data of De Sutter *et al.* (2000) used as they used clay-sand mixture. Hence the proposed Eq. (4.15) is well applicable to sediment mixtures having clay-gravel, clay-sand-gravel, clay-silt-gravel and clay-silt-sand-gravel i.e. cohesive sediment mixture having presence of gravel in the mixture. The proposed Eq. (4.15) shows the better results over the existing Eq. (2.49) for computation of critical shear stress of cohesive sediment mixtures having gravel as per statistics shown in Table 4.5. And most importantly the proposed Eq. (4.15) shows the easily computable parameters compared to the existing Eq. (2.49) of Kothyari and Jain (2008).

**Table 4.5** Statistical analysis of computed and observed $(r_{cc}/r_{co})$ as per Eqs. (4.17) - (4.19)

| Equation | Data | Cohesive sediment mixture | N | Discrepancy ratio | | | | |
|---|---|---|---|---|---|---|---|---|
| | | | | $\overline{R}$ | % of data in range | | | $\sigma_{cc}$ |
| | | | | | 0.75 – 1.25 | 0.75 – 1.50 | 0.50 – 1.50 | |
| Proposed Eq. (4.15) | Present study | Clay-silt-gravel | 22 | 1.175 | 36 | 82 | 91 | 0.287 |
| | | Clay-silt-sand-gravel | 20 | 1.090 | 70 | 90 | 95 | 0.256 |
| | Kothyari and Jain (2008) | Clay-gravel mixture | 62 | 1.020 | 97 | 100 | 100 | 0.105 |
| | | Clay-sand-gravel | 46 | 1.011 | 89 | 96 | 98 | 0.168 |
| | Ansari (1999) | Clay-sand | 25 | 0.728 | 32 | 44 | 68 | 0.325 |
| | De Sutter *et al.* (2000) | Clay-VDV sand | 04 | 0.131 | 00 | 00 | 00 | 0.022 |
| | De Sutter *et al.* (2000) | Clay-SIB sand | 04 | 0.144 | 00 | 00 | 00 | 0.018 |
| Kothyari and Jain (2008) (Eq. (2.49)) | Present study | Clay-silt-gravel | 22 | 1.213 | 27 | 59 | 73 | 0.351 |
| | | Clay-silt-sand-gravel | 20 | 1.046 | 65 | 85 | 95 | 0.291 |
| | Kothyari and Jain (2008) | Clay-gravel | 62 | 1.061 | 100 | 100 | 100 | 0.079 |
| | | Clay-sand-gravel | 46 | 0.940 | 98 | 98 | 100 | 0.122 |
| Proposed Eq. (4.16) | Present study | Clay-silt-sand- | 22 | 0.901 | 77 | 77 | 100 | 0.168 |
| | Ansari (1999) | Clay-sand | 25 | 1.373 | 28 | 56 | 68 | 0.517 |
| | De Sutter *et al.* (2000) | Clay-VDV sand | 04 | 0.219 | 00 | 00 | 00 | 0.044 |
| | De Sutter *et al.* (2000) | Clay-SIB sand | 04 | 0.280 | 00 | 00 | 00 | 0.030 |
| Smerdon and Beasley (1961) (Eq. (2.39)) | Present study | Clay-silt-gravel | 22 | 0.965 | 59 | 73 | 95 | 0.294 |
| | | Clay-silt-sand-gravel | 20 | 1.118 | 30 | 50 | 80 | 0.506 |
| | | Clay-silt-sand- | 22 | 2.952 | 05 | 14 | 14 | 1.403 |
| | Kothyari and Jain (2008) | Clay-gravel | 62 | 0.955 | 42 | 45 | 69 | 0.489 |
| | | Clay-sand-gravel | 46 | 1.538 | 37 | 46 | 63 | 0.971 |
| | Ansari (1999) | Clay-sand | 25 | 3.019 | 08 | 12 | 12 | 1.545 |
| | De Sutter *et al.* (2000) | Clay-VDV sand | 04 | 0.905 | 25 | 25 | 75 | 0.452 |
| | De Sutter *et al.* (2000) | Clay-SIB sand | 04 | 0.882 | 25 | 50 | 100 | 0.426 |
| | Torfs *et al.* (2001) | Kaolinite clay-sand | 08 | 0.654 | 25 | 25 | 50 | 0.282 |
| | Torfs *et al.* (2001) | Montmorillonite clay-sand | 15 | 1.502 | 40 | 67 | 67 | 0.776 |

Similar procedure has been adopted for the checking the applicability of proposed Eq. (4.16). It is found that the proposed Eq. (4.16) is applicable to clay-silt-sand mixture as 77% data

of present study lies in the range of 0.75 to 1.50 of discrepancy ratio and other statistics are also in good and acceptable range as reported in Table 4.5. Even the 56% data of Ansari (1999) lies in that range. However no one data lies in that range for clay-sand mixture of De Sutter *et al.* (2000). Hence, Eq. (4.16) can be used for computation of critical shear stress for the cohesive sediment mixture consisting of clay-silt-sand. It can be seen from the statistics in Table 4.5 that the proposed Eq. (4.16) shows better results for Ansari (1999) data over the existing Eq. (2.39) of Smerdon and Beasley (1961) which may be because of compaction level used in the experiments. However, Eq. (2.39) shows the good results for data of De Sutter *et al.* (2000) and Torfs *et al.* (2001) which may be attributed to compaction level in clay-sand mixture bed and less number of data used in their study.

## 4.4 TRANSPORT OF SEDIMENT FROM COHESIVE CHANNEL BED

Transport of sediment, from the channel bed, starts when the developed shear stress, due to incoming flow, exceeds the critical shear stress of that channel bed. It was observed that initially the transport rate of sediment is higher; however, it is decreasing with the passes of time and a time comes when there is nearly no or very less transport of sediment observed i.e. the channel bed comes in an equilibrium condition. So, this section deals with the process of sediment transport that includes the sub-section in the form of equilibrium time, initial transport rate and transport rate of bed load and suspended load etc.

### 4.4.1 Equilibrium Time

A stream in equilibrium is defined as the one in which channel dimensions and slope are so adjusted over a period of time that it carries incoming sediment load and water without appreciable erosion or deposition (Mackin, 1948). Garde and Ranga Raju (2000) defined the equilibrium condition of a reach as "a certain length of an alluvial stream is said to be in equilibrium if the amount of sediment coming into this reach is equal to the sediment going out from the same". However, a deviation from equilibrium conditions allows the alluvial river system for changing the channel geometry that may causes aggradation and / or degradation till the equilibrium condition reached so that it restores the balance between inflowing and outflowing water and sediment discharges. Equilibrium time is treated as the time taken by the flow to reach in equilibrium condition.

In the present study, the erosion from the channel bed starts after a given flow rate or discharge allowed in the flume. The rate of erosion from the channel bed is higher initially and then decreases with time as collection of bed load in the trap was observed to be decreases with time. And a condition reached after a time where the variation in the bed level becomes negligible as illustrated in Fig. 4.9 and also the transport of bed load and suspended load becomes very low as shown in Fig. 4.10. This condition is treated as equilibrium condition and the corresponding total time taken is called an equilibrium time. The equilibrium time for the present study varied with the clay percentage in the mixture. It is observed that the equilibrium time increases with the increase of clay percentage as illustrated in Fig. 4.11. This section focuses on the computation of the equilibrium time for three cohesive mixture i.e. clay-silt-gravel, clay-silt-sand-gravel, and clay-silt-sand.

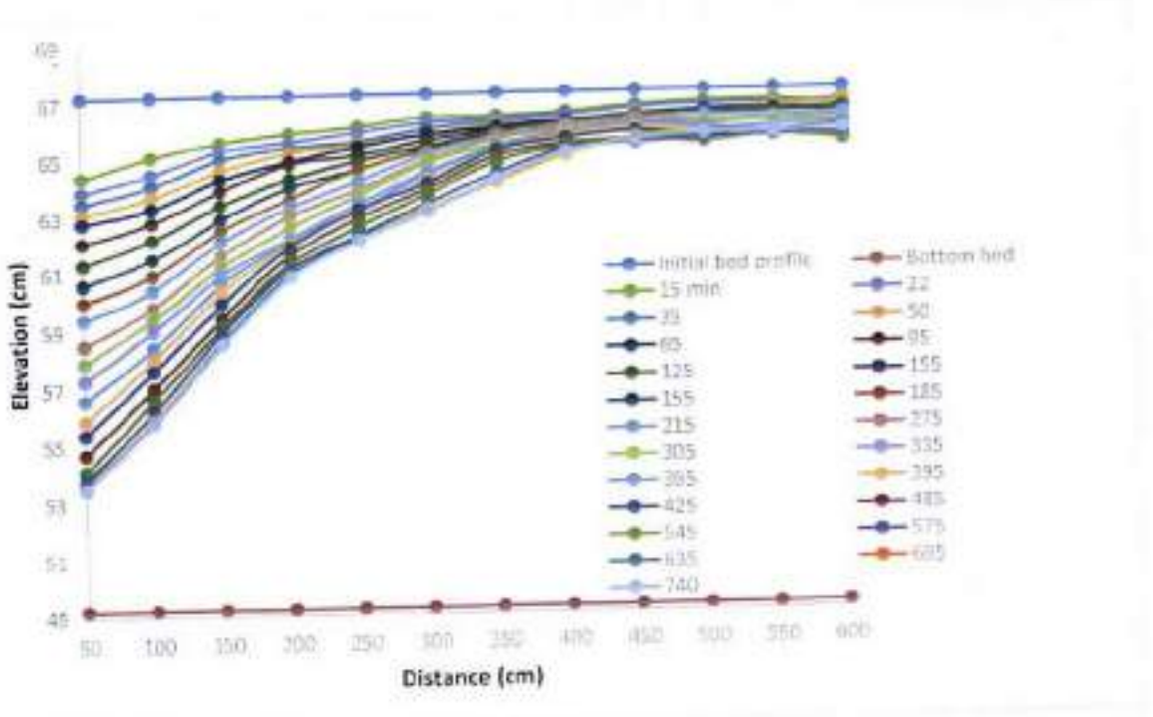


Fig. 4.9 Bed level variations for clay-silt-gravel mixture having 10% clay content

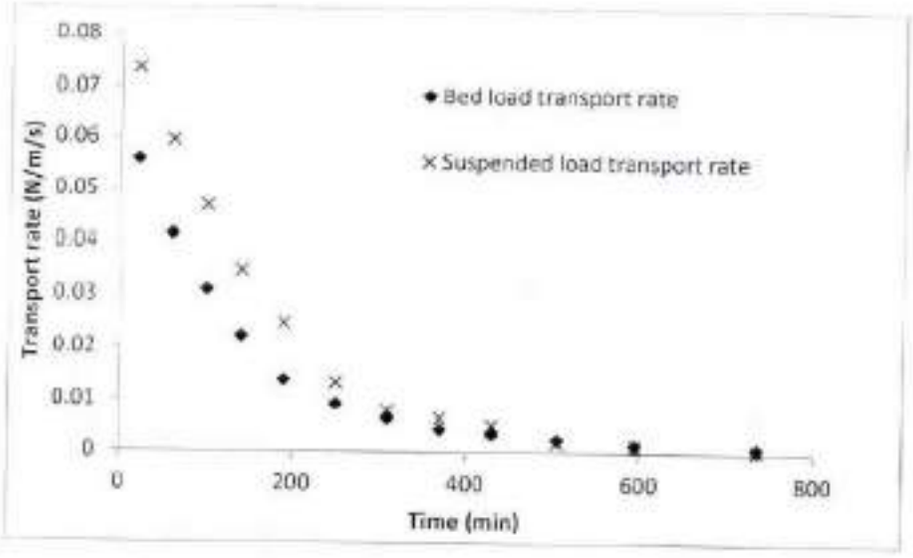


Fig. 4.10 Variation of sediment transport rate for clay-silt-gravel mixture having 50% clay content

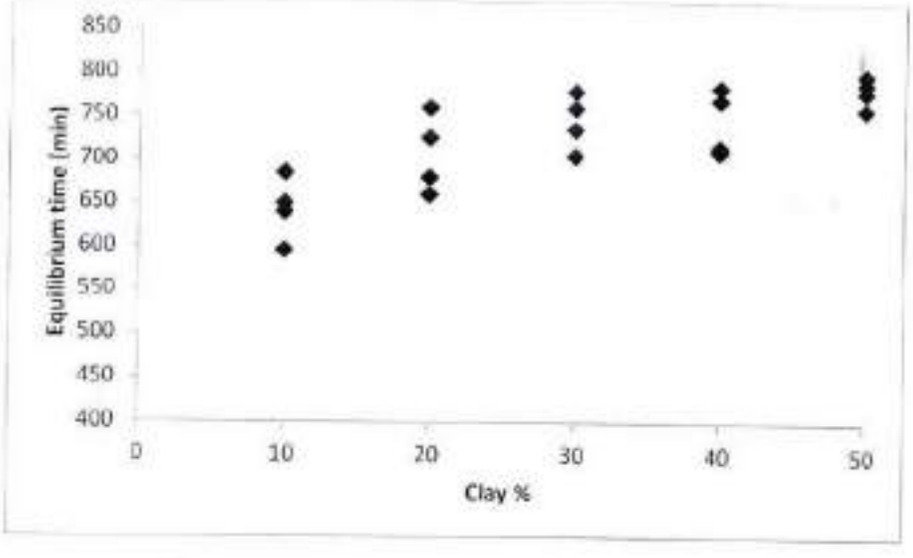


Fig. 4.11 Equilibrium time plot w.r.t. clay % for clay-silt-sand-gravel mixture

The following parameters have been considered in the development of formulation for the computation of equilibrium time.

$$t_e = f(P_c, \tau, \tau_{cr}, \rho, \rho_s, d_{cr}, g) \tag{4.20}$$

Here, $t_e$ is the equilibrium time (min); $P_c$ is the clay percentage in fraction; $\tau$ is the shear stress (N/m$^2$) developed on the test section of the channel bed due to the incoming flow; $\tau_{ce}$ is the critical shear stress (N/m$^2$) for cohesive sediment mixture; $\rho_s$ and $\rho$ are particle and fluid densities (kg/m$^3$) respectively; $d_a$ is arithmetic mean size (m) of the cohesive sediment mixture; and $g$ is gravitational acceleration (m/s$^2$).

Equation (4.20) can be represented in the dimensionless form using dimensional analysis as below:

$$t_e^* = f(P_c, \tau_e^*) \tag{4.21}$$

Here, $t_e^*$ is the dimensionless equilibrium time and computed as

$$t_e^* = \left( \sqrt{\frac{g t_e^2}{(S-1) d_a}} \right)^{1/2} \tag{4.22}$$

Here, $S = \frac{\rho_s - \rho}{\rho}$

$\tau_e^*$ is the dimensionless excess shear stress on the test section of channel bed and computed as

$$\tau_e^* = \frac{\tau - \tau_{ce}}{(\rho_s - \rho) g d_a} \tag{4.23}$$

Equation (4.21) represents the functional relationship in the dimensionless form for the equilibrium time. The parameter $P_c$ has been taken in account to consider the effects of various percentage of clay while the parameter $\tau_e^*$ accounts for the sediment transport phenomena. The variation of parameters $P_c$ with the dimensionless equilibrium time has been illustrated in Fig. 4.12. And the variation of parameters $\tau_e^*$ with the dimensionless equilibrium time has shown in Figs. 4.13a, 4.13b, and 4.13c for the cohesive sediment mixture; clay-silt-gravel, clay-silt-sand-gravel, and clay-silt-sand respectively. Only the present study data has been used as the other investigators's data has not been available for the equilibrium time computation.

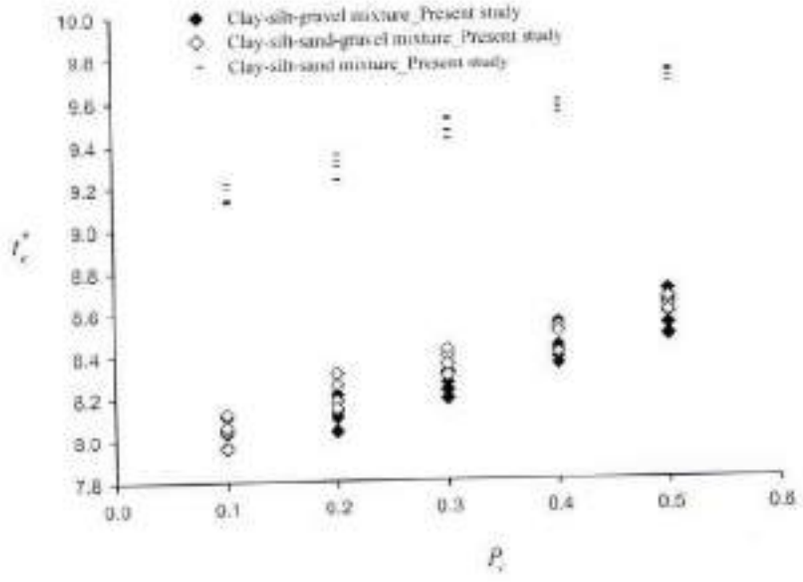


Fig. 4.12 Variation of clay fraction with dimensionless equilibrium time

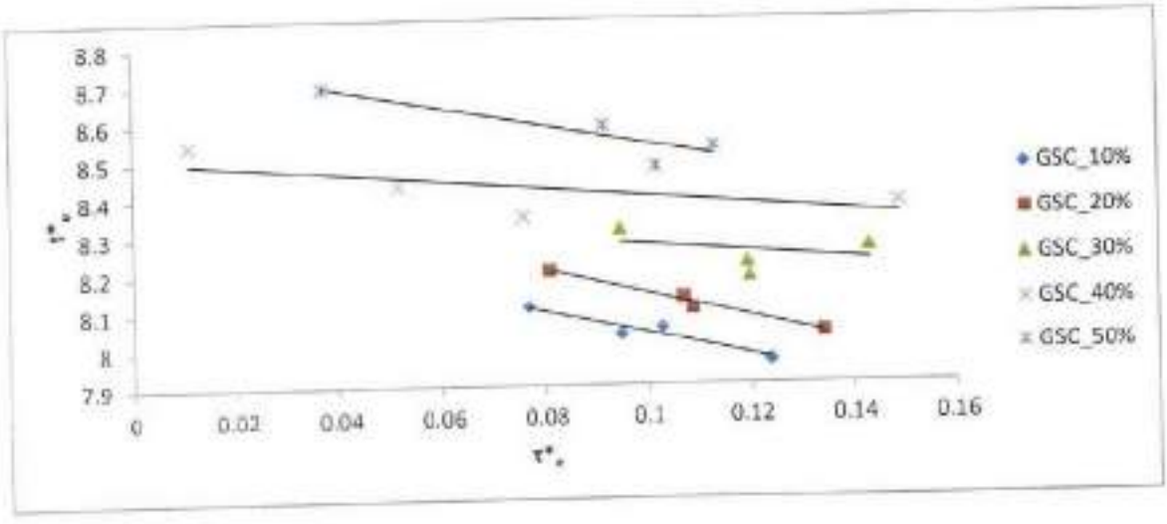


Fig. 4.13a Variation of $t_c^*$ with $\tau_c^*$ for different % of clay in clay-silt-gravel (GSC) mixture

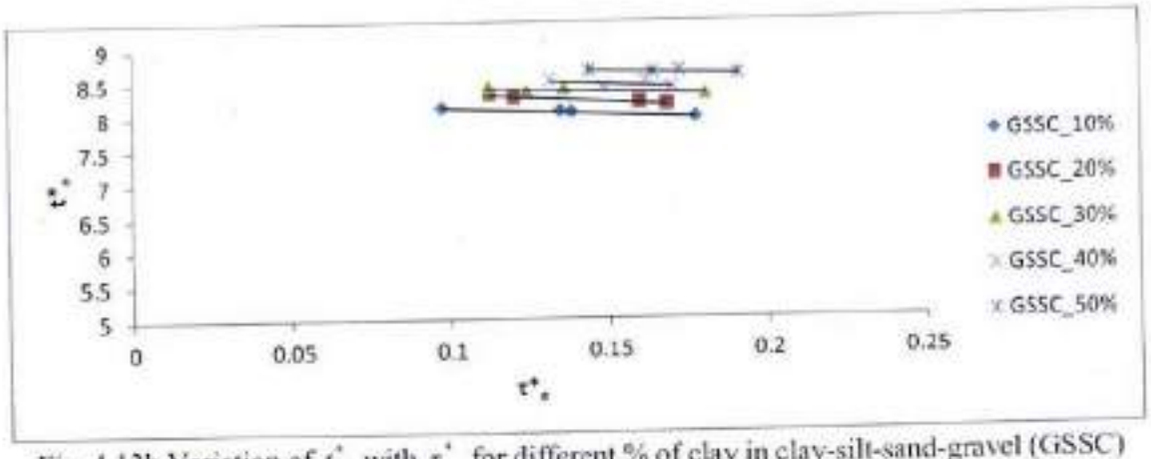


Fig. 4.13b Variation of $t_e^*$ with $\tau_e^*$ for different % of clay in clay-silt-sand-gravel (GSSC) mixture

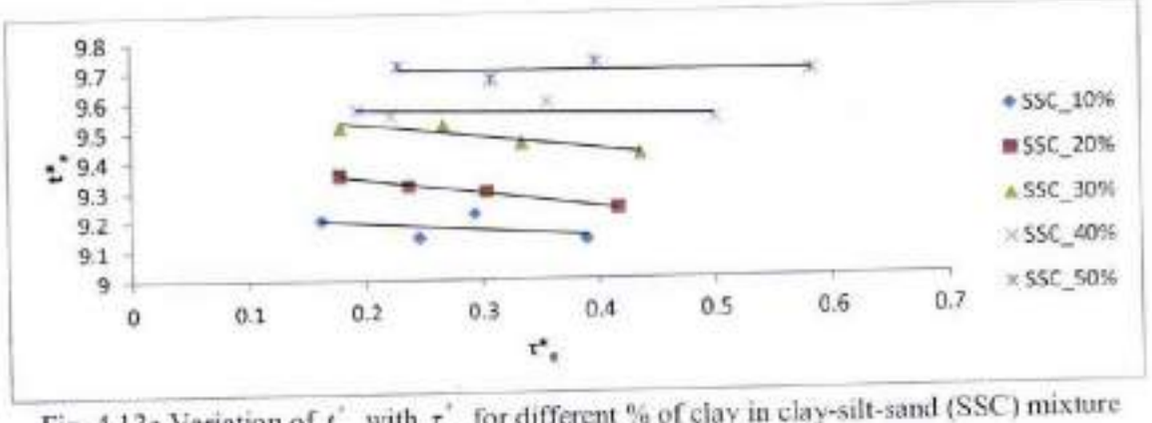


Fig. 4.13c Variation of $t_e^*$ with $\tau_e^*$ for different % of clay in clay-silt-sand (SSC) mixture

Figure 4.12 shows that the dimensionless equilibrium time increases with clay percentage for all the three sediment mixture in the present study. The cohesive channel bed has becomes more resistance against the erosion for higher clay content in bed which may take more time to reach an equilibrium condition. Figures 4.13(a), (b), and (c) shows the decreasing trend for $t_e^*$ with the increase of dimensionless excess shear stress for each percentage of clay. A higher excess shear stress developed on the channel bed leads to higher erosion rate and consequently reaches equilibrium state relatively faster. The present section deals with the formulation for the computation of $t_e^*$ for all the three cohesive sediment mixture in the present study.

After a large number of trials the following relationships are proposed for the computation of $t_e^*$ for the cohesive sediment mixture in the present study:

$$t_e^* = 7.668(1+P_c)^{0.137}(\tau_c^*)^{-0.011} \quad (4.24)$$

$$t_e^* = 7.371(1+P_c)^{0.259}(\tau_c^*)^{-0.032} \quad (4.25)$$

$$t_e^* = 8.925(1+P_c)^{0.198}(\tau_c^*)^{-0.065} \quad (4.26)$$

Equations (4.24), (4.25), and (4.26) represent the relationship for the computation of $t_e^*$ for the cohesive sediment mixture of clay-silt-gravel, clay-silt-sand-gravel, and clay-silt-sand respectively based on the present study data. The computed value from equations (4.24), (4.25), and (4.26) for $t_e^*$ shows a good agreement with the observed data as well as good regression coefficient as illustrated in Fig. 4.14.

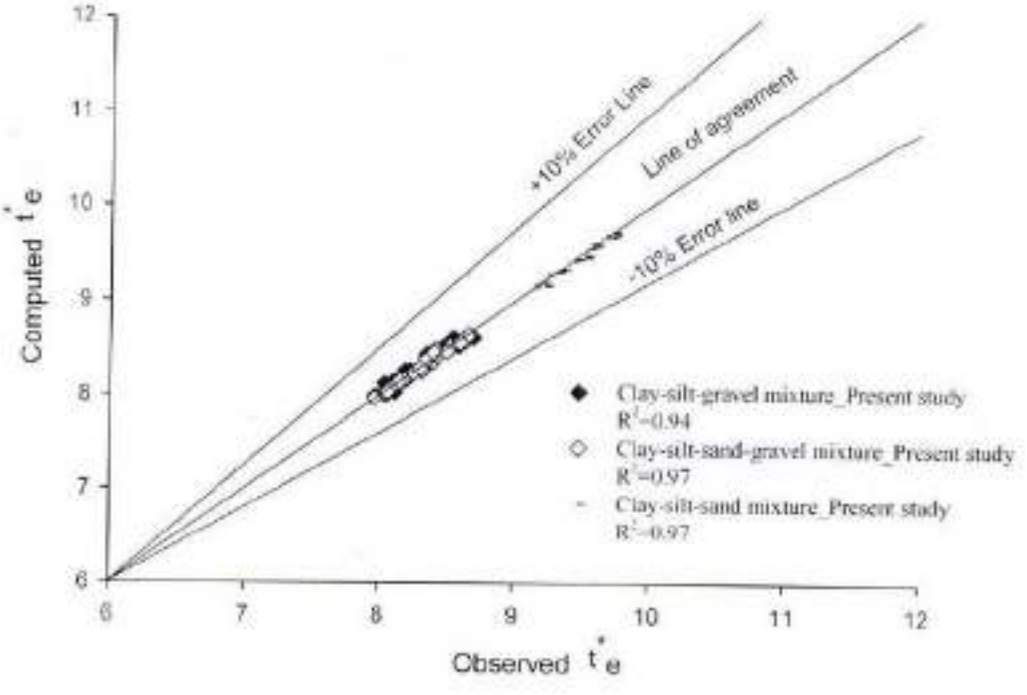


Fig. 4.14 Comparison between computed and observed dimensionless equilibrium time

### 4.4.2 Bed Load Transport

#### 4.4.2.1 Initial bed load transport rate

This section deals with the development of a formulation for the computation of initial bed load transport rate form the cohesive channel bed in response to a given flow rate in the channel. It was observed that the transport rate of sediment decreases with the increase of time i.e. transport rate will be higher in the initial period of time. Initial transport rate of sediment is an important aspect in sediment transport study as higher initial transport rate may lead to higher degradation in the channel bed. Hence, the total erosion from the channel bed as well as transport rate of sediment depends on the initial transport rate of sediment. However, studies have not been performed for the computation of initial transport rate of sediment from the cohesive channel bed consisting of sediment mixture clay-silt-gravel, clay-silt-sand-gravel, and clay-silt-sand.

The initial bed load transport rate is influenced by the cohesion, so varied with the clay percentage in the sediment mixture. Figure 4.15 shows the initial bed load transport rate decreases with the increase of clay percentage for all the three cohesive mixture i.e. clay-silt-gravel, clay-silt-sand-gravel, and clay-silt-sand in the present study. Higher percentage of clay in the mixture binds the particles together more tightly and that responded to decreasing initial bed load transport with increase of clay percentage. The initial bed load transport rate also depends on the shear stress developed by the incoming flow and for this plot has been made between dimensionless initial bed load transport rate and dimensionless excess shear stress of incoming flow in the channel. Dimensionless initial bed load transport rate was found to be increases with the increase of dimensionless excess shear stress for all the percentage of clay as illustrated in Figs. 4.16, 4.17, and 4.18 for sediment mixture clay-silt-gravel, clay-silt-sand-gravel, and clay-silt-sand respectively.

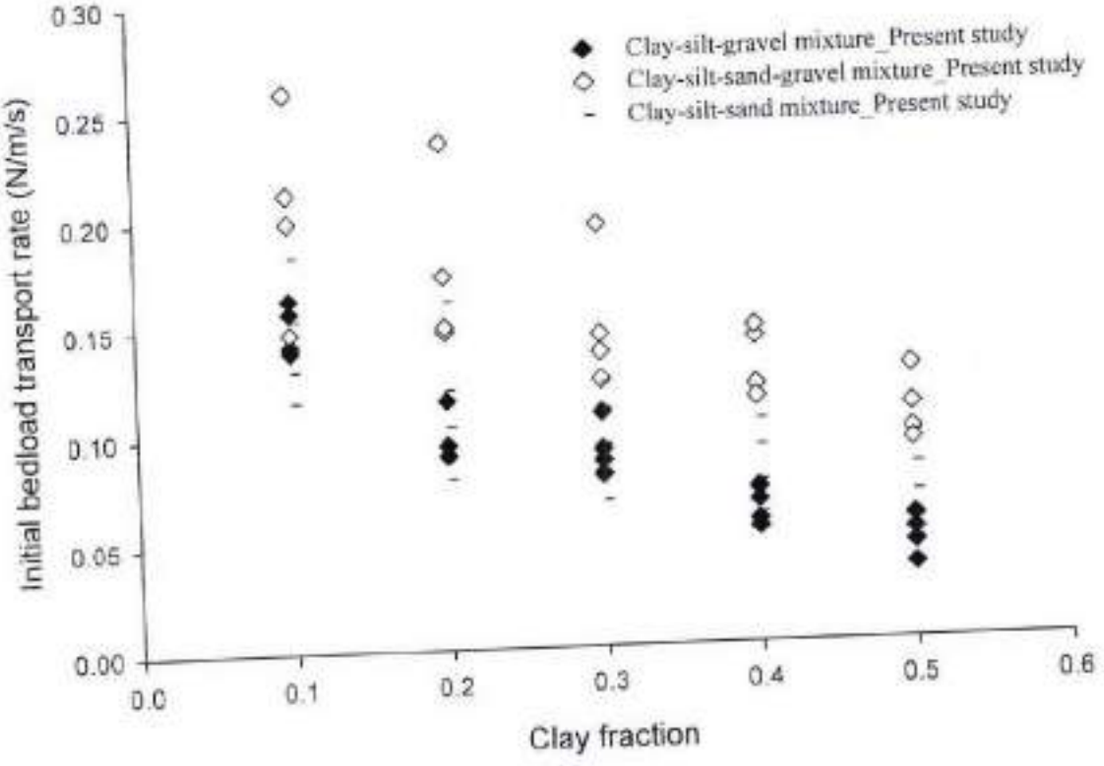


Fig. 4.15 Variation of initial bed load transport rate with clay percentage

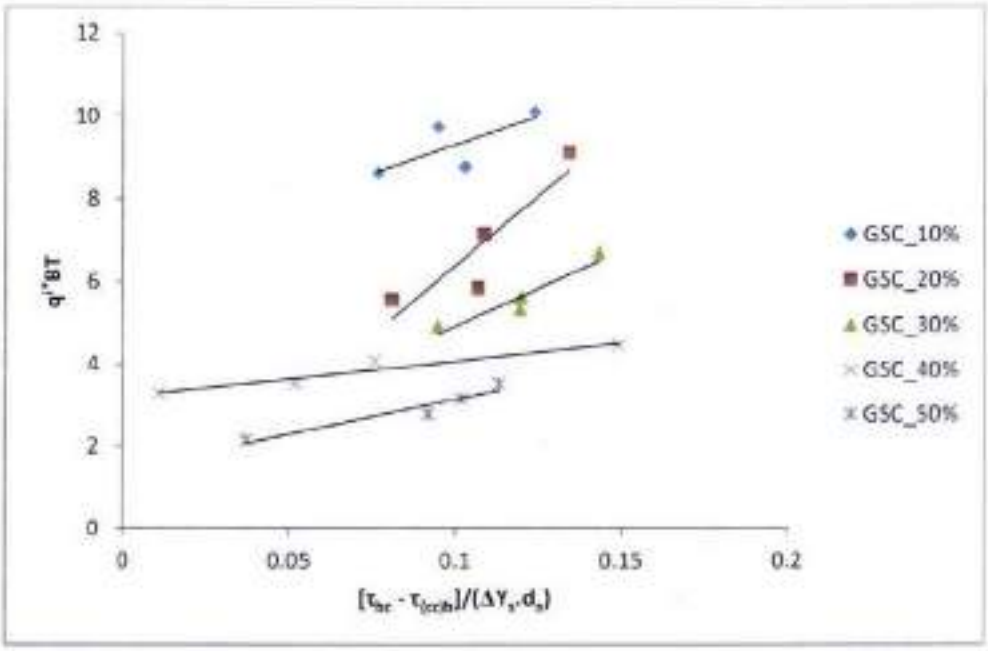


Fig. 4.16 Variation of initial bed load transport rate with dimensionless excess shear stress for clay-silt-gravel (GSC) mixture

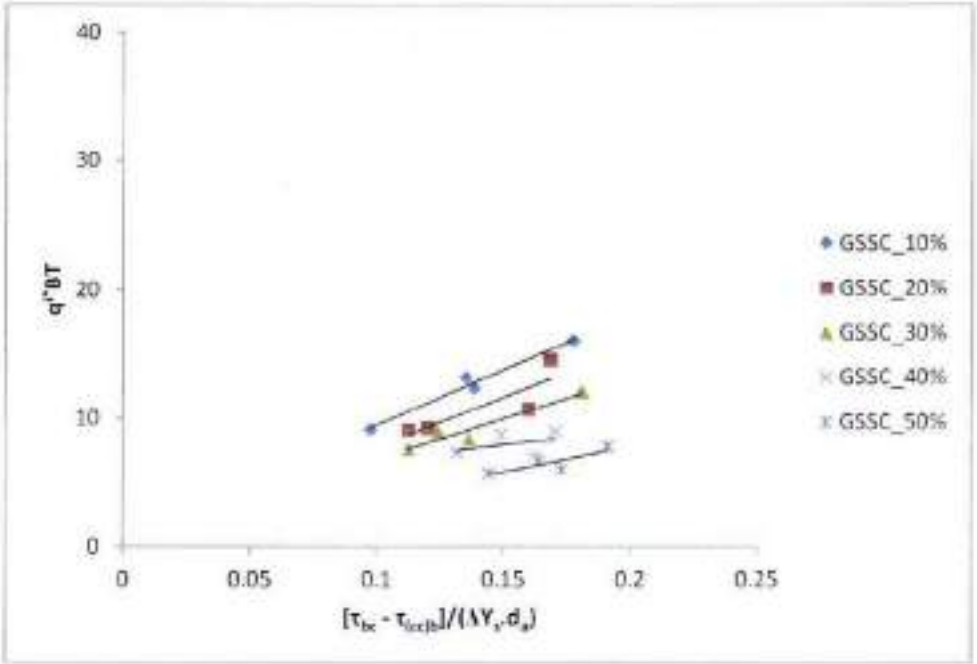


Fig. 4.17 Variation of initial bed load transport rate with dimensionless excess shear stress for clay-silt-sand-gravel (GSSC) mixture

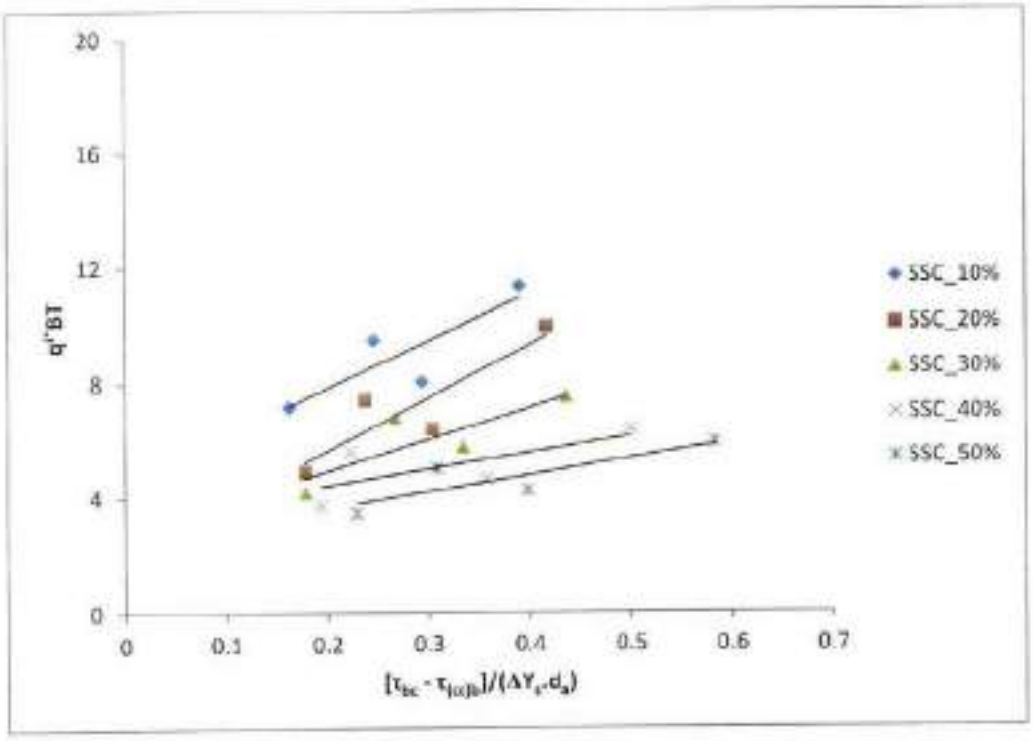


Fig. 4.18 Variation of initial bed load transport rate with dimensionless excess shear stress for clay-silt-sand (SSC) mixture

The following parameters have been considered in the development of formulation for the computation of initial bed load transport rate.

$$q'_{BI} = f(P_c, \tau, \tau_{cr}, \rho, \rho_s, d_a, g, \upsilon) \tag{4.27}$$

Here, $q'_{BI}$ is the initial bed load transport rate (N/m-s); $P_c$ is the clay percentage in fraction; $\tau$ is the shear stress (N/m$^2$) developed due to the incoming flow; $\tau_{cr}$ is the critical shear stress (N/m$^2$) for cohesive sediment mixture; $\rho_s$ and $\rho$ are particle and fluid densities (Kg/m$^3$) respectively; $d_a$ is arithmetic mean size (m) of the cohesive sediment mixture; $g$ is gravitational acceleration (m/s$^2$), and $\upsilon$ is the kinematic viscosity of fluid (m$^2$/s).

Equation (4.27) represented in the dimensionless form using dimensional analysis as below:

$$q^*_{BI} = f(P_c, \tau^*_c) \tag{4.28}$$

Here, $q_{BT}^{*}$ is the dimensionless initial bed load transport rate and computed as

$$q_{BT}^{*} = \frac{q_{BT}'}{(\rho_s - \rho)g\upsilon} \tag{4.29}$$

$\tau_e^{*}$ is the dimensionless excess shear stress and computed as

$$\tau_e^{*} = \frac{\tau - \tau_{ce}}{(\rho_s - \rho)gd_e} \tag{4.30}$$

After a large number of trials the following relationships are proposed for the computation of $q_{BT}^{*}$ for the cohesive sediment mixture in the present study:

$$q_{BT}^{*} = 25.446(1 + P_c)^{-3.36}\left(\tau_e^{*}\right)^{0.298} \tag{4.31}$$

$$q_{BT}^{*} = 96.219(1 + P_c)^{-2.499}\left(\tau_e^{*}\right)^{0.187} \tag{4.32}$$

$$q_{BT}^{*} = 23.33(1 + P_c)^{-2.793}\left(\tau_e^{*}\right)^{0.527} \tag{4.33}$$

Equations (4.31), (4.32), and (4.33) represent the relationship for the computation of $q_{BT}^{*}$ for the cohesive sediment mixture of clay-silt-gravel, clay-silt-sand-gravel, and clay-silt-sand respectively based on the present study data. The computed value from equations (4.31), (4.32), and (4.33) for $q_{BT}^{*}$ shows a good agreement with the observed data as well as good regression coefficient as illustrated in Fig. 4.19.

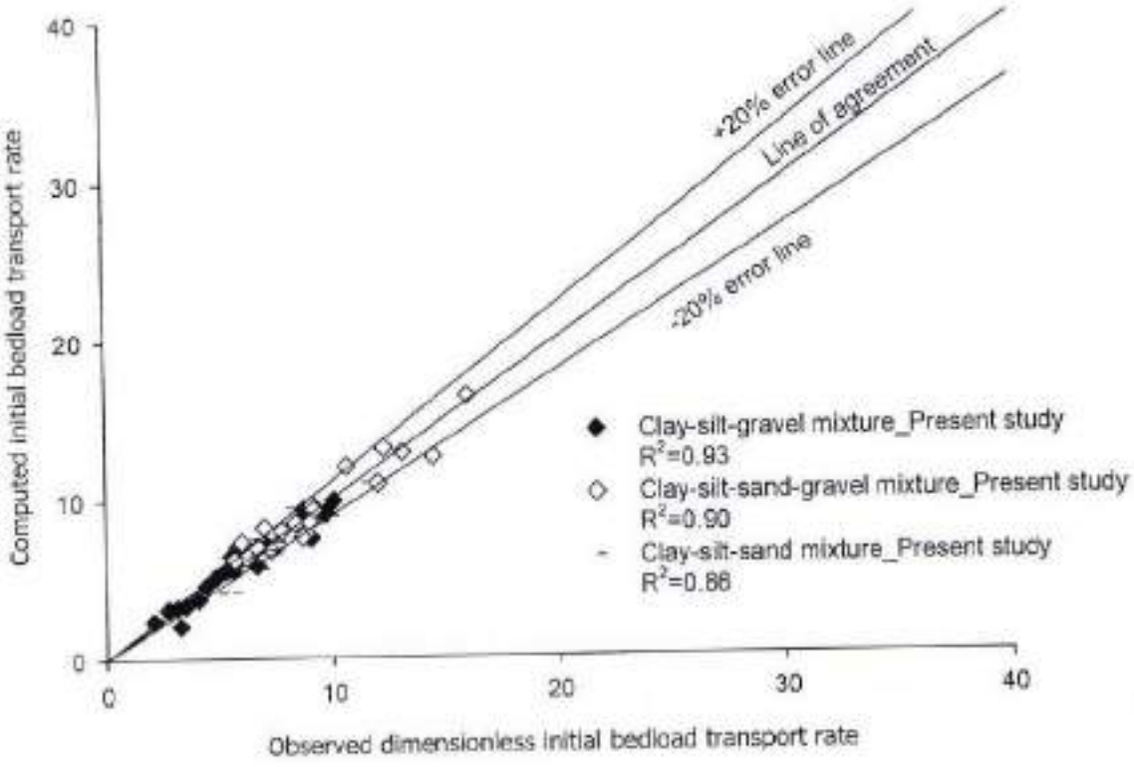


Fig. 4.19 Comparison between computed and observed value of $q_{BI}^{*}$

### 4.4.2.2 Cumulative bed load

The bed load eroded and transported from the channel bed is collected in the trap located at the end of the flume at different time intervals for each experimental run. Cumulative bed load is the sum of bed load collected at different time intervals from the start of the run to the end of run. End of run in each experiment corresponds to the equilibrium condition. The formulation for the computation of the cumulative bed load for cohesive sediment mixture (clay-silt-gravel, clay-silt-sand-gravel and clay-silt-sand) has not been reported yet. Hence, this section made an attempt to develop a relationship for the computation of cumulative bed load transport for all the three cohesive mixture in the present study.

Several parameters has been considered to develop a formulation for the computation of cumulative bed load, however, only the parameters which shows good results for the formulation were considered and represented in the analysis as below:

$$M^{c}_{BL,e} = f(P_c, \tau, \tau_{cr}, q, \rho, \rho_s, d_a, b, l, g) \quad (4.34)$$

Here, $M^{c}_{BL,e}$ is the cumulative bed load (kg) collected till the equilibrium condition reached; $P_c$ is the clay percentage in fraction; $\tau$ is the shear stress (N/m$^2$) developed on the test section of the channel bed due to the incoming flow; $\tau_{cr}$ is the critical shear stress (N/m$^2$) for cohesive sediment mixture; $q$ is the unit discharge (m$^2$/s) i.e. discharge per unit width of the channel; $\rho_s$ and $\rho$ are particle and fluid densities (kg/m$^3$) respectively; $d_a$ is arithmetic mean size (m) of the cohesive sediment mixture; $b$ is the width (m) of the test section; $l$ is the length (m) of the test section; and $g$ is gravitational acceleration (m/s$^2$).

Equation (4.34) represented in the dimensionless form using dimensional analysis as below:

$$M^{c*}_{BL,e} = f(P_c, \tau^*_e, h^*) \quad (4.35)$$

Here, $M^{c*}_{BL,e}$ is the dimensionless cumulative bed load till equilibrium condition of flow reached which can be computed as

$$M^{c*}_{BL,e} = \frac{(M^{c}_{BL,e} g / bl)}{(\rho_s - \rho) g d_a} \quad (4.36)$$

$\tau^*_e$ is the dimensionless excess shear stress on the test section of channel bed and computed as

$$\tau^*_e = \frac{\tau - \tau_{cr}}{(\rho_s - \rho) g d_a} \quad (4.37)$$

$h^*$ is the dimensionless form of flow depth in terms of unit discharge and computed as

$$h^* = \frac{(q^2/g)^{1/3}}{d_a} \quad (4.38)$$

Equation (4.35) represents the functional relationship for the dimensionless cumulative bed load. The change in clay percentage in the cohesive bed influences the bed load transport; hence, to account the influence of cohesion the parameter $P_c$ has been considered. As the transport of sediment occurs when the developed shear stress on the channel bed exceeds in fair amount from

the critical shear stress, so to account this transport phenomena of sediment the parameter $\tau_c^*$ has been taken into consideration for the formulation development. Excess shear stress, developed due to discharge; is responsible for the sediment transport; however, it is found not enough to represent the phenomena and hence an additional parameter in terms of discharge included which plays a significant role in the support of sediment transport phenomena. In this view, the third parameter $h^*$ has been considered in the formulation which represents the dimensionless depth of flow in terms of unit discharge and it acts as a catalyst which enhances the accuracy in the computation towards the observed data.

The effect of parameters involved in Eq. (4.35) i.e. $P_c, \tau_c^*$, and $h^*$ on $M_{BT,c}^*$ has been shown in Fig. 4.20, Fig. 4.21 and Fig. 4.22 respectively. For this purpose, the data of present study for all the three mixture (clay-silt-gravel, clay-silt-sand-gravel, and clay-silt-sand) has been used along with the data of Jain (2008).

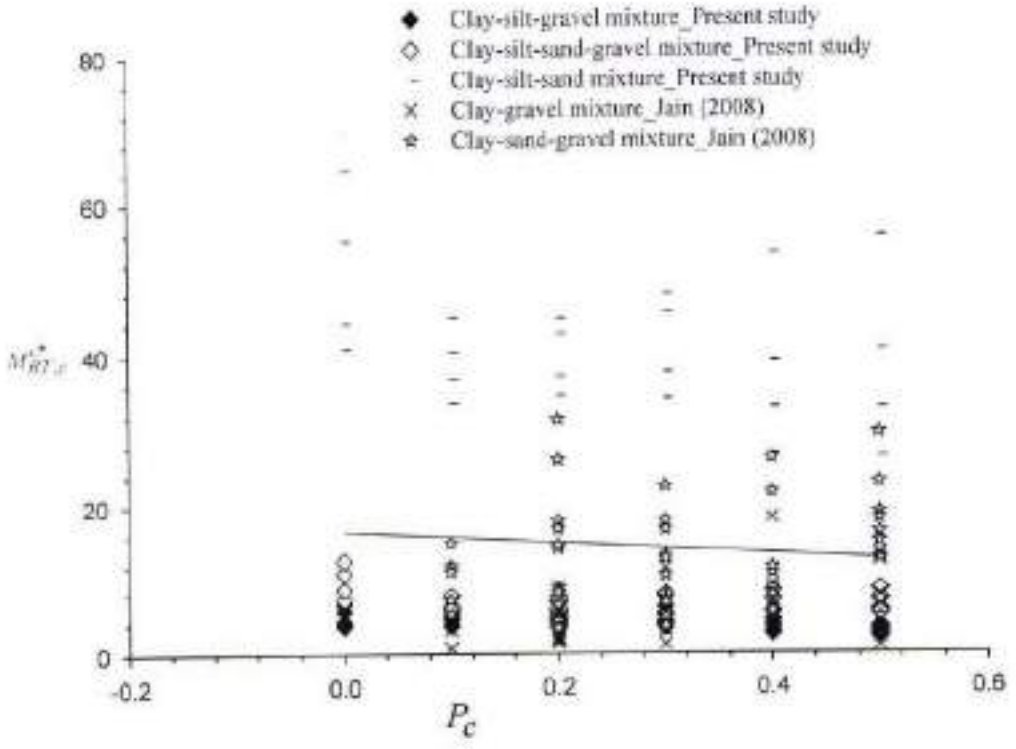


Fig. 4.20 Variation of $M_{BT,c}^*$ with $P_c$

Figure 4.20 shows the decreasing trends line i.e. the value of $M_{BT,e}^{*}$ decreases with the increase of $P_c$. The increase of clay content in the cohesive bed may leads to stronger bond among the particles in the sediment mixture which resulted in increased erosion resistance against the flow and hence responded to less erosion and transport of sediment and consequently $M_{BT,e}^{*}$ decreases with the increase of $P_c$. The decreasing trend line in Fig. 4.20 corresponds to the combined data of Jain (2008) along with the present study data.

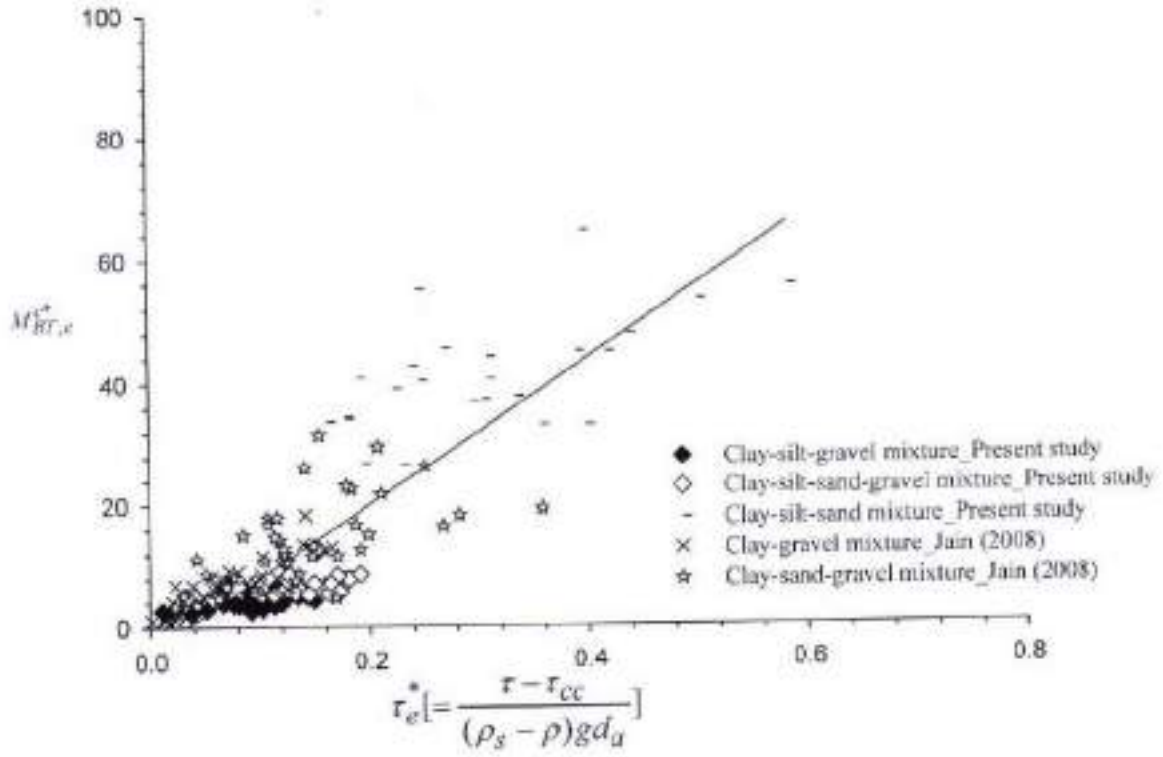


Fig. 4.21 Variation of $M_{BT,e}^{*}$ with $\tau_e^*$

Figure 4.21 shows the increasing trend of $M_{BT,e}^{*}$ with $\tau_e^*$. The present study data is supported by Jain (2008) that showing the increasing trend line as illustrated in Fig. 4.21. The increasing value of excess shear stress on the channel bed leads to the phenomenon of increasing trend line.

The variation of third parameter $h^*$ with $M_{BL,e}^{c*}$ has the increasing trend line as illustrated in Fig. 4.22 which includes the data of present study as well as Jain (2008) data. Since $h^*$ is the function of unit discharge, so $h^*$ increase as the discharge increases and increase in discharge resulted in more erosion and transport of sediment which resulted into this increasing trend phenomenon.

Figures 4.20 – 4.22 indicates that the variation of $M_{BL,e}^{c*}$ with the parameters $P_c$ $\tau_e^*$, and $h^*$ differed for each sediment mixture. Hence, separate formulation for each sediment mixture in the present study has been developed.

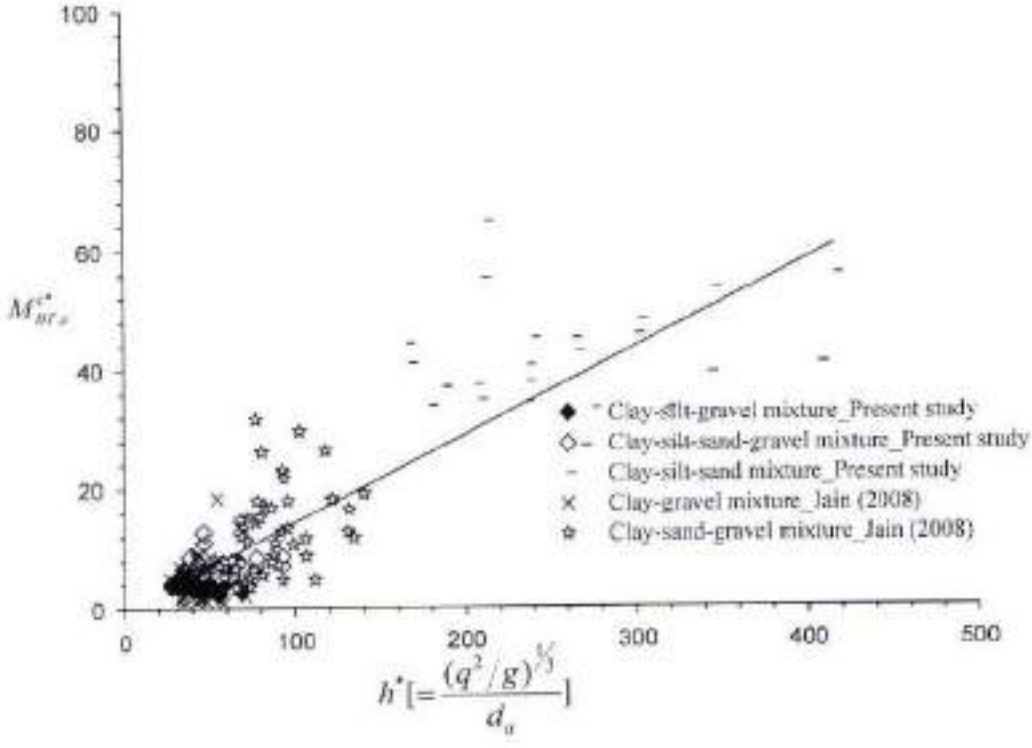


Fig. 4.22 Variation of $M_{BL,e}^{c*}$ with $h^*$

Large number of trials led into the following relationships as formulation for the computation of $M_{BL,e}^{c*}$ for the cohesive sediment mixture in the present study:

$$M_{BL,g}^{c*} = 1.207(1+P_c)^{-2.4}(\tau_c^*)^{0.24}(h^*)^{0.609} \quad (4.39)$$

$$M_{BL,s}^{c*} = 0.267(1+P_c)^{-1.609}(\tau_c^*)^{0.25}(h^*) \quad (4.40)$$

$$M_{BL,g}^{c*} = 0.783(1+P_c)^{-1.61}(\tau_c^*)^{0.272}(h^*)^{0.831} \quad (4.41)$$

Equations (4.39), (4.40), and (4.41) are proposed, using the present study data, for the computation of $M_{BL,g}^{c*}$ for the cohesive sediment mixture of clay-silt-gravel, clay-silt-sand-gravel, and clay-silt-sand respectively.

The computed value of $M_{BL,g}^{c*}$ were plotted against the observed ones for cohesive mixture of clay-silt-gravel, clay-silt-sand-gravel, and clay-silt-sand as shown in Fig. 4.23, Fig.4.24, and Fig. 4.25 respectively. The mean discrepancy ratio, standard deviation and percentage of data within the error line of 0.5 fold and 2.0 fold were computed for the proposed equations in the present study to test the goodness of fit as per Yang *et al.* (1996) and reported in Table 4.6.

$$\text{Discrepancy ratio, } R_i = \frac{(M_{BL,g}^{c*})_{c,i}}{(M_{BL,g}^{c*})_{o,i}} \quad (4.42)$$

Here, $(M_{BL,g}^{c*})_{c,i}$ and $(M_{BL,g}^{c*})_{o,i}$ are the computed and observed value of $(M_{BL,g}^{c*})$respectively.

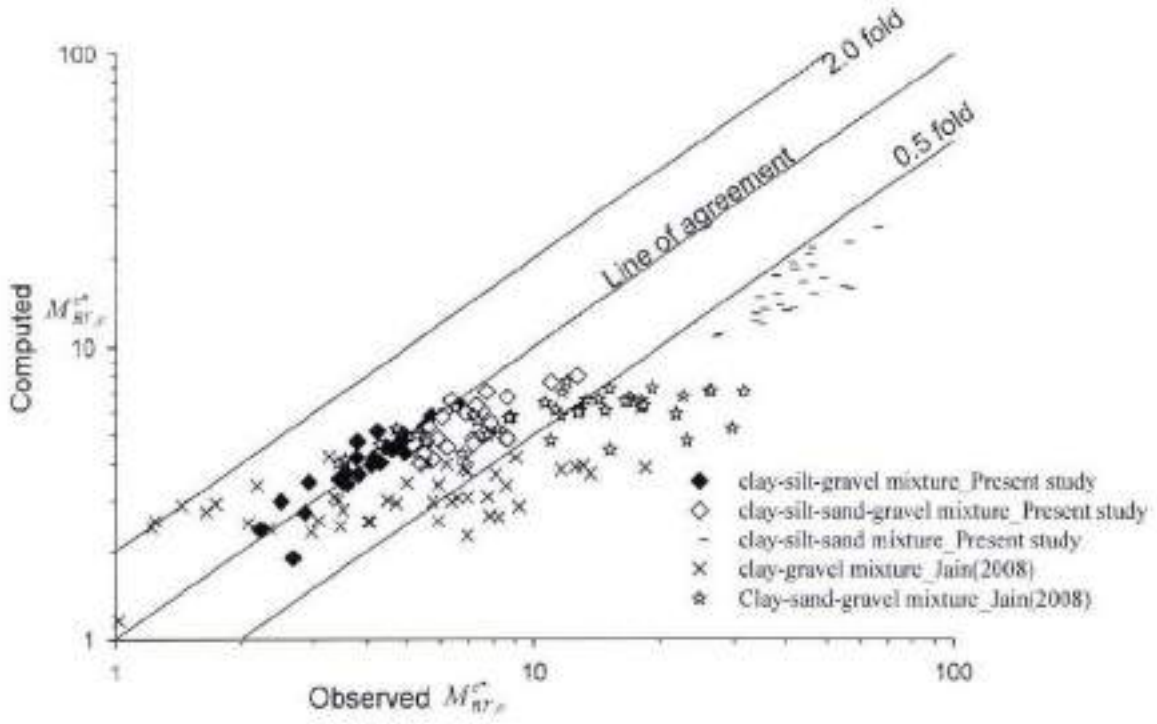


Fig. 4.23 Comparison of observed and computed value of $M^*_{BT,e}$ using Eq. (4.39)

Figure 4.23 shows the plot of computed value of $M^*_{BT,e}$ against the observed ones for present study data as well as for Jain (2008) data as per the proposed Eq. (4.39). Table 4.6 shows a good value of regression coefficient ( $R^2$ = 0.87) for the cohesive sediment mixture of clay-silt-gravel. It also shows that 95%, 95%, and 100% data lies in the range for discrepancy ratio of 0.75-1.25, 0.75-1.50, and 0.50-2.0 respectively for the clay-silt-gravel mixture. Hence, the proposed Eq. (4.39) well predicts the value of $M^*_{BT,e}$ for the sediment mixture of clay-silt-gravel in the present study.

**Table 4.6** Statistical analysis of computed and observed value of $M^{*}_{BL,e}$

| Equation | Data | Cohesive sediment mixture | Clay % | N | Discrepancy ratio | | | | | $R^2$ |
|---|---|---|---|---|---|---|---|---|---|---|
| | | | | | $\bar{R}$ | % of data in range | | | $\sigma_{ln}$ | |
| | | | | | | 0.75 – 1.25 | 0.75 – 1.50 | 0.50 – 2.00 | | |
| Proposed Eq. (4.39) | Present study | Clay-silt-gravel | 10-50 | 20 | 1.002 | 95.00 | 95.00 | 100.00 | 0.1043 | 0.87 |
| | | Clay-silt-sand-gravel | 10-50 | 20 | 0.780 | 50.00 | 100.00 | 100.00 | 0.128 | 0.16 |
| | | Clay-silt-sand | 10-50 | 20 | 0.383 | 00.00 | 00.00 | 00.00 | 0.055 | 0.35 |
| | Jain (2008) | Clay-gravel | 10-50 | 46 | 0.831 | 17.39 | 19.57 | 47.83 | 0.543 | 0.27 |
| | | Clay-sand-gravel | 10-50 | 43 | 0.582 | 25.58 | 25.58 | 48.84 | 0.291 | 0.31 |
| Proposed Eq. (4.40) | Present study | Clay-silt-gravel | 10-50 | 20 | 1.189 | 70.00 | 85.00 | 85.00 | 0.251 | 0.43 |
| | | Clay-silt-sand-gravel | 10-50 | 20 | 1.005 | 100.00 | 100.00 | 100.00 | 0.081 | 0.76 |
| | | Clay-silt-sand | 10-50 | 20 | 0.887 | 100.00 | 100.00 | 100.00 | 0.093 | 0.79 |
| | Jain (2008) | Clay-gravel | 10-50 | 46 | 0.963 | 23.91 | 26.09 | 56.52 | 0.722 | 0.51 |
| | | Clay-sand-gravel | 10-50 | 43 | 0.870 | 34.88 | 41.86 | 67.44 | 0.418 | 0.26 |
| Proposed Eq. (4.41) | Present study | Clay-silt-gravel | 10-50 | 20 | 1.736 | 5.00 | 20.00 | 20.00 | 0.340 | 0.52 |
| | | Clay-silt-sand-gravel | 10-50 | 20 | 1.436 | 5.00 | 75.00 | 75.00 | 0.116 | 0.75 |
| | | Clay-silt-sand | 10-50 | 20 | 1.009 | 95.00 | 100.00 | 100.00 | 0.102 | 0.79 |
| | Jain (2008) | Clay-gravel | 10-50 | 46 | 1.354 | 36.96 | 45.65 | 71.74 | 0.977 | 0.56 |
| | | Clay-sand-gravel | 10-50 | 43 | 1.150 | 37.21 | 51.16 | 72.09 | 0.544 | 0.30 |

For the wide applicability of the proposed Eq. (4.39) the data of other sediment mixture were also considered. The data of present sediment mixture of clay-silt-sand-gravel, clay-silt-sand along with the Jain (2008) data were used for the computation of $M^{*}_{BL,e}$ using Eq. (4.39) and plot has been illustrated in Fig. 4.23 which shows the computation of $M^{*}_{BL,e}$ for sediment mixture other than clay-silt-gravel not well predicted by proposed Eq. (4.39) as low value of regression coefficient ($R^2$ = 0.16, 0.35, 0.27, 0.31) found for those data as shown in Table 4.6.

Hence, the proposed Eq. (4.39) can be exclusively applicable to the sediment mixture of clay-silt-gravel of present study.

Figure 4.24 shows the plot between computed and observed value of $M_{BL,e}^{*}$ as per proposed Eq. (4.40) for the present study data along with Jain (2008) data. The good value of regression coefficient ($R^2$ = 0.76) found for the sediment mixture of clay-silt-sand-gravel in the present study as shown in Table 4.6. This table also indicated the 100 % data lies with the error line which also illustrated in Fig. 4.24. Hence, the proposed Eq. (4.40) well predicts the computed value of $M_{BL,e}^{*}$ for the sediment mixture of clay-silt-sand-gravel in the present study. Table 4.6 shows the good value of $R^2$ (= 0.79) for clay-silt-sand mixture in the present study and also 100% data lies within the error line as illustrated in Fig. 4.24 corresponding to the proposed Eq. (4.40), however, deviation of data from line of agreement (i.e. under predicted) for clay-silt-sand mixture shows the non-applicability of proposed Eq. (4.40) to this sediment mixture. Equation (4.40) also not applicable to the sediment mixture of clay-silt-gravel in the present study as well as to Jain (2008) data as low value of $R^2$ found for them as shown in Table 4.6. Hence, the proposed Eq. (4.40) is applicable to clay-silt-sand-gravel mixture of the present study.

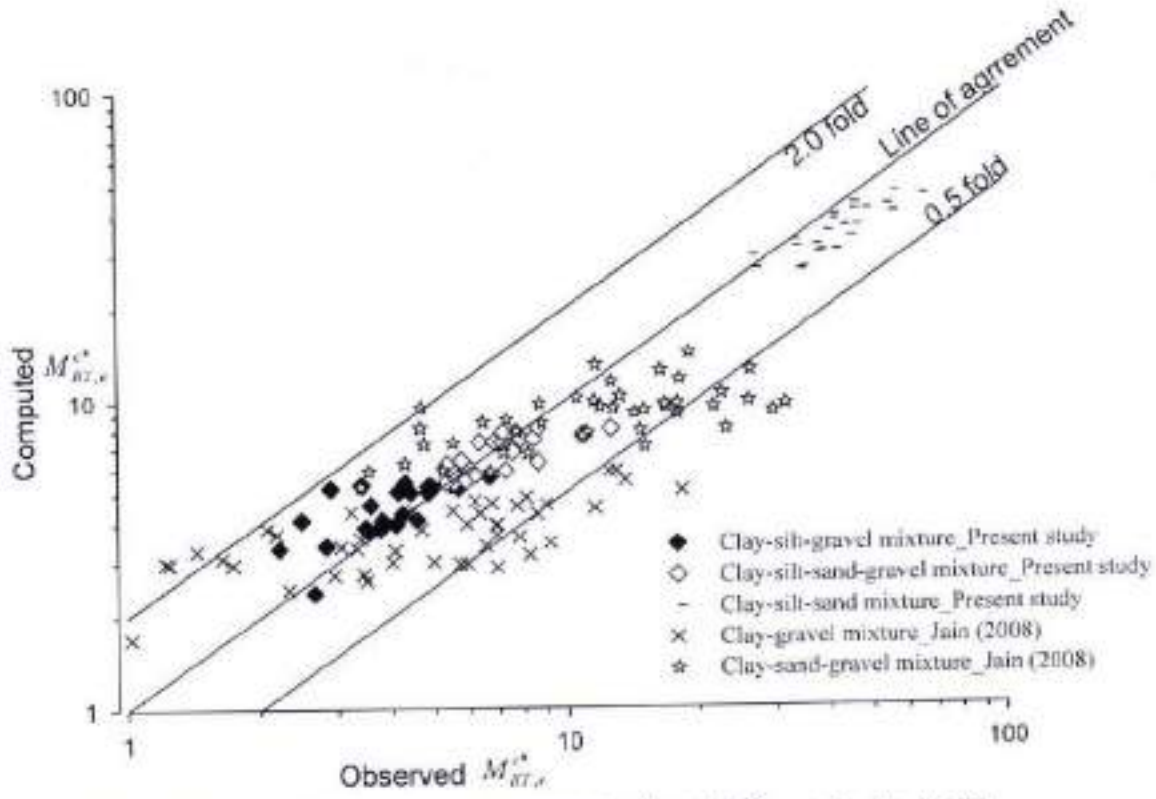


Fig. 4.24 Comparison of observed and computed value of $M^*_{BT,c}$ using Eq. (4.40)

Similarly, the proposed Eq. (4.41) well applicable to the clay-silt-sand mixture of the present study as good value of $R^2$ (= 0.79) found for the this mixture as shown in Table 4.6 and also 100% data lies within the error line and around the line of agreement for this mixture as illustrated in Fig. 4.25. The good value of $R^2$ (= 0.75) found for the sediment mixture of clay-silt-sand-gravel corresponding to proposed Eq. (4.41) as shown in Table 4.6 and also 75% data lies within the error line as plotted in Fig. 4.25 for this sediment mixture, however, deviation from the line of agreement doesn't allow the applicability of proposed Eq. (4.41) to the sediment mixture of clay-silt-sand-gravel. The low value of $R^2$ found for the sediment mixture of clay-silt-gravel and Jain (2008) data as shown in Table 4.6. Hence, the applicability of Eq. (4.41) found for the clay-silt-sand mixture in the present study.

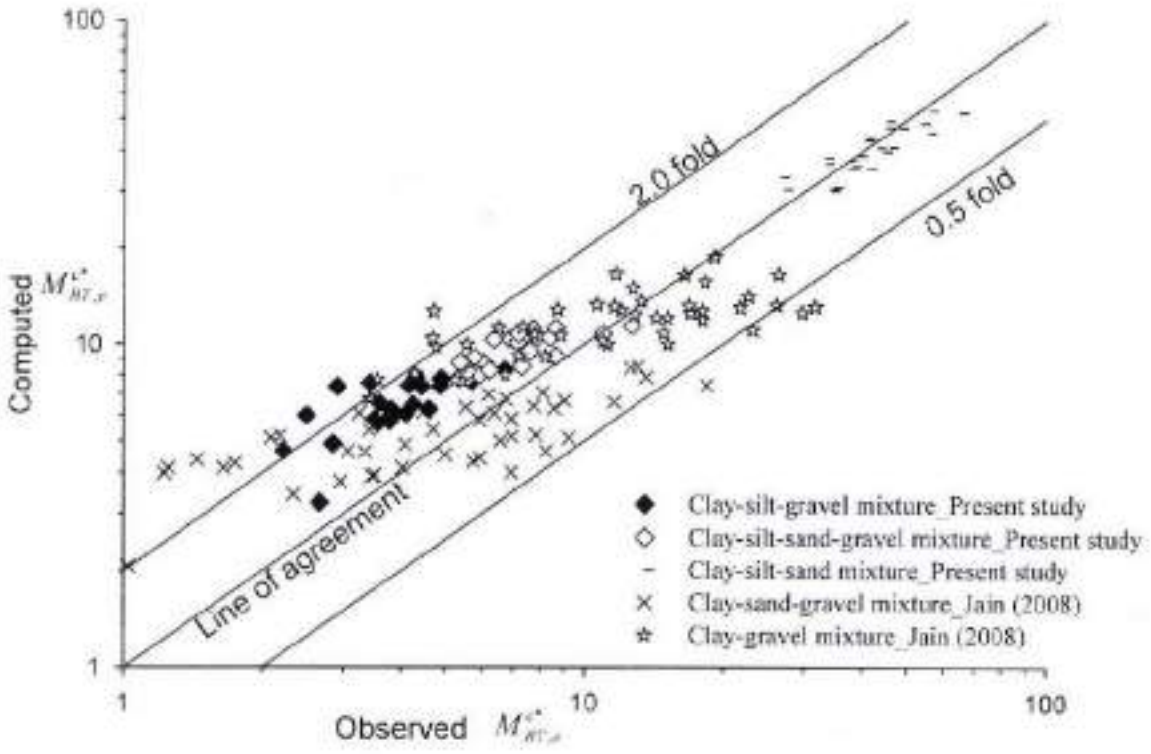


Fig. 4.25 Comparison of observed and computed value of $M_{BT,e}^{*}$ using Eq. (4.41)

### 4.4.2.3 Bed load transport rate

This section deals with the transport rate of bed load and it depends on the various factors like clay percentage, sediment size, shear stress, etc. The variation of bed load transport rate with clay percentage, time, and excess shear stress has been shown in Fig. 4.26, 4.27, and 4.28 respectively. The transport rate of bed load decreases with the increase of the clay percentage as illustrated in Fig. 4.26 for all the three cohesive sediment mixture used in the present study. The increase of the clay percentage in the sediment mixture increases the influence of cohesion which leads to stronger bond among the particles and resulted in low transport rate.

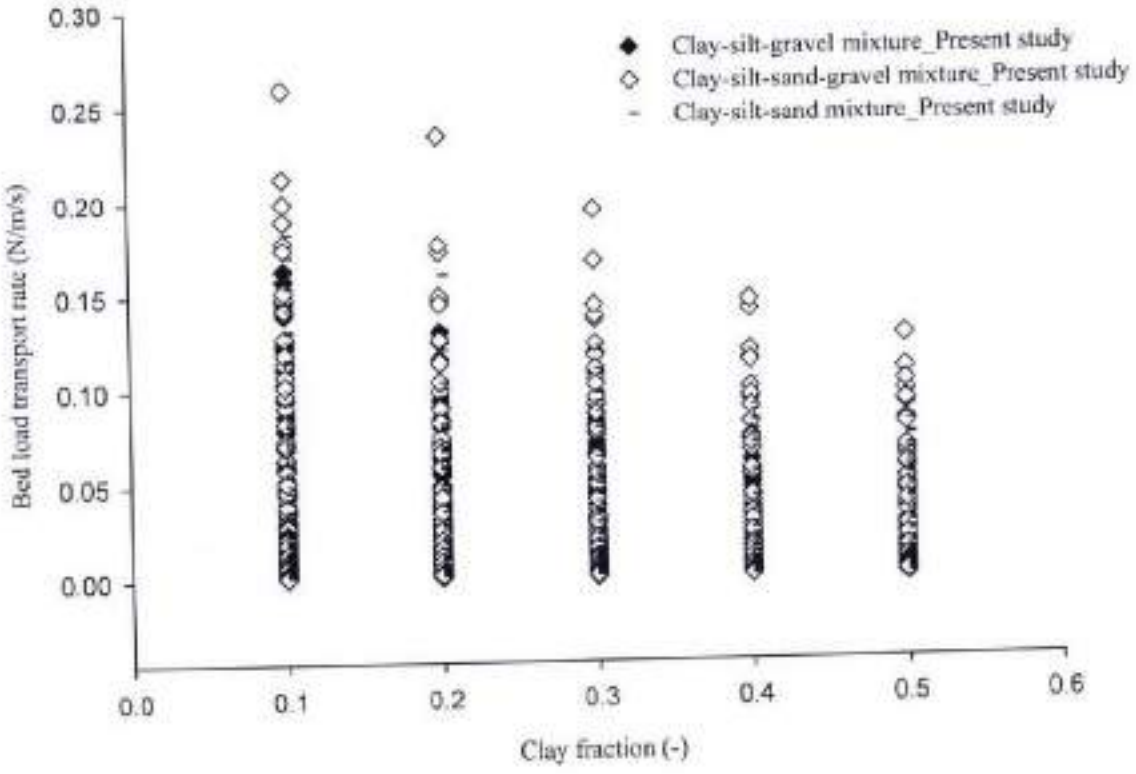


Fig. 4.26 Variation of bed load transport rate with clay fraction for the present study

Transport rate is found to be decreases with time and it supported by Jain (2008) data as illustrated in Fig. 4.27. With the increase of time the degradation in the upstream of working section increases and resulted in lowering the shear stress that leads to decrease in the transport rate of sediment.

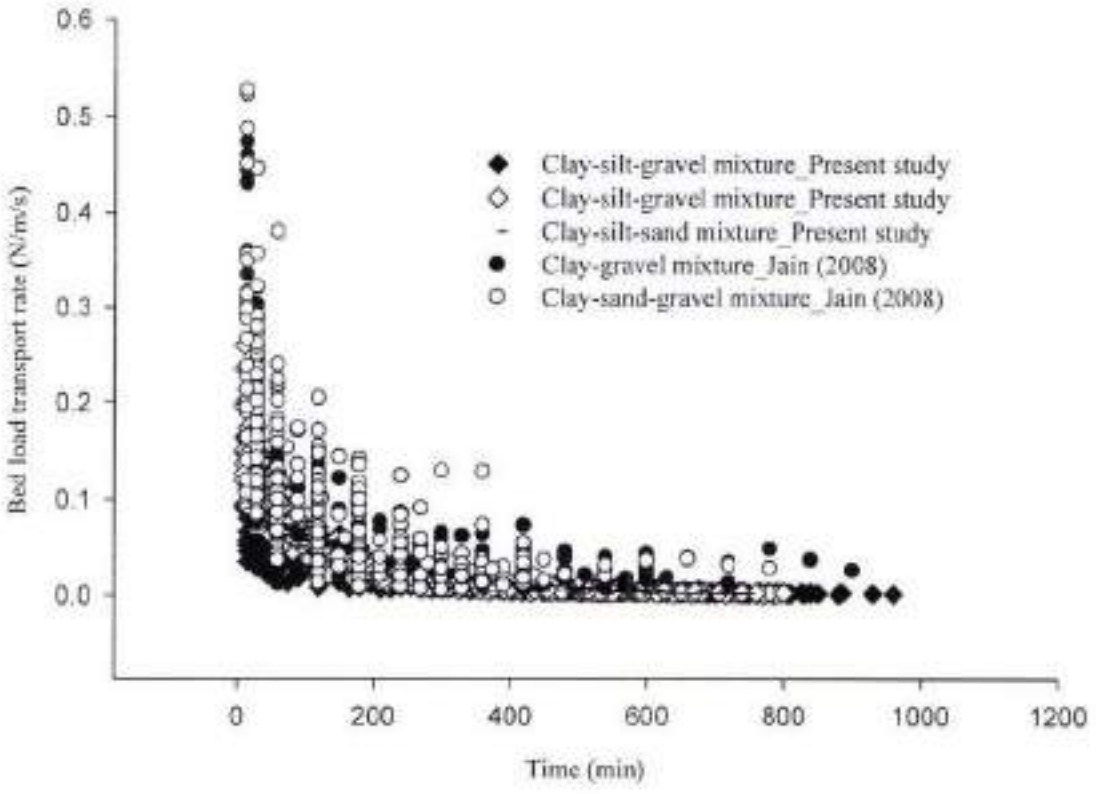


Fig. 4.27 Variation of bed load transport rate with time

Figure 4.28 shows the transport rate increases with the increase of excess shear stress as higher shear stress leads to higher transport of sediment.

This section deals with the formulation for the computation of the bed load transport rate. Since the transport rate depends on the clay percentage, excess shear stress, and time. And equilibrium time is the function of clay percentage and excess shear stress. Hence, bed load transport rate can be represented in the terms of time and equilibrium time as shown in Eq. (4.43).

$$q_{BT} = f(t, t_e, q'_{BT}) \tag{4.43}$$

Here, $q_{BT}$ is the bed load transport rate (N/m/s); $t$ is time (s); $t_e$ is equilibrium time (s); and $q'_{BT}$ is the initial bed load transport rate (N/m/s).

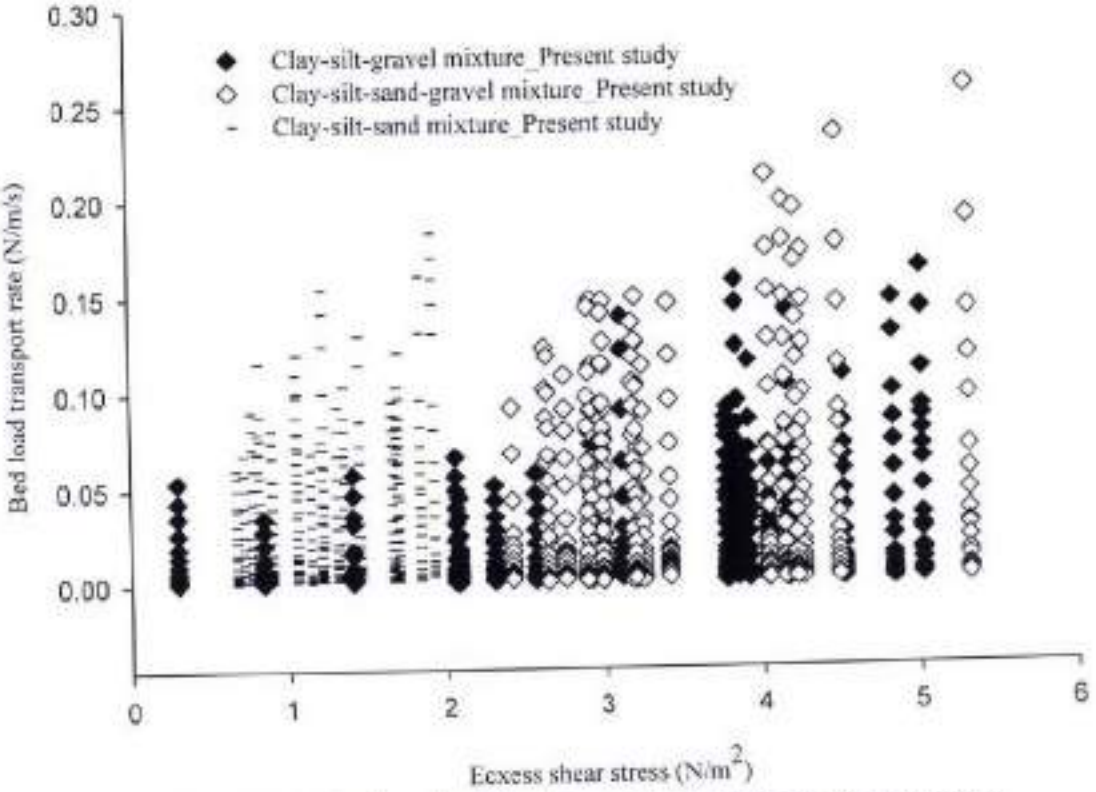


Fig. 4.28 Variation of bed load transport rate with excess shear stress

Equation (4.43) represented in the dimensionless as below:

$$q^*_{BT} = f\left(\frac{t}{t_c}\right) \tag{4.44}$$

Here, $q^*_{BT}$ is the dimensionless bed load transport rate and computed as

$$q^*_{BT} = \frac{q_{BT}}{q'_{BT}} \tag{4.45}$$

Equation (4.44) represents the functional relationship for the dimensionless bed load transport rate. Plot has been made between observed dimensionless bed load transport rate and functional parameter of $\frac{t}{t_c}$ and curve is fitted between them which represent the formulation for the

computation of dimensionless bed load transport rate $\left(q_{BT}^{*}\right)$. The fitted curve is illustrated in Fig. 4.29, 4.30, and 4.31 for the cohesive sediment mixture of clay-silt-gravel, clay-silt-sand-gravel, and clay-silt-sand respectively and the corresponding formulation from the fitted curve has been represented as Eqs. (4.46), (4.47), & (4.48) respectively.

$$q_{BT}^{*} = 1 - 0.97\left[1 - e^{-6.889\left(\frac{t}{t_c}\right)}\right] \tag{4.46}$$

$$q_{BT}^{*} = 1 - 0.984\left[1 - e^{-7.133\left(\frac{t}{t_c}\right)}\right] \tag{4.47}$$

$$q_{BT}^{*} = 1 - 0.992\left[1 - e^{-4.298\left(\frac{t}{t_c}\right)}\right] \tag{4.48}$$

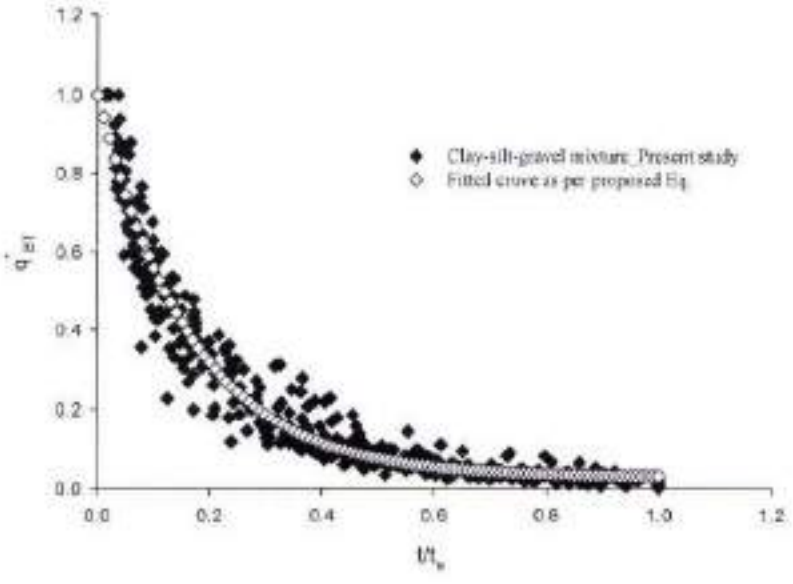


Fig. 4.29 Fitted curve for clay-silt-gravel mixture in the present study

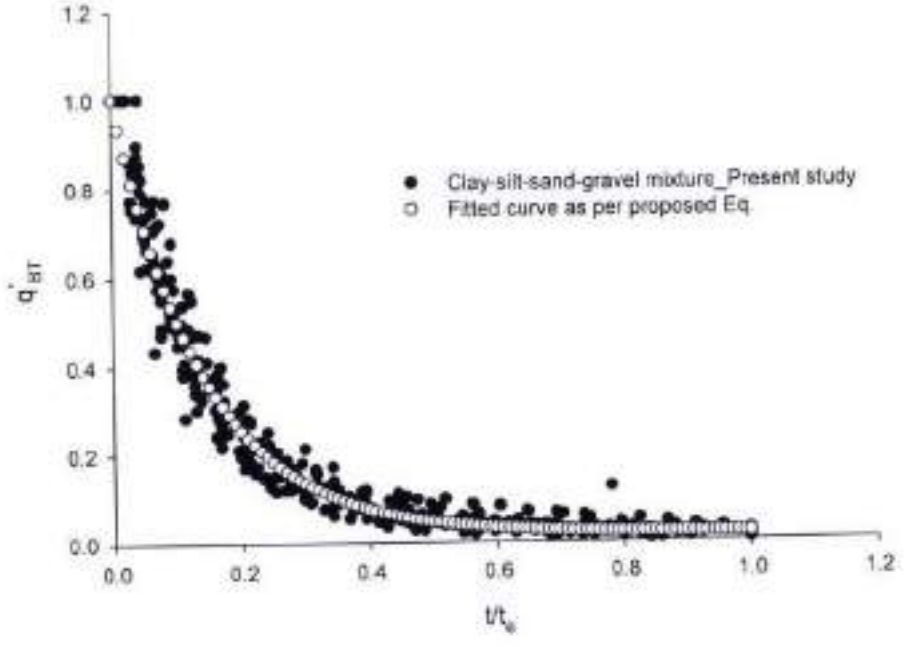


Fig. 4.30 Fitted curve for clay-silt-sand-gravel mixture in the present study

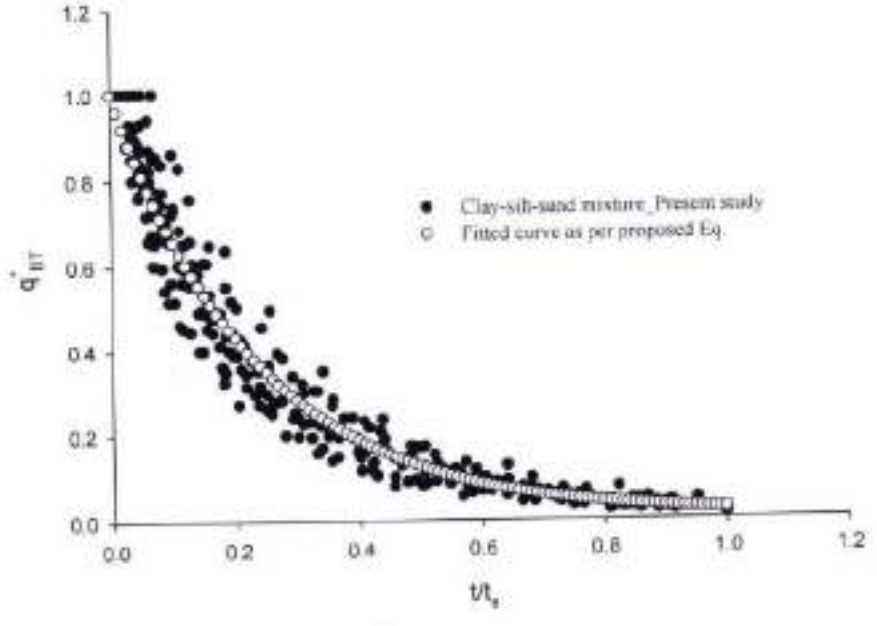


Fig. 4.31 Fitted curve for clay-silt-sand mixture in the present study

The plot has been between the observed and computed value of dimensionless bed load transport rate and regression analysis is done which shows the good regression coefficient as illustrated in Fig. 4.32 for all the three cohesive mixture used in the present study. Hence, the proposed formulation as Eq. (4.46), (4.47), & (4.48) is applicable to clay-silt-gravel, clay-silt-sand-gravel, and clay-silt-sand mixture respectively for the present study.

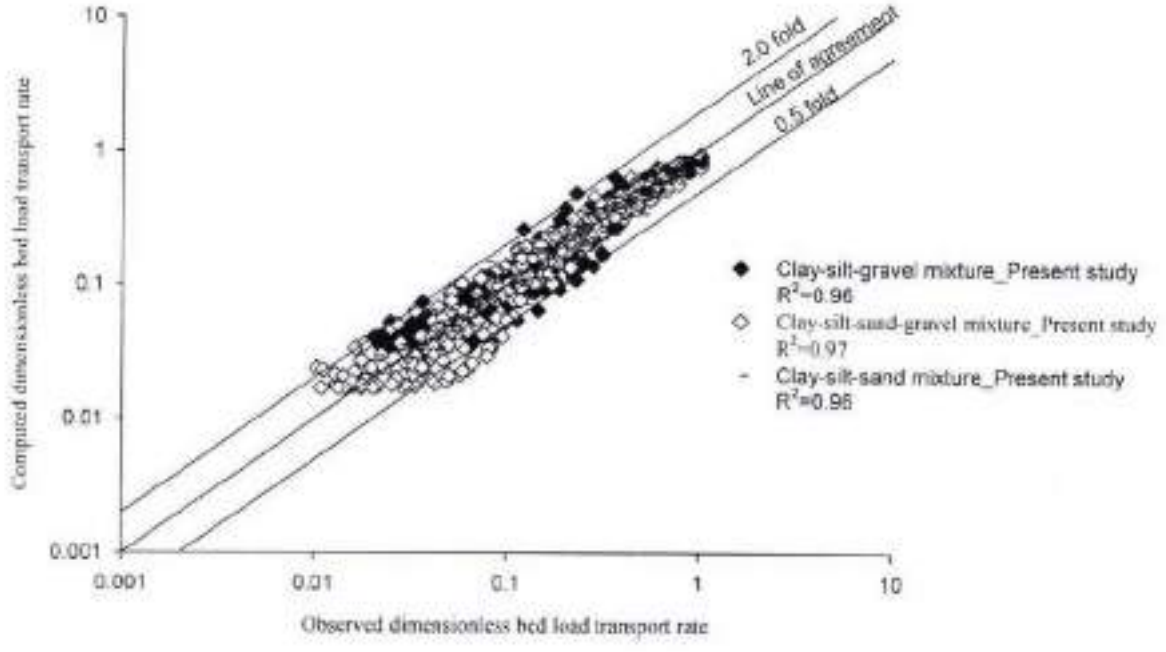


Fig. 4.32 Comparison between computed and observed value of $q_{sr}^{*}$

## 4.4.3 Suspended Load Transport

### 4.4.3.1 Initial suspended load transport rate

Sediment is transported as bed load and suspended load along with the flow in the channel. Initial bed load transport rate is already discussed in the earlier section. This section deals with the initial suspended load transport rate.

The main purpose of the study of the initial transport rate of sediment is to know about the instantly transport of sediment from the channel bed in the response to a given flow rate. This instant transport rate is here treated as the initial transport rate. Generally, clear water flows in

the downstream of a dam which causes the erosion instantly in the channel bed in the downstream of dam. So, the study of this initial or instantly transport rate gives the idea of how much sediment will be eroded from the channel bed so that it can be controlled by adjusting the flow rate in such a way that the channel bed downstream of dam remains safe.

Initial transport rate of suspended load is found to be the function of clay percentage in the sediment mixture as well as shear stress. It decreases with the increase of clay percentage as illustrated in Fig. 4.33 for all the three cohesive sediment mixture used in the present study. Variation of initial suspended load transport rate with excess shear stress is shown in Fig. 4.34, 4.35, and 4.36 for clay-silt-gravel, clay-silt-sand-gravel, and clay-silt-sand mixture respectively which indicates the transport rate increases with the dimensionless excess shear.

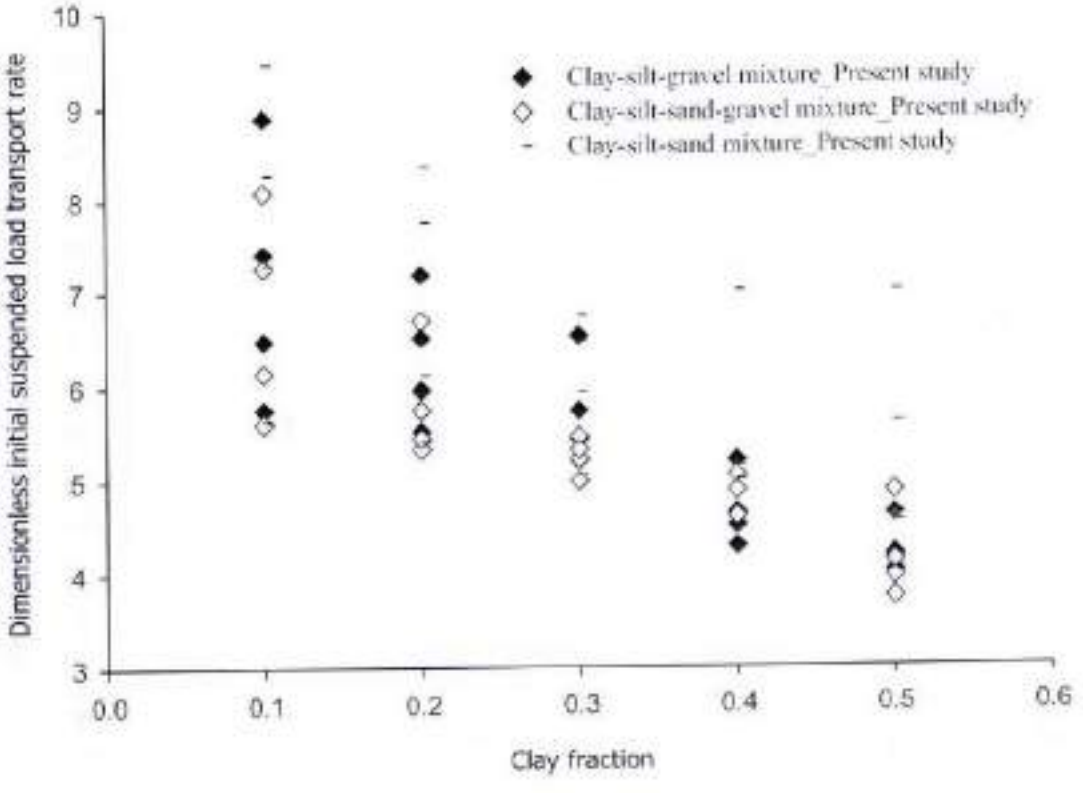


Fig. 4.33 Variation of initial suspended load transport rate with clay fraction in dimensionless form

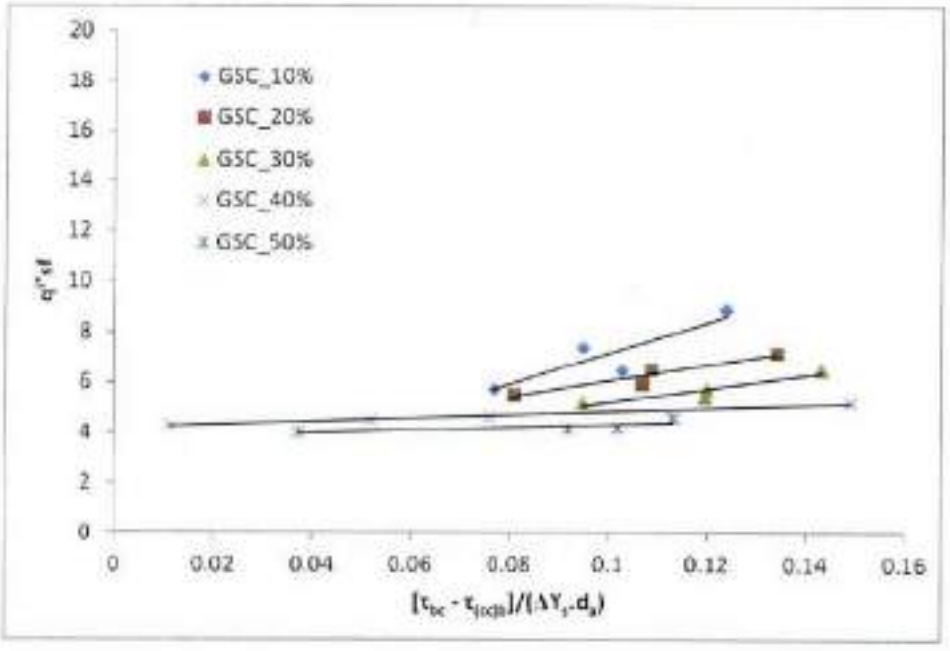


Fig. 4.34 Variation of initial suspended load transport rate with excess shear stress in dimensionless form for clay-silt-gravel (GSC) mixture

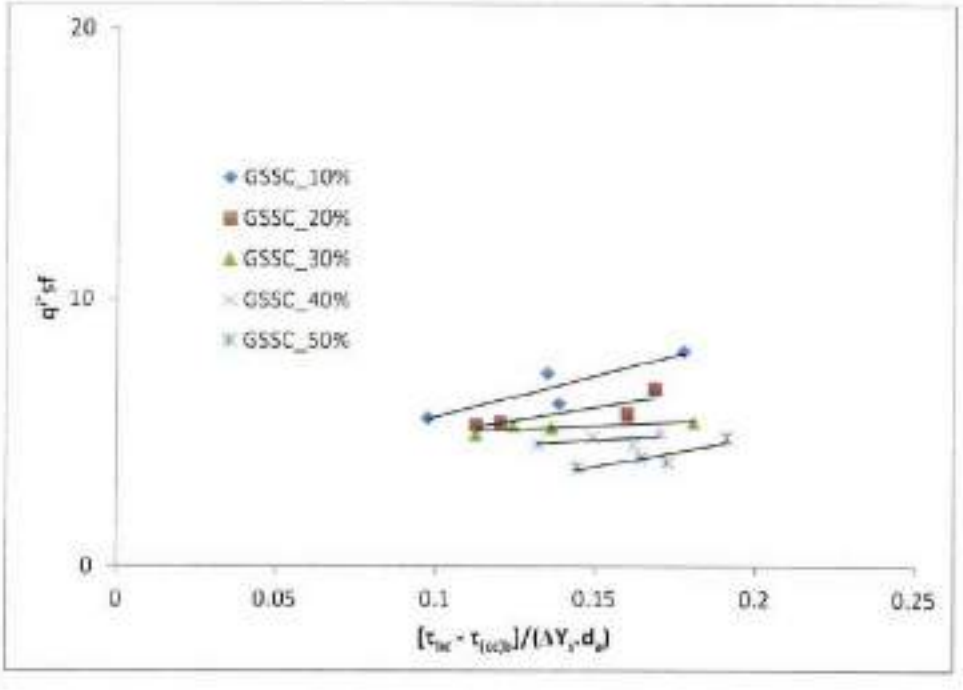


Fig. 4.35 Variation of initial suspended load transport rate with excess shear stress in dimensionless form for clay-silt-sand-gravel (GSSC) mixture

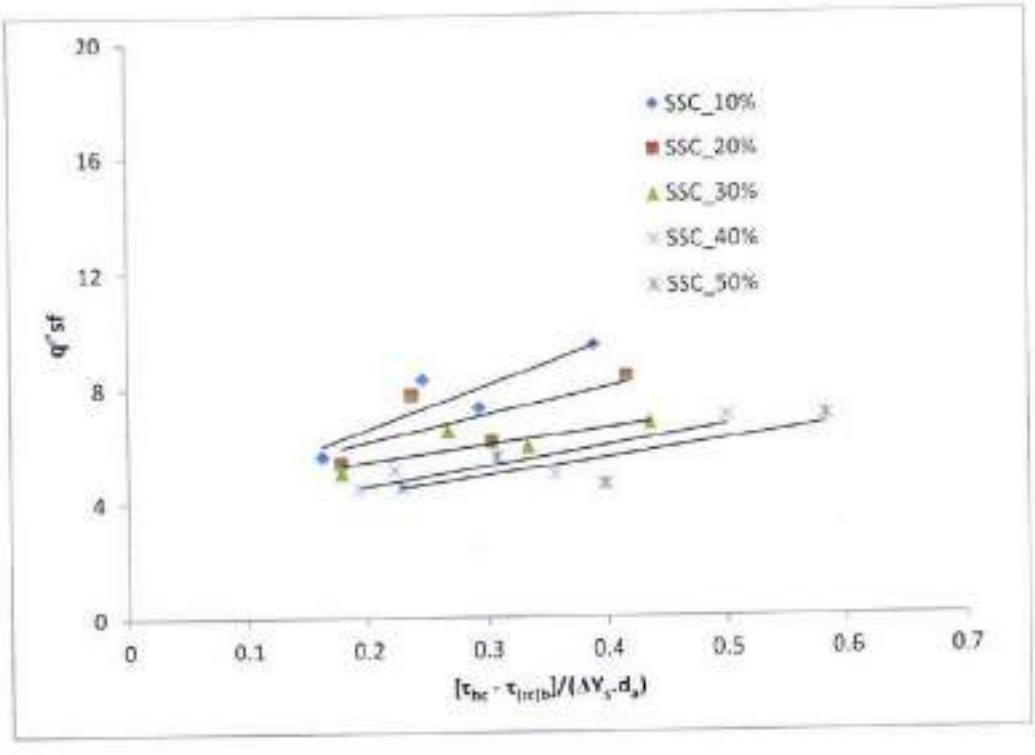


Fig. 4.36 Variation of initial suspended load transport rate with excess shear stress in dimensionless form for clay-silt-sand (SSC) mixture

The formulation for the computation of initial suspended load transport rate has been made in the similar way as in case of formulation of initial bed load transport rate. The following parameters have been considered for the formulation development:

$$q'_{sf} = f(P_c, \tau, \tau_{cr}, \rho, \rho_s, d_s, g, \upsilon) \tag{4.49}$$

Here, $q'_{sf}$ is the initial suspended load transport rate (N/m/s).

Equation (4.49) represented in the dimensionless form using dimensional analysis as below:

$$q^*_{sf} = f(P_c, \tau^*_c) \tag{4.50}$$

Here, $q^*_{sf}$ is the dimensionless initial bed load transport rate and computed as

$$q^*_{sf} = \frac{q'_{sf}}{(\rho_s - \rho)g\upsilon} \tag{4.51}$$

After a large number of trials the following relationships are proposed for the computation of $q_{ci}^{*}$ for the cohesive sediment mixture in the present study:

$$q_{ci}^{*} = 12.018(1+P_c)^{-1.512}(\tau_c^{*})^{0.161} \tag{4.52}$$

$$q_{ci}^{*} = 19.743(1+P_c)^{-1.260}(\tau_c^{*})^{0.449} \tag{4.53}$$

$$q_{ci}^{*} = 15.596(1+P_c)^{-1.628}(\tau_c^{*})^{0.415} \tag{4.54}$$

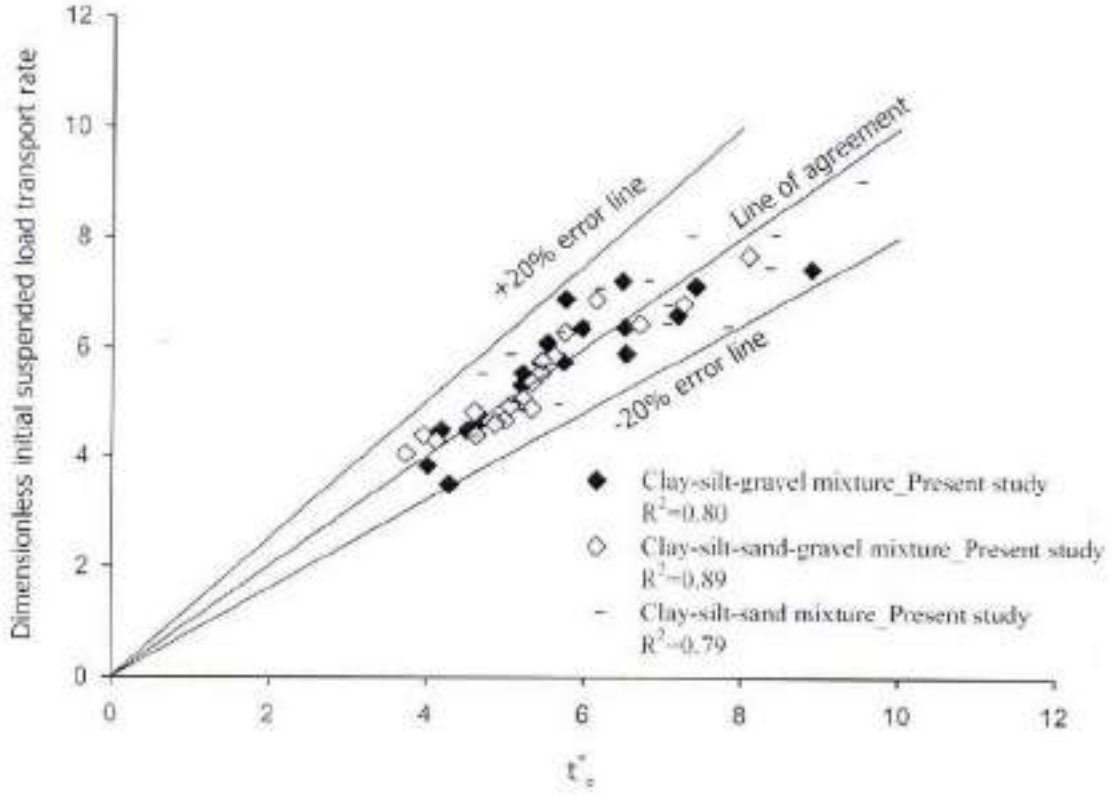


Fig. 4.37 Comparison between computed and observed value of $q_{ci}^{*}$

Equations (4.52), (4.53), and (4.54) represent the relationship for the computation of $q_{ci}^{*}$ for the cohesive sediment mixture of clay-silt-gravel, clay-silt-sand-gravel, and clay-silt-sand respectively based on the present study data. The computed value from equations (4.52), (4.53),

and (4.54) for $q_{sl}^{*}$ has been plotted against the observed ones as illustrated in Fig. 4.37. Figure 4.37 shows that the most of the present study data lies between the $\pm 20\%$ error line and having a good regression coefficient which indicates a good match between computed and observed value for the present study.

### 4.4.3.2 Suspended load transport rate

Transport rate of sediment studied separately for the bed load and suspended load. Bed load transport rate has already been discussed in the earlier section and this section deals with the transport rate of suspended load. In the similar way as in the case of bed load transport rate, the suspended load transport rate also depends on the parameters like clay percentage, sediment size, shear stress, etc. The variation of suspended load transport rate with clay percentage, time, and excess shear stress has been shown in Fig. 4.38, 4.39, and 4.40 respectively for all the cohesive mixture used in the present study. The transport rate of suspended load decreases with the increase of the clay percentage as illustrated in Fig. 4.38.

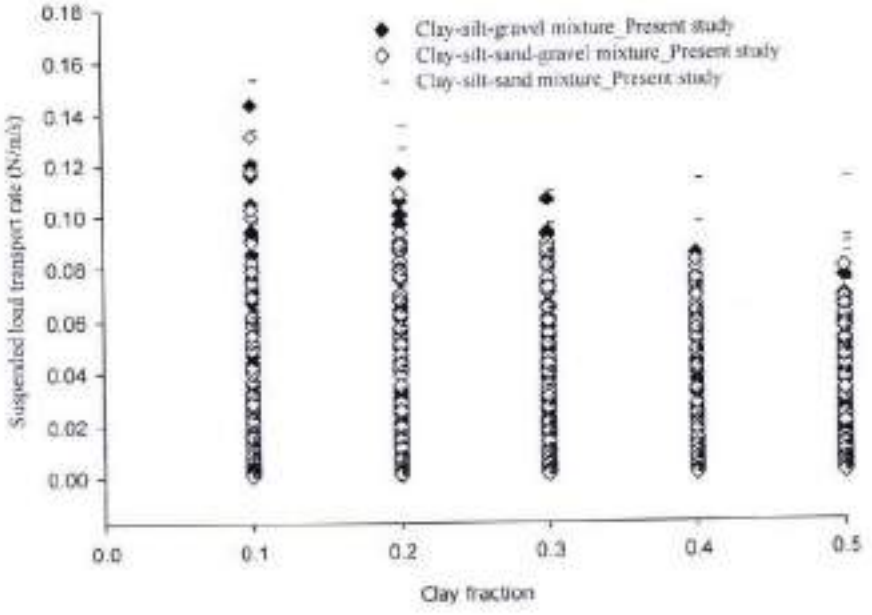


Fig. 4.38 Variation of suspended load transport rate with clay fraction for the present study

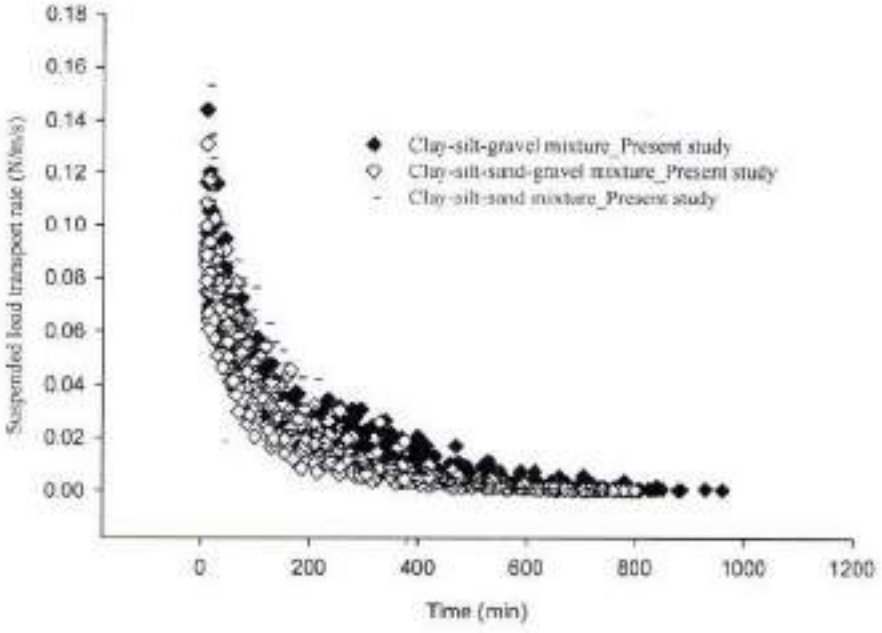


Fig. 4.39 Variation of suspended load transport rate with time for the present study

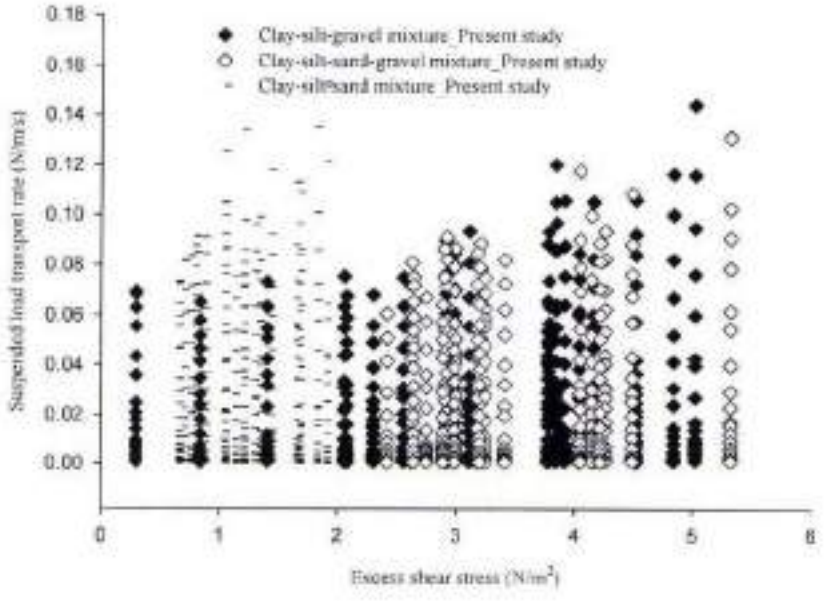


Fig. 4.40 Variation of suspended load transport rate with excess shear stress for the present study

Transport rate is found to be decreases with time similar as in case of bed load transport rate and it supported by Jain (2008) data as illustrated in Fig. 4.39. Figure 4.40 shows the transport rate increases with the increase of excess shear stress as higher shear stress leads to higher transport of sediment.

This section deals with the formulation for the computation of the suspended load transport rate. Since the transport rate depends on the clay percentage, excess shear stress, and time. And equilibrium time is the function of clay percentage as well as excess shear stress. Hence, bed load transport rate can be represented in the terms of time and equilibrium time as shown in Eq. (4.55).

$$q_{sf} = f(t, t_e, q'_{sf}) \tag{4.55}$$

Here, $q_{sf}$ is the bed load transport rate (N/m-s); $t$ is time (s); $t_e$ is equilibrium time (s); and $q'_{sf}$ is the initial bed load transport rate (N/m/s).

Equation (4.55) represented in the dimensionless as below:

$$q^*_{sf} = f\left(\frac{t}{t_e}\right) \tag{4.56}$$

Here, $q^*_{sf}$ is the dimensionless bed load transport rate and computed as

$$q^*_{sf} = \frac{q_{sf}}{q'_{sf}} \tag{4.57}$$

Equation (4.56) represents the functional relationship for the dimensionless suspended load transport rate. Plot has been made between observed dimensionless suspended load transport rate and functional parameter of $\frac{t}{t_e}$ and curve is fitted between them which represent the formulation for the computation of dimensionless suspended load transport rate $\left(q^*_{sf}\right)$. The fitted curve is illustrated in Figs. 4.41, 4.42, and 4.43 for the cohesive sediment mixture of clay-silt-gravel, clay-silt-sand-gravel, and clay-silt-sand respectively and the corresponding

formulation from the fitted curve has been represented as Eq. (4.58), (4.59), & (4.60) respectively.

$$q_{ij}^{*} = 1 - 0.365\left[1 - e^{-1.134\left(\frac{t}{t_v}\right)}\right] - 0.754\left[1 - e^{-6.97\left(\frac{t}{t_v}\right)}\right] \tag{4.58}$$

$$q_{ij}^{*} = 1 - 0.996\left[1 - e^{-5.3\left(\frac{t}{t_v}\right)}\right] \tag{4.59}$$

$$q_{ij}^{*} = 1 - 0.238\left[1 - e^{-0.22\left(\frac{t}{t_v}\right)}\right] - 0.956\left[1 - e^{-5.067\left(\frac{t}{t_v}\right)}\right] \tag{4.60}$$

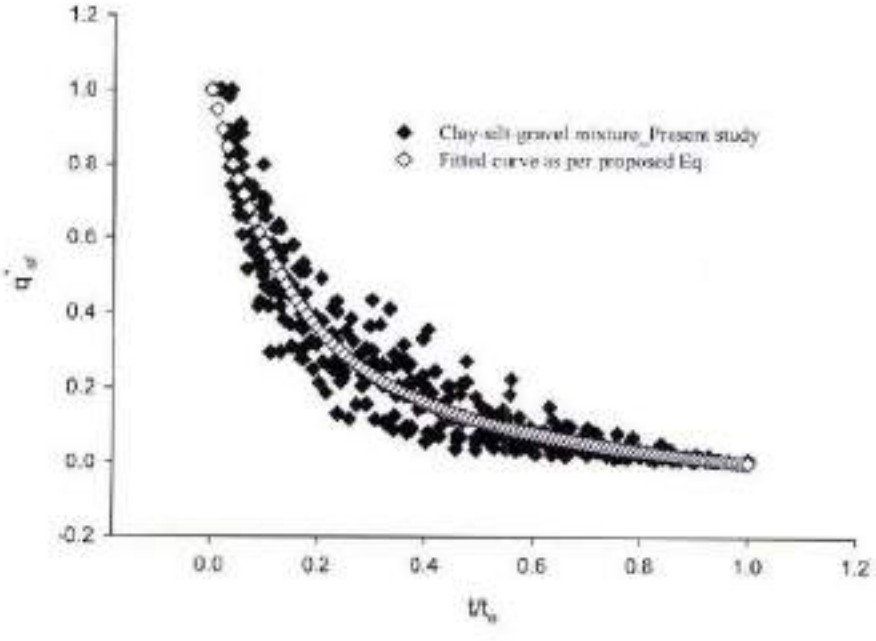


Fig. 4.41 Fitted curve for clay-silt-gravel mixture in the present study

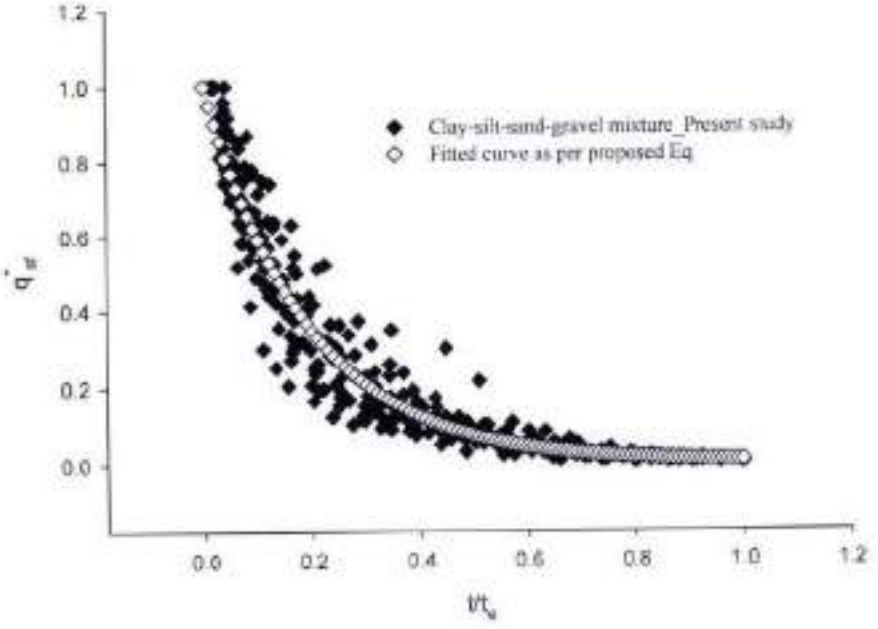


Fig. 4.42 Fitted curve for clay-silt-sand-gravel mixture in the present study

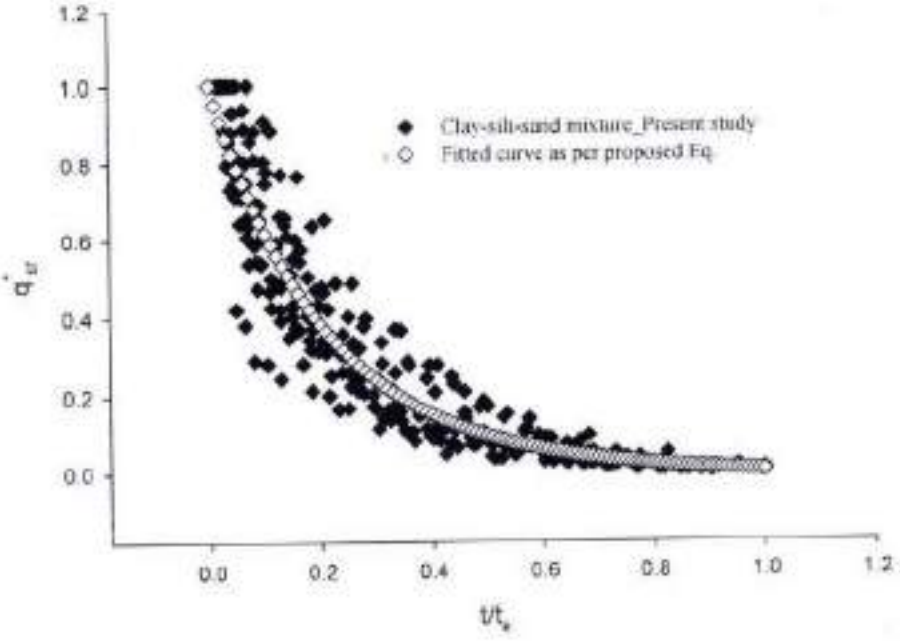


Fig. 4.43 Fitted curve for clay-silt-sand mixture in the present study

The plot has been made between the observed and computed value of dimensionless suspended load transport rate and regression analysis is done which shows the good regression coefficient as illustrated in Fig. 4.44 for all the three cohesive mixture used in the present study. Hence, the proposed formulation in the present study as Eqs. (4.58), (4.59), & (4.60) is applicable to clay-silt-gravel, clay-silt-sand-gravel, and clay-silt-sand mixture respectively for the present study.

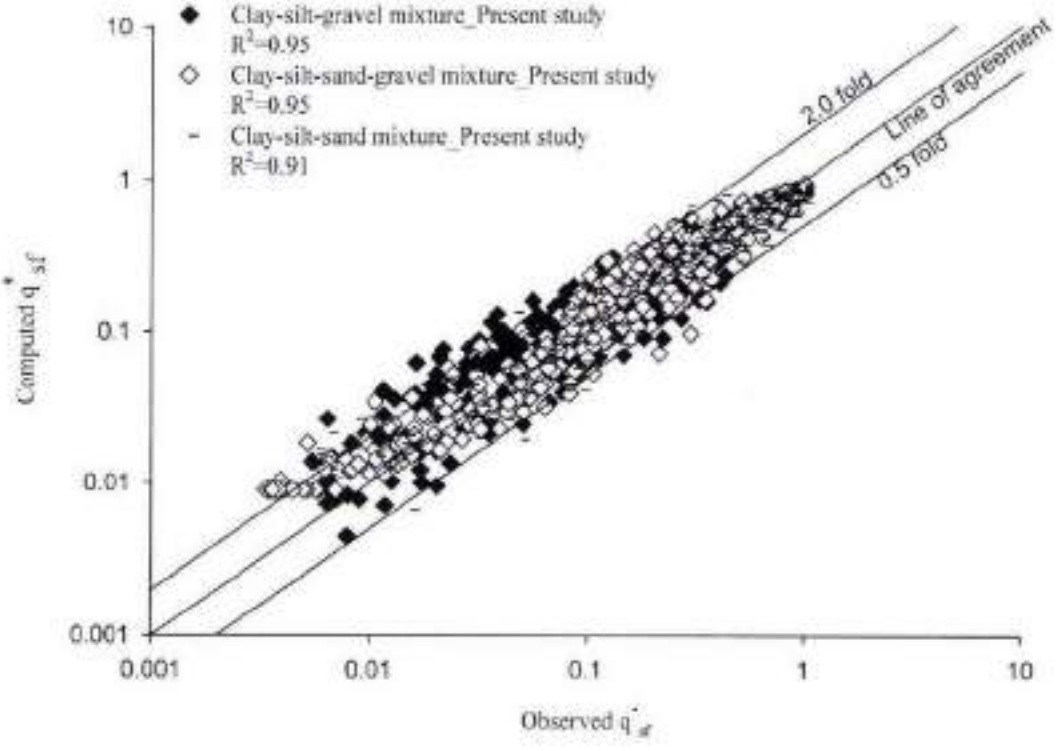


Fig. 4.44 Comparison between computed and observed value of $q^*_{sf}$

## 4.5 TRANSIENT BED SURFACE PROFILES

Degradation in the channel bed occurs when the developed shear stress on the channel bed is sufficiently large enough to mobilize and transport the bed particles and this degradation continues till a stable bed condition reached. This section discuss the transient bed profiles at the mid of flume width at a longitudinal interval of 50 cm along the flow direction for different percentage of clay in the sediment mixture of clay-silt-gravel, clay-silt-sand-gravel, and clay-silt-sand. Transient bed profile varied with the clay percentage in the sediment mixture as well as

with the excess shear stress which provides the power to erode the channel bed. The variation of transient bed surface profile with the clay percentage has been shown in Fig. 4.45 which indicates that degradation of channel bed decreases with the increase of clay percentage.

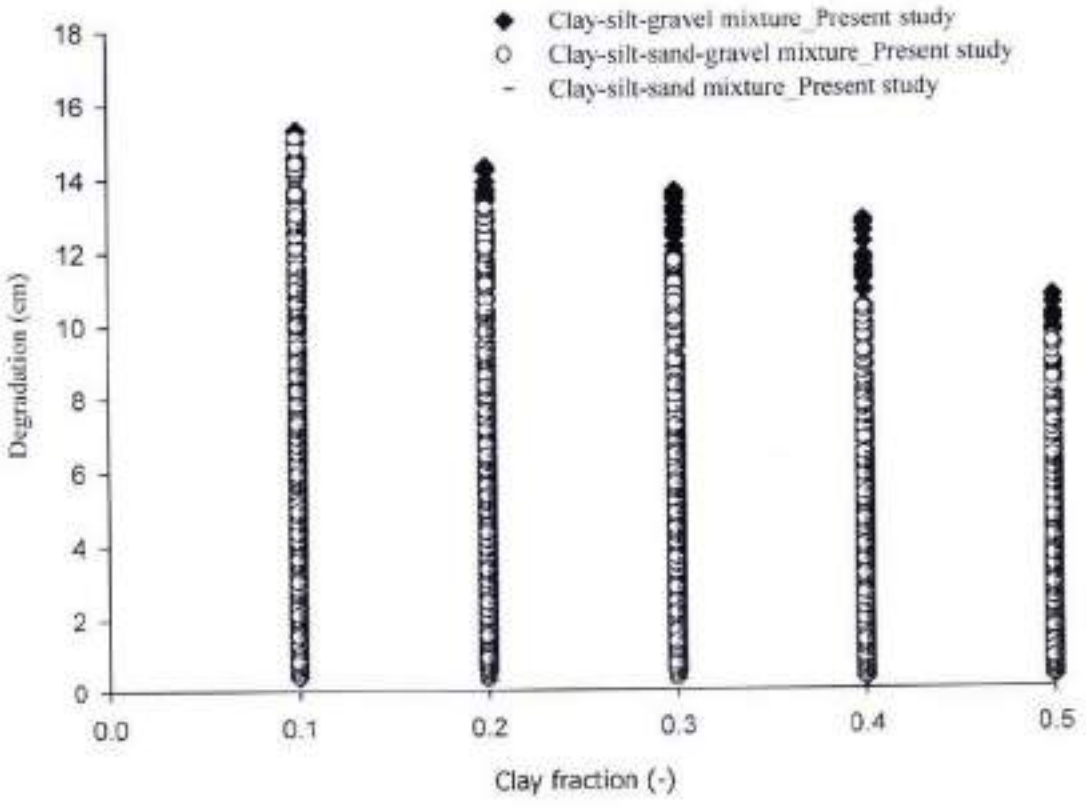


Fig. 4.45 Variation of degradation with clay fraction for present study

Figure 4.46 shows the variation of transient bed surface profile with excess shear stress developed by the incoming flow. It indicates that the channel bed degradation increases with the increase of excess shear stress as obvious.

Time parameter has also been considered to compute the bed profile in respect of time as bed profile varied with time. The variation of bed profile with time has been illustrated in Fig. 4.47 which shows the variation in bed profiles decreases with the increases of time i.e. higher variation observed in the initial period of time and after that it is decreases. In Fig. 4.47, only data of sediment mixtures having 10% clay is included for the purpose of clarity of trend of data.

It is observed that maximum degradation in the channel bed is occurred towards the end of time i.e. at equilibrium time.

A plot has been made for degradation along the channel bed as illustrated in Fig. 4.48. Figure 4.48 shows the maximum degradation occurred at 50cm longitudinally from the entrance of upstream working section for all the three cohesive sediment mixture in the present study.

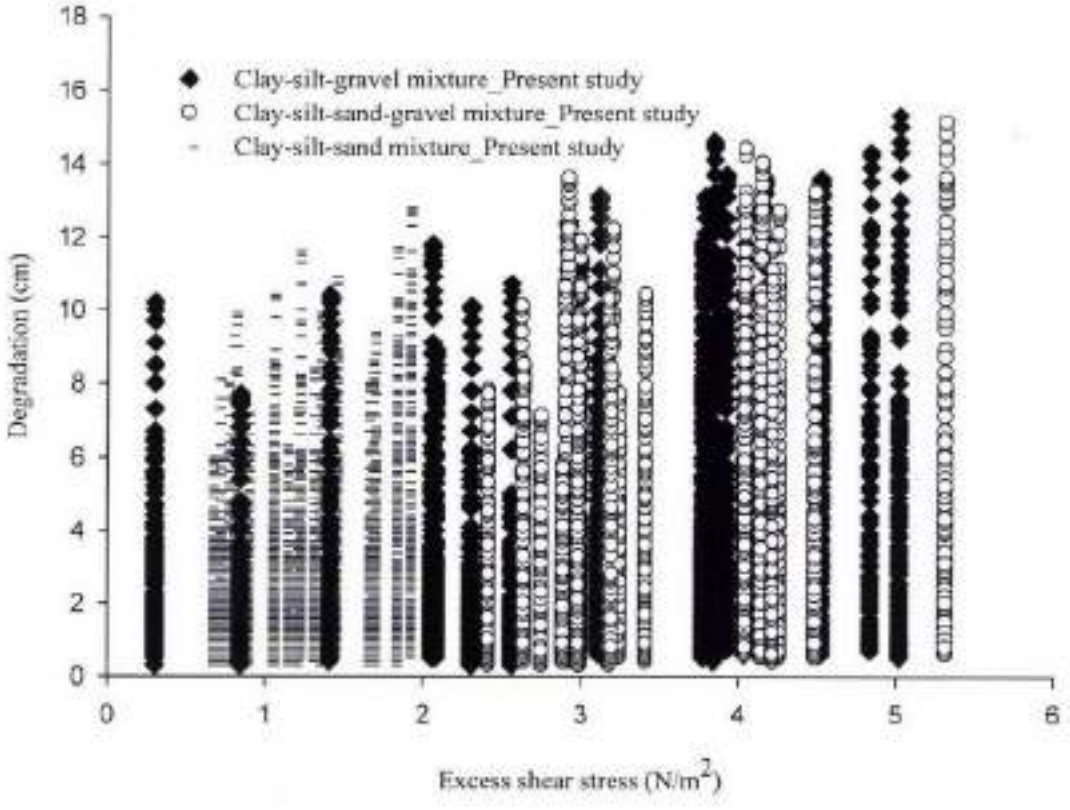


Fig. 4.46 Variation of degradation with excess shear stress for present study

As the channel bed profile is varied with the clay percentage, excess shear stress, and time. So, the following parameters have been considered in the formulation for the computation of transient bed profile.

$$z = f(z_{max}, t, t_e, X, L_{max}) \tag{4.61}$$

Here, $z$ is the bed degradation at given location $X$ and time $t$; $z_{max}$ is the maximum degradation in the channel bed which is the function of clay percentage and excess shear stress; $t_e$ is the equilibrium time for which computation has been made in previous section; $L_{max}$ is the location point of maximum degradation which is 50 cm as per Fig. 4.48.

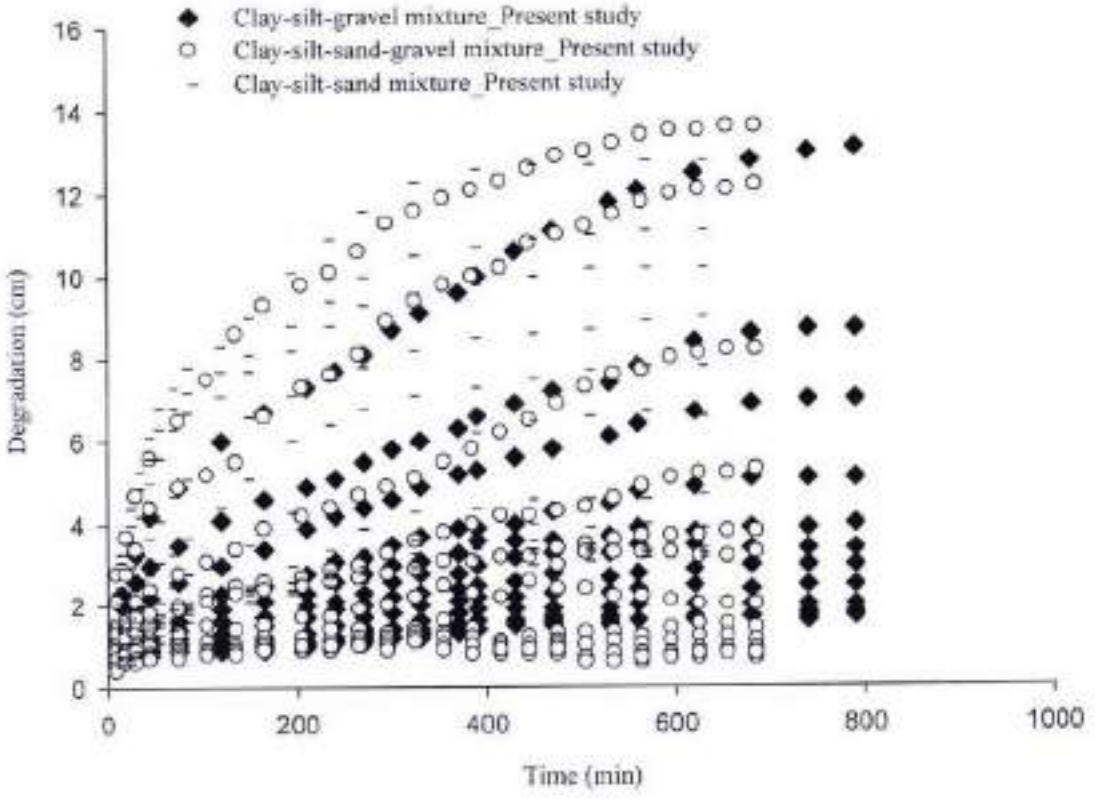


Fig. 4.47 Variation of degradation with time for 10% clay in mixtures

Before the development of relationship for the computation of bed profile $z$, the formulation has to be made for the computation of maximum degradation $(z_{max})$ in the cohesive channel bed. Maximum degradation of the channel bed is dependent on the clay percentage in the mixture as well as shear stress developed by incoming flow. In this view, the variation of $z_{max}$ with $P_c$ and $\tau_c^*$ has been shown in Fig. 4.49 and 4.50 respectively. Figure 4.49 shows that $z_{max}$ decreases with the increases of clay content in the mixture due to cohesion influence. Figure

4.50 illustrated that $z_{max}$ increases with the increase of dimensionless excess shear stress $(\tau_e^*)$ for each cohesive bed in the present study. Hence, the following parameters are considered for the computation of maximum degradation:

$$z_{max} = f(P_e, \tau_e, \rho_s, \rho, g, d_a, q) \tag{4.62}$$

Here, $q$ is the unit discharge ($m^2/s$).

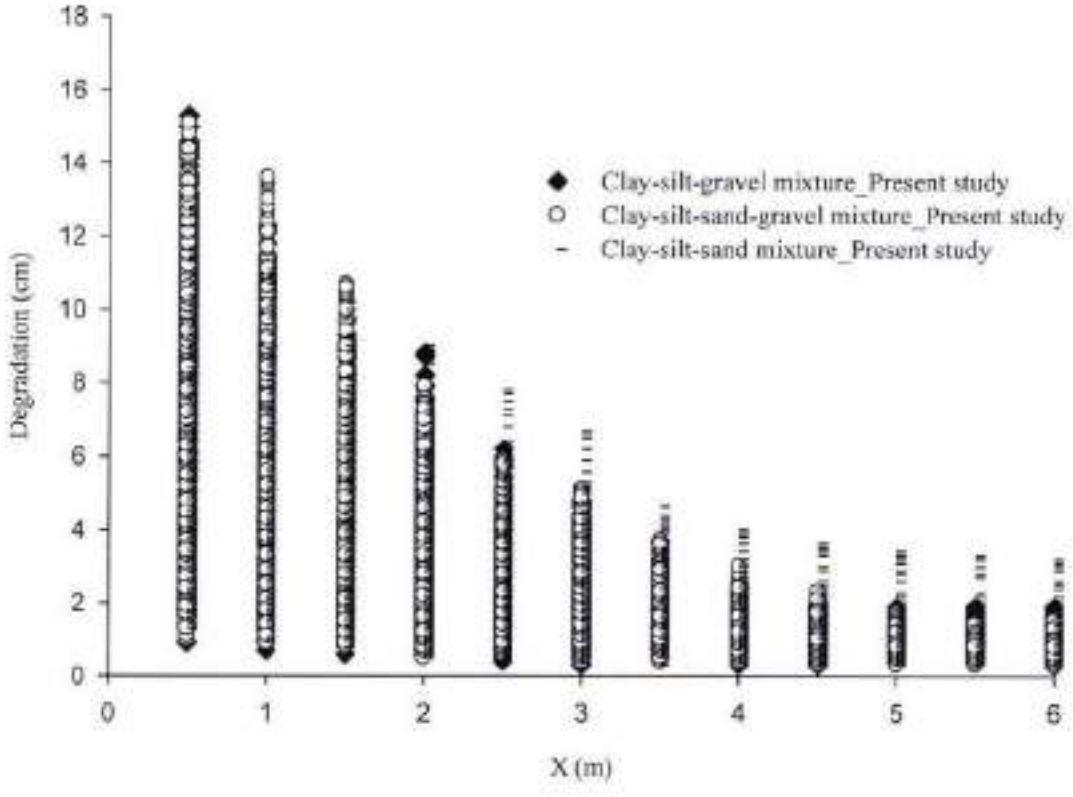


Fig. 4.48 Variation of degradation along the channel bed for present study

The functional form of Eq. (4.62) can be represented in the dimensionless form as following:

$$\frac{z_{max}}{\left(\frac{q^2}{g}\right)^{\frac{1}{3}}} = f\left(P_c, \tau_c^*\right) \tag{4.63}$$

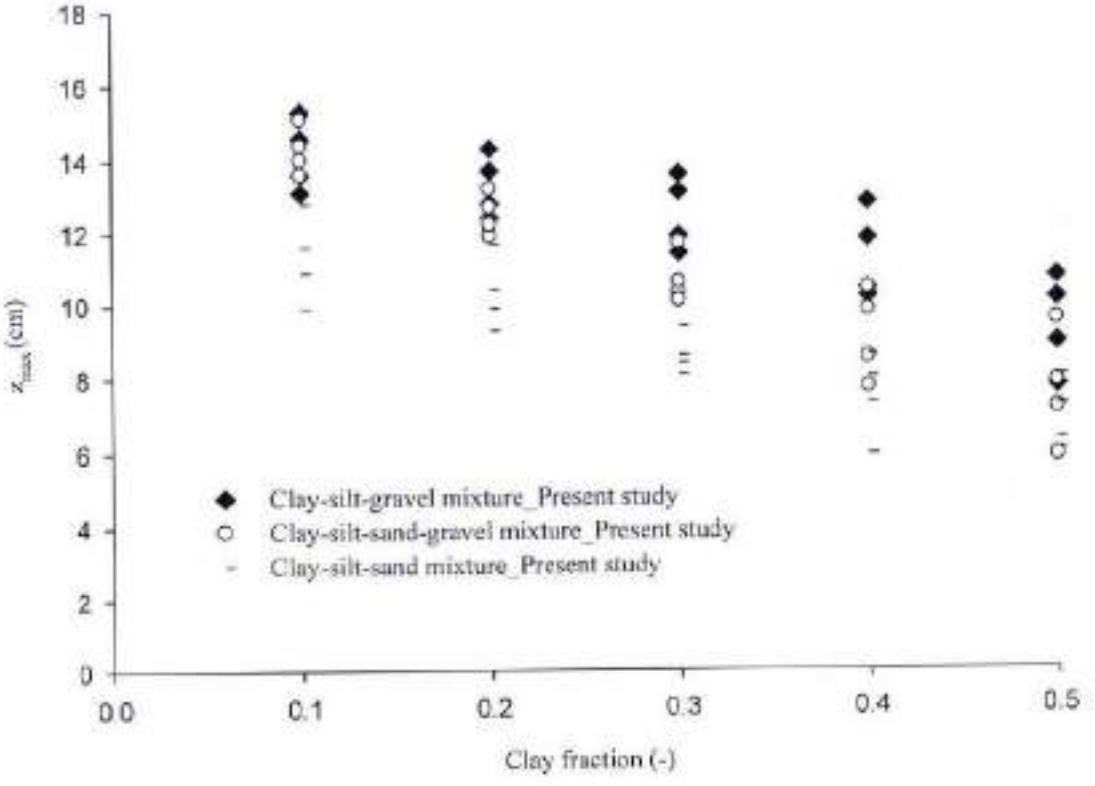


Fig. 4.49 Variation of maximum degradation with clay fraction for the present study

After a large number of trials the following relationships are proposed for the computation of $z_{max}$ for the cohesive sediment mixture in the present study:

$$\frac{z_{max}}{\left(\frac{q^2}{g}\right)^{\frac{1}{3}}} = 1.902(1 + P_c)^{-1.173}(\tau_c^*)^{0.005} \tag{4.64}$$

$$\frac{z_{max}}{\left(\frac{q^2}{g}\right)^{1/3}} = 1.354(1+P_c)^{-1.894}(\tau_c^*)^{-0.199} \tag{4.65}$$

$$\frac{z_{max}}{\left(\frac{q^2}{g}\right)^{1/3}} = 2.281(1+P_c)^{-1.720}(\tau_c^*)^{0.041} \tag{4.66}$$

Equations (4.64), (4.65), and (4.66) represent the relationship for the computation of $z_{max}$ for the cohesive sediment mixture of clay-silt-gravel, clay-silt-sand-gravel, and clay-silt-sand respectively based on the present study data. The computed value from equations (4.64), (4.65), and (4.66) for $z_{max}$ shows a good agreement with the observed data as well as good regression coefficient as illustrated in Fig. 4.51.

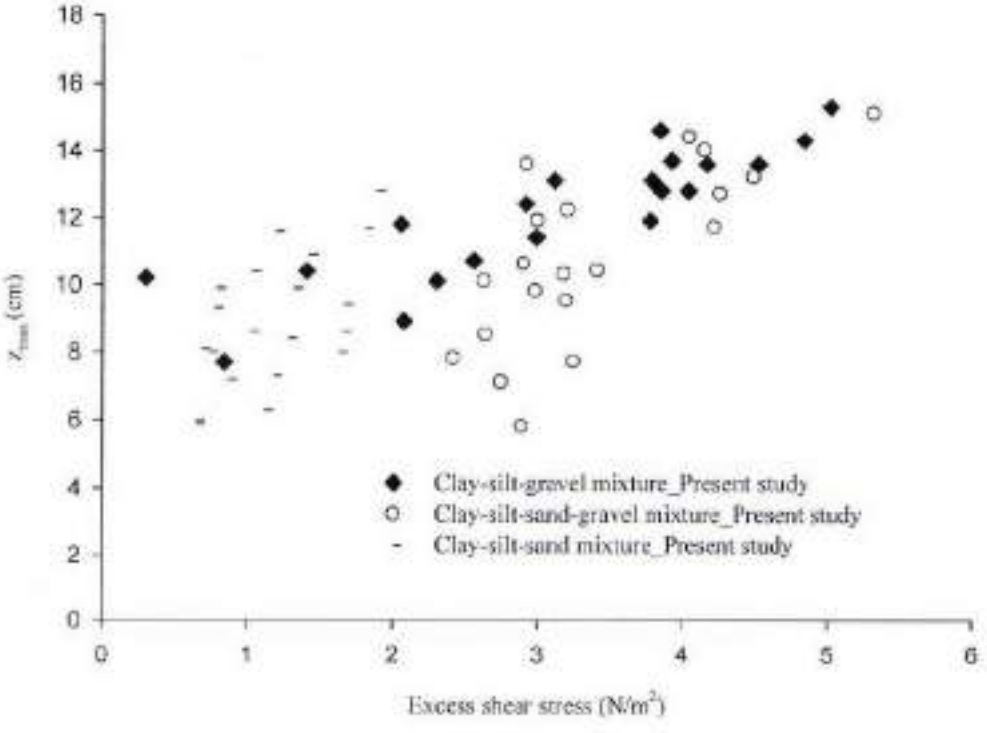


Fig. 4.50 Variation of maximum degradation with excess shear stress for present study

After the computation of $z_{max}$ the formulation for the computation of transient bed profile has been proposed. Equation (4.61) can be represented in the dimensionless form as following:

$$\frac{z}{z_{max}} = f\left(\frac{t}{t_e}, \frac{X}{L_{max}}\right) \tag{4.67}$$

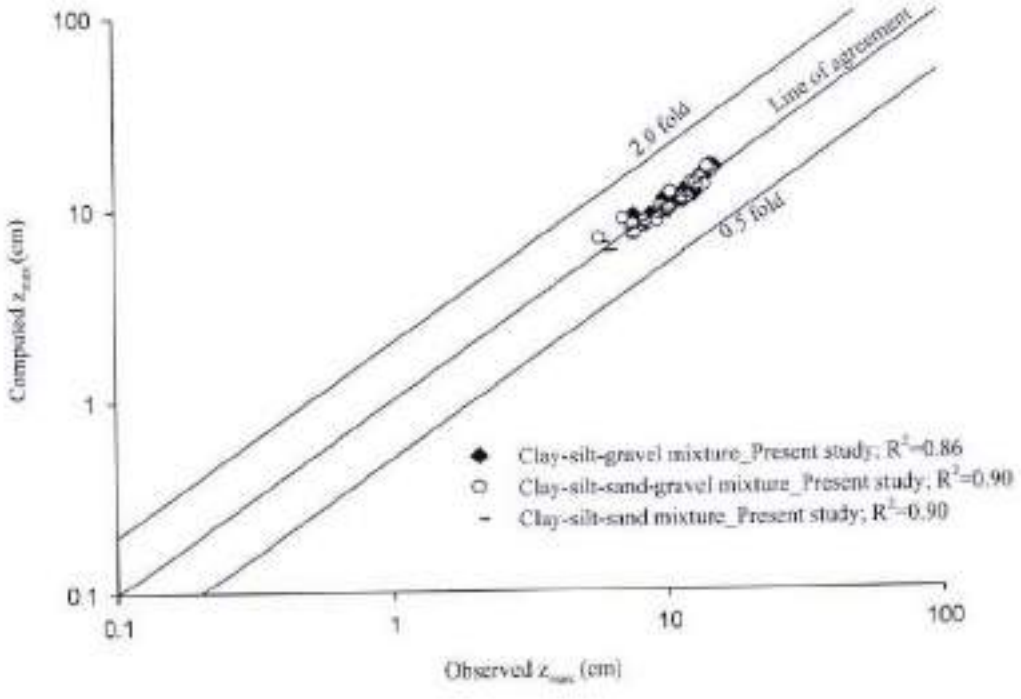


Fig. 4.51 Comparison between computed and observed $z_{max}$

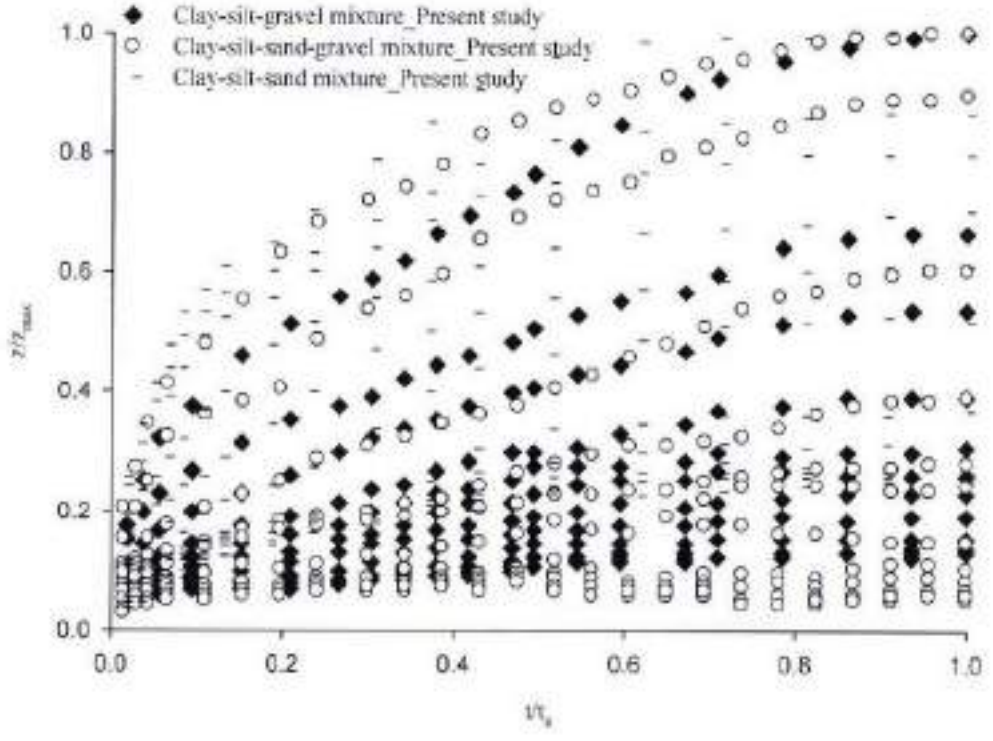


Fig. 4.52 Variation of $\frac{z}{z_{max}}$ with $\frac{t}{t_e}$ for 10% clay in the mixtures

The variation of $z/z_{max}$ with dimensionless parameters $t/t_e$ and $x/L_{max}$ has been plotted in Fig. 4.52 and 4.53 respectively. Figure 4.52 shows the channel bed degradation increases with the increase of time as the degradation building up with progress of time. In Fig. 4.52 only data of sediment mixtures having 10% clay is included for the purpose of clarity of data trend. Figure 4.53 shows the degradation in the channel bed decreases as moved from upstream to downstream end longitudinally in an exponential fashion i.e. more degradation occurred towards upstream compared to downstream of working section. The flow of water is clear at the entrance of working section so it has enough capacity to erode and carry the sediment along with the flow, however, its eroding capacity decreases as moved longitudinally from upstream to downstream end of working section due to carrying of sediment with it. That's why comparatively more degradation occurred towards upstream of working section.

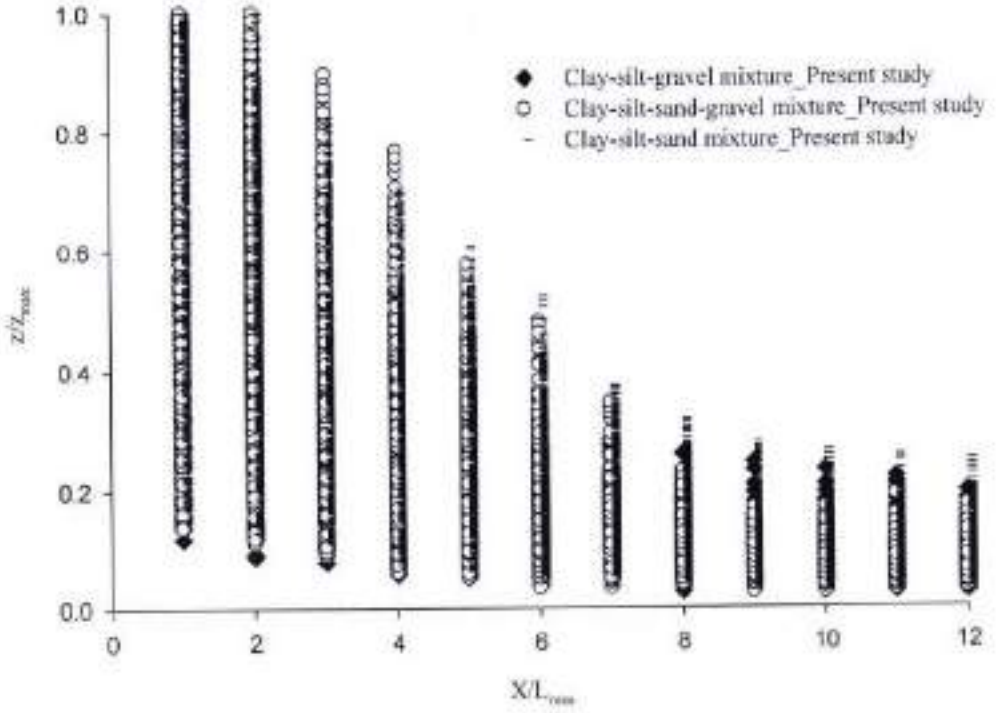


Fig. 4.53 Variation of $\frac{z}{z_{max}}$ of with $\frac{X}{L_{max}}$

The following relationships are proposed for the computation of transient bed profile for the cohesive sediment mixture in the present study based on functional relationship Eq. (4.67):

$$\frac{z}{z_{max}} = 1.256\left(\frac{t}{t_e}\right)^{0.383} e^{-0.235\frac{X}{L_{max}}} \tag{4.68}$$

$$\frac{z}{z_{max}} = 1.29\left(\frac{t}{t_e}\right)^{0.253} e^{-0.261\frac{X}{L_{max}}} \tag{4.69}$$

$$\frac{z}{z_{max}} = 1.205\left(\frac{t}{t_e}\right)^{0.365} e^{-0.19\frac{X}{L_{max}}} \tag{4.70}$$

Equations (4.68), (4.69), and (4.70) represent the relationship for the computation of transient bed profile for the cohesive sediment mixture of clay-silt-gravel, clay-silt-sand-gravel,

and clay-silt-sand respectively based on the present study data. The computed value from equations (4.68), (4.69), and (4.70) for $z/z_{max}$ shows a good agreement with the observed data as well as good regression coefficient as illustrated in Fig. 4.54(a-c) for all the three cohesive sediment mixture used in the present study. The plot has also been made between computed and observed value of degradation along the channel bed at each point of 50 cm interval as illustrated in Figs. 4.55 – 4.69 for the cohesive mixture of clay-silt-gravel, clay-silt-sand-gravel, and clay-silt-sand which shows a good match between observed and computed bed profiles. The plot has been made for bed profiles for three different time period i.e. during initial period of run, mid period, and end of run for ex. Figs. 4.55, 4.56, 4.57, 4.58, and 4.59 shows the bed profiles for 10%, 20%, 30%, 40%, & 50% clay respectively in the mixture of clay-silt-gravel for initial, mid, and end period of time.

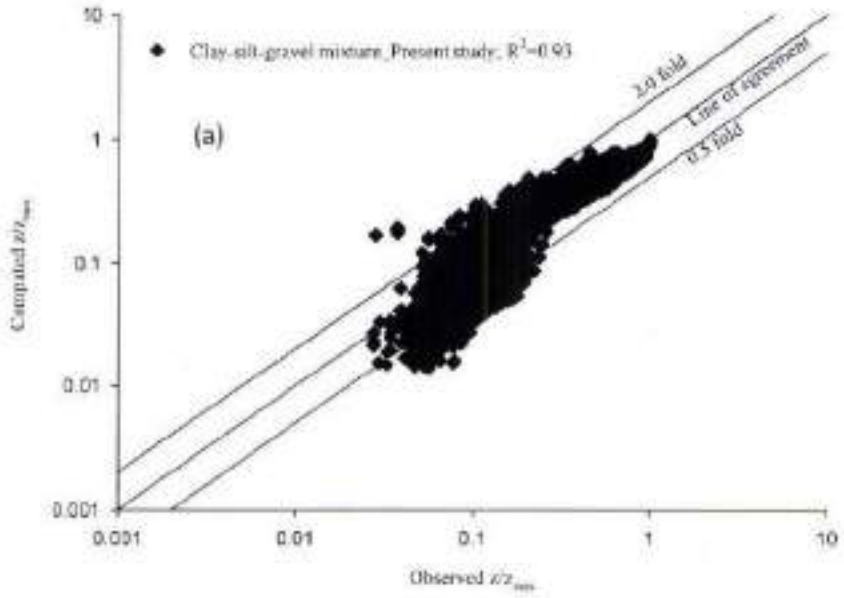


Fig. 4.54a Comparison between computed and observed $\frac{z}{z_{max}}$

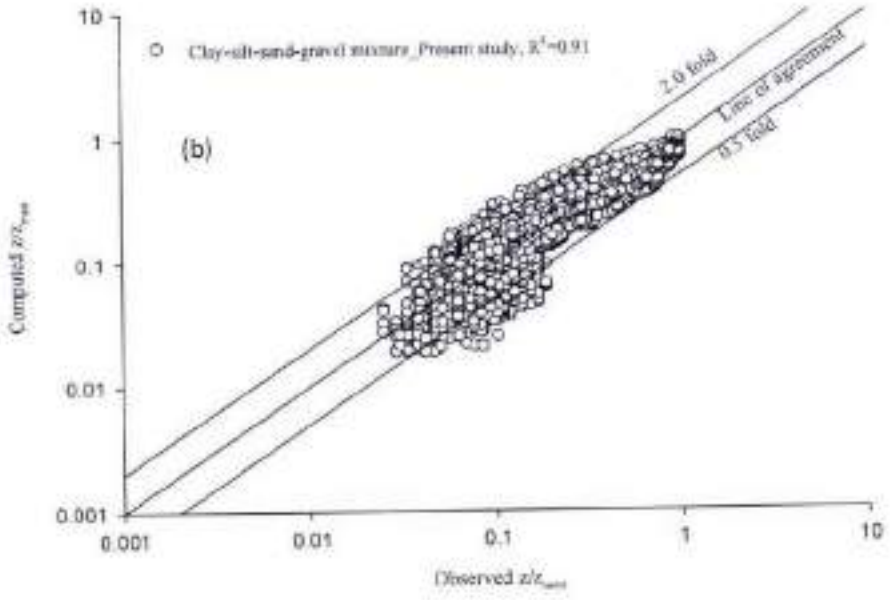


Fig. 4.54b Comparison between computed and observed $\frac{z}{z_{max}}$

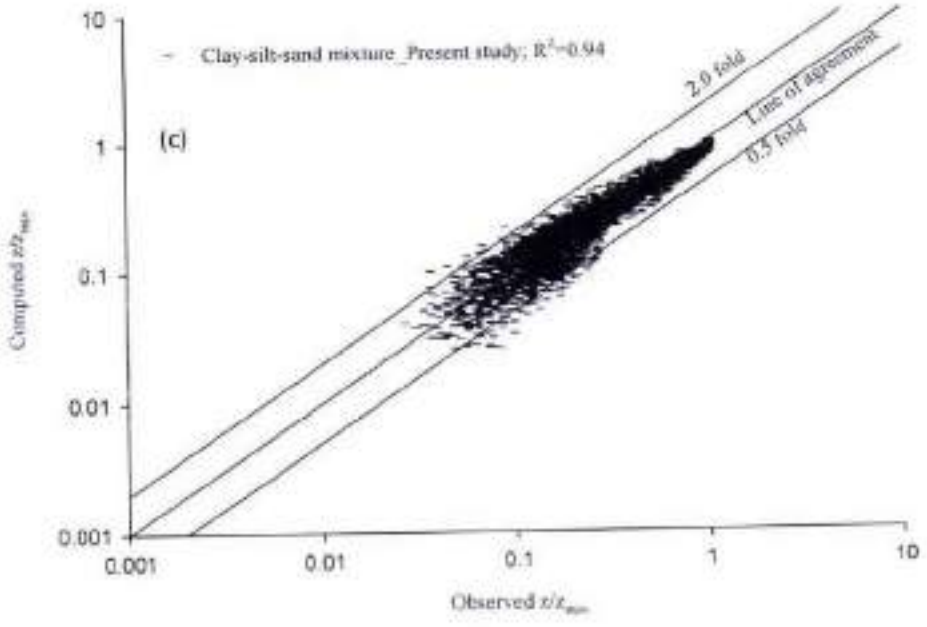


Fig. 4.54c Comparison between computed and observed $\frac{z}{z_{max}}$

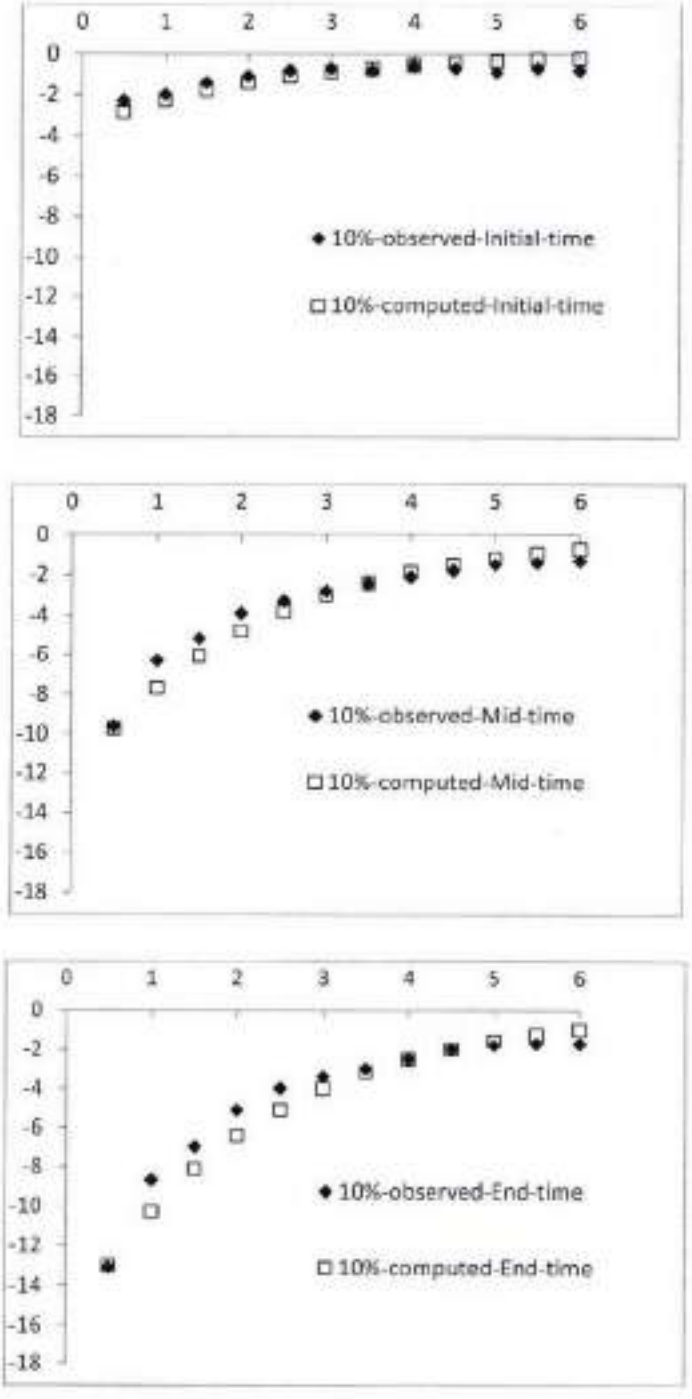


Fig. 4.55 Comparison between computed and observed bed profile for 10% clay in clay-silt-gravel mixture

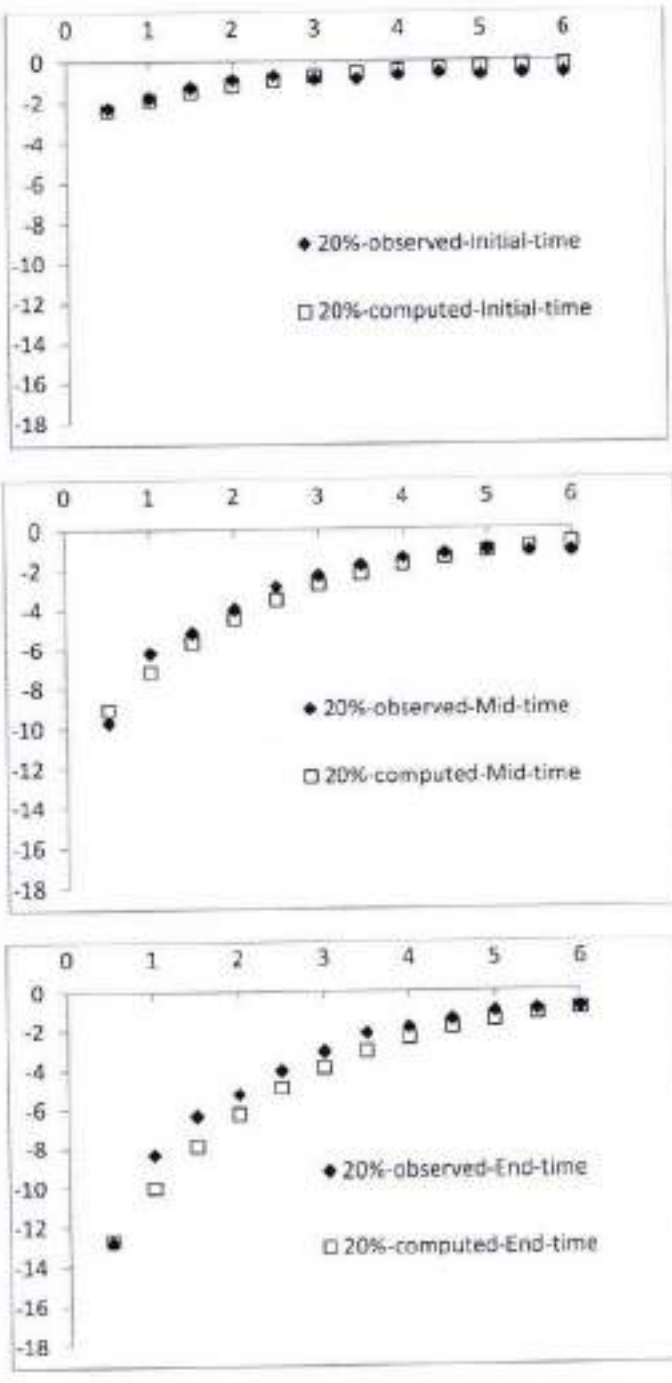


Fig. 4.56 Comparison between computed and observed bed profile for 20% clay in clay-silt-gravel mixture

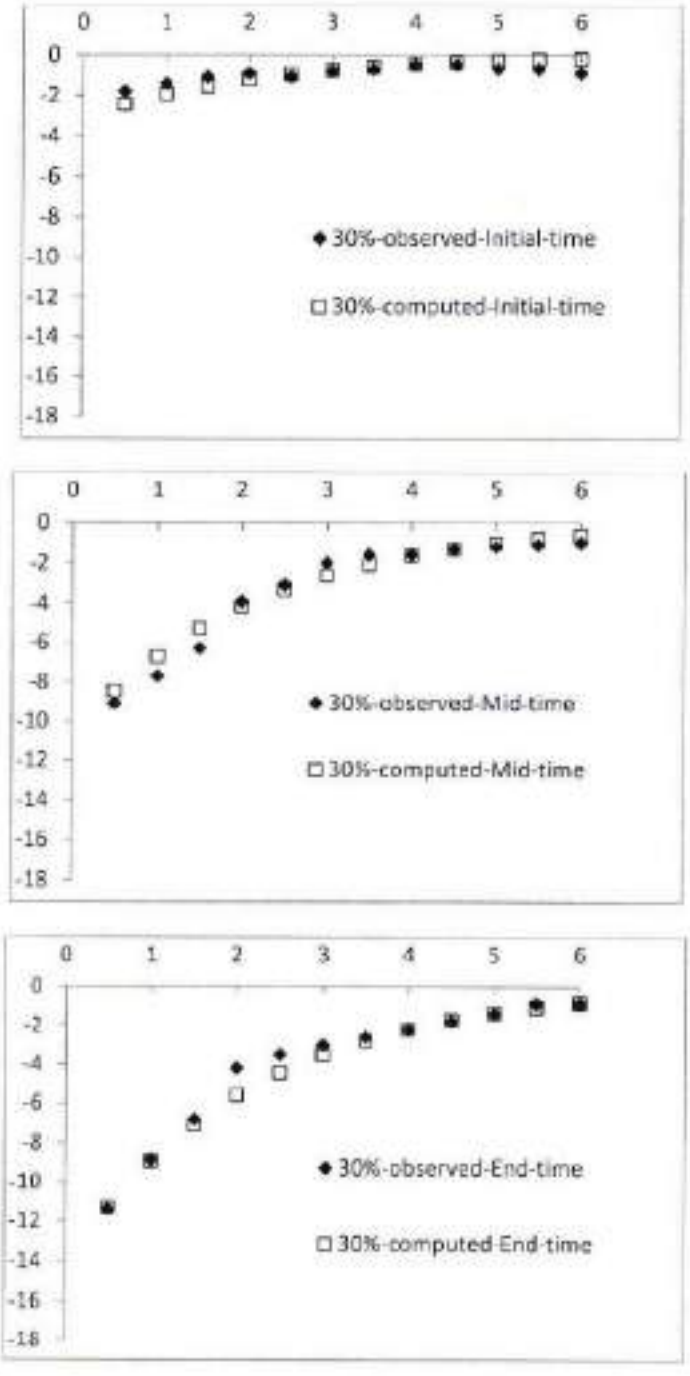


Fig. 4.57 Comparison between computed and observed bed profile for 30% clay in clay-silt-gravel mixture

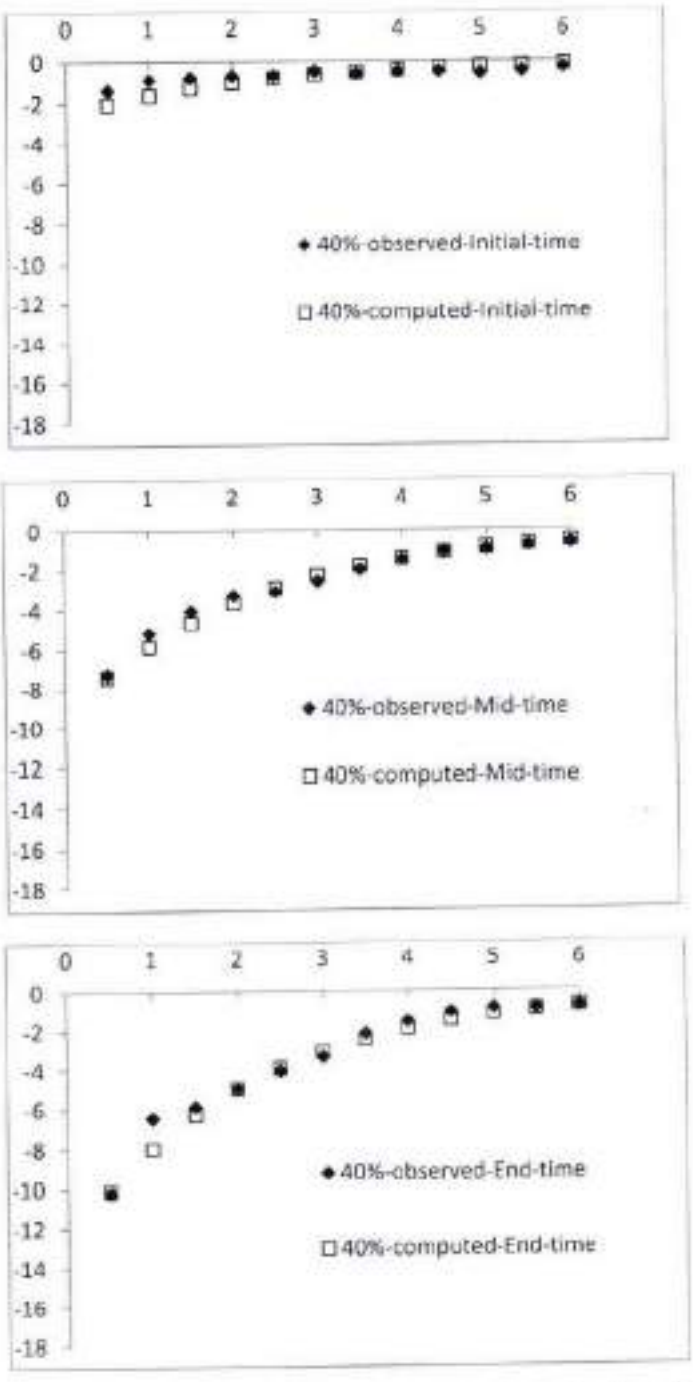


Fig. 4.58 Comparison between computed and observed bed profile for 40% clay in clay-silt-gravel mixture

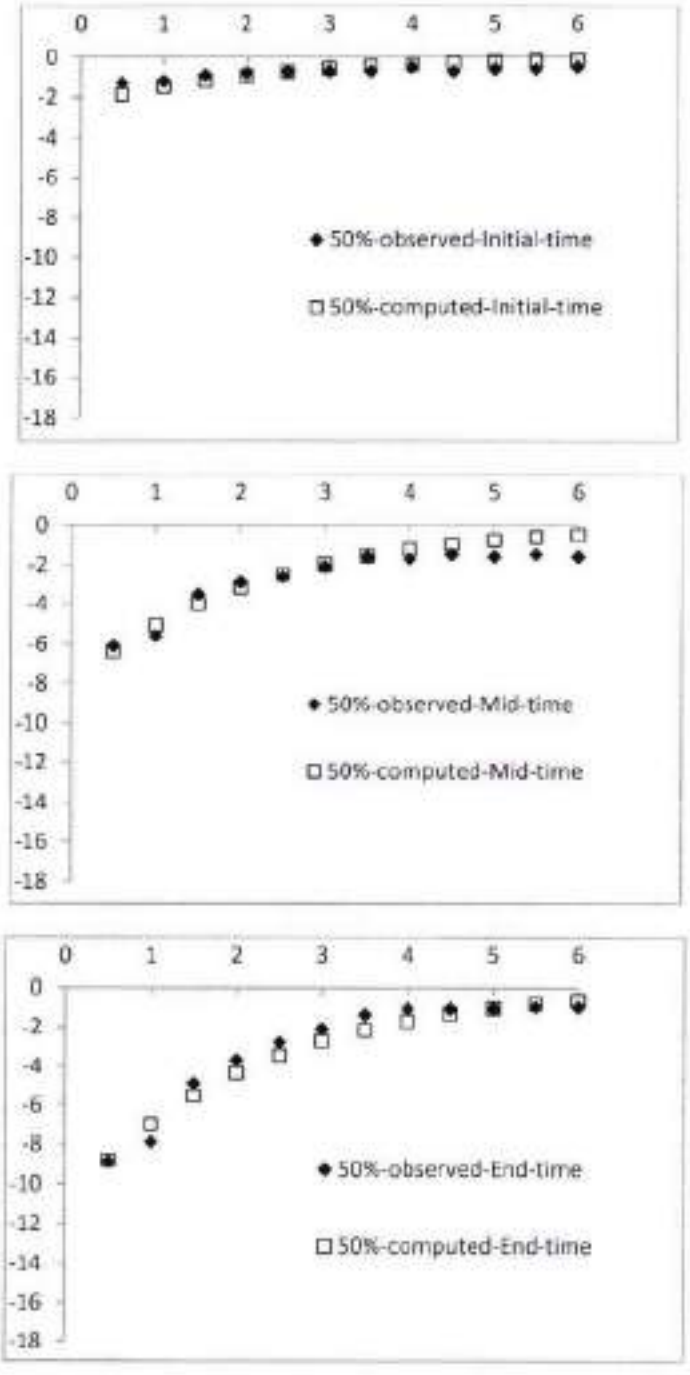


Fig. 4.59 Comparison between computed and observed bed profile for 50% clay in clay-silt-gravel mixture

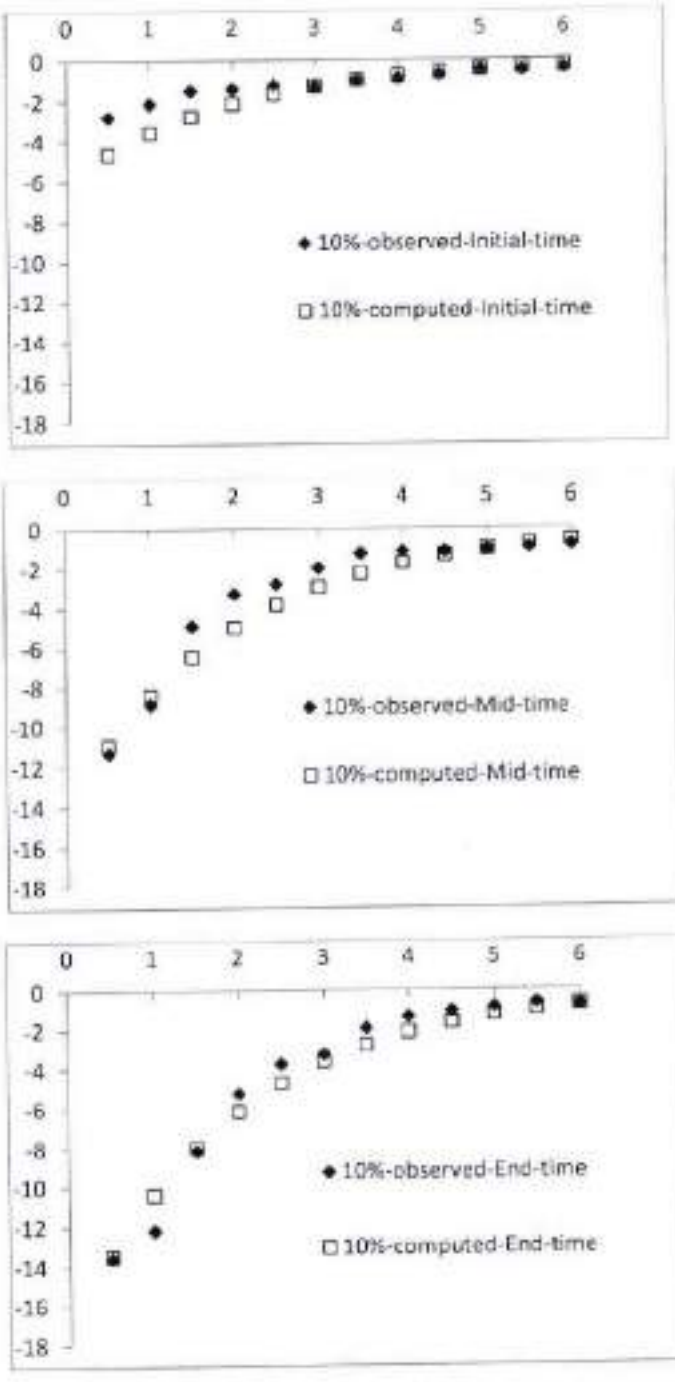


Fig. 4.60 Comparison between computed and observed bed profile for 10% clay in clay-silt-sand-gravel mixture

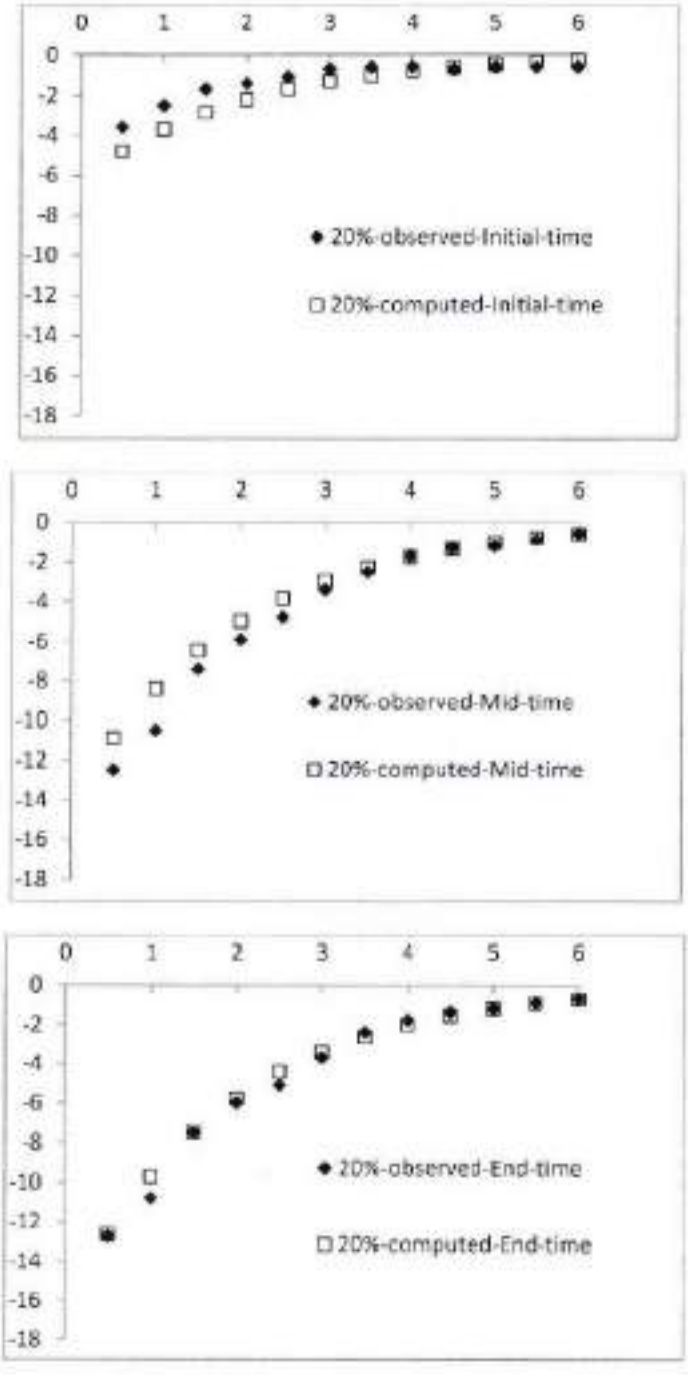


Fig. 4.61 Comparison between computed and observed bed profile for 20% clay in clay-silt-sand-gravel mixture

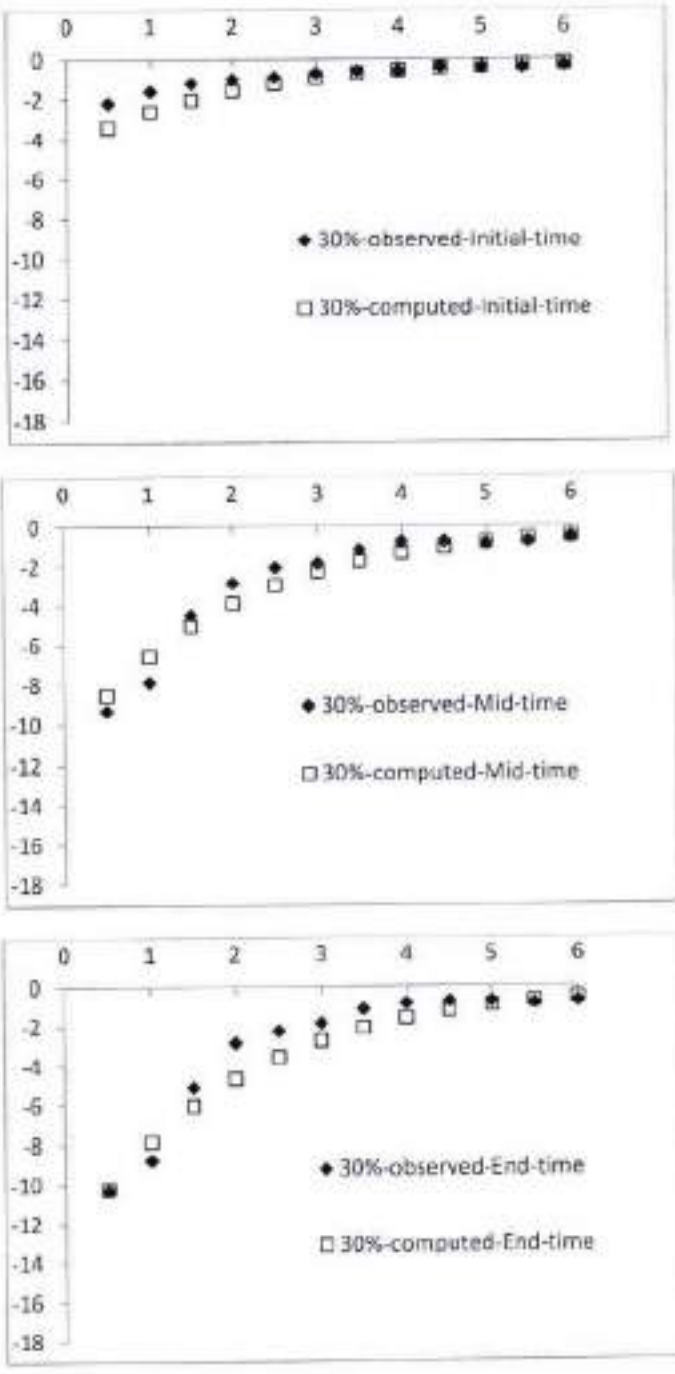


Fig. 4.62 Comparison between computed and observed bed profile for 30% clay in clay-silt-sand-gravel mixture

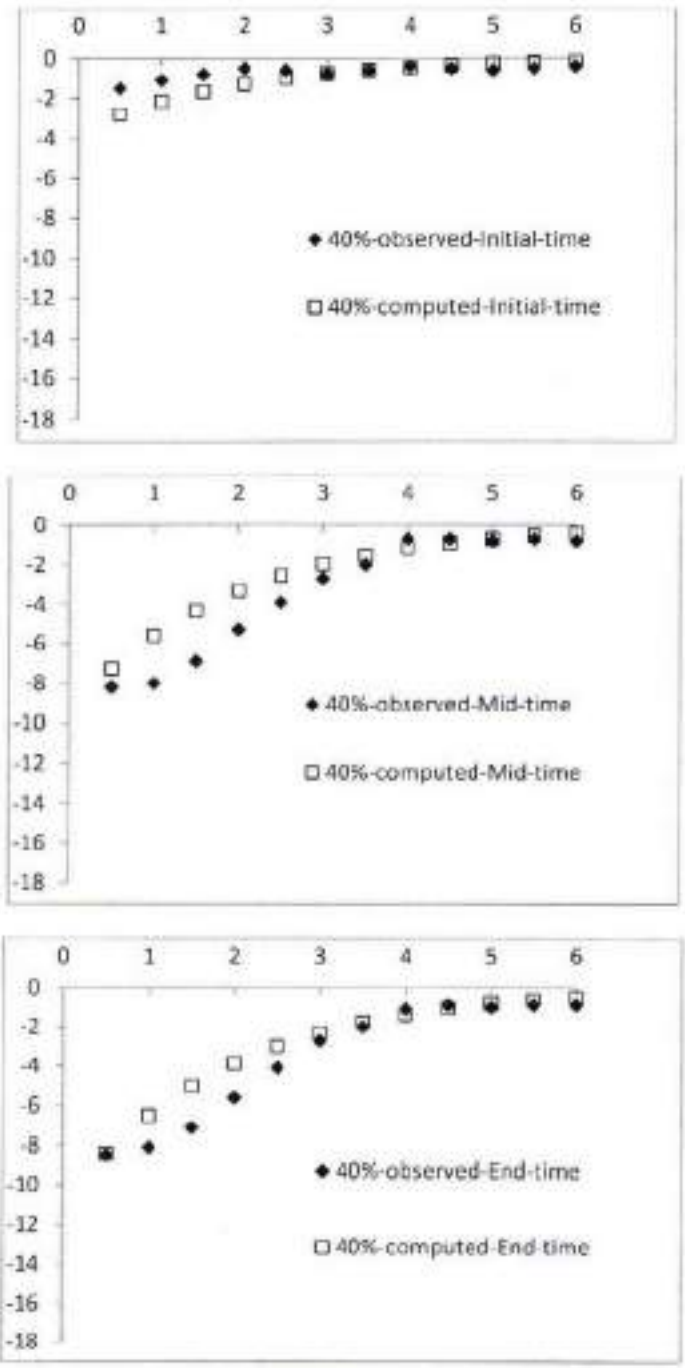


Fig. 4.63 Comparison between computed and observed bed profile for 40% clay in clay-silt-sand-gravel mixture

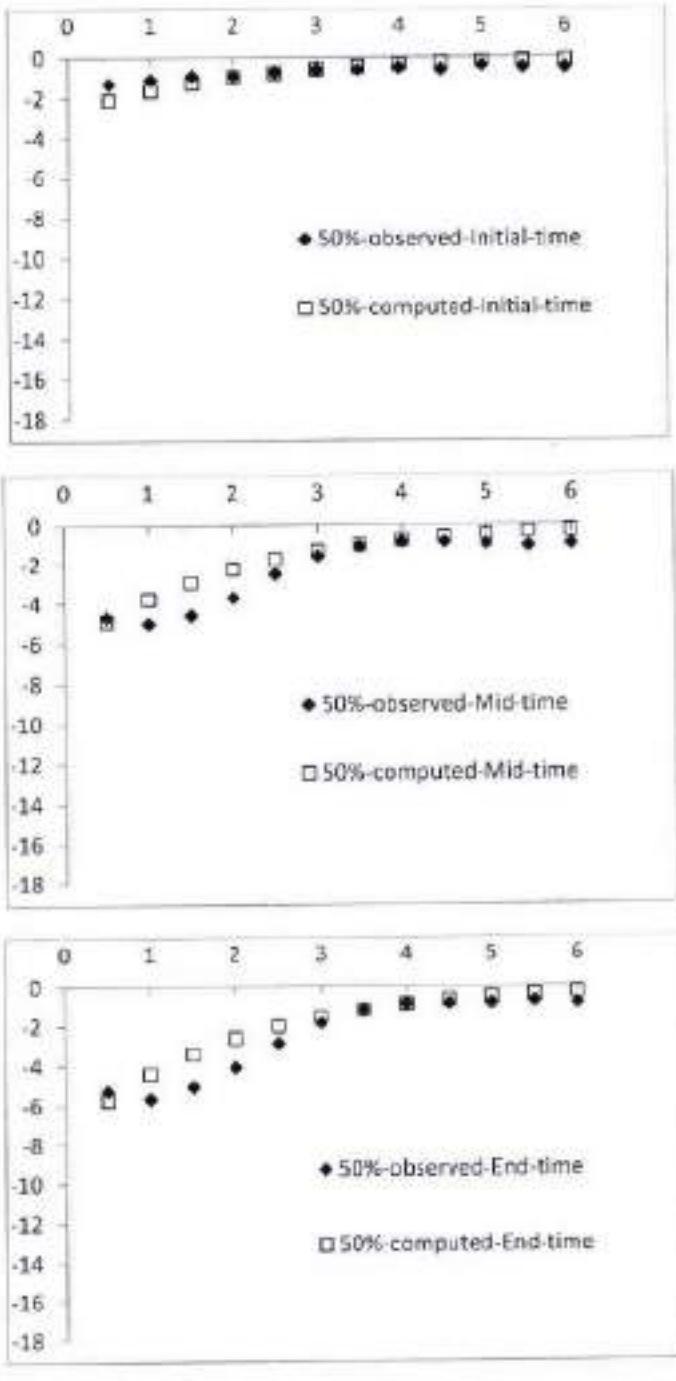


Fig. 4.64 Comparison between computed and observed bed profile for 50% clay in clay-silt-sand-gravel mixture

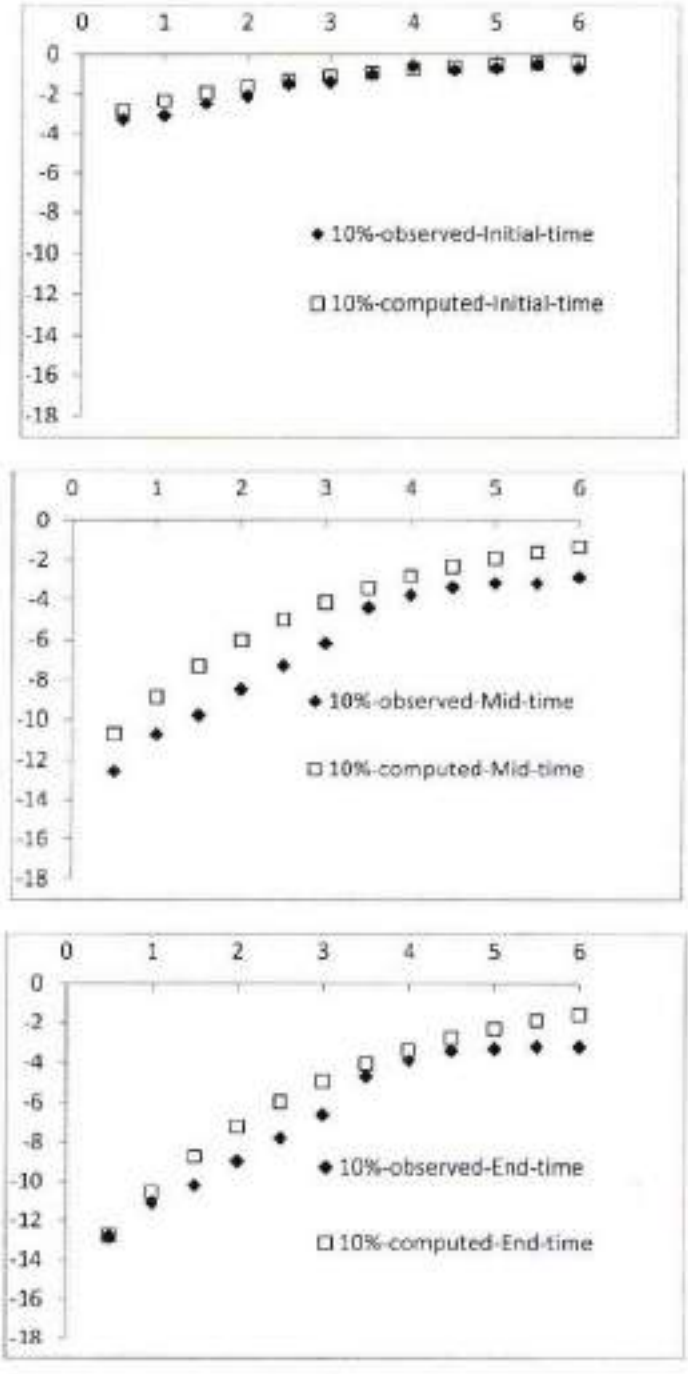


Fig. 4.65 Comparison between computed and observed bed profile for 10% clay in clay-silt-sand mixture

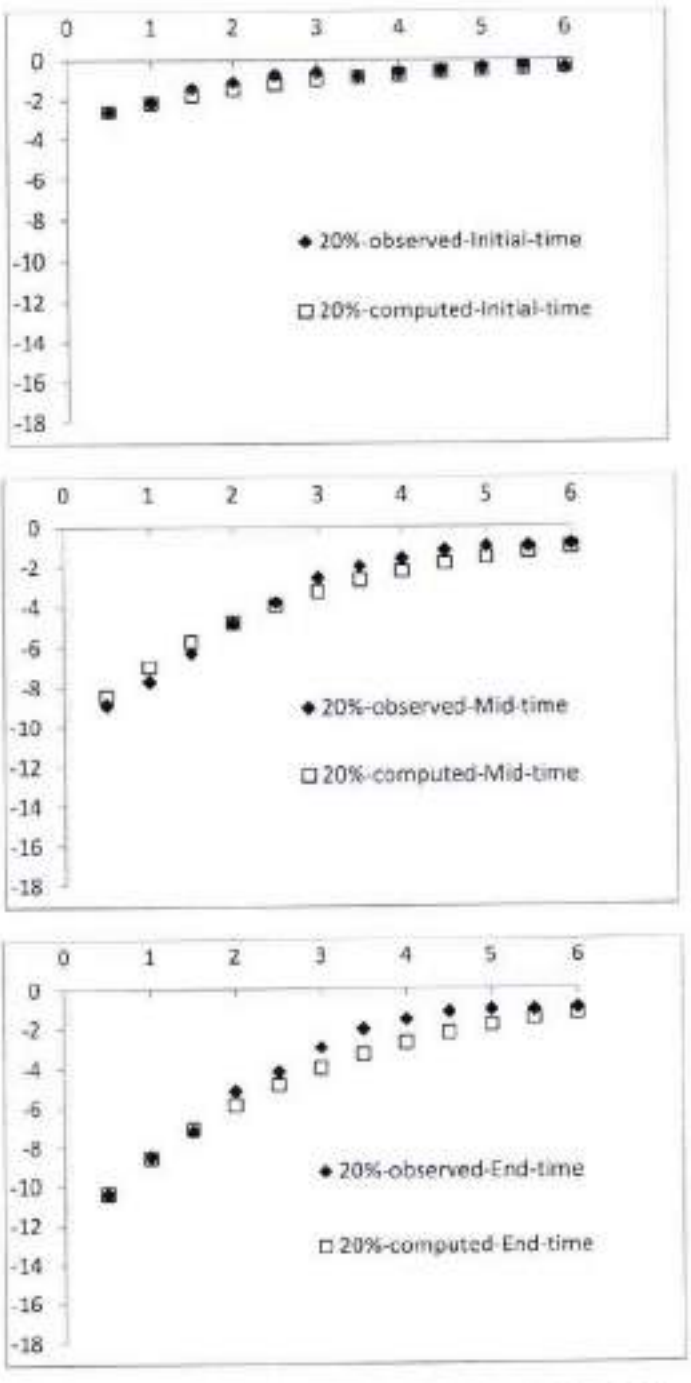


Fig. 4.66 Comparison between computed and observed bed profile for 20% clay in clay-silt-sand mixture

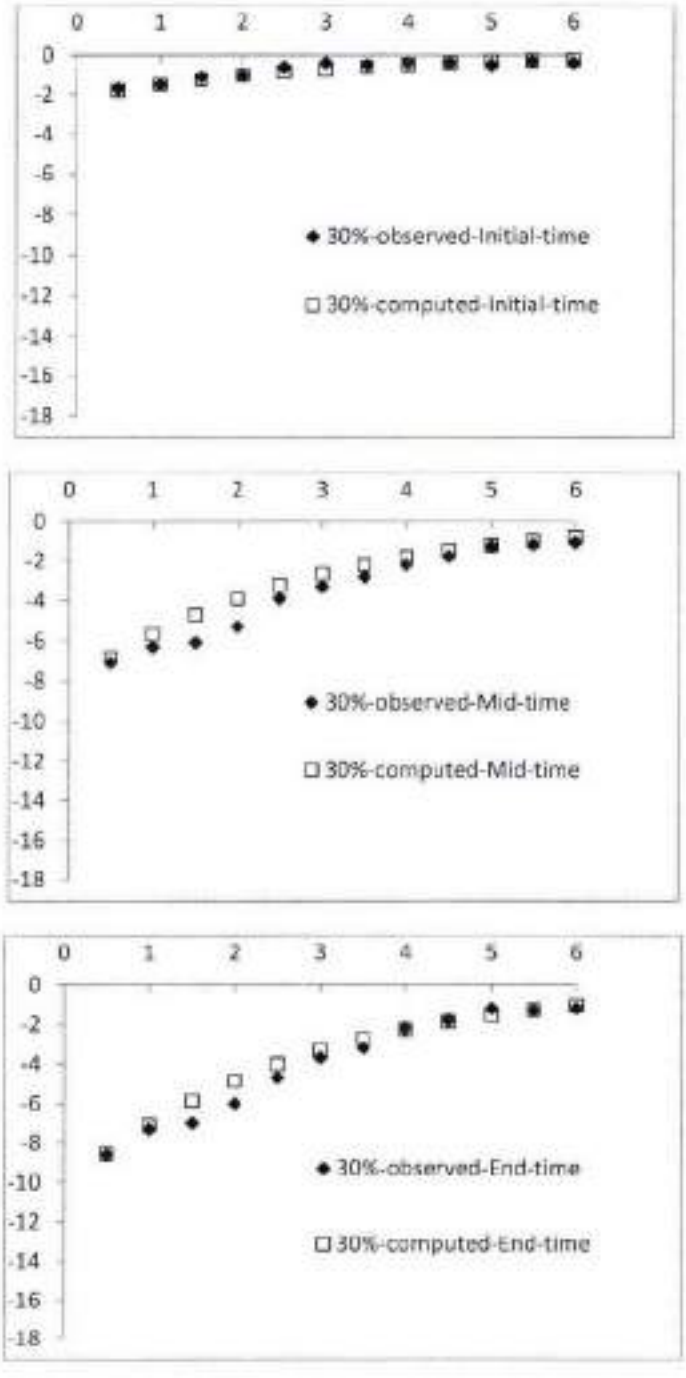


Fig. 4.67 Comparison between computed and observed bed profile for 30% clay in clay-silt-sand mixture

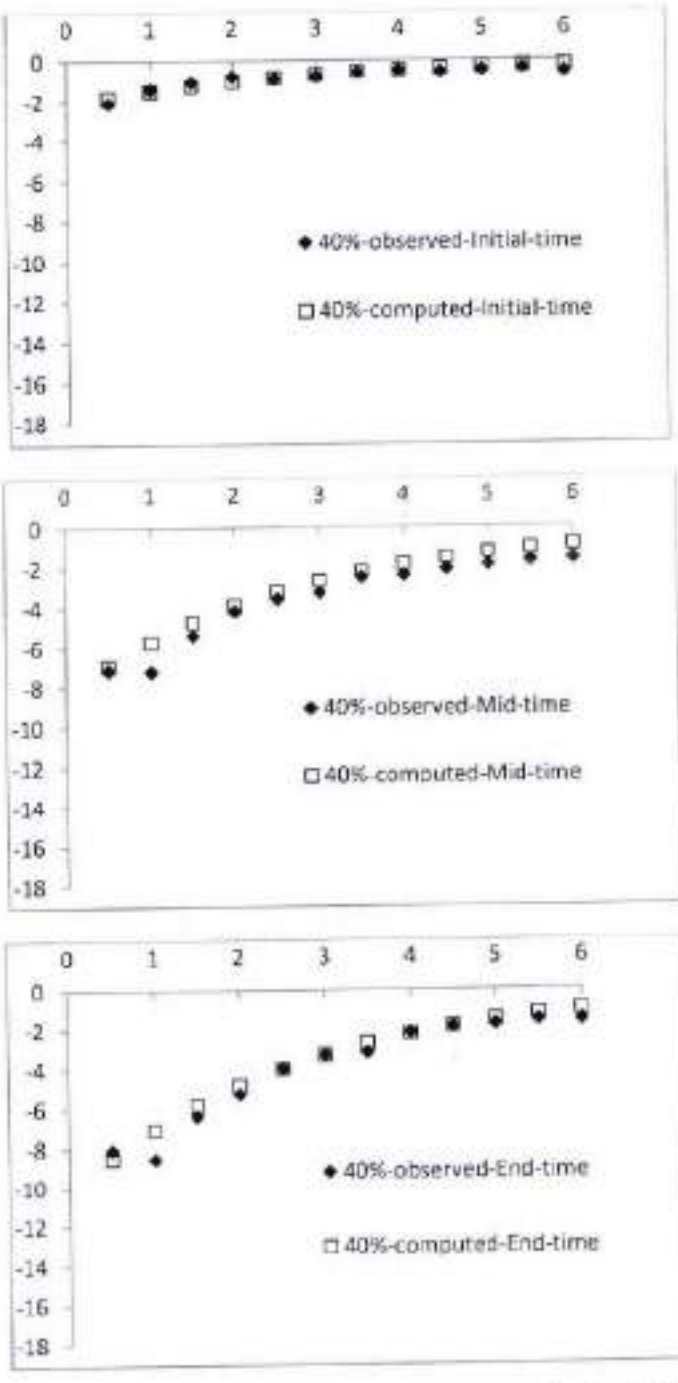


Fig. 4.68 Comparison between computed and observed bed profile for 40% clay in clay-silt-sand mixture

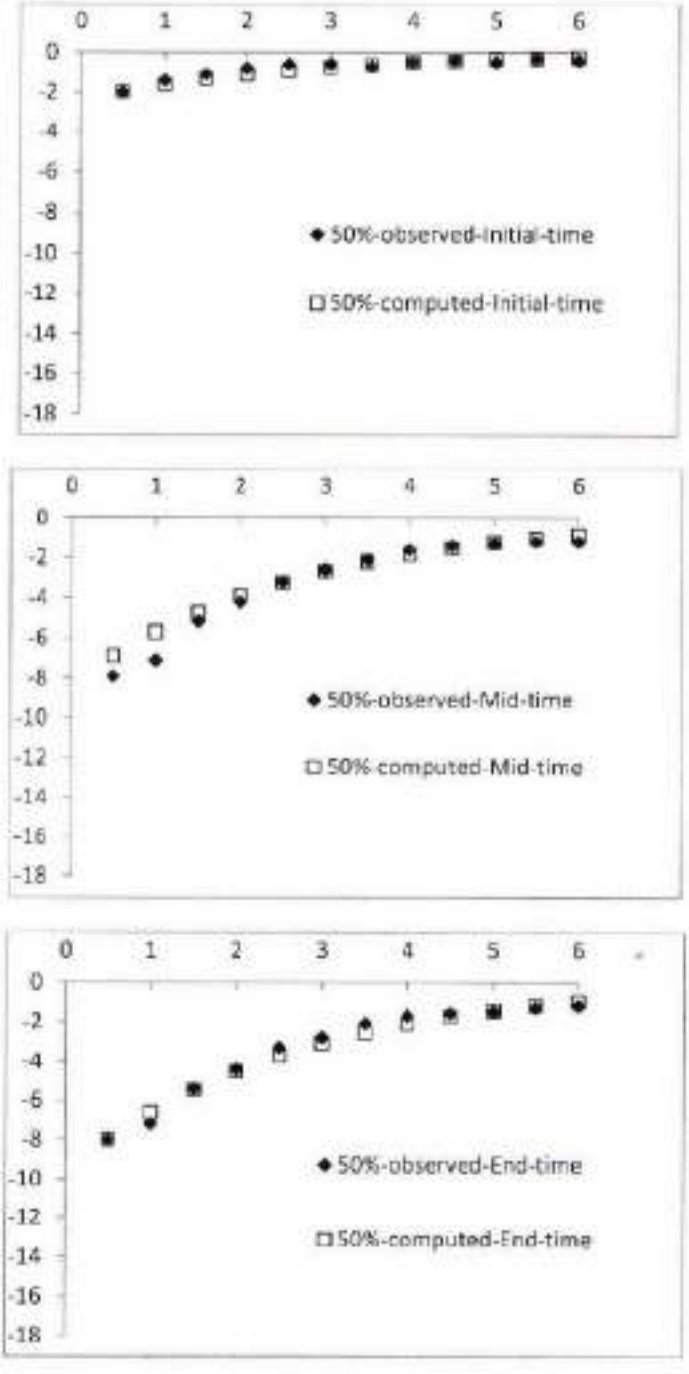


Fig. 4.69 Comparison between computed and observed bed profile for 50% clay in clay-silt-sand mixture

## 4.6 CONCLUDING REMARKS

This chapter discusses the results on incipient motion, transport rate of sediment, and transient bed profile.

- The analysis of present study reveals that initiation of detachment of particles from the cohesive bed governed by the clay percentage, weighted geometric standard deviation, and bulk density of the cohesive mixture.
- A relationship has also been developed for the computation of critical shear stress of gravel particles in cohesive mixture of clay-silt-gravel and clay-silt-sand-gravel; and for sand particles in cohesive mixture of clay-silt-sand.
- Transport rate of sediment is found to be higher in the initial period of time; however, it decreases with time. A relationship has been proposed for the computation of bed load transport rate and suspended load transport rate in terms of time, initial transport rate, equilibrium time. Formulations has also been proposed for the computation of initial transport rate and equilibrium time which has the function of clay content and excess shear stress.
- The variation of bed surface profile has been studied with time for cohesive mixture of clay-silt-gravel, clay-silt-sand-gravel, and clay-silt-sand. Degradation is observed to be higher in the upstream working section than that of downstream working section. The degradation in channel bed is higher in the initial period of time; however, it decreases with time and attained nearly static bed profile at an equilibrium time. Degradation of channel bed decreases with the increase of clay percentage. Relationship has been proposed based on the present study data for the computation of transient bed profile for cohesive sediment mixture of clay-silt-gravel, clay-silt-sand-gravel, and clay-silt-sand.

CHAPTER – V

# TURBULENCE CHARACTERISTICS OF FLOW

## 5.1 INTRODUCTION

The velocity data has been collected over degraded bed of clay-silt-sand, clay-silt-sand-gravel, and clay-silt-gravel mixtures in which clay content varies as 0%, 30%, and 50%. The results for distribution of velocity, turbulence intensity, turbulence kinetic energy, and turbulence Reynolds shear stresses over degraded bed have been presented for clay-silt-gravel, clay-silt-sand-gravel, and clay-silt-sand mixture. The results turbulence characteristics have been presented in graphical form for few runs; however, data of all runs has been incorporated in Appendix D.

## 5.2 FLOW VELOCITY

The experimentally collected raw data of flow velocity were filtered before analysis it using WinADV at the minimum signal-to-noise ratio of 17 and the minimum correlations coefficient of 70%. The points at which 3D-velocity measurements were taken illustrated in Fig. 3.14 of Chapter 3. The average velocity in three directions at these points could be computed as

$$\bar{u} = \frac{1}{N}\sum_{i=1}^{N} u_i \tag{5.1}$$

$$\bar{v} = \frac{1}{N}\sum_{i=1}^{N} v_i \tag{5.2}$$

$$\bar{w} = \frac{1}{N}\sum_{i=1}^{N} w_i \tag{5.3}$$

Where, $\bar{u}$ , $\bar{v}$ and $\bar{w}$ are the average velocity at any point in x, y and z direction respectively; $u_i$, $v_i$, and $w_i$ represents the instantaneous velocity in respective directions; and $N$ is the number of data samples collected at that point.

The instantaneous velocity fluctuations in longitudinal, lateral, and vertical directions ( $u_i', v_i', w_i'$ ) of the respective recorded instantaneous velocities ( $u_i, v_i, w_i$ ) was computed from the time averaged velocities ( $\bar{u}, \bar{v}, \bar{w}$ ) as per following equations

$$u_i' = \bar{u} - u_i \tag{5.4}$$

$$v_i' = \bar{v} - v_i \tag{5.5}$$

$$w_i' = \bar{w} - w_i \tag{5.6}$$

### 5.2.1 Longitudinal Velocity Profile

The longitudinal scaled velocity profile has been plotted against the degradation at different sections over the degraded bed for all the three mixtures used in the present study as illustrated in Figs. 5.1 to 5.8. In these figures, z is the vertical distance above or below the initial bed and z = 0 indicated the initial bed level i.e. bed level before beginning of erosion from channel bed. These plots have been made corresponding to 0%, 30% and 50% clay content in the mixture. For ex., Fig. 5.4 shows the velocity profile at different sections of the channel bed for run no. SSC 9 having 30% clay content in the mixture of clay-silt-sand. The velocity plot has been made for clay-silt-sand-gravel mixture for 50% clay content and for clay-silt-gravel mixture for 30% clay content as illustrated in Fig. 5.7 and 5.8 respectively. Velocity is found to be lower just above the bed. However, it increases as moved horizontally towards downstream or moved vertically across the flow depth towards the free surface. Due to higher degradation at the upstream section the depth of flow increases at that section which accounts for the reduction in velocity at that section; however, degradation decreases towards the downstream section that causes increase in velocity towards downstream section.

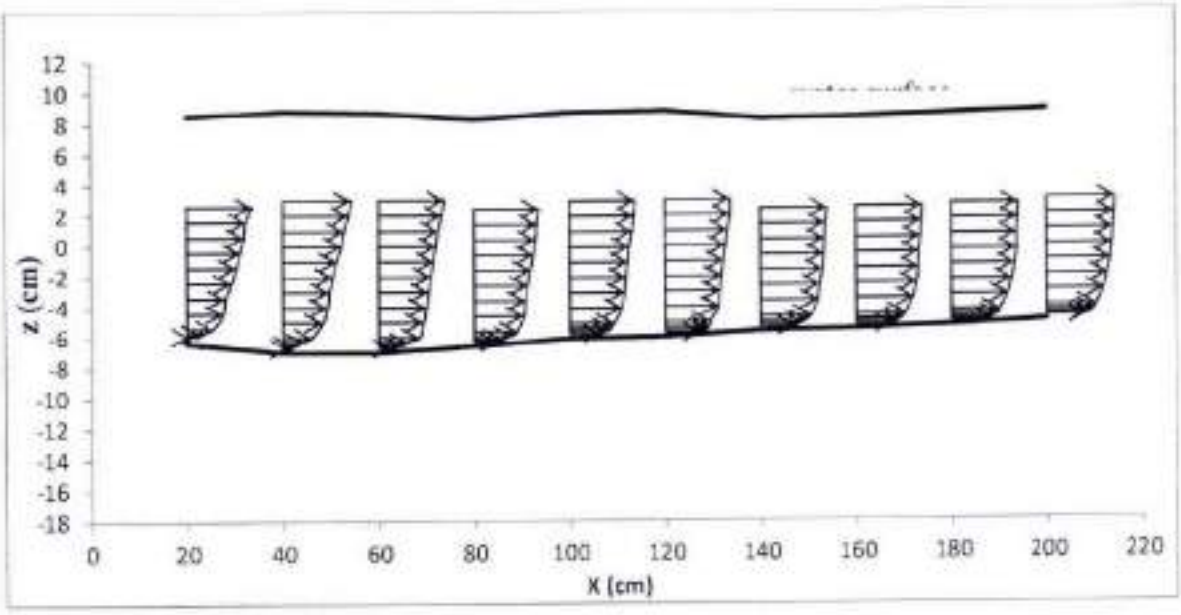


Fig. 5.1 Velocity profile over degraded bed of clay-silt-sand mixture for run no. SSC 9

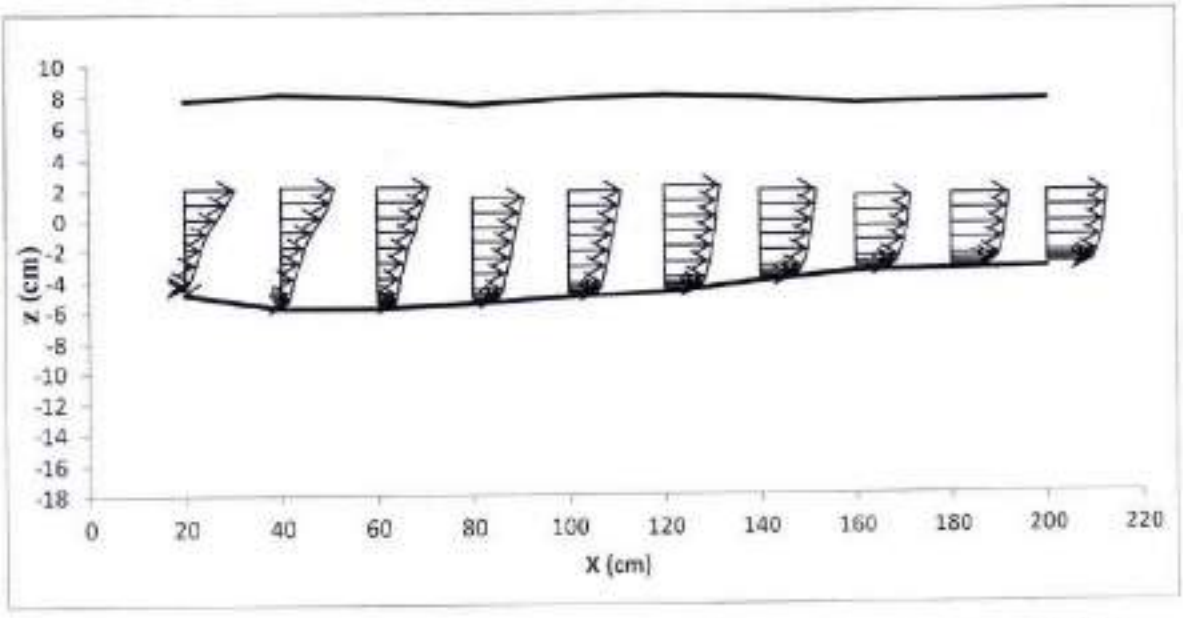


Fig. 5.2 Velocity profile over degraded bed of clay-silt-sand mixture for run no. SSC 12

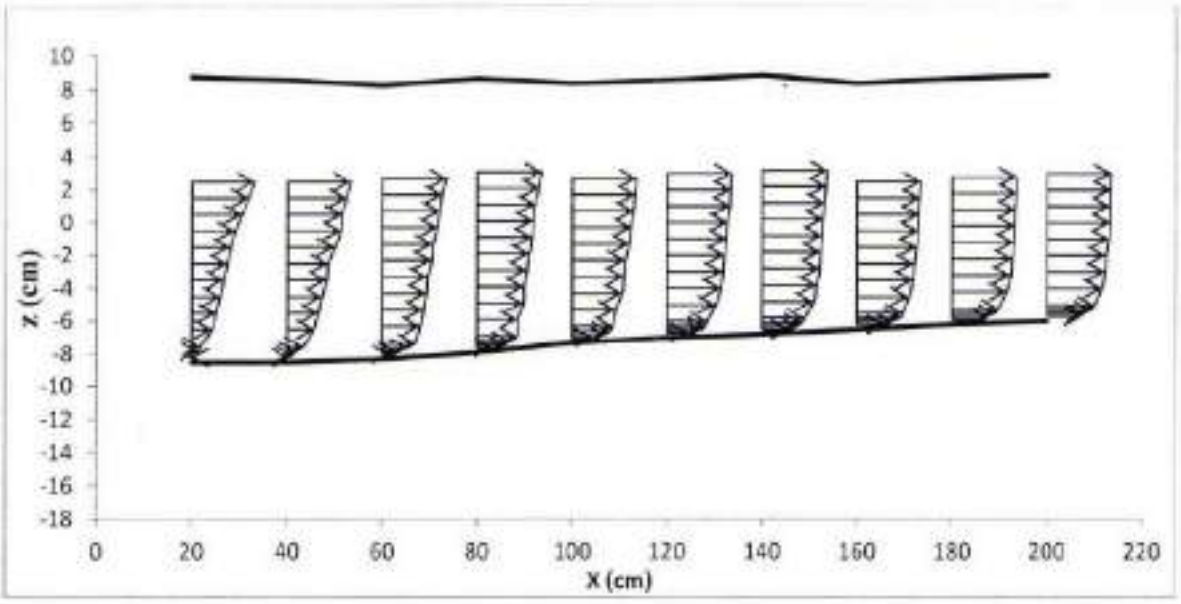


Fig. 5.3 Velocity profile over degraded bed of clay-silt-sand mixture for run no. SSC 20

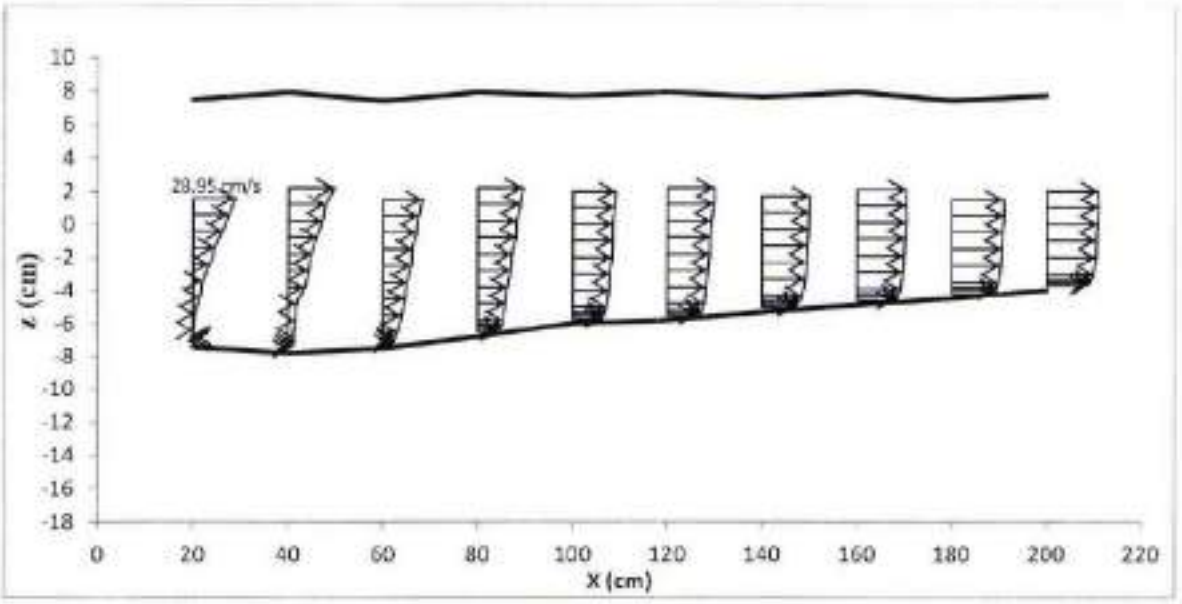


Fig. 5.4 Velocity profile over degraded bed of clay-silt-sand mixture for run no. SSC 19

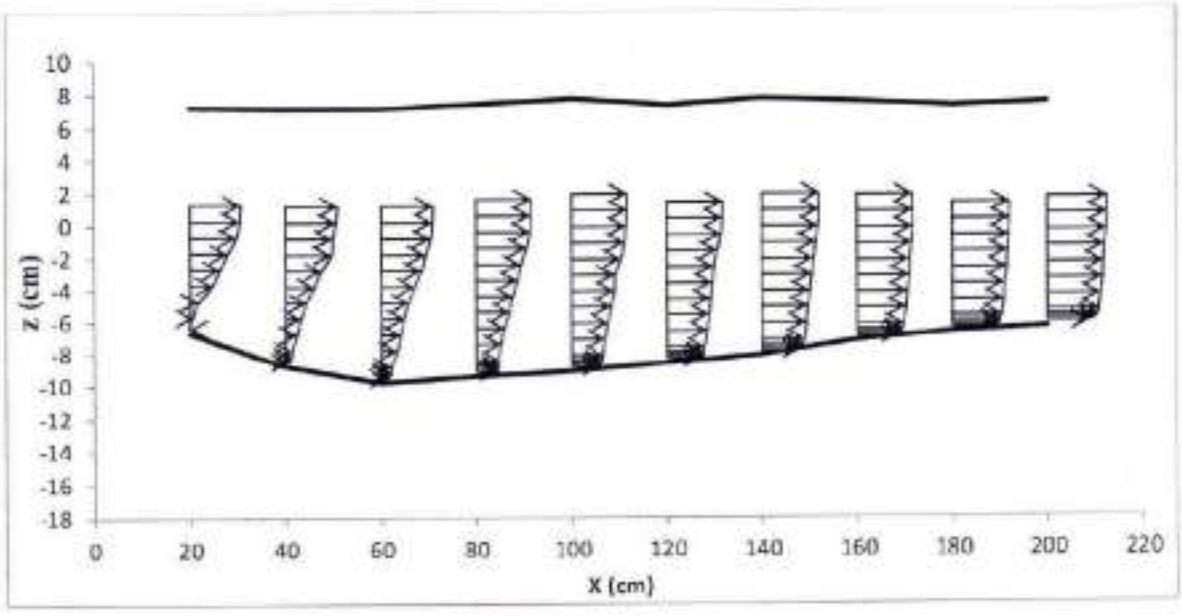


Fig. 5.5 Velocity profile over degraded bed of clay-silt-sand mixture for run no. SSC 21

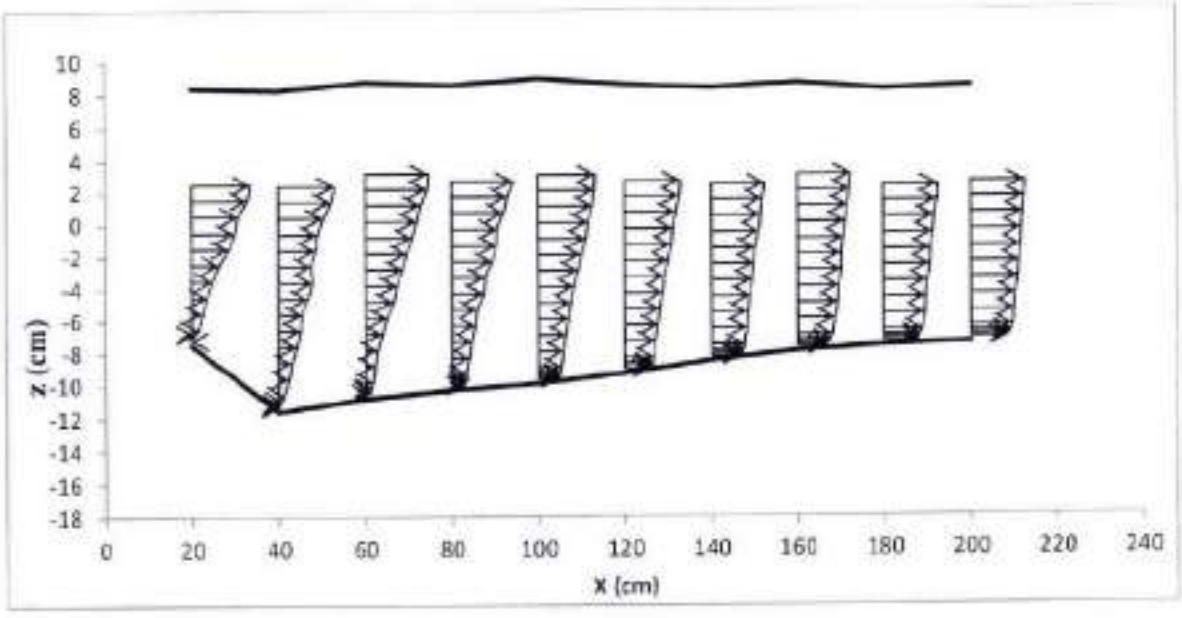


Fig. 5.6 Velocity profile over degraded bed of clay-silt-sand mixture for run no. SSC 22

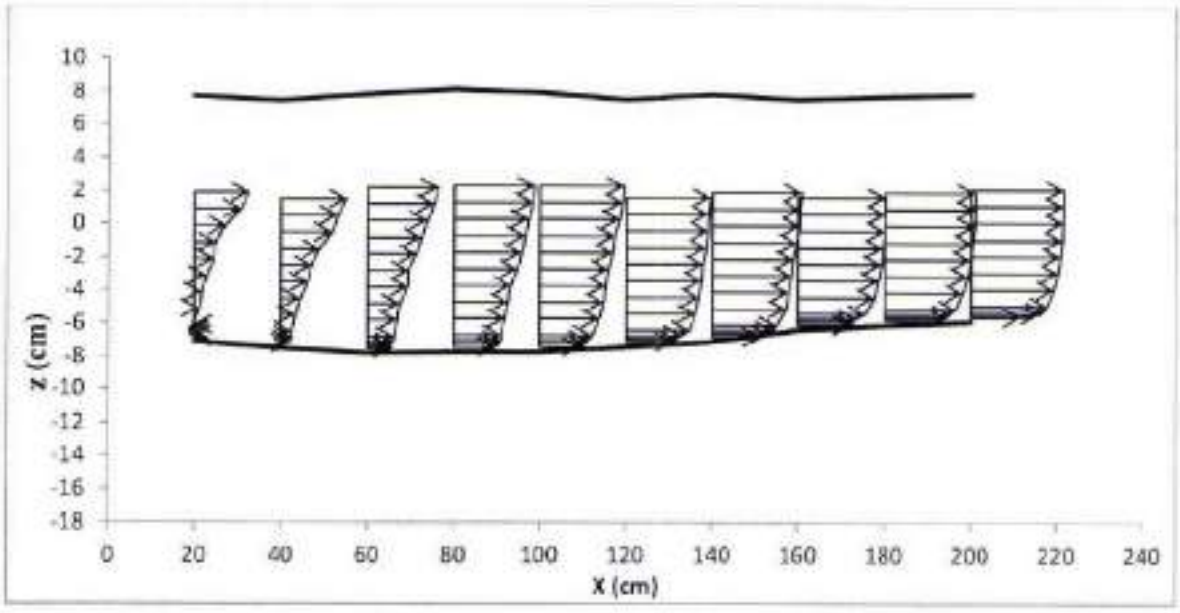


Fig. 5.7 Velocity profile over degraded bed of clay-silt-sand-gravel mixture for run no. GSSC 19

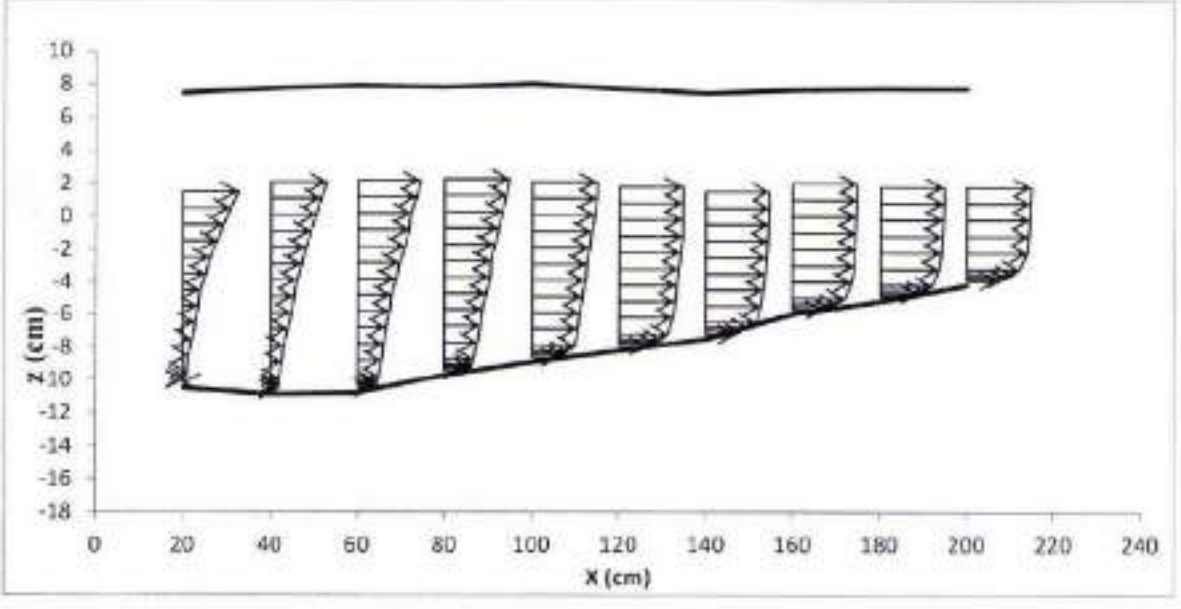


Fig. 5.8 Velocity profile over degraded bed of clay-silt-gravel mixture for run no. GSC 9

Velocity is found to be lower just above the degraded bed at upstream section. It is due to higher degradation in the upstream section of the channel bed that resulted in the higher flow depth which leads to lowering the flow velocity. However, velocity increases as moved from

upstream to downstream along the channel bed and velocity also increases as moved vertically from the channel bed to free water surface. Similar trend of data has been observed for all the runs.

### 5.2.2 Vector Plot for Resultant Velocity

The vertical distribution of resultant velocity (resultant of x-z plane) was plotted across the depth of flow at different sections together along the degraded bed corresponding to 50%, 30% and 0% clay content in the channel bed for all the mixture as illustrated in Figs. 5.9 to 5.16. For ex. Fig. 5.9 shows the plot corresponding to run number SSC 9 which has 50% clay in the sediment mixture of clay-silt-sand. The resultant flow velocity (in x-z plane) was found to be reversal near the bed surface especially in the upstream of working section. This reversal flow mainly observed around the section where maximum degradation taken place. The magnitude of velocity is low near the bed surface; however, it increases as moved towards downstream section. Velocity is increases across the depth of flow at each section as moved towards free water surface from the bottom bed. However, variation in velocity was significantly noticeable in the upstream part of working section. The variation in velocity was found to be minimum over the degraded bed having 50% clay content. The variation in velocity was reduced as the clay percentage in the channel bed increases from 0% to 50%. This variation in velocity is attributed to the level of degradation in the channel bed which found to be decreases as clay percentage rise from 0% to 50%. The similar trend of data pattern has been found for all the three mixture.

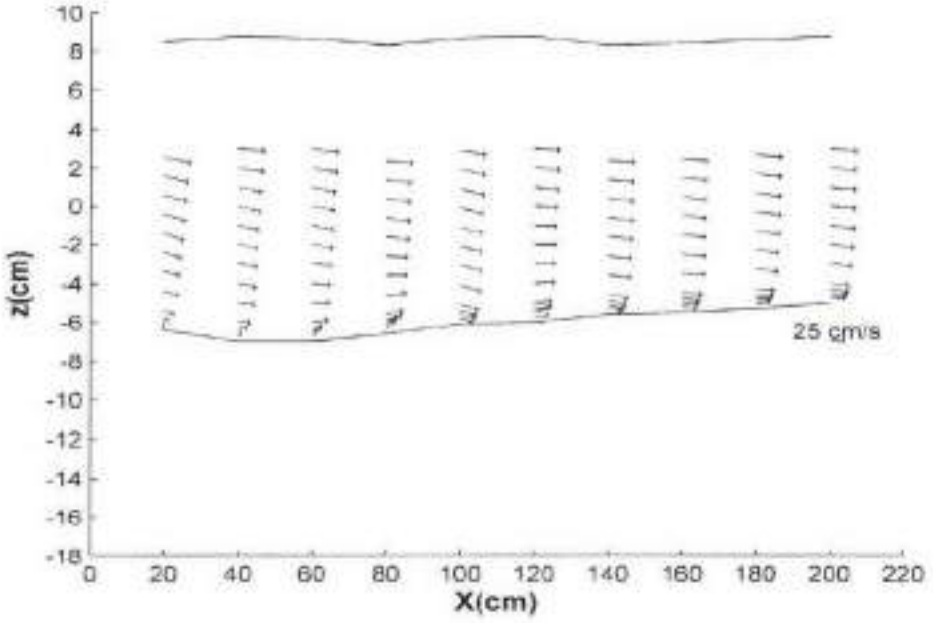


Fig. 5.9 Distribution of resultant velocity for clay-silt-sand mixture for run no. SSC 9

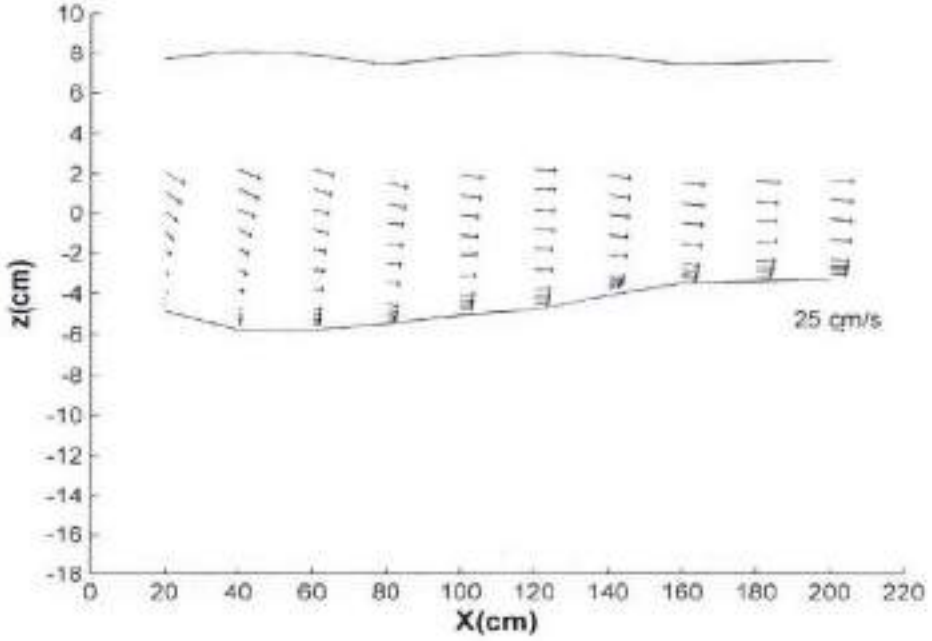


Fig. 5.10 Distribution of resultant velocity for clay-silt-sand mixture for run no. SSC 12

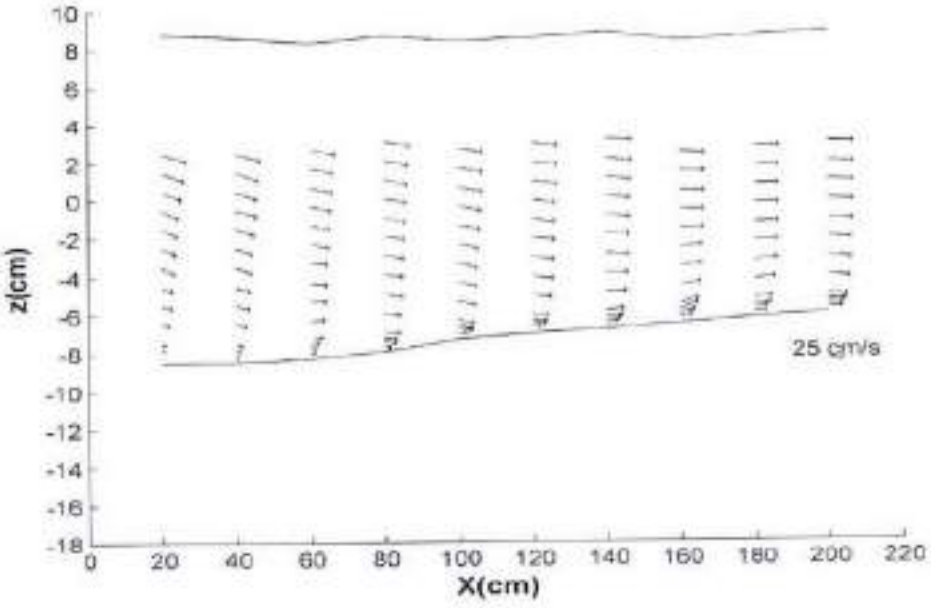


Fig. 5.11 Distribution of resultant velocity for clay-silt-sand mixture for run no. SSC 20

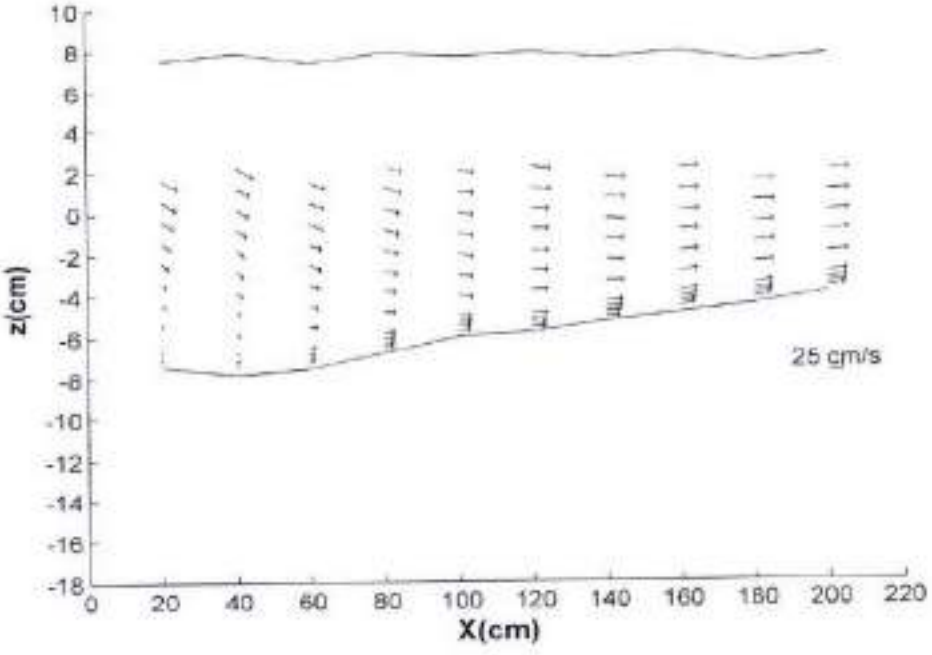


Fig. 5.12 Distribution of resultant velocity for clay-silt-sand mixture for run no. SSC 19

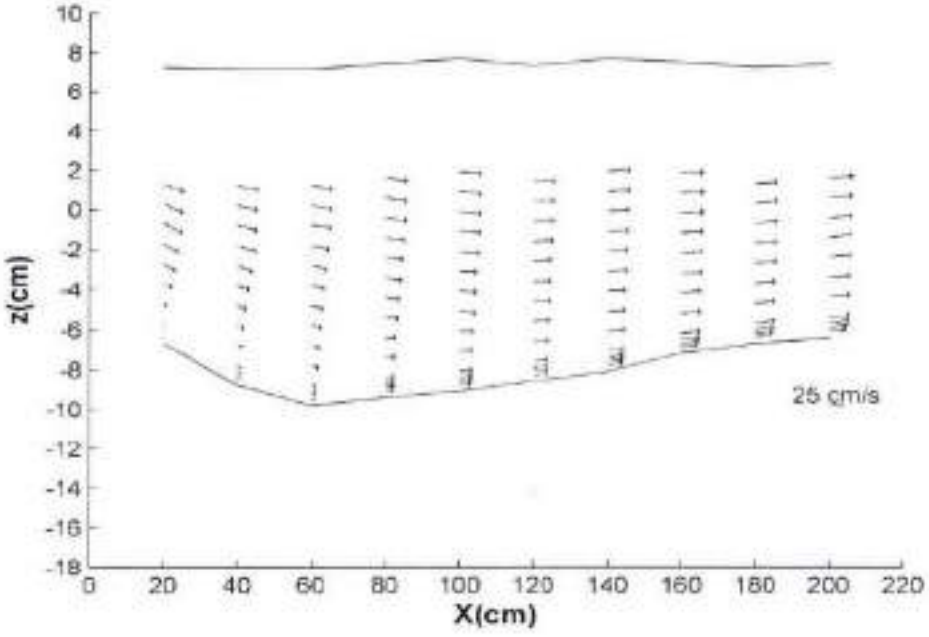


Fig. 5.13 Distribution of resultant velocity for clay-silt-sand mixture for run no. SSC 21

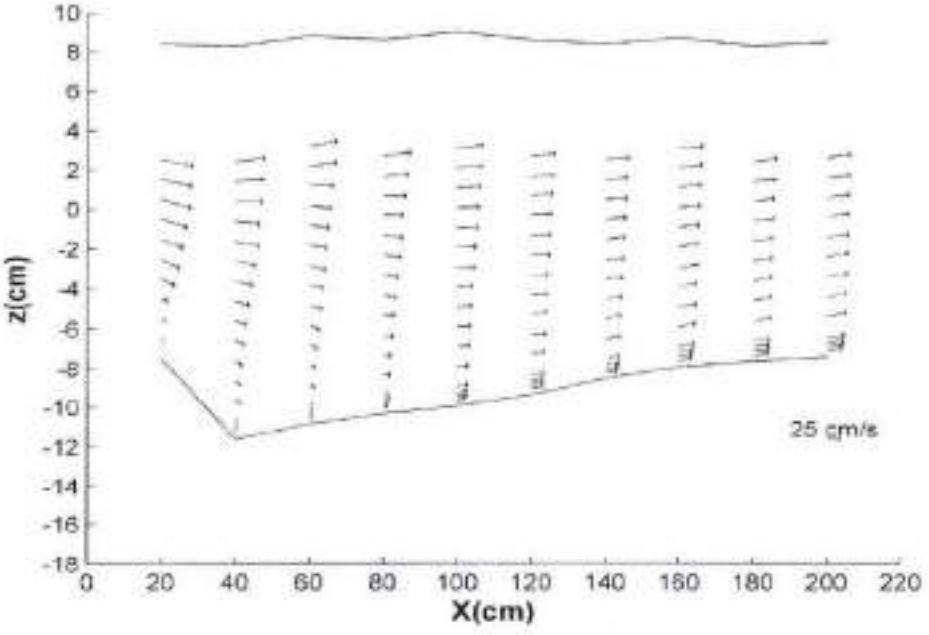


Fig. 5.14 Distribution of resultant velocity for clay-silt-sand mixture for run no. SSC 22

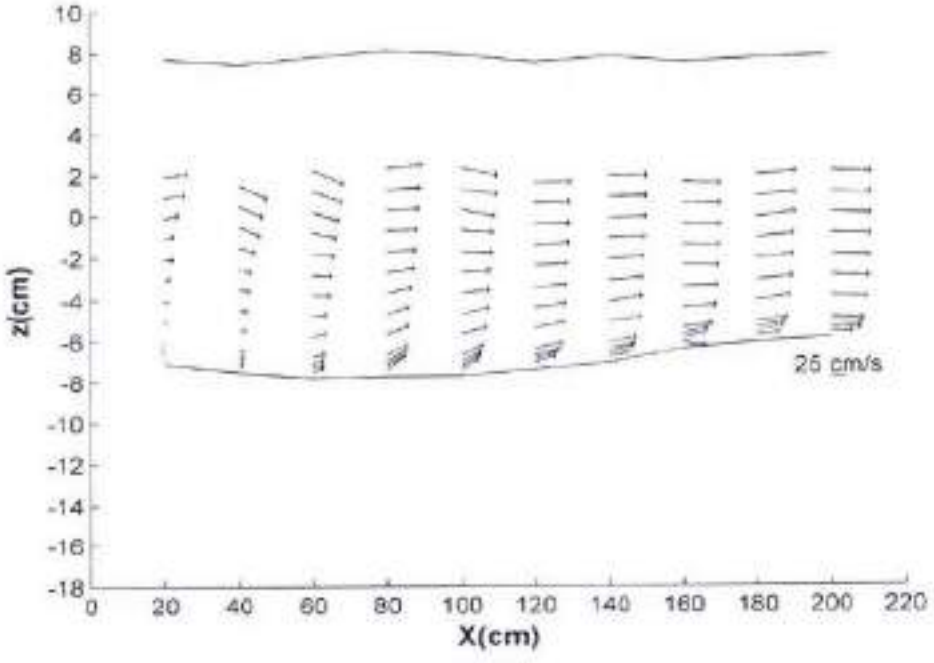


Fig. 5.15 Distribution of resultant velocity for clay-silt-sand-gravel mixture for run run no. GSSC 19

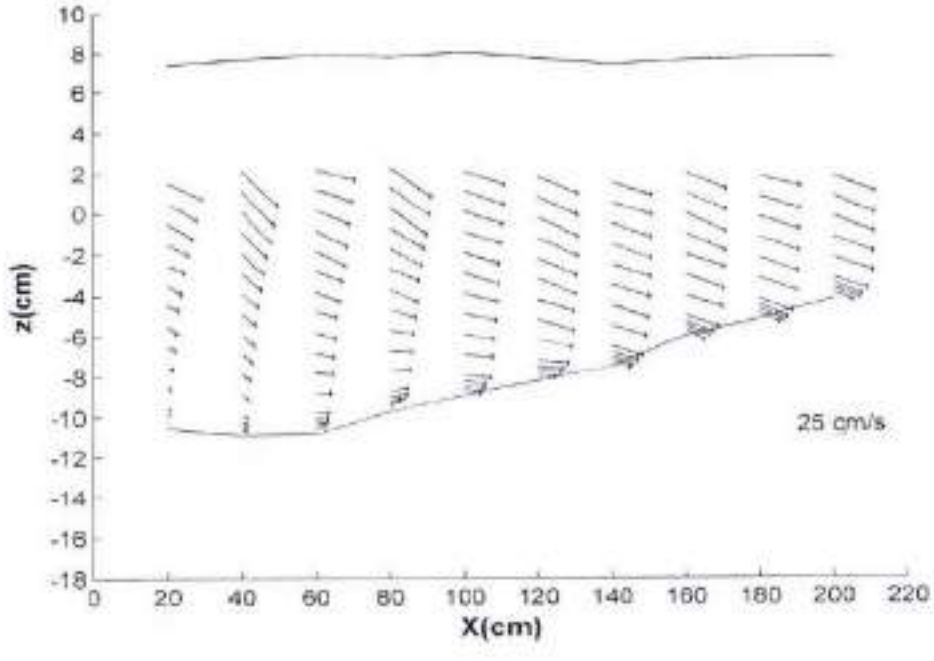


Fig. 5.16 Distribution of resultant velocity for clay-silt-gravel mixture for run no. GSC 9

### 5.2.3 Turbulence Characteristics

After filtering the raw data of velocity, turbulence parameters like turbulence intensity (TI), turbulence kinetic energy (TKE), and Reynolds shear stresses (RSS) were computed and normalized with the parameter of shear velocity of approach flow. Shear velocity ($u_*$) of approach flow was computed by $\sqrt{gRS_o}$ ; where g is acceleration gravity, $R$ is hydraulic radius, and $S_o$ is bed slope.

The turbulence intensity components in the x, y and z directions can be represented as follows:

$$TI_u = \sqrt{\overline{u'^2}} = [\frac{1}{N}\sum_{i=1}^{N}(u_i - \bar{u})^2]^{0.5} \tag{5.7}$$

$$TI_v = \sqrt{\overline{v'^2}} = [\frac{1}{N}\sum_{i=1}^{N}(v_i - \bar{v})^2]^{0.5} \tag{5.8}$$

$$TI_w = \sqrt{\overline{w'^2}} = [\frac{1}{N}\sum_{i=1}^{N}(w_i - \bar{w})^2]^{0.5} \tag{5.9}$$

Where $TI_u, TI_v$, and $TI_w$ are the turbulence intensity in x, y, and z directions respectively. The turbulence intensity in x, y, and z direction were normalized with the shear velocity of approach flow ($u_*$) and represented as

$$TI_u^+ = TI_u/u_* \tag{5.10}$$

$$TI_v^+ = TI_v/u_* \tag{5.11}$$

$$TI_w^+ = TI_w/u_* \tag{5.12}$$

Turbulent kinetic energy is one of the parameter of turbulence flow and is computed as

$$TKE = \frac{(\overline{u'^2} + \overline{v'^2} + \overline{w'^2})}{2} \tag{5.13}$$

Turbulence kinetic energy is normalized with square of shear velocity corresponding to approach flow as represented below:

$$TKE^{+} = \frac{TKE}{u_*^2} \tag{5.14}$$

Where, $TKE^{+}$ is the normalized turbulence kinetic energy.

Reynolds shear stress in x-z plane $= -u'w'$ (5.15)

$$u'w'^{+} = -u'w' / u_*^2 \tag{5.16}$$

Where, $u'w'^{+}$ is the normalized Reynolds shear stress in x-z plane.

The parameters considered for turbulence characteristics of flow are $u^{+}$, $v^{+}$, $w^{+}$, $TI_u^{+}$, $TI_v^{+}$, $TI_w^{+}$, $TKE^{+}$, and $u'w'^{+}$ in the present study. Figures 5.17(a-d) to 5.24(e-f) show the plot for turbulence parameters over the degraded channel bed for all three mixtures i.e. clay-silt-sand (SSC) mixture, clay-silt-sand-gravel (GSSC) mixture, and clay-silt-gravel (GSC) mixture. Figures 5.17(a-d) to 5.22(a-e) denote the plot for turbulence parameters over the degraded cohesive channel bed made of clay-silt-sand mixture while Fig. 5.23(a-d)-(e-f) and 5.24(a-d)-(e-f) shows the turbulence characteristics plot for clay-silt-sand-gravel mixture with 50% clay content and for clay-silt-gravel mixture with 30% clay content respectively. The parameter $u^{+}$ increases longitudinally along the flow as well as vertically across the depth of flow towards the free surface of water shown in Fig. 5.17(a). However, velocity distribution in transverse and vertical directions denoted as $v^{+}$ and $w^{+}$ found to be near to zero as illustrated in Fig. 5.17(b) and 5.17(c) respectively. The vertical normalized profiles of the turbulence intensities measured in the streamwise, transverse, and vertical directions were plotted as illustrated in Fig. 5.17(d), 5.17(e), and 5.17(f) respectively for clay-silt-sand mixture corresponding to run SSC 9.

The value of $TI_u^{+}$, $TI_v^{+}$ and $TI_w^{+}$ was found to be maximum at section near to upstream (i.e. 20 cm) and their value decreases as moved longitudinally towards downstream section as shown in Fig. 5.17(d). The similar trend has been found over the degraded bed having clay content 0%, 30%, and 50% in case of clay-silt-sand mixture. The maximum value of $TI_u^{+}$, $TI_v^{+}$ and $TI_w^{+}$ was noticed around the initial bed level (i.e. z = 0) at all sections for 30% and 50% clay content degraded bed. However, in case of 0% clay content bed the maximum value of

turbulence intensities were observed below the initial bed level for upstream sections (i.e. up to 80 cm) and their maximum value lies around initial bed level for remaining downstream sections as illustrated in Fig. 5.17(d). The magnitude of maximum value of $TI_u^+$ was noticed higher compared to $TI_v^+$ and $TI_w^+$. The maximum value of $TI_u^+$ was found near to upstream section which indicates the higher fluctuation in velocity exist there and this may be attributed to transition of bed from solid to mobile. The variation of turbulence intensity found to be increasing across the depth of flow (when moved towards free water surface from the bottom bed) and reaches to maximum and then again decreasing. This trend has been seen for few sections towards upstream (i.e. up to 80 cm), however, as moved towards downstream then it increases in fairly uniform manner with less variations. At upstream section (i.e. up to 100 cm), the value of $TI_u^+$ was noticed higher over 0% clay content bed when compared to 30% and 50% clay content bed. However, this increment in turbulence intensity reduces as moved towards the downstream section as shown in Fig. 5.17(d).

$TKE^+$ has been plotted at all sections together over each degraded bed for all the three mixture as shown in Figs. 5.17(g) to 5.24(g). The maximum value of $TKE^+$ was found around the initial bed level (i.e. $z = 0$) for 30% and 50% clay content bed. In case of 0% clay, the maximum value of $TKE^+$ was obtained below the initial bed level for upstream section (i.e. up to 80 cm) and then maximum value shifted to occurs around initial bed level for the remaining sections towards downstream. The higher variation in the value of $TKE^+$ exist for upstream section across the depth of flow (when moved from bottom bed to free water surface), however, this variation reduces as moved towards downstream section for all the three 0%, 30%, and 50% clay content degraded bed.

The plot has been made for the distribution of normalized Reynolds shear stress $u'w'^+$ at all sections for all three mixture as illustrated in Figs. 5.17(h) to 5.24(h). The maximum value of $u'w'^+$ at all section lies around the initial bed level for 30% and 50% clay content bed, however, there is different trend exist for 0% clay content bed. In case of 0% clay content bed, the maximum value of $u'w'^+$ occurs below the level of initial bed for upstream section (i.e. up to 120 cm), however, this maximum value of $u'w'^+$ shifted to occur around initial bed level as moved towards downstream section. The Reynolds shear stress $u'w'^+$ has its maximum value at all

section (except at 20 and 40 cm) for 0 % clay content bed when compared to 30% and 50% clay content bed. More variation (across the depth of flow) in the value of $u'w''$ has been observed at upstream sections (i.e. up to 100 cm), however, this variation across the depth of flow reduces as moved towards downstream section. This trend has been found similar for 0%, 30%, and 50% clay content bed.

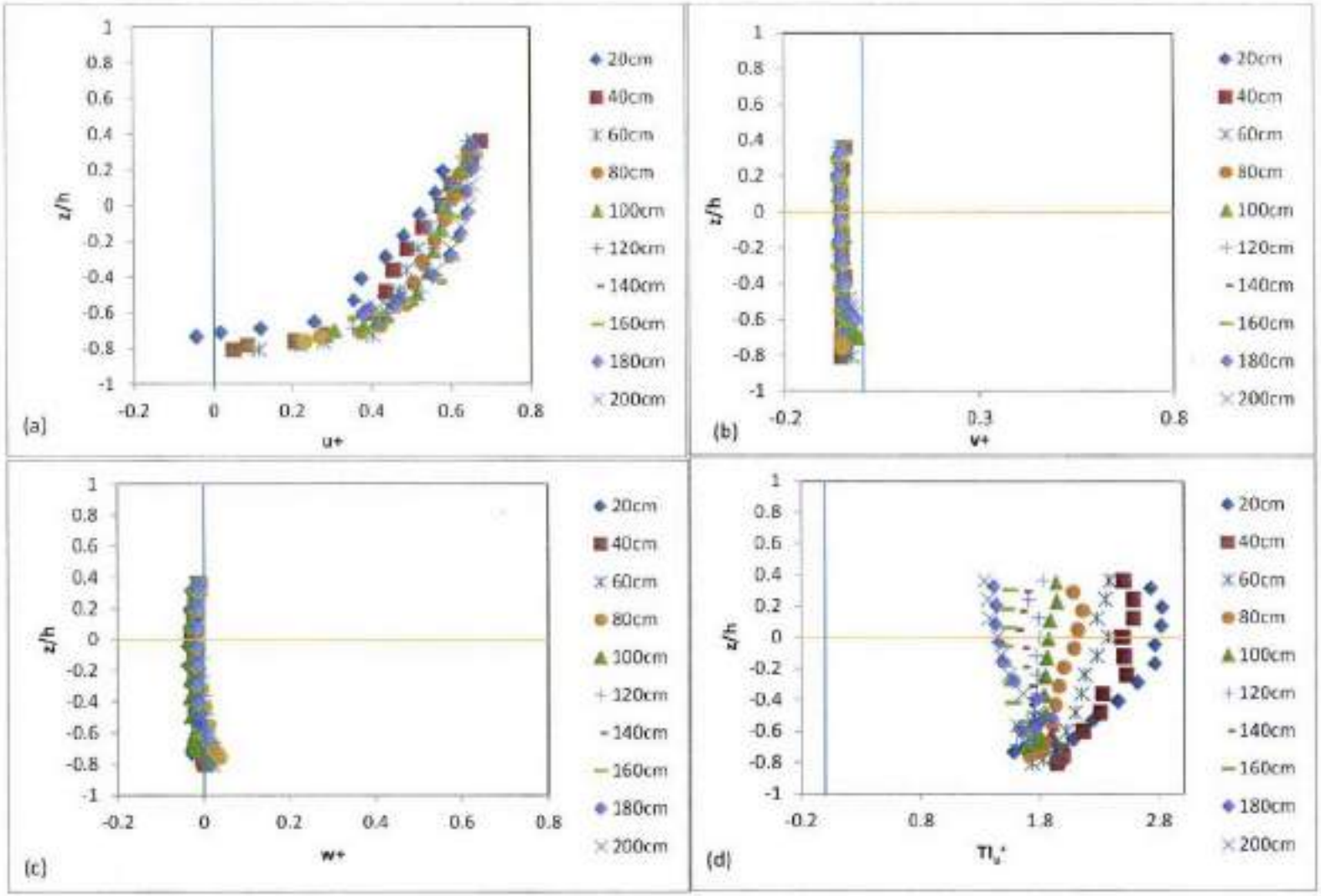


Fig. 5.17(a-d) Distribution of turbulence parameters over degraded bed of clay-silt-sand mixture for run no. SSC 9

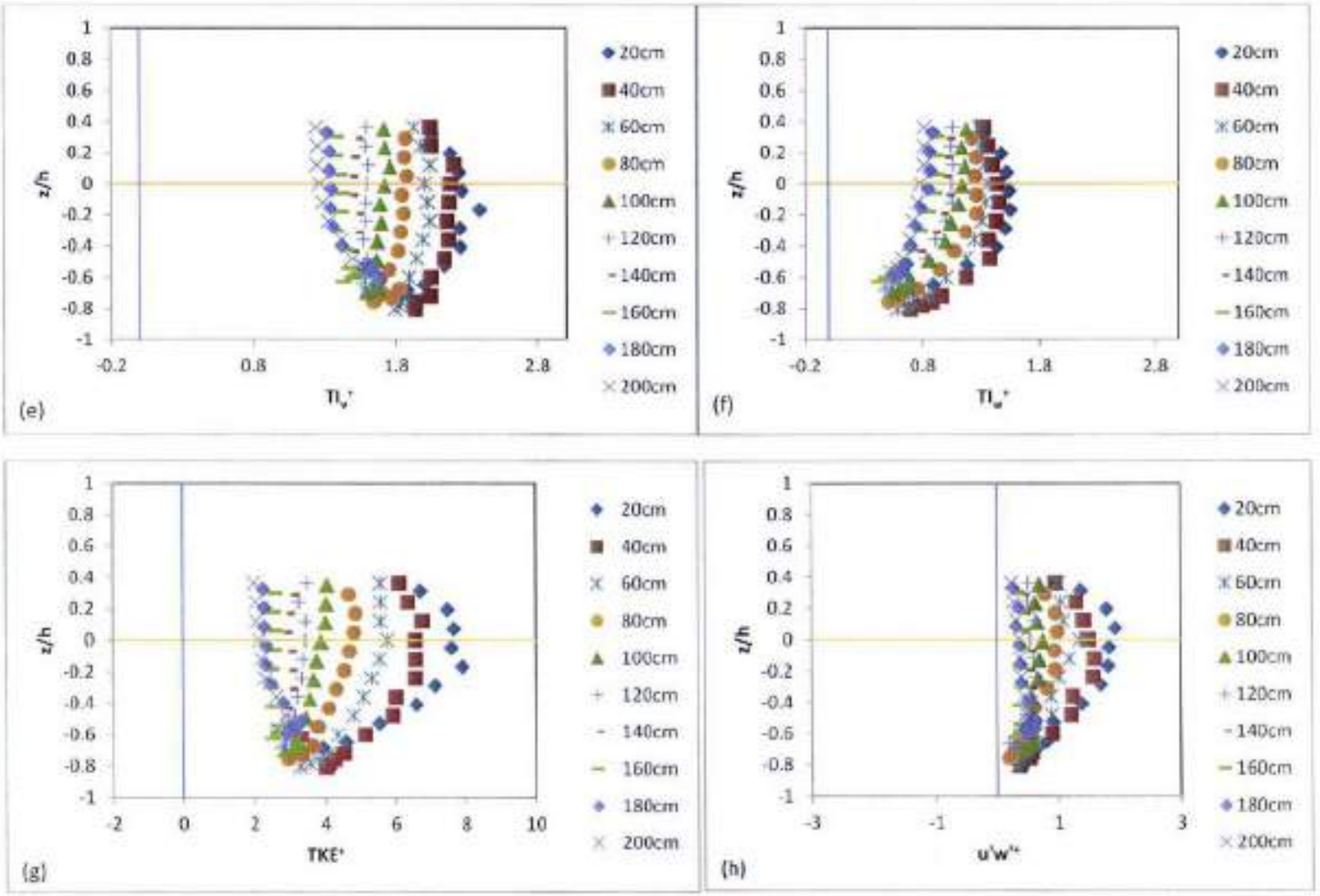


Fig. 5.17(e-h) Distribution of turbulence parameters over degraded bed of clay-silt-sand mixture for run no. SSC 9

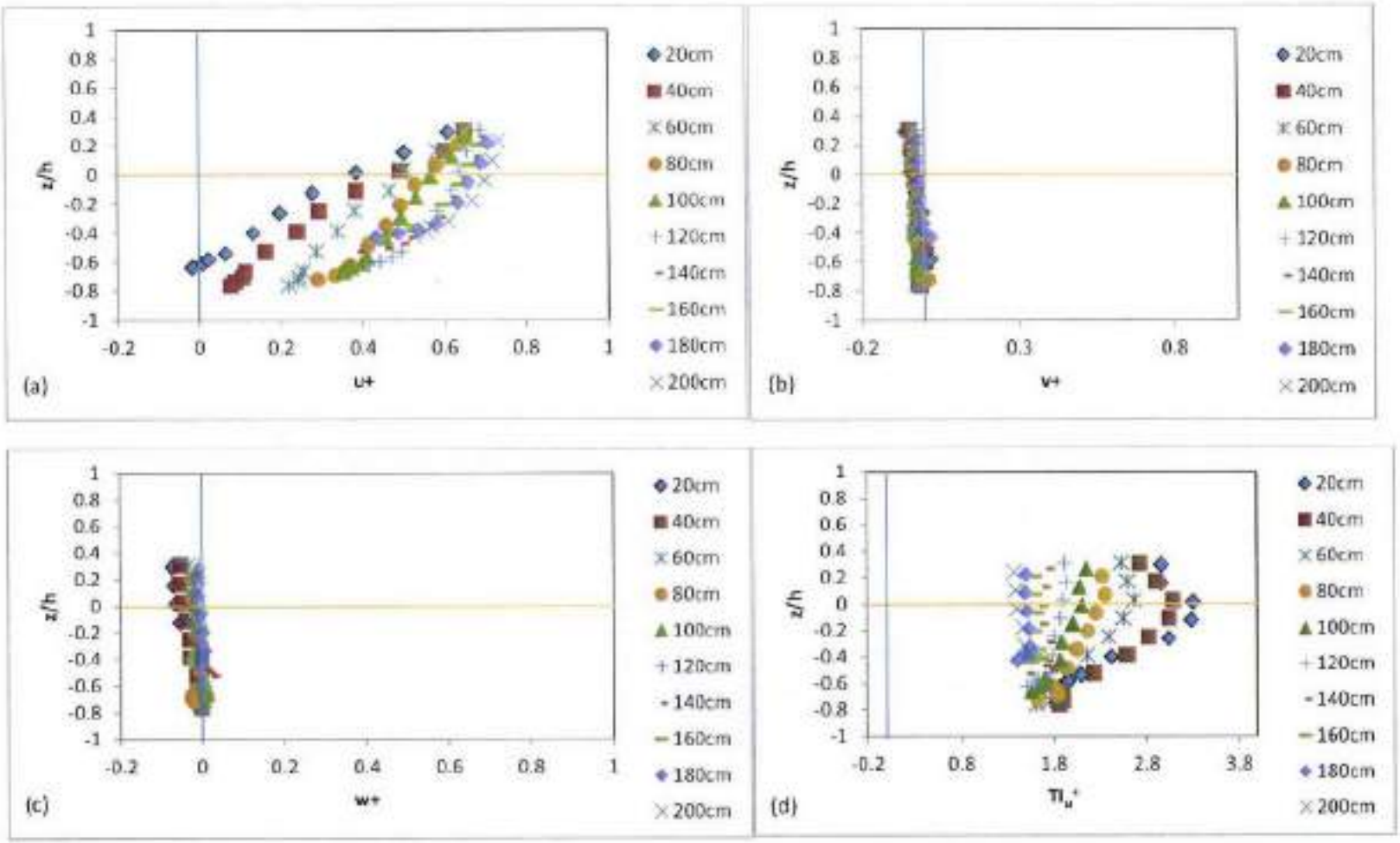


Fig. 5.18(a-d) Distribution of turbulence parameters over degraded bed of clay-silt-sand mixture for run no. SSC 12

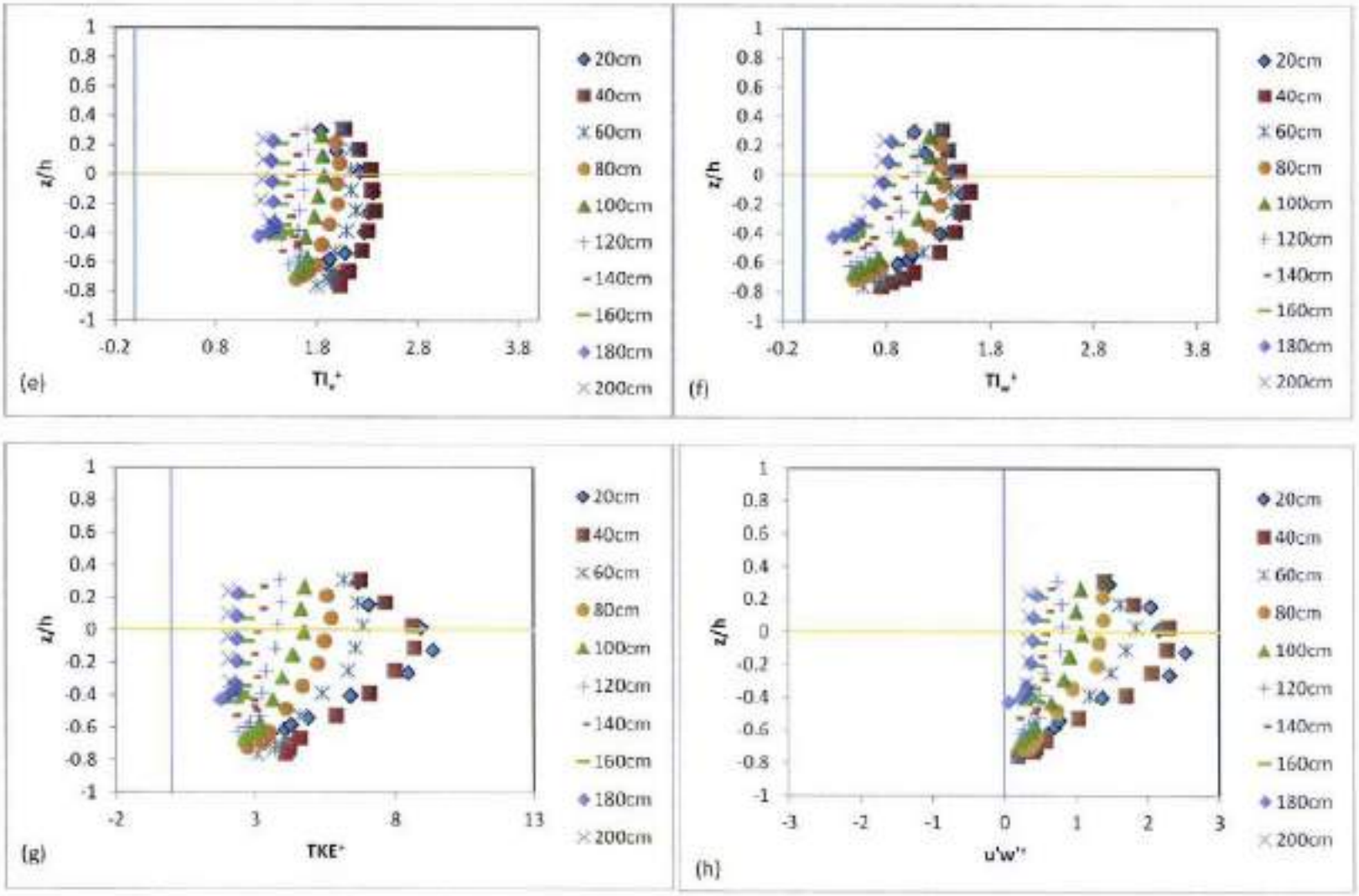


Fig. 5.18(e-h) Distribution of turbulence parameters over degraded bed of clay-silt-sand mixture for run no. SSC 12

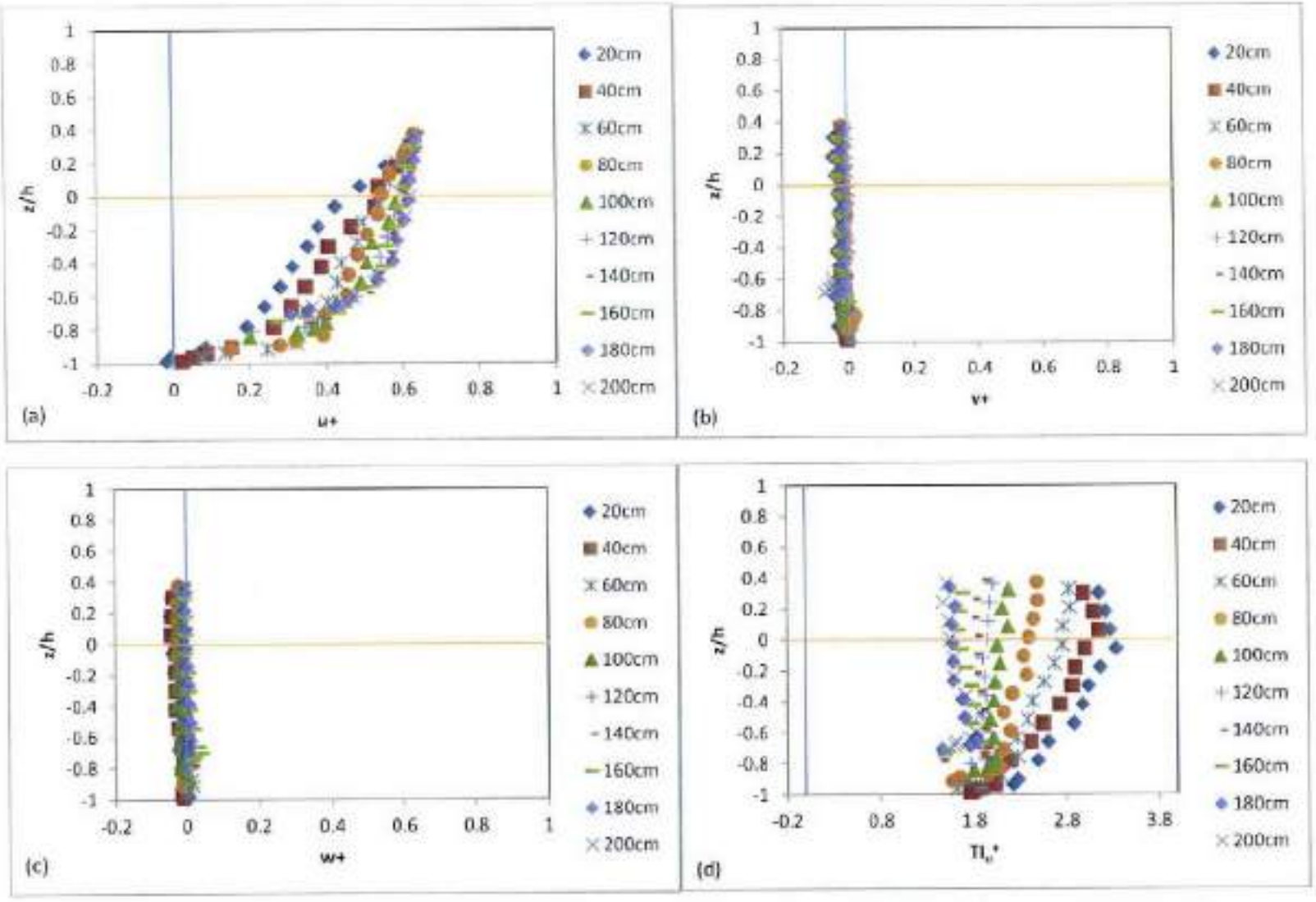


Fig. 5.19(a-d) Distribution of turbulence parameters over degraded bed of clay-silt-sand mixture for run no. SSC 20

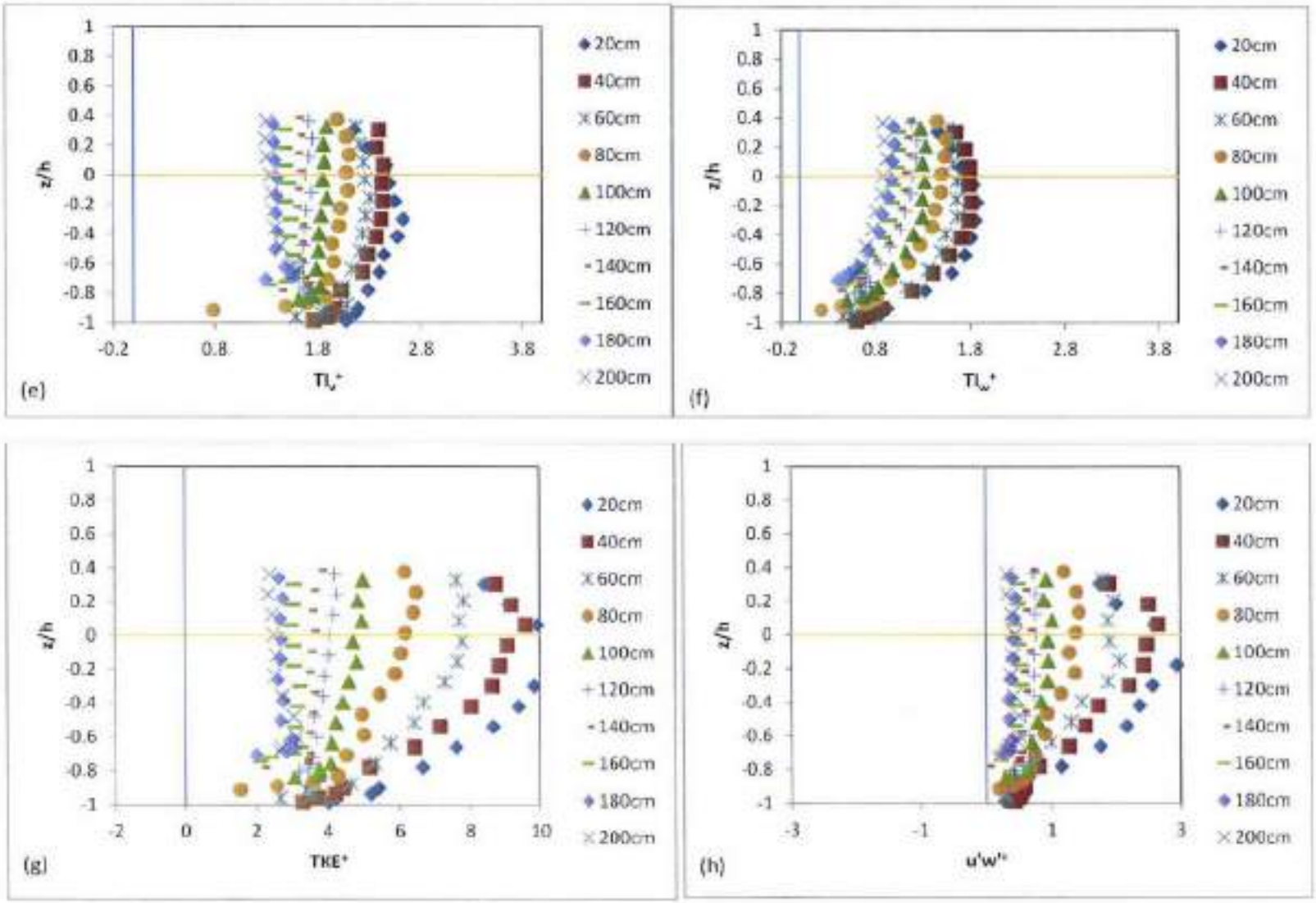


Fig. 5.19(e-h) Distribution of turbulence parameters over degraded bed of clay-silt-sand mixture for run no. SSC 20

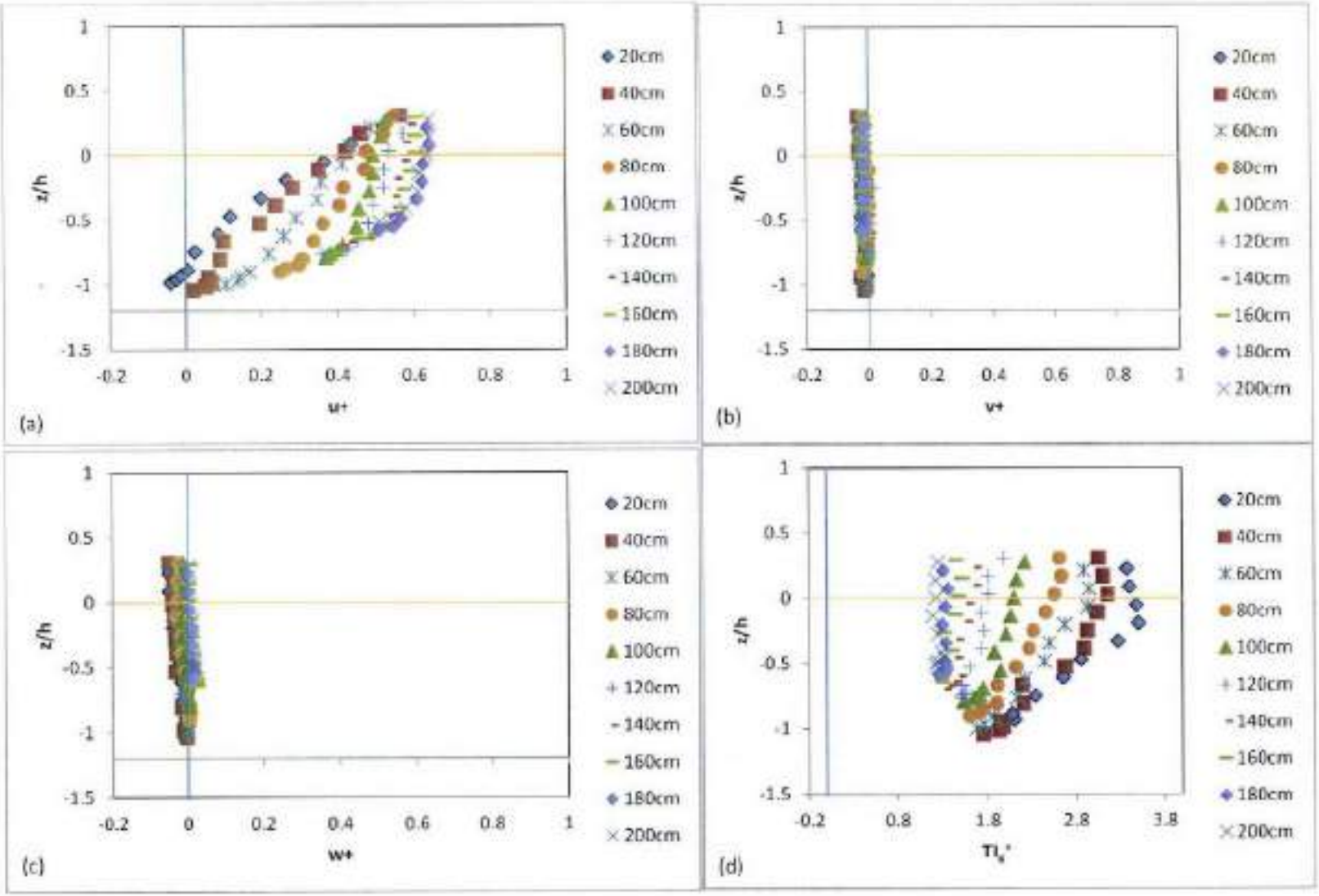


Fig. 5.20(a-d) Distribution of turbulence parameters over degraded bed of clay-silt-sand mixture for run no. SSC 19

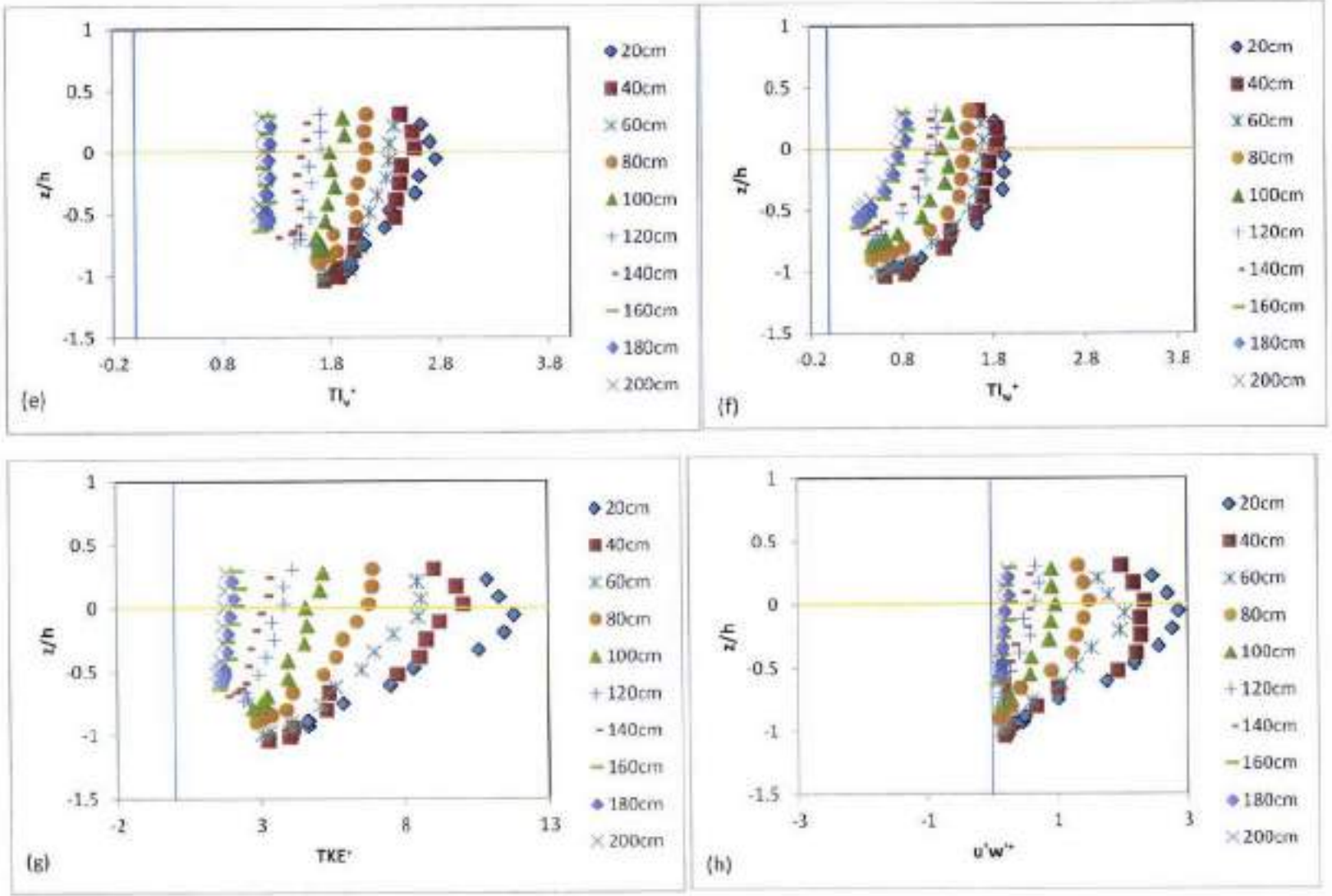


Fig. 5.20(e-h) Distribution of turbulence parameters over degraded bed of clay-silt-sand mixture for run no. SSC 19

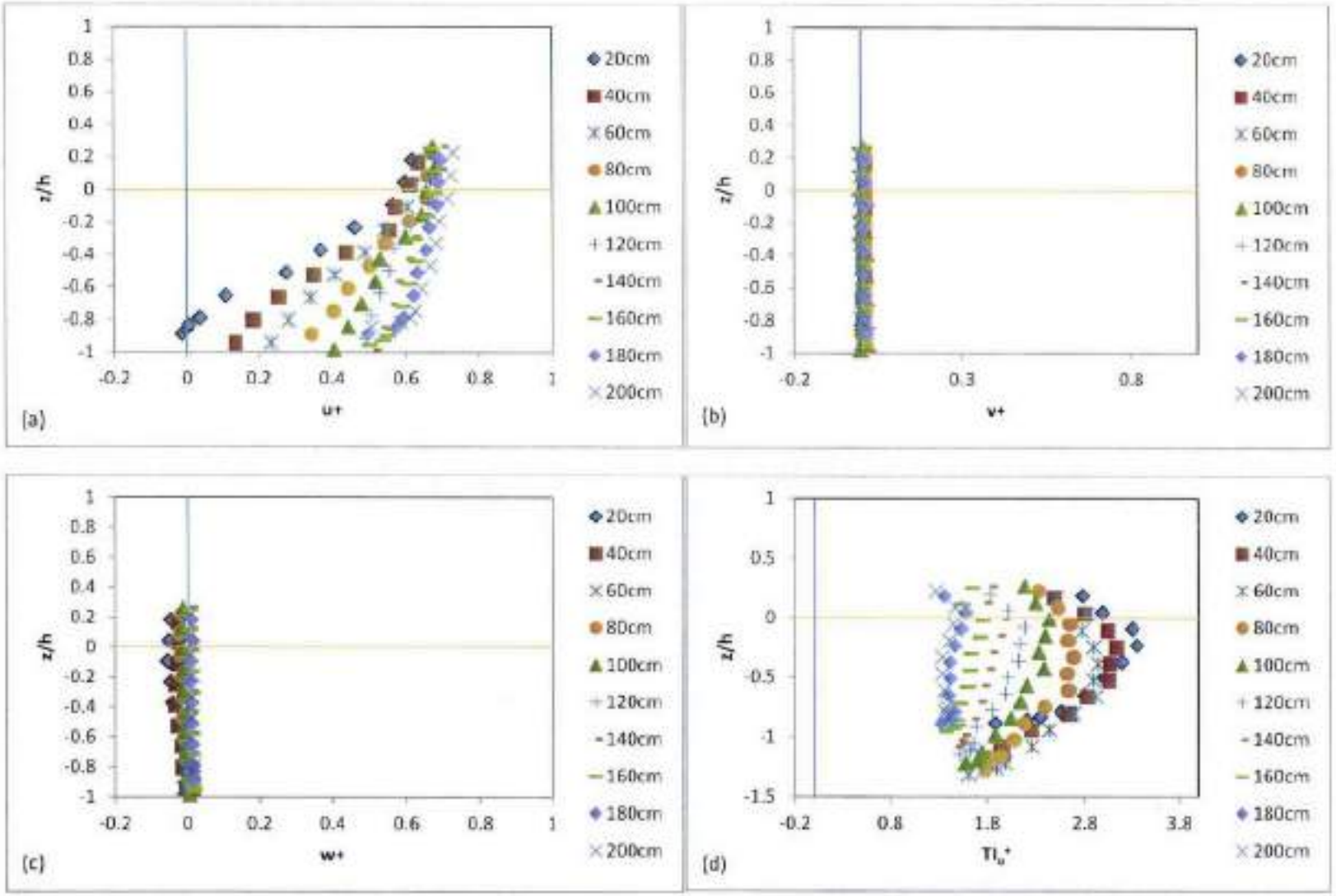


Fig. 5.21(a-d) Distribution of turbulence parameters over degraded bed of clay-silt-sand mixture for run no. SSC 21

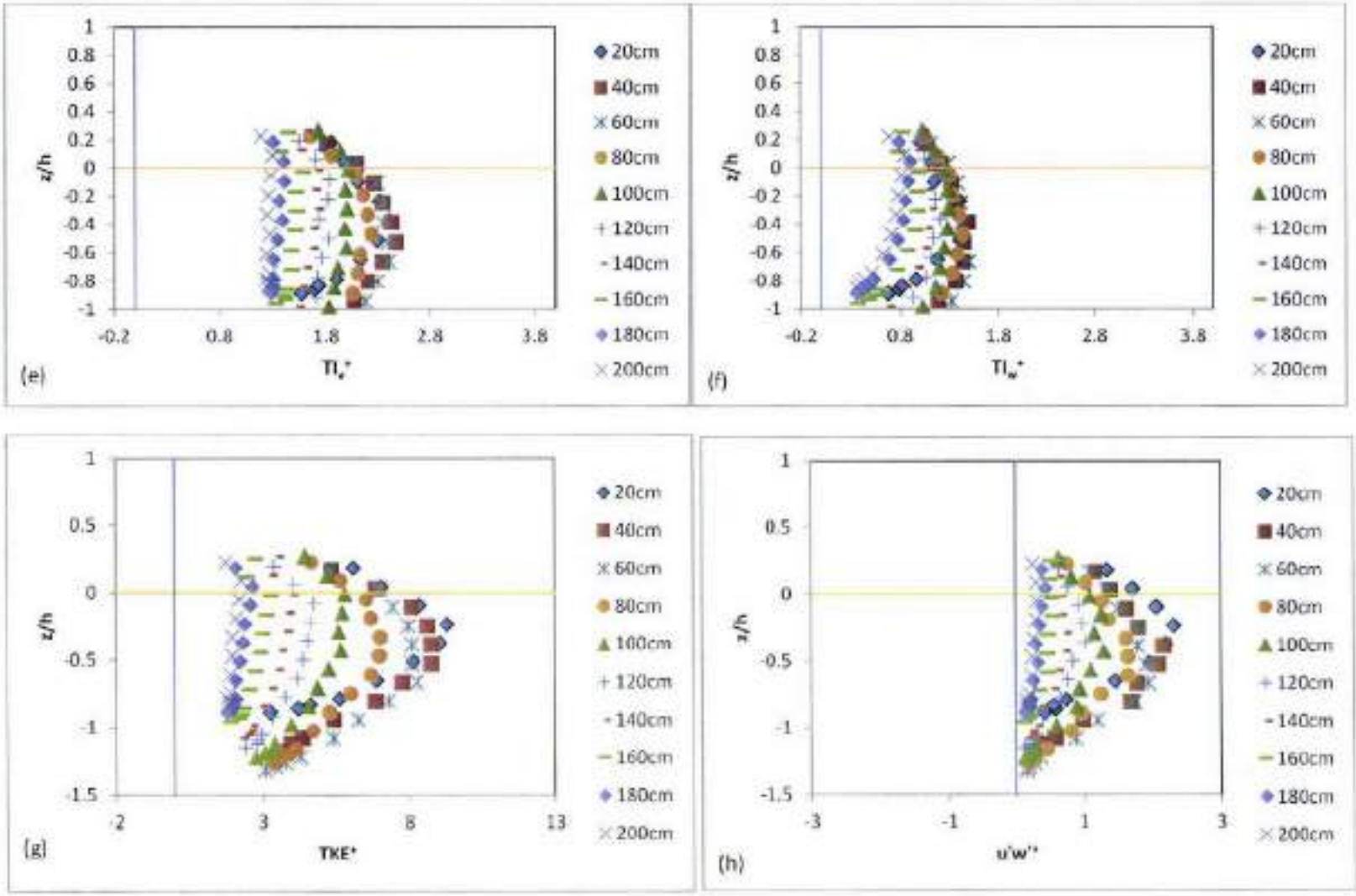


Fig. 5.21(e-h) Distribution of turbulence parameters over degraded bed of clay-silt-sand mixture for run no. SSC 21

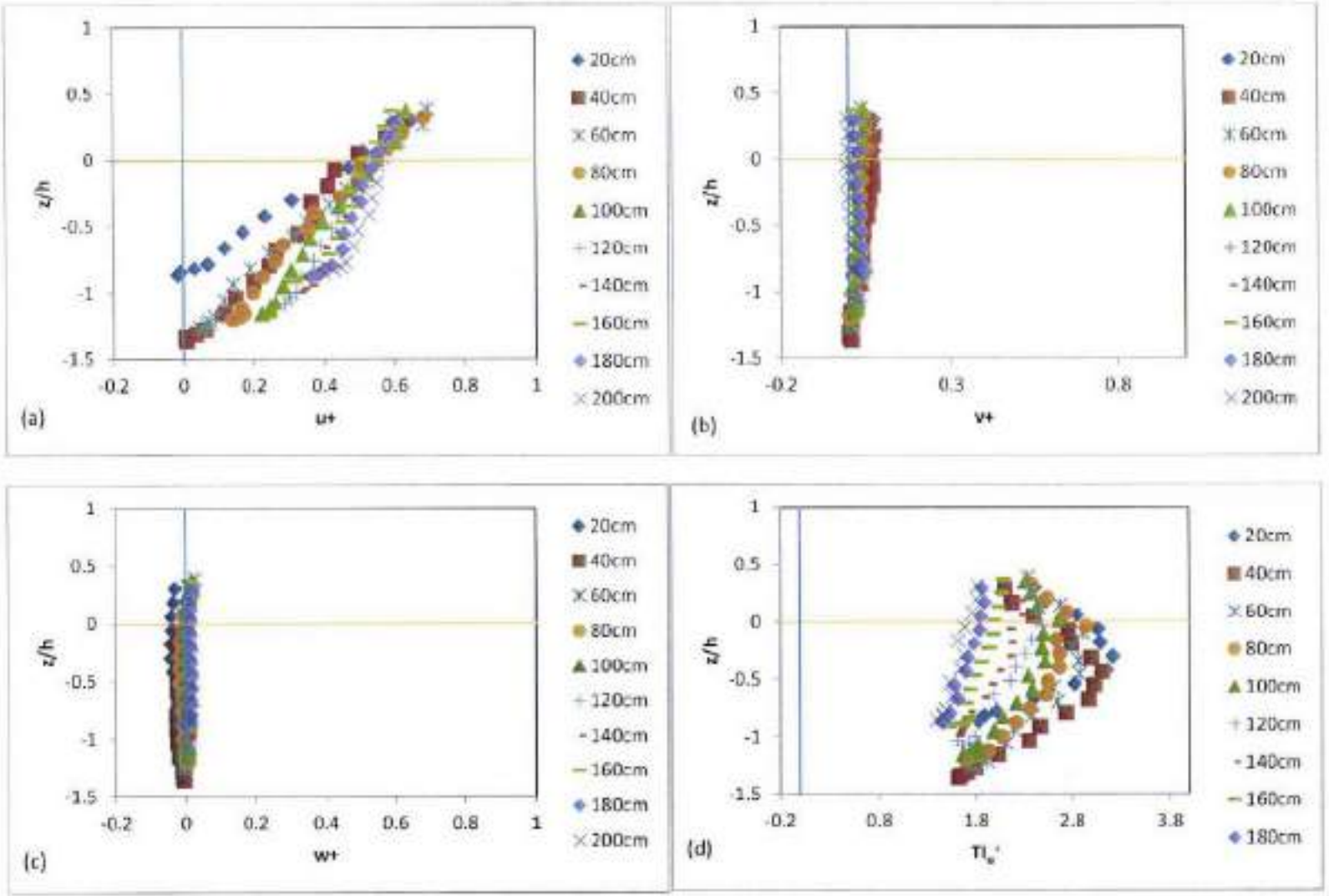


Fig. 5.22(a-d) Distribution of turbulence parameters over degraded bed of clay-silt-sand mixture for run no. SSC 22

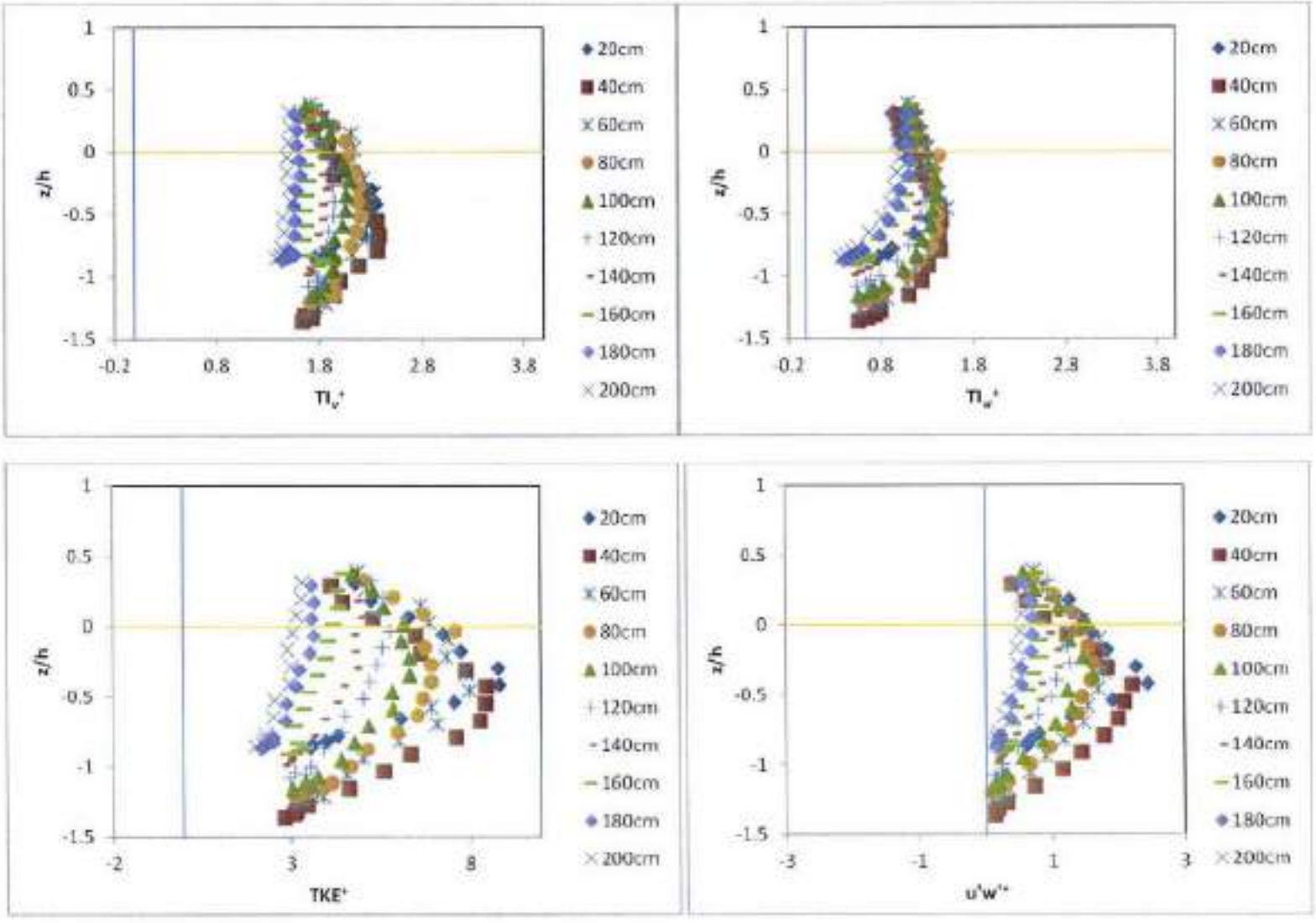


Fig. 5.22(e-h) Distribution of turbulence parameters over degraded bed of clay-silt-sand mixture for run no. SSC 22

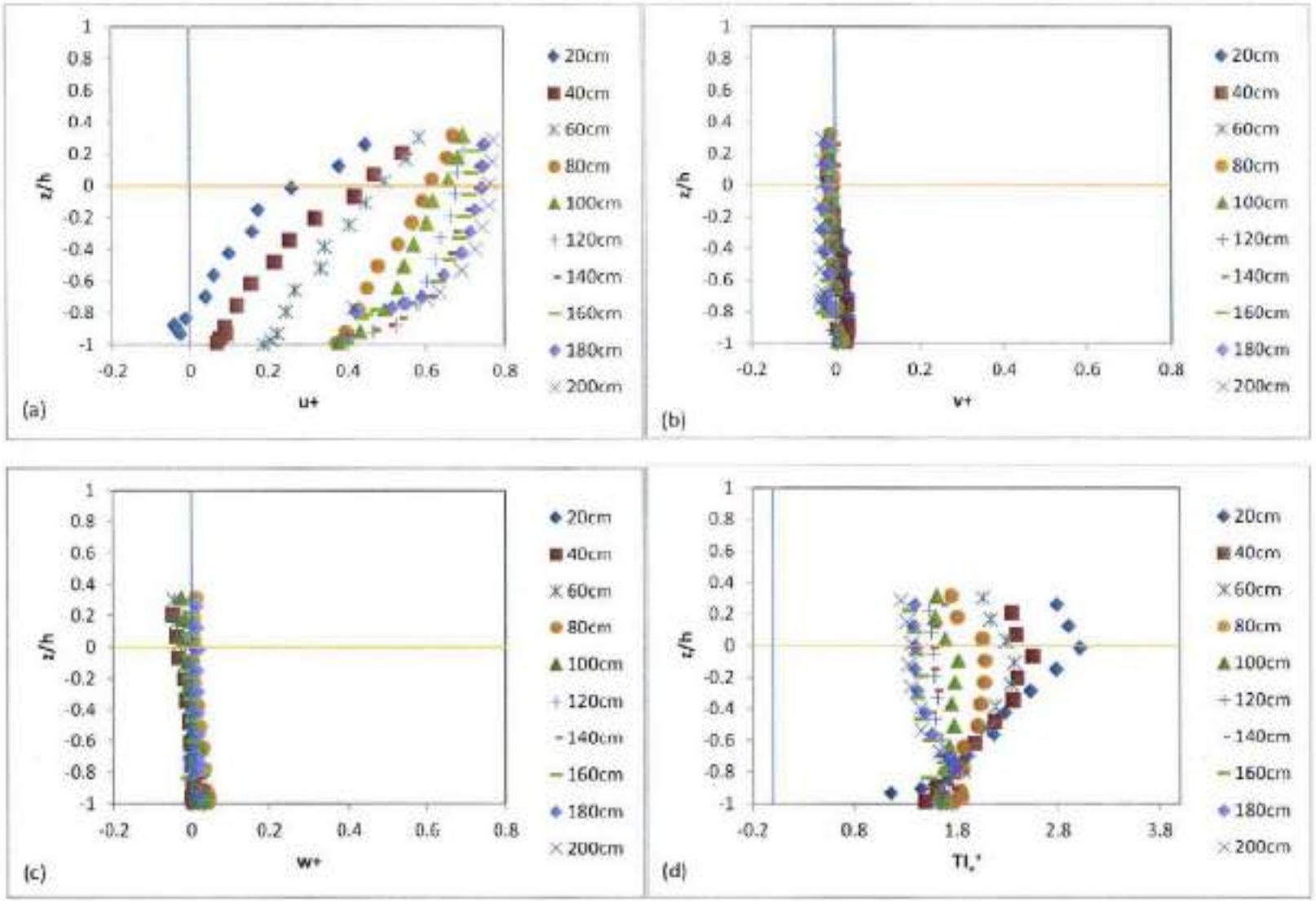


Fig. 5.23(a-d) Distribution of turbulence parameters over degraded bed of clay-silt-sand-gravel mixture for run no. GSSC 19

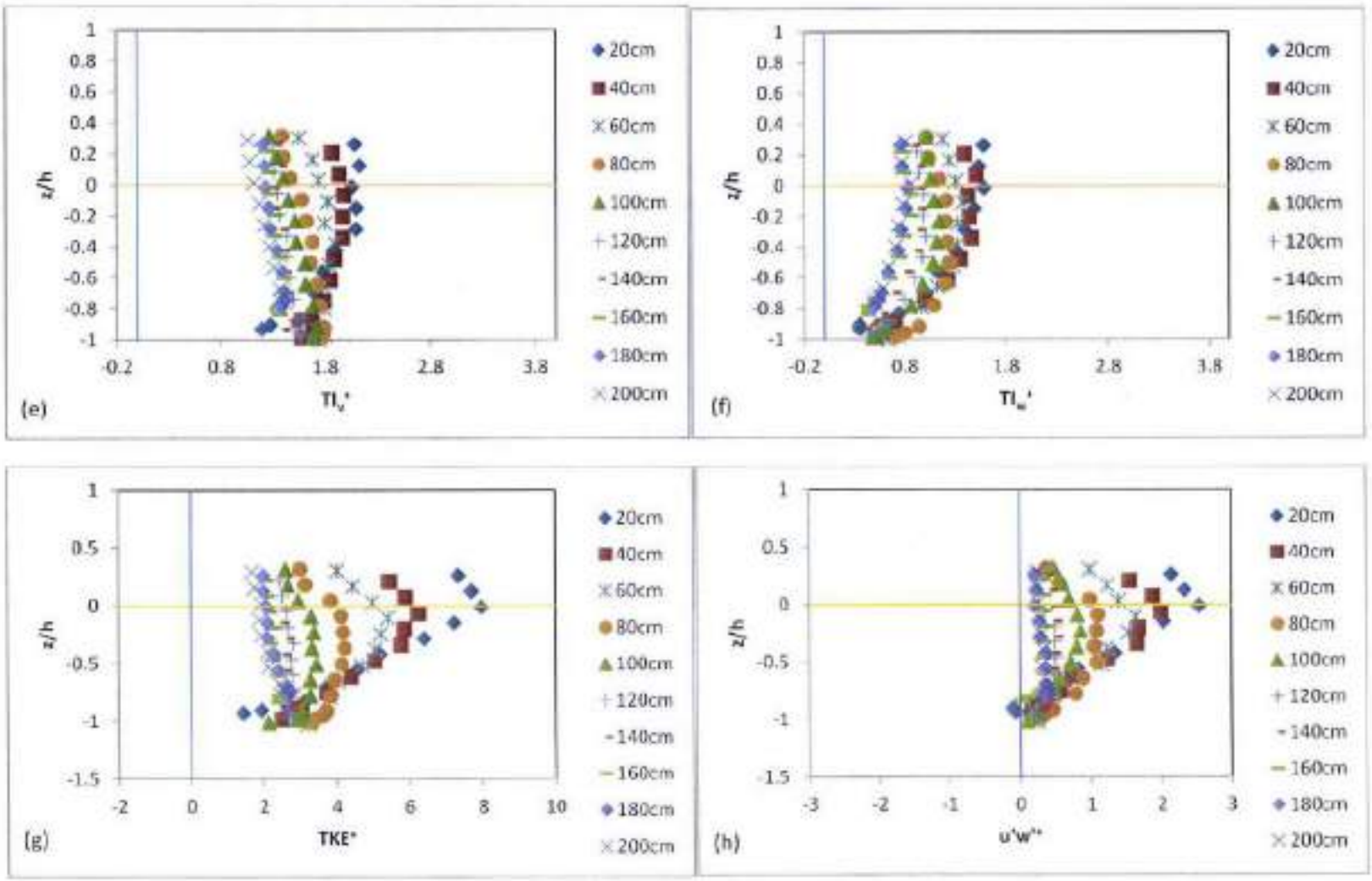


Fig. 5.23(e-h) Distribution of turbulence parameters over degraded bed of clay-silt-sand-gravel mixture for run no. GSSC 19

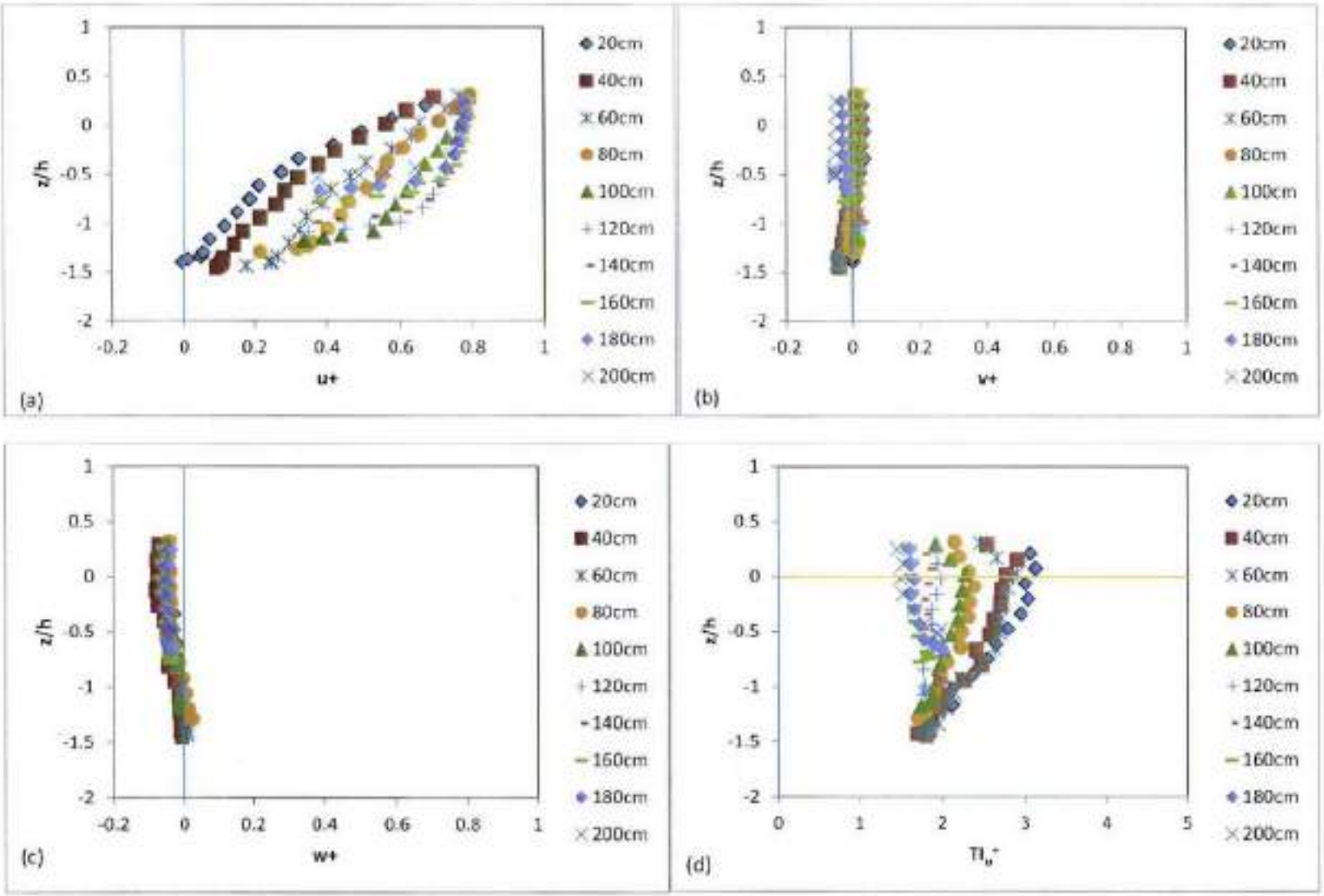


Fig. 5.24(a-d) Distribution of turbulence parameters over degraded bed of clay-silt-gravel mixture for run no. GSC 9

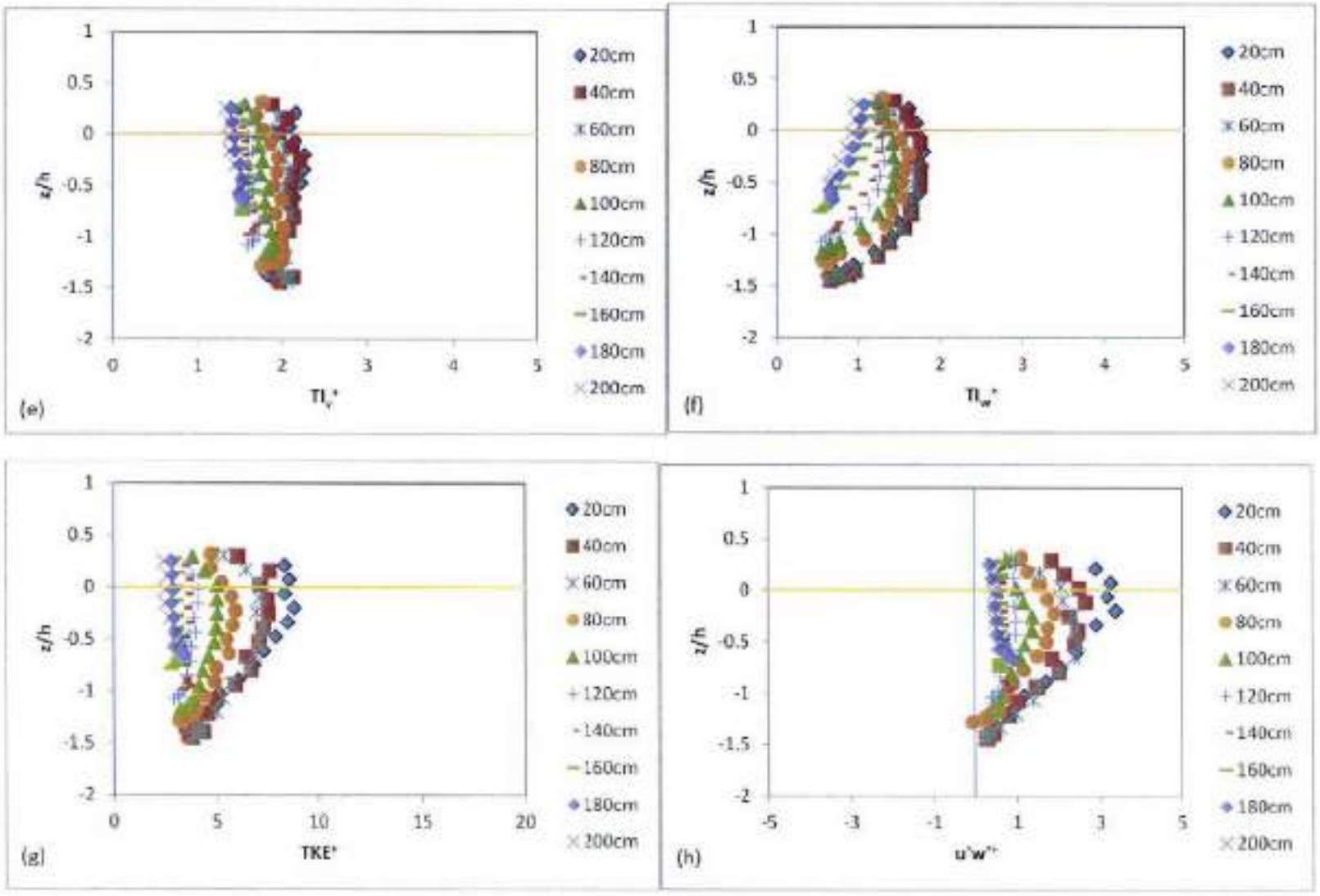


Fig. 5.24(e-h) Distribution of turbulence parameters over degraded bed of clay-silt-gravel mixture for run no. GSC 9

## 5.3 CONCLUDING REMARKS

This chapter includes the study of turbulence characteristics of flow over degraded channel bed.

- ADV was used for collecting the 3D velocity data over the degraded bed of clay-silt-gravel, clay-silt-sand-gravel, and clay-silt-sand mixture in which clay is varied as 0%, 30%, and 50%. WinADV was used for filtering the collected velocity raw data and data processing which gives the output in terms of turbulence parameters i.e. turbulence intensity, turbulence kinetic energy, and Reynolds shear stresses.
- Velocity is found to be lower just above the bed; however, it increases as moved horizontally towards downstream or moved vertically across the flow depth towards the free surface.
- Normalized turbulence intensity ( $u_*^+$ ) decreases longitudinally as moved from upstream to downstream end; as more degradation resulted in more velocity fluctuations.
- The position of maximum value of $TI_*^+$ has been found around the initial bed level (i.e. z = 0) for cohesive mixture in the present study; however, this position of maximum value occurs below the initial bed level, especially in the upstream sections, in case of 0% clay content in the mixture. Normalized turbulence kinetic energy ( $TKE^+$ ) and normalized Reynolds shear stress ( $u'w'^+$ ) has the similar trend of data as that of $TI_*^+$.

# CHAPTER – VI

## CONCLUSIONS

*The following conclusions have been drawn from the present study:*

- **For incipient motion in case of cohesionless sediment mixture**
  - ✓ Critical shear stress for gravel particles has been studied in presence of silt for non-uniform cohesionless mixture i.e. for sediment mixture of gravel-silt and gravel-sand-silt.
  - ✓ The critical shear stress for the gravel particles was found to be low in presence of silt which may be attributed to early dislodging of silt and subsequent exposure of the gravel particles which causes movement of gravel particles at low critical shear stress.
  - ✓ The visual observations of the channel bed after the end of incipient motion reveals the dominancy of gravel particles on the top surface of the channel bed due to removal of silt particles from the top layer of channel bed.
  - ✓ The critical shear stress of gravel particles in case of non-uniform sediment deviates from that of uniform sediment. Therefore, a new relationship in the form of Eq. (4.8) is proposed for predicting the critical shear stress of gravel particle in non-uniform cohesionless sediment.
  - ✓ The critical shear stress computed from the proposed relationship shows a good agreement between observed and computed values for data of Misri (1981) and Kuhnle (1993) along with the present study. Thus it is concluded that the proposed relationship predicts well the critical shear stress of gravel particles in sediment mixture of gravel-silt, gravel-sand, and gravel-sand-silt.
  - ✓ The proposed relationship developed in such a way that it converges into Brownlie (1981) equation in case of uniform sediment.
- **For incipient motion in case of cohesive sediment mixture**
  - ✓ The experimental study has been conducted for incipient motion of coarser particles present in cohesive sediment mixture for clay-silt-gravel, clay-silt-sand-

gravel, and clay-silt-sand. The clay content in theses mixture varied from 10% to 50%.

- ✓ High clay percentage significantly increases the critical shear stress. It may be attributed to strong cohesive bond among the particles present in the mixture that resulted in higher resistance of erosion against the flow and leads to higher value of critical shear stress.
- ✓ The presence of silt lowers the critical shear stress especially when there is low clay content (up to 20%) in the mixture. This is attributed to exposure of gravel particles due to dislodging of silt at lower tractive shear stress.
- ✓ Clay content, water content, and compaction are the main factors that govern the incipient motion, however, effect of clay content is more pronounced. As water content in the mixture and *UCS* govern the bulk density, it is appropriate to consider clay content and bulk density as governing parameters for studying the incipient motion of cohesive mixture in addition to the sediment size.
- ✓ The appearance of the top surface of bed was found different for varying percentage of the clay in the sediment mixture. The dominancy of gravel particles were noticed on the top surface of the bed for 10% and 20% clay content in clay-silt-gravel mixture and clay-silt-sand-gravel mixture. However, the dominancy of gravel particles on the top surface was decreases with increase of clay percentage in the sediment mixture. Pattern of mass erosion was observed for higher clay content i.e. 40% and 50% of clay content in the mixture.
- ✓ A relationship has been developed in the form of Eq. (4.15) for the computation of critical shear stress of gravel particles that is suited to cohesive sediment mixture of clay-gravel, clay-sand-gravel, clay-silt-gravel, and clay-silt-sand-gravel. A relationship has also been developed in the form of Eq. (4.16) for the computation of critical shear stress of sand particles in cohesive sediment mixture of clay-silt-sand.

➢ **For transport rate of sediment**

- ✓ High transport rate of sediment was found in the initial period of time which called here initial transport rate. However, initial transport rate decreases with the increase of clay percentage in the mixture.

- ✓ Equilibrium time i.e. time required for allotment of final scour is affected by the clay content in the mixture and found to be increases with the increase of clay content in the mixture.
- ✓ Clay content and excess shear stress was found to be governing parameters for the transport rate of sediment.
- ✓ Relationships have been developed as Eqs. (4.46) – (4.48) and Eqs. (4.52) – (4.54) for the computation of bed load transport rate and suspended load transport rate respectively for clay-silt-gravel mixture, clay-silt-sand-gravel mixture, and clay-silt-sand mixture.

➢ **For transient bed profile**

- ✓ The transient bed profiles at the mid of flume width at a longitudinal interval of 50 cm along the flow direction for different percentage of clay in the sediment mixture of clay-silt-gravel, clay-silt-sand-gravel, and clay-silt-sand has been studied.
- ✓ Clay percentage, excess shear stress, and time are the main parameters that govern the transient bed profile. Degradation of channel bed decreases with the increase of clay percentage. Increase in excess shear stress accelerates the degradation, and the bed degradation decreases with the increases of time i.e. higher degradation observed in the initial period of time and after that it is low.
- ✓ The maximum degradation was found to occur at 50 cm from the entrance of upstream working section for all the three cohesive sediment mixture in the present study.
- ✓ The relationships have been proposed in form of Eqs. (4.68) – (4.70) for the computation of bed profile for cohesive mixture of clay-silt-gravel, clay-silt-sand-gravel, and clay-silt-sand.
- ✓ The relationships have also been proposed as Eqs. (4.24) – (4.26) & Eqs. (4.64) – (4.66) for the computation of equilibrium time and maximum degradation respectively for all the three cohesive mixtures in the present study.

➢ **For turbulence characteristics of flow**

- ✓ Turbulence characteristics of flow; in terms of distribution of velocity, turbulence intensity, turbulence kinetic energy, and Reynolds shear stress; using Acoustic

Doppler Velocimeter over the degraded cohesive bed has been made in which clay varied as 0%, 30%, and 50%.

- ✓ Velocity is found to be low just above the degraded bed especially at upstream sections. However, velocity increases as moved to downstream along the channel bed as well as moved vertically from the channel bed to free water surface.
- ✓ The velocity fluctuation is higher in upstream sections than that of downstream sections for vertical distribution of longitudinal velocity over the degraded bed.
- ✓ The fluctuation in vertical distribution of velocity was reduced as the clay percentage in the channel bed increases from 0% to 50%. It may be attributed to the level of degraded bed which found to be decreases as clay percentage rise from 0% to 50%.
- ✓ The turbulence intensity decreases longitudinally as moved from upstream to downstream end; as more degradation resulted in higher velocity fluctuations. The position of maximum value of turbulence intensity has been found around the initial bed level for cohesive mixture; however, this position of maximum value occurs below the initial bed level, especially in the upstream sections, in case of 0% clay content in the mixture.
- ✓ Normalized turbulence kinetic energy and normalized Reyonlds shear stress has the similar trend as that of turbulence intensity.

# REFERENCES


Aberle, J., Nikora, V., and Walters, R. (2004). "Effects of bed material properties on cohesive sediment erosion." *Marine Geology*, 207(1–4), 83–93.

Ackers, P., and White, W. R. (1973). "Sediment transport: New approach and analysis." *Journal of the Hydraulics Division*, 99(11), 2041–2060.

Ahmad, M. F., Dong, P., Mamat, M., Nik, W. B. W., and Mohd, M. H. (2011). "The critical shear stresses for sand and mud mixture." *Applied Mathematical Sciences*, 5(2), 53–71.

Ahmad, Z., Sharma, H., and Westrich, B. (2013). "Turbulence characteristics of flow over a block ramp." *Journal of Water Resource and Hydraulic Engineering*, 2(1), 21–29.

Ahmed, F., and Rajaratnam, N. (1998). "Flow around Bridge Piers." *Journal of Hydraulic Engineering*, 124(3), 288–300.

Ansari, S. A. (1999). "Influence of cohesion on local scour." IIT Roorkee. Ph.D. Thesis, Department of Civil Engineering, Indian Institute of Technology Roorkee, Roorkee, India.

Ansari, S. A., Kothyari, U. C., and Ranga Raju, K. G. (2003). "Influence of cohesion on scour under submerged circular vertical jets." *Journal of Hydraulic Engineering*, 129(12), 1014–1019.

Ansari, S. A., Kothyari, U. C., and Ranga Raju, K. G. (2007). "Incipient motion characteristics of cohesive sediments." *ISH Journal of Hydraulic Engineering*, 13(2), 108–121.

Aricò, C., and Tucciarelli, T. (2008). "Diffusive modeling of aggradation and degradation in artificial channels." *Journal of Hydraulic Engineering*, 134(8), 1079–1088.

Ashida, K., and Michiue, M. (1971). "An investigation of river bed degradation downstream of dam." *Proceeding of 14th Congress of IAHR*, Paris, France, 247–256.

Ashida, K., and Michiue, M. (1972). "Study on hydraulic resistance and bed-load transport rate in alluvial streams." *Proceedings of the Japan Society of Civil Engineers*, 59–69.

Beck, J. S., and Basson, G. R. (2003). *The hydraulics of the impacts of dam development on the river morphology. Water Research Comission Report No. 1102/1/03, South Africa.*

Begin, Z. B., Meyer, D. F., and Schumm, S. A. (1981). "Development of longitudinal profiles of alluvial channels in response to base-level lowering." *Earth Surface Processes and Landforms*, 6(1), 49–68.

Beheshti, A. A., and Ataie-Ashtiani, B. (2008). "Analysis of threshold and incipient conditions for sediment movement." *Coastal Engineering*, 55(5), 423–430.

Bhallamudi, S. M., and Chaudhry, M. H. (1991). "Numerical modeling of aggradation and

degradation in alluvial channels." *Journal of Hydraulic Engineering*, 117(9), 1145–1164.

Bigillon, F., Nino, Y., and Garcia, M. H. (2006). "Measurements of turbulence characteristics in an open-channel flow over a transitionally-rough bed using particle image velocimetry." *Exp Fluids*, 41, 857–867.

Bridge, J. S., and Bennett, S. J. (1992). "A model for the entrainment and transport of sediment grains of mixed sizes, shapes, and densities." *Water Resources Research*, 28(2), 337–363.

Brownlie, W. R. (1981). *Prediction of flow depth and sediment discharge*.

Cao, Z., Day, R., and Egashira, S. (2002). "Coupled and decoupled numerical modeling of flow and morphological evolution in alluvial rivers." *Journal of Hydraulic Engineering*, 128(3), 306–321.

Carollo, F. G., Ferro, V., and Termini, D. (2005). "Analyzing turbulence intensity in gravel bed channels." *Journal of Hydraulic Engineering*, 131(12), 1050–1061.

Cellino, M., and Lemmin, U. (2004). "Influence of coherent flow structures on the dynamics of suspended sediment transport in open-channel flow." *Journal of Hydraulic Engineering*, 130(11), 1077–1088.

Chollet, J.-P., and Cunge, J. A. (1980). "Simulation of unsteady flow in alluvial streams." *Applied Mathematical Modelling*, 4(4), 234–244.

Colby, B. R. (1964). *Sediment transport in alluvial channels. U.S. Geological Survey*. Report No. 462-A, 47 pp.

Cui, Y., Paola, C., and Parker, G. (1996). "Numerical simulation of aggradation and downstream fining." *Journal of Hydraulic Research*, 34(2), 185–204.

Cunge, J. A., and Perdreau, N. (1973). "Mobile bed fluvial mathematical models."

Debnath, K., Nikora, V., and Elliott, A. (2007). "Stream bank erosion: In Situ flume tests." *Journal of Irrigation and Drainage Engineering*, 133(3), 256–264.

Dey, S., and Barbhuiya, A. K. (2006). "Velocity and turbulence in a scour hole at a vertical-wall abutment." *Flow Measurement and Instrumentation*, 17(1), 13–21.

Dey, S., and Debnath, K. (2000). "Influence of streamwise bed slope on sediment threshold under stream flow." *Journal of Irrigation and Drainage Engineering*, 126(4), 255–263.

Dey, S., and Raju, U. V. (2002). "Incipient motion of gravel and coal beds." *Sadhana*, 27(5), 559–568.

Dey, S., Sarkar, S., and Solari, L. (2011). "Near-bed turbulence characteristics at the entrainment threshold of sediment beds." *Journal of Hydraulic Engineering*, 137(9), 945–958.

Dietrich, W. E. (1982). "Settling velocity of natural particles." *Water Resources Research*, 18(6), 1615–1626.

Dong, P. (2007). "Two-fraction formulation of critical shear stresses for sand and silt mixtures." *Journal of Waterway, Port, Coastal, and Ocean Engineering*, 133(3), 238–241.

Dunn, I. S. (1959). "Tractive resistance of cohesive channels." *Journal of Geotechnical Engineering*, 85(3), 1–24.

Durgunoğlu, A., and Singh, K. P. (1993). *The economics of using sediment-entrapment reduction measures in lake and reservoir design.WRC report no. 216, Project No. G-2017-03, University of Illinois.*

Egiazaroff, I. V. (1965). "Calculation of nonuniform sediment concentration." *Journal of Hydraulic Division*, 91(4), 225–247.

Einstein, H. A. (1942). "Formulas for the transportation of bed load." *Transactions of the American Society of Civil Engineers*, 107(1), 561–577.

Einstein, H. A. (1950). *The bed-load function for sediment transportation in open channel flows. Technical Bulletin No. 1026, USDA, Soil Conservation Service, Washington.*

Engelund, F., and Fredsoe, J. (1976). "A sediment transport model for straight alluvial channels." *Hydrology Research*, 7(5), 293–306.

Engelund, F., and Hansen, E. (1967). *A monograph on sediment transport in alluvial streams. Teknisk Forlag.*

Ferguson, R. I., and Church, M. (2004). "A simple universal equation for grain settling velocity." *Journal of Sedimentary Research*, 74(6), 933–937.

Ferro, V. (2003). "ADV measurements of velocity distributions in a gravel-bed flume." *Earth Surface Processes and Landforms*, 28, 707–722.

Garde, R. J., and Ranga Raju, K. G. (2000). *Mechanics of sediment transportation and alluvial stream problems*. New Age International, New Delhi.

Gaucher, J., Marche, C., and Mahdi, T.-F. (2010). "Experimental investigation of the hydraulic erosion of noncohesive compacted soils." *Journal of Hydraulic Engineering*, 136(11), 901–913.

Guan, D., Melville, B. W., and Friedrich, H. (2014). "Flow patterns and turbulence structures in a scour hole downstream of a submerged weir." *Journal of Hydraulic Engineering*, 140(1), 68–76.

Guo, J., and Julien, P. Y. (2001). "Guo-JulienIAHR01.pdf." *Journal of Hydraulic Research*, 39(1), 11–23.

Hayashi, T., Ozaki, S., and Ichibashi, T. (1980). "Study on bed load transport of sediment mixtures." *Proceeding of 24th Japanese Conference on Hydraulics*, Japan, 35–43.

Holtorff, G. (1983). "Steady bed material transport in alluvial channels." *Journal of Hydraulic Division*, 109(3), 368–384.

Houssais, M., and Lajeunesse, E. (2012). "Bedload transport of a bimodal sediment bed." *Journal of Geophysical Research*, 117(F04015), 1–13.

IS, B. of I. S. (1970). "Classification and identification of soils for general engineering purposes." *IS : 1498*.

IS, B. of I. S. (1975). "Determination of dry density od soils In-place by the core-cutter method." *IS : 2720*, Part XXIX.

IS, B. of I. S. (1991). "Determination of unconfined compressive strength." *IS : 2720*, Part X.

Iwagaki, Y. (1956). "Hydrodynamical study on critical tractive force." *Trans. of JSCE*, 41, 1–21.

Jain, R. K. (2008). "Influence of cohesion on detachment and transport of clay-sand-gravel mixtures." Ph.D. Thesis, Department of Civil Engineering, Indian Institute of Technology Roorkee, Roorkee, India.

Jain, R. K., and Kothyari, U. C. (2009). "Cohesion influences on erosion and bed load transport." *Water Resources Research*, 45(W06410), 1–17.

Jain, R. K., and Kothyari, U. C. (2010). "Influence of cohesion on suspended load transport of non-uniform sediments." *Journal of Hydraulic Research*, 48(1), 33–43.

Jain, R. K., Kumar, A., and Kothyari, U. C. (2015). "Turbulence statistics of flow through degraded channel bed of sand-gravel mixture." *Journal of Hydro-environment Research*, International Association for Hydro-environment Engineering and Research, Asia Pacific Division, 9, 508–518.

James, C. S. (1990). "Prediction of entrainment conditions for nonuniform, noncohesive sediments." *Journal of Hydraulic Research*, 28(1), 25–41.

Jepsen, R., Roberts, J., and Gailani, J. (2010). "Effects of bed load and suspended load on separation of sands and fines in mixed sediment." *Journal of waterway, port, coastal, and ocean engineering*, 136(6), 319–326.

Jepsen, R., Roberts, J., and Lick, W. (1997). "Effects of bulk density on sediment erosion rates." *Water, Air and Soil Pollution*, 99(1), 21–31.

Julian, J. P., and Torres, R. (2006). "Hydraulic erosion of cohesive riverbanks." *Geomorphology*, 76(1–2), 193–206.

Julien, P. Y. (2002). *River Mechanics. Water*, Cambridge University Press, New York, 434 pp.

Kamphuis, J. W., and Hall, K. R. (1983). "Cohesive material erosion by unidirectional current." *Journal of Hydraulic Engineering*, 109(1), 49–61.

Kassem, A. A., and Chaudhry, M. H. (1998). "Comparison of coupled and semicoupled numerical models for alluvial channels." *Journal of Hydraulic Engineering*, 124(8), 794–802.

Khullar, N. K., Kothyari, U. C., and Ranga Raju, K. G. (2010). "Influence of cohesion on

suspended load transport of non-uniform sediments." *Journal of Hydraulic Engineering*, 136(8), 534–543.

Kirkil, G., and Constantinescu, G. (2010). "Flow and turbulence structure around an in-stream rectangular cylinder with scour hole." *Water Resources Research*, 46, 1–20.

Köse, Ö. (2011). "Distribution of turbulence statistics in open-channel flow." *International Journal of the Physical Sciences*, 6(14), 3426–3436.

Kothyari, U. C. (1996). "Erosion and sedimentation problems in India." *Erosion and Sediment Yield: Global and Regional Perspectives, IAHS Publ. no. 236, 1996*, 531–540.

Kothyari, U. C., and Jain, R. K. (2008). "Influence of cohesion on the incipient motion condition of sediment mixtures." *Water Resources Research*, 44, 1–15.

Kothyari, U. C., and Jain, R. K. (2010a). "Erosion characteristics of cohesive sediment mixtures." *River Flow*, 815–821.

Kothyari, U. C., and Jain, R. K. (2010b). "Experimental and numerical investigations on degradation of channel bed of cohesive sediment mixtures." *Water Resources Research*, 46(12), 1–15.

Kothyari, U. C., Kumar, A., and Jain, R. K. (2014). "Influence of Cohesion on River Bed Scour in the Wake Region of Piers." *Journal of Hydraulic Engineering*, 140(1), 1–13.

Krishnappan, B. G. (1985). "Modeling of unsteady flows in alluvial streams." *Journal of Hydraulic Engineering*, 111(2), 257–266.

Kuhnle, R. A. (1993). "Incipient motion of sand-gravel sediment mixtures." *Journal of Hydraulic Engineering*, 119(12), 1400–1415.

Kumar, A., and Kothyari, U. C. (2012). "Three-dimensional flow characteristics within the scour hole around circular uniform and compound piers." *Journal of Hydraulic Engineering*, 138(5), 420–429.

Lyle, W. M., and Smerdon, E. T. (1965). "Relation of compaction and other soil properties to erosion resistance of soils." *Trans. ASAE*, 419–422.

Lyn, D. A. (1987). "Unsteady sediment-transport modeling." *Journal of Hydraulic Engineering*, 113(1), 1–15.

Lyn, D. A. (1993). "Turbulence measurements in open-channel flows over artificial bed forms." *Journal of Hydraulic Engineering*, 119(3), 306–326.

Mackin, J. H. (1948). "Concept of the graded river." *Bulletin of the Geological Society of America*, 59, 463–511.

Mazumder, B. S., and Ojha, S. P. (2007). "Turbulence statistics of flow due to wave-current interaction." *Flow Measurement and Instrumentation*, 18, 129–138.

Mehta, A. J., Hayter, E. J., Parker, W. R., Krone, R. B., and Teeter, A. M. (1989). "Cohesive

sediment transport. I: process description." *Journal of Hydraulic Engineering*, 115(8), 1076–1093.

Meyer-Peter, E., and Müller, R. (1948). "Formulas for bed-load transport." *Proceedings of the 2nd Meeting of the International Association of Hydraulic Research*, IAHR, Stockholm, 39–64.

Misri, R. L. (1981). "Partial bed load transport of coarse nonuniform sediment." IIT Roorkee.

Misri, R. L., Garde, R. J., and Ranga Raju, K. G. (1984). "Bed load transport of coarse nonuniform sediment." *Journal of Hydraulic Engineering*, 110(3), 312–328.

Mitchener, H., and Torfs, H. (1996). "Erosion of mud/sand mixtures." *Coastal Engineering*, 29(1–2), 1–25.

Mostafa, T. S., Imran, J., Chaudhry, M. H., and Kahn, I. B. (2008). "Erosion resistance of cohesive soils." *Journal of Hydraulic Research*, 46(6), 777–787.

Murray, W. A. (1976). *Erodibility of coarse Sand / clayey silt mixtures*. Report No. 411.2, 25 pp.

Muzzammil, M., and Gangadhariah, T. (2003). "The mean characteristics of horseshoe vortex at a cylindrical pier." *Journal of Hydraulic Research*, 41(3), 285–297.

Nezu, I. (1977). "Turbulent Structure in Compound Open-Channel Flows." Ph.D. Thesis. Department of Civil Engineering, Kyoto university, Japan.

Nikora, V., and Goring, D. (2000). "Flow turbulence over fixed and weakly mobile gravel beds." *Journal of Hydraulic Engineering*, 126(9), 679–690.

Nujić, M. (1995). "Efficient implementation of non-oscillatory schemes for the computation of free-surface flows." *Journal of Hydraulic Research*, 33(1), 101–111.

Ojha, S. P., and Mazumder, B. S. (2010). "Turbulence characteristics of flow over a series of 2-D bed forms in the presence of surface waves." *Journal of Geophysical Research*, 115(F04016), 1–15.

Owens, P. N., Batalla, R. J., Collins, A. J., Gomez, B., Hicks, D. M., Horowitz, A. J., Kondolf, G. M., Marden, M., Page, M. J., Peacock, D. H., Petticrew, E. L., Salomons, W., and Trustrum, N. A. (2005). "Fine-grained sediment in river systems: environmental significance and management issues." *River Research and Applications*, 21, 693–717.

Paintal, A. S. (1971). "A Stochastic Model Of Bed Load Transport." *Journal of Hydraulic Research*, 9(4), 527–554.

Panagiotopoulos, I., Voulgaris, G., and Collins, M. B. (1997). "The influence of clay on the threshold of movement of fine sandy beds." *Coastal Engineering*, 32(1), 19–43.

Parchure, T. M., and Mehta, A. J. (1985). "Erosion of soft cohesive sediment deposits." *Journal of Hydraulic Engineering*, 111(10), 1308–1326.

Parker, G. (1979). "Hydraulic geometry of active gravel rivers." *Journal of Hydraulic Division*,

105(9), 1185–1201.

Parker, G. (1990). "Surface-based bedload transport relation for gravel rivers." *Journal of Hydraulic Research*, 28(4), 417–436.

Parker, G., Klingeman, P. C., and McLean, D. G. (1982). "Bedload and size distribution in paved gravel-bed streams." *Journal of the Hydraulics Division*, 108(4), 544–571.

Patel, P. L., Porey, P. D., Ghare, A. D., and Patel, S. B. (2009). "Entrainment characteristics of nonuniform unimodal and bimodal sediments." *KSCE Journal of Civil Engineering*, 13(3), 189–194.

Patel, P. L., and Ranga Raju, K. G. (1999). "Critical tractive stress of nonuniform sediments." *Journal of Hydraulic Research*, 37(1), 39–58.

Proffitt, G. T., and Sutherland, A. J. (1983). "Transport of non-uniform sediments." *Journal of Hydraulic Research*, 21(1), 33–43.

Van Prooijen, B. C., and Winterwerp, J. C. (2010). "A stochastic formulation for erosion of cohesive sediments." *Journal of Geophysical Research*, 115, 1–15.

Qian, H., Cao, Z., Pender, G., Liu, H., and Hu, P. (2015). "Well-balanced numerical modelling of non-uniform sediment transport in alluvial rivers." *International Journal of Sediment Research*, Elsevier, 30(2), 117–130.

Ramesh, B. (2012). "Near bed particle motion over transitionally rough bed using high speed imaging." Ph.D. Thesis, Civil Engineering, IIT Roorkee, India.

Ravisangar, V., Sturm, T. W., and Amirtharajah, A. (2005). "Influence of sediment structure on erosional strength and density of kaolinite sediment beds." *Journal of Hydraulic Engineering*, 131(5), 356–365.

Roberts, J., Jepsen, R., Gotthard, D., and Lick, W. (1998). "Effects of particle size and bulk density on erosion of quartz particles." *Journal of Hydraulic Engineering*, 124(12), 1261–1267.

Rodriguez, J. F., and Garcia, M. H. (2008). "Laboratory measurements of 3-D flow patterns and turbulence in straight open channel with rough bed." *Journal of Hydraulic Research*, 46(4), 454–465.

Samaga, B. R., Ranga Raju, K. G., and Garde, R. J. (1986a). "Bed load transport of sediment mixtures." *Journal of Hydraulic Engineering*, 112(11), 1003–1018.

Samaga, B. R., Ranga Raju, K. G., and Garde, R. J. (1986b). "Suspended load transport of sediment mixtures." *Journal of Hydraulic Engineering*, 112(11), 1019–1035.

Sanford, L. P., and Maa, J. P.-Y. (2001). "A unified erosion formulation for fine sediments." *Marine Geology*, 179(1–2), 9–23.

Shields, I. A. (1936). *Application of similarity principles and turbulence research to bed-load movement. Publication no. 167.*

Shvidchenko, A. B., Pender, G., and Hoey, T. B. (2001). "Critical shear stress for incipient motion of sand/gravel streambeds." *Water Resources Research*, 37(8), 2273–2283.

Simões, F. J. M. (2014). "Shear velocity criterion for incipient motion of sediment." *Water Science and Engineering*, Hohai University. Production and hosting by Elsevier B.V., 7(2), 183–193.

Simons, D. B., Richardson, E. V, and Haushild, W. L. (1963). *Some effects of fine sediment on flow phenomena*.

Singh, A. K., Kothyari, U. C., and Ranga Raju, K. G. (2004). "Rapidly varying transient flows in alluvial rivers." *Journal of Hydraulic Research*, 42(5), 473–486.

Singh, M., Singh, I. B., and Müller, G. (2007). "Sediment characteristics and transportation dynamics of the Ganga River." *Geomorphology*, 86(1–2), 144–175.

Singh, S. K., Debnath, K., and Mazumder, B. S. (2016). "Turbulence statistics of wave-current flow over a submerged cube." *Journal of Waterway, Port, Coastal, and Ocean Engineering*, 142(3), 1–20.

Singh, U. K., Ahmad, Z., and Kumar, A. (2013). "Turbulence structures over mobile-bed of cohesive sediment mixture." *Hydro 2013 Iinternational*, IIT Madras, Chennai, 714–720.

Singh, V., and Bhallamudi, S. M. (1997). "Hydrodynamic modeling of basin irrigation." *Journal of Irrigation and Drainage Engineering*, 123(6), 407–414.

Song, T., and Chiew, Y. M. (2001). "Turbulence measurement in nonuniform open-channel flow using acoustic Doppler velocimeter (ADV)." *Journal of Engineering Mechanics*, 127(3), 219–232.

Song, T., and Graf, W. H. (1996). "Velocity and turbulence distribution in unsteady open-channel flows." *Journal of Hydraulic Engineering*, 122(3), 141–154.

Soni, J. P., Garde, R. J., and Raju Raju, K. G. (1980). "Aggradation in streams due to overloading." *Journal of Hydraulic Division*, 106, 117–132.

De Sutter, R., Huygens, M., and Verhoeven, R. (2000). "Transport of sediment mixtures." *The role of erosion and sediment transport in nutrient and contaminant transfer, IAHS Publication No. 263*, Waterloo, Canada.

Swamee, P. K., and Ojha, C. S. P. (1991). "Bed-load and suspended-load transport of nonuniform sediments." *Journal of Hydraulic Engineering*, 117(6), 774–787.

Tominaga, A., Nezu, I., Ezaki, K., and Nakagawa, H. (1989). "Three-dimensional turbulent structure in straight open channel flows." *Journal of Hydraulic Research*, 27(1), 149–173.

Torfs, J., Jiang, J., and Mehta, A. J. (2000). "Assessment of the erodibility of fine/coarse sediment mixtures." *Proceedings in Marine Science*, 109–123.

Vogel, K. R., Niekerk, A. van, Slingerland, R. L., and Bridge, J. S. (1992). "Routing of heterogeneous sediments over movable bed: Model verification." *Journal of Hydraulic*

*Engineering*, 118(2), 263–279.

Wan, C. F., and Fell, R. (2004). "Investigation of rate of erosion of soils in embankment dams." *Journal of Hydraulic Engineering*, 130(4), 373–380.

Wang, J., Guo, W., Xu, H., Jin, Z., and Zhou, Y. (2012). "Study on incipient motion of consolidated cohesive fine sediment." *Applied Mechanics and Materials*, 204–208, 354–358.

Wiberg, P. L., and Smith, J. D. (1987). "Calculations of the critical shear stress for motion of uniform and heterogeneous sediments." *Water Resources Research*, 23(8), 1471–1480.

Wijetunge, J. J., and Sleath, J. F. A. (1998). "Effects of sediment transport on bed friction and turbulence." *Journal of waterway, port, coastal, and ocean engineering*, 124(4), 172–178.

Wilcock, P. R. (1993). "Critical shear stress of natural sediments." *Journal of Hydraulic Engineering*, 119(4), 491–505.

Wilcock, P. R., Kenworthy, S. T., and Crowe, J. C. (2001). "Experimental study of the transport of mixed sand and gravel." *Water Resources Research*, 37(12), 3349–3358.

Wilcock, P. R., and Southard, J. B. (1988). "Experimental study of incipient motion in mixed-size sediment." *Water Resources Research*, 24(7), 1137–1151.

Winterwerp, J. C., van Kesteren, W. G. M., van Prooijen, B., and Jacobs, W. (2012). "A conceptual framework for shear flow–induced erosion of soft cohesive sediment beds." *Journal of Geophysical Research*, 117(C10), C10020.

Wong, M., and Parker, G. (2006). "Reanalysis and correction of bed-load relation of Meyer-Peter and Müller using their own database." *Journal of Hydraulic Engineering*, 132(11), 1159–1168.

Woo, H., Julien, P. Y., and Richardson, E. V. (1987). "Transport of bed sediment in clay suspensions." *Journal of Hydraulic Engineering*, 113(8), 1061–1066.

Wu, B., Molinas, A., and Julien, P. Y. (2004). "Bed-material load computations for nonuniform sediments." *Journal of Hydraulic Engineering*, 130(10), 1002–1012.

Wu, B., Molinas, A., and Shu, A. (2003). "Fractional transport of sediment mixtures." *International Journal of Sediment Research*, 18(3), 232–247.

Wu, W., Wang, S. S. Y., and Jia, Y. (2000). "Nonuniform sediment transport in alluvial rivers." *Journal of Hydraulic Research*, 38(6), 427–434.

Xu, D., Bai, Y., Ji, C., and Williams, J. (2015). "Experimental study of the density influence on the incipient motion and erosion modes of muds in unidirectional flows: the case of Huangmaohai Estuary." *Ocean Dynamics*, 65(2), 187–201.

Xu, Y., Jiand, H., Chu, F., and Liu, C. (2014). "Fractal model for surface erosion of cohesive sediments." *Fractals*, 22(3), 1440006.

Yalin, M. S., and Karahan, E. (1979). "Inception of sediment transport." *Journal of the Hydraulics Division, ASCE*, 105(11), 1433–1443.

Yang, C. T. (1973). "Incipient motion and sediment transport." *Journal of the Hydraulics Division*, 99(10), 1679–1704.

Yang, C. T., Molinas, A., and Wu, B. (1996). "Sediment transport in the Yellow River." *Journal of Hydraulic Engineering*, 122(5), 237–244.

Zanke, U. C. E. (2003). "On the influence of turbulence on the initiation of sediment motion." *International Journal of Sediment Research*, 18(1), 17–31.

Zhu, Y. H., Lu, J. Y., Liao, H. Z., Wang, J. S., Fan, B. L., and Yao, S. M. (2008). "Research on cohesive sediment erosion by flow: An overview." *Science in China, Series E: Technological Sciences*, 51(11), 2001–2012.

# APPENDIX – A

**Sediment and hydraulics parameters for incipient motion**

| Run No. | Sediment proportions (%) | | | | $d_{50}$ | $w$ | $\gamma_s$ | $GS$ | $h$ | $Q$ | $S_f$ | $\tau_{*cr}$ |
|---|---|---|---|---|---|---|---|---|---|---|---|---|
| | Clay | Silt | Sand | Gravel | (mm) | (%) | (kN/m$^3$) | (kN/m$^3$) | (m) | (m$^3$/s) | (-) | (-) |
| (1) | (2) | (3) | (4) | (5) | (6) | (7) | (8) | (9) | (10) | (11) | (12) | (13) |
| 1 | 10.00 | 45.00 | - | 45.00 | 2.5043 | 16.03 | 17.30 | 0.00 | 0.0363 | 0.0110 | 0.0067 | 0.0341 |
| 2 | 10.00 | 45.00 | - | 45.00 | 2.5043 | 10.23 | 16.56 | 0.00 | 0.0333 | 0.0105 | 0.0075 | 0.0376 |
| 3 | 10.00 | 45.00 | - | 45.00 | 2.5043 | 15.15 | 17.19 | 0.00 | 0.0285 | 0.0079 | 0.0079 | 0.0321 |
| 4 | 10.00 | 45.00 | - | 45.00 | 2.5043 | 14.29 | 18.21 | 0.00 | 0.0295 | 0.0083 | 0.0094 | 0.0335 |
| 5 | 10.00 | 45.00 | - | 45.00 | 2.5043 | 11.84 | 16.39 | 0.00 | 0.0272 | 0.0087 | 0.0084 | 0.0392 |
| 6 | 20.00 | 40.00 | - | 40.00 | 2.2276 | 12.13 | 17.64 | 7.03 | 0.0298 | 0.0096 | 0.0099 | 0.0446 |
| 7 | 20.00 | 40.00 | - | 40.00 | 2.2276 | 12.46 | 17.76 | 5.95 | 0.0303 | 0.0093 | 0.0120 | 0.0438 |
| 8 | 20.00 | 40.00 | - | 40.00 | 2.2276 | 11.39 | 17.87 | 5.41 | 0.0483 | 0.0143 | 0.0089 | 0.0385 |
| 9 | 20.00 | 40.00 | - | 40.00 | 2.2276 | 11.25 | 16.62 | 7.57 | 0.0384 | 0.0137 | 0.0045 | 0.0427 |
| 10 | 30.00 | 35.00 | - | 35.00 | 1.9509 | 10.61 | 17.30 | 10.81 | 0.0317 | 0.0099 | 0.0080 | 0.0455 |
| 11 | 30.00 | 35.00 | - | 35.00 | 1.9509 | 11.92 | 17.87 | 10.27 | 0.0378 | 0.0121 | 0.0079 | 0.0466 |
| 12 | 30.00 | 35.00 | - | 35.00 | 1.9509 | 7.72 | 17.76 | 11.35 | 0.0418 | 0.0131 | 0.0122 | 0.0526 |
| 13 | 30.00 | 35.00 | - | 35.00 | 1.9509 | 10.64 | 18.55 | 11.89 | 0.0381 | 0.0134 | 0.0117 | 0.0597 |
| 14 | 30.00 | 35.00 | - | 35.00 | 1.9509 | 12.09 | 17.41 | 18.38 | 0.0378 | 0.0123 | 0.0097 | 0.0505 |
| 15 | 40.00 | 30.00 | - | 30.00 | 1.6742 | 16.20 | 18.78 | 22.17 | 0.0485 | 0.0327 | 0.0060 | 0.1487 |
| 16 | 40.00 | 30.00 | - | 30.00 | 1.6742 | 13.82 | 19.35 | 21.09 | 0.0587 | 0.0308 | 0.0088 | 0.1136 |
| 17 | 40.00 | 30.00 | - | 30.00 | 1.6742 | 14.64 | 19.01 | 18.92 | 0.0397 | 0.0230 | 0.0104 | 0.1424 |
| 18 | 40.00 | 30.00 | - | 30.00 | 1.6742 | 11.06 | 18.78 | 18.92 | 0.0309 | 0.0134 | 0.0081 | 0.0837 |
| 19 | 50.00 | 25.00 | - | 25.00 | 1.3975 | 12.74 | 20.37 | 30.28 | 0.0228 | 0.0123 | 0.0094 | 0.1371 |
| 20 | 50.00 | 25.00 | - | 25.00 | 1.3975 | 14.42 | 20.60 | 42.17 | 0.0398 | 0.0220 | 0.0123 | 0.1604 |
| 21 | 50.00 | 25.00 | - | 25.00 | 1.3975 | 16.45 | 20.54 | 38.39 | 0.0407 | 0.0221 | 0.0057 | 0.1218 |
| 22 | 50.00 | 25.00 | - | 25.00 | 1.3975 | 15.53 | 20.49 | 32.44 | 0.0383 | 0.0246 | 0.0050 | 0.1510 |
| 23 | 10.00 | 30.00 | 30.00 | 30.00 | 1.8500 | 10.64 | 17.53 | 0.00 | 0.0503 | 0.0169 | 0.0061 | 0.0489 |
| 24 | 10.00 | 30.00 | 30.00 | 30.00 | 1.8500 | 8.13 | 18.67 | 0.00 | 0.0542 | 0.0137 | 0.0138 | 0.0390 |
| 25 | 10.00 | 30.00 | 30.00 | 30.00 | 1.8500 | 7.88 | 18.21 | 0.00 | 0.0452 | 0.0109 | 0.0096 | 0.0336 |
| 26 | 10.00 | 30.00 | 30.00 | 30.00 | 1.8500 | 9.60 | 17.76 | 0.00 | 0.0582 | 0.0129 | 0.0160 | 0.0373 |

| (1) | (2) | (3) | (4) | (5) | (6) | (7) | (8) | (9) | (10) | (11) | (12) | (13) |
|---|---|---|---|---|---|---|---|---|---|---|---|---|
| 27 | 20.00 | 26.67 | 26.67 | 26.67 | 1.6460 | 10.44 | 18.35 | 7.57 | 0.0662 | 0.0131 | 0.0144 | 0.0320 |
| 28 | 20.00 | 26.67 | 26.67 | 26.67 | 1.6460 | 16.58 | 19.46 | 9.73 | 0.0486 | 0.0130 | 0.0136 | 0.0490 |
| 29 | 20.00 | 26.67 | 26.67 | 26.67 | 1.6460 | 12.65 | 16.96 | 6.49 | 0.0406 | 0.0133 | 0.0165 | 0.0761 |
| 30 | 20.00 | 26.67 | 26.67 | 26.67 | 1.6460 | 11.20 | 18.44 | 8.65 | 0.0331 | 0.0117 | 0.0102 | 0.0673 |
| 31 | 30.00 | 23.33 | 23.33 | 23.33 | 1.4420 | 13.31 | 19.86 | 19.46 | 0.0348 | 0.0141 | 0.0093 | 0.0872 |
| 32 | 30.00 | 23.33 | 23.33 | 23.33 | 1.4420 | 13.07 | 19.69 | 20.00 | 0.0334 | 0.0129 | 0.0104 | 0.0846 |
| 33 | 30.00 | 23.33 | 23.33 | 23.33 | 1.4420 | 18.25 | 19.92 | 18.92 | 0.0296 | 0.0135 | 0.0048 | 0.0920 |
| 34 | 30.00 | 23.33 | 23.33 | 23.33 | 1.4420 | 12.62 | 19.80 | 17.84 | 0.0361 | 0.0127 | 0.0087 | 0.0709 |
| 35 | 40.00 | 20.00 | 20.00 | 20.00 | 1.2380 | 12.11 | 19.12 | 16.76 | 0.0415 | 0.0155 | 0.0066 | 0.0789 |
| 36 | 40.00 | 20.00 | 20.00 | 20.00 | 1.2380 | 13.78 | 20.20 | 27.03 | 0.0368 | 0.0165 | 0.0060 | 0.1012 |
| 37 | 40.00 | 20.00 | 20.00 | 20.00 | 1.2380 | 14.01 | 20.37 | 28.12 | 0.0325 | 0.0162 | 0.0098 | 0.1344 |
| 38 | 40.00 | 20.00 | 20.00 | 20.00 | 1.2380 | 13.10 | 20.15 | 29.74 | 0.0358 | 0.0142 | 0.0087 | 0.0938 |
| 39 | 50.00 | 16.67 | 16.67 | 16.67 | 1.0340 | 14.79 | 20.77 | 40.01 | 0.0425 | 0.0185 | 0.0107 | 0.1283 |
| 40 | 50.00 | 16.67 | 16.67 | 16.67 | 1.0340 | 14.63 | 21.06 | 43.25 | 0.0470 | 0.0217 | 0.0081 | 0.1303 |
| 41 | 50.00 | 16.67 | 16.67 | 16.67 | 1.0340 | 12.43 | 18.55 | 19.46 | 0.0553 | 0.0217 | 0.0085 | 0.1030 |
| 42 | 50.00 | 16.67 | 16.67 | 16.67 | 1.0340 | 14.66 | 20.03 | 25.41 | 0.0423 | 0.0297 | 0.0084 | 0.1680 |
| 43 | 10.00 | 45.00 | 45.00 | - | 0.2993 | 13.62 | 19.18 | 6.49 | 0.0277 | 0.0071 | 0.0054 | 0.1235 |
| 44 | 10.00 | 45.00 | 45.00 | - | 0.2993 | 12.50 | 17.41 | 6.49 | 0.0283 | 0.0070 | 0.0058 | 0.1191 |
| 45 | 10.00 | 45.00 | 45.00 | - | 0.2993 | 12.20 | 17.30 | 5.95 | 0.0354 | 0.0090 | 0.0041 | 0.1168 |
| 46 | 10.00 | 45.00 | 45.00 | - | 0.2993 | 14.18 | 18.32 | 7.03 | 0.0309 | 0.0072 | 0.0040 | 0.1007 |
| 47 | 20.00 | 40.00 | 40.00 | - | 0.2676 | 13.16 | 19.58 | 11.89 | 0.0266 | 0.0077 | 0.0037 | 0.1450 |
| 48 | 20.00 | 40.00 | 40.00 | - | 0.2676 | 16.50 | 18.10 | 8.11 | 0.0263 | 0.0077 | 0.0027 | 0.1366 |
| 49 | 20.00 | 40.00 | 40.00 | - | 0.2676 | 18.71 | 18.78 | 8.65 | 0.0325 | 0.0082 | 0.0063 | 0.1477 |
| 50 | 20.00 | 40.00 | 40.00 | - | 0.2676 | 14.71 | 17.76 | 7.57 | 0.0271 | 0.0078 | 0.0053 | 0.1603 |
| 51 | 30.00 | 35.00 | 35.00 | - | 0.2359 | 15.23 | 19.58 | 24.33 | 0.0398 | 0.0115 | 0.0044 | 0.1673 |
| 52 | 30.00 | 35.00 | 35.00 | - | 0.2359 | 16.78 | 20.20 | 30.28 | 0.0376 | 0.0122 | 0.0051 | 0.2059 |
| 53 | 30.00 | 35.00 | 35.00 | - | 0.2359 | 12.41 | 18.04 | 18.38 | 0.0397 | 0.0119 | 0.0054 | 0.1913 |
| 54 | 30.00 | 35.00 | 35.00 | - | 0.2359 | 15.61 | 19.80 | 17.84 | 0.0403 | 0.0128 | 0.0029 | 0.1740 |
| 55 | 40.00 | 30.00 | 30.00 | - | 0.2042 | 14.86 | 19.35 | 23.25 | 0.0365 | 0.0117 | 0.0052 | 0.2270 |
| 56 | 40.00 | 30.00 | 30.00 | - | 0.2042 | 17.22 | 20.15 | 31.36 | 0.0522 | 0.0195 | 0.0042 | 0.2710 |
| 57 | 40.00 | 30.00 | 30.00 | - | 0.2042 | 16.85 | 19.80 | 34.06 | 0.0373 | 0.0123 | 0.0059 | 0.2452 |
| 58 | 40.00 | 30.00 | 30.00 | - | 0.2042 | 17.00 | 19.92 | 29.20 | 0.0368 | 0.0119 | 0.0034 | 0.2081 |

| (1) | (2) | (3) | (4) | (5) | (6) | (7) | (8) | (9) | (10) | (11) | (12) | (13) |
|---|---|---|---|---|---|---|---|---|---|---|---|---|
| 59 | 50.00 | 25.00 | 25.00 | - | 0.1725 | 15.92 | 19.92 | 32.98 | 0.0267 | 0.0090 | 0.0122 | 0.3708 |
| 60 | 50.00 | 25.00 | 25.00 | - | 0.1725 | 19.38 | 19.80 | 32.44 | 0.0344 | 0.0113 | 0.0118 | 0.3360 |
| 61 | 50.00 | 25.00 | 25.00 | - | 0.1725 | 17.13 | 19.46 | 31.36 | 0.0250 | 0.0079 | 0.0102 | 0.2973 |
| 62 | 50.00 | 25.00 | 25.00 | - | 0.1725 | 17.72 | 19.01 | 23.79 | 0.0403 | 0.0128 | 0.0075 | 0.2762 |
| 63 | 50.00 | 25.00 | 25.00 | - | 0.1725 | 17.14 | 18.67 | 20.55 | 0.0243 | 0.0091 | 0.0034 | 0.2936 |
| 64 | 50.00 | 25.00 | 25.00 | - | 0.1725 | 15.91 | 18.67 | 19.46 | 0.0271 | 0.0088 | 0.0039 | 0.2447 |
| 65 | - | - | - | 100.00 | 5.5000 | - | - | - | 0.0971 | 0.0644 | 0.0051 | 0.0517 |
| 66 | - | - | - | | 5.5000 | - | - | - | 0.0701 | 0.0429 | 0.0085 | 0.0519 |
| 67 | - | - | - | | 5.5000 | - | - | - | 0.0758 | 0.0469 | 0.0075 | 0.0511 |
| 68 | - | - | - | | 5.5000 | - | - | - | 0.0783 | 0.0504 | 0.0062 | 0.0518 |
| 69 | - | 33.33 | 33.33 | 33.33 | 2.0540 | - | - | - | 0.0263 | 0.0075 | 0.0071 | 0.0368 |
| 70 | - | 33.33 | 33.33 | 33.33 | 2.0540 | - | - | - | 0.0253 | 0.0071 | 0.0067 | 0.0354 |
| 71 | - | 33.33 | 33.33 | 33.33 | 2.0540 | - | - | - | 0.0257 | 0.0069 | 0.0092 | 0.0361 |
| 72 | - | 33.33 | 33.33 | 33.33 | 2.0540 | - | - | - | 0.0252 | 0.0072 | 0.0082 | 0.0377 |
| 73 | - | 50.00 | - | 50.00 | 2.7810 | - | - | - | 0.0242 | 0.0072 | 0.0105 | 0.0344 |
| 74 | - | 50.00 | - | 50.00 | 2.7810 | - | - | - | 0.0253 | 0.0069 | 0.0078 | 0.0278 |
| 75 | - | 50.00 | - | 50.00 | 2.7810 | - | - | - | 0.0248 | 0.0071 | 0.0077 | 0.0303 |
| 76 | - | 50.00 | - | 50.00 | 2.7810 | - | - | - | 0.0240 | 0.0071 | 0.0093 | 0.0332 |
| 77 | - | 50.00 | 50.00 | - | 0.3310 | - | - | - | 0.0375 | 0.0069 | 0.0055 | 0.0722 |
| 78 | - | 50.00 | 50.00 | - | 0.3310 | - | - | - | 0.0370 | 0.0069 | 0.0056 | 0.0733 |
| 79 | - | 50.00 | 50.00 | - | 0.3310 | - | - | - | 0.0372 | 0.0068 | 0.0074 | 0.0759 |
| 80 | - | 50.00 | 50.00 | - | 0.3310 | - | - | - | 0.0369 | 0.0068 | 0.0086 | 0.0783 |

# APPENDIX – B

Sediment and hydraulic parameters for transport rate of sediment

| Run No. | Observation No. | Clay | $d_{50}$ | Time | Discharge | Bed slope | $\gamma_s$ | Water content | UCS | $q_{Bg}$ | $q_{Bv}$ | $q_{Bf}$ |
|---|---|---|---|---|---|---|---|---|---|---|---|---|
| | | (%) | (m) | (min) | ($m^3$/s) | (-) | (kN/$m^3$) | (-) | (kN/$m^2$) | (N/m/s) | (N/m/s) | (N/m/s) |
| (1) | (2) | (3) | (4) | (5) | (6) | (7) | (8) | (9) | (10) | (11) | (12) | (13) |
| GSC 1 | GSC_1.1 | 10 | 0.002504 | 15 | 0.0503 | 0.00721 | 17.30 | 0.16 | 0.00 | 0.1394 | - | 0.0932 |
| | GSC_1.2 | 10 | 0.002504 | 30 | 0.0503 | 0.00721 | 17.30 | 0.16 | 0.00 | 0.1218 | - | 0.0806 |
| | GSC_1.3 | 10 | 0.002504 | 45 | 0.0503 | 0.00721 | 17.30 | 0.16 | 0.00 | 0.0905 | - | 0.0667 |
| | GSC_1.4 | 10 | 0.002504 | 75 | 0.0503 | 0.00721 | 17.30 | 0.16 | 0.00 | 0.0629 | - | 0.0553 |
| | GSC_1.5 | 10 | 0.002504 | 120 | 0.0503 | 0.00721 | 17.30 | 0.16 | 0.00 | 0.0443 | - | 0.0441 |
| | GSC_1.6 | 10 | 0.002504 | 165 | 0.0503 | 0.00721 | 17.30 | 0.16 | 0.00 | 0.0283 | - | 0.0352 |
| | GSC_1.7 | 10 | 0.002504 | 210 | 0.0503 | 0.00721 | 17.30 | 0.16 | 0.00 | 0.0204 | - | 0.0302 |
| | GSC_1.8 | 10 | 0.002504 | 240 | 0.0503 | 0.00721 | 17.30 | 0.16 | 0.00 | 0.0158 | - | 0.0254 |
| | GSC_1.9 | 10 | 0.002504 | 270 | 0.0503 | 0.00721 | 17.30 | 0.16 | 0.00 | 0.0162 | - | 0.0238 |
| | GSC_1.10 | 10 | 0.002504 | 300 | 0.0503 | 0.00721 | 17.30 | 0.16 | 0.00 | 0.0136 | - | 0.0200 |
| | GSC_1.11 | 10 | 0.002504 | 330 | 0.0503 | 0.00721 | 17.30 | 0.16 | 0.00 | 0.0111 | - | 0.0227 |
| | GSC_1.12 | 10 | 0.002504 | 370 | 0.0503 | 0.00721 | 17.30 | 0.16 | 0.00 | 0.0086 | - | 0.0197 |
| | GSC_1.13 | 10 | 0.002504 | 390 | 0.0503 | 0.00721 | 17.30 | 0.16 | 0.00 | 0.0082 | - | 0.0163 |
| | GSC_1.14 | 10 | 0.002504 | 430 | 0.0503 | 0.00721 | 17.30 | 0.16 | 0.00 | 0.0077 | - | 0.0131 |
| | GSC_1.15 | 10 | 0.002504 | 470 | 0.0503 | 0.00721 | 17.30 | 0.16 | 0.00 | 0.0060 | - | 0.0089 |
| | GSC_1.16 | 10 | 0.002504 | 530 | 0.0503 | 0.00721 | 17.30 | 0.16 | 0.00 | 0.0049 | - | 0.0089 |
| | GSC_1.17 | 10 | 0.002504 | 560 | 0.0503 | 0.00721 | 17.30 | 0.16 | 0.00 | 0.0044 | - | 0.0042 |
| | GSC_1.18 | 10 | 0.002504 | 620 | 0.0503 | 0.00721 | 17.30 | 0.16 | 0.00 | 0.0040 | - | 0.0029 |
| | GSC_1.19 | 10 | 0.002504 | 680 | 0.0503 | 0.00721 | 17.30 | 0.16 | 0.00 | 0.0035 | - | 0.0014 |
| | GSC_1.20 | 10 | 0.002504 | 740 | 0.0503 | 0.00721 | 17.30 | 0.16 | 0.00 | 0.0031 | - | 0.0007 |
| | GSC_1.21 | 10 | 0.002504 | 790 | 0.0503 | 0.00721 | 17.30 | 0.16 | 0.00 | 0.0021 | - | 0.0004 |

| (1) | (2) | (3) | (4) | (5) | (6) | (7) | (8) | (9) | (10) | (11) | (12) | (13) |
|---|---|---|---|---|---|---|---|---|---|---|---|---|
| GSC 2 | GSC_1.22 | 10 | 0.002504 | 15 | 0.0708 | 0.00721 | 16.56 | 0.10 | 0.00 | 0.1573 | - | 0.1199 |
| | GSC_1.23 | 10 | 0.002504 | 22 | 0.0708 | 0.00721 | 16.56 | 0.10 | 0.00 | 0.1454 | - | 0.1047 |
| | GSC_1.24 | 10 | 0.002504 | 35 | 0.0708 | 0.00721 | 16.56 | 0.10 | 0.00 | 0.1234 | - | 0.0853 |
| | GSC_1.25 | 10 | 0.002504 | 50 | 0.0708 | 0.00721 | 16.56 | 0.10 | 0.00 | 0.0949 | - | 0.0619 |
| | GSC_1.26 | 10 | 0.002504 | 65 | 0.0708 | 0.00721 | 16.56 | 0.10 | 0.00 | 0.0824 | - | 0.0499 |
| | GSC_1.27 | 10 | 0.002504 | 95 | 0.0708 | 0.00721 | 16.56 | 0.10 | 0.00 | 0.0703 | - | 0.0500 |
| | GSC_1.28 | 10 | 0.002504 | 125 | 0.0708 | 0.00721 | 16.56 | 0.10 | 0.00 | 0.0593 | - | 0.0333 |
| | GSC_1.29 | 10 | 0.002504 | 155 | 0.0708 | 0.00721 | 16.56 | 0.10 | 0.00 | 0.0455 | - | 0.0324 |
| | GSC_1.30 | 10 | 0.002504 | 185 | 0.0708 | 0.00721 | 16.56 | 0.10 | 0.00 | 0.0385 | - | 0.0291 |
| | GSC_1.31 | 10 | 0.002504 | 215 | 0.0708 | 0.00721 | 16.56 | 0.10 | 0.00 | 0.0305 | - | 0.0307 |
| | GSC_1.32 | 10 | 0.002504 | 275 | 0.0708 | 0.00721 | 16.56 | 0.10 | 0.00 | 0.0246 | - | 0.0263 |
| | GSC_1.33 | 10 | 0.002504 | 305 | 0.0708 | 0.00721 | 16.56 | 0.10 | 0.00 | 0.0187 | - | 0.0224 |
| | GSC_1.34 | 10 | 0.002504 | 335 | 0.0708 | 0.00721 | 16.56 | 0.10 | 0.00 | 0.0149 | - | 0.0157 |
| | GSC_1.35 | 10 | 0.002504 | 365 | 0.0708 | 0.00721 | 16.56 | 0.10 | 0.00 | 0.0113 | - | 0.0079 |
| | GSC_1.36 | 10 | 0.002504 | 395 | 0.0708 | 0.00721 | 16.56 | 0.10 | 0.00 | 0.0091 | - | 0.0082 |
| | GSC_1.37 | 10 | 0.002504 | 425 | 0.0708 | 0.00721 | 16.56 | 0.10 | 0.00 | 0.0083 | - | 0.0058 |
| | GSC_1.38 | 10 | 0.002504 | 485 | 0.0708 | 0.00721 | 16.56 | 0.10 | 0.00 | 0.0073 | - | 0.0037 |
| | GSC_1.39 | 10 | 0.002504 | 545 | 0.0708 | 0.00721 | 16.56 | 0.10 | 0.00 | 0.0061 | - | 0.0023 |
| | GSC_1.40 | 10 | 0.002504 | 575 | 0.0708 | 0.00721 | 16.56 | 0.10 | 0.00 | 0.0041 | - | 0.0016 |
| | GSC_1.41 | 10 | 0.002504 | 635 | 0.0708 | 0.00721 | 16.56 | 0.10 | 0.00 | 0.0036 | - | 0.0015 |
| | GSC_1.42 | 10 | 0.002504 | 695 | 0.0708 | 0.00721 | 16.56 | 0.10 | 0.00 | 0.0023 | - | 0.0009 |
| | GSC_1.43 | 10 | 0.002504 | 740 | 0.0708 | 0.00721 | 16.56 | 0.10 | 0.00 | 0.0016 | - | 0.0004 |
| GSC 3 | GSC_1.44 | 10 | 0.002504 | 15 | 0.0504 | 0.00946 | 17.19 | 0.15 | 0.00 | 0.1418 | - | 0.1049 |
| | GSC_1.45 | 10 | 0.002504 | 35 | 0.0504 | 0.00946 | 17.19 | 0.15 | 0.00 | 0.1033 | - | 0.0821 |
| | GSC_1.46 | 10 | 0.002504 | 50 | 0.0504 | 0.00946 | 17.19 | 0.15 | 0.00 | 0.0791 | - | 0.0707 |
| | GSC_1.47 | 10 | 0.002504 | 65 | 0.0504 | 0.00946 | 17.19 | 0.15 | 0.00 | 0.0691 | - | 0.0598 |
| | GSC_1.48 | 10 | 0.002504 | 80 | 0.0504 | 0.00946 | 17.19 | 0.15 | 0.00 | 0.0604 | - | 0.0553 |
| | GSC_1.49 | 10 | 0.002504 | 110 | 0.0504 | 0.00946 | 17.19 | 0.15 | 0.00 | 0.0521 | - | 0.0468 |

| (1) | (2) | (3) | (4) | (5) | (6) | (7) | (8) | (9) | (10) | (11) | (12) | (13) |
|---|---|---|---|---|---|---|---|---|---|---|---|---|
| | GSC_1.50 | 10 | 0.002504 | 125 | 0.0504 | 0.00946 | 17.19 | 0.15 | 0.00 | 0.0473 | - | 0.0314 |
| | GSC_1.51 | 10 | 0.002504 | 170 | 0.0504 | 0.00946 | 17.19 | 0.15 | 0.00 | 0.0403 | - | 0.0262 |
| | GSC_1.52 | 10 | 0.002504 | 260 | 0.0504 | 0.00946 | 17.19 | 0.15 | 0.00 | 0.0354 | - | 0.0188 |
| | GSC_1.53 | 10 | 0.002504 | 290 | 0.0504 | 0.00946 | 17.19 | 0.15 | 0.00 | 0.0313 | - | 0.0150 |
| | GSC_1.54 | 10 | 0.002504 | 320 | 0.0504 | 0.00946 | 17.19 | 0.15 | 0.00 | 0.0254 | - | 0.0143 |
| | GSC_1.55 | 10 | 0.002504 | 350 | 0.0504 | 0.00946 | 17.19 | 0.15 | 0.00 | 0.0187 | - | 0.0132 |
| | GSC_1.56 | 10 | 0.002504 | 380 | 0.0504 | 0.00946 | 17.19 | 0.15 | 0.00 | 0.0139 | - | 0.0084 |
| | GSC_1.57 | 10 | 0.002504 | 415 | 0.0504 | 0.00946 | 17.19 | 0.15 | 0.00 | 0.0105 | - | 0.0066 |
| | GSC_1.58 | 10 | 0.002504 | 445 | 0.0504 | 0.00946 | 17.19 | 0.15 | 0.00 | 0.0071 | - | 0.0048 |
| | GSC_1.59 | 10 | 0.002504 | 475 | 0.0504 | 0.00946 | 17.19 | 0.15 | 0.00 | 0.0045 | - | 0.0038 |
| | GSC_1.60 | 10 | 0.002504 | 525 | 0.0504 | 0.00946 | 17.19 | 0.15 | 0.00 | 0.0033 | - | 0.0024 |
| | GSC_1.61 | 10 | 0.002504 | 585 | 0.0504 | 0.00946 | 17.19 | 0.15 | 0.00 | 0.0025 | - | 0.0017 |
| | GSC_1.62 | 10 | 0.002504 | 645 | 0.0504 | 0.00946 | 17.19 | 0.15 | 0.00 | 0.0019 | - | 0.0011 |
| | GSC_1.63 | 10 | 0.002504 | 705 | 0.0504 | 0.00946 | 17.19 | 0.15 | 0.00 | 0.0014 | - | 0.0009 |
| | GSC_1.64 | 10 | 0.002504 | 750 | 0.0504 | 0.00946 | 17.19 | 0.15 | 0.00 | 0.0008 | - | 0.0006 |
| GSC 4 | GSC_1.65 | 10 | 0.002504 | 10 | 0.0702 | 0.00946 | 16.39 | 0.12 | 0.00 | 0.1635 | - | 0.1438 |
| | GSC_1.66 | 10 | 0.002504 | 30 | 0.0702 | 0.00946 | 16.39 | 0.12 | 0.00 | 0.1424 | - | 0.1158 |
| | GSC_1.67 | 10 | 0.002504 | 45 | 0.0702 | 0.00946 | 16.39 | 0.12 | 0.00 | 0.1109 | - | 0.0944 |
| | GSC_1.68 | 10 | 0.002504 | 60 | 0.0702 | 0.00946 | 16.39 | 0.12 | 0.00 | 0.0908 | - | 0.0760 |
| | GSC_1.69 | 10 | 0.002504 | 75 | 0.0702 | 0.00946 | 16.39 | 0.12 | 0.00 | 0.0863 | - | 0.0598 |
| | GSC_1.70 | 10 | 0.002504 | 90 | 0.0702 | 0.00946 | 16.39 | 0.12 | 0.00 | 0.0787 | - | 0.0425 |
| | GSC_1.71 | 10 | 0.002504 | 120 | 0.0702 | 0.00946 | 16.39 | 0.12 | 0.00 | 0.0701 | - | 0.0396 |
| | GSC_1.72 | 10 | 0.002504 | 150 | 0.0702 | 0.00946 | 16.39 | 0.12 | 0.00 | 0.0631 | - | 0.0268 |
| | GSC_1.73 | 10 | 0.002504 | 180 | 0.0702 | 0.00946 | 16.39 | 0.12 | 0.00 | 0.0490 | - | 0.0168 |
| | GSC_1.74 | 10 | 0.002504 | 260 | 0.0702 | 0.00946 | 16.39 | 0.12 | 0.00 | 0.0339 | - | 0.0140 |
| | GSC_1.75 | 10 | 0.002504 | 290 | 0.0702 | 0.00946 | 16.39 | 0.12 | 0.00 | 0.0277 | - | 0.0106 |
| | GSC_1.76 | 10 | 0.002504 | 320 | 0.0702 | 0.00946 | 16.39 | 0.12 | 0.00 | 0.0259 | - | 0.0086 |
| | GSC_1.77 | 10 | 0.002504 | 365 | 0.0702 | 0.00946 | 16.39 | 0.12 | 0.00 | 0.0161 | - | 0.0091 |

| (1) | (2) | (3) | (4) | (5) | (6) | (7) | (8) | (9) | (10) | (11) | (12) | (13) |
|---|---|---|---|---|---|---|---|---|---|---|---|---|
| | GSC_1.78 | 10 | 0.002504 | 410 | 0.0702 | 0.00946 | 16.39 | 0.12 | 0.00 | 0.0135 | - | 0.0072 |
| | GSC_1.79 | 10 | 0.002504 | 440 | 0.0702 | 0.00946 | 16.39 | 0.12 | 0.00 | 0.0097 | - | 0.0058 |
| | GSC_1.80 | 10 | 0.002504 | 500 | 0.0702 | 0.00946 | 16.39 | 0.12 | 0.00 | 0.0050 | - | 0.0041 |
| | GSC_1.81 | 10 | 0.002504 | 570 | 0.0702 | 0.00946 | 16.39 | 0.12 | 0.00 | 0.0030 | - | 0.0030 |
| | GSC_1.82 | 10 | 0.002504 | 695 | 0.0702 | 0.00946 | 16.39 | 0.12 | 0.00 | 0.0025 | - | 0.0011 |
| GSC 5 | GSC_2.1 | 20 | 0.002228 | 10 | 0.0502 | 0.00946 | 17.64 | 0.12 | 7.03 | 0.0944 | - | 0.0965 |
| | GSC_2.2 | 20 | 0.002228 | 25 | 0.0502 | 0.00946 | 17.64 | 0.12 | 7.03 | 0.0719 | - | 0.0858 |
| | GSC_2.3 | 20 | 0.002228 | 40 | 0.0502 | 0.00946 | 17.64 | 0.12 | 7.03 | 0.0633 | - | 0.0639 |
| | GSC_2.4 | 20 | 0.002228 | 55 | 0.0502 | 0.00946 | 17.64 | 0.12 | 7.03 | 0.0547 | - | 0.0549 |
| | GSC_2.5 | 20 | 0.002228 | 70 | 0.0502 | 0.00946 | 17.64 | 0.12 | 7.03 | 0.0487 | - | 0.0415 |
| | GSC_2.6 | 20 | 0.002228 | 85 | 0.0502 | 0.00946 | 17.64 | 0.12 | 7.03 | 0.0407 | - | 0.0284 |
| | GSC_2.7 | 20 | 0.002228 | 115 | 0.0502 | 0.00946 | 17.64 | 0.12 | 7.03 | 0.0356 | - | 0.0299 |
| | GSC_2.8 | 20 | 0.002228 | 145 | 0.0502 | 0.00946 | 17.64 | 0.12 | 7.03 | 0.0300 | - | 0.0240 |
| | GSC_2.9 | 20 | 0.002228 | 175 | 0.0502 | 0.00946 | 17.64 | 0.12 | 7.03 | 0.0276 | - | 0.0261 |
| | GSC_2.10 | 20 | 0.002228 | 215 | 0.0502 | 0.00946 | 17.64 | 0.12 | 7.03 | 0.0257 | - | 0.0199 |
| | GSC_2.11 | 20 | 0.002228 | 275 | 0.0502 | 0.00946 | 17.64 | 0.12 | 7.03 | 0.0230 | - | 0.0171 |
| | GSC_2.12 | 20 | 0.002228 | 315 | 0.0502 | 0.00946 | 17.64 | 0.12 | 7.03 | 0.0215 | - | 0.0156 |
| | GSC_2.13 | 20 | 0.002228 | 345 | 0.0502 | 0.00946 | 17.64 | 0.12 | 7.03 | 0.0176 | - | 0.0120 |
| | GSC_2.14 | 20 | 0.002228 | 420 | 0.0502 | 0.00946 | 17.64 | 0.12 | 7.03 | 0.0136 | - | 0.0117 |
| | GSC_2.15 | 20 | 0.002228 | 465 | 0.0502 | 0.00946 | 17.64 | 0.12 | 7.03 | 0.0106 | - | 0.0076 |
| | GSC_2.16 | 20 | 0.002228 | 555 | 0.0502 | 0.00946 | 17.64 | 0.12 | 7.03 | 0.0078 | - | 0.0047 |
| | GSC_2.17 | 20 | 0.002228 | 615 | 0.0502 | 0.00946 | 17.64 | 0.12 | 7.03 | 0.0063 | - | 0.0026 |
| | GSC_2.18 | 20 | 0.002228 | 675 | 0.0502 | 0.00946 | 17.64 | 0.12 | 7.03 | 0.0049 | - | 0.0014 |
| | GSC_2.19 | 20 | 0.002228 | 760 | 0.0502 | 0.00946 | 17.64 | 0.12 | 7.03 | 0.0017 | - | 0.0008 |
| GSC 6 | GSC_2.20 | 20 | 0.002228 | 10 | 0.0708 | 0.00946 | 17.76 | 0.12 | 5.95 | 0.1473 | - | 0.1162 |
| | GSC_2.21 | 20 | 0.002228 | 25 | 0.0708 | 0.00946 | 17.76 | 0.12 | 5.95 | 0.1300 | - | 0.0999 |
| | GSC_2.22 | 20 | 0.002228 | 45 | 0.0708 | 0.00946 | 17.76 | 0.12 | 5.95 | 0.0993 | - | 0.0819 |
| | GSC_2.23 | 20 | 0.002228 | 75 | 0.0708 | 0.00946 | 17.76 | 0.12 | 5.95 | 0.0847 | - | 0.0667 |

| (1) | (2) | (3) | (4) | (5) | (6) | (7) | (8) | (9) | (10) | (11) | (12) | (13) |
|---|---|---|---|---|---|---|---|---|---|---|---|---|
| | GSC_2.24 | 20 | 0.002228 | 90 | 0.0708 | 0.00946 | 17.76 | 0.12 | 5.95 | 0.0728 | - | 0.0519 |
| | GSC_2.25 | 20 | 0.002228 | 120 | 0.0708 | 0.00946 | 17.76 | 0.12 | 5.95 | 0.0583 | - | 0.0412 |
| | GSC_2.26 | 20 | 0.002228 | 165 | 0.0708 | 0.00946 | 17.76 | 0.12 | 5.95 | 0.0426 | - | 0.0306 |
| | GSC_2.27 | 20 | 0.002228 | 225 | 0.0708 | 0.00946 | 17.76 | 0.12 | 5.95 | 0.0302 | - | 0.0238 |
| | GSC_2.28 | 20 | 0.002228 | 240 | 0.0708 | 0.00946 | 17.76 | 0.12 | 5.95 | 0.0232 | - | 0.0145 |
| | GSC_2.29 | 20 | 0.002228 | 300 | 0.0708 | 0.00946 | 17.76 | 0.12 | 5.95 | 0.0130 | - | 0.0115 |
| | GSC_2.30 | 20 | 0.002228 | 360 | 0.0708 | 0.00946 | 17.76 | 0.12 | 5.95 | 0.0103 | - | 0.0083 |
| | GSC_2.31 | 20 | 0.002228 | 420 | 0.0708 | 0.00946 | 17.76 | 0.12 | 5.95 | 0.0074 | - | 0.0051 |
| | GSC_2.32 | 20 | 0.002228 | 480 | 0.0708 | 0.00946 | 17.76 | 0.12 | 5.95 | 0.0055 | - | 0.0043 |
| | GSC_2.33 | 20 | 0.002228 | 540 | 0.0708 | 0.00946 | 17.76 | 0.12 | 5.95 | 0.0039 | - | 0.0022 |
| | GSC_2.34 | 20 | 0.002228 | 600 | 0.0708 | 0.00946 | 17.76 | 0.12 | 5.95 | 0.0025 | - | 0.0011 |
| | GSC_2.35 | 20 | 0.002228 | 700 | 0.0708 | 0.00946 | 17.76 | 0.12 | 5.95 | 0.0009 | - | 0.0006 |
| GSC 7 | GSC_2.36 | 20 | 0.002228 | 15 | 0.0712 | 0.00721 | 17.87 | 0.11 | 5.41 | 0.1154 | - | 0.1054 |
| | GSC_2.37 | 20 | 0.002228 | 30 | 0.0712 | 0.00721 | 17.87 | 0.11 | 5.41 | 0.0847 | - | 0.0874 |
| | GSC_2.38 | 20 | 0.002228 | 45 | 0.0712 | 0.00721 | 17.87 | 0.11 | 5.41 | 0.0691 | - | 0.0752 |
| | GSC_2.39 | 20 | 0.002228 | 60 | 0.0712 | 0.00721 | 17.87 | 0.11 | 5.41 | 0.0587 | - | 0.0639 |
| | GSC_2.40 | 20 | 0.002228 | 75 | 0.0712 | 0.00721 | 17.87 | 0.11 | 5.41 | 0.0497 | - | 0.0497 |
| | GSC_2.41 | 20 | 0.002228 | 100 | 0.0712 | 0.00721 | 17.87 | 0.11 | 5.41 | 0.0466 | - | 0.0404 |
| | GSC_2.42 | 20 | 0.002228 | 130 | 0.0712 | 0.00721 | 17.87 | 0.11 | 5.41 | 0.0436 | - | 0.0325 |
| | GSC_2.43 | 20 | 0.002228 | 150 | 0.0712 | 0.00721 | 17.87 | 0.11 | 5.41 | 0.0391 | - | 0.0225 |
| | GSC_2.44 | 20 | 0.002228 | 175 | 0.0712 | 0.00721 | 17.87 | 0.11 | 5.41 | 0.0368 | - | 0.0138 |
| | GSC_2.45 | 20 | 0.002228 | 240 | 0.0712 | 0.00721 | 17.87 | 0.11 | 5.41 | 0.0359 | - | 0.0116 |
| | GSC_2.46 | 20 | 0.002228 | 270 | 0.0712 | 0.00721 | 17.87 | 0.11 | 5.41 | 0.0321 | - | 0.0084 |
| | GSC_2.47 | 20 | 0.002228 | 300 | 0.0712 | 0.00721 | 17.87 | 0.11 | 5.41 | 0.0252 | - | 0.0084 |
| | GSC_2.48 | 20 | 0.002228 | 345 | 0.0712 | 0.00721 | 17.87 | 0.11 | 5.41 | 0.0161 | - | 0.0072 |
| | GSC_2.49 | 20 | 0.002228 | 385 | 0.0712 | 0.00721 | 17.87 | 0.11 | 5.41 | 0.0116 | - | 0.0058 |
| | GSC_2.50 | 20 | 0.002228 | 430 | 0.0712 | 0.00721 | 17.87 | 0.11 | 5.41 | 0.0056 | - | 0.0044 |
| | GSC_2.51 | 20 | 0.002228 | 490 | 0.0712 | 0.00721 | 17.87 | 0.11 | 5.41 | 0.0034 | - | 0.0029 |

| (1) | (2) | (3) | (4) | (5) | (6) | (7) | (8) | (9) | (10) | (11) | (12) | (13) |
|---|---|---|---|---|---|---|---|---|---|---|---|---|
| | GSC_2.52 | 20 | 0.002228 | 565 | 0.0712 | 0.00721 | 17.87 | 0.11 | 5.41 | 0.0023 | - | 0.0017 |
| | GSC_2.53 | 20 | 0.002228 | 640 | 0.0712 | 0.00721 | 17.87 | 0.11 | 5.41 | 0.0017 | - | 0.0012 |
| | GSC_2.54 | 20 | 0.002228 | 740 | 0.0712 | 0.00721 | 17.87 | 0.11 | 5.41 | 0.0009 | - | 0.0005 |
| GSC 8 | GSC_2.55 | 20 | 0.002228 | 10 | 0.0511 | 0.00721 | 16.62 | 0.11 | 7.57 | 0.0899 | - | 0.0895 |
| | GSC_2.56 | 20 | 0.002228 | 25 | 0.0511 | 0.00721 | 16.62 | 0.11 | 7.57 | 0.0804 | - | 0.0760 |
| | GSC_2.57 | 20 | 0.002228 | 40 | 0.0511 | 0.00721 | 16.62 | 0.11 | 7.57 | 0.0725 | - | 0.0683 |
| | GSC_2.58 | 20 | 0.002228 | 55 | 0.0511 | 0.00721 | 16.62 | 0.11 | 7.57 | 0.0650 | - | 0.0604 |
| | GSC_2.59 | 20 | 0.002228 | 80 | 0.0511 | 0.00721 | 16.62 | 0.11 | 7.57 | 0.0566 | - | 0.0487 |
| | GSC_2.60 | 20 | 0.002228 | 110 | 0.0511 | 0.00721 | 16.62 | 0.11 | 7.57 | 0.0476 | - | 0.0430 |
| | GSC_2.61 | 20 | 0.002228 | 140 | 0.0511 | 0.00721 | 16.62 | 0.11 | 7.57 | 0.0400 | - | 0.0329 |
| | GSC_2.62 | 20 | 0.002228 | 200 | 0.0511 | 0.00721 | 16.62 | 0.11 | 7.57 | 0.0291 | - | 0.0202 |
| | GSC_2.63 | 20 | 0.002228 | 230 | 0.0511 | 0.00721 | 16.62 | 0.11 | 7.57 | 0.0196 | - | 0.0210 |
| | GSC_2.64 | 20 | 0.002228 | 265 | 0.0511 | 0.00721 | 16.62 | 0.11 | 7.57 | 0.0149 | - | 0.0188 |
| | GSC_2.65 | 20 | 0.002228 | 295 | 0.0511 | 0.00721 | 16.62 | 0.11 | 7.57 | 0.0104 | - | 0.0166 |
| | GSC_2.66 | 20 | 0.002228 | 325 | 0.0511 | 0.00721 | 16.62 | 0.11 | 7.57 | 0.0072 | - | 0.0148 |
| | GSC_2.67 | 20 | 0.002228 | 355 | 0.0511 | 0.00721 | 16.62 | 0.11 | 7.57 | 0.0054 | - | 0.0126 |
| | GSC_2.68 | 20 | 0.002228 | 385 | 0.0511 | 0.00721 | 16.62 | 0.11 | 7.57 | 0.0045 | - | 0.0110 |
| | GSC_2.69 | 20 | 0.002228 | 415 | 0.0511 | 0.00721 | 16.62 | 0.11 | 7.57 | 0.0033 | - | 0.0088 |
| | GSC_2.70 | 20 | 0.002228 | 445 | 0.0511 | 0.00721 | 16.62 | 0.11 | 7.57 | 0.0043 | - | 0.0063 |
| | GSC_2.71 | 20 | 0.002228 | 475 | 0.0511 | 0.00721 | 16.62 | 0.11 | 7.57 | 0.0034 | - | 0.0054 |
| | GSC_2.72 | 20 | 0.002228 | 505 | 0.0511 | 0.00721 | 16.62 | 0.11 | 7.57 | 0.0022 | - | 0.0046 |
| | GSC_2.73 | 20 | 0.002228 | 550 | 0.0511 | 0.00721 | 16.62 | 0.11 | 7.57 | 0.0024 | - | 0.0051 |
| | GSC_2.74 | 20 | 0.002228 | 615 | 0.0511 | 0.00721 | 16.62 | 0.11 | 7.57 | 0.0019 | - | 0.0037 |
| | GSC_2.75 | 20 | 0.002228 | 675 | 0.0511 | 0.00721 | 16.62 | 0.11 | 7.57 | 0.0019 | - | 0.0026 |
| | GSC_2.76 | 20 | 0.002228 | 720 | 0.0511 | 0.00721 | 16.62 | 0.11 | 7.57 | 0.0017 | - | 0.0015 |
| | GSC_2.77 | 20 | 0.002228 | 765 | 0.0511 | 0.00721 | 16.62 | 0.11 | 7.57 | 0.0014 | - | 0.0011 |
| | GSC_2.78 | 20 | 0.002228 | 810 | 0.0511 | 0.00721 | 16.62 | 0.11 | 7.57 | 0.0010 | - | 0.0008 |
| GSC 9 | GSC_3.1 | 30 | 0.001951 | 15 | 0.0516 | 0.00721 | 17.30 | 0.11 | 10.81 | 0.0796 | - | 0.0845 |

| (1) | (2) | (3) | (4) | (5) | (6) | (7) | (8) | (9) | (10) | (11) | (12) | (13) |
|---|---|---|---|---|---|---|---|---|---|---|---|---|
| | GSC_3.2 | 30 | 0.001951 | 30 | 0.0516 | 0.00721 | 17.30 | 0.11 | 10.81 | 0.0686 | - | 0.0705 |
| | GSC_3.3 | 30 | 0.001951 | 45 | 0.0516 | 0.00721 | 17.30 | 0.11 | 10.81 | 0.0578 | - | 0.0700 |
| | GSC_3.4 | 30 | 0.001951 | 60 | 0.0516 | 0.00721 | 17.30 | 0.11 | 10.81 | 0.0512 | - | 0.0605 |
| | GSC_3.5 | 30 | 0.001951 | 80 | 0.0516 | 0.00721 | 17.30 | 0.11 | 10.81 | 0.0449 | - | 0.0496 |
| | GSC_3.6 | 30 | 0.001951 | 110 | 0.0516 | 0.00721 | 17.30 | 0.11 | 10.81 | 0.0388 | - | 0.0423 |
| | GSC_3.7 | 30 | 0.001951 | 140 | 0.0516 | 0.00721 | 17.30 | 0.11 | 10.81 | 0.0308 | - | 0.0308 |
| | GSC_3.8 | 30 | 0.001951 | 210 | 0.0516 | 0.00721 | 17.30 | 0.11 | 10.81 | 0.0203 | - | 0.0292 |
| | GSC_3.9 | 30 | 0.001951 | 240 | 0.0516 | 0.00721 | 17.30 | 0.11 | 10.81 | 0.0132 | - | 0.0258 |
| | GSC_3.10 | 30 | 0.001951 | 270 | 0.0516 | 0.00721 | 17.30 | 0.11 | 10.81 | 0.0093 | - | 0.0216 |
| | GSC_3.11 | 30 | 0.001951 | 300 | 0.0516 | 0.00721 | 17.30 | 0.11 | 10.81 | 0.0078 | - | 0.0167 |
| | GSC_3.12 | 30 | 0.001951 | 330 | 0.0516 | 0.00721 | 17.30 | 0.11 | 10.81 | 0.0070 | - | 0.0127 |
| | GSC_3.13 | 30 | 0.001951 | 390 | 0.0516 | 0.00721 | 17.30 | 0.11 | 10.81 | 0.0055 | - | 0.0092 |
| | GSC_3.14 | 30 | 0.001951 | 425 | 0.0516 | 0.00721 | 17.30 | 0.11 | 10.81 | 0.0054 | - | 0.0071 |
| | GSC_3.15 | 30 | 0.001951 | 455 | 0.0516 | 0.00721 | 17.30 | 0.11 | 10.81 | 0.0039 | - | 0.0076 |
| | GSC_3.16 | 30 | 0.001951 | 495 | 0.0516 | 0.00721 | 17.30 | 0.11 | 10.81 | 0.0041 | - | 0.0056 |
| | GSC_3.17 | 30 | 0.001951 | 525 | 0.0516 | 0.00721 | 17.30 | 0.11 | 10.81 | 0.0037 | - | 0.0042 |
| | GSC_3.18 | 30 | 0.001951 | 555 | 0.0516 | 0.00721 | 17.30 | 0.11 | 10.81 | 0.0035 | - | 0.0028 |
| | GSC_3.19 | 30 | 0.001951 | 585 | 0.0516 | 0.00721 | 17.30 | 0.11 | 10.81 | 0.0033 | - | 0.0022 |
| | GSC_3.20 | 30 | 0.001951 | 665 | 0.0516 | 0.00721 | 17.30 | 0.11 | 10.81 | 0.0028 | - | 0.0015 |
| | GSC_3.21 | 30 | 0.001951 | 710 | 0.0516 | 0.00721 | 17.30 | 0.11 | 10.81 | 0.0025 | - | 0.0010 |
| | GSC_3.22 | 30 | 0.001951 | 775 | 0.0516 | 0.00721 | 17.30 | 0.11 | 10.81 | 0.0019 | - | 0.0006 |
| | GSC_3.23 | 30 | 0.001951 | 830 | 0.0516 | 0.00721 | 17.30 | 0.11 | 10.81 | 0.0011 | - | 0.0004 |
| GSC 10 | GSC_3.24 | 30 | 0.001951 | 10 | 0.0711 | 0.00721 | 17.87 | 0.12 | 10.27 | 0.0909 | - | 0.0929 |
| | GSC_3.25 | 30 | 0.001951 | 25 | 0.0711 | 0.00721 | 17.87 | 0.12 | 10.27 | 0.0770 | - | 0.0735 |
| | GSC_3.26 | 30 | 0.001951 | 40 | 0.0711 | 0.00721 | 17.87 | 0.12 | 10.27 | 0.0642 | - | 0.0634 |
| | GSC_3.27 | 30 | 0.001951 | 55 | 0.0711 | 0.00721 | 17.87 | 0.12 | 10.27 | 0.0579 | - | 0.0566 |
| | GSC_3.28 | 30 | 0.001951 | 75 | 0.0711 | 0.00721 | 17.87 | 0.12 | 10.27 | 0.0520 | - | 0.0482 |
| | GSC_3.29 | 30 | 0.001951 | 100 | 0.0711 | 0.00721 | 17.87 | 0.12 | 10.27 | 0.0437 | - | 0.0525 |

| (1) | (2) | (3) | (4) | (5) | (6) | (7) | (8) | (9) | (10) | (11) | (12) | (13) |
|---|---|---|---|---|---|---|---|---|---|---|---|---|
| | GSC_3.30 | 30 | 0.001951 | 130 | 0.0711 | 0.00721 | 17.87 | 0.12 | 10.27 | 0.0363 | - | 0.0475 |
| | GSC_3.31 | 30 | 0.001951 | 175 | 0.0711 | 0.00721 | 17.87 | 0.12 | 10.27 | 0.0329 | - | 0.0373 |
| | GSC_3.32 | 30 | 0.001951 | 235 | 0.0711 | 0.00721 | 17.87 | 0.12 | 10.27 | 0.0280 | - | 0.0343 |
| | GSC_3.33 | 30 | 0.001951 | 295 | 0.0711 | 0.00721 | 17.87 | 0.12 | 10.27 | 0.0143 | - | 0.0307 |
| | GSC_3.34 | 30 | 0.001951 | 355 | 0.0711 | 0.00721 | 17.87 | 0.12 | 10.27 | 0.0101 | - | 0.0201 |
| | GSC_3.35 | 30 | 0.001951 | 415 | 0.0711 | 0.00721 | 17.87 | 0.12 | 10.27 | 0.0073 | - | 0.0170 |
| | GSC_3.36 | 30 | 0.001951 | 475 | 0.0711 | 0.00721 | 17.87 | 0.12 | 10.27 | 0.0057 | - | 0.0105 |
| | GSC_3.37 | 30 | 0.001951 | 535 | 0.0711 | 0.00721 | 17.87 | 0.12 | 10.27 | 0.0035 | - | 0.0072 |
| | GSC_3.38 | 30 | 0.001951 | 595 | 0.0711 | 0.00721 | 17.87 | 0.12 | 10.27 | 0.0029 | - | 0.0034 |
| | GSC_3.39 | 30 | 0.001951 | 655 | 0.0711 | 0.00721 | 17.87 | 0.12 | 10.27 | 0.0018 | - | 0.0016 |
| | GSC_3.40 | 30 | 0.001951 | 745 | 0.0711 | 0.00721 | 17.87 | 0.12 | 10.27 | 0.0008 | - | 0.0007 |
| GSC 11 | GSC_3.41 | 30 | 0.001951 | 15 | 0.0518 | 0.00946 | 17.76 | 0.08 | 11.35 | 0.0861 | - | 0.0881 |
| | GSC_3.42 | 30 | 0.001951 | 30 | 0.0518 | 0.00946 | 17.76 | 0.08 | 11.35 | 0.0807 | - | 0.0654 |
| | GSC_3.43 | 30 | 0.001951 | 45 | 0.0518 | 0.00946 | 17.76 | 0.08 | 11.35 | 0.0755 | - | 0.0535 |
| | GSC_3.44 | 30 | 0.001951 | 60 | 0.0518 | 0.00946 | 17.76 | 0.08 | 11.35 | 0.0660 | - | 0.0494 |
| | GSC_3.45 | 30 | 0.001951 | 75 | 0.0518 | 0.00946 | 17.76 | 0.08 | 11.35 | 0.0583 | - | 0.0438 |
| | GSC_3.46 | 30 | 0.001951 | 90 | 0.0518 | 0.00946 | 17.76 | 0.08 | 11.35 | 0.0513 | - | 0.0417 |
| | GSC_3.47 | 30 | 0.001951 | 105 | 0.0518 | 0.00946 | 17.76 | 0.08 | 11.35 | 0.0457 | - | 0.0438 |
| | GSC_3.48 | 30 | 0.001951 | 120 | 0.0518 | 0.00946 | 17.76 | 0.08 | 11.35 | 0.0419 | - | 0.0404 |
| | GSC_3.49 | 30 | 0.001951 | 135 | 0.0518 | 0.00946 | 17.76 | 0.08 | 11.35 | 0.0358 | - | 0.0399 |
| | GSC_3.50 | 30 | 0.001951 | 150 | 0.0518 | 0.00946 | 17.76 | 0.08 | 11.35 | 0.0298 | - | 0.0344 |
| | GSC_3.51 | 30 | 0.001951 | 180 | 0.0518 | 0.00946 | 17.76 | 0.08 | 11.35 | 0.0234 | - | 0.0287 |
| | GSC_3.52 | 30 | 0.001951 | 210 | 0.0518 | 0.00946 | 17.76 | 0.08 | 11.35 | 0.0172 | - | 0.0249 |
| | GSC_3.53 | 30 | 0.001951 | 240 | 0.0518 | 0.00946 | 17.76 | 0.08 | 11.35 | 0.0138 | - | 0.0225 |
| | GSC_3.54 | 30 | 0.001951 | 270 | 0.0518 | 0.00946 | 17.76 | 0.08 | 11.35 | 0.0101 | - | 0.0181 |
| | GSC_3.55 | 30 | 0.001951 | 300 | 0.0518 | 0.00946 | 17.76 | 0.08 | 11.35 | 0.0076 | - | 0.0155 |
| | GSC_3.56 | 30 | 0.001951 | 345 | 0.0518 | 0.00946 | 17.76 | 0.08 | 11.35 | 0.0065 | - | 0.0102 |
| | GSC_3.57 | 30 | 0.001951 | 375 | 0.0518 | 0.00946 | 17.76 | 0.08 | 11.35 | 0.0056 | - | 0.0101 |

| (1) | (2) | (3) | (4) | (5) | (6) | (7) | (8) | (9) | (10) | (11) | (12) | (13) |
|---|---|---|---|---|---|---|---|---|---|---|---|---|
| | GSC_3.58 | 30 | 0.001951 | 405 | 0.0518 | 0.00946 | 17.76 | 0.08 | 11.35 | 0.0053 | - | 0.0070 |
| | GSC_3.59 | 30 | 0.001951 | 450 | 0.0518 | 0.00946 | 17.76 | 0.08 | 11.35 | 0.0047 | - | 0.0057 |
| | GSC_3.60 | 30 | 0.001951 | 480 | 0.0518 | 0.00946 | 17.76 | 0.08 | 11.35 | 0.0039 | - | 0.0046 |
| | GSC_3.61 | 30 | 0.001951 | 510 | 0.0518 | 0.00946 | 17.76 | 0.08 | 11.35 | 0.0030 | - | 0.0033 |
| | GSC_3.62 | 30 | 0.001951 | 540 | 0.0518 | 0.00946 | 17.76 | 0.08 | 11.35 | 0.0022 | - | 0.0018 |
| | GSC_3.63 | 30 | 0.001951 | 585 | 0.0518 | 0.00946 | 17.76 | 0.08 | 11.35 | 0.0017 | - | 0.0019 |
| | GSC_3.64 | 30 | 0.001951 | 630 | 0.0518 | 0.00946 | 17.76 | 0.08 | 11.35 | 0.0010 | - | 0.0010 |
| | GSC_3.65 | 30 | 0.001951 | 690 | 0.0518 | 0.00946 | 17.76 | 0.08 | 11.35 | 0.0005 | - | 0.0006 |
| | GSC_3.66 | 30 | 0.001951 | 770 | 0.0518 | 0.00946 | 17.76 | 0.08 | 11.35 | 0.0002 | - | 0.0003 |
| GSC 12 | GSC_3.67 | 30 | 0.001951 | 15 | 0.0706 | 0.00946 | 18.55 | 0.11 | 11.89 | 0.1082 | - | 0.1057 |
| | GSC_3.68 | 30 | 0.001951 | 30 | 0.0706 | 0.00946 | 18.55 | 0.11 | 11.89 | 0.0829 | - | 0.0918 |
| | GSC_3.69 | 30 | 0.001951 | 45 | 0.0706 | 0.00946 | 18.55 | 0.11 | 11.89 | 0.0713 | - | 0.0838 |
| | GSC_3.70 | 30 | 0.001951 | 75 | 0.0706 | 0.00946 | 18.55 | 0.11 | 11.89 | 0.0649 | - | 0.0721 |
| | GSC_3.71 | 30 | 0.001951 | 105 | 0.0706 | 0.00946 | 18.55 | 0.11 | 11.89 | 0.0578 | - | 0.0572 |
| | GSC_3.72 | 30 | 0.001951 | 135 | 0.0706 | 0.00946 | 18.55 | 0.11 | 11.89 | 0.0470 | - | 0.0418 |
| | GSC_3.73 | 30 | 0.001951 | 180 | 0.0706 | 0.00946 | 18.55 | 0.11 | 11.89 | 0.0382 | - | 0.0365 |
| | GSC_3.74 | 30 | 0.001951 | 225 | 0.0706 | 0.00946 | 18.55 | 0.11 | 11.89 | 0.0253 | - | 0.0310 |
| | GSC_3.75 | 30 | 0.001951 | 255 | 0.0706 | 0.00946 | 18.55 | 0.11 | 11.89 | 0.0189 | - | 0.0282 |
| | GSC_3.76 | 30 | 0.001951 | 285 | 0.0706 | 0.00946 | 18.55 | 0.11 | 11.89 | 0.0118 | - | 0.0280 |
| | GSC_3.77 | 30 | 0.001951 | 315 | 0.0706 | 0.00946 | 18.55 | 0.11 | 11.89 | 0.0105 | - | 0.0246 |
| | GSC_3.78 | 30 | 0.001951 | 350 | 0.0706 | 0.00946 | 18.55 | 0.11 | 11.89 | 0.0092 | - | 0.0216 |
| | GSC_3.79 | 30 | 0.001951 | 370 | 0.0706 | 0.00946 | 18.55 | 0.11 | 11.89 | 0.0090 | - | 0.0193 |
| | GSC_3.80 | 30 | 0.001951 | 400 | 0.0706 | 0.00946 | 18.55 | 0.11 | 11.89 | 0.0075 | - | 0.0161 |
| | GSC_3.81 | 30 | 0.001951 | 430 | 0.0706 | 0.00946 | 18.55 | 0.11 | 11.89 | 0.0067 | - | 0.0125 |
| | GSC_3.82 | 30 | 0.001951 | 460 | 0.0706 | 0.00946 | 18.55 | 0.11 | 11.89 | 0.0090 | - | 0.0100 |
| | GSC_3.83 | 30 | 0.001951 | 490 | 0.0706 | 0.00946 | 18.55 | 0.11 | 11.89 | 0.0060 | - | 0.0088 |
| | GSC_3.84 | 30 | 0.001951 | 520 | 0.0706 | 0.00946 | 18.55 | 0.11 | 11.89 | 0.0056 | - | 0.0089 |
| | GSC_3.85 | 30 | 0.001951 | 550 | 0.0706 | 0.00946 | 18.55 | 0.11 | 11.89 | 0.0046 | - | 0.0072 |

| (1) | (2) | (3) | (4) | (5) | (6) | (7) | (8) | (9) | (10) | (11) | (12) | (13) |
|---|---|---|---|---|---|---|---|---|---|---|---|---|
| | GSC_3.86 | 30 | 0.001951 | 615 | 0.0706 | 0.00946 | 18.55 | 0.11 | 11.89 | 0.0037 | - | 0.0045 |
| | GSC_3.87 | 30 | 0.001951 | 645 | 0.0706 | 0.00946 | 18.55 | 0.11 | 11.89 | 0.0032 | - | 0.0034 |
| | GSC_3.88 | 30 | 0.001951 | 675 | 0.0706 | 0.00946 | 18.55 | 0.11 | 11.89 | 0.0031 | - | 0.0028 |
| | GSC_3.89 | 30 | 0.001951 | 705 | 0.0706 | 0.00946 | 18.55 | 0.11 | 11.89 | 0.0029 | - | 0.0022 |
| | GSC_3.90 | 30 | 0.001951 | 735 | 0.0706 | 0.00946 | 18.55 | 0.11 | 11.89 | 0.0026 | - | 0.0013 |
| | GSC_3.91 | 30 | 0.001951 | 765 | 0.0706 | 0.00946 | 18.55 | 0.11 | 11.89 | 0.0019 | - | 0.0008 |
| | GSC_3.92 | 30 | 0.001951 | 795 | 0.0706 | 0.00946 | 18.55 | 0.11 | 11.89 | 0.0013 | - | 0.0003 |
| GSC 13 | GSC_4.1 | 40 | 0.001674 | 15 | 0.0508 | 0.00721 | 18.78 | 0.16 | 22.17 | 0.0535 | - | 0.0694 |
| | GSC_4.2 | 40 | 0.001674 | 30 | 0.0508 | 0.00721 | 18.78 | 0.16 | 22.17 | 0.0436 | - | 0.0681 |
| | GSC_4.3 | 40 | 0.001674 | 50 | 0.0508 | 0.00721 | 18.78 | 0.16 | 22.17 | 0.0354 | - | 0.0629 |
| | GSC_4.4 | 40 | 0.001674 | 90 | 0.0508 | 0.00721 | 18.78 | 0.16 | 22.17 | 0.0267 | - | 0.0554 |
| | GSC_4.5 | 40 | 0.001674 | 120 | 0.0508 | 0.00721 | 18.78 | 0.16 | 22.17 | 0.0189 | - | 0.0433 |
| | GSC_4.6 | 40 | 0.001674 | 150 | 0.0508 | 0.00721 | 18.78 | 0.16 | 22.17 | 0.0144 | - | 0.0358 |
| | GSC_4.7 | 40 | 0.001674 | 235 | 0.0508 | 0.00721 | 18.78 | 0.16 | 22.17 | 0.0100 | - | 0.0246 |
| | GSC_4.8 | 40 | 0.001674 | 280 | 0.0508 | 0.00721 | 18.78 | 0.16 | 22.17 | 0.0069 | - | 0.0208 |
| | GSC_4.9 | 40 | 0.001674 | 340 | 0.0508 | 0.00721 | 18.78 | 0.16 | 22.17 | 0.0052 | - | 0.0178 |
| | GSC_4.10 | 40 | 0.001674 | 415 | 0.0508 | 0.00721 | 18.78 | 0.16 | 22.17 | 0.0036 | - | 0.0142 |
| | GSC_4.11 | 40 | 0.001674 | 475 | 0.0508 | 0.00721 | 18.78 | 0.16 | 22.17 | 0.0035 | - | 0.0100 |
| | GSC_4.12 | 40 | 0.001674 | 535 | 0.0508 | 0.00721 | 18.78 | 0.16 | 22.17 | 0.0030 | - | 0.0085 |
| | GSC_4.13 | 40 | 0.001674 | 615 | 0.0508 | 0.00721 | 18.78 | 0.16 | 22.17 | 0.0028 | - | 0.0070 |
| | GSC_4.14 | 40 | 0.001674 | 705 | 0.0508 | 0.00721 | 18.78 | 0.16 | 22.17 | 0.0026 | - | 0.0054 |
| | GSC_4.15 | 40 | 0.001674 | 780 | 0.0508 | 0.00721 | 18.78 | 0.16 | 22.17 | 0.0023 | - | 0.0035 |
| | GSC_4.16 | 40 | 0.001674 | 840 | 0.0508 | 0.00721 | 18.78 | 0.16 | 22.17 | 0.0020 | - | 0.0016 |
| | GSC_4.17 | 40 | 0.001674 | 930 | 0.0508 | 0.00721 | 18.78 | 0.16 | 22.17 | 0.0010 | - | 0.0007 |
| GSC 14 | GSC_4.18 | 40 | 0.001674 | 15 | 0.0697 | 0.00721 | 19.35 | 0.14 | 21.09 | 0.0660 | - | 0.0753 |
| | GSC_4.19 | 40 | 0.001674 | 30 | 0.0697 | 0.00721 | 19.35 | 0.14 | 21.09 | 0.0560 | - | 0.0631 |
| | GSC_4.20 | 40 | 0.001674 | 60 | 0.0697 | 0.00721 | 19.35 | 0.14 | 21.09 | 0.0489 | - | 0.0546 |
| | GSC_4.21 | 40 | 0.001674 | 90 | 0.0697 | 0.00721 | 19.35 | 0.14 | 21.09 | 0.0396 | - | 0.0438 |

| (1) | (2) | (3) | (4) | (5) | (6) | (7) | (8) | (9) | (10) | (11) | (12) | (13) |
|---|---|---|---|---|---|---|---|---|---|---|---|---|
| | GSC_4.22 | 40 | 0.001674 | 135 | 0.0697 | 0.00721 | 19.35 | 0.14 | 21.09 | 0.0314 | - | 0.0334 |
| | GSC_4.23 | 40 | 0.001674 | 180 | 0.0697 | 0.00721 | 19.35 | 0.14 | 21.09 | 0.0228 | - | 0.0310 |
| | GSC_4.24 | 40 | 0.001674 | 270 | 0.0697 | 0.00721 | 19.35 | 0.14 | 21.09 | 0.0126 | - | 0.0218 |
| | GSC_4.25 | 40 | 0.001674 | 315 | 0.0697 | 0.00721 | 19.35 | 0.14 | 21.09 | 0.0078 | - | 0.0157 |
| | GSC_4.26 | 40 | 0.001674 | 405 | 0.0697 | 0.00721 | 19.35 | 0.14 | 21.09 | 0.0052 | - | 0.0102 |
| | GSC_4.27 | 40 | 0.001674 | 465 | 0.0697 | 0.00721 | 19.35 | 0.14 | 21.09 | 0.0046 | - | 0.0063 |
| | GSC_4.28 | 40 | 0.001674 | 540 | 0.0697 | 0.00721 | 19.35 | 0.14 | 21.09 | 0.0028 | - | 0.0044 |
| | GSC_4.29 | 40 | 0.001674 | 615 | 0.0697 | 0.00721 | 19.35 | 0.14 | 21.09 | 0.0022 | - | 0.0022 |
| | GSC_4.30 | 40 | 0.001674 | 690 | 0.0697 | 0.00721 | 19.35 | 0.14 | 21.09 | 0.0013 | - | 0.0012 |
| | GSC_4.31 | 40 | 0.001674 | 790 | 0.0697 | 0.00721 | 19.35 | 0.14 | 21.09 | 0.0007 | - | 0.0004 |
| GSC 15 | GSC_4.32 | 40 | 0.001674 | 15 | 0.0501 | 0.00946 | 19.01 | 0.15 | 18.92 | 0.0571 | - | 0.0731 |
| | GSC_4.33 | 40 | 0.001674 | 35 | 0.0501 | 0.00946 | 19.01 | 0.15 | 18.92 | 0.0465 | - | 0.0631 |
| | GSC_4.34 | 40 | 0.001674 | 55 | 0.0501 | 0.00946 | 19.01 | 0.15 | 18.92 | 0.0354 | - | 0.0545 |
| | GSC_4.35 | 40 | 0.001674 | 85 | 0.0501 | 0.00946 | 19.01 | 0.15 | 18.92 | 0.0312 | - | 0.0507 |
| | GSC_4.36 | 40 | 0.001674 | 130 | 0.0501 | 0.00946 | 19.01 | 0.15 | 18.92 | 0.0173 | - | 0.0424 |
| | GSC_4.37 | 40 | 0.001674 | 175 | 0.0501 | 0.00946 | 19.01 | 0.15 | 18.92 | 0.0149 | - | 0.0360 |
| | GSC_4.38 | 40 | 0.001674 | 255 | 0.0501 | 0.00946 | 19.01 | 0.15 | 18.92 | 0.0082 | - | 0.0317 |
| | GSC_4.39 | 40 | 0.001674 | 305 | 0.0501 | 0.00946 | 19.01 | 0.15 | 18.92 | 0.0073 | - | 0.0230 |
| | GSC_4.40 | 40 | 0.001674 | 370 | 0.0501 | 0.00946 | 19.01 | 0.15 | 18.92 | 0.0067 | - | 0.0118 |
| | GSC_4.41 | 40 | 0.001674 | 430 | 0.0501 | 0.00946 | 19.01 | 0.15 | 18.92 | 0.0049 | - | 0.0091 |
| | GSC_4.42 | 40 | 0.001674 | 490 | 0.0501 | 0.00946 | 19.01 | 0.15 | 18.92 | 0.0054 | - | 0.0072 |
| | GSC_4.43 | 40 | 0.001674 | 550 | 0.0501 | 0.00946 | 19.01 | 0.15 | 18.92 | 0.0030 | - | 0.0065 |
| | GSC_4.44 | 40 | 0.001674 | 610 | 0.0501 | 0.00946 | 19.01 | 0.15 | 18.92 | 0.0027 | - | 0.0037 |
| | GSC_4.45 | 40 | 0.001674 | 715 | 0.0501 | 0.00946 | 19.01 | 0.15 | 18.92 | 0.0021 | - | 0.0022 |
| | GSC_4.46 | 40 | 0.001674 | 775 | 0.0501 | 0.00946 | 19.01 | 0.15 | 18.92 | 0.0016 | - | 0.0013 |
| | GSC_4.47 | 40 | 0.001674 | 850 | 0.0501 | 0.00946 | 19.01 | 0.15 | 18.92 | 0.0010 | - | 0.0006 |
| GSC 16 | GSC_4.48 | 40 | 0.001674 | 30 | 0.0702 | 0.00946 | 18.78 | 0.11 | 18.92 | 0.0719 | - | 0.0843 |
| | GSC_4.49 | 40 | 0.001674 | 45 | 0.0702 | 0.00946 | 18.78 | 0.11 | 18.92 | 0.0611 | - | 0.0743 |

| (1) | (2) | (3) | (4) | (5) | (6) | (7) | (8) | (9) | (10) | (11) | (12) | (13) |
|---|---|---|---|---|---|---|---|---|---|---|---|---|
| | GSC_4.50 | 40 | 0.001674 | 65 | 0.0702 | 0.00946 | 18.78 | 0.11 | 18.92 | 0.0511 | - | 0.0612 |
| | GSC_4.51 | 40 | 0.001674 | 80 | 0.0702 | 0.00946 | 18.78 | 0.11 | 18.92 | 0.0434 | - | 0.0597 |
| | GSC_4.52 | 40 | 0.001674 | 100 | 0.0702 | 0.00946 | 18.78 | 0.11 | 18.92 | 0.0371 | - | 0.0477 |
| | GSC_4.53 | 40 | 0.001674 | 120 | 0.0702 | 0.00946 | 18.78 | 0.11 | 18.92 | 0.0325 | - | 0.0383 |
| | GSC_4.54 | 40 | 0.001674 | 140 | 0.0702 | 0.00946 | 18.78 | 0.11 | 18.92 | 0.0293 | - | 0.0316 |
| | GSC_4.55 | 40 | 0.001674 | 160 | 0.0702 | 0.00946 | 18.78 | 0.11 | 18.92 | 0.0266 | - | 0.0265 |
| | GSC_4.56 | 40 | 0.001674 | 195 | 0.0702 | 0.00946 | 18.78 | 0.11 | 18.92 | 0.0211 | - | 0.0220 |
| | GSC_4.57 | 40 | 0.001674 | 235 | 0.0702 | 0.00946 | 18.78 | 0.11 | 18.92 | 0.0183 | - | 0.0131 |
| | GSC_4.58 | 40 | 0.001674 | 265 | 0.0702 | 0.00946 | 18.78 | 0.11 | 18.92 | 0.0155 | - | 0.0086 |
| | GSC_4.59 | 40 | 0.001674 | 295 | 0.0702 | 0.00946 | 18.78 | 0.11 | 18.92 | 0.0127 | - | 0.0083 |
| | GSC_4.60 | 40 | 0.001674 | 325 | 0.0702 | 0.00946 | 18.78 | 0.11 | 18.92 | 0.0092 | - | 0.0047 |
| | GSC_4.61 | 40 | 0.001674 | 370 | 0.0702 | 0.00946 | 18.78 | 0.11 | 18.92 | 0.0079 | - | 0.0033 |
| | GSC_4.62 | 40 | 0.001674 | 400 | 0.0702 | 0.00946 | 18.78 | 0.11 | 18.92 | 0.0070 | - | 0.0031 |
| | GSC_4.63 | 40 | 0.001674 | 445 | 0.0702 | 0.00946 | 18.78 | 0.11 | 18.92 | 0.0061 | - | 0.0033 |
| | GSC_4.64 | 40 | 0.001674 | 490 | 0.0702 | 0.00946 | 18.78 | 0.11 | 18.92 | 0.0052 | - | 0.0018 |
| | GSC_4.65 | 40 | 0.001674 | 535 | 0.0702 | 0.00946 | 18.78 | 0.11 | 18.92 | 0.0044 | - | 0.0014 |
| | GSC_4.66 | 40 | 0.001674 | 610 | 0.0702 | 0.00946 | 18.78 | 0.11 | 18.92 | 0.0033 | - | 0.0010 |
| | GSC_4.67 | 40 | 0.001674 | 670 | 0.0702 | 0.00946 | 18.78 | 0.11 | 18.92 | 0.0019 | - | 0.0005 |
| | GSC_4.68 | 40 | 0.001674 | 730 | 0.0702 | 0.00946 | 18.78 | 0.11 | 18.92 | 0.0014 | - | 0.0005 |
| | GSC_4.69 | 40 | 0.001674 | 810 | 0.0702 | 0.00946 | 18.78 | 0.11 | 18.92 | 0.0008 | - | 0.0003 |
| GSC 17 | GSC_5.1 | 50 | 0.001398 | 15 | 0.0507 | 0.00946 | 20.37 | 0.13 | 30.28 | 0.0449 | - | 0.0673 |
| | GSC_5.2 | 50 | 0.001398 | 30 | 0.0507 | 0.00946 | 20.37 | 0.13 | 30.28 | 0.0349 | - | 0.0589 |
| | GSC_5.3 | 50 | 0.001398 | 60 | 0.0507 | 0.00946 | 20.37 | 0.13 | 30.28 | 0.0252 | - | 0.0489 |
| | GSC_5.4 | 50 | 0.001398 | 90 | 0.0507 | 0.00946 | 20.37 | 0.13 | 30.28 | 0.0172 | - | 0.0442 |
| | GSC_5.5 | 50 | 0.001398 | 120 | 0.0507 | 0.00946 | 20.37 | 0.13 | 30.28 | 0.0149 | - | 0.0318 |
| | GSC_5.6 | 50 | 0.001398 | 150 | 0.0507 | 0.00946 | 20.37 | 0.13 | 30.28 | 0.0129 | - | 0.0280 |
| | GSC_5.7 | 50 | 0.001398 | 180 | 0.0507 | 0.00946 | 20.37 | 0.13 | 30.28 | 0.0084 | - | 0.0235 |
| | GSC_5.8 | 50 | 0.001398 | 210 | 0.0507 | 0.00946 | 20.37 | 0.13 | 30.28 | 0.0054 | - | 0.0161 |

| (1) | (2) | (3) | (4) | (5) | (6) | (7) | (8) | (9) | (10) | (11) | (12) | (13) |
|---|---|---|---|---|---|---|---|---|---|---|---|---|
| | GSC_5.9 | 50 | 0.001398 | 240 | 0.0507 | 0.00946 | 20.37 | 0.13 | 30.28 | 0.0099 | - | 0.0103 |
| | GSC_5.10 | 50 | 0.001398 | 270 | 0.0507 | 0.00946 | 20.37 | 0.13 | 30.28 | 0.0059 | - | 0.0078 |
| | GSC_5.11 | 50 | 0.001398 | 300 | 0.0507 | 0.00946 | 20.37 | 0.13 | 30.28 | 0.0059 | - | 0.0058 |
| | GSC_5.12 | 50 | 0.001398 | 330 | 0.0507 | 0.00946 | 20.37 | 0.13 | 30.28 | 0.0065 | - | 0.0059 |
| | GSC_5.13 | 50 | 0.001398 | 375 | 0.0507 | 0.00946 | 20.37 | 0.13 | 30.28 | 0.0057 | - | 0.0048 |
| | GSC_5.14 | 50 | 0.001398 | 405 | 0.0507 | 0.00946 | 20.37 | 0.13 | 30.28 | 0.0036 | - | 0.0051 |
| | GSC_5.15 | 50 | 0.001398 | 435 | 0.0507 | 0.00946 | 20.37 | 0.13 | 30.28 | 0.0043 | - | 0.0036 |
| | GSC_5.16 | 50 | 0.001398 | 465 | 0.0507 | 0.00946 | 20.37 | 0.13 | 30.28 | 0.0044 | - | 0.0028 |
| | GSC_5.17 | 50 | 0.001398 | 500 | 0.0507 | 0.00946 | 20.37 | 0.13 | 30.28 | 0.0032 | - | 0.0021 |
| | GSC_5.18 | 50 | 0.001398 | 530 | 0.0507 | 0.00946 | 20.37 | 0.13 | 30.28 | 0.0016 | - | 0.0019 |
| | GSC_5.19 | 50 | 0.001398 | 560 | 0.0507 | 0.00946 | 20.37 | 0.13 | 30.28 | 0.0018 | - | 0.0014 |
| | GSC_5.20 | 50 | 0.001398 | 620 | 0.0507 | 0.00946 | 20.37 | 0.13 | 30.28 | 0.0014 | - | 0.0018 |
| | GSC_5.21 | 50 | 0.001398 | 650 | 0.0507 | 0.00946 | 20.37 | 0.13 | 30.28 | 0.0011 | - | 0.0014 |
| | GSC_5.22 | 50 | 0.001398 | 680 | 0.0507 | 0.00946 | 20.37 | 0.13 | 30.28 | 0.0009 | - | 0.0010 |
| | GSC_5.23 | 50 | 0.001398 | 740 | 0.0507 | 0.00946 | 20.37 | 0.13 | 30.28 | 0.0005 | - | 0.0009 |
| | GSC_5.24 | 50 | 0.001398 | 770 | 0.0507 | 0.00946 | 20.37 | 0.13 | 30.28 | 0.0005 | - | 0.0006 |
| | GSC_5.25 | 50 | 0.001398 | 830 | 0.0507 | 0.00946 | 20.37 | 0.13 | 30.28 | 0.0004 | - | 0.0004 |
| | GSC_5.26 | 50 | 0.001398 | 880 | 0.0507 | 0.00946 | 20.37 | 0.13 | 30.28 | 0.0003 | - | 0.0003 |
| GSC 18 | GSC_5.27 | 50 | 0.001398 | 15 | 0.0695 | 0.00946 | 20.60 | 0.14 | 42.17 | 0.0573 | - | 0.0748 |
| | GSC_5.28 | 50 | 0.001398 | 35 | 0.0695 | 0.00946 | 20.60 | 0.14 | 42.17 | 0.0467 | - | 0.0633 |
| | GSC_5.29 | 50 | 0.001398 | 65 | 0.0695 | 0.00946 | 20.60 | 0.14 | 42.17 | 0.0370 | - | 0.0554 |
| | GSC_5.30 | 50 | 0.001398 | 100 | 0.0695 | 0.00946 | 20.60 | 0.14 | 42.17 | 0.0278 | - | 0.0467 |
| | GSC_5.31 | 50 | 0.001398 | 140 | 0.0695 | 0.00946 | 20.60 | 0.14 | 42.17 | 0.0204 | - | 0.0381 |
| | GSC_5.32 | 50 | 0.001398 | 220 | 0.0695 | 0.00946 | 20.60 | 0.14 | 42.17 | 0.0126 | - | 0.0288 |
| | GSC_5.33 | 50 | 0.001398 | 280 | 0.0695 | 0.00946 | 20.60 | 0.14 | 42.17 | 0.0079 | - | 0.0306 |
| | GSC_5.34 | 50 | 0.001398 | 340 | 0.0695 | 0.00946 | 20.60 | 0.14 | 42.17 | 0.0042 | - | 0.0266 |
| | GSC_5.35 | 50 | 0.001398 | 400 | 0.0695 | 0.00946 | 20.60 | 0.14 | 42.17 | 0.0036 | - | 0.0203 |
| | GSC_5.36 | 50 | 0.001398 | 470 | 0.0695 | 0.00946 | 20.60 | 0.14 | 42.17 | 0.0031 | - | 0.0168 |

| (1) | (2) | (3) | (4) | (5) | (6) | (7) | (8) | (9) | (10) | (11) | (12) | (13) |
|---|---|---|---|---|---|---|---|---|---|---|---|---|
| | GSC_5.37 | 50 | 0.001398 | 530 | 0.0695 | 0.00946 | 20.60 | 0.14 | 42.17 | 0.0036 | - | 0.0111 |
| | GSC_5.38 | 50 | 0.001398 | 590 | 0.0695 | 0.00946 | 20.60 | 0.14 | 42.17 | 0.0034 | - | 0.0070 |
| | GSC_5.39 | 50 | 0.001398 | 660 | 0.0695 | 0.00946 | 20.60 | 0.14 | 42.17 | 0.0026 | - | 0.0050 |
| | GSC_5.40 | 50 | 0.001398 | 720 | 0.0695 | 0.00946 | 20.60 | 0.14 | 42.17 | 0.0020 | - | 0.0026 |
| | GSC_5.41 | 50 | 0.001398 | 780 | 0.0695 | 0.00946 | 20.60 | 0.14 | 42.17 | 0.0014 | - | 0.0015 |
| | GSC_5.42 | 50 | 0.001398 | 840 | 0.0695 | 0.00946 | 20.60 | 0.14 | 42.17 | 0.0010 | - | 0.0006 |
| GSC 19 | GSC_5.43 | 50 | 0.001398 | 15 | 0.0696 | 0.00721 | 20.54 | 0.16 | 38.39 | 0.0512 | - | 0.0678 |
| | GSC_5.44 | 50 | 0.001398 | 30 | 0.0696 | 0.00721 | 20.54 | 0.16 | 38.39 | 0.0434 | - | 0.0557 |
| | GSC_5.45 | 50 | 0.001398 | 45 | 0.0696 | 0.00721 | 20.54 | 0.16 | 38.39 | 0.0346 | - | 0.0489 |
| | GSC_5.46 | 50 | 0.001398 | 60 | 0.0696 | 0.00721 | 20.54 | 0.16 | 38.39 | 0.0279 | - | 0.0388 |
| | GSC_5.47 | 50 | 0.001398 | 90 | 0.0696 | 0.00721 | 20.54 | 0.16 | 38.39 | 0.0229 | - | 0.0309 |
| | GSC_5.48 | 50 | 0.001398 | 120 | 0.0696 | 0.00721 | 20.54 | 0.16 | 38.39 | 0.0207 | - | 0.0250 |
| | GSC_5.49 | 50 | 0.001398 | 150 | 0.0696 | 0.00721 | 20.54 | 0.16 | 38.39 | 0.0156 | - | 0.0219 |
| | GSC_5.50 | 50 | 0.001398 | 195 | 0.0696 | 0.00721 | 20.54 | 0.16 | 38.39 | 0.0111 | - | 0.0147 |
| | GSC_5.51 | 50 | 0.001398 | 240 | 0.0696 | 0.00721 | 20.54 | 0.16 | 38.39 | 0.0083 | - | 0.0155 |
| | GSC_5.52 | 50 | 0.001398 | 300 | 0.0696 | 0.00721 | 20.54 | 0.16 | 38.39 | 0.0070 | - | 0.0178 |
| | GSC_5.53 | 50 | 0.001398 | 360 | 0.0696 | 0.00721 | 20.54 | 0.16 | 38.39 | 0.0054 | - | 0.0120 |
| | GSC_5.54 | 50 | 0.001398 | 420 | 0.0696 | 0.00721 | 20.54 | 0.16 | 38.39 | 0.0031 | - | 0.0091 |
| | GSC_5.55 | 50 | 0.001398 | 500 | 0.0696 | 0.00721 | 20.54 | 0.16 | 38.39 | 0.0025 | - | 0.0058 |
| | GSC_5.56 | 50 | 0.001398 | 580 | 0.0696 | 0.00721 | 20.54 | 0.16 | 38.39 | 0.0019 | - | 0.0035 |
| | GSC_5.57 | 50 | 0.001398 | 670 | 0.0696 | 0.00721 | 20.54 | 0.16 | 38.39 | 0.0015 | - | 0.0024 |
| | GSC_5.58 | 50 | 0.001398 | 745 | 0.0696 | 0.00721 | 20.54 | 0.16 | 38.39 | 0.0012 | - | 0.0012 |
| | GSC_5.59 | 50 | 0.001398 | 805 | 0.0696 | 0.00721 | 20.54 | 0.16 | 38.39 | 0.0008 | - | 0.0005 |
| GSC 20 | GSC_5.60 | 50 | 0.001398 | 15 | 0.0503 | 0.00721 | 20.49 | 0.16 | 32.44 | 0.0346 | - | 0.0650 |
| | GSC_5.61 | 50 | 0.001398 | 30 | 0.0503 | 0.00721 | 20.49 | 0.16 | 32.44 | 0.0281 | - | 0.0578 |
| | GSC_5.62 | 50 | 0.001398 | 45 | 0.0503 | 0.00721 | 20.49 | 0.16 | 32.44 | 0.0205 | - | 0.0516 |
| | GSC_5.63 | 50 | 0.001398 | 75 | 0.0503 | 0.00721 | 20.49 | 0.16 | 32.44 | 0.0124 | - | 0.0467 |
| | GSC_5.64 | 50 | 0.001398 | 120 | 0.0503 | 0.00721 | 20.49 | 0.16 | 32.44 | 0.0078 | - | 0.0414 |

| (1) | (2) | (3) | (4) | (5) | (6) | (7) | (8) | (9) | (10) | (11) | (12) | (13) |
|---|---|---|---|---|---|---|---|---|---|---|---|---|
| | GSC_5.65 | 50 | 0.001398 | 165 | 0.0503 | 0.00721 | 20.49 | 0.16 | 32.44 | 0.0069 | - | 0.0346 |
| | GSC_5.66 | 50 | 0.001398 | 225 | 0.0503 | 0.00721 | 20.49 | 0.16 | 32.44 | 0.0062 | - | 0.0279 |
| | GSC_5.67 | 50 | 0.001398 | 285 | 0.0503 | 0.00721 | 20.49 | 0.16 | 32.44 | 0.0054 | - | 0.0237 |
| | GSC_5.68 | 50 | 0.001398 | 345 | 0.0503 | 0.00721 | 20.49 | 0.16 | 32.44 | 0.0048 | - | 0.0181 |
| | GSC_5.69 | 50 | 0.001398 | 390 | 0.0503 | 0.00721 | 20.49 | 0.16 | 32.44 | 0.0046 | - | 0.0123 |
| | GSC_5.70 | 50 | 0.001398 | 435 | 0.0503 | 0.00721 | 20.49 | 0.16 | 32.44 | 0.0042 | - | 0.0077 |
| | GSC_5.71 | 50 | 0.001398 | 485 | 0.0503 | 0.00721 | 20.49 | 0.16 | 32.44 | 0.0038 | - | 0.0055 |
| | GSC_5.72 | 50 | 0.001398 | 545 | 0.0503 | 0.00721 | 20.49 | 0.16 | 32.44 | 0.0034 | - | 0.0030 |
| | GSC_5.73 | 50 | 0.001398 | 625 | 0.0503 | 0.00721 | 20.49 | 0.16 | 32.44 | 0.0033 | - | 0.0029 |
| | GSC_5.74 | 50 | 0.001398 | 705 | 0.0503 | 0.00721 | 20.49 | 0.16 | 32.44 | 0.0031 | - | 0.0017 |
| | GSC_5.75 | 50 | 0.001398 | 765 | 0.0503 | 0.00721 | 20.49 | 0.16 | 32.44 | 0.0028 | - | 0.0012 |
| | GSC_5.76 | 50 | 0.001398 | 825 | 0.0503 | 0.00721 | 20.49 | 0.16 | 32.44 | 0.0023 | - | 0.0007 |
| | GSC_5.77 | 50 | 0.001398 | 885 | 0.0503 | 0.00721 | 20.49 | 0.16 | 32.44 | 0.0015 | - | 0.0004 |
| | GSC_5.78 | 50 | 0.001398 | 960 | 0.0503 | 0.00721 | 20.49 | 0.16 | 32.44 | 0.0007 | - | 0.0003 |
| GSC 21 | GSC_0.1 | 0 | 0.002781 | 15 | 0.0510 | 0.00946 | 16.50 | 0.12 | 0.00 | 0.1640 | - | 0.1174 |
| | GSC_0.2 | 0 | 0.002781 | 30 | 0.0510 | 0.00946 | 16.50 | 0.12 | 0.00 | 0.1163 | - | 0.0835 |
| | GSC_0.3 | 0 | 0.002781 | 60 | 0.0510 | 0.00946 | 16.50 | 0.12 | 0.00 | 0.0813 | - | 0.0518 |
| | GSC_0.4 | 0 | 0.002781 | 115 | 0.0510 | 0.00946 | 16.50 | 0.12 | 0.00 | 0.0672 | - | 0.0378 |
| | GSC_0.5 | 0 | 0.002781 | 165 | 0.0510 | 0.00946 | 16.50 | 0.12 | 0.00 | 0.0531 | - | 0.0255 |
| | GSC_0.6 | 0 | 0.002781 | 240 | 0.0510 | 0.00946 | 16.50 | 0.12 | 0.00 | 0.0372 | - | 0.0146 |
| | GSC_0.7 | 0 | 0.002781 | 320 | 0.0510 | 0.00946 | 16.50 | 0.12 | 0.00 | 0.0235 | - | 0.0096 |
| | GSC_0.8 | 0 | 0.002781 | 390 | 0.0510 | 0.00946 | 16.50 | 0.12 | 0.00 | 0.0120 | - | 0.0069 |
| | GSC_0.9 | 0 | 0.002781 | 420 | 0.0510 | 0.00946 | 16.50 | 0.12 | 0.00 | 0.0077 | - | 0.0029 |
| | GSC_0.10 | 0 | 0.002781 | 450 | 0.0510 | 0.00946 | 16.50 | 0.12 | 0.00 | 0.0055 | - | 0.0011 |
| | GSC_0.11 | 0 | 0.002781 | 550 | 0.0510 | 0.00946 | 16.50 | 0.12 | 0.00 | 0.0014 | - | 0.0003 |
| GSC 22 | GSC_0.12 | 0 | 0.002781 | 35 | 0.0683 | 0.00721 | 16.84 | 0.13 | 0.00 | 0.1774 | - | 0.1484 |
| | GSC_0.13 | 0 | 0.002781 | 80 | 0.0683 | 0.00721 | 16.84 | 0.13 | 0.00 | 0.1037 | - | 0.1233 |
| | GSC_0.14 | 0 | 0.002781 | 140 | 0.0683 | 0.00721 | 16.84 | 0.13 | 0.00 | 0.0750 | - | 0.0932 |

| (1) | (2) | (3) | (4) | (5) | (6) | (7) | (8) | (9) | (10) | (11) | (12) | (13) |
|---|---|---|---|---|---|---|---|---|---|---|---|---|
| | GSC_0.15 | 0 | 0.002781 | 175 | 0.0683 | 0.00721 | 16.84 | 0.13 | 0.00 | 0.0491 | - | 0.0773 |
| | GSC_0.16 | 0 | 0.002781 | 295 | 0.0683 | 0.00721 | 16.84 | 0.13 | 0.00 | 0.0370 | - | 0.0579 |
| | GSC_0.17 | 0 | 0.002781 | 365 | 0.0683 | 0.00721 | 16.84 | 0.13 | 0.00 | 0.0280 | - | 0.0350 |
| | GSC_0.18 | 0 | 0.002781 | 395 | 0.0683 | 0.00721 | 16.84 | 0.13 | 0.00 | 0.0183 | - | 0.0214 |
| | GSC_0.19 | 0 | 0.002781 | 475 | 0.0683 | 0.00721 | 16.84 | 0.13 | 0.00 | 0.0121 | - | 0.0109 |
| | GSC_0.20 | 0 | 0.002781 | 535 | 0.0683 | 0.00721 | 16.84 | 0.13 | 0.00 | 0.0072 | - | 0.0043 |
| | GSC_0.21 | 0 | 0.002781 | 575 | 0.0683 | 0.00721 | 16.84 | 0.13 | 0.00 | 0.0029 | - | 0.0006 |
| GSC 23 | GSC_0.22 | 0 | 0.002781 | 30 | 0.0703 | 0.00946 | 16.28 | 0.12 | 0.00 | 0.1961 | - | 0.1605 |
| | GSC_0.23 | 0 | 0.002781 | 60 | 0.0703 | 0.00946 | 16.28 | 0.12 | 0.00 | 0.1526 | - | 0.1255 |
| | GSC_0.24 | 0 | 0.002781 | 100 | 0.0703 | 0.00946 | 16.28 | 0.12 | 0.00 | 0.1071 | - | 0.0991 |
| | GSC_0.25 | 0 | 0.002781 | 160 | 0.0703 | 0.00946 | 16.28 | 0.12 | 0.00 | 0.0722 | - | 0.0732 |
| | GSC_0.26 | 0 | 0.002781 | 220 | 0.0703 | 0.00946 | 16.28 | 0.12 | 0.00 | 0.0595 | - | 0.0551 |
| | GSC_0.27 | 0 | 0.002781 | 290 | 0.0703 | 0.00946 | 16.28 | 0.12 | 0.00 | 0.0467 | - | 0.0365 |
| | GSC_0.28 | 0 | 0.002781 | 360 | 0.0703 | 0.00946 | 16.28 | 0.12 | 0.00 | 0.0312 | - | 0.0182 |
| | GSC_0.29 | 0 | 0.002781 | 420 | 0.0703 | 0.00946 | 16.28 | 0.12 | 0.00 | 0.0191 | - | 0.0079 |
| | GSC_0.30 | 0 | 0.002781 | 490 | 0.0703 | 0.00946 | 16.28 | 0.12 | 0.00 | 0.0093 | - | 0.0029 |
| | GSC_0.31 | 0 | 0.002781 | 560 | 0.0703 | 0.00946 | 16.28 | 0.12 | 0.00 | 0.0031 | - | 0.0004 |
| GSC 24 | GSC_0.32 | 0 | 0.002781 | 15 | 0.0500 | 0.00721 | 16.62 | 0.12 | 0.00 | 0.1524 | - | 0.1066 |
| | GSC_0.33 | 0 | 0.002781 | 30 | 0.0500 | 0.00721 | 16.62 | 0.12 | 0.00 | 0.1062 | - | 0.0764 |
| | GSC_0.34 | 0 | 0.002781 | 60 | 0.0500 | 0.00721 | 16.62 | 0.12 | 0.00 | 0.0665 | - | 0.0637 |
| | GSC_0.35 | 0 | 0.002781 | 110 | 0.0500 | 0.00721 | 16.62 | 0.12 | 0.00 | 0.0574 | - | 0.0510 |
| | GSC_0.36 | 0 | 0.002781 | 160 | 0.0500 | 0.00721 | 16.62 | 0.12 | 0.00 | 0.0481 | - | 0.0362 |
| | GSC_0.37 | 0 | 0.002781 | 230 | 0.0500 | 0.00721 | 16.62 | 0.12 | 0.00 | 0.0374 | - | 0.0194 |
| | GSC_0.38 | 0 | 0.002781 | 300 | 0.0500 | 0.00721 | 16.62 | 0.12 | 0.00 | 0.0253 | - | 0.0093 |
| | GSC_0.39 | 0 | 0.002781 | 370 | 0.0500 | 0.00721 | 16.62 | 0.12 | 0.00 | 0.0120 | - | 0.0051 |
| | GSC_0.40 | 0 | 0.002781 | 430 | 0.0500 | 0.00721 | 16.62 | 0.12 | 0.00 | 0.0063 | - | 0.0023 |
| | GSC_0.41 | 0 | 0.002781 | 490 | 0.0500 | 0.00721 | 16.62 | 0.12 | 0.00 | 0.0029 | - | 0.0012 |
| | GSC_0.42 | 0 | 0.002781 | 540 | 0.0500 | 0.00721 | 16.62 | 0.12 | 0.00 | 0.0018 | - | 0.0003 |

| (1) | (2) | (3) | (4) | (5) | (6) | (7) | (8) | (9) | (10) | (11) | (12) | (13) |
|---|---|---|---|---|---|---|---|---|---|---|---|---|
| GSSC 1 | GSSC_1.1 | 10 | 0.001850 | 10 | 0.0507 | 0.00721 | 17.53 | 0.11 | 0.00 | 0.0745 | 0.0732 | 0.0909 |
| | GSSC_1.2 | 10 | 0.001850 | 20 | 0.0507 | 0.00721 | 17.53 | 0.11 | 0.00 | 0.0578 | 0.0560 | 0.0820 |
| | GSSC_1.3 | 10 | 0.001850 | 30 | 0.0507 | 0.00721 | 17.53 | 0.11 | 0.00 | 0.0449 | 0.0460 | 0.0716 |
| | GSSC_1.4 | 10 | 0.001850 | 45 | 0.0507 | 0.00721 | 17.53 | 0.11 | 0.00 | 0.0347 | 0.0293 | 0.0581 |
| | GSSC_1.5 | 10 | 0.001850 | 75 | 0.0507 | 0.00721 | 17.53 | 0.11 | 0.00 | 0.0321 | 0.0262 | 0.0488 |
| | GSSC_1.6 | 10 | 0.001850 | 105 | 0.0507 | 0.00721 | 17.53 | 0.11 | 0.00 | 0.0290 | 0.0226 | 0.0367 |
| | GSSC_1.7 | 10 | 0.001850 | 135 | 0.0507 | 0.00721 | 17.53 | 0.11 | 0.00 | 0.0233 | 0.0209 | 0.0271 |
| | GSSC_1.8 | 10 | 0.001850 | 165 | 0.0507 | 0.00721 | 17.53 | 0.11 | 0.00 | 0.0193 | 0.0175 | 0.0249 |
| | GSSC_1.9 | 10 | 0.001850 | 205 | 0.0507 | 0.00721 | 17.53 | 0.11 | 0.00 | 0.0145 | 0.0169 | 0.0206 |
| | GSSC_1.10 | 10 | 0.001850 | 235 | 0.0507 | 0.00721 | 17.53 | 0.11 | 0.00 | 0.0120 | 0.0132 | 0.0210 |
| | GSSC_1.11 | 10 | 0.001850 | 265 | 0.0507 | 0.00721 | 17.53 | 0.11 | 0.00 | 0.0092 | 0.0072 | 0.0175 |
| | GSSC_1.12 | 10 | 0.001850 | 295 | 0.0507 | 0.00721 | 17.53 | 0.11 | 0.00 | 0.0076 | 0.0059 | 0.0132 |
| | GSSC_1.13 | 10 | 0.001850 | 325 | 0.0507 | 0.00721 | 17.53 | 0.11 | 0.00 | 0.0073 | 0.0064 | 0.0106 |
| | GSSC_1.14 | 10 | 0.001850 | 355 | 0.0507 | 0.00721 | 17.53 | 0.11 | 0.00 | 0.0066 | 0.0074 | 0.0091 |
| | GSSC_1.15 | 10 | 0.001850 | 385 | 0.0507 | 0.00721 | 17.53 | 0.11 | 0.00 | 0.0070 | 0.0052 | 0.0080 |
| | GSSC_1.16 | 10 | 0.001850 | 415 | 0.0507 | 0.00721 | 17.53 | 0.11 | 0.00 | 0.0065 | 0.0050 | 0.0058 |
| | GSSC_1.17 | 10 | 0.001850 | 445 | 0.0507 | 0.00721 | 17.53 | 0.11 | 0.00 | 0.0060 | 0.0036 | 0.0044 |
| | GSSC_1.18 | 10 | 0.001850 | 475 | 0.0507 | 0.00721 | 17.53 | 0.11 | 0.00 | 0.0058 | 0.0034 | 0.0032 |
| | GSSC_1.19 | 10 | 0.001850 | 505 | 0.0507 | 0.00721 | 17.53 | 0.11 | 0.00 | 0.0050 | 0.0033 | 0.0026 |
| | GSSC_1.20 | 10 | 0.001850 | 535 | 0.0507 | 0.00721 | 17.53 | 0.11 | 0.00 | 0.0103 | 0.0077 | 0.0019 |
| | GSSC_1.21 | 10 | 0.001850 | 565 | 0.0507 | 0.00721 | 17.53 | 0.11 | 0.00 | 0.0039 | 0.0032 | 0.0012 |
| | GSSC_1.22 | 10 | 0.001850 | 595 | 0.0507 | 0.00721 | 17.53 | 0.11 | 0.00 | 0.0039 | 0.0023 | 0.0010 |
| | GSSC_1.23 | 10 | 0.001850 | 625 | 0.0507 | 0.00721 | 17.53 | 0.11 | 0.00 | 0.0028 | 0.0021 | 0.0007 |
| | GSSC_1.24 | 10 | 0.001850 | 655 | 0.0507 | 0.00721 | 17.53 | 0.11 | 0.00 | 0.0021 | 0.0021 | 0.0004 |
| | GSSC_1.25 | 10 | 0.001850 | 685 | 0.0507 | 0.00721 | 17.53 | 0.11 | 0.00 | 0.0015 | 0.0011 | 0.0003 |
| GSSC 2 | GSSC_1.26 | 10 | 0.001850 | 10 | 0.0502 | 0.00946 | 18.67 | 0.08 | 0.00 | 0.0989 | 0.1004 | 0.0995 |
| | GSSC_1.27 | 10 | 0.001850 | 25 | 0.0502 | 0.00946 | 18.67 | 0.08 | 0.00 | 0.0892 | 0.0891 | 0.0739 |
| | GSSC_1.28 | 10 | 0.001850 | 40 | 0.0502 | 0.00946 | 18.67 | 0.08 | 0.00 | 0.0738 | 0.0750 | 0.0517 |

| (1) | (2) | (3) | (4) | (5) | (6) | (7) | (8) | (9) | (10) | (11) | (12) | (13) |
|---|---|---|---|---|---|---|---|---|---|---|---|---|
| | GSSC_1.29 | 10 | 0.001850 | 55 | 0.0502 | 0.00946 | 18.67 | 0.08 | 0.00 | 0.0635 | 0.0632 | 0.0411 |
| | GSSC_1.30 | 10 | 0.001850 | 70 | 0.0502 | 0.00946 | 18.67 | 0.08 | 0.00 | 0.0555 | 0.0513 | 0.0299 |
| | GSSC_1.31 | 10 | 0.001850 | 85 | 0.0502 | 0.00946 | 18.67 | 0.08 | 0.00 | 0.0436 | 0.0389 | 0.0251 |
| | GSSC_1.32 | 10 | 0.001850 | 100 | 0.0502 | 0.00946 | 18.67 | 0.08 | 0.00 | 0.0392 | 0.0343 | 0.0203 |
| | GSSC_1.33 | 10 | 0.001850 | 130 | 0.0502 | 0.00946 | 18.67 | 0.08 | 0.00 | 0.0237 | 0.0247 | 0.0163 |
| | GSSC_1.34 | 10 | 0.001850 | 160 | 0.0502 | 0.00946 | 18.67 | 0.08 | 0.00 | 0.0152 | 0.0135 | 0.0151 |
| | GSSC_1.35 | 10 | 0.001850 | 190 | 0.0502 | 0.00946 | 18.67 | 0.08 | 0.00 | 0.0095 | 0.0100 | 0.0113 |
| | GSSC_1.36 | 10 | 0.001850 | 220 | 0.0502 | 0.00946 | 18.67 | 0.08 | 0.00 | 0.0042 | 0.0073 | 0.0105 |
| | GSSC_1.37 | 10 | 0.001850 | 265 | 0.0502 | 0.00946 | 18.67 | 0.08 | 0.00 | 0.0039 | 0.0047 | 0.0079 |
| | GSSC_1.38 | 10 | 0.001850 | 295 | 0.0502 | 0.00946 | 18.67 | 0.08 | 0.00 | 0.0037 | 0.0045 | 0.0089 |
| | GSSC_1.39 | 10 | 0.001850 | 340 | 0.0502 | 0.00946 | 18.67 | 0.08 | 0.00 | 0.0032 | 0.0039 | 0.0071 |
| | GSSC_1.40 | 10 | 0.001850 | 415 | 0.0502 | 0.00946 | 18.67 | 0.08 | 0.00 | 0.0029 | 0.0034 | 0.0054 |
| | GSSC_1.41 | 10 | 0.001850 | 445 | 0.0502 | 0.00946 | 18.67 | 0.08 | 0.00 | 0.0018 | 0.0024 | 0.0035 |
| | GSSC_1.42 | 10 | 0.001850 | 505 | 0.0502 | 0.00946 | 18.67 | 0.08 | 0.00 | 0.0019 | 0.0025 | 0.0027 |
| | GSSC_1.43 | 10 | 0.001850 | 565 | 0.0502 | 0.00946 | 18.67 | 0.08 | 0.00 | 0.0014 | 0.0015 | 0.0013 |
| | GSSC_1.44 | 10 | 0.001850 | 640 | 0.0502 | 0.00946 | 18.67 | 0.08 | 0.00 | 0.0008 | 0.0006 | 0.0006 |
| GSSC 3 | GSSC_1.45 | 10 | 0.001850 | 10 | 0.0695 | 0.00946 | 18.21 | 0.08 | 0.00 | 0.1232 | 0.1360 | 0.1308 |
| | GSSC_1.46 | 10 | 0.001850 | 25 | 0.0695 | 0.00946 | 18.21 | 0.08 | 0.00 | 0.0974 | 0.0926 | 0.1023 |
| | GSSC_1.47 | 10 | 0.001850 | 45 | 0.0695 | 0.00946 | 18.21 | 0.08 | 0.00 | 0.0745 | 0.0676 | 0.0905 |
| | GSSC_1.48 | 10 | 0.001850 | 65 | 0.0695 | 0.00946 | 18.21 | 0.08 | 0.00 | 0.0616 | 0.0565 | 0.0784 |
| | GSSC_1.49 | 10 | 0.001850 | 85 | 0.0695 | 0.00946 | 18.21 | 0.08 | 0.00 | 0.0526 | 0.0446 | 0.0614 |
| | GSSC_1.50 | 10 | 0.001850 | 115 | 0.0695 | 0.00946 | 18.21 | 0.08 | 0.00 | 0.0376 | 0.0321 | 0.0542 |
| | GSSC_1.51 | 10 | 0.001850 | 145 | 0.0695 | 0.00946 | 18.21 | 0.08 | 0.00 | 0.0311 | 0.0262 | 0.0398 |
| | GSSC_1.52 | 10 | 0.001850 | 175 | 0.0695 | 0.00946 | 18.21 | 0.08 | 0.00 | 0.0243 | 0.0222 | 0.0290 |
| | GSSC_1.53 | 10 | 0.001850 | 205 | 0.0695 | 0.00946 | 18.21 | 0.08 | 0.00 | 0.0161 | 0.0198 | 0.0229 |
| | GSSC_1.54 | 10 | 0.001850 | 235 | 0.0695 | 0.00946 | 18.21 | 0.08 | 0.00 | 0.0139 | 0.0154 | 0.0169 |
| | GSSC_1.55 | 10 | 0.001850 | 265 | 0.0695 | 0.00946 | 18.21 | 0.08 | 0.00 | 0.0116 | 0.0161 | 0.0156 |
| | GSSC_1.56 | 10 | 0.001850 | 295 | 0.0695 | 0.00946 | 18.21 | 0.08 | 0.00 | 0.0100 | 0.0117 | 0.0124 |

| (1) | (2) | (3) | (4) | (5) | (6) | (7) | (8) | (9) | (10) | (11) | (12) | (13) |
|---|---|---|---|---|---|---|---|---|---|---|---|---|
| | GSSC_1.57 | 10 | 0.001850 | 325 | 0.0695 | 0.00946 | 18.21 | 0.08 | 0.00 | 0.0067 | 0.0079 | 0.0093 |
| | GSSC_1.58 | 10 | 0.001850 | 355 | 0.0695 | 0.00946 | 18.21 | 0.08 | 0.00 | 0.0046 | 0.0069 | 0.0066 |
| | GSSC_1.59 | 10 | 0.001850 | 415 | 0.0695 | 0.00946 | 18.21 | 0.08 | 0.00 | 0.0027 | 0.0033 | 0.0049 |
| | GSSC_1.60 | 10 | 0.001850 | 475 | 0.0695 | 0.00946 | 18.21 | 0.08 | 0.00 | 0.0025 | 0.0026 | 0.0030 |
| | GSSC_1.61 | 10 | 0.001850 | 535 | 0.0695 | 0.00946 | 18.21 | 0.08 | 0.00 | 0.0018 | 0.0016 | 0.0015 |
| | GSSC_1.62 | 10 | 0.001850 | 595 | 0.0695 | 0.00946 | 18.21 | 0.08 | 0.00 | 0.0012 | 0.0011 | 0.0008 |
| GSSC 4 | GSSC_1.63 | 10 | 0.001850 | 15 | 0.0691 | 0.00721 | 17.76 | 0.10 | 0.00 | 0.1022 | 0.1103 | 0.1175 |
| | GSSC_1.64 | 10 | 0.001850 | 30 | 0.0691 | 0.00721 | 17.76 | 0.10 | 0.00 | 0.0856 | 0.0887 | 0.0898 |
| | GSSC_1.65 | 10 | 0.001850 | 45 | 0.0691 | 0.00721 | 17.76 | 0.10 | 0.00 | 0.0743 | 0.0776 | 0.0786 |
| | GSSC_1.66 | 10 | 0.001850 | 60 | 0.0691 | 0.00721 | 17.76 | 0.10 | 0.00 | 0.0614 | 0.0657 | 0.0691 |
| | GSSC_1.67 | 10 | 0.001850 | 75 | 0.0691 | 0.00721 | 17.76 | 0.10 | 0.00 | 0.0493 | 0.0524 | 0.0542 |
| | GSSC_1.68 | 10 | 0.001850 | 90 | 0.0691 | 0.00721 | 17.76 | 0.10 | 0.00 | 0.0285 | 0.0422 | 0.0419 |
| | GSSC_1.69 | 10 | 0.001850 | 105 | 0.0691 | 0.00721 | 17.76 | 0.10 | 0.00 | 0.0237 | 0.0274 | 0.0319 |
| | GSSC_1.70 | 10 | 0.001850 | 135 | 0.0691 | 0.00721 | 17.76 | 0.10 | 0.00 | 0.0204 | 0.0183 | 0.0283 |
| | GSSC_1.71 | 10 | 0.001850 | 165 | 0.0691 | 0.00721 | 17.76 | 0.10 | 0.00 | 0.0130 | 0.0111 | 0.0222 |
| | GSSC_1.72 | 10 | 0.001850 | 195 | 0.0691 | 0.00721 | 17.76 | 0.10 | 0.00 | 0.0133 | 0.0096 | 0.0153 |
| | GSSC_1.73 | 10 | 0.001850 | 225 | 0.0691 | 0.00721 | 17.76 | 0.10 | 0.00 | 0.0125 | 0.0089 | 0.0105 |
| | GSSC_1.74 | 10 | 0.001850 | 255 | 0.0691 | 0.00721 | 17.76 | 0.10 | 0.00 | 0.0113 | 0.0071 | 0.0088 |
| | GSSC_1.75 | 10 | 0.001850 | 285 | 0.0691 | 0.00721 | 17.76 | 0.10 | 0.00 | 0.0074 | 0.0058 | 0.0058 |
| | GSSC_1.76 | 10 | 0.001850 | 315 | 0.0691 | 0.00721 | 17.76 | 0.10 | 0.00 | 0.0054 | 0.0043 | 0.0038 |
| | GSSC_1.77 | 10 | 0.001850 | 360 | 0.0691 | 0.00721 | 17.76 | 0.10 | 0.00 | 0.0047 | 0.0032 | 0.0027 |
| | GSSC_1.78 | 10 | 0.001850 | 420 | 0.0691 | 0.00721 | 17.76 | 0.10 | 0.00 | 0.0035 | 0.0030 | 0.0018 |
| | GSSC_1.79 | 10 | 0.001850 | 480 | 0.0691 | 0.00721 | 17.76 | 0.10 | 0.00 | 0.0018 | 0.0016 | 0.0012 |
| | GSSC_1.80 | 10 | 0.001850 | 560 | 0.0691 | 0.00721 | 17.76 | 0.10 | 0.00 | 0.0010 | 0.0009 | 0.0008 |
| | GSSC_1.81 | 10 | 0.001850 | 650 | 0.0691 | 0.00721 | 17.76 | 0.10 | 0.00 | 0.0006 | 0.0004 | 0.0005 |
| GSSC 5 | GSSC_2.1 | 20 | 0.001646 | 15 | 0.0691 | 0.00721 | 18.35 | 0.10 | 7.57 | 0.0826 | 0.0903 | 0.0932 |
| | GSSC_2.2 | 20 | 0.001646 | 30 | 0.0691 | 0.00721 | 18.35 | 0.10 | 7.57 | 0.0697 | 0.0772 | 0.0821 |
| | GSSC_2.3 | 20 | 0.001646 | 50 | 0.0691 | 0.00721 | 18.35 | 0.10 | 7.57 | 0.0598 | 0.0648 | 0.0698 |

| (1) | (2) | (3) | (4) | (5) | (6) | (7) | (8) | (9) | (10) | (11) | (12) | (13) |
|---|---|---|---|---|---|---|---|---|---|---|---|---|
| | GSSC_2.4 | 20 | 0.001646 | 65 | 0.0691 | 0.00721 | 18.35 | 0.10 | 7.57 | 0.0488 | 0.0502 | 0.0620 |
| | GSSC_2.5 | 20 | 0.001646 | 80 | 0.0691 | 0.00721 | 18.35 | 0.10 | 7.57 | 0.0415 | 0.0420 | 0.0532 |
| | GSSC_2.6 | 20 | 0.001646 | 100 | 0.0691 | 0.00721 | 18.35 | 0.10 | 7.57 | 0.0341 | 0.0365 | 0.0438 |
| | GSSC_2.7 | 20 | 0.001646 | 110 | 0.0691 | 0.00721 | 18.35 | 0.10 | 7.57 | 0.0276 | 0.0325 | 0.0402 |
| | GSSC_2.8 | 20 | 0.001646 | 145 | 0.0691 | 0.00721 | 18.35 | 0.10 | 7.57 | 0.0211 | 0.0264 | 0.0307 |
| | GSSC_2.9 | 20 | 0.001646 | 155 | 0.0691 | 0.00721 | 18.35 | 0.10 | 7.57 | 0.0178 | 0.0217 | 0.0301 |
| | GSSC_2.10 | 20 | 0.001646 | 190 | 0.0691 | 0.00721 | 18.35 | 0.10 | 7.57 | 0.0124 | 0.0164 | 0.0266 |
| | GSSC_2.11 | 20 | 0.001646 | 215 | 0.0691 | 0.00721 | 18.35 | 0.10 | 7.57 | 0.0114 | 0.0095 | 0.0225 |
| | GSSC_2.12 | 20 | 0.001646 | 250 | 0.0691 | 0.00721 | 18.35 | 0.10 | 7.57 | 0.0097 | 0.0077 | 0.0168 |
| | GSSC_2.13 | 20 | 0.001646 | 275 | 0.0691 | 0.00721 | 18.35 | 0.10 | 7.57 | 0.0072 | 0.0054 | 0.0137 |
| | GSSC_2.14 | 20 | 0.001646 | 320 | 0.0691 | 0.00721 | 18.35 | 0.10 | 7.57 | 0.0061 | 0.0037 | 0.0073 |
| | GSSC_2.15 | 20 | 0.001646 | 380 | 0.0691 | 0.00721 | 18.35 | 0.10 | 7.57 | 0.0042 | 0.0030 | 0.0046 |
| | GSSC_2.16 | 20 | 0.001646 | 455 | 0.0691 | 0.00721 | 18.35 | 0.10 | 7.57 | 0.0028 | 0.0021 | 0.0034 |
| | GSSC_2.17 | 20 | 0.001646 | 545 | 0.0691 | 0.00721 | 18.35 | 0.10 | 7.57 | 0.0018 | 0.0014 | 0.0013 |
| | GSSC_2.18 | 20 | 0.001646 | 680 | 0.0691 | 0.00721 | 18.35 | 0.10 | 7.57 | 0.0008 | 0.0007 | 0.0006 |
| GSSC 6 | GSSC_2.19 | 20 | 0.001646 | 10 | 0.0500 | 0.00721 | 19.46 | 0.17 | 9.73 | 0.0723 | 0.0747 | 0.0865 |
| | GSSC_2.20 | 20 | 0.001646 | 25 | 0.0500 | 0.00721 | 19.46 | 0.17 | 9.73 | 0.0614 | 0.0647 | 0.0794 |
| | GSSC_2.21 | 20 | 0.001646 | 40 | 0.0500 | 0.00721 | 19.46 | 0.17 | 9.73 | 0.0547 | 0.0590 | 0.0696 |
| | GSSC_2.22 | 20 | 0.001646 | 55 | 0.0500 | 0.00721 | 19.46 | 0.17 | 9.73 | 0.0420 | 0.0491 | 0.0570 |
| | GSSC_2.23 | 20 | 0.001646 | 70 | 0.0500 | 0.00721 | 19.46 | 0.17 | 9.73 | 0.0336 | 0.0413 | 0.0505 |
| | GSSC_2.24 | 20 | 0.001646 | 85 | 0.0500 | 0.00721 | 19.46 | 0.17 | 9.73 | 0.0241 | 0.0355 | 0.0446 |
| | GSSC_2.25 | 20 | 0.001646 | 105 | 0.0500 | 0.00721 | 19.46 | 0.17 | 9.73 | 0.0176 | 0.0297 | 0.0409 |
| | GSSC_2.26 | 20 | 0.001646 | 135 | 0.0500 | 0.00721 | 19.46 | 0.17 | 9.73 | 0.0115 | 0.0249 | 0.0343 |
| | GSSC_2.27 | 20 | 0.001646 | 170 | 0.0500 | 0.00721 | 19.46 | 0.17 | 9.73 | 0.0063 | 0.0188 | 0.0275 |
| | GSSC_2.28 | 20 | 0.001646 | 210 | 0.0500 | 0.00721 | 19.46 | 0.17 | 9.73 | 0.0047 | 0.0125 | 0.0206 |
| | GSSC_2.29 | 20 | 0.001646 | 250 | 0.0500 | 0.00721 | 19.46 | 0.17 | 9.73 | 0.0024 | 0.0082 | 0.0135 |
| | GSSC_2.30 | 20 | 0.001646 | 320 | 0.0500 | 0.00721 | 19.46 | 0.17 | 9.73 | 0.0022 | 0.0056 | 0.0101 |
| | GSSC_2.31 | 20 | 0.001646 | 380 | 0.0500 | 0.00721 | 19.46 | 0.17 | 9.73 | 0.0015 | 0.0050 | 0.0070 |

| (1) | (2) | (3) | (4) | (5) | (6) | (7) | (8) | (9) | (10) | (11) | (12) | (13) |
|---|---|---|---|---|---|---|---|---|---|---|---|---|
| | GSSC_2.32 | 20 | 0.001646 | 470 | 0.0500 | 0.00721 | 19.46 | 0.17 | 9.73 | 0.0013 | 0.0046 | 0.0045 |
| | GSSC_2.33 | 20 | 0.001646 | 560 | 0.0500 | 0.00721 | 19.46 | 0.17 | 9.73 | 0.0008 | 0.0040 | 0.0028 |
| | GSSC_2.34 | 20 | 0.001646 | 660 | 0.0500 | 0.00721 | 19.46 | 0.17 | 9.73 | 0.0006 | 0.0023 | 0.0013 |
| | GSSC_2.35 | 20 | 0.001646 | 760 | 0.0500 | 0.00721 | 19.46 | 0.17 | 9.73 | 0.0003 | 0.0009 | 0.0006 |
| GSSC 7 | GSSC_2.36 | 20 | 0.001646 | 10 | 0.0497 | 0.00946 | 16.96 | 0.13 | 6.49 | 0.0746 | 0.0745 | 0.0883 |
| | GSSC_2.37 | 20 | 0.001646 | 25 | 0.0497 | 0.00946 | 16.96 | 0.13 | 6.49 | 0.0627 | 0.0630 | 0.0785 |
| | GSSC_2.38 | 20 | 0.001646 | 35 | 0.0497 | 0.00946 | 16.96 | 0.13 | 6.49 | 0.0523 | 0.0514 | 0.0673 |
| | GSSC_2.39 | 20 | 0.001646 | 55 | 0.0497 | 0.00946 | 16.96 | 0.13 | 6.49 | 0.0459 | 0.0447 | 0.0561 |
| | GSSC_2.40 | 20 | 0.001646 | 75 | 0.0497 | 0.00946 | 16.96 | 0.13 | 6.49 | 0.0344 | 0.0356 | 0.0504 |
| | GSSC_2.41 | 20 | 0.001646 | 95 | 0.0497 | 0.00946 | 16.96 | 0.13 | 6.49 | 0.0297 | 0.0296 | 0.0465 |
| | GSSC_2.42 | 20 | 0.001646 | 125 | 0.0497 | 0.00946 | 16.96 | 0.13 | 6.49 | 0.0240 | 0.0238 | 0.0384 |
| | GSSC_2.43 | 20 | 0.001646 | 155 | 0.0497 | 0.00946 | 16.96 | 0.13 | 6.49 | 0.0213 | 0.0190 | 0.0293 |
| | GSSC_2.44 | 20 | 0.001646 | 185 | 0.0497 | 0.00946 | 16.96 | 0.13 | 6.49 | 0.0149 | 0.0156 | 0.0247 |
| | GSSC_2.45 | 20 | 0.001646 | 230 | 0.0497 | 0.00946 | 16.96 | 0.13 | 6.49 | 0.0100 | 0.0130 | 0.0180 |
| | GSSC_2.46 | 20 | 0.001646 | 280 | 0.0497 | 0.00946 | 16.96 | 0.13 | 6.49 | 0.0034 | 0.0090 | 0.0109 |
| | GSSC_2.47 | 20 | 0.001646 | 320 | 0.0497 | 0.00946 | 16.96 | 0.13 | 6.49 | 0.0023 | 0.0075 | 0.0074 |
| | GSSC_2.48 | 20 | 0.001646 | 365 | 0.0497 | 0.00946 | 16.96 | 0.13 | 6.49 | 0.0018 | 0.0064 | 0.0049 |
| | GSSC_2.49 | 20 | 0.001646 | 425 | 0.0497 | 0.00946 | 16.96 | 0.13 | 6.49 | 0.0012 | 0.0041 | 0.0035 |
| | GSSC_2.50 | 20 | 0.001646 | 500 | 0.0497 | 0.00946 | 16.96 | 0.13 | 6.49 | 0.0009 | 0.0030 | 0.0020 |
| | GSSC_2.51 | 20 | 0.001646 | 600 | 0.0497 | 0.00946 | 16.96 | 0.13 | 6.49 | 0.0005 | 0.0015 | 0.0009 |
| | GSSC_2.52 | 20 | 0.001646 | 725 | 0.0497 | 0.00946 | 16.96 | 0.13 | 6.49 | 0.0003 | 0.0007 | 0.0003 |
| GSSC 8 | GSSC_2.53 | 20 | 0.001646 | 10 | 0.0694 | 0.00946 | 18.44 | 0.11 | 8.65 | 0.1183 | 0.1164 | 0.1084 |
| | GSSC_2.54 | 20 | 0.001646 | 20 | 0.0694 | 0.00946 | 18.44 | 0.11 | 8.65 | 0.0955 | 0.0812 | 0.0880 |
| | GSSC_2.55 | 20 | 0.001646 | 35 | 0.0694 | 0.00946 | 18.44 | 0.11 | 8.65 | 0.0754 | 0.0700 | 0.0761 |
| | GSSC_2.56 | 20 | 0.001646 | 50 | 0.0694 | 0.00946 | 18.44 | 0.11 | 8.65 | 0.0582 | 0.0556 | 0.0672 |
| | GSSC_2.57 | 20 | 0.001646 | 80 | 0.0694 | 0.00946 | 18.44 | 0.11 | 8.65 | 0.0478 | 0.0422 | 0.0569 |
| | GSSC_2.58 | 20 | 0.001646 | 100 | 0.0694 | 0.00946 | 18.44 | 0.11 | 8.65 | 0.0448 | 0.0378 | 0.0430 |
| | GSSC_2.59 | 20 | 0.001646 | 120 | 0.0694 | 0.00946 | 18.44 | 0.11 | 8.65 | 0.0329 | 0.0336 | 0.0348 |

| (1) | (2) | (3) | (4) | (5) | (6) | (7) | (8) | (9) | (10) | (11) | (12) | (13) |
|---|---|---|---|---|---|---|---|---|---|---|---|---|
| | GSSC_2.60 | 20 | 0.001646 | 140 | 0.0694 | 0.00946 | 18.44 | 0.11 | 8.65 | 0.0200 | 0.0231 | 0.0283 |
| | GSSC_2.61 | 20 | 0.001646 | 170 | 0.0694 | 0.00946 | 18.44 | 0.11 | 8.65 | 0.0171 | 0.0180 | 0.0252 |
| | GSSC_2.62 | 20 | 0.001646 | 200 | 0.0694 | 0.00946 | 18.44 | 0.11 | 8.65 | 0.0112 | 0.0149 | 0.0193 |
| | GSSC_2.63 | 20 | 0.001646 | 250 | 0.0694 | 0.00946 | 18.44 | 0.11 | 8.65 | 0.0085 | 0.0116 | 0.0141 |
| | GSSC_2.64 | 20 | 0.001646 | 290 | 0.0694 | 0.00946 | 18.44 | 0.11 | 8.65 | 0.0065 | 0.0092 | 0.0108 |
| | GSSC_2.65 | 20 | 0.001646 | 335 | 0.0694 | 0.00946 | 18.44 | 0.11 | 8.65 | 0.0048 | 0.0070 | 0.0067 |
| | GSSC_2.66 | 20 | 0.001646 | 380 | 0.0694 | 0.00946 | 18.44 | 0.11 | 8.65 | 0.0041 | 0.0050 | 0.0034 |
| | GSSC_2.67 | 20 | 0.001646 | 470 | 0.0694 | 0.00946 | 18.44 | 0.11 | 8.65 | 0.0027 | 0.0028 | 0.0020 |
| | GSSC_2.68 | 20 | 0.001646 | 570 | 0.0694 | 0.00946 | 18.44 | 0.11 | 8.65 | 0.0017 | 0.0014 | 0.0012 |
| | GSSC_2.69 | 20 | 0.001646 | 660 | 0.0694 | 0.00946 | 18.44 | 0.11 | 8.65 | 0.0011 | 0.0010 | 0.0006 |
| GSSC 9 | GSSC_3.1 | 30 | 0.001442 | 10 | 0.0515 | 0.00946 | 19.86 | 0.13 | 19.46 | 0.0681 | 0.0678 | 0.0846 |
| | GSSC_3.2 | 30 | 0.001442 | 30 | 0.0515 | 0.00946 | 19.86 | 0.13 | 19.46 | 0.0605 | 0.0578 | 0.0792 |
| | GSSC_3.3 | 30 | 0.001442 | 50 | 0.0515 | 0.00946 | 19.86 | 0.13 | 19.46 | 0.0531 | 0.0517 | 0.0721 |
| | GSSC_3.4 | 30 | 0.001442 | 70 | 0.0515 | 0.00946 | 19.86 | 0.13 | 19.46 | 0.0477 | 0.0444 | 0.0650 |
| | GSSC_3.5 | 30 | 0.001442 | 90 | 0.0515 | 0.00946 | 19.86 | 0.13 | 19.46 | 0.0412 | 0.0354 | 0.0544 |
| | GSSC_3.6 | 30 | 0.001442 | 110 | 0.0515 | 0.00946 | 19.86 | 0.13 | 19.46 | 0.0370 | 0.0265 | 0.0501 |
| | GSSC_3.7 | 30 | 0.001442 | 130 | 0.0515 | 0.00946 | 19.86 | 0.13 | 19.46 | 0.0308 | 0.0182 | 0.0424 |
| | GSSC_3.8 | 30 | 0.001442 | 160 | 0.0515 | 0.00946 | 19.86 | 0.13 | 19.46 | 0.0174 | 0.0101 | 0.0435 |
| | GSSC_3.9 | 30 | 0.001442 | 190 | 0.0515 | 0.00946 | 19.86 | 0.13 | 19.46 | 0.0115 | 0.0085 | 0.0308 |
| | GSSC_3.10 | 30 | 0.001442 | 235 | 0.0515 | 0.00946 | 19.86 | 0.13 | 19.46 | 0.0072 | 0.0049 | 0.0265 |
| | GSSC_3.11 | 30 | 0.001442 | 280 | 0.0515 | 0.00946 | 19.86 | 0.13 | 19.46 | 0.0042 | 0.0028 | 0.0202 |
| | GSSC_3.12 | 30 | 0.001442 | 325 | 0.0515 | 0.00946 | 19.86 | 0.13 | 19.46 | 0.0026 | 0.0019 | 0.0145 |
| | GSSC_3.13 | 30 | 0.001442 | 370 | 0.0515 | 0.00946 | 19.86 | 0.13 | 19.46 | 0.0016 | 0.0017 | 0.0091 |
| | GSSC_3.14 | 30 | 0.001442 | 430 | 0.0515 | 0.00946 | 19.86 | 0.13 | 19.46 | 0.0012 | 0.0011 | 0.0049 |
| | GSSC_3.15 | 30 | 0.001442 | 520 | 0.0515 | 0.00946 | 19.86 | 0.13 | 19.46 | 0.0007 | 0.0007 | 0.0025 |
| | GSSC_3.16 | 30 | 0.001442 | 640 | 0.0515 | 0.00946 | 19.86 | 0.13 | 19.46 | 0.0004 | 0.0004 | 0.0010 |
| | GSSC_3.17 | 30 | 0.001442 | 760 | 0.0515 | 0.00946 | 19.86 | 0.13 | 19.46 | 0.0002 | 0.0003 | 0.0003 |
| GSSC 10 | GSSC_3.18 | 30 | 0.001442 | 10 | 0.0696 | 0.00946 | 19.69 | 0.13 | 20.00 | 0.0958 | 0.0992 | 0.0886 |

| (1) | (2) | (3) | (4) | (5) | (6) | (7) | (8) | (9) | (10) | (11) | (12) | (13) |
|---|---|---|---|---|---|---|---|---|---|---|---|---|
| | GSSC_3.19 | 30 | 0.001442 | 20 | 0.0696 | 0.00946 | 19.69 | 0.13 | 20.00 | 0.0812 | 0.0863 | 0.0811 |
| | GSSC_3.20 | 30 | 0.001442 | 35 | 0.0696 | 0.00946 | 19.69 | 0.13 | 20.00 | 0.0662 | 0.0717 | 0.0702 |
| | GSSC_3.21 | 30 | 0.001442 | 50 | 0.0696 | 0.00946 | 19.69 | 0.13 | 20.00 | 0.0553 | 0.0614 | 0.0598 |
| | GSSC_3.22 | 30 | 0.001442 | 65 | 0.0696 | 0.00946 | 19.69 | 0.13 | 20.00 | 0.0469 | 0.0484 | 0.0503 |
| | GSSC_3.23 | 30 | 0.001442 | 85 | 0.0696 | 0.00946 | 19.69 | 0.13 | 20.00 | 0.0414 | 0.0351 | 0.0391 |
| | GSSC_3.24 | 30 | 0.001442 | 115 | 0.0696 | 0.00946 | 19.69 | 0.13 | 20.00 | 0.0337 | 0.0241 | 0.0344 |
| | GSSC_3.25 | 30 | 0.001442 | 145 | 0.0696 | 0.00946 | 19.69 | 0.13 | 20.00 | 0.0233 | 0.0187 | 0.0208 |
| | GSSC_3.26 | 30 | 0.001442 | 190 | 0.0696 | 0.00946 | 19.69 | 0.13 | 20.00 | 0.0189 | 0.0173 | 0.0148 |
| | GSSC_3.27 | 30 | 0.001442 | 235 | 0.0696 | 0.00946 | 19.69 | 0.13 | 20.00 | 0.0127 | 0.0119 | 0.0103 |
| | GSSC_3.28 | 30 | 0.001442 | 275 | 0.0696 | 0.00946 | 19.69 | 0.13 | 20.00 | 0.0073 | 0.0069 | 0.0086 |
| | GSSC_3.29 | 30 | 0.001442 | 320 | 0.0696 | 0.00946 | 19.69 | 0.13 | 20.00 | 0.0046 | 0.0048 | 0.0070 |
| | GSSC_3.30 | 30 | 0.001442 | 365 | 0.0696 | 0.00946 | 19.69 | 0.13 | 20.00 | 0.0036 | 0.0033 | 0.0048 |
| | GSSC_3.31 | 30 | 0.001442 | 405 | 0.0696 | 0.00946 | 19.69 | 0.13 | 20.00 | 0.0029 | 0.0028 | 0.0021 |
| | GSSC_3.32 | 30 | 0.001442 | 465 | 0.0696 | 0.00946 | 19.69 | 0.13 | 20.00 | 0.0021 | 0.0023 | 0.0009 |
| | GSSC_3.33 | 30 | 0.001442 | 565 | 0.0696 | 0.00946 | 19.69 | 0.13 | 20.00 | 0.0013 | 0.0013 | 0.0005 |
| | GSSC_3.34 | 30 | 0.001442 | 705 | 0.0696 | 0.00946 | 19.69 | 0.13 | 20.00 | 0.0008 | 0.0008 | 0.0003 |
| GSSC 11 | GSSC_3.35 | 30 | 0.001442 | 30 | 0.0690 | 0.00721 | 19.92 | 0.18 | 18.92 | 0.0693 | 0.0748 | 0.0863 |
| | GSSC_3.36 | 30 | 0.001442 | 60 | 0.0690 | 0.00721 | 19.92 | 0.18 | 18.92 | 0.0494 | 0.0609 | 0.0749 |
| | GSSC_3.37 | 30 | 0.001442 | 90 | 0.0690 | 0.00721 | 19.92 | 0.18 | 18.92 | 0.0338 | 0.0451 | 0.0639 |
| | GSSC_3.38 | 30 | 0.001442 | 120 | 0.0690 | 0.00721 | 19.92 | 0.18 | 18.92 | 0.0220 | 0.0331 | 0.0545 |
| | GSSC_3.39 | 30 | 0.001442 | 165 | 0.0690 | 0.00721 | 19.92 | 0.18 | 18.92 | 0.0139 | 0.0178 | 0.0453 |
| | GSSC_3.40 | 30 | 0.001442 | 210 | 0.0690 | 0.00721 | 19.92 | 0.18 | 18.92 | 0.0091 | 0.0128 | 0.0323 |
| | GSSC_3.41 | 30 | 0.001442 | 255 | 0.0690 | 0.00721 | 19.92 | 0.18 | 18.92 | 0.0076 | 0.0087 | 0.0303 |
| | GSSC_3.42 | 30 | 0.001442 | 330 | 0.0690 | 0.00721 | 19.92 | 0.18 | 18.92 | 0.0068 | 0.0057 | 0.0260 |
| | GSSC_3.43 | 30 | 0.001442 | 375 | 0.0690 | 0.00721 | 19.92 | 0.18 | 18.92 | 0.0060 | 0.0049 | 0.0186 |
| | GSSC_3.44 | 30 | 0.001442 | 420 | 0.0690 | 0.00721 | 19.92 | 0.18 | 18.92 | 0.0043 | 0.0044 | 0.0093 |
| | GSSC_3.45 | 30 | 0.001442 | 465 | 0.0690 | 0.00721 | 19.92 | 0.18 | 18.92 | 0.0037 | 0.0030 | 0.0072 |
| | GSSC_3.46 | 30 | 0.001442 | 510 | 0.0690 | 0.00721 | 19.92 | 0.18 | 18.92 | 0.0031 | 0.0022 | 0.0039 |

| (1) | (2) | (3) | (4) | (5) | (6) | (7) | (8) | (9) | (10) | (11) | (12) | (13) |
|---|---|---|---|---|---|---|---|---|---|---|---|---|
| | GSSC_3.47 | 30 | 0.001442 | 555 | 0.0690 | 0.00721 | 19.92 | 0.18 | 18.92 | 0.0024 | 0.0015 | 0.0028 |
| | GSSC_3.48 | 30 | 0.001442 | 615 | 0.0690 | 0.00721 | 19.92 | 0.18 | 18.92 | 0.0018 | 0.0012 | 0.0013 |
| | GSSC_3.49 | 30 | 0.001442 | 735 | 0.0690 | 0.00721 | 19.92 | 0.18 | 18.92 | 0.0007 | 0.0006 | 0.0006 |
| GSSC 12 | GSSC_3.50 | 30 | 0.001442 | 15 | 0.0512 | 0.00721 | 19.80 | 0.13 | 17.84 | 0.0631 | 0.0601 | 0.0808 |
| | GSSC_3.51 | 30 | 0.001442 | 35 | 0.0512 | 0.00721 | 19.80 | 0.13 | 17.84 | 0.0489 | 0.0528 | 0.0716 |
| | GSSC_3.52 | 30 | 0.001442 | 50 | 0.0512 | 0.00721 | 19.80 | 0.13 | 17.84 | 0.0414 | 0.0453 | 0.0591 |
| | GSSC_3.53 | 30 | 0.001442 | 70 | 0.0512 | 0.00721 | 19.80 | 0.13 | 17.84 | 0.0317 | 0.0315 | 0.0502 |
| | GSSC_3.54 | 30 | 0.001442 | 100 | 0.0512 | 0.00721 | 19.80 | 0.13 | 17.84 | 0.0209 | 0.0207 | 0.0428 |
| | GSSC_3.55 | 30 | 0.001442 | 130 | 0.0512 | 0.00721 | 19.80 | 0.13 | 17.84 | 0.0146 | 0.0143 | 0.0304 |
| | GSSC_3.56 | 30 | 0.001442 | 160 | 0.0512 | 0.00721 | 19.80 | 0.13 | 17.84 | 0.0107 | 0.0100 | 0.0206 |
| | GSSC_3.57 | 30 | 0.001442 | 190 | 0.0512 | 0.00721 | 19.80 | 0.13 | 17.84 | 0.0069 | 0.0085 | 0.0168 |
| | GSSC_3.58 | 30 | 0.001442 | 240 | 0.0512 | 0.00721 | 19.80 | 0.13 | 17.84 | 0.0041 | 0.0067 | 0.0129 |
| | GSSC_3.59 | 30 | 0.001442 | 300 | 0.0512 | 0.00721 | 19.80 | 0.13 | 17.84 | 0.0032 | 0.0059 | 0.0087 |
| | GSSC_3.60 | 30 | 0.001442 | 360 | 0.0512 | 0.00721 | 19.80 | 0.13 | 17.84 | 0.0026 | 0.0043 | 0.0069 |
| | GSSC_3.61 | 30 | 0.001442 | 420 | 0.0512 | 0.00721 | 19.80 | 0.13 | 17.84 | 0.0023 | 0.0037 | 0.0045 |
| | GSSC_3.62 | 30 | 0.001442 | 480 | 0.0512 | 0.00721 | 19.80 | 0.13 | 17.84 | 0.0015 | 0.0024 | 0.0050 |
| | GSSC_3.63 | 30 | 0.001442 | 540 | 0.0512 | 0.00721 | 19.80 | 0.13 | 17.84 | 0.0014 | 0.0019 | 0.0041 |
| | GSSC_3.64 | 30 | 0.001442 | 600 | 0.0512 | 0.00721 | 19.80 | 0.13 | 17.84 | 0.0013 | 0.0015 | 0.0016 |
| | GSSC_3.65 | 30 | 0.001442 | 660 | 0.0512 | 0.00721 | 19.80 | 0.13 | 17.84 | 0.0010 | 0.0015 | 0.0013 |
| | GSSC_3.66 | 30 | 0.001442 | 720 | 0.0512 | 0.00721 | 19.80 | 0.13 | 17.84 | 0.0008 | 0.0012 | 0.0008 |
| | GSSC_3.67 | 30 | 0.001442 | 780 | 0.0512 | 0.00721 | 19.80 | 0.13 | 17.84 | 0.0005 | 0.0008 | 0.0003 |
| GSSC 13 | GSSC_4.1 | 40 | 0.001238 | 10 | 0.0510 | 0.00721 | 19.12 | 0.12 | 16.76 | 0.0618 | 0.0570 | 0.0749 |
| | GSSC_4.2 | 40 | 0.001238 | 30 | 0.0510 | 0.00721 | 19.12 | 0.12 | 16.76 | 0.0508 | 0.0485 | 0.0718 |
| | GSSC_4.3 | 40 | 0.001238 | 40 | 0.0510 | 0.00721 | 19.12 | 0.12 | 16.76 | 0.0402 | 0.0410 | 0.0652 |
| | GSSC_4.4 | 40 | 0.001238 | 60 | 0.0510 | 0.00721 | 19.12 | 0.12 | 16.76 | 0.0297 | 0.0370 | 0.0592 |
| | GSSC_4.5 | 40 | 0.001238 | 80 | 0.0510 | 0.00721 | 19.12 | 0.12 | 16.76 | 0.0217 | 0.0313 | 0.0536 |
| | GSSC_4.6 | 40 | 0.001238 | 100 | 0.0510 | 0.00721 | 19.12 | 0.12 | 16.76 | 0.0177 | 0.0245 | 0.0470 |

| (1) | (2) | (3) | (4) | (5) | (6) | (7) | (8) | (9) | (10) | (11) | (12) | (13) |
|---|---|---|---|---|---|---|---|---|---|---|---|---|
| | GSSC_4.7 | 40 | 0.001238 | 130 | 0.0510 | 0.00721 | 19.12 | 0.12 | 16.76 | 0.0142 | 0.0194 | 0.0388 |
| | GSSC_4.8 | 40 | 0.001238 | 160 | 0.0510 | 0.00721 | 19.12 | 0.12 | 16.76 | 0.0095 | 0.0145 | 0.0313 |
| | GSSC_4.9 | 40 | 0.001238 | 210 | 0.0510 | 0.00721 | 19.12 | 0.12 | 16.76 | 0.0056 | 0.0083 | 0.0254 |
| | GSSC_4.10 | 40 | 0.001238 | 270 | 0.0510 | 0.00721 | 19.12 | 0.12 | 16.76 | 0.0034 | 0.0064 | 0.0195 |
| | GSSC_4.11 | 40 | 0.001238 | 310 | 0.0510 | 0.00721 | 19.12 | 0.12 | 16.76 | 0.0031 | 0.0030 | 0.0122 |
| | GSSC_4.12 | 40 | 0.001238 | 370 | 0.0510 | 0.00721 | 19.12 | 0.12 | 16.76 | 0.0014 | 0.0017 | 0.0091 |
| | GSSC_4.13 | 40 | 0.001238 | 430 | 0.0510 | 0.00721 | 19.12 | 0.12 | 16.76 | 0.0008 | 0.0014 | 0.0057 |
| | GSSC_4.14 | 40 | 0.001238 | 545 | 0.0510 | 0.00721 | 19.12 | 0.12 | 16.76 | 0.0004 | 0.0009 | 0.0032 |
| | GSSC_4.15 | 40 | 0.001238 | 665 | 0.0510 | 0.00721 | 19.12 | 0.12 | 16.76 | 0.0003 | 0.0005 | 0.0012 |
| | GSSC_4.16 | 40 | 0.001238 | 785 | 0.0510 | 0.00721 | 19.12 | 0.12 | 16.76 | 0.0002 | 0.0003 | 0.0004 |
| GSSC 14 | GSSC_4.17 | 40 | 0.001238 | 15 | 0.0697 | 0.00721 | 20.20 | 0.14 | 27.03 | 0.0707 | 0.0704 | 0.0790 |
| | GSSC_4.18 | 40 | 0.001238 | 30 | 0.0697 | 0.00721 | 20.20 | 0.14 | 27.03 | 0.0587 | 0.0559 | 0.0695 |
| | GSSC_4.19 | 40 | 0.001238 | 38 | 0.0697 | 0.00721 | 20.20 | 0.14 | 27.03 | 0.0495 | 0.0441 | 0.0568 |
| | GSSC_4.20 | 40 | 0.001238 | 50 | 0.0697 | 0.00721 | 20.20 | 0.14 | 27.03 | 0.0425 | 0.0383 | 0.0461 |
| | GSSC_4.21 | 40 | 0.001238 | 70 | 0.0697 | 0.00721 | 20.20 | 0.14 | 27.03 | 0.0398 | 0.0343 | 0.0387 |
| | GSSC_4.22 | 40 | 0.001238 | 95 | 0.0697 | 0.00721 | 20.20 | 0.14 | 27.03 | 0.0358 | 0.0307 | 0.0333 |
| | GSSC_4.23 | 40 | 0.001238 | 120 | 0.0697 | 0.00721 | 20.20 | 0.14 | 27.03 | 0.0315 | 0.0247 | 0.0243 |
| | GSSC_4.24 | 40 | 0.001238 | 150 | 0.0697 | 0.00721 | 20.20 | 0.14 | 27.03 | 0.0225 | 0.0171 | 0.0191 |
| | GSSC_4.25 | 40 | 0.001238 | 180 | 0.0697 | 0.00721 | 20.20 | 0.14 | 27.03 | 0.0144 | 0.0123 | 0.0138 |
| | GSSC_4.26 | 40 | 0.001238 | 210 | 0.0697 | 0.00721 | 20.20 | 0.14 | 27.03 | 0.0084 | 0.0083 | 0.0099 |
| | GSSC_4.27 | 40 | 0.001238 | 250 | 0.0697 | 0.00721 | 20.20 | 0.14 | 27.03 | 0.0052 | 0.0066 | 0.0092 |
| | GSSC_4.28 | 40 | 0.001238 | 310 | 0.0697 | 0.00721 | 20.20 | 0.14 | 27.03 | 0.0025 | 0.0046 | 0.0068 |
| | GSSC_4.29 | 40 | 0.001238 | 350 | 0.0697 | 0.00721 | 20.20 | 0.14 | 27.03 | 0.0024 | 0.0038 | 0.0054 |
| | GSSC_4.30 | 40 | 0.001238 | 390 | 0.0697 | 0.00721 | 20.20 | 0.14 | 27.03 | 0.0013 | 0.0026 | 0.0034 |
| | GSSC_4.31 | 40 | 0.001238 | 450 | 0.0697 | 0.00721 | 20.20 | 0.14 | 27.03 | 0.0008 | 0.0017 | 0.0025 |
| | GSSC_4.32 | 40 | 0.001238 | 525 | 0.0697 | 0.00721 | 20.20 | 0.14 | 27.03 | 0.0006 | 0.0012 | 0.0010 |
| | GSSC_4.33 | 40 | 0.001238 | 615 | 0.0697 | 0.00721 | 20.20 | 0.14 | 27.03 | 0.0003 | 0.0007 | 0.0006 |
| | GSSC_4.34 | 40 | 0.001238 | 715 | 0.0697 | 0.00721 | 20.20 | 0.14 | 27.03 | 0.0002 | 0.0003 | 0.0003 |

| (1) | (2) | (3) | (4) | (5) | (6) | (7) | (8) | (9) | (10) | (11) | (12) | (13) |
|---|---|---|---|---|---|---|---|---|---|---|---|---|
| GSSC 15 | GSSC_4.35 | 40 | 0.001238 | 15 | 0.0696 | 0.00946 | 20.37 | 0.14 | 28.12 | 0.0732 | 0.0727 | 0.0818 |
| | GSSC_4.36 | 40 | 0.001238 | 30 | 0.0696 | 0.00946 | 20.37 | 0.14 | 28.12 | 0.0637 | 0.0551 | 0.0724 |
| | GSSC_4.37 | 40 | 0.001238 | 45 | 0.0696 | 0.00946 | 20.37 | 0.14 | 28.12 | 0.0530 | 0.0423 | 0.0619 |
| | GSSC_4.38 | 40 | 0.001238 | 75 | 0.0696 | 0.00946 | 20.37 | 0.14 | 28.12 | 0.0414 | 0.0312 | 0.0519 |
| | GSSC_4.39 | 40 | 0.001238 | 105 | 0.0696 | 0.00946 | 20.37 | 0.14 | 28.12 | 0.0308 | 0.0236 | 0.0398 |
| | GSSC_4.40 | 40 | 0.001238 | 135 | 0.0696 | 0.00946 | 20.37 | 0.14 | 28.12 | 0.0226 | 0.0202 | 0.0320 |
| | GSSC_4.41 | 40 | 0.001238 | 165 | 0.0696 | 0.00946 | 20.37 | 0.14 | 28.12 | 0.0151 | 0.0154 | 0.0234 |
| | GSSC_4.42 | 40 | 0.001238 | 195 | 0.0696 | 0.00946 | 20.37 | 0.14 | 28.12 | 0.0114 | 0.0106 | 0.0195 |
| | GSSC_4.43 | 40 | 0.001238 | 250 | 0.0696 | 0.00946 | 20.37 | 0.14 | 28.12 | 0.0095 | 0.0075 | 0.0102 |
| | GSSC_4.44 | 40 | 0.001238 | 280 | 0.0696 | 0.00946 | 20.37 | 0.14 | 28.12 | 0.0086 | 0.0072 | 0.0068 |
| | GSSC_4.45 | 40 | 0.001238 | 325 | 0.0696 | 0.00946 | 20.37 | 0.14 | 28.12 | 0.0079 | 0.0067 | 0.0053 |
| | GSSC_4.46 | 40 | 0.001238 | 400 | 0.0696 | 0.00946 | 20.37 | 0.14 | 28.12 | 0.0067 | 0.0049 | 0.0041 |
| | GSSC_4.47 | 40 | 0.001238 | 430 | 0.0696 | 0.00946 | 20.37 | 0.14 | 28.12 | 0.0065 | 0.0050 | 0.0026 |
| | GSSC_4.48 | 40 | 0.001238 | 460 | 0.0696 | 0.00946 | 20.37 | 0.14 | 28.12 | 0.0056 | 0.0040 | 0.0019 |
| | GSSC_4.49 | 40 | 0.001238 | 500 | 0.0696 | 0.00946 | 20.37 | 0.14 | 28.12 | 0.0047 | 0.0038 | 0.0014 |
| | GSSC_4.50 | 40 | 0.001238 | 530 | 0.0696 | 0.00946 | 20.37 | 0.14 | 28.12 | 0.0041 | 0.0032 | 0.0010 |
| | GSSC_4.51 | 40 | 0.001238 | 565 | 0.0696 | 0.00946 | 20.37 | 0.14 | 28.12 | 0.0032 | 0.0027 | 0.0008 |
| | GSSC_4.52 | 40 | 0.001238 | 625 | 0.0696 | 0.00946 | 20.37 | 0.14 | 28.12 | 0.0021 | 0.0022 | 0.0005 |
| | GSSC_4.53 | 40 | 0.001238 | 710 | 0.0696 | 0.00946 | 20.37 | 0.14 | 28.12 | 0.0010 | 0.0012 | 0.0003 |
| GSSC 16 | GSSC_4.54 | 40 | 0.001238 | 15 | 0.0512 | 0.00946 | 20.15 | 0.13 | 29.74 | 0.0589 | 0.0546 | 0.0746 |
| | GSSC_4.55 | 40 | 0.001238 | 35 | 0.0512 | 0.00946 | 20.15 | 0.13 | 29.74 | 0.0448 | 0.0448 | 0.0683 |
| | GSSC_4.56 | 40 | 0.001238 | 50 | 0.0512 | 0.00946 | 20.15 | 0.13 | 29.74 | 0.0367 | 0.0330 | 0.0624 |
| | GSSC_4.57 | 40 | 0.001238 | 70 | 0.0512 | 0.00946 | 20.15 | 0.13 | 29.74 | 0.0303 | 0.0266 | 0.0582 |
| | GSSC_4.58 | 40 | 0.001238 | 85 | 0.0512 | 0.00946 | 20.15 | 0.13 | 29.74 | 0.0232 | 0.0197 | 0.0558 |
| | GSSC_4.59 | 40 | 0.001238 | 100 | 0.0512 | 0.00946 | 20.15 | 0.13 | 29.74 | 0.0188 | 0.0151 | 0.0477 |
| | GSSC_4.60 | 40 | 0.001238 | 130 | 0.0512 | 0.00946 | 20.15 | 0.13 | 29.74 | 0.0151 | 0.0149 | 0.0411 |
| | GSSC_4.61 | 40 | 0.001238 | 150 | 0.0512 | 0.00946 | 20.15 | 0.13 | 29.74 | 0.0121 | 0.0117 | 0.0328 |

| (1) | (2) | (3) | (4) | (5) | (6) | (7) | (8) | (9) | (10) | (11) | (12) | (13) |
|---|---|---|---|---|---|---|---|---|---|---|---|---|
| | GSSC_4.62 | 40 | 0.001238 | 180 | 0.0512 | 0.00946 | 20.15 | 0.13 | 29.74 | 0.0075 | 0.0089 | 0.0272 |
| | GSSC_4.63 | 40 | 0.001238 | 210 | 0.0512 | 0.00946 | 20.15 | 0.13 | 29.74 | 0.0060 | 0.0074 | 0.0176 |
| | GSSC_4.64 | 40 | 0.001238 | 270 | 0.0512 | 0.00946 | 20.15 | 0.13 | 29.74 | 0.0048 | 0.0053 | 0.0111 |
| | GSSC_4.65 | 40 | 0.001238 | 330 | 0.0512 | 0.00946 | 20.15 | 0.13 | 29.74 | 0.0031 | 0.0036 | 0.0084 |
| | GSSC_4.66 | 40 | 0.001238 | 390 | 0.0512 | 0.00946 | 20.15 | 0.13 | 29.74 | 0.0022 | 0.0025 | 0.0062 |
| | GSSC_4.67 | 40 | 0.001238 | 460 | 0.0512 | 0.00946 | 20.15 | 0.13 | 29.74 | 0.0013 | 0.0013 | 0.0039 |
| | GSSC_4.68 | 40 | 0.001238 | 550 | 0.0512 | 0.00946 | 20.15 | 0.13 | 29.74 | 0.0009 | 0.0009 | 0.0020 |
| | GSSC_4.69 | 40 | 0.001238 | 650 | 0.0512 | 0.00946 | 20.15 | 0.13 | 29.74 | 0.0005 | 0.0006 | 0.0009 |
| | GSSC_4.70 | 40 | 0.001238 | 770 | 0.0512 | 0.00946 | 20.15 | 0.13 | 29.74 | 0.0003 | 0.0004 | 0.0003 |
| GSSC 17 | GSSC_5.1 | 50 | 0.001034 | 15 | 0.0501 | 0.00946 | 20.77 | 0.15 | 40.01 | 0.0510 | 0.0462 | 0.0640 |
| | GSSC_5.2 | 50 | 0.001034 | 30 | 0.0501 | 0.00946 | 20.77 | 0.15 | 40.01 | 0.0449 | 0.0367 | 0.0571 |
| | GSSC_5.3 | 50 | 0.001034 | 50 | 0.0501 | 0.00946 | 20.77 | 0.15 | 40.01 | 0.0334 | 0.0292 | 0.0503 |
| | GSSC_5.4 | 50 | 0.001034 | 70 | 0.0501 | 0.00946 | 20.77 | 0.15 | 40.01 | 0.0304 | 0.0210 | 0.0428 |
| | GSSC_5.5 | 50 | 0.001034 | 100 | 0.0501 | 0.00946 | 20.77 | 0.15 | 40.01 | 0.0246 | 0.0120 | 0.0290 |
| | GSSC_5.6 | 50 | 0.001034 | 130 | 0.0501 | 0.00946 | 20.77 | 0.15 | 40.01 | 0.0196 | 0.0077 | 0.0188 |
| | GSSC_5.7 | 50 | 0.001034 | 175 | 0.0501 | 0.00946 | 20.77 | 0.15 | 40.01 | 0.0117 | 0.0035 | 0.0125 |
| | GSSC_5.8 | 50 | 0.001034 | 235 | 0.0501 | 0.00946 | 20.77 | 0.15 | 40.01 | 0.0072 | 0.0022 | 0.0097 |
| | GSSC_5.9 | 50 | 0.001034 | 295 | 0.0501 | 0.00946 | 20.77 | 0.15 | 40.01 | 0.0054 | 0.0014 | 0.0074 |
| | GSSC_5.10 | 50 | 0.001034 | 355 | 0.0501 | 0.00946 | 20.77 | 0.15 | 40.01 | 0.0034 | 0.0011 | 0.0077 |
| | GSSC_5.11 | 50 | 0.001034 | 415 | 0.0501 | 0.00946 | 20.77 | 0.15 | 40.01 | 0.0031 | 0.0008 | 0.0064 |
| | GSSC_5.12 | 50 | 0.001034 | 475 | 0.0501 | 0.00946 | 20.77 | 0.15 | 40.01 | 0.0026 | 0.0007 | 0.0054 |
| | GSSC_5.13 | 50 | 0.001034 | 535 | 0.0501 | 0.00946 | 20.77 | 0.15 | 40.01 | 0.0014 | 0.0005 | 0.0041 |
| | GSSC_5.14 | 50 | 0.001034 | 595 | 0.0501 | 0.00946 | 20.77 | 0.15 | 40.01 | 0.0010 | 0.0003 | 0.0025 |
| | GSSC_5.15 | 50 | 0.001034 | 655 | 0.0501 | 0.00946 | 20.77 | 0.15 | 40.01 | 0.0012 | 0.0003 | 0.0014 |
| | GSSC_5.16 | 50 | 0.001034 | 715 | 0.0501 | 0.00946 | 20.77 | 0.15 | 40.01 | 0.0006 | 0.0002 | 0.0005 |
| | GSSC_5.17 | 50 | 0.001034 | 790 | 0.0501 | 0.00946 | 20.77 | 0.15 | 40.01 | 0.0007 | 0.0002 | 0.0003 |
| GSSC 18 | GSSC_5.18 | 50 | 0.001034 | 15 | 0.0697 | 0.00721 | 21.06 | 0.15 | 43.25 | 0.0570 | 0.0517 | 0.0668 |

| (1) | (2) | (3) | (4) | (5) | (6) | (7) | (8) | (9) | (10) | (11) | (12) | (13) |
|---|---|---|---|---|---|---|---|---|---|---|---|---|
| | GSSC_5.19 | 50 | 0.001034 | 25 | 0.0697 | 0.00721 | 21.06 | 0.15 | 43.25 | 0.0492 | 0.0419 | 0.0572 |
| | GSSC_5.20 | 50 | 0.001034 | 40 | 0.0697 | 0.00721 | 21.06 | 0.15 | 43.25 | 0.0438 | 0.0360 | 0.0463 |
| | GSSC_5.21 | 50 | 0.001034 | 65 | 0.0697 | 0.00721 | 21.06 | 0.15 | 43.25 | 0.0363 | 0.0285 | 0.0360 |
| | GSSC_5.22 | 50 | 0.001034 | 95 | 0.0697 | 0.00721 | 21.06 | 0.15 | 43.25 | 0.0260 | 0.0248 | 0.0307 |
| | GSSC_5.23 | 50 | 0.001034 | 125 | 0.0697 | 0.00721 | 21.06 | 0.15 | 43.25 | 0.0194 | 0.0134 | 0.0225 |
| | GSSC_5.24 | 50 | 0.001034 | 155 | 0.0697 | 0.00721 | 21.06 | 0.15 | 43.25 | 0.0131 | 0.0080 | 0.0138 |
| | GSSC_5.25 | 50 | 0.001034 | 185 | 0.0697 | 0.00721 | 21.06 | 0.15 | 43.25 | 0.0105 | 0.0056 | 0.0083 |
| | GSSC_5.26 | 50 | 0.001034 | 215 | 0.0697 | 0.00721 | 21.06 | 0.15 | 43.25 | 0.0104 | 0.0042 | 0.0069 |
| | GSSC_5.27 | 50 | 0.001034 | 255 | 0.0697 | 0.00721 | 21.06 | 0.15 | 43.25 | 0.0091 | 0.0037 | 0.0063 |
| | GSSC_5.28 | 50 | 0.001034 | 295 | 0.0697 | 0.00721 | 21.06 | 0.15 | 43.25 | 0.0069 | 0.0031 | 0.0057 |
| | GSSC_5.29 | 50 | 0.001034 | 375 | 0.0697 | 0.00721 | 21.06 | 0.15 | 43.25 | 0.0049 | 0.0017 | 0.0044 |
| | GSSC_5.30 | 50 | 0.001034 | 435 | 0.0697 | 0.00721 | 21.06 | 0.15 | 43.25 | 0.0041 | 0.0004 | 0.0032 |
| | GSSC_5.31 | 50 | 0.001034 | 510 | 0.0697 | 0.00721 | 21.06 | 0.15 | 43.25 | 0.0035 | 0.0004 | 0.0022 |
| | GSSC_5.32 | 50 | 0.001034 | 585 | 0.0697 | 0.00721 | 21.06 | 0.15 | 43.25 | 0.0028 | 0.0003 | 0.0011 |
| | GSSC_5.33 | 50 | 0.001034 | 705 | 0.0697 | 0.00721 | 21.06 | 0.15 | 43.25 | 0.0016 | 0.0003 | 0.0004 |
| | GSSC_5.34 | 50 | 0.001034 | 780 | 0.0697 | 0.00721 | 21.06 | 0.15 | 43.25 | 0.0012 | 0.0003 | 0.0003 |
| GSSC 19 | GSSC_5.35 | 50 | 0.001034 | 15 | 0.0512 | 0.00721 | 18.55 | 0.12 | 19.46 | 0.0454 | 0.0467 | 0.0605 |
| | GSSC_5.36 | 50 | 0.001034 | 30 | 0.0512 | 0.00721 | 18.55 | 0.12 | 19.46 | 0.0332 | 0.0345 | 0.0507 |
| | GSSC_5.37 | 50 | 0.001034 | 60 | 0.0512 | 0.00721 | 18.55 | 0.12 | 19.46 | 0.0170 | 0.0262 | 0.0415 |
| | GSSC_5.38 | 50 | 0.001034 | 90 | 0.0512 | 0.00721 | 18.55 | 0.12 | 19.46 | 0.0098 | 0.0161 | 0.0287 |
| | GSSC_5.39 | 50 | 0.001034 | 135 | 0.0512 | 0.00721 | 18.55 | 0.12 | 19.46 | 0.0063 | 0.0137 | 0.0195 |
| | GSSC_5.40 | 50 | 0.001034 | 170 | 0.0512 | 0.00721 | 18.55 | 0.12 | 19.46 | 0.0047 | 0.0114 | 0.0117 |
| | GSSC_5.41 | 50 | 0.001034 | 255 | 0.0512 | 0.00721 | 18.55 | 0.12 | 19.46 | 0.0028 | 0.0090 | 0.0089 |
| | GSSC_5.42 | 50 | 0.001034 | 305 | 0.0512 | 0.00721 | 18.55 | 0.12 | 19.46 | 0.0024 | 0.0063 | 0.0063 |
| | GSSC_5.43 | 50 | 0.001034 | 400 | 0.0512 | 0.00721 | 18.55 | 0.12 | 19.46 | 0.0016 | 0.0041 | 0.0045 |
| | GSSC_5.44 | 50 | 0.001034 | 450 | 0.0512 | 0.00721 | 18.55 | 0.12 | 19.46 | 0.0012 | 0.0033 | 0.0043 |
| | GSSC_5.45 | 50 | 0.001034 | 530 | 0.0512 | 0.00721 | 18.55 | 0.12 | 19.46 | 0.0010 | 0.0020 | 0.0026 |
| | GSSC_5.46 | 50 | 0.001034 | 650 | 0.0512 | 0.00721 | 18.55 | 0.12 | 19.46 | 0.0009 | 0.0016 | 0.0011 |

| (1) | (2) | (3) | (4) | (5) | (6) | (7) | (8) | (9) | (10) | (11) | (12) | (13) |
|---|---|---|---|---|---|---|---|---|---|---|---|---|
| | GSSC_5.47 | 50 | 0.001034 | 740 | 0.0512 | 0.00721 | 18.55 | 0.12 | 19.46 | 0.0008 | 0.0011 | 0.0007 |
| | GSSC_5.48 | 50 | 0.001034 | 800 | 0.0512 | 0.00721 | 18.55 | 0.12 | 19.46 | 0.0009 | 0.0010 | 0.0002 |
| GSSC 20 | GSSC_5.49 | 50 | 0.001034 | 10 | 0.0697 | 0.00946 | 20.03 | 0.15 | 25.41 | 0.0630 | 0.0634 | 0.0788 |
| | GSSC_5.50 | 50 | 0.001034 | 25 | 0.0697 | 0.00946 | 20.03 | 0.15 | 25.41 | 0.0519 | 0.0503 | 0.0641 |
| | GSSC_5.51 | 50 | 0.001034 | 50 | 0.0697 | 0.00946 | 20.03 | 0.15 | 25.41 | 0.0398 | 0.0400 | 0.0560 |
| | GSSC_5.52 | 50 | 0.001034 | 85 | 0.0697 | 0.00946 | 20.03 | 0.15 | 25.41 | 0.0265 | 0.0316 | 0.0446 |
| | GSSC_5.53 | 50 | 0.001034 | 125 | 0.0697 | 0.00946 | 20.03 | 0.15 | 25.41 | 0.0233 | 0.0218 | 0.0320 |
| | GSSC_5.54 | 50 | 0.001034 | 155 | 0.0697 | 0.00946 | 20.03 | 0.15 | 25.41 | 0.0202 | 0.0191 | 0.0195 |
| | GSSC_5.55 | 50 | 0.001034 | 240 | 0.0697 | 0.00946 | 20.03 | 0.15 | 25.41 | 0.0125 | 0.0083 | 0.0107 |
| | GSSC_5.56 | 50 | 0.001034 | 300 | 0.0697 | 0.00946 | 20.03 | 0.15 | 25.41 | 0.0100 | 0.0047 | 0.0110 |
| | GSSC_5.57 | 50 | 0.001034 | 350 | 0.0697 | 0.00946 | 20.03 | 0.15 | 25.41 | 0.0056 | 0.0034 | 0.0085 |
| | GSSC_5.58 | 50 | 0.001034 | 420 | 0.0697 | 0.00946 | 20.03 | 0.15 | 25.41 | 0.0042 | 0.0020 | 0.0052 |
| | GSSC_5.59 | 50 | 0.001034 | 455 | 0.0697 | 0.00946 | 20.03 | 0.15 | 25.41 | 0.0036 | 0.0016 | 0.0039 |
| | GSSC_5.60 | 50 | 0.001034 | 515 | 0.0697 | 0.00946 | 20.03 | 0.15 | 25.41 | 0.0031 | 0.0015 | 0.0026 |
| | GSSC_5.61 | 50 | 0.001034 | 590 | 0.0697 | 0.00946 | 20.03 | 0.15 | 25.41 | 0.0022 | 0.0011 | 0.0013 |
| | GSSC_5.62 | 50 | 0.001034 | 670 | 0.0697 | 0.00946 | 20.03 | 0.15 | 25.41 | 0.0023 | 0.0009 | 0.0007 |
| | GSSC_5.63 | 50 | 0.001034 | 760 | 0.0697 | 0.00946 | 20.03 | 0.15 | 25.41 | 0.0010 | 0.0007 | 0.0003 |
| GSSC 21 | GSSC_0.1 | 0 | 0.002054 | 20 | 0.0511 | 0.00721 | 16.96 | 0.09 | 0.00 | 0.1034 | 0.1537 | 0.0962 |
| | GSSC_0.2 | 0 | 0.002054 | 40 | 0.0511 | 0.00721 | 16.96 | 0.09 | 0.00 | 0.0813 | 0.1159 | 0.0889 |
| | GSSC_0.3 | 0 | 0.002054 | 60 | 0.0511 | 0.00721 | 16.96 | 0.09 | 0.00 | 0.0624 | 0.0739 | 0.0663 |
| | GSSC_0.4 | 0 | 0.002054 | 90 | 0.0511 | 0.00721 | 16.96 | 0.09 | 0.00 | 0.0426 | 0.0403 | 0.0548 |
| | GSSC_0.5 | 0 | 0.002054 | 135 | 0.0511 | 0.00721 | 16.96 | 0.09 | 0.00 | 0.0278 | 0.0209 | 0.0406 |
| | GSSC_0.6 | 0 | 0.002054 | 210 | 0.0511 | 0.00721 | 16.96 | 0.09 | 0.00 | 0.0160 | 0.0124 | 0.0271 |
| | GSSC_0.7 | 0 | 0.002054 | 270 | 0.0511 | 0.00721 | 16.96 | 0.09 | 0.00 | 0.0106 | 0.0080 | 0.0207 |
| | GSSC_0.8 | 0 | 0.002054 | 350 | 0.0511 | 0.00721 | 16.96 | 0.09 | 0.00 | 0.0083 | 0.0074 | 0.0143 |
| | GSSC_0.9 | 0 | 0.002054 | 390 | 0.0511 | 0.00721 | 16.96 | 0.09 | 0.00 | 0.0074 | 0.0057 | 0.0074 |
| | GSSC_0.10 | 0 | 0.002054 | 470 | 0.0511 | 0.00721 | 16.96 | 0.09 | 0.00 | 0.0063 | 0.0043 | 0.0047 |

| (1) | (2) | (3) | (4) | (5) | (6) | (7) | (8) | (9) | (10) | (11) | (12) | (13) |
|---|---|---|---|---|---|---|---|---|---|---|---|---|
| | GSSC_0.11 | 0 | 0.002054 | 540 | 0.0511 | 0.00721 | 16.96 | 0.09 | 0.00 | 0.0051 | 0.0036 | 0.0020 |
| | GSSC_0.12 | 0 | 0.002054 | 660 | 0.0511 | 0.00721 | 16.96 | 0.09 | 0.00 | 0.0036 | 0.0020 | 0.0008 |
| | GSSC_0.13 | 0 | 0.002054 | 830 | 0.0511 | 0.00721 | 16.96 | 0.09 | 0.00 | 0.0017 | 0.0017 | 0.0007 |
| GSSC 22 | GSSC_0.14 | 0 | 0.002054 | 25 | 0.0698 | 0.00721 | 17.07 | 0.09 | 0.00 | 0.1808 | 0.1878 | 0.1229 |
| | GSSC_0.15 | 0 | 0.002054 | 40 | 0.0698 | 0.00721 | 17.07 | 0.09 | 0.00 | 0.1470 | 0.1690 | 0.1009 |
| | GSSC_0.16 | 0 | 0.002054 | 60 | 0.0698 | 0.00721 | 17.07 | 0.09 | 0.00 | 0.1326 | 0.1415 | 0.0771 |
| | GSSC_0.17 | 0 | 0.002054 | 83 | 0.0698 | 0.00721 | 17.07 | 0.09 | 0.00 | 0.1018 | 0.0932 | 0.0518 |
| | GSSC_0.18 | 0 | 0.002054 | 123 | 0.0698 | 0.00721 | 17.07 | 0.09 | 0.00 | 0.0754 | 0.0631 | 0.0323 |
| | GSSC_0.19 | 0 | 0.002054 | 143 | 0.0698 | 0.00721 | 17.07 | 0.09 | 0.00 | 0.0495 | 0.0398 | 0.0206 |
| | GSSC_0.20 | 0 | 0.002054 | 183 | 0.0698 | 0.00721 | 17.07 | 0.09 | 0.00 | 0.0320 | 0.0267 | 0.0111 |
| | GSSC_0.21 | 0 | 0.002054 | 228 | 0.0698 | 0.00721 | 17.07 | 0.09 | 0.00 | 0.0209 | 0.0154 | 0.0054 |
| | GSSC_0.22 | 0 | 0.002054 | 283 | 0.0698 | 0.00721 | 17.07 | 0.09 | 0.00 | 0.0101 | 0.0058 | 0.0024 |
| | GSSC_0.23 | 0 | 0.002054 | 328 | 0.0698 | 0.00721 | 17.07 | 0.09 | 0.00 | 0.0036 | 0.0035 | 0.0007 |
| GSSC 23 | GSSC_0.24 | 0 | 0.002054 | 15 | 0.0509 | 0.00946 | 17.30 | 0.11 | 0.00 | 0.1299 | 0.1655 | 0.1058 |
| | GSSC_0.25 | 0 | 0.002054 | 33 | 0.0509 | 0.00946 | 17.30 | 0.11 | 0.00 | 0.1330 | 0.1355 | 0.0855 |
| | GSSC_0.26 | 0 | 0.002054 | 59 | 0.0509 | 0.00946 | 17.30 | 0.11 | 0.00 | 0.1001 | 0.1103 | 0.0738 |
| | GSSC_0.27 | 0 | 0.002054 | 87 | 0.0509 | 0.00946 | 17.30 | 0.11 | 0.00 | 0.0707 | 0.0701 | 0.0560 |
| | GSSC_0.28 | 0 | 0.002054 | 143 | 0.0509 | 0.00946 | 17.30 | 0.11 | 0.00 | 0.0454 | 0.0420 | 0.0387 |
| | GSSC_0.29 | 0 | 0.002054 | 192 | 0.0509 | 0.00946 | 17.30 | 0.11 | 0.00 | 0.0244 | 0.0236 | 0.0246 |
| | GSSC_0.30 | 0 | 0.002054 | 272 | 0.0509 | 0.00946 | 17.30 | 0.11 | 0.00 | 0.0120 | 0.0109 | 0.0101 |
| | GSSC_0.31 | 0 | 0.002054 | 325 | 0.0509 | 0.00946 | 17.30 | 0.11 | 0.00 | 0.0052 | 0.0065 | 0.0030 |
| | GSSC_0.32 | 0 | 0.002054 | 380 | 0.0509 | 0.00946 | 17.30 | 0.11 | 0.00 | 0.0023 | 0.0031 | 0.0007 |
| GSSC 24 | GSSC_0.33 | 0 | 0.002054 | 14 | 0.0692 | 0.00946 | 17.19 | 0.09 | 0.00 | 0.2214 | 0.2439 | 0.1412 |
| | GSSC_0.34 | 0 | 0.002054 | 30 | 0.0692 | 0.00946 | 17.19 | 0.09 | 0.00 | 0.2148 | 0.2237 | 0.1175 |
| | GSSC_0.35 | 0 | 0.002054 | 49 | 0.0692 | 0.00946 | 17.19 | 0.09 | 0.00 | 0.2095 | 0.1928 | 0.0841 |
| | GSSC_0.36 | 0 | 0.002054 | 69 | 0.0692 | 0.00946 | 17.19 | 0.09 | 0.00 | 0.1805 | 0.1631 | 0.0580 |
| | GSSC_0.37 | 0 | 0.002054 | 89 | 0.0692 | 0.00946 | 17.19 | 0.09 | 0.00 | 0.1551 | 0.1228 | 0.0446 |

| (1) | (2) | (3) | (4) | (5) | (6) | (7) | (8) | (9) | (10) | (11) | (12) | (13) |
|---|---|---|---|---|---|---|---|---|---|---|---|---|
| | GSSC_0.38 | 0 | 0.002054 | 113 | 0.0692 | 0.00946 | 17.19 | 0.09 | 0.00 | 0.0983 | 0.0862 | 0.0355 |
| | GSSC_0.39 | 0 | 0.002054 | 141 | 0.0692 | 0.00946 | 17.19 | 0.09 | 0.00 | 0.0536 | 0.0485 | 0.0092 |
| | GSSC_0.40 | 0 | 0.002054 | 170 | 0.0692 | 0.00946 | 17.19 | 0.09 | 0.00 | 0.0145 | 0.0195 | 0.0024 |
| | GSSC_0.41 | 0 | 0.002054 | 194 | 0.0692 | 0.00946 | 17.19 | 0.09 | 0.00 | 0.0038 | 0.0049 | 0.0007 |
| SSC 1 | SSC_1.1 | 10 | 0.000299 | 10 | 0.0451 | 0.00465 | 19.18 | 0.14 | 6.49 | - | 0.1834 | 0.1530 |
| | SSC_1.2 | 10 | 0.000299 | 20 | 0.0451 | 0.00465 | 19.18 | 0.14 | 6.49 | - | 0.1704 | 0.1216 |
| | SSC_1.3 | 10 | 0.000299 | 30 | 0.0451 | 0.00465 | 19.18 | 0.14 | 6.49 | - | 0.1595 | 0.0643 |
| | SSC_1.4 | 10 | 0.000299 | 40 | 0.0451 | 0.00465 | 19.18 | 0.14 | 6.49 | - | 0.1465 | 0.0582 |
| | SSC_1.5 | 10 | 0.000299 | 50 | 0.0451 | 0.00465 | 19.18 | 0.14 | 6.49 | - | 0.1312 | 0.0442 |
| | SSC_1.6 | 10 | 0.000299 | 65 | 0.0451 | 0.00465 | 19.18 | 0.14 | 6.49 | - | 0.0940 | 0.0428 |
| | SSC_1.7 | 10 | 0.000299 | 80 | 0.0451 | 0.00465 | 19.18 | 0.14 | 6.49 | - | 0.0811 | 0.0371 |
| | SSC_1.8 | 10 | 0.000299 | 115 | 0.0451 | 0.00465 | 19.18 | 0.14 | 6.49 | - | 0.0636 | 0.0325 |
| | SSC_1.9 | 10 | 0.000299 | 145 | 0.0451 | 0.00465 | 19.18 | 0.14 | 6.49 | - | 0.0542 | 0.0251 |
| | SSC_1.10 | 10 | 0.000299 | 190 | 0.0451 | 0.00465 | 19.18 | 0.14 | 6.49 | - | 0.0435 | 0.0175 |
| | SSC_1.11 | 10 | 0.000299 | 230 | 0.0451 | 0.00465 | 19.18 | 0.14 | 6.49 | - | 0.0353 | 0.0124 |
| | SSC_1.12 | 10 | 0.000299 | 265 | 0.0451 | 0.00465 | 19.18 | 0.14 | 6.49 | - | 0.0242 | 0.0071 |
| | SSC_1.13 | 10 | 0.000299 | 320 | 0.0451 | 0.00465 | 19.18 | 0.14 | 6.49 | - | 0.0155 | 0.0054 |
| | SSC_1.14 | 10 | 0.000299 | 385 | 0.0451 | 0.00465 | 19.18 | 0.14 | 6.49 | - | 0.0120 | 0.0044 |
| | SSC_1.15 | 10 | 0.000299 | 445 | 0.0451 | 0.00465 | 19.18 | 0.14 | 6.49 | - | 0.0097 | 0.0020 |
| | SSC_1.16 | 10 | 0.000299 | 505 | 0.0451 | 0.00465 | 19.18 | 0.14 | 6.49 | - | 0.0073 | 0.0010 |
| | SSC_1.17 | 10 | 0.000299 | 565 | 0.0451 | 0.00465 | 19.18 | 0.14 | 6.49 | - | 0.0057 | 0.0005 |
| | SSC_1.18 | 10 | 0.000299 | 625 | 0.0451 | 0.00465 | 19.18 | 0.14 | 6.49 | - | 0.0035 | 0.0002 |
| SSC 2 | SSC_1.19 | 10 | 0.000299 | 15 | 0.0313 | 0.00465 | 17.41 | 0.13 | 6.49 | - | 0.1302 | 0.1181 |
| | SSC_1.20 | 10 | 0.000299 | 30 | 0.0313 | 0.00465 | 17.41 | 0.13 | 6.49 | - | 0.1149 | 0.0920 |
| | SSC_1.21 | 10 | 0.000299 | 45 | 0.0313 | 0.00465 | 17.41 | 0.13 | 6.49 | - | 0.0855 | 0.0843 |
| | SSC_1.22 | 10 | 0.000299 | 65 | 0.0313 | 0.00465 | 17.41 | 0.13 | 6.49 | - | 0.0729 | 0.0712 |
| | SSC_1.23 | 10 | 0.000299 | 95 | 0.0313 | 0.00465 | 17.41 | 0.13 | 6.49 | - | 0.0637 | 0.0596 |
| | SSC_1.24 | 10 | 0.000299 | 125 | 0.0313 | 0.00465 | 17.41 | 0.13 | 6.49 | - | 0.0565 | 0.0462 |

| (1) | (2) | (3) | (4) | (5) | (6) | (7) | (8) | (9) | (10) | (11) | (12) | (13) |
|---|---|---|---|---|---|---|---|---|---|---|---|---|
| | SSC_1.25 | 10 | 0.000299 | 170 | 0.0313 | 0.00465 | 17.41 | 0.13 | 6.49 | - | 0.0463 | 0.0300 |
| | SSC_1.26 | 10 | 0.000299 | 200 | 0.0313 | 0.00465 | 17.41 | 0.13 | 6.49 | - | 0.0320 | 0.0197 |
| | SSC_1.27 | 10 | 0.000299 | 235 | 0.0313 | 0.00465 | 17.41 | 0.13 | 6.49 | - | 0.0254 | 0.0129 |
| | SSC_1.28 | 10 | 0.000299 | 275 | 0.0313 | 0.00465 | 17.41 | 0.13 | 6.49 | - | 0.0204 | 0.0140 |
| | SSC_1.29 | 10 | 0.000299 | 315 | 0.0313 | 0.00465 | 17.41 | 0.13 | 6.49 | - | 0.0177 | 0.0102 |
| | SSC_1.30 | 10 | 0.000299 | 340 | 0.0313 | 0.00465 | 17.41 | 0.13 | 6.49 | - | 0.0144 | 0.0094 |
| | SSC_1.31 | 10 | 0.000299 | 400 | 0.0313 | 0.00465 | 17.41 | 0.13 | 6.49 | - | 0.0096 | 0.0073 |
| | SSC_1.32 | 10 | 0.000299 | 460 | 0.0313 | 0.00465 | 17.41 | 0.13 | 6.49 | - | 0.0084 | 0.0051 |
| | SSC_1.33 | 10 | 0.000299 | 520 | 0.0313 | 0.00465 | 17.41 | 0.13 | 6.49 | - | 0.0067 | 0.0032 |
| | SSC_1.34 | 10 | 0.000299 | 610 | 0.0313 | 0.00465 | 17.41 | 0.13 | 6.49 | - | 0.0049 | 0.0015 |
| | SSC_1.35 | 10 | 0.000299 | 670 | 0.0313 | 0.00465 | 17.41 | 0.13 | 6.49 | - | 0.0021 | 0.0006 |
| SSC 3 | SSC_1.36 | 10 | 0.000299 | 10 | 0.0292 | 0.00272 | 17.30 | 0.12 | 5.95 | - | 0.1162 | 0.0913 |
| | SSC_1.37 | 10 | 0.000299 | 30 | 0.0292 | 0.00272 | 17.30 | 0.12 | 5.95 | - | 0.0881 | 0.0850 |
| | SSC_1.38 | 10 | 0.000299 | 40 | 0.0292 | 0.00272 | 17.30 | 0.12 | 5.95 | - | 0.0763 | 0.0725 |
| | SSC_1.39 | 10 | 0.000299 | 55 | 0.0292 | 0.00272 | 17.30 | 0.12 | 5.95 | - | 0.0689 | 0.0612 |
| | SSC_1.40 | 10 | 0.000299 | 100 | 0.0292 | 0.00272 | 17.30 | 0.12 | 5.95 | - | 0.0565 | 0.0503 |
| | SSC_1.41 | 10 | 0.000299 | 150 | 0.0292 | 0.00272 | 17.30 | 0.12 | 5.95 | - | 0.0434 | 0.0444 |
| | SSC_1.42 | 10 | 0.000299 | 220 | 0.0292 | 0.00272 | 17.30 | 0.12 | 5.95 | - | 0.0352 | 0.0336 |
| | SSC_1.43 | 10 | 0.000299 | 270 | 0.0292 | 0.00272 | 17.30 | 0.12 | 5.95 | - | 0.0268 | 0.0252 |
| | SSC_1.44 | 10 | 0.000299 | 330 | 0.0292 | 0.00272 | 17.30 | 0.12 | 5.95 | - | 0.0195 | 0.0156 |
| | SSC_1.45 | 10 | 0.000299 | 390 | 0.0292 | 0.00272 | 17.30 | 0.12 | 5.95 | - | 0.0132 | 0.0088 |
| | SSC_1.46 | 10 | 0.000299 | 450 | 0.0292 | 0.00272 | 17.30 | 0.12 | 5.95 | - | 0.0083 | 0.0045 |
| | SSC_1.47 | 10 | 0.000299 | 510 | 0.0292 | 0.00272 | 17.30 | 0.12 | 5.95 | - | 0.0060 | 0.0032 |
| | SSC_1.48 | 10 | 0.000299 | 570 | 0.0292 | 0.00272 | 17.30 | 0.12 | 5.95 | - | 0.0034 | 0.0010 |
| | SSC_1.49 | 10 | 0.000299 | 660 | 0.0292 | 0.00272 | 17.30 | 0.12 | 5.95 | - | 0.0013 | 0.0003 |
| SSC 4 | SSC_1.50 | 10 | 0.000299 | 10 | 0.0443 | 0.00272 | 18.32 | 0.14 | 7.03 | - | 0.1538 | 0.1340 |
| | SSC_1.51 | 10 | 0.000299 | 25 | 0.0443 | 0.00272 | 18.32 | 0.14 | 7.03 | - | 0.1421 | 0.0977 |
| | SSC_1.52 | 10 | 0.000299 | 35 | 0.0443 | 0.00272 | 18.32 | 0.14 | 7.03 | - | 0.1251 | 0.0859 |

| (1) | (2) | (3) | (4) | (5) | (6) | (7) | (8) | (9) | (10) | (11) | (12) | (13) |
|---|---|---|---|---|---|---|---|---|---|---|---|---|
| | SSC_1.53 | 10 | 0.000299 | 45 | 0.0443 | 0.00272 | 18.32 | 0.14 | 7.03 | - | 0.1000 | 0.0719 |
| | SSC_1.54 | 10 | 0.000299 | 55 | 0.0443 | 0.00272 | 18.32 | 0.14 | 7.03 | - | 0.0832 | 0.0634 |
| | SSC_1.55 | 10 | 0.000299 | 70 | 0.0443 | 0.00272 | 18.32 | 0.14 | 7.03 | - | 0.0706 | 0.0569 |
| | SSC_1.56 | 10 | 0.000299 | 90 | 0.0443 | 0.00272 | 18.32 | 0.14 | 7.03 | - | 0.0612 | 0.0466 |
| | SSC_1.57 | 10 | 0.000299 | 115 | 0.0443 | 0.00272 | 18.32 | 0.14 | 7.03 | - | 0.0499 | 0.0425 |
| | SSC_1.58 | 10 | 0.000299 | 150 | 0.0443 | 0.00272 | 18.32 | 0.14 | 7.03 | - | 0.0415 | 0.0347 |
| | SSC_1.59 | 10 | 0.000299 | 185 | 0.0443 | 0.00272 | 18.32 | 0.14 | 7.03 | - | 0.0366 | 0.0230 |
| | SSC_1.60 | 10 | 0.000299 | 230 | 0.0443 | 0.00272 | 18.32 | 0.14 | 7.03 | - | 0.0319 | 0.0143 |
| | SSC_1.61 | 10 | 0.000299 | 275 | 0.0443 | 0.00272 | 18.32 | 0.14 | 7.03 | - | 0.0263 | 0.0101 |
| | SSC_1.62 | 10 | 0.000299 | 330 | 0.0443 | 0.00272 | 18.32 | 0.14 | 7.03 | - | 0.0229 | 0.0048 |
| | SSC_1.63 | 10 | 0.000299 | 405 | 0.0443 | 0.00272 | 18.32 | 0.14 | 7.03 | - | 0.0189 | 0.0030 |
| | SSC_1.64 | 10 | 0.000299 | 485 | 0.0443 | 0.00272 | 18.32 | 0.14 | 7.03 | - | 0.0103 | 0.0012 |
| | SSC_1.65 | 10 | 0.000299 | 555 | 0.0443 | 0.00272 | 18.32 | 0.14 | 7.03 | - | 0.0046 | 0.0008 |
| | SSC_1.66 | 10 | 0.000299 | 630 | 0.0443 | 0.00272 | 18.32 | 0.14 | 7.03 | - | 0.0020 | 0.0001 |
| SSC 5 | SSC_2.1 | 20 | 0.000268 | 15 | 0.0445 | 0.00272 | 19.58 | 0.13 | 11.89 | - | 0.1204 | 0.1256 |
| | SSC_2.2 | 20 | 0.000268 | 35 | 0.0445 | 0.00272 | 19.58 | 0.13 | 11.89 | - | 0.1002 | 0.0997 |
| | SSC_2.3 | 20 | 0.000268 | 60 | 0.0445 | 0.00272 | 19.58 | 0.13 | 11.89 | - | 0.0798 | 0.0867 |
| | SSC_2.4 | 20 | 0.000268 | 95 | 0.0445 | 0.00272 | 19.58 | 0.13 | 11.89 | - | 0.0699 | 0.0765 |
| | SSC_2.5 | 20 | 0.000268 | 120 | 0.0445 | 0.00272 | 19.58 | 0.13 | 11.89 | - | 0.0587 | 0.0631 |
| | SSC_2.6 | 20 | 0.000268 | 145 | 0.0445 | 0.00272 | 19.58 | 0.13 | 11.89 | - | 0.0495 | 0.0527 |
| | SSC_2.7 | 20 | 0.000268 | 210 | 0.0445 | 0.00272 | 19.58 | 0.13 | 11.89 | - | 0.0385 | 0.0421 |
| | SSC_2.8 | 20 | 0.000268 | 265 | 0.0445 | 0.00272 | 19.58 | 0.13 | 11.89 | - | 0.0288 | 0.0304 |
| | SSC_2.9 | 20 | 0.000268 | 330 | 0.0445 | 0.00272 | 19.58 | 0.13 | 11.89 | - | 0.0206 | 0.0212 |
| | SSC_2.10 | 20 | 0.000268 | 385 | 0.0445 | 0.00272 | 19.58 | 0.13 | 11.89 | - | 0.0128 | 0.0132 |
| | SSC_2.11 | 20 | 0.000268 | 445 | 0.0445 | 0.00272 | 19.58 | 0.13 | 11.89 | - | 0.0082 | 0.0071 |
| | SSC_2.12 | 20 | 0.000268 | 515 | 0.0445 | 0.00272 | 19.58 | 0.13 | 11.89 | - | 0.0067 | 0.0037 |
| | SSC_2.13 | 20 | 0.000268 | 585 | 0.0445 | 0.00272 | 19.58 | 0.13 | 11.89 | - | 0.0041 | 0.0018 |
| | SSC_2.14 | 20 | 0.000268 | 680 | 0.0445 | 0.00272 | 19.58 | 0.13 | 11.89 | - | 0.0021 | 0.0006 |

| (1) | (2) | (3) | (4) | (5) | (6) | (7) | (8) | (9) | (10) | (11) | (12) | (13) |
|---|---|---|---|---|---|---|---|---|---|---|---|---|
| SSC 6 | SSC_2.15 | 20 | 0.000268 | 35 | 0.0309 | 0.00272 | 18.10 | 0.17 | 8.11 | - | 0.0794 | 0.0877 |
| | SSC_2.16 | 20 | 0.000268 | 70 | 0.0309 | 0.00272 | 18.10 | 0.17 | 8.11 | - | 0.0683 | 0.0796 |
| | SSC_2.17 | 20 | 0.000268 | 90 | 0.0309 | 0.00272 | 18.10 | 0.17 | 8.11 | - | 0.0599 | 0.0675 |
| | SSC_2.18 | 20 | 0.000268 | 130 | 0.0309 | 0.00272 | 18.10 | 0.17 | 8.11 | - | 0.0504 | 0.0556 |
| | SSC_2.19 | 20 | 0.000268 | 180 | 0.0309 | 0.00272 | 18.10 | 0.17 | 8.11 | - | 0.0392 | 0.0426 |
| | SSC_2.20 | 20 | 0.000268 | 240 | 0.0309 | 0.00272 | 18.10 | 0.17 | 8.11 | - | 0.0277 | 0.0320 |
| | SSC_2.21 | 20 | 0.000268 | 305 | 0.0309 | 0.00272 | 18.10 | 0.17 | 8.11 | - | 0.0164 | 0.0216 |
| | SSC_2.22 | 20 | 0.000268 | 370 | 0.0309 | 0.00272 | 18.10 | 0.17 | 8.11 | - | 0.0101 | 0.0125 |
| | SSC_2.23 | 20 | 0.000268 | 430 | 0.0309 | 0.00272 | 18.10 | 0.17 | 8.11 | - | 0.0067 | 0.0076 |
| | SSC_2.24 | 20 | 0.000268 | 495 | 0.0309 | 0.00272 | 18.10 | 0.17 | 8.11 | - | 0.0051 | 0.0035 |
| | SSC_2.25 | 20 | 0.000268 | 610 | 0.0309 | 0.00272 | 18.10 | 0.17 | 8.11 | - | 0.0038 | 0.0012 |
| | SSC_2.26 | 20 | 0.000268 | 700 | 0.0309 | 0.00272 | 18.10 | 0.17 | 8.11 | - | 0.0017 | 0.0003 |
| SSC 7 | SSC_2.27 | 20 | 0.000268 | 15 | 0.0440 | 0.00465 | 18.78 | 0.19 | 8.65 | - | 0.1610 | 0.1353 |
| | SSC_2.28 | 20 | 0.000268 | 30 | 0.0440 | 0.00465 | 18.78 | 0.19 | 8.65 | - | 0.1317 | 0.1007 |
| | SSC_2.29 | 20 | 0.000268 | 45 | 0.0440 | 0.00465 | 18.78 | 0.19 | 8.65 | - | 0.0966 | 0.0857 |
| | SSC_2.30 | 20 | 0.000268 | 60 | 0.0440 | 0.00465 | 18.78 | 0.19 | 8.65 | - | 0.0825 | 0.0725 |
| | SSC_2.31 | 20 | 0.000268 | 75 | 0.0440 | 0.00465 | 18.78 | 0.19 | 8.65 | - | 0.0723 | 0.0658 |
| | SSC_2.32 | 20 | 0.000268 | 95 | 0.0440 | 0.00465 | 18.78 | 0.19 | 8.65 | - | 0.0641 | 0.0578 |
| | SSC_2.33 | 20 | 0.000268 | 115 | 0.0440 | 0.00465 | 18.78 | 0.19 | 8.65 | - | 0.0580 | 0.0461 |
| | SSC_2.34 | 20 | 0.000268 | 140 | 0.0440 | 0.00465 | 18.78 | 0.19 | 8.65 | - | 0.0504 | 0.0338 |
| | SSC_2.35 | 20 | 0.000268 | 160 | 0.0440 | 0.00465 | 18.78 | 0.19 | 8.65 | - | 0.0477 | 0.0225 |
| | SSC_2.36 | 20 | 0.000268 | 190 | 0.0440 | 0.00465 | 18.78 | 0.19 | 8.65 | - | 0.0404 | 0.0233 |
| | SSC_2.37 | 20 | 0.000268 | 220 | 0.0440 | 0.00465 | 18.78 | 0.19 | 8.65 | - | 0.0355 | 0.0180 |
| | SSC_2.38 | 20 | 0.000268 | 250 | 0.0440 | 0.00465 | 18.78 | 0.19 | 8.65 | - | 0.0311 | 0.0154 |
| | SSC_2.39 | 20 | 0.000268 | 285 | 0.0440 | 0.00465 | 18.78 | 0.19 | 8.65 | - | 0.0257 | 0.0088 |
| | SSC_2.40 | 20 | 0.000268 | 325 | 0.0440 | 0.00465 | 18.78 | 0.19 | 8.65 | - | 0.0193 | 0.0056 |
| | SSC_2.41 | 20 | 0.000268 | 385 | 0.0440 | 0.00465 | 18.78 | 0.19 | 8.65 | - | 0.0118 | 0.0038 |
| | SSC_2.42 | 20 | 0.000268 | 430 | 0.0440 | 0.00465 | 18.78 | 0.19 | 8.65 | - | 0.0079 | 0.0026 |

| (1) | (2) | (3) | (4) | (5) | (6) | (7) | (8) | (9) | (10) | (11) | (12) | (13) |
|---|---|---|---|---|---|---|---|---|---|---|---|---|
| | SSC_2.43 | 20 | 0.000268 | 490 | 0.0440 | 0.00465 | 18.78 | 0.19 | 8.65 | - | 0.0053 | 0.0014 |
| | SSC_2.44 | 20 | 0.000268 | 550 | 0.0440 | 0.00465 | 18.78 | 0.19 | 8.65 | - | 0.0037 | 0.0008 |
| | SSC_2.45 | 20 | 0.000268 | 640 | 0.0440 | 0.00465 | 18.78 | 0.19 | 8.65 | - | 0.0019 | 0.0003 |
| SSC 8 | SSC_2.46 | 20 | 0.000268 | 15 | 0.0305 | 0.00465 | 17.76 | 0.15 | 7.57 | - | 0.1036 | 0.0992 |
| | SSC_2.47 | 20 | 0.000268 | 30 | 0.0305 | 0.00465 | 17.76 | 0.15 | 7.57 | - | 0.0871 | 0.0814 |
| | SSC_2.48 | 20 | 0.000268 | 45 | 0.0305 | 0.00465 | 17.76 | 0.15 | 7.57 | - | 0.0807 | 0.0740 |
| | SSC_2.49 | 20 | 0.000268 | 60 | 0.0305 | 0.00465 | 17.76 | 0.15 | 7.57 | - | 0.0724 | 0.0647 |
| | SSC_2.50 | 20 | 0.000268 | 80 | 0.0305 | 0.00465 | 17.76 | 0.15 | 7.57 | - | 0.0673 | 0.0575 |
| | SSC_2.51 | 20 | 0.000268 | 100 | 0.0305 | 0.00465 | 17.76 | 0.15 | 7.57 | - | 0.0627 | 0.0398 |
| | SSC_2.52 | 20 | 0.000268 | 130 | 0.0305 | 0.00465 | 17.76 | 0.15 | 7.57 | - | 0.0533 | 0.0428 |
| | SSC_2.53 | 20 | 0.000268 | 180 | 0.0305 | 0.00465 | 17.76 | 0.15 | 7.57 | - | 0.0405 | 0.0318 |
| | SSC_2.54 | 20 | 0.000268 | 220 | 0.0305 | 0.00465 | 17.76 | 0.15 | 7.57 | - | 0.0315 | 0.0211 |
| | SSC_2.55 | 20 | 0.000268 | 280 | 0.0305 | 0.00465 | 17.76 | 0.15 | 7.57 | - | 0.0223 | 0.0134 |
| | SSC_2.56 | 20 | 0.000268 | 325 | 0.0305 | 0.00465 | 17.76 | 0.15 | 7.57 | - | 0.0155 | 0.0101 |
| | SSC_2.57 | 20 | 0.000268 | 370 | 0.0305 | 0.00465 | 17.76 | 0.15 | 7.57 | - | 0.0104 | 0.0069 |
| | SSC_2.58 | 20 | 0.000268 | 430 | 0.0305 | 0.00465 | 17.76 | 0.15 | 7.57 | - | 0.0056 | 0.0073 |
| | SSC_2.59 | 20 | 0.000268 | 490 | 0.0305 | 0.00465 | 17.76 | 0.15 | 7.57 | - | 0.0042 | 0.0049 |
| | SSC_2.60 | 20 | 0.000268 | 550 | 0.0305 | 0.00465 | 17.76 | 0.15 | 7.57 | - | 0.0031 | 0.0031 |
| | SSC_2.61 | 20 | 0.000268 | 610 | 0.0305 | 0.00465 | 17.76 | 0.15 | 7.57 | - | 0.0023 | 0.0013 |
| | SSC_2.62 | 20 | 0.000268 | 670 | 0.0305 | 0.00465 | 17.76 | 0.15 | 7.57 | - | 0.0015 | 0.0004 |
| SSC 9 | SSC_3.1 | 30 | 0.000236 | 10 | 0.0443 | 0.00272 | 19.58 | 0.15 | 24.33 | - | 0.1101 | 0.1049 |
| | SSC_3.2 | 30 | 0.000236 | 30 | 0.0443 | 0.00272 | 19.58 | 0.15 | 24.33 | - | 0.0983 | 0.0920 |
| | SSC_3.3 | 30 | 0.000236 | 40 | 0.0443 | 0.00272 | 19.58 | 0.15 | 24.33 | - | 0.0873 | 0.0798 |
| | SSC_3.4 | 30 | 0.000236 | 50 | 0.0443 | 0.00272 | 19.58 | 0.15 | 24.33 | - | 0.0792 | 0.0686 |
| | SSC_3.5 | 30 | 0.000236 | 70 | 0.0443 | 0.00272 | 19.58 | 0.15 | 24.33 | - | 0.0722 | 0.0564 |
| | SSC_3.6 | 30 | 0.000236 | 95 | 0.0443 | 0.00272 | 19.58 | 0.15 | 24.33 | - | 0.0638 | 0.0411 |
| | SSC_3.7 | 30 | 0.000236 | 125 | 0.0443 | 0.00272 | 19.58 | 0.15 | 24.33 | - | 0.0540 | 0.0294 |
| | SSC_3.8 | 30 | 0.000236 | 160 | 0.0443 | 0.00272 | 19.58 | 0.15 | 24.33 | - | 0.0453 | 0.0210 |

| (1) | (2) | (3) | (4) | (5) | (6) | (7) | (8) | (9) | (10) | (11) | (12) | (13) |
|---|---|---|---|---|---|---|---|---|---|---|---|---|
| | SSC_3.9 | 30 | 0.000236 | 200 | 0.0443 | 0.00272 | 19.58 | 0.15 | 24.33 | - | 0.0353 | 0.0221 |
| | SSC_3.10 | 30 | 0.000236 | 240 | 0.0443 | 0.00272 | 19.58 | 0.15 | 24.33 | - | 0.0252 | 0.0171 |
| | SSC_3.11 | 30 | 0.000236 | 300 | 0.0443 | 0.00272 | 19.58 | 0.15 | 24.33 | - | 0.0159 | 0.0109 |
| | SSC_3.12 | 30 | 0.000236 | 350 | 0.0443 | 0.00272 | 19.58 | 0.15 | 24.33 | - | 0.0138 | 0.0095 |
| | SSC_3.13 | 30 | 0.000236 | 405 | 0.0443 | 0.00272 | 19.58 | 0.15 | 24.33 | - | 0.0120 | 0.0067 |
| | SSC_3.14 | 30 | 0.000236 | 455 | 0.0443 | 0.00272 | 19.58 | 0.15 | 24.33 | - | 0.0082 | 0.0048 |
| | SSC_3.15 | 30 | 0.000236 | 515 | 0.0443 | 0.00272 | 19.58 | 0.15 | 24.33 | - | 0.0074 | 0.0025 |
| | SSC_3.16 | 30 | 0.000236 | 575 | 0.0443 | 0.00272 | 19.58 | 0.15 | 24.33 | - | 0.0061 | 0.0011 |
| | SSC_3.17 | 30 | 0.000236 | 675 | 0.0443 | 0.00272 | 19.58 | 0.15 | 24.33 | - | 0.0040 | 0.0007 |
| | SSC_3.18 | 30 | 0.000236 | 745 | 0.0443 | 0.00272 | 19.58 | 0.15 | 24.33 | - | 0.0016 | 0.0004 |
| SSC 10 | SSC_3.19 | 30 | 0.000236 | 10 | 0.0447 | 0.00465 | 20.20 | 0.17 | 30.28 | - | 0.1216 | 0.1092 |
| | SSC_3.20 | 30 | 0.000236 | 25 | 0.0447 | 0.00465 | 20.20 | 0.17 | 30.28 | - | 0.0973 | 0.0863 |
| | SSC_3.21 | 30 | 0.000236 | 40 | 0.0447 | 0.00465 | 20.20 | 0.17 | 30.28 | - | 0.0871 | 0.0774 |
| | SSC_3.22 | 30 | 0.000236 | 55 | 0.0447 | 0.00465 | 20.20 | 0.17 | 30.28 | - | 0.0818 | 0.0640 |
| | SSC_3.23 | 30 | 0.000236 | 75 | 0.0447 | 0.00465 | 20.20 | 0.17 | 30.28 | - | 0.0729 | 0.0508 |
| | SSC_3.24 | 30 | 0.000236 | 105 | 0.0447 | 0.00465 | 20.20 | 0.17 | 30.28 | - | 0.0639 | 0.0391 |
| | SSC_3.25 | 30 | 0.000236 | 135 | 0.0447 | 0.00465 | 20.20 | 0.17 | 30.28 | - | 0.0531 | 0.0342 |
| | SSC_3.26 | 30 | 0.000236 | 175 | 0.0447 | 0.00465 | 20.20 | 0.17 | 30.28 | - | 0.0442 | 0.0243 |
| | SSC_3.27 | 30 | 0.000236 | 215 | 0.0447 | 0.00465 | 20.20 | 0.17 | 30.28 | - | 0.0363 | 0.0152 |
| | SSC_3.28 | 30 | 0.000236 | 260 | 0.0447 | 0.00465 | 20.20 | 0.17 | 30.28 | - | 0.0290 | 0.0162 |
| | SSC_3.29 | 30 | 0.000236 | 305 | 0.0447 | 0.00465 | 20.20 | 0.17 | 30.28 | - | 0.0228 | 0.0120 |
| | SSC_3.30 | 30 | 0.000236 | 365 | 0.0447 | 0.00465 | 20.20 | 0.17 | 30.28 | - | 0.0147 | 0.0074 |
| | SSC_3.31 | 30 | 0.000236 | 425 | 0.0447 | 0.00465 | 20.20 | 0.17 | 30.28 | - | 0.0092 | 0.0036 |
| | SSC_3.32 | 30 | 0.000236 | 495 | 0.0447 | 0.00465 | 20.20 | 0.17 | 30.28 | - | 0.0070 | 0.0015 |
| | SSC_3.33 | 30 | 0.000236 | 585 | 0.0447 | 0.00465 | 20.20 | 0.17 | 30.28 | - | 0.0053 | 0.0006 |
| | SSC_3.34 | 30 | 0.000236 | 690 | 0.0447 | 0.00465 | 20.20 | 0.17 | 30.28 | - | 0.0018 | 0.0001 |
| SSC 11 | SSC_3.35 | 30 | 0.000236 | 20 | 0.0310 | 0.00465 | 18.04 | 0.12 | 18.38 | - | 0.0933 | 0.0962 |
| | SSC_3.36 | 30 | 0.000236 | 45 | 0.0310 | 0.00465 | 18.04 | 0.12 | 18.38 | - | 0.0811 | 0.0854 |

| (1) | (2) | (3) | (4) | (5) | (6) | (7) | (8) | (9) | (10) | (11) | (12) | (13) |
|---|---|---|---|---|---|---|---|---|---|---|---|---|
| | SSC_3.37 | 30 | 0.000236 | 70 | 0.0310 | 0.00465 | 18.04 | 0.12 | 18.38 | - | 0.0672 | 0.0772 |
| | SSC_3.38 | 30 | 0.000236 | 90 | 0.0310 | 0.00465 | 18.04 | 0.12 | 18.38 | - | 0.0558 | 0.0634 |
| | SSC_3.39 | 30 | 0.000236 | 115 | 0.0310 | 0.00465 | 18.04 | 0.12 | 18.38 | - | 0.0464 | 0.0521 |
| | SSC_3.40 | 30 | 0.000236 | 140 | 0.0310 | 0.00465 | 18.04 | 0.12 | 18.38 | - | 0.0360 | 0.0414 |
| | SSC_3.41 | 30 | 0.000236 | 170 | 0.0310 | 0.00465 | 18.04 | 0.12 | 18.38 | - | 0.0294 | 0.0342 |
| | SSC_3.42 | 30 | 0.000236 | 220 | 0.0310 | 0.00465 | 18.04 | 0.12 | 18.38 | - | 0.0208 | 0.0271 |
| | SSC_3.43 | 30 | 0.000236 | 280 | 0.0310 | 0.00465 | 18.04 | 0.12 | 18.38 | - | 0.0179 | 0.0265 |
| | SSC_3.44 | 30 | 0.000236 | 325 | 0.0310 | 0.00465 | 18.04 | 0.12 | 18.38 | - | 0.0132 | 0.0200 |
| | SSC_3.45 | 30 | 0.000236 | 380 | 0.0310 | 0.00465 | 18.04 | 0.12 | 18.38 | - | 0.0107 | 0.0145 |
| | SSC_3.46 | 30 | 0.000236 | 430 | 0.0310 | 0.00465 | 18.04 | 0.12 | 18.38 | - | 0.0090 | 0.0086 |
| | SSC_3.47 | 30 | 0.000236 | 490 | 0.0310 | 0.00465 | 18.04 | 0.12 | 18.38 | - | 0.0063 | 0.0049 |
| | SSC_3.48 | 30 | 0.000236 | 550 | 0.0310 | 0.00465 | 18.04 | 0.12 | 18.38 | - | 0.0046 | 0.0036 |
| | SSC_3.49 | 30 | 0.000236 | 630 | 0.0310 | 0.00465 | 18.04 | 0.12 | 18.38 | - | 0.0033 | 0.0012 |
| | SSC_3.50 | 30 | 0.000236 | 710 | 0.0310 | 0.00465 | 18.04 | 0.12 | 18.38 | - | 0.0016 | 0.0006 |
| SSC 12 | SSC_3.51 | 30 | 0.000236 | 25 | 0.0308 | 0.00272 | 19.80 | 0.16 | 17.84 | - | 0.0676 | 0.0817 |
| | SSC_3.52 | 30 | 0.000236 | 55 | 0.0308 | 0.00272 | 19.80 | 0.16 | 17.84 | - | 0.0577 | 0.0699 |
| | SSC_3.53 | 30 | 0.000236 | 75 | 0.0308 | 0.00272 | 19.80 | 0.16 | 17.84 | - | 0.0497 | 0.0609 |
| | SSC_3.54 | 30 | 0.000236 | 115 | 0.0308 | 0.00272 | 19.80 | 0.16 | 17.84 | - | 0.0409 | 0.0489 |
| | SSC_3.55 | 30 | 0.000236 | 150 | 0.0308 | 0.00272 | 19.80 | 0.16 | 17.84 | - | 0.0338 | 0.0389 |
| | SSC_3.56 | 30 | 0.000236 | 205 | 0.0308 | 0.00272 | 19.80 | 0.16 | 17.84 | - | 0.0257 | 0.0308 |
| | SSC_3.57 | 30 | 0.000236 | 265 | 0.0308 | 0.00272 | 19.80 | 0.16 | 17.84 | - | 0.0191 | 0.0226 |
| | SSC_3.58 | 30 | 0.000236 | 325 | 0.0308 | 0.00272 | 19.80 | 0.16 | 17.84 | - | 0.0159 | 0.0186 |
| | SSC_3.59 | 30 | 0.000236 | 365 | 0.0308 | 0.00272 | 19.80 | 0.16 | 17.84 | - | 0.0113 | 0.0150 |
| | SSC_3.60 | 30 | 0.000236 | 425 | 0.0308 | 0.00272 | 19.80 | 0.16 | 17.84 | - | 0.0089 | 0.0113 |
| | SSC_3.61 | 30 | 0.000236 | 505 | 0.0308 | 0.00272 | 19.80 | 0.16 | 17.84 | - | 0.0064 | 0.0077 |
| | SSC_3.62 | 30 | 0.000236 | 610 | 0.0308 | 0.00272 | 19.80 | 0.16 | 17.84 | - | 0.0050 | 0.0041 |
| | SSC_3.63 | 30 | 0.000236 | 705 | 0.0308 | 0.00272 | 19.80 | 0.16 | 17.84 | - | 0.0031 | 0.0013 |
| | SSC_3.64 | 30 | 0.000236 | 740 | 0.0308 | 0.00272 | 19.80 | 0.16 | 17.84 | - | 0.0012 | 0.0007 |

| (1) | (2) | (3) | (4) | (5) | (6) | (7) | (8) | (9) | (10) | (11) | (12) | (13) |
|---|---|---|---|---|---|---|---|---|---|---|---|---|
| SSC 13 | SSC_4.1 | 40 | 0.000204 | 10 | 0.0441 | 0.00465 | 19.35 | 0.15 | 23.25 | - | 0.1032 | 0.1132 |
| | SSC_4.2 | 40 | 0.000204 | 25 | 0.0441 | 0.00465 | 19.35 | 0.15 | 23.25 | - | 0.0877 | 0.0963 |
| | SSC_4.3 | 40 | 0.000204 | 35 | 0.0441 | 0.00465 | 19.35 | 0.15 | 23.25 | - | 0.0826 | 0.0845 |
| | SSC_4.4 | 40 | 0.000204 | 50 | 0.0441 | 0.00465 | 19.35 | 0.15 | 23.25 | - | 0.0775 | 0.0727 |
| | SSC_4.5 | 40 | 0.000204 | 60 | 0.0441 | 0.00465 | 19.35 | 0.15 | 23.25 | - | 0.0710 | 0.0615 |
| | SSC_4.6 | 40 | 0.000204 | 90 | 0.0441 | 0.00465 | 19.35 | 0.15 | 23.25 | - | 0.0678 | 0.0540 |
| | SSC_4.7 | 40 | 0.000204 | 105 | 0.0441 | 0.00465 | 19.35 | 0.15 | 23.25 | - | 0.0627 | 0.0480 |
| | SSC_4.8 | 40 | 0.000204 | 130 | 0.0441 | 0.00465 | 19.35 | 0.15 | 23.25 | - | 0.0567 | 0.0418 |
| | SSC_4.9 | 40 | 0.000204 | 170 | 0.0441 | 0.00465 | 19.35 | 0.15 | 23.25 | - | 0.0468 | 0.0341 |
| | SSC_4.10 | 40 | 0.000204 | 205 | 0.0441 | 0.00465 | 19.35 | 0.15 | 23.25 | - | 0.0348 | 0.0228 |
| | SSC_4.11 | 40 | 0.000204 | 250 | 0.0441 | 0.00465 | 19.35 | 0.15 | 23.25 | - | 0.0276 | 0.0111 |
| | SSC_4.12 | 40 | 0.000204 | 290 | 0.0441 | 0.00465 | 19.35 | 0.15 | 23.25 | - | 0.0225 | 0.0092 |
| | SSC_4.13 | 40 | 0.000204 | 355 | 0.0441 | 0.00465 | 19.35 | 0.15 | 23.25 | - | 0.0175 | 0.0079 |
| | SSC_4.14 | 40 | 0.000204 | 390 | 0.0441 | 0.00465 | 19.35 | 0.15 | 23.25 | - | 0.0119 | 0.0062 |
| | SSC_4.15 | 40 | 0.000204 | 450 | 0.0441 | 0.00465 | 19.35 | 0.15 | 23.25 | - | 0.0093 | 0.0057 |
| | SSC_4.16 | 40 | 0.000204 | 510 | 0.0441 | 0.00465 | 19.35 | 0.15 | 23.25 | - | 0.0064 | 0.0038 |
| | SSC_4.17 | 40 | 0.000204 | 570 | 0.0441 | 0.00465 | 19.35 | 0.15 | 23.25 | - | 0.0041 | 0.0017 |
| | SSC_4.18 | 40 | 0.000204 | 630 | 0.0441 | 0.00465 | 19.35 | 0.15 | 23.25 | - | 0.0029 | 0.0007 |
| | SSC_4.19 | 40 | 0.000204 | 700 | 0.0441 | 0.00465 | 19.35 | 0.15 | 23.25 | - | 0.0013 | 0.0005 |
| SSC 14 | SSC_4.20 | 40 | 0.000204 | 10 | 0.0435 | 0.00272 | 20.15 | 0.17 | 31.36 | - | 0.0906 | 0.0835 |
| | SSC_4.21 | 40 | 0.000204 | 25 | 0.0435 | 0.00272 | 20.15 | 0.17 | 31.36 | - | 0.0819 | 0.0717 |
| | SSC_4.22 | 40 | 0.000204 | 40 | 0.0435 | 0.00272 | 20.15 | 0.17 | 31.36 | - | 0.0709 | 0.0616 |
| | SSC_4.23 | 40 | 0.000204 | 60 | 0.0435 | 0.00272 | 20.15 | 0.17 | 31.36 | - | 0.0601 | 0.0490 |
| | SSC_4.24 | 40 | 0.000204 | 90 | 0.0435 | 0.00272 | 20.15 | 0.17 | 31.36 | - | 0.0501 | 0.0350 |
| | SSC_4.25 | 40 | 0.000204 | 115 | 0.0435 | 0.00272 | 20.15 | 0.17 | 31.36 | - | 0.0429 | 0.0307 |
| | SSC_4.26 | 40 | 0.000204 | 145 | 0.0435 | 0.00272 | 20.15 | 0.17 | 31.36 | - | 0.0349 | 0.0284 |
| | SSC_4.27 | 40 | 0.000204 | 195 | 0.0435 | 0.00272 | 20.15 | 0.17 | 31.36 | - | 0.0253 | 0.0207 |
| | SSC_4.28 | 40 | 0.000204 | 240 | 0.0435 | 0.00272 | 20.15 | 0.17 | 31.36 | - | 0.0199 | 0.0122 |

| (1) | (2) | (3) | (4) | (5) | (6) | (7) | (8) | (9) | (10) | (11) | (12) | (13) |
|---|---|---|---|---|---|---|---|---|---|---|---|---|
| | SSC_4.29 | 40 | 0.000204 | 285 | 0.0435 | 0.00272 | 20.15 | 0.17 | 31.36 | - | 0.0151 | 0.0072 |
| | SSC_4.30 | 40 | 0.000204 | 335 | 0.0435 | 0.00272 | 20.15 | 0.17 | 31.36 | - | 0.0127 | 0.0061 |
| | SSC_4.31 | 40 | 0.000204 | 390 | 0.0435 | 0.00272 | 20.15 | 0.17 | 31.36 | - | 0.0075 | 0.0037 |
| | SSC_4.32 | 40 | 0.000204 | 440 | 0.0435 | 0.00272 | 20.15 | 0.17 | 31.36 | - | 0.0066 | 0.0025 |
| | SSC_4.33 | 40 | 0.000204 | 515 | 0.0435 | 0.00272 | 20.15 | 0.17 | 31.36 | - | 0.0046 | 0.0015 |
| | SSC_4.34 | 40 | 0.000204 | 580 | 0.0435 | 0.00272 | 20.15 | 0.17 | 31.36 | - | 0.0029 | 0.0007 |
| | SSC_4.35 | 40 | 0.000204 | 710 | 0.0435 | 0.00272 | 20.15 | 0.17 | 31.36 | - | 0.0013 | 0.0003 |
| SSC 15 | SSC_4.36 | 40 | 0.000204 | 30 | 0.0312 | 0.00465 | 19.80 | 0.17 | 34.06 | - | 0.0750 | 0.0810 |
| | SSC_4.37 | 40 | 0.000204 | 45 | 0.0312 | 0.00465 | 19.80 | 0.17 | 34.06 | - | 0.0705 | 0.0761 |
| | SSC_4.38 | 40 | 0.000204 | 60 | 0.0312 | 0.00465 | 19.80 | 0.17 | 34.06 | - | 0.0626 | 0.0715 |
| | SSC_4.39 | 40 | 0.000204 | 75 | 0.0312 | 0.00465 | 19.80 | 0.17 | 34.06 | - | 0.0549 | 0.0629 |
| | SSC_4.40 | 40 | 0.000204 | 100 | 0.0312 | 0.00465 | 19.80 | 0.17 | 34.06 | - | 0.0424 | 0.0531 |
| | SSC_4.41 | 40 | 0.000204 | 120 | 0.0312 | 0.00465 | 19.80 | 0.17 | 34.06 | - | 0.0330 | 0.0464 |
| | SSC_4.42 | 40 | 0.000204 | 150 | 0.0312 | 0.00465 | 19.80 | 0.17 | 34.06 | - | 0.0202 | 0.0376 |
| | SSC_4.43 | 40 | 0.000204 | 205 | 0.0312 | 0.00465 | 19.80 | 0.17 | 34.06 | - | 0.0149 | 0.0321 |
| | SSC_4.44 | 40 | 0.000204 | 260 | 0.0312 | 0.00465 | 19.80 | 0.17 | 34.06 | - | 0.0103 | 0.0231 |
| | SSC_4.45 | 40 | 0.000204 | 295 | 0.0312 | 0.00465 | 19.80 | 0.17 | 34.06 | - | 0.0086 | 0.0168 |
| | SSC_4.46 | 40 | 0.000204 | 335 | 0.0312 | 0.00465 | 19.80 | 0.17 | 34.06 | - | 0.0074 | 0.0113 |
| | SSC_4.47 | 40 | 0.000204 | 385 | 0.0312 | 0.00465 | 19.80 | 0.17 | 34.06 | - | 0.0068 | 0.0069 |
| | SSC_4.48 | 40 | 0.000204 | 445 | 0.0312 | 0.00465 | 19.80 | 0.17 | 34.06 | - | 0.0054 | 0.0034 |
| | SSC_4.49 | 40 | 0.000204 | 535 | 0.0312 | 0.00465 | 19.80 | 0.17 | 34.06 | - | 0.0053 | 0.0016 |
| | SSC_4.50 | 40 | 0.000204 | 625 | 0.0312 | 0.00465 | 19.80 | 0.17 | 34.06 | - | 0.0032 | 0.0009 |
| | SSC_4.51 | 40 | 0.000204 | 730 | 0.0312 | 0.00465 | 19.80 | 0.17 | 34.06 | - | 0.0016 | 0.0003 |
| SSC 16 | SSC_4.52 | 40 | 0.000204 | 50 | 0.0301 | 0.00272 | 19.92 | 0.17 | 29.20 | - | 0.0601 | 0.0729 |
| | SSC_4.53 | 40 | 0.000204 | 80 | 0.0301 | 0.00272 | 19.92 | 0.17 | 29.20 | - | 0.0497 | 0.0644 |
| | SSC_4.54 | 40 | 0.000204 | 115 | 0.0301 | 0.00272 | 19.92 | 0.17 | 29.20 | - | 0.0388 | 0.0556 |
| | SSC_4.55 | 40 | 0.000204 | 150 | 0.0301 | 0.00272 | 19.92 | 0.17 | 29.20 | - | 0.0255 | 0.0474 |
| | SSC_4.56 | 40 | 0.000204 | 180 | 0.0301 | 0.00272 | 19.92 | 0.17 | 29.20 | - | 0.0157 | 0.0292 |

| (1) | (2) | (3) | (4) | (5) | (6) | (7) | (8) | (9) | (10) | (11) | (12) | (13) |
|---|---|---|---|---|---|---|---|---|---|---|---|---|
| | SSC_4.57 | 40 | 0.000204 | 240 | 0.0301 | 0.00272 | 19.92 | 0.17 | 29.20 | - | 0.0093 | 0.0187 |
| | SSC_4.58 | 40 | 0.000204 | 330 | 0.0301 | 0.00272 | 19.92 | 0.17 | 29.20 | - | 0.0047 | 0.0112 |
| | SSC_4.59 | 40 | 0.000204 | 410 | 0.0301 | 0.00272 | 19.92 | 0.17 | 29.20 | - | 0.0032 | 0.0083 |
| | SSC_4.60 | 40 | 0.000204 | 480 | 0.0301 | 0.00272 | 19.92 | 0.17 | 29.20 | - | 0.0024 | 0.0058 |
| | SSC_4.61 | 40 | 0.000204 | 540 | 0.0301 | 0.00272 | 19.92 | 0.17 | 29.20 | - | 0.0019 | 0.0026 |
| | SSC_4.62 | 40 | 0.000204 | 600 | 0.0301 | 0.00272 | 19.92 | 0.17 | 29.20 | - | 0.0016 | 0.0010 |
| | SSC_4.63 | 40 | 0.000204 | 720 | 0.0301 | 0.00272 | 19.92 | 0.17 | 29.20 | - | 0.0006 | 0.0002 |
| SSC 17 | SSC_5.13 | 50 | 0.000173 | 15 | 0.0452 | 0.00465 | 19.01 | 0.18 | 23.79 | - | 0.0955 | 0.1131 |
| | SSC_5.14 | 50 | 0.000173 | 35 | 0.0452 | 0.00465 | 19.01 | 0.18 | 23.79 | - | 0.0889 | 0.0879 |
| | SSC_5.15 | 50 | 0.000173 | 50 | 0.0452 | 0.00465 | 19.01 | 0.18 | 23.79 | - | 0.0810 | 0.0738 |
| | SSC_5.16 | 50 | 0.000173 | 60 | 0.0452 | 0.00465 | 19.01 | 0.18 | 23.79 | - | 0.0737 | 0.0664 |
| | SSC_5.17 | 50 | 0.000173 | 80 | 0.0452 | 0.00465 | 19.01 | 0.18 | 23.79 | - | 0.0652 | 0.0563 |
| | SSC_5.18 | 50 | 0.000173 | 95 | 0.0452 | 0.00465 | 19.01 | 0.18 | 23.79 | - | 0.0578 | 0.0549 |
| | SSC_5.19 | 50 | 0.000173 | 115 | 0.0452 | 0.00465 | 19.01 | 0.18 | 23.79 | - | 0.0507 | 0.0496 |
| | SSC_5.20 | 50 | 0.000173 | 140 | 0.0452 | 0.00465 | 19.01 | 0.18 | 23.79 | - | 0.0421 | 0.0431 |
| | SSC_5.21 | 50 | 0.000173 | 170 | 0.0452 | 0.00465 | 19.01 | 0.18 | 23.79 | - | 0.0335 | 0.0345 |
| | SSC_5.22 | 50 | 0.000173 | 200 | 0.0452 | 0.00465 | 19.01 | 0.18 | 23.79 | - | 0.0274 | 0.0233 |
| | SSC_5.23 | 50 | 0.000173 | 245 | 0.0452 | 0.00465 | 19.01 | 0.18 | 23.79 | - | 0.0224 | 0.0178 |
| | SSC_5.24 | 50 | 0.000173 | 285 | 0.0452 | 0.00465 | 19.01 | 0.18 | 23.79 | - | 0.0179 | 0.0106 |
| | SSC_5.25 | 50 | 0.000173 | 340 | 0.0452 | 0.00465 | 19.01 | 0.18 | 23.79 | - | 0.0134 | 0.0080 |
| | SSC_5.26 | 50 | 0.000173 | 390 | 0.0452 | 0.00465 | 19.01 | 0.18 | 23.79 | - | 0.0104 | 0.0067 |
| | SSC_5.27 | 50 | 0.000173 | 450 | 0.0452 | 0.00465 | 19.01 | 0.18 | 23.79 | - | 0.0082 | 0.0043 |
| | SSC_5.28 | 50 | 0.000173 | 480 | 0.0452 | 0.00465 | 19.01 | 0.18 | 23.79 | - | 0.0071 | 0.0033 |
| | SSC_5.29 | 50 | 0.000173 | 560 | 0.0452 | 0.00465 | 19.01 | 0.18 | 23.79 | - | 0.0044 | 0.0021 |
| | SSC_5.30 | 50 | 0.000173 | 640 | 0.0452 | 0.00465 | 19.01 | 0.18 | 23.79 | - | 0.0020 | 0.0007 |
| | SSC_5.31 | 50 | 0.000173 | 720 | 0.0452 | 0.00465 | 19.01 | 0.18 | 23.79 | - | 0.0014 | 0.0004 |
| SSC 18 | SSC_5.32 | 50 | 0.000173 | 10 | 0.0302 | 0.00465 | 18.67 | 0.17 | 20.55 | - | 0.0685 | 0.0752 |
| | SSC_5.33 | 50 | 0.000173 | 20 | 0.0302 | 0.00465 | 18.67 | 0.17 | 20.55 | - | 0.0602 | 0.0664 |

| (1) | (2) | (3) | (4) | (5) | (6) | (7) | (8) | (9) | (10) | (11) | (12) | (13) |
|---|---|---|---|---|---|---|---|---|---|---|---|---|
| | SSC_5.34 | 50 | 0.000173 | 35 | 0.0302 | 0.00465 | 18.67 | 0.17 | 20.55 | - | 0.0525 | 0.0535 |
| | SSC_5.35 | 50 | 0.000173 | 50 | 0.0302 | 0.00465 | 18.67 | 0.17 | 20.55 | - | 0.0460 | 0.0456 |
| | SSC_5.36 | 50 | 0.000173 | 85 | 0.0302 | 0.00465 | 18.67 | 0.17 | 20.55 | - | 0.0383 | 0.0371 |
| | SSC_5.37 | 50 | 0.000173 | 115 | 0.0302 | 0.00465 | 18.67 | 0.17 | 20.55 | - | 0.0308 | 0.0282 |
| | SSC_5.38 | 50 | 0.000173 | 155 | 0.0302 | 0.00465 | 18.67 | 0.17 | 20.55 | - | 0.0243 | 0.0232 |
| | SSC_5.39 | 50 | 0.000173 | 195 | 0.0302 | 0.00465 | 18.67 | 0.17 | 20.55 | - | 0.0187 | 0.0173 |
| | SSC_5.40 | 50 | 0.000173 | 240 | 0.0302 | 0.00465 | 18.67 | 0.17 | 20.55 | - | 0.0131 | 0.0102 |
| | SSC_5.41 | 50 | 0.000173 | 295 | 0.0302 | 0.00465 | 18.67 | 0.17 | 20.55 | - | 0.0108 | 0.0075 |
| | SSC_5.42 | 50 | 0.000173 | 355 | 0.0302 | 0.00465 | 18.67 | 0.17 | 20.55 | - | 0.0060 | 0.0054 |
| | SSC_5.43 | 50 | 0.000173 | 445 | 0.0302 | 0.00465 | 18.67 | 0.17 | 20.55 | - | 0.0046 | 0.0033 |
| | SSC_5.44 | 50 | 0.000173 | 535 | 0.0302 | 0.00465 | 18.67 | 0.17 | 20.55 | - | 0.0030 | 0.0014 |
| | SSC_5.45 | 50 | 0.000173 | 625 | 0.0302 | 0.00465 | 18.67 | 0.17 | 20.55 | - | 0.0020 | 0.0006 |
| | SSC_5.46 | 50 | 0.000173 | 740 | 0.0302 | 0.00465 | 18.67 | 0.17 | 20.55 | - | 0.0008 | 0.0002 |
| SSC 19 | SSC_5.47 | 50 | 0.000173 | 20 | 0.0308 | 0.00272 | 18.67 | 0.16 | 19.46 | - | 0.0559 | 0.0737 |
| | SSC_5.48 | 50 | 0.000173 | 60 | 0.0308 | 0.00272 | 18.67 | 0.16 | 19.46 | - | 0.0415 | 0.0596 |
| | SSC_5.49 | 50 | 0.000173 | 100 | 0.0308 | 0.00272 | 18.67 | 0.16 | 19.46 | - | 0.0310 | 0.0469 |
| | SSC_5.50 | 50 | 0.000173 | 140 | 0.0308 | 0.00272 | 18.67 | 0.16 | 19.46 | - | 0.0222 | 0.0346 |
| | SSC_5.51 | 50 | 0.000173 | 190 | 0.0308 | 0.00272 | 18.67 | 0.16 | 19.46 | - | 0.0139 | 0.0246 |
| | SSC_5.52 | 50 | 0.000173 | 250 | 0.0308 | 0.00272 | 18.67 | 0.16 | 19.46 | - | 0.0094 | 0.0133 |
| | SSC_5.53 | 50 | 0.000173 | 310 | 0.0308 | 0.00272 | 18.67 | 0.16 | 19.46 | - | 0.0065 | 0.0081 |
| | SSC_5.54 | 50 | 0.000173 | 370 | 0.0308 | 0.00272 | 18.67 | 0.16 | 19.46 | - | 0.0043 | 0.0065 |
| | SSC_5.55 | 50 | 0.000173 | 430 | 0.0308 | 0.00272 | 18.67 | 0.16 | 19.46 | - | 0.0034 | 0.0051 |
| | SSC_5.56 | 50 | 0.000173 | 505 | 0.0308 | 0.00272 | 18.67 | 0.16 | 19.46 | - | 0.0023 | 0.0017 |
| | SSC_5.57 | 50 | 0.000173 | 595 | 0.0308 | 0.00272 | 18.67 | 0.16 | 19.46 | - | 0.0012 | 0.0012 |
| | SSC_5.58 | 50 | 0.000173 | 735 | 0.0308 | 0.00272 | 18.67 | 0.16 | 19.46 | - | 0.0007 | 0.0005 |
| SSC 20 | SSC_5.59 | 50 | 0.000173 | 15 | 0.0438 | 0.00272 | 18.81 | 0.17 | 25.95 | - | 0.0811 | 0.0908 |
| | SSC_5.60 | 50 | 0.000173 | 30 | 0.0438 | 0.00272 | 18.81 | 0.17 | 25.95 | - | 0.0748 | 0.0846 |
| | SSC_5.61 | 50 | 0.000173 | 45 | 0.0438 | 0.00272 | 18.81 | 0.17 | 25.95 | - | 0.0665 | 0.0728 |

| (1) | (2) | (3) | (4) | (5) | (6) | (7) | (8) | (9) | (10) | (11) | (12) | (13) |
|---|---|---|---|---|---|---|---|---|---|---|---|---|
| | SSC_5.62 | 50 | 0.000173 | 65 | 0.0438 | 0.00272 | 18.81 | 0.17 | 25.95 | - | 0.0543 | 0.0624 |
| | SSC_5.63 | 50 | 0.000173 | 85 | 0.0438 | 0.00272 | 18.81 | 0.17 | 25.95 | - | 0.0478 | 0.0536 |
| | SSC_5.64 | 50 | 0.000173 | 105 | 0.0438 | 0.00272 | 18.81 | 0.17 | 25.95 | - | 0.0400 | 0.0463 |
| | SSC_5.65 | 50 | 0.000173 | 125 | 0.0438 | 0.00272 | 18.81 | 0.17 | 25.95 | - | 0.0332 | 0.0366 |
| | SSC_5.66 | 50 | 0.000173 | 155 | 0.0438 | 0.00272 | 18.81 | 0.17 | 25.95 | - | 0.0278 | 0.0298 |
| | SSC_5.67 | 50 | 0.000173 | 185 | 0.0438 | 0.00272 | 18.81 | 0.17 | 25.95 | - | 0.0226 | 0.0246 |
| | SSC_5.68 | 50 | 0.000173 | 215 | 0.0438 | 0.00272 | 18.81 | 0.17 | 25.95 | - | 0.0158 | 0.0218 |
| | SSC_5.69 | 50 | 0.000173 | 260 | 0.0438 | 0.00272 | 18.81 | 0.17 | 25.95 | - | 0.0118 | 0.0159 |
| | SSC_5.70 | 50 | 0.000173 | 305 | 0.0438 | 0.00272 | 18.81 | 0.17 | 25.95 | - | 0.0083 | 0.0114 |
| | SSC_5.71 | 50 | 0.000173 | 350 | 0.0438 | 0.00272 | 18.81 | 0.17 | 25.95 | - | 0.0075 | 0.0094 |
| | SSC_5.72 | 50 | 0.000173 | 410 | 0.0438 | 0.00272 | 18.81 | 0.17 | 25.95 | - | 0.0064 | 0.0059 |
| | SSC_5.73 | 50 | 0.000173 | 470 | 0.0438 | 0.00272 | 18.81 | 0.17 | 25.95 | - | 0.0053 | 0.0045 |
| | SSC_5.74 | 50 | 0.000173 | 530 | 0.0438 | 0.00272 | 18.81 | 0.17 | 25.95 | - | 0.0043 | 0.0026 |
| | SSC_5.75 | 50 | 0.000173 | 590 | 0.0438 | 0.00272 | 18.81 | 0.17 | 25.95 | - | 0.0029 | 0.0014 |
| | SSC_5.76 | 50 | 0.000173 | 650 | 0.0438 | 0.00272 | 18.81 | 0.17 | 25.95 | - | 0.0016 | 0.0007 |
| | SSC_5.77 | 50 | 0.000173 | 710 | 0.0438 | 0.00272 | 18.81 | 0.17 | 25.95 | - | 0.0009 | 0.0003 |
| SSC 21 | SSC_0.1 | 0 | 0.000331 | 30 | 0.0308 | 0.00272 | 16.96 | 0.10 | 0.00 | - | 0.1222 | 0.1058 |
| | SSC_0.2 | 0 | 0.000331 | 45 | 0.0308 | 0.00272 | 16.96 | 0.10 | 0.00 | - | 0.1013 | 0.0853 |
| | SSC_0.3 | 0 | 0.000331 | 75 | 0.0308 | 0.00272 | 16.96 | 0.10 | 0.00 | - | 0.0819 | 0.0718 |
| | SSC_0.4 | 0 | 0.000331 | 110 | 0.0308 | 0.00272 | 16.96 | 0.10 | 0.00 | - | 0.0693 | 0.0482 |
| | SSC_0.5 | 0 | 0.000331 | 185 | 0.0308 | 0.00272 | 16.96 | 0.10 | 0.00 | - | 0.0514 | 0.0330 |
| | SSC_0.6 | 0 | 0.000331 | 220 | 0.0308 | 0.00272 | 16.96 | 0.10 | 0.00 | - | 0.0378 | 0.0230 |
| | SSC_0.7 | 0 | 0.000331 | 305 | 0.0308 | 0.00272 | 16.96 | 0.10 | 0.00 | - | 0.0248 | 0.0162 |
| | SSC_0.8 | 0 | 0.000331 | 365 | 0.0308 | 0.00272 | 16.96 | 0.10 | 0.00 | - | 0.0179 | 0.0106 |
| | SSC_0.9 | 0 | 0.000331 | 430 | 0.0308 | 0.00272 | 16.96 | 0.10 | 0.00 | - | 0.0148 | 0.0079 |
| | SSC_0.10 | 0 | 0.000331 | 465 | 0.0308 | 0.00272 | 16.96 | 0.10 | 0.00 | - | 0.0121 | 0.0064 |
| | SSC_0.11 | 0 | 0.000331 | 525 | 0.0308 | 0.00272 | 16.96 | 0.10 | 0.00 | - | 0.0095 | 0.0041 |
| | SSC_0.12 | 0 | 0.000331 | 630 | 0.0308 | 0.00272 | 16.96 | 0.10 | 0.00 | - | 0.0074 | 0.0024 |

| (1) | (2) | (3) | (4) | (5) | (6) | (7) | (8) | (9) | (10) | (11) | (12) | (13) |
|---|---|---|---|---|---|---|---|---|---|---|---|---|
| | SSC_0.13 | 0 | 0.000331 | 755 | 0.0308 | 0.00272 | 16.96 | 0.10 | 0.00 | - | 0.0043 | 0.0010 |
| | SSC_0.14 | 0 | 0.000331 | 870 | 0.0308 | 0.00272 | 16.96 | 0.10 | 0.00 | - | 0.0021 | 0.0002 |
| SSC 22 | SSC_0.15 | 0 | 0.000331 | 15 | 0.0432 | 0.00272 | 17.19 | 0.11 | 0.00 | - | 0.1786 | 0.1577 |
| | SSC_0.16 | 0 | 0.000331 | 35 | 0.0432 | 0.00272 | 17.19 | 0.11 | 0.00 | - | 0.1523 | 0.1073 |
| | SSC_0.17 | 0 | 0.000331 | 55 | 0.0432 | 0.00272 | 17.19 | 0.11 | 0.00 | - | 0.1322 | 0.0814 |
| | SSC_0.18 | 0 | 0.000331 | 90 | 0.0432 | 0.00272 | 17.19 | 0.11 | 0.00 | - | 0.1178 | 0.0663 |
| | SSC_0.19 | 0 | 0.000331 | 145 | 0.0432 | 0.00272 | 17.19 | 0.11 | 0.00 | - | 0.0889 | 0.0524 |
| | SSC_0.20 | 0 | 0.000331 | 175 | 0.0432 | 0.00272 | 17.19 | 0.11 | 0.00 | - | 0.0666 | 0.0388 |
| | SSC_0.21 | 0 | 0.000331 | 275 | 0.0432 | 0.00272 | 17.19 | 0.11 | 0.00 | - | 0.0422 | 0.0272 |
| | SSC_0.22 | 0 | 0.000331 | 335 | 0.0432 | 0.00272 | 17.19 | 0.11 | 0.00 | - | 0.0313 | 0.0136 |
| | SSC_0.23 | 0 | 0.000331 | 395 | 0.0432 | 0.00272 | 17.19 | 0.11 | 0.00 | - | 0.0201 | 0.0097 |
| | SSC_0.24 | 0 | 0.000331 | 440 | 0.0432 | 0.00272 | 17.19 | 0.11 | 0.00 | - | 0.0148 | 0.0069 |
| | SSC_0.25 | 0 | 0.000331 | 570 | 0.0432 | 0.00272 | 17.19 | 0.11 | 0.00 | - | 0.0082 | 0.0037 |
| | SSC_0.26 | 0 | 0.000331 | 710 | 0.0432 | 0.00272 | 17.19 | 0.11 | 0.00 | - | 0.0061 | 0.0012 |
| | SSC_0.27 | 0 | 0.000331 | 815 | 0.0432 | 0.00272 | 17.19 | 0.11 | 0.00 | - | 0.0027 | 0.0004 |
| SSC 23 | SSC_0.28 | 0 | 0.000331 | 15 | 0.0439 | 0.00465 | 17.07 | 0.11 | 0.00 | - | 0.1960 | 0.1736 |
| | SSC_0.29 | 0 | 0.000331 | 30 | 0.0439 | 0.00465 | 17.07 | 0.11 | 0.00 | - | 0.1566 | 0.1355 |
| | SSC_0.30 | 0 | 0.000331 | 60 | 0.0439 | 0.00465 | 17.07 | 0.11 | 0.00 | - | 0.1199 | 0.1128 |
| | SSC_0.31 | 0 | 0.000331 | 90 | 0.0439 | 0.00465 | 17.07 | 0.11 | 0.00 | - | 0.0902 | 0.0879 |
| | SSC_0.32 | 0 | 0.000331 | 135 | 0.0439 | 0.00465 | 17.07 | 0.11 | 0.00 | - | 0.0825 | 0.0696 |
| | SSC_0.33 | 0 | 0.000331 | 195 | 0.0439 | 0.00465 | 17.07 | 0.11 | 0.00 | - | 0.0725 | 0.0543 |
| | SSC_0.34 | 0 | 0.000331 | 275 | 0.0439 | 0.00465 | 17.07 | 0.11 | 0.00 | - | 0.0636 | 0.0426 |
| | SSC_0.35 | 0 | 0.000331 | 355 | 0.0439 | 0.00465 | 17.07 | 0.11 | 0.00 | - | 0.0519 | 0.0287 |
| | SSC_0.36 | 0 | 0.000331 | 435 | 0.0439 | 0.00465 | 17.07 | 0.11 | 0.00 | - | 0.0351 | 0.0146 |
| | SSC_0.37 | 0 | 0.000331 | 495 | 0.0439 | 0.00465 | 17.07 | 0.11 | 0.00 | - | 0.0179 | 0.0070 |
| | SSC_0.38 | 0 | 0.000331 | 585 | 0.0439 | 0.00465 | 17.07 | 0.11 | 0.00 | - | 0.0087 | 0.0033 |
| | SSC_0.39 | 0 | 0.000331 | 675 | 0.0439 | 0.00465 | 17.07 | 0.11 | 0.00 | - | 0.0068 | 0.0014 |
| | SSC_0.40 | 0 | 0.000331 | 795 | 0.0439 | 0.00465 | 17.07 | 0.11 | 0.00 | - | 0.0039 | 0.0003 |

| (1) | (2) | (3) | (4) | (5) | (6) | (7) | (8) | (9) | (10) | (11) | (12) | (13) |
|---|---|---|---|---|---|---|---|---|---|---|---|---|
| SSC 24 | SSC_0.41 | 0 | 0.000331 | 30 | 0.0303 | 0.00465 | 16.73 | 0.11 | 0.00 | - | 0.1410 | 0.1268 |
| | SSC_0.42 | 0 | 0.000331 | 45 | 0.0303 | 0.00465 | 16.73 | 0.11 | 0.00 | - | 0.1065 | 0.1032 |
| | SSC_0.43 | 0 | 0.000331 | 75 | 0.0303 | 0.00465 | 16.73 | 0.11 | 0.00 | - | 0.0797 | 0.0804 |
| | SSC_0.44 | 0 | 0.000331 | 110 | 0.0303 | 0.00465 | 16.73 | 0.11 | 0.00 | - | 0.0692 | 0.0654 |
| | SSC_0.45 | 0 | 0.000331 | 155 | 0.0303 | 0.00465 | 16.73 | 0.11 | 0.00 | - | 0.0589 | 0.0473 |
| | SSC_0.46 | 0 | 0.000331 | 215 | 0.0303 | 0.00465 | 16.73 | 0.11 | 0.00 | - | 0.0482 | 0.0385 |
| | SSC_0.47 | 0 | 0.000331 | 295 | 0.0303 | 0.00465 | 16.73 | 0.11 | 0.00 | - | 0.0353 | 0.0238 |
| | SSC_0.48 | 0 | 0.000331 | 370 | 0.0303 | 0.00465 | 16.73 | 0.11 | 0.00 | - | 0.0230 | 0.0182 |
| | SSC_0.49 | 0 | 0.000331 | 445 | 0.0303 | 0.00465 | 16.73 | 0.11 | 0.00 | - | 0.0140 | 0.0126 |
| | SSC_0.50 | 0 | 0.000331 | 485 | 0.0303 | 0.00465 | 16.73 | 0.11 | 0.00 | - | 0.0097 | 0.0083 |
| | SSC_0.51 | 0 | 0.000331 | 545 | 0.0303 | 0.00465 | 16.73 | 0.11 | 0.00 | - | 0.0075 | 0.0041 |
| | SSC_0.52 | 0 | 0.000331 | 620 | 0.0303 | 0.00465 | 16.73 | 0.11 | 0.00 | - | 0.0060 | 0.0028 |
| | SSC_0.53 | 0 | 0.000331 | 720 | 0.0303 | 0.00465 | 16.73 | 0.11 | 0.00 | - | 0.0040 | 0.0010 |
| | SSC_0.54 | 0 | 0.000331 | 840 | 0.0303 | 0.00465 | 16.73 | 0.11 | 0.00 | - | 0.0019 | 0.0002 |

# APPENDIX - C

Observations for transient bed surface profile

| Observation | Time | Degradation (cm) at different sections | | | | | | | | | | | |
|---|---|---|---|---|---|---|---|---|---|---|---|---|---|
| No. | (min) | 0.5 m | 1.0 m | 1.5 m | 2.0 m | 2.5 m | 3.0 m | 3.5 m | 4.0 m | 4.5 m | 5.0 m | 5.5 m | 6.0 m |
| (1) | (2) | (3) | (4) | (5) | (6) | (7) | (8) | (9) | (10) | (11) | (12) | (13) | (14) |
| GSC_1.1 | 15 | 2.3 | 2.0 | 1.4 | 1.1 | 0.8 | 0.7 | 0.8 | 0.6 | 0.7 | 0.9 | 0.7 | 0.8 |
| GSC_1.2 | 30 | 3.3 | 2.6 | 1.9 | 1.3 | 1.1 | 0.9 | 0.8 | 0.8 | 0.7 | 0.8 | 0.8 | 0.8 |
| GSC_1.3 | 45 | 4.2 | 3.0 | 2.2 | 1.6 | 1.5 | 1.2 | 1.0 | 1.0 | 0.8 | 0.8 | 0.9 | 0.8 |
| GSC_1.4 | 75 | 4.9 | 3.5 | 2.6 | 1.9 | 1.6 | 1.4 | 1.1 | 1.2 | 1.0 | 0.9 | 0.9 | 0.9 |
| GSC_1.5 | 120 | 6.0 | 4.1 | 3.0 | 2.3 | 1.9 | 1.6 | 1.3 | 1.1 | 1.0 | 0.9 | 1.0 | 0.9 |
| GSC_1.6 | 165 | 6.7 | 4.6 | 3.4 | 2.5 | 2.1 | 1.7 | 1.5 | 1.2 | 1.1 | 1.0 | 0.9 | 0.9 |
| GSC_1.7 | 210 | 7.3 | 4.9 | 3.9 | 2.8 | 2.3 | 2.0 | 1.7 | 1.3 | 1.0 | 1.1 | 1.0 | 1.0 |
| GSC_1.8 | 240 | 7.7 | 5.1 | 4.2 | 3.1 | 2.6 | 2.1 | 1.9 | 1.5 | 1.2 | 1.2 | 1.1 | 1.1 |
| GSC_1.9 | 270 | 8.1 | 5.5 | 4.4 | 3.2 | 2.8 | 2.3 | 2.0 | 1.7 | 1.4 | 1.3 | 1.1 | 1.2 |
| GSC_1.10 | 300 | 8.7 | 5.8 | 4.6 | 3.5 | 3.0 | 2.6 | 2.2 | 1.8 | 1.4 | 1.4 | 1.2 | 1.2 |
| GSC_1.11 | 330 | 9.1 | 6.0 | 4.9 | 3.7 | 3.1 | 2.8 | 2.3 | 2.0 | 1.6 | 1.4 | 1.3 | 1.2 |
| GSC_1.12 | 370 | 9.6 | 6.3 | 5.2 | 3.9 | 3.3 | 2.8 | 2.4 | 2.1 | 1.8 | 1.5 | 1.4 | 1.3 |
| GSC_1.13 | 390 | 10.0 | 6.6 | 5.3 | 3.9 | 3.6 | 3.0 | 2.5 | 2.2 | 1.9 | 1.6 | 1.4 | 1.4 |
| GSC_1.14 | 430 | 10.6 | 6.9 | 5.6 | 4.0 | 3.6 | 3.2 | 2.6 | 2.2 | 1.9 | 1.6 | 1.5 | 1.5 |
| GSC_1.15 | 470 | 11.1 | 7.2 | 5.8 | 4.3 | 3.6 | 3.3 | 2.8 | 2.3 | 1.9 | 1.7 | 1.5 | 1.6 |
| GSC_1.16 | 530 | 11.8 | 7.4 | 6.1 | 4.5 | 3.7 | 3.3 | 2.7 | 2.3 | 1.9 | 1.7 | 1.6 | 1.5 |
| GSC_1.17 | 560 | 12.1 | 7.8 | 6.4 | 4.8 | 3.9 | 3.5 | 2.8 | 2.4 | 2.0 | 1.6 | 1.6 | 1.6 |
| GSC_1.18 | 620 | 12.5 | 8.4 | 6.7 | 4.9 | 3.8 | 3.5 | 2.9 | 2.5 | 2.0 | 1.7 | 1.6 | 1.7 |
| GSC_1.19 | 680 | 12.8 | 8.6 | 6.9 | 5.1 | 3.9 | 3.4 | 3.0 | 2.4 | 2.0 | 1.7 | 1.7 | 1.7 |
| GSC_1.20 | 740 | 13.0 | 8.7 | 7.0 | 5.1 | 3.9 | 3.4 | 3.0 | 2.5 | 2.0 | 1.8 | 1.7 | 1.6 |
| GSC_1.21 | 790 | 13.1 | 8.7 | 7.0 | 5.1 | 4.0 | 3.4 | 3.0 | 2.5 | 2.0 | 1.8 | 1.7 | 1.7 |
| GSC_1.22 | 15 | 2.8 | 2.1 | 1.6 | 1.3 | 1.1 | 0.8 | 0.8 | 0.7 | 0.5 | 0.4 | 0.4 | 0.6 |
| GSC_1.23 | 22 | 3.6 | 2.7 | 1.9 | 1.6 | 1.3 | 1.0 | 0.9 | 0.8 | 0.6 | 0.5 | 0.5 | 0.5 |

| (1) | (2) | (3) | (4) | (5) | (6) | (7) | (8) | (9) | (10) | (11) | (12) | (13) | (14) |
|---|---|---|---|---|---|---|---|---|---|---|---|---|---|
| GSC_1.24 | 35 | 4.7 | 3.1 | 2.2 | 1.8 | 1.6 | 1.2 | 1.0 | 1.0 | 0.8 | 0.7 | 0.6 | 0.4 |
| GSC_1.25 | 50 | 5.6 | 3.5 | 2.6 | 2.0 | 1.7 | 1.4 | 1.1 | 1.1 | 0.9 | 0.7 | 0.6 | 0.5 |
| GSC_1.26 | 65 | 6.4 | 3.9 | 2.9 | 2.3 | 1.8 | 1.4 | 1.2 | 1.0 | 0.9 | 0.7 | 0.7 | 0.7 |
| GSC_1.27 | 95 | 7.4 | 4.4 | 3.3 | 2.4 | 2.1 | 1.6 | 1.3 | 1.1 | 0.9 | 0.8 | 0.7 | 0.8 |
| GSC_1.28 | 125 | 8.2 | 5.0 | 3.8 | 2.9 | 2.3 | 1.8 | 1.4 | 1.3 | 1.0 | 0.8 | 0.8 | 0.7 |
| GSC_1.29 | 155 | 8.9 | 5.7 | 4.3 | 3.2 | 2.6 | 1.9 | 1.4 | 1.2 | 1.0 | 0.8 | 0.8 | 0.8 |
| GSC_1.30 | 185 | 9.6 | 6.3 | 4.7 | 3.6 | 2.6 | 2.0 | 1.5 | 1.1 | 0.9 | 0.9 | 1.0 | 1.0 |
| GSC_1.31 | 215 | 10.2 | 6.8 | 5.1 | 3.9 | 3.0 | 2.1 | 1.5 | 1.2 | 1.0 | 0.9 | 1.0 | 0.9 |
| GSC_1.32 | 275 | 11.1 | 7.4 | 5.6 | 4.2 | 3.3 | 2.3 | 1.6 | 1.3 | 1.0 | 1.1 | 1.1 | 1.2 |
| GSC_1.33 | 305 | 11.6 | 7.8 | 6.0 | 4.6 | 3.5 | 2.4 | 1.8 | 1.4 | 1.1 | 1.2 | 1.1 | 1.3 |
| GSC_1.34 | 335 | 12.1 | 8.2 | 6.3 | 5.0 | 3.8 | 2.7 | 1.9 | 1.4 | 1.2 | 1.4 | 1.3 | 1.2 |
| GSC_1.35 | 365 | 12.5 | 8.8 | 6.6 | 5.1 | 4.0 | 2.8 | 1.9 | 1.4 | 1.1 | 1.3 | 1.5 | 1.4 |
| GSC_1.36 | 395 | 12.9 | 9.2 | 6.9 | 5.2 | 4.1 | 3.0 | 2.0 | 1.5 | 1.3 | 1.5 | 1.6 | 1.6 |
| GSC_1.37 | 425 | 13.2 | 9.6 | 7.3 | 5.3 | 4.0 | 3.1 | 2.0 | 1.6 | 1.4 | 1.6 | 1.5 | 1.7 |
| GSC_1.38 | 485 | 13.7 | 10.2 | 7.8 | 5.6 | 4.3 | 3.3 | 2.2 | 1.8 | 1.7 | 1.8 | 1.6 | 1.8 |
| GSC_1.39 | 545 | 14.1 | 10.6 | 8.1 | 5.9 | 4.6 | 3.5 | 2.4 | 1.9 | 1.7 | 1.6 | 1.6 | 1.7 |
| GSC_1.40 | 575 | 14.4 | 11.0 | 8.3 | 6.1 | 4.9 | 3.8 | 2.8 | 2.0 | 1.8 | 1.7 | 1.6 | 1.6 |
| GSC_1.41 | 635 | 14.5 | 11.3 | 8.6 | 6.3 | 5.0 | 4.0 | 3.1 | 2.1 | 1.7 | 1.6 | 1.5 | 1.3 |
| GSC_1.42 | 695 | 14.6 | 11.3 | 8.7 | 6.4 | 5.1 | 4.0 | 3.1 | 2.2 | 1.6 | 1.5 | 1.5 | 1.4 |
| GSC_1.43 | 740 | 14.6 | 11.4 | 8.7 | 6.4 | 5.1 | 4.0 | 3.1 | 2.1 | 1.6 | 1.5 | 1.5 | 1.4 |
| GSC_1.44 | 15 | 2.9 | 2.1 | 1.6 | 1.1 | 0.9 | 0.8 | 1.0 | 0.8 | 0.7 | 0.8 | 0.6 | 0.7 |
| GSC_1.45 | 35 | 3.8 | 2.8 | 2.1 | 1.4 | 1.0 | 0.7 | 0.8 | 0.7 | 0.9 | 0.9 | 0.9 | 1.0 |
| GSC_1.46 | 50 | 4.3 | 3.2 | 2.6 | 1.6 | 1.1 | 0.8 | 0.8 | 0.8 | 0.9 | 1.0 | 1.0 | 1.0 |
| GSC_1.47 | 65 | 4.9 | 3.6 | 2.9 | 1.9 | 1.2 | 0.7 | 0.8 | 0.9 | 0.9 | 1.0 | 1.1 | 1.2 |
| GSC_1.48 | 80 | 5.5 | 4.0 | 3.2 | 2.2 | 1.3 | 0.9 | 0.9 | 0.9 | 1.0 | 1.0 | 1.2 | 1.2 |
| GSC_1.49 | 110 | 6.1 | 4.5 | 3.5 | 2.6 | 1.5 | 1.1 | 1.0 | 1.0 | 0.9 | 1.1 | 1.1 | 1.2 |
| GSC_1.50 | 125 | 6.8 | 4.9 | 3.9 | 2.9 | 1.7 | 1.2 | 1.0 | 0.8 | 0.9 | 1.0 | 1.1 | 1.3 |
| GSC_1.51 | 170 | 7.5 | 5.4 | 4.3 | 3.2 | 1.9 | 1.4 | 1.2 | 1.0 | 0.8 | 0.8 | 0.9 | 1.2 |
| GSC_1.52 | 260 | 8.8 | 6.1 | 4.9 | 3.6 | 2.3 | 1.6 | 1.3 | 1.1 | 1.1 | 1.0 | 1.0 | 1.1 |

| (1) | (2) | (3) | (4) | (5) | (6) | (7) | (8) | (9) | (10) | (11) | (12) | (13) | (14) |
|---|---|---|---|---|---|---|---|---|---|---|---|---|---|
| GSC_1.53 | 290 | 9.4 | 6.7 | 5.3 | 3.9 | 2.5 | 1.6 | 1.2 | 1.1 | 1.0 | 1.0 | 1.0 | 1.0 |
| GSC_1.54 | 320 | 10.0 | 7.1 | 5.6 | 4.0 | 2.8 | 1.9 | 1.3 | 1.0 | 0.9 | 1.0 | 1.1 | 1.0 |
| GSC_1.55 | 350 | 10.6 | 7.6 | 5.8 | 4.2 | 3.1 | 2.0 | 1.5 | 1.2 | 1.0 | 1.1 | 1.0 | 1.1 |
| GSC_1.56 | 380 | 11.2 | 8.1 | 6.2 | 4.4 | 3.4 | 2.3 | 1.7 | 1.4 | 1.2 | 1.1 | 1.0 | 0.9 |
| GSC_1.57 | 415 | 11.9 | 8.8 | 6.6 | 4.6 | 3.8 | 2.6 | 1.8 | 1.4 | 1.3 | 1.0 | 1.0 | 1.0 |
| GSC_1.58 | 445 | 12.8 | 9.3 | 7.1 | 5.0 | 4.1 | 2.8 | 1.4 | 1.2 | 0.9 | 0.9 | 1.0 | 0.9 |
| GSC_1.59 | 475 | 13.2 | 9.9 | 7.0 | 5.1 | 4.2 | 3.0 | 1.7 | 1.3 | 1.1 | 1.0 | 0.9 | 0.8 |
| GSC_1.60 | 525 | 13.4 | 10.1 | 7.2 | 5.3 | 4.3 | 3.0 | 1.8 | 1.4 | 1.2 | 1.0 | 0.8 | 0.9 |
| GSC_1.61 | 585 | 13.5 | 10.2 | 7.2 | 5.6 | 4.2 | 3.1 | 1.9 | 1.5 | 1.2 | 1.0 | 0.9 | 0.9 |
| GSC_1.62 | 645 | 13.5 | 10.2 | 7.4 | 5.8 | 4.3 | 3.2 | 2.0 | 1.4 | 1.2 | 1.0 | 1.0 | 0.9 |
| GSC_1.63 | 705 | 13.6 | 10.3 | 7.4 | 5.9 | 4.3 | 3.2 | 2.1 | 1.4 | 1.2 | 1.0 | 1.0 | 0.9 |
| GSC_1.64 | 750 | 13.6 | 10.3 | 7.5 | 5.9 | 4.2 | 3.2 | 2.1 | 1.4 | 1.1 | 1.0 | 1.0 | 0.9 |
| GSC_1.65 | 10 | 3.4 | 2.3 | 1.6 | 1.1 | 0.9 | 1.0 | 0.9 | 0.8 | 0.6 | 0.7 | 0.5 | 0.5 |
| GSC_1.66 | 30 | 4.9 | 3.1 | 2.2 | 1.3 | 1.0 | 0.9 | 0.9 | 1.0 | 0.8 | 0.7 | 0.7 | 0.6 |
| GSC_1.67 | 45 | 5.8 | 4.3 | 3.1 | 1.6 | 1.3 | 1.0 | 0.9 | 1.0 | 0.9 | 0.8 | 0.7 | 0.7 |
| GSC_1.68 | 60 | 6.8 | 5.3 | 3.5 | 2.4 | 1.6 | 1.2 | 1.0 | 0.9 | 0.9 | 0.8 | 0.8 | 0.7 |
| GSC_1.69 | 75 | 7.6 | 5.9 | 3.8 | 2.8 | 1.9 | 1.4 | 1.1 | 1.0 | 0.8 | 0.9 | 0.9 | 0.8 |
| GSC_1.70 | 90 | 8.3 | 6.6 | 4.1 | 3.2 | 2.2 | 1.6 | 1.2 | 0.9 | 1.0 | 1.0 | 0.9 | 0.9 |
| GSC_1.71 | 120 | 9.4 | 7.2 | 4.7 | 3.9 | 2.6 | 2.0 | 1.4 | 1.0 | 1.1 | 0.9 | 1.0 | 0.9 |
| GSC_1.72 | 150 | 10.2 | 8.0 | 5.2 | 4.1 | 3.0 | 2.2 | 1.6 | 1.3 | 1.1 | 1.0 | 0.9 | 1.1 |
| GSC_1.73 | 180 | 11.0 | 9.2 | 5.6 | 4.5 | 3.3 | 2.5 | 1.7 | 1.4 | 1.2 | 1.0 | 1.0 | 0.9 |
| GSC_1.74 | 260 | 12.2 | 10.0 | 6.2 | 5.1 | 3.8 | 2.8 | 2.1 | 1.5 | 1.3 | 1.2 | 1.1 | 1.1 |
| GSC_1.75 | 290 | 12.6 | 10.5 | 6.6 | 5.4 | 4.1 | 3.0 | 2.3 | 1.6 | 1.4 | 1.4 | 1.3 | 1.4 |
| GSC_1.76 | 320 | 13.0 | 10.8 | 7.0 | 5.7 | 4.2 | 3.1 | 2.5 | 1.7 | 1.4 | 1.6 | 1.5 | 1.4 |
| GSC_1.77 | 365 | 13.7 | 11.1 | 7.3 | 6.0 | 4.4 | 3.3 | 2.5 | 1.6 | 1.5 | 1.5 | 1.6 | 1.5 |
| GSC_1.78 | 410 | 14.3 | 11.2 | 7.2 | 6.4 | 4.6 | 3.6 | 2.6 | 1.5 | 1.6 | 1.6 | 1.7 | 1.5 |
| GSC_1.79 | 440 | 14.6 | 11.5 | 7.4 | 6.5 | 4.9 | 3.8 | 2.9 | 1.7 | 1.7 | 1.7 | 1.8 | 1.6 |
| GSC_1.80 | 500 | 15.0 | 11.8 | 7.6 | 6.7 | 5.1 | 4.2 | 3.1 | 2.1 | 1.9 | 1.9 | 1.8 | 1.9 |
| GSC_1.81 | 570 | 15.3 | 12.1 | 7.4 | 6.9 | 5.2 | 4.1 | 3.0 | 2.2 | 1.9 | 1.9 | 1.9 | 1.8 |

| (1) | (2) | (3) | (4) | (5) | (6) | (7) | (8) | (9) | (10) | (11) | (12) | (13) | (14) |
|---|---|---|---|---|---|---|---|---|---|---|---|---|---|
| GSC_1.82 | 695 | 15.3 | 12.1 | 7.5 | 6.9 | 5.2 | 4.1 | 3.1 | 2.2 | 2.0 | 1.9 | 1.9 | 1.8 |
| GSC_2.1 | 10 | 2.3 | 1.8 | 1.3 | 0.9 | 0.7 | 0.9 | 0.9 | 0.7 | 0.6 | 0.7 | 0.6 | 0.6 |
| GSC_2.2 | 25 | 3.5 | 2.3 | 1.7 | 1.3 | 1.0 | 1.1 | 1.0 | 0.9 | 0.9 | 0.8 | 0.7 | 0.8 |
| GSC_2.3 | 40 | 4.4 | 2.7 | 2.0 | 1.7 | 1.2 | 1.0 | 1.0 | 1.1 | 1.0 | 1.0 | 0.9 | 0.9 |
| GSC_2.4 | 55 | 5.1 | 3.1 | 2.3 | 2.1 | 1.4 | 1.1 | 1.2 | 1.1 | 0.9 | 0.9 | 1.0 | 0.9 |
| GSC_2.5 | 70 | 5.7 | 3.3 | 2.7 | 2.4 | 1.7 | 1.3 | 1.2 | 1.2 | 1.0 | 0.9 | 1.0 | 1.0 |
| GSC_2.6 | 85 | 6.2 | 3.8 | 3.0 | 2.8 | 1.9 | 1.6 | 1.3 | 1.4 | 1.3 | 1.0 | 1.1 | 1.1 |
| GSC_2.7 | 115 | 6.9 | 4.1 | 3.2 | 2.7 | 2.1 | 1.8 | 1.6 | 1.4 | 1.2 | 1.1 | 1.1 | 1.3 |
| GSC_2.8 | 145 | 7.5 | 3.9 | 3.4 | 3.0 | 2.4 | 1.9 | 1.6 | 1.6 | 1.3 | 1.2 | 0.9 | 1.1 |
| GSC_2.9 | 175 | 8.0 | 4.2 | 3.9 | 2.9 | 2.5 | 2.1 | 1.8 | 1.6 | 1.4 | 1.1 | 1.0 | 1.0 |
| GSC_2.10 | 215 | 8.6 | 4.8 | 4.3 | 3.3 | 2.7 | 2.3 | 1.9 | 1.6 | 1.3 | 1.1 | 0.9 | 1.1 |
| GSC_2.11 | 275 | 9.3 | 5.5 | 4.7 | 3.6 | 2.8 | 2.4 | 1.8 | 1.5 | 1.3 | 1.1 | 1.0 | 1.2 |
| GSC_2.12 | 315 | 9.7 | 6.2 | 5.2 | 4.0 | 2.9 | 2.3 | 1.8 | 1.4 | 1.2 | 1.0 | 1.1 | 1.1 |
| GSC_2.13 | 345 | 10.1 | 6.8 | 5.5 | 4.4 | 3.2 | 2.5 | 2.0 | 1.5 | 1.2 | 1.0 | 1.0 | 0.9 |
| GSC_2.14 | 420 | 11.0 | 7.4 | 5.9 | 4.9 | 3.4 | 2.5 | 2.1 | 1.4 | 1.1 | 1.0 | 0.9 | 0.9 |
| GSC_2.15 | 465 | 11.5 | 7.8 | 6.3 | 5.0 | 3.8 | 2.7 | 2.1 | 1.6 | 1.2 | 0.9 | 0.9 | 0.9 |
| GSC_2.16 | 555 | 12.2 | 8.1 | 6.4 | 5.2 | 4.1 | 2.9 | 2.2 | 1.8 | 1.4 | 1.0 | 0.9 | 0.8 |
| GSC_2.17 | 615 | 12.6 | 8.3 | 6.3 | 5.4 | 4.2 | 3.0 | 2.3 | 2.0 | 1.5 | 1.1 | 1.0 | 0.8 |
| GSC_2.18 | 675 | 12.8 | 8.4 | 6.4 | 5.3 | 4.2 | 3.1 | 2.1 | 1.9 | 1.5 | 1.1 | 1.0 | 0.9 |
| GSC_2.19 | 760 | 12.8 | 8.4 | 6.4 | 5.3 | 4.1 | 3.1 | 2.2 | 1.9 | 1.5 | 1.1 | 1.0 | 0.9 |
| GSC_2.20 | 10 | 3.1 | 2.2 | 1.6 | 1.2 | 1.0 | 1.0 | 0.9 | 0.9 | 0.7 | 0.7 | 0.7 | 0.8 |
| GSC_2.21 | 25 | 4.4 | 3.6 | 2.4 | 1.4 | 1.1 | 1.2 | 1.0 | 1.1 | 0.9 | 1.0 | 0.9 | 0.8 |
| GSC_2.22 | 45 | 5.6 | 4.8 | 3.3 | 2.0 | 1.5 | 1.3 | 1.1 | 1.0 | 1.1 | 1.2 | 1.0 | 1.0 |
| GSC_2.23 | 75 | 6.6 | 6.1 | 4.2 | 2.8 | 2.1 | 1.5 | 1.3 | 1.2 | 1.0 | 1.1 | 1.2 | 1.1 |
| GSC_2.24 | 90 | 7.1 | 6.9 | 4.8 | 3.1 | 2.3 | 1.6 | 1.4 | 1.2 | 1.3 | 1.3 | 1.4 | 1.3 |
| GSC_2.25 | 120 | 7.9 | 7.8 | 5.6 | 3.7 | 2.7 | 1.9 | 1.4 | 1.3 | 1.1 | 1.2 | 1.2 | 1.4 |
| GSC_2.26 | 165 | 9.2 | 8.5 | 6.3 | 4.3 | 3.4 | 2.2 | 1.6 | 1.4 | 1.2 | 1.0 | 1.1 | 1.1 |
| GSC_2.27 | 225 | 10.3 | 9.3 | 6.9 | 5.1 | 3.9 | 2.5 | 1.8 | 1.5 | 1.3 | 1.0 | 0.9 | 1.0 |
| GSC_2.28 | 240 | 11.3 | 10.1 | 7.4 | 5.5 | 4.2 | 2.7 | 2.1 | 1.5 | 1.4 | 1.1 | 1.0 | 1.0 |

| (1) | (2) | (3) | (4) | (5) | (6) | (7) | (8) | (9) | (10) | (11) | (12) | (13) | (14) |
|---|---|---|---|---|---|---|---|---|---|---|---|---|---|
| GSC_2.29 | 300 | 12.1 | 10.8 | 7.9 | 5.8 | 4.4 | 2.8 | 2.4 | 1.6 | 1.3 | 1.2 | 1.1 | 1.2 |
| GSC_2.30 | 360 | 12.9 | 11.4 | 8.3 | 6.2 | 4.8 | 3.0 | 2.5 | 1.9 | 1.5 | 1.3 | 1.2 | 1.4 |
| GSC_2.31 | 420 | 13.5 | 11.8 | 8.8 | 6.7 | 5.1 | 3.4 | 2.6 | 1.8 | 1.4 | 1.3 | 1.2 | 1.2 |
| GSC_2.32 | 480 | 13.9 | 12.1 | 9.0 | 7.0 | 5.2 | 3.7 | 2.8 | 1.9 | 1.5 | 1.2 | 1.1 | 1.0 |
| GSC_2.33 | 540 | 14.2 | 12.3 | 9.0 | 7.1 | 5.5 | 3.8 | 3.0 | 2.0 | 1.4 | 1.1 | 1.0 | 1.0 |
| GSC_2.34 | 600 | 14.3 | 12.2 | 9.1 | 7.0 | 5.7 | 3.9 | 3.0 | 2.1 | 1.2 | 1.0 | 0.9 | 1.0 |
| GSC_2.35 | 700 | 14.3 | 12.2 | 9.1 | 7.0 | 5.8 | 3.9 | 3.0 | 2.0 | 1.2 | 1.0 | 0.9 | 0.9 |
| GSC_2.36 | 15 | 2.5 | 2.0 | 1.5 | 1.2 | 1.1 | 0.9 | 0.9 | 1.0 | 0.8 | 0.7 | 0.7 | 0.8 |
| GSC_2.37 | 30 | 3.8 | 2.9 | 2.1 | 1.5 | 1.2 | 1.0 | 1.1 | 0.9 | 0.8 | 0.8 | 0.9 | 1.0 |
| GSC_2.38 | 45 | 4.9 | 3.6 | 2.8 | 1.9 | 1.3 | 1.1 | 1.0 | 0.9 | 1.0 | 0.9 | 1.0 | 1.2 |
| GSC_2.39 | 60 | 5.7 | 4.3 | 3.2 | 2.2 | 1.5 | 1.2 | 1.0 | 0.9 | 0.9 | 1.0 | 1.1 | 1.1 |
| GSC_2.40 | 75 | 6.6 | 4.9 | 3.6 | 2.7 | 1.8 | 1.3 | 1.1 | 1.0 | 0.9 | 0.9 | 1.0 | 1.2 |
| GSC_2.41 | 100 | 7.6 | 5.6 | 3.9 | 3.1 | 2.0 | 1.4 | 1.2 | 1.1 | 1.0 | 1.0 | 0.9 | 1.0 |
| GSC_2.42 | 130 | 8.7 | 6.4 | 4.5 | 3.6 | 2.4 | 1.6 | 1.3 | 1.0 | 0.8 | 0.9 | 0.9 | 0.9 |
| GSC_2.43 | 150 | 9.2 | 6.8 | 5.0 | 4.0 | 2.7 | 1.9 | 1.4 | 1.1 | 0.9 | 0.9 | 1.0 | 0.9 |
| GSC_2.44 | 175 | 9.7 | 7.3 | 5.7 | 4.4 | 3.1 | 2.2 | 1.6 | 1.2 | 1.0 | 1.0 | 1.2 | 0.9 |
| GSC_2.45 | 240 | 10.7 | 7.9 | 6.3 | 4.8 | 3.5 | 2.4 | 1.7 | 1.3 | 1.2 | 1.1 | 0.9 | 1.0 |
| GSC_2.46 | 270 | 11.1 | 8.4 | 6.7 | 5.2 | 3.9 | 2.6 | 1.7 | 1.3 | 1.2 | 1.3 | 1.1 | 1.1 |
| GSC_2.47 | 300 | 11.5 | 8.9 | 7.3 | 5.8 | 3.9 | 2.8 | 2.0 | 1.5 | 1.3 | 1.2 | 1.0 | 1.1 |
| GSC_2.48 | 345 | 12.1 | 9.5 | 7.9 | 6.2 | 4.3 | 3.2 | 2.1 | 1.6 | 1.4 | 1.3 | 1.3 | 1.2 |
| GSC_2.49 | 385 | 12.5 | 9.9 | 8.4 | 7.3 | 4.6 | 3.4 | 2.1 | 1.7 | 1.7 | 1.6 | 1.6 | 1.5 |
| GSC_2.50 | 430 | 13.1 | 10.4 | 9.0 | 7.9 | 5.1 | 3.6 | 2.3 | 1.8 | 1.5 | 1.4 | 1.4 | 1.4 |
| GSC_2.51 | 490 | 13.4 | 10.8 | 9.3 | 8.2 | 5.4 | 3.8 | 2.5 | 1.9 | 1.5 | 1.4 | 1.6 | 1.5 |
| GSC_2.52 | 565 | 13.6 | 11.1 | 9.7 | 8.7 | 5.8 | 4.1 | 2.8 | 2.0 | 1.4 | 1.2 | 1.4 | 1.5 |
| GSC_2.53 | 640 | 13.7 | 11.2 | 9.7 | 8.8 | 5.8 | 4.2 | 3.0 | 2.0 | 1.3 | 1.1 | 1.2 | 1.3 |
| GSC_2.54 | 740 | 13.7 | 11.2 | 9.7 | 8.8 | 5.8 | 4.3 | 3.0 | 2.0 | 1.3 | 1.1 | 1.2 | 1.2 |
| GSC_2.55 | 10 | 1.9 | 1.6 | 1.2 | 0.7 | 0.9 | 0.6 | 0.8 | 0.7 | 0.6 | 0.8 | 0.7 | 0.7 |
| GSC_2.56 | 25 | 3.0 | 2.1 | 1.6 | 1.0 | 0.8 | 0.7 | 0.8 | 0.9 | 0.8 | 0.8 | 0.8 | 0.7 |
| GSC_2.57 | 40 | 3.7 | 2.6 | 2.0 | 1.4 | 0.9 | 0.9 | 0.8 | 0.8 | 1.0 | 0.9 | 0.9 | 0.8 |

| (1) | (2) | (3) | (4) | (5) | (6) | (7) | (8) | (9) | (10) | (11) | (12) | (13) | (14) |
|---|---|---|---|---|---|---|---|---|---|---|---|---|---|
| GSC_2.58 | 55 | 4.3 | 3.1 | 2.3 | 1.5 | 1.2 | 1.0 | 0.8 | 0.7 | 0.9 | 1.0 | 0.9 | 0.9 |
| GSC_2.59 | 80 | 5.4 | 3.7 | 2.1 | 1.8 | 1.4 | 1.1 | 0.9 | 1.0 | 0.9 | 0.9 | 1.0 | 1.1 |
| GSC_2.60 | 110 | 5.9 | 4.0 | 2.5 | 2.2 | 1.6 | 1.3 | 1.0 | 1.1 | 1.0 | 0.9 | 1.0 | 1.1 |
| GSC_2.61 | 140 | 6.6 | 3.9 | 2.9 | 2.6 | 2.1 | 1.5 | 1.3 | 1.2 | 1.0 | 1.1 | 1.0 | 1.0 |
| GSC_2.62 | 200 | 7.6 | 4.3 | 3.4 | 2.9 | 2.4 | 1.7 | 1.4 | 1.1 | 1.1 | 1.0 | 1.1 | 1.2 |
| GSC_2.63 | 230 | 8.1 | 4.6 | 3.9 | 3.1 | 2.5 | 2.1 | 1.6 | 1.2 | 1.0 | 0.9 | 1.1 | 1.1 |
| GSC_2.64 | 265 | 8.6 | 5.0 | 4.2 | 3.3 | 2.8 | 2.2 | 1.8 | 1.4 | 1.1 | 1.0 | 1.0 | 1.0 |
| GSC_2.65 | 295 | 8.9 | 5.4 | 4.5 | 3.6 | 2.8 | 2.3 | 1.5 | 1.3 | 1.1 | 1.1 | 0.9 | 1.0 |
| GSC_2.66 | 325 | 9.1 | 5.8 | 4.6 | 4.0 | 3.0 | 2.6 | 1.6 | 1.3 | 1.2 | 1.0 | 1.0 | 1.1 |
| GSC_2.67 | 355 | 9.4 | 4.7 | 3.3 | 2.3 | 2.3 | 1.8 | 1.5 | 1.2 | 1.2 | 0.8 | 0.7 | 0.6 |
| GSC_2.68 | 385 | 9.8 | 4.9 | 3.6 | 2.7 | 2.4 | 1.9 | 1.4 | 1.1 | 1.1 | 0.9 | 0.9 | 0.7 |
| GSC_2.69 | 415 | 10.2 | 5.1 | 3.7 | 3.0 | 2.6 | 2.0 | 1.6 | 1.2 | 1.0 | 0.8 | 0.8 | 0.8 |
| GSC_2.70 | 445 | 10.4 | 5.1 | 4.1 | 3.3 | 3.0 | 2.1 | 1.7 | 1.3 | 1.1 | 0.9 | 0.9 | 0.8 |
| GSC_2.71 | 475 | 10.8 | 5.8 | 4.6 | 3.6 | 3.2 | 2.1 | 1.7 | 1.4 | 1.1 | 1.0 | 1.0 | 0.8 |
| GSC_2.72 | 505 | 11.1 | 6.2 | 5.1 | 4.0 | 3.4 | 2.3 | 1.8 | 1.3 | 1.0 | 1.0 | 1.1 | 1.0 |
| GSC_2.73 | 550 | 11.6 | 6.6 | 5.5 | 4.4 | 3.6 | 2.6 | 2.0 | 1.4 | 1.2 | 0.9 | 0.9 | 0.9 |
| GSC_2.74 | 615 | 12.0 | 7.0 | 5.8 | 4.8 | 3.7 | 2.7 | 2.1 | 1.6 | 1.1 | 1.0 | 0.8 | 0.8 |
| GSC_2.75 | 675 | 12.3 | 7.3 | 6.0 | 5.1 | 4.0 | 2.8 | 2.2 | 1.5 | 1.2 | 0.9 | 0.8 | 0.9 |
| GSC_2.76 | 720 | 12.4 | 7.4 | 6.2 | 5.2 | 4.1 | 2.8 | 2.1 | 1.6 | 1.3 | 1.0 | 0.9 | 0.9 |
| GSC_2.77 | 765 | 12.4 | 7.5 | 6.3 | 5.1 | 4.1 | 3.0 | 2.0 | 1.6 | 1.3 | 1.1 | 0.9 | 0.8 |
| GSC_2.78 | 810 | 12.4 | 7.5 | 6.3 | 5.1 | 4.1 | 3.0 | 2.1 | 1.6 | 1.3 | 1.1 | 0.9 | 0.8 |
| GSC_3.1 | 15 | 1.8 | 1.4 | 1.1 | 0.9 | 1.1 | 0.8 | 0.7 | 0.5 | 0.5 | 0.7 | 0.7 | 0.9 |
| GSC_3.2 | 30 | 2.7 | 2.0 | 1.7 | 1.4 | 1.2 | 0.9 | 0.7 | 0.7 | 0.8 | 0.9 | 0.9 | 0.9 |
| GSC_3.3 | 45 | 3.5 | 2.8 | 2.3 | 1.7 | 1.4 | 1.0 | 0.8 | 0.9 | 0.8 | 0.9 | 1.0 | 1.0 |
| GSC_3.4 | 60 | 4.3 | 3.7 | 2.9 | 2.1 | 1.6 | 1.2 | 1.1 | 0.9 | 0.9 | 1.0 | 1.0 | 1.1 |
| GSC_3.5 | 80 | 5.1 | 4.3 | 3.4 | 2.6 | 2.0 | 1.5 | 1.1 | 1.0 | 1.0 | 0.9 | 1.1 | 1.0 |
| GSC_3.6 | 110 | 5.7 | 4.8 | 3.9 | 2.9 | 2.2 | 1.8 | 1.2 | 1.1 | 0.9 | 1.1 | 1.2 | 1.2 |
| GSC_3.7 | 140 | 6.1 | 5.3 | 4.4 | 3.2 | 2.3 | 1.8 | 1.3 | 1.2 | 1.0 | 1.0 | 1.1 | 1.3 |
| GSC_3.8 | 210 | 6.9 | 5.9 | 4.9 | 3.1 | 2.5 | 1.7 | 1.4 | 1.1 | 1.0 | 1.1 | 1.1 | 1.2 |

| (1) | (2) | (3) | (4) | (5) | (6) | (7) | (8) | (9) | (10) | (11) | (12) | (13) | (14) |
|---|---|---|---|---|---|---|---|---|---|---|---|---|---|
| GSC_3.9 | 240 | 7.3 | 6.4 | 5.3 | 3.3 | 2.7 | 1.6 | 1.2 | 1.1 | 1.0 | 1.0 | 1.1 | 1.1 |
| GSC_3.10 | 270 | 7.8 | 6.7 | 5.6 | 3.4 | 2.8 | 1.9 | 1.4 | 1.2 | 1.0 | 1.1 | 1.0 | 1.1 |
| GSC_3.11 | 300 | 8.2 | 7.1 | 5.8 | 3.6 | 2.8 | 1.9 | 1.6 | 1.3 | 1.1 | 1.1 | 1.2 | 1.2 |
| GSC_3.12 | 330 | 8.5 | 7.4 | 6.0 | 3.7 | 3.0 | 2.1 | 1.7 | 1.5 | 1.2 | 1.1 | 1.1 | 1.1 |
| GSC_3.13 | 390 | 9.1 | 7.7 | 6.3 | 3.9 | 3.1 | 2.0 | 1.6 | 1.6 | 1.3 | 1.2 | 1.1 | 1.0 |
| GSC_3.14 | 425 | 9.5 | 7.6 | 6.1 | 3.8 | 3.0 | 2.2 | 1.8 | 1.7 | 1.4 | 1.2 | 1.0 | 1.0 |
| GSC_3.15 | 455 | 9.9 | 7.8 | 6.4 | 3.5 | 2.9 | 2.4 | 2.1 | 1.6 | 1.3 | 1.1 | 1.1 | 1.0 |
| GSC_3.16 | 495 | 10.3 | 8.1 | 6.5 | 3.6 | 3.1 | 2.4 | 2.0 | 1.7 | 1.3 | 1.2 | 1.1 | 1.1 |
| GSC_3.17 | 525 | 10.6 | 8.4 | 6.7 | 3.8 | 3.2 | 2.5 | 2.2 | 1.8 | 1.4 | 1.1 | 1.0 | 1.0 |
| GSC_3.18 | 555 | 10.9 | 8.6 | 6.8 | 3.9 | 3.2 | 2.6 | 2.2 | 1.8 | 1.5 | 1.3 | 1.0 | 0.9 |
| GSC_3.19 | 585 | 11.1 | 8.5 | 6.7 | 4.0 | 3.2 | 2.7 | 2.3 | 2.0 | 1.6 | 1.4 | 0.9 | 1.0 |
| GSC_3.20 | 665 | 11.2 | 8.7 | 6.6 | 4.1 | 3.3 | 2.8 | 2.4 | 2.0 | 1.7 | 1.4 | 1.0 | 0.9 |
| GSC_3.21 | 710 | 11.3 | 8.9 | 6.7 | 4.3 | 3.4 | 3.0 | 2.6 | 2.2 | 1.8 | 1.3 | 0.9 | 0.9 |
| GSC_3.22 | 775 | 11.4 | 8.9 | 6.8 | 4.2 | 3.6 | 3.0 | 2.6 | 2.3 | 1.8 | 1.4 | 1.0 | 0.9 |
| GSC_3.23 | 830 | 11.4 | 8.9 | 6.8 | 4.2 | 3.5 | 3.0 | 2.6 | 2.2 | 1.8 | 1.4 | 0.9 | 0.9 |
| GSC_3.24 | 10 | 2.5 | 1.8 | 1.4 | 1.1 | 0.9 | 0.8 | 0.8 | 0.6 | 0.7 | 0.6 | 0.7 | 0.7 |
| GSC_3.25 | 25 | 3.5 | 2.7 | 2.1 | 1.6 | 1.4 | 1.1 | 0.9 | 0.8 | 0.7 | 0.7 | 0.6 | 0.6 |
| GSC_3.26 | 40 | 4.3 | 3.5 | 2.8 | 2.0 | 1.5 | 1.2 | 1.0 | 0.8 | 0.8 | 0.7 | 0.7 | 0.6 |
| GSC_3.27 | 55 | 5.1 | 4.0 | 3.4 | 2.6 | 1.9 | 1.4 | 1.1 | 0.9 | 0.8 | 0.7 | 0.7 | 0.7 |
| GSC_3.28 | 75 | 5.9 | 4.6 | 4.1 | 3.0 | 2.3 | 1.6 | 1.1 | 0.9 | 0.8 | 0.8 | 0.7 | 0.6 |
| GSC_3.29 | 100 | 6.7 | 5.2 | 4.6 | 3.5 | 2.7 | 1.9 | 1.3 | 1.0 | 1.0 | 0.9 | 0.8 | 0.8 |
| GSC_3.30 | 130 | 7.6 | 6.2 | 5.0 | 3.9 | 3.0 | 2.3 | 1.4 | 1.0 | 0.9 | 0.9 | 1.0 | 0.9 |
| GSC_3.31 | 175 | 8.5 | 6.9 | 5.3 | 4.4 | 3.4 | 2.6 | 1.5 | 1.1 | 1.0 | 1.0 | 1.1 | 1.1 |
| GSC_3.32 | 235 | 9.4 | 7.6 | 5.8 | 4.7 | 3.8 | 2.9 | 1.7 | 1.3 | 1.1 | 1.1 | 1.0 | 1.0 |
| GSC_3.33 | 295 | 10.1 | 8.4 | 6.5 | 5.2 | 4.2 | 3.1 | 1.9 | 1.4 | 1.2 | 1.0 | 1.0 | 1.0 |
| GSC_3.34 | 355 | 10.9 | 9.0 | 7.0 | 5.7 | 4.9 | 3.5 | 2.2 | 1.6 | 1.3 | 1.1 | 1.0 | 0.9 |
| GSC_3.35 | 415 | 11.5 | 9.6 | 7.3 | 5.9 | 5.2 | 4.0 | 2.6 | 1.9 | 1.4 | 1.0 | 0.9 | 0.9 |
| GSC_3.36 | 475 | 12.1 | 10.2 | 7.9 | 6.2 | 5.2 | 4.4 | 2.8 | 2.2 | 1.3 | 1.1 | 1.0 | 0.9 |
| GSC_3.37 | 535 | 12.5 | 10.9 | 7.6 | 6.4 | 5.5 | 4.6 | 3.0 | 2.1 | 1.4 | 1.2 | 1.1 | 1.1 |

| (1) | (2) | (3) | (4) | (5) | (6) | (7) | (8) | (9) | (10) | (11) | (12) | (13) | (14) |
|---|---|---|---|---|---|---|---|---|---|---|---|---|---|
| GSC_3.38 | 595 | 12.8 | 11.2 | 7.5 | 6.8 | 5.7 | 4.7 | 3.4 | 2.3 | 1.6 | 1.2 | 1.0 | 1.0 |
| GSC_3.39 | 655 | 13.0 | 11.3 | 7.7 | 6.9 | 5.9 | 4.8 | 3.6 | 2.2 | 1.7 | 1.1 | 1.0 | 0.9 |
| GSC_3.40 | 745 | 13.1 | 11.3 | 7.7 | 6.9 | 5.9 | 4.8 | 3.7 | 2.2 | 1.7 | 1.1 | 1.0 | 1.0 |
| GSC_3.41 | 15 | 2.0 | 1.6 | 1.2 | 0.9 | 0.9 | 0.8 | 0.9 | 0.6 | 0.7 | 0.6 | 0.6 | 0.5 |
| GSC_3.42 | 30 | 3.0 | 2.3 | 1.8 | 1.4 | 1.1 | 0.9 | 0.8 | 0.7 | 0.8 | 0.7 | 0.6 | 0.6 |
| GSC_3.43 | 45 | 3.8 | 3.0 | 2.3 | 1.9 | 1.3 | 1.0 | 0.9 | 0.8 | 0.8 | 0.7 | 0.8 | 0.7 |
| GSC_3.44 | 60 | 4.5 | 3.6 | 2.9 | 2.4 | 1.4 | 1.2 | 1.0 | 0.9 | 0.7 | 0.8 | 0.8 | 0.8 |
| GSC_3.45 | 75 | 5.3 | 4.2 | 3.4 | 2.8 | 1.7 | 1.4 | 1.1 | 1.1 | 0.8 | 0.9 | 0.9 | 0.8 |
| GSC_3.46 | 90 | 6.0 | 4.9 | 4.0 | 3.0 | 2.0 | 1.5 | 1.1 | 1.0 | 0.9 | 0.9 | 0.8 | 0.8 |
| GSC_3.47 | 105 | 6.6 | 5.4 | 4.3 | 3.3 | 1.9 | 1.5 | 1.2 | 1.0 | 1.1 | 1.0 | 1.0 | 0.9 |
| GSC_3.48 | 120 | 7.2 | 6.0 | 4.6 | 3.5 | 2.1 | 1.6 | 1.3 | 1.2 | 1.0 | 1.0 | 1.1 | 1.1 |
| GSC_3.49 | 135 | 7.6 | 6.7 | 5.0 | 3.7 | 2.2 | 1.8 | 1.4 | 1.3 | 1.1 | 1.1 | 1.0 | 0.9 |
| GSC_3.50 | 150 | 7.9 | 7.0 | 5.3 | 3.8 | 2.1 | 1.7 | 1.4 | 1.2 | 1.1 | 1.1 | 1.0 | 1.0 |
| GSC_3.51 | 180 | 8.4 | 7.4 | 5.5 | 3.8 | 2.4 | 1.9 | 1.5 | 1.2 | 1.0 | 1.0 | 0.9 | 1.0 |
| GSC_3.52 | 210 | 8.8 | 7.7 | 5.8 | 4.0 | 2.4 | 2.1 | 1.5 | 1.3 | 1.1 | 1.1 | 1.0 | 0.9 |
| GSC_3.53 | 240 | 9.1 | 8.1 | 6.0 | 3.9 | 2.8 | 2.2 | 1.7 | 1.4 | 1.2 | 1.1 | 1.0 | 1.0 |
| GSC_3.54 | 270 | 9.5 | 8.6 | 6.4 | 3.8 | 3.0 | 2.5 | 1.9 | 1.5 | 1.2 | 1.2 | 1.1 | 1.0 |
| GSC_3.55 | 300 | 9.8 | 9.0 | 6.7 | 4.0 | 3.1 | 2.5 | 2.0 | 1.5 | 1.3 | 1.3 | 1.2 | 1.0 |
| GSC_3.56 | 345 | 10.3 | 9.4 | 6.9 | 4.1 | 3.3 | 2.6 | 2.1 | 1.6 | 1.4 | 1.3 | 1.3 | 1.2 |
| GSC_3.57 | 375 | 10.6 | 9.7 | 7.0 | 4.0 | 3.5 | 2.7 | 2.2 | 1.7 | 1.4 | 1.3 | 1.2 | 1.1 |
| GSC_3.58 | 405 | 10.9 | 9.8 | 7.2 | 4.0 | 3.8 | 2.8 | 2.4 | 2.0 | 1.5 | 1.2 | 1.1 | 1.1 |
| GSC_3.59 | 450 | 11.3 | 10.1 | 7.5 | 4.2 | 3.8 | 3.0 | 2.5 | 2.1 | 1.6 | 1.3 | 1.2 | 1.0 |
| GSC_3.60 | 480 | 11.5 | 10.4 | 7.8 | 4.3 | 4.1 | 3.0 | 2.6 | 2.3 | 1.7 | 1.3 | 1.1 | 1.0 |
| GSC_3.61 | 510 | 11.6 | 10.5 | 7.9 | 4.5 | 3.9 | 3.2 | 2.6 | 2.2 | 1.8 | 1.4 | 1.1 | 1.1 |
| GSC_3.62 | 540 | 11.7 | 10.6 | 8.0 | 4.6 | 4.1 | 3.3 | 2.5 | 2.1 | 1.8 | 1.3 | 1.2 | 1.2 |
| GSC_3.63 | 585 | 11.8 | 10.8 | 8.2 | 4.7 | 4.2 | 3.2 | 2.6 | 2.2 | 1.7 | 1.4 | 1.2 | 1.1 |
| GSC_3.64 | 630 | 11.9 | 11.0 | 8.1 | 4.7 | 4.2 | 3.1 | 2.6 | 2.1 | 1.7 | 1.3 | 1.0 | 1.0 |
| GSC_3.65 | 690 | 11.9 | 11.2 | 8.1 | 4.7 | 4.3 | 3.1 | 2.6 | 2.2 | 1.7 | 1.2 | 1.0 | 0.9 |
| GSC_3.66 | 770 | 11.9 | 11.2 | 8.1 | 4.7 | 4.3 | 3.1 | 2.6 | 2.1 | 1.7 | 1.2 | 1.0 | 0.9 |

| (1) | (2) | (3) | (4) | (5) | (6) | (7) | (8) | (9) | (10) | (11) | (12) | (13) | (14) |
|---|---|---|---|---|---|---|---|---|---|---|---|---|---|
| GSC_3.67 | 15 | 2.8 | 2.1 | 2.2 | 1.6 | 1.1 | 0.8 | 0.9 | 0.7 | 0.7 | 0.6 | 0.6 | 0.7 |
| GSC_3.68 | 30 | 4.0 | 2.9 | 2.6 | 1.9 | 1.4 | 1.0 | 1.0 | 0.9 | 0.8 | 0.8 | 0.9 | 0.9 |
| GSC_3.69 | 45 | 4.9 | 3.7 | 3.2 | 2.2 | 1.5 | 1.2 | 1.0 | 0.8 | 0.9 | 0.9 | 0.8 | 0.9 |
| GSC_3.70 | 75 | 5.9 | 4.6 | 3.7 | 2.6 | 1.7 | 1.3 | 1.2 | 1.0 | 0.9 | 0.8 | 0.9 | 0.9 |
| GSC_3.71 | 105 | 6.7 | 5.2 | 4.2 | 3.0 | 1.9 | 1.4 | 1.1 | 1.0 | 1.0 | 0.9 | 1.0 | 1.1 |
| GSC_3.72 | 135 | 7.4 | 5.7 | 4.6 | 3.5 | 2.4 | 1.5 | 1.2 | 0.9 | 1.1 | 1.1 | 1.1 | 1.0 |
| GSC_3.73 | 180 | 8.4 | 6.3 | 5.0 | 4.0 | 2.8 | 1.7 | 1.3 | 1.1 | 1.1 | 1.0 | 1.1 | 1.1 |
| GSC_3.74 | 225 | 9.1 | 6.8 | 5.5 | 4.4 | 3.1 | 2.0 | 1.5 | 1.3 | 1.2 | 1.1 | 1.2 | 1.0 |
| GSC_3.75 | 255 | 9.6 | 7.4 | 6.0 | 4.8 | 3.4 | 2.4 | 1.7 | 1.3 | 1.1 | 0.9 | 1.0 | 0.9 |
| GSC_3.76 | 285 | 10.0 | 7.9 | 5.4 | 5.0 | 3.7 | 2.8 | 1.9 | 1.4 | 1.1 | 1.0 | 0.9 | 0.9 |
| GSC_3.77 | 315 | 10.4 | 8.2 | 5.8 | 5.2 | 3.8 | 2.7 | 2.0 | 1.4 | 1.0 | 0.9 | 1.0 | 0.9 |
| GSC_3.78 | 350 | 10.9 | 8.5 | 6.1 | 5.4 | 4.1 | 3.0 | 2.1 | 1.6 | 1.0 | 0.9 | 0.9 | 0.8 |
| GSC_3.79 | 370 | 11.1 | 8.7 | 6.2 | 5.4 | 4.2 | 3.0 | 2.0 | 1.6 | 1.1 | 1.0 | 0.9 | 0.9 |
| GSC_3.80 | 400 | 11.5 | 8.6 | 6.4 | 5.7 | 4.4 | 3.2 | 2.0 | 1.5 | 1.2 | 1.1 | 1.0 | 0.9 |
| GSC_3.81 | 430 | 11.8 | 9.0 | 6.7 | 5.8 | 4.6 | 3.3 | 2.2 | 1.5 | 1.1 | 1.1 | 1.0 | 1.0 |
| GSC_3.82 | 460 | 12.1 | 9.4 | 7.0 | 5.9 | 4.7 | 3.2 | 2.2 | 1.6 | 1.2 | 1.0 | 1.0 | 0.9 |
| GSC_3.83 | 490 | 12.4 | 9.7 | 7.2 | 6.2 | 5.0 | 3.3 | 2.4 | 1.6 | 1.3 | 1.1 | 1.0 | 1.0 |
| GSC_3.84 | 520 | 12.6 | 9.8 | 7.4 | 6.3 | 5.2 | 3.5 | 2.6 | 1.7 | 1.2 | 1.0 | 1.0 | 0.9 |
| GSC_3.85 | 550 | 12.8 | 10.1 | 7.7 | 6.6 | 5.4 | 3.7 | 2.7 | 1.6 | 1.3 | 1.1 | 1.1 | 1.0 |
| GSC_3.86 | 615 | 13.1 | 10.4 | 8.1 | 7.0 | 5.7 | 3.8 | 2.6 | 1.7 | 1.3 | 0.9 | 0.8 | 1.0 |
| GSC_3.87 | 645 | 13.2 | 10.7 | 8.2 | 7.3 | 5.9 | 4.0 | 2.8 | 1.7 | 1.2 | 1.0 | 0.8 | 0.9 |
| GSC_3.88 | 675 | 13.4 | 11.1 | 8.3 | 7.2 | 6.0 | 4.0 | 2.9 | 2.0 | 1.4 | 1.3 | 1.0 | 1.0 |
| GSC_3.89 | 705 | 13.5 | 11.2 | 8.6 | 7.3 | 6.2 | 4.2 | 3.0 | 2.2 | 1.6 | 1.2 | 0.9 | 0.9 |
| GSC_3.90 | 735 | 13.5 | 11.4 | 8.7 | 7.5 | 6.2 | 4.3 | 3.0 | 2.1 | 1.5 | 1.2 | 1.0 | 0.9 |
| GSC_3.91 | 765 | 13.6 | 11.4 | 8.9 | 7.6 | 6.2 | 4.2 | 3.2 | 2.2 | 1.7 | 1.3 | 0.9 | 0.8 |
| GSC_3.92 | 795 | 13.6 | 11.4 | 9.0 | 7.6 | 6.2 | 4.2 | 3.1 | 2.2 | 1.7 | 1.3 | 0.9 | 0.8 |
| GSC_4.1 | 15 | 1.4 | 0.9 | 0.8 | 0.7 | 0.7 | 0.5 | 0.6 | 0.5 | 0.5 | 0.6 | 0.5 | 0.3 |
| GSC_4.2 | 30 | 2.2 | 1.3 | 1.2 | 1.0 | 1.1 | 0.9 | 0.7 | 0.6 | 0.7 | 0.8 | 0.6 | 0.5 |
| GSC_4.3 | 50 | 2.8 | 1.2 | 1.7 | 1.4 | 1.3 | 1.1 | 1.0 | 0.8 | 0.8 | 0.9 | 0.6 | 0.6 |

| (1) | (2) | (3) | (4) | (5) | (6) | (7) | (8) | (9) | (10) | (11) | (12) | (13) | (14) |
|---|---|---|---|---|---|---|---|---|---|---|---|---|---|
| GSC_4.4 | 90 | 3.6 | 2.0 | 1.6 | 1.6 | 1.4 | 1.5 | 1.2 | 1.1 | 0.9 | 0.9 | 0.8 | 0.7 |
| GSC_4.5 | 120 | 4.2 | 2.2 | 1.9 | 1.8 | 1.7 | 1.7 | 1.4 | 1.2 | 1.0 | 1.1 | 1.0 | 0.9 |
| GSC_4.6 | 150 | 4.6 | 2.8 | 2.2 | 1.9 | 2.0 | 1.9 | 1.5 | 1.3 | 1.1 | 1.0 | 1.0 | 0.9 |
| GSC_4.7 | 235 | 5.4 | 3.6 | 2.6 | 2.2 | 1.9 | 1.7 | 1.6 | 1.4 | 1.2 | 1.1 | 1.0 | 0.9 |
| GSC_4.8 | 280 | 6.0 | 4.0 | 3.1 | 2.6 | 2.3 | 2.0 | 1.7 | 1.4 | 1.1 | 1.0 | 0.9 | 0.9 |
| GSC_4.9 | 340 | 6.7 | 4.6 | 3.5 | 2.9 | 2.6 | 2.2 | 1.8 | 1.5 | 1.2 | 1.0 | 0.9 | 0.9 |
| GSC_4.10 | 415 | 7.3 | 5.2 | 4.1 | 3.3 | 3.1 | 2.6 | 2.0 | 1.5 | 1.1 | 1.0 | 0.8 | 0.7 |
| GSC_4.11 | 475 | 8.0 | 5.4 | 4.6 | 3.7 | 3.2 | 2.5 | 1.9 | 1.6 | 1.2 | 1.1 | 0.8 | 0.8 |
| GSC_4.12 | 535 | 8.5 | 5.6 | 5.0 | 4.1 | 3.3 | 2.7 | 1.8 | 1.4 | 1.1 | 1.0 | 0.9 | 0.9 |
| GSC_4.13 | 615 | 9.1 | 5.5 | 5.2 | 4.4 | 3.5 | 3.0 | 1.9 | 1.3 | 1.0 | 0.9 | 0.9 | 0.8 |
| GSC_4.14 | 705 | 9.7 | 6.2 | 5.6 | 4.7 | 3.8 | 3.2 | 2.1 | 1.5 | 1.2 | 0.9 | 0.8 | 0.7 |
| GSC_4.15 | 780 | 10.0 | 6.4 | 5.9 | 5.0 | 4.0 | 3.3 | 2.1 | 1.4 | 1.1 | 0.9 | 0.8 | 0.8 |
| GSC_4.16 | 840 | 10.2 | 6.5 | 5.9 | 5.0 | 4.0 | 3.4 | 2.2 | 1.6 | 1.2 | 0.9 | 0.9 | 0.8 |
| GSC_4.17 | 930 | 10.2 | 6.5 | 5.9 | 5.0 | 4.1 | 3.4 | 2.2 | 1.6 | 1.1 | 0.9 | 0.9 | 0.8 |
| GSC_4.18 | 15 | 2.1 | 1.7 | 1.3 | 1.2 | 0.9 | 0.8 | 0.7 | 0.6 | 0.6 | 0.5 | 0.7 | 0.7 |
| GSC_4.19 | 30 | 3.2 | 2.5 | 1.9 | 1.8 | 1.7 | 1.4 | 1.2 | 1.1 | 1.0 | 0.7 | 0.8 | 0.9 |
| GSC_4.20 | 60 | 4.2 | 3.3 | 2.7 | 2.4 | 2.1 | 1.8 | 1.5 | 1.1 | 1.0 | 0.8 | 0.9 | 0.9 |
| GSC_4.21 | 90 | 5.0 | 4.0 | 3.3 | 3.0 | 2.4 | 2.0 | 1.7 | 1.3 | 1.1 | 0.9 | 0.9 | 1.0 |
| GSC_4.22 | 135 | 6.1 | 4.7 | 3.8 | 3.6 | 2.5 | 2.2 | 2.0 | 1.4 | 1.2 | 1.1 | 0.9 | 1.1 |
| GSC_4.23 | 180 | 7.0 | 5.6 | 4.4 | 4.4 | 2.5 | 2.4 | 2.0 | 1.6 | 1.5 | 1.2 | 1.0 | 1.0 |
| GSC_4.24 | 270 | 8.1 | 6.7 | 5.2 | 4.8 | 2.7 | 2.5 | 2.3 | 1.7 | 1.6 | 1.4 | 1.4 | 1.1 |
| GSC_4.25 | 315 | 8.8 | 7.8 | 5.8 | 5.1 | 2.9 | 2.7 | 2.5 | 1.8 | 1.5 | 1.3 | 1.3 | 1.2 |
| GSC_4.26 | 405 | 9.8 | 9.1 | 6.3 | 5.3 | 3.1 | 3.1 | 2.6 | 1.7 | 1.4 | 1.2 | 1.1 | 1.2 |
| GSC_4.27 | 465 | 10.5 | 10.2 | 6.8 | 5.5 | 3.4 | 3.3 | 2.8 | 1.7 | 1.4 | 1.2 | 1.0 | 1.0 |
| GSC_4.28 | 540 | 11.2 | 10.9 | 7.1 | 5.6 | 3.4 | 3.2 | 3.0 | 1.9 | 1.6 | 1.1 | 1.0 | 0.9 |
| GSC_4.29 | 615 | 11.5 | 11.3 | 7.0 | 5.8 | 3.5 | 3.3 | 3.2 | 2.0 | 1.4 | 1.0 | 0.9 | 0.9 |
| GSC_4.30 | 690 | 11.7 | 11.3 | 7.1 | 5.8 | 3.6 | 3.4 | 3.1 | 1.9 | 1.4 | 1.0 | 0.9 | 0.9 |
| GSC_4.31 | 790 | 11.8 | 11.3 | 7.1 | 5.8 | 3.6 | 3.4 | 3.1 | 1.9 | 1.3 | 1.0 | 0.9 | 0.9 |
| GSC_4.32 | 15 | 1.6 | 1.9 | 1.1 | 0.9 | 0.8 | 0.7 | 0.7 | 0.4 | 0.6 | 0.6 | 0.5 | 0.5 |

| (1) | (2) | (3) | (4) | (5) | (6) | (7) | (8) | (9) | (10) | (11) | (12) | (13) | (14) |
|---|---|---|---|---|---|---|---|---|---|---|---|---|---|
| GSC_4.33 | 35 | 2.6 | 2.4 | 1.7 | 1.3 | 1.5 | 1.0 | 0.7 | 0.6 | 0.8 | 0.7 | 0.8 | 0.9 |
| GSC_4.34 | 55 | 3.3 | 3.1 | 2.5 | 1.7 | 1.3 | 1.1 | 0.8 | 0.7 | 0.9 | 0.9 | 1.0 | 0.9 |
| GSC_4.35 | 85 | 4.0 | 3.8 | 3.0 | 2.1 | 1.5 | 1.2 | 1.1 | 1.0 | 0.6 | 0.7 | 0.8 | 1.0 |
| GSC_4.36 | 130 | 4.8 | 4.6 | 3.7 | 2.5 | 1.6 | 1.4 | 1.0 | 0.9 | 0.7 | 0.7 | 0.9 | 1.0 |
| GSC_4.37 | 175 | 5.4 | 5.1 | 4.2 | 2.9 | 1.8 | 1.5 | 1.5 | 1.1 | 0.9 | 0.8 | 0.7 | 0.9 |
| GSC_4.38 | 255 | 6.4 | 5.8 | 4.9 | 2.7 | 2.0 | 1.7 | 1.4 | 1.1 | 0.9 | 0.9 | 0.8 | 0.8 |
| GSC_4.39 | 305 | 7.1 | 6.2 | 5.4 | 3.3 | 2.7 | 2.0 | 1.5 | 1.2 | 1.0 | 0.8 | 0.8 | 1.0 |
| GSC_4.40 | 370 | 7.8 | 7.2 | 5.9 | 3.9 | 2.8 | 1.9 | 1.4 | 1.1 | 1.0 | 0.9 | 0.9 | 0.9 |
| GSC_4.41 | 430 | 8.4 | 7.7 | 6.4 | 4.3 | 3.2 | 2.0 | 1.6 | 1.3 | 1.1 | 1.0 | 0.9 | 0.9 |
| GSC_4.42 | 490 | 9.3 | 8.2 | 6.9 | 4.8 | 3.5 | 2.2 | 1.7 | 1.2 | 1.0 | 1.0 | 1.0 | 1.1 |
| GSC_4.43 | 550 | 9.6 | 8.9 | 7.2 | 4.7 | 3.7 | 2.6 | 2.0 | 1.4 | 1.2 | 1.1 | 1.0 | 0.9 |
| GSC_4.44 | 610 | 9.9 | 9.1 | 7.3 | 5.0 | 4.0 | 2.9 | 2.2 | 1.6 | 1.3 | 1.2 | 1.0 | 1.0 |
| GSC_4.45 | 715 | 10.2 | 9.2 | 7.6 | 5.2 | 4.1 | 3.0 | 2.0 | 1.6 | 1.4 | 1.1 | 0.9 | 0.9 |
| GSC_4.46 | 775 | 10.3 | 9.3 | 7.6 | 5.0 | 4.0 | 3.0 | 2.1 | 1.6 | 1.3 | 1.0 | 0.9 | 0.8 |
| GSC_4.47 | 850 | 10.4 | 9.6 | 7.7 | 5.0 | 4.1 | 3.0 | 2.1 | 1.6 | 1.3 | 1.0 | 0.9 | 0.8 |
| GSC_4.48 | 30 | 2.4 | 1.9 | 1.6 | 1.4 | 1.0 | 0.8 | 0.8 | 0.7 | 0.6 | 0.6 | 0.7 | 0.8 |
| GSC_4.49 | 45 | 3.3 | 2.5 | 2.2 | 1.8 | 1.2 | 0.9 | 0.8 | 0.9 | 0.8 | 1.0 | 0.9 | 1.0 |
| GSC_4.50 | 65 | 4.1 | 3.0 | 2.9 | 2.2 | 1.4 | 1.1 | 0.9 | 1.0 | 0.9 | 1.0 | 1.0 | 0.9 |
| GSC_4.51 | 80 | 4.9 | 3.8 | 3.2 | 2.6 | 1.7 | 1.3 | 1.0 | 1.1 | 1.1 | 0.9 | 0.9 | 0.9 |
| GSC_4.52 | 100 | 5.5 | 4.6 | 3.9 | 3.2 | 2.0 | 1.7 | 1.2 | 1.3 | 1.2 | 1.0 | 0.8 | 0.9 |
| GSC_4.53 | 120 | 6.0 | 5.2 | 3.9 | 3.6 | 2.2 | 1.6 | 1.8 | 1.3 | 1.4 | 1.2 | 1.0 | 0.8 |
| GSC_4.54 | 140 | 6.5 | 5.9 | 4.3 | 3.8 | 2.6 | 1.7 | 1.8 | 1.3 | 1.2 | 1.1 | 0.9 | 0.8 |
| GSC_4.55 | 160 | 6.9 | 6.5 | 4.5 | 4.2 | 2.7 | 2.0 | 1.9 | 1.3 | 1.3 | 1.0 | 0.9 | 1.0 |
| GSC_4.56 | 195 | 7.4 | 7.1 | 4.8 | 4.2 | 3.0 | 2.2 | 2.0 | 1.4 | 1.3 | 1.0 | 0.9 | 1.0 |
| GSC_4.57 | 235 | 8.0 | 7.6 | 4.8 | 4.1 | 3.3 | 2.3 | 1.7 | 1.4 | 1.2 | 1.0 | 0.9 | 0.9 |
| GSC_4.58 | 265 | 8.5 | 7.9 | 5.4 | 4.3 | 3.5 | 2.4 | 2.2 | 1.6 | 1.1 | 0.9 | 0.9 | 0.8 |
| GSC_4.59 | 295 | 9.1 | 8.5 | 5.2 | 4.8 | 3.7 | 2.6 | 2.4 | 1.8 | 1.0 | 1.1 | 1.0 | 1.0 |
| GSC_4.60 | 325 | 9.5 | 8.8 | 5.3 | 5.2 | 4.0 | 2.8 | 2.2 | 1.9 | 1.1 | 1.2 | 1.0 | 1.0 |
| GSC_4.61 | 370 | 10.0 | 9.2 | 5.6 | 5.3 | 4.2 | 2.9 | 2.4 | 1.9 | 1.1 | 1.2 | 1.0 | 0.8 |

| (1) | (2) | (3) | (4) | (5) | (6) | (7) | (8) | (9) | (10) | (11) | (12) | (13) | (14) |
|---|---|---|---|---|---|---|---|---|---|---|---|---|---|
| GSC_4.62 | 400 | 10.5 | 9.5 | 5.9 | 5.4 | 4.5 | 3.0 | 2.4 | 1.8 | 1.0 | 1.1 | 0.9 | 0.9 |
| GSC_4.63 | 445 | 10.9 | 9.8 | 5.7 | 5.5 | 4.8 | 3.2 | 2.2 | 1.7 | 1.2 | 1.0 | 1.1 | 1.0 |
| GSC_4.64 | 490 | 11.4 | 10.0 | 5.8 | 5.7 | 4.8 | 3.2 | 2.3 | 1.7 | 1.0 | 1.2 | 1.1 | 1.1 |
| GSC_4.65 | 535 | 11.8 | 10.3 | 5.9 | 5.7 | 4.9 | 3.1 | 2.4 | 1.9 | 1.0 | 1.2 | 1.1 | 1.2 |
| GSC_4.66 | 610 | 12.2 | 10.3 | 6.0 | 5.7 | 5.0 | 3.0 | 2.3 | 2.0 | 1.4 | 1.3 | 1.1 | 1.0 |
| GSC_4.67 | 670 | 12.5 | 10.4 | 6.0 | 5.8 | 5.0 | 2.9 | 2.5 | 2.0 | 1.4 | 1.0 | 1.0 | 0.9 |
| GSC_4.68 | 730 | 12.7 | 10.4 | 6.0 | 5.7 | 5.0 | 3.0 | 2.6 | 2.0 | 1.5 | 1.1 | 1.0 | 0.9 |
| GSC_4.69 | 810 | 12.8 | 10.4 | 6.0 | 5.7 | 5.0 | 3.1 | 2.6 | 2.0 | 1.5 | 1.1 | 1.0 | 0.9 |
| GSC_5.1 | 15 | 1.3 | 1.2 | 0.9 | 0.8 | 0.7 | 0.7 | 0.7 | 0.5 | 0.7 | 0.6 | 0.6 | 0.5 |
| GSC_5.2 | 30 | 1.9 | 1.6 | 1.4 | 1.2 | 0.9 | 0.8 | 0.7 | 0.5 | 0.7 | 0.7 | 0.6 | 0.5 |
| GSC_5.3 | 60 | 2.6 | 2.0 | 1.9 | 1.7 | 1.0 | 0.9 | 1.0 | 0.7 | 0.7 | 0.8 | 0.6 | 0.6 |
| GSC_5.4 | 90 | 3.2 | 2.4 | 2.0 | 1.9 | 1.3 | 1.2 | 1.1 | 0.9 | 0.9 | 0.7 | 0.8 | 0.7 |
| GSC_5.5 | 120 | 3.6 | 2.8 | 2.2 | 2.2 | 1.8 | 1.3 | 1.2 | 1.0 | 1.0 | 1.1 | 0.9 | 0.7 |
| GSC_5.6 | 150 | 4.0 | 3.1 | 2.5 | 2.4 | 2.1 | 1.4 | 1.0 | 1.3 | 1.2 | 1.3 | 1.1 | 1.0 |
| GSC_5.7 | 180 | 4.4 | 3.5 | 2.5 | 2.4 | 2.2 | 1.7 | 1.3 | 1.1 | 1.2 | 1.2 | 1.0 | 1.1 |
| GSC_5.8 | 210 | 4.7 | 3.7 | 2.7 | 2.6 | 2.3 | 1.6 | 1.5 | 1.4 | 1.3 | 1.1 | 1.1 | 1.2 |
| GSC_5.9 | 240 | 5.0 | 4.0 | 2.8 | 2.7 | 2.4 | 1.8 | 1.5 | 1.5 | 1.6 | 1.4 | 1.2 | 1.1 |
| GSC_5.10 | 270 | 5.3 | 4.5 | 2.8 | 2.6 | 2.4 | 1.6 | 1.5 | 1.6 | 1.3 | 1.1 | 1.5 | 1.3 |
| GSC_5.11 | 300 | 5.5 | 4.7 | 3.3 | 2.9 | 2.5 | 1.9 | 1.7 | 1.7 | 1.2 | 1.0 | 1.5 | 1.4 |
| GSC_5.12 | 330 | 5.7 | 5.0 | 3.2 | 3.0 | 2.4 | 2.0 | 1.8 | 1.4 | 1.2 | 1.3 | 1.5 | 1.5 |
| GSC_5.13 | 375 | 6.1 | 5.6 | 3.5 | 2.9 | 2.6 | 2.1 | 1.6 | 1.7 | 1.5 | 1.6 | 1.5 | 1.6 |
| GSC_5.14 | 405 | 6.5 | 6.0 | 3.6 | 3.2 | 2.7 | 2.4 | 1.6 | 1.4 | 1.3 | 1.1 | 1.4 | 1.4 |
| GSC_5.15 | 435 | 6.8 | 6.1 | 4.0 | 3.3 | 2.6 | 2.4 | 1.5 | 1.3 | 1.2 | 1.3 | 1.2 | 1.3 |
| GSC_5.16 | 465 | 7.1 | 6.5 | 4.3 | 3.5 | 2.8 | 2.3 | 1.6 | 1.3 | 1.2 | 1.1 | 1.1 | 1.3 |
| GSC_5.17 | 500 | 7.4 | 7.2 | 4.5 | 3.5 | 2.7 | 2.1 | 1.4 | 1.3 | 1.2 | 0.9 | 1.0 | 1.1 |
| GSC_5.18 | 530 | 7.6 | 7.5 | 4.4 | 3.6 | 2.7 | 2.3 | 1.5 | 1.3 | 1.0 | 0.9 | 0.9 | 1.0 |
| GSC_5.19 | 560 | 8.0 | 7.6 | 4.6 | 3.6 | 2.8 | 2.2 | 1.6 | 1.4 | 1.1 | 0.8 | 0.9 | 1.1 |
| GSC_5.20 | 620 | 8.3 | 7.7 | 4.7 | 3.5 | 2.9 | 2.3 | 1.7 | 1.4 | 1.2 | 1.0 | 1.0 | 1.3 |
| GSC_5.21 | 650 | 8.5 | 7.8 | 4.7 | 3.5 | 2.9 | 2.3 | 1.6 | 1.5 | 1.4 | 1.1 | 0.9 | 0.9 |

| (1) | (2) | (3) | (4) | (5) | (6) | (7) | (8) | (9) | (10) | (11) | (12) | (13) | (14) |
|---|---|---|---|---|---|---|---|---|---|---|---|---|---|
| GSC_5.22 | 680 | 8.7 | 7.8 | 4.6 | 3.6 | 2.9 | 2.1 | 1.6 | 1.5 | 1.5 | 1.1 | 1.0 | 0.9 |
| GSC_5.23 | 740 | 8.8 | 7.9 | 4.7 | 3.6 | 2.7 | 2.1 | 1.5 | 1.4 | 1.5 | 1.0 | 0.9 | 1.1 |
| GSC_5.24 | 770 | 8.8 | 7.9 | 4.9 | 3.6 | 2.8 | 2.0 | 1.3 | 1.3 | 1.4 | 1.0 | 0.9 | 1.0 |
| GSC_5.25 | 830 | 8.9 | 7.9 | 4.9 | 3.7 | 2.8 | 2.0 | 1.4 | 1.1 | 1.2 | 1.1 | 0.9 | 1.0 |
| GSC_5.26 | 880 | 8.9 | 7.9 | 4.9 | 3.7 | 2.8 | 2.1 | 1.4 | 1.1 | 1.1 | 1.1 | 1.0 | 1.0 |
| GSC_5.27 | 15 | 1.7 | 1.5 | 1.1 | 0.7 | 0.7 | 0.6 | 0.7 | 0.6 | 0.4 | 0.5 | 0.6 | 0.7 |
| GSC_5.28 | 35 | 2.6 | 2.0 | 1.7 | 1.1 | 1.0 | 0.8 | 0.8 | 0.8 | 0.5 | 0.6 | 0.7 | 0.7 |
| GSC_5.29 | 65 | 3.6 | 2.5 | 2.0 | 1.3 | 1.1 | 0.9 | 1.0 | 0.6 | 0.5 | 0.7 | 0.7 | 0.8 |
| GSC_5.30 | 100 | 4.3 | 2.9 | 2.2 | 1.5 | 1.2 | 1.0 | 1.2 | 0.7 | 0.7 | 0.7 | 0.8 | 0.8 |
| GSC_5.31 | 140 | 5.0 | 3.3 | 2.5 | 1.7 | 1.4 | 0.8 | 1.1 | 0.6 | 0.7 | 0.8 | 0.9 | 0.8 |
| GSC_5.32 | 220 | 6.2 | 3.7 | 2.8 | 1.9 | 1.5 | 1.0 | 0.9 | 0.9 | 0.8 | 0.9 | 0.9 | 1.0 |
| GSC_5.33 | 280 | 7.1 | 4.1 | 3.0 | 2.0 | 1.5 | 1.1 | 0.9 | 0.9 | 0.8 | 0.9 | 1.1 | 1.0 |
| GSC_5.34 | 340 | 7.8 | 4.4 | 3.2 | 2.0 | 1.6 | 1.1 | 0.7 | 1.0 | 0.9 | 1.1 | 1.0 | 1.1 |
| GSC_5.35 | 400 | 8.4 | 4.6 | 3.3 | 2.1 | 1.6 | 1.2 | 0.9 | 0.8 | 1.0 | 1.1 | 1.1 | 1.3 |
| GSC_5.36 | 470 | 8.9 | 4.8 | 3.3 | 1.9 | 1.8 | 0.9 | 0.8 | 0.6 | 0.9 | 0.9 | 1.0 | 1.2 |
| GSC_5.37 | 530 | 9.4 | 4.9 | 3.5 | 2.0 | 1.7 | 1.1 | 0.8 | 0.6 | 1.0 | 0.9 | 1.1 | 1.1 |
| GSC_5.38 | 590 | 9.8 | 4.8 | 3.5 | 2.1 | 1.7 | 1.2 | 0.8 | 0.3 | 1.1 | 1.0 | 1.0 | 0.9 |
| GSC_5.39 | 660 | 10.2 | 4.9 | 3.4 | 2.2 | 1.6 | 1.1 | 0.9 | 0.4 | 0.9 | 0.9 | 0.8 | 0.9 |
| GSC_5.40 | 720 | 10.5 | 4.9 | 3.5 | 2.2 | 1.7 | 1.1 | 0.9 | 0.4 | 0.8 | 0.8 | 0.8 | 0.7 |
| GSC_5.41 | 780 | 10.7 | 4.9 | 3.6 | 2.2 | 1.7 | 1.1 | 1.0 | 0.4 | 0.7 | 0.8 | 0.7 | 0.7 |
| GSC_5.42 | 840 | 10.7 | 4.9 | 3.6 | 2.2 | 1.7 | 1.2 | 0.9 | 0.4 | 0.7 | 0.7 | 0.6 | 0.7 |
| GSC_5.43 | 15 | 1.6 | 1.3 | 0.9 | 0.6 | 0.8 | 0.7 | 0.5 | 0.4 | 0.3 | 0.7 | 0.6 | 0.6 |
| GSC_5.44 | 30 | 2.5 | 1.9 | 1.2 | 0.9 | 0.7 | 0.8 | 0.6 | 0.6 | 0.7 | 0.6 | 0.7 | 0.5 |
| GSC_5.45 | 45 | 3.3 | 2.3 | 1.6 | 1.2 | 0.8 | 0.9 | 0.7 | 0.7 | 0.9 | 0.7 | 0.7 | 0.6 |
| GSC_5.46 | 60 | 3.9 | 2.6 | 1.9 | 1.4 | 0.9 | 0.8 | 0.7 | 0.6 | 0.8 | 0.8 | 0.9 | 0.8 |
| GSC_5.47 | 90 | 4.7 | 2.9 | 2.1 | 1.5 | 1.0 | 0.9 | 0.9 | 0.7 | 1.0 | 0.9 | 0.9 | 0.8 |
| GSC_5.48 | 120 | 5.4 | 3.1 | 2.0 | 1.4 | 1.2 | 1.0 | 0.9 | 0.8 | 0.8 | 0.9 | 1.0 | 0.9 |
| GSC_5.49 | 150 | 6.2 | 3.5 | 2.3 | 1.6 | 1.4 | 1.1 | 1.1 | 1.0 | 1.1 | 1.0 | 1.0 | 1.0 |
| GSC_5.50 | 195 | 6.7 | 3.8 | 2.5 | 1.8 | 1.5 | 1.2 | 1.2 | 1.1 | 1.1 | 1.3 | 1.2 | 1.1 |

| (1) | (2) | (3) | (4) | (5) | (6) | (7) | (8) | (9) | (10) | (11) | (12) | (13) | (14) |
|---|---|---|---|---|---|---|---|---|---|---|---|---|---|
| GSC_5.51 | 240 | 7.2 | 4.1 | 2.7 | 1.9 | 1.6 | 1.4 | 1.3 | 1.2 | 1.1 | 1.2 | 1.4 | 1.3 |
| GSC_5.52 | 300 | 7.8 | 4.6 | 2.8 | 2.2 | 1.7 | 1.4 | 1.3 | 1.4 | 1.4 | 1.5 | 1.5 | 1.4 |
| GSC_5.53 | 360 | 8.4 | 4.9 | 3.0 | 2.1 | 1.8 | 1.3 | 1.3 | 1.4 | 1.2 | 1.5 | 1.6 | 1.5 |
| GSC_5.54 | 420 | 8.9 | 5.2 | 3.1 | 2.1 | 2.0 | 1.4 | 1.4 | 1.3 | 1.4 | 1.6 | 1.6 | 1.5 |
| GSC_5.55 | 500 | 9.3 | 5.6 | 3.3 | 2.4 | 1.9 | 1.6 | 1.5 | 1.4 | 1.5 | 1.5 | 1.6 | 1.6 |
| GSC_5.56 | 580 | 9.7 | 5.9 | 3.5 | 2.6 | 1.9 | 1.7 | 1.5 | 1.4 | 1.4 | 1.3 | 1.5 | 1.6 |
| GSC_5.57 | 670 | 10.0 | 6.1 | 3.6 | 2.7 | 2.0 | 1.7 | 1.5 | 1.4 | 1.5 | 1.4 | 1.5 | 1.4 |
| GSC_5.58 | 745 | 10.1 | 6.2 | 3.6 | 2.7 | 2.0 | 1.8 | 1.5 | 1.4 | 1.4 | 1.3 | 1.4 | 1.4 |
| GSC_5.59 | 805 | 10.1 | 6.2 | 3.6 | 2.7 | 2.1 | 1.8 | 1.5 | 1.4 | 1.4 | 1.3 | 1.4 | 1.4 |
| GSC_5.60 | 15 | 0.9 | 0.7 | 0.6 | 0.6 | 0.4 | 0.3 | 0.6 | 0.5 | 0.4 | 0.6 | 0.5 | 0.6 |
| GSC_5.61 | 30 | 1.4 | 0.9 | 0.8 | 0.6 | 0.5 | 0.5 | 0.6 | 0.5 | 0.5 | 0.6 | 0.6 | 0.5 |
| GSC_5.62 | 45 | 2.0 | 1.0 | 0.8 | 0.7 | 0.5 | 0.6 | 0.6 | 0.5 | 0.6 | 0.6 | 0.7 | 0.6 |
| GSC_5.63 | 75 | 2.5 | 1.3 | 1.0 | 0.8 | 0.6 | 0.6 | 0.5 | 0.6 | 0.7 | 0.7 | 0.6 | 0.7 |
| GSC_5.64 | 120 | 3.0 | 1.8 | 1.2 | 0.9 | 0.8 | 0.7 | 0.6 | 0.7 | 0.6 | 0.7 | 0.7 | 0.7 |
| GSC_5.65 | 165 | 3.5 | 2.3 | 1.4 | 1.0 | 0.9 | 0.7 | 0.7 | 0.9 | 0.8 | 0.9 | 0.8 | 0.9 |
| GSC_5.66 | 225 | 4.1 | 2.6 | 1.8 | 0.9 | 1.0 | 0.8 | 1.0 | 1.2 | 1.1 | 0.9 | 0.9 | 0.9 |
| GSC_5.67 | 285 | 4.8 | 2.8 | 1.7 | 1.1 | 1.2 | 1.0 | 1.1 | 1.0 | 1.2 | 1.1 | 1.1 | 1.0 |
| GSC_5.68 | 345 | 5.4 | 3.1 | 2.1 | 1.2 | 1.5 | 1.1 | 1.1 | 1.2 | 1.1 | 1.2 | 1.2 | 1.1 |
| GSC_5.69 | 390 | 5.8 | 3.3 | 2.4 | 1.3 | 1.5 | 1.2 | 1.2 | 1.1 | 1.2 | 1.1 | 1.2 | 1.2 |
| GSC_5.70 | 435 | 6.1 | 3.6 | 2.7 | 1.5 | 1.7 | 1.4 | 1.3 | 1.4 | 1.3 | 1.2 | 1.1 | 1.1 |
| GSC_5.71 | 485 | 6.4 | 4.0 | 2.9 | 1.6 | 1.6 | 1.4 | 1.4 | 1.4 | 1.5 | 1.3 | 1.3 | 1.2 |
| GSC_5.72 | 545 | 6.8 | 4.4 | 3.0 | 1.5 | 1.8 | 1.5 | 1.5 | 1.4 | 1.3 | 1.5 | 1.4 | 1.3 |
| GSC_5.73 | 625 | 7.1 | 4.6 | 3.2 | 1.7 | 1.9 | 1.7 | 1.6 | 1.6 | 1.5 | 1.4 | 1.5 | 1.4 |
| GSC_5.74 | 705 | 7.4 | 4.7 | 3.3 | 1.8 | 2.1 | 1.8 | 1.8 | 1.7 | 1.5 | 1.6 | 1.6 | 1.4 |
| GSC_5.75 | 765 | 7.5 | 4.6 | 3.3 | 1.8 | 2.1 | 1.9 | 2.0 | 2.0 | 1.8 | 1.8 | 1.7 | 1.5 |
| GSC_5.76 | 825 | 7.6 | 4.7 | 3.4 | 1.9 | 2.0 | 1.8 | 2.2 | 2.0 | 1.9 | 1.8 | 1.6 | 1.5 |
| GSC_5.77 | 885 | 7.7 | 4.8 | 3.4 | 1.9 | 2.0 | 1.8 | 2.0 | 1.8 | 1.6 | 1.6 | 1.5 | 1.5 |
| GSC_5.78 | 960 | 7.7 | 4.8 | 3.4 | 1.9 | 2.1 | 1.7 | 1.8 | 1.7 | 1.6 | 1.5 | 1.5 | 1.4 |
| GSC_0.1 | 15 | 2.5 | 1.8 | 1.1 | 0.8 | 0.7 | 0.8 | 0.8 | 0.7 | 0.5 | 0.6 | 0.4 | 0.4 |

| (1) | (2) | (3) | (4) | (5) | (6) | (7) | (8) | (9) | (10) | (11) | (12) | (13) | (14) |
|---|---|---|---|---|---|---|---|---|---|---|---|---|---|
| GSC_0.2 | 30 | 4.2 | 3.3 | 1.6 | 1.2 | 0.8 | 0.8 | 0.8 | 0.7 | 0.6 | 0.7 | 0.6 | 0.5 |
| GSC_0.3 | 60 | 5.7 | 4.9 | 2.8 | 2.1 | 1.3 | 1.2 | 1.1 | 0.8 | 0.5 | 0.6 | 0.6 | 0.7 |
| GSC_0.4 | 115 | 7.4 | 6.2 | 4.1 | 3.1 | 1.9 | 1.5 | 1.1 | 1.0 | 0.8 | 0.7 | 0.5 | 0.8 |
| GSC_0.5 | 165 | 8.7 | 7.2 | 5.0 | 3.8 | 2.5 | 1.8 | 1.3 | 1.0 | 0.8 | 0.7 | 0.8 | 0.7 |
| GSC_0.6 | 240 | 10.1 | 8.3 | 6.1 | 4.7 | 3.2 | 2.2 | 1.3 | 1.1 | 1.0 | 1.0 | 0.9 | 0.7 |
| GSC_0.7 | 320 | 11.3 | 9.2 | 7.2 | 5.5 | 3.9 | 2.5 | 1.4 | 1.1 | 0.9 | 0.8 | 0.8 | 0.8 |
| GSC_0.8 | 390 | 12.4 | 9.9 | 7.8 | 6.3 | 4.3 | 2.7 | 1.7 | 1.2 | 0.9 | 0.6 | 0.7 | 0.8 |
| GSC_0.9 | 420 | 12.6 | 10.3 | 8.1 | 6.5 | 4.4 | 2.6 | 1.7 | 1.1 | 0.7 | 0.7 | 0.6 | 0.6 |
| GSC_0.10 | 450 | 12.8 | 10.4 | 8.2 | 6.5 | 4.4 | 2.6 | 1.7 | 1.1 | 0.8 | 0.7 | 0.7 | 0.6 |
| GSC_0.11 | 550 | 13.0 | 10.5 | 8.3 | 6.5 | 4.4 | 2.6 | 1.7 | 1.1 | 0.8 | 0.7 | 0.6 | 0.6 |
| GSC_0.12 | 35 | 3.2 | 2.5 | 1.7 | 1.4 | 1.1 | 0.8 | 0.5 | 0.4 | 0.6 | 0.3 | 0.5 | 0.3 |
| GSC_0.13 | 80 | 5.2 | 3.9 | 3.0 | 2.2 | 1.3 | 1.1 | 0.8 | 0.6 | 0.7 | 0.5 | 0.6 | 0.4 |
| GSC_0.14 | 140 | 7.1 | 5.5 | 4.2 | 3.1 | 1.6 | 1.2 | 0.7 | 0.8 | 0.6 | 0.6 | 0.8 | 0.6 |
| GSC_0.15 | 175 | 7.9 | 6.7 | 4.9 | 3.6 | 1.7 | 1.3 | 0.8 | 0.7 | 0.6 | 0.7 | 0.7 | 0.6 |
| GSC_0.16 | 295 | 10.8 | 8.2 | 6.0 | 4.6 | 2.2 | 1.5 | 1.1 | 1.0 | 0.8 | 0.8 | 0.8 | 0.9 |
| GSC_0.17 | 365 | 12.2 | 9.4 | 6.9 | 5.4 | 2.5 | 1.6 | 1.2 | 0.9 | 0.9 | 0.9 | 0.8 | 1.0 |
| GSC_0.18 | 395 | 12.7 | 10.4 | 7.7 | 6.1 | 2.6 | 1.7 | 1.2 | 0.9 | 0.9 | 0.9 | 0.8 | 0.9 |
| GSC_0.19 | 475 | 13.5 | 11.6 | 8.8 | 6.6 | 2.8 | 1.7 | 1.3 | 1.1 | 0.8 | 1.0 | 1.1 | 1.0 |
| GSC_0.20 | 535 | 13.8 | 12.0 | 9.4 | 6.8 | 2.9 | 1.8 | 1.3 | 1.2 | 0.8 | 1.0 | 0.9 | 0.9 |
| GSC_0.21 | 575 | 14.0 | 12.2 | 9.5 | 6.8 | 2.9 | 1.8 | 1.3 | 1.2 | 0.8 | 0.9 | 0.9 | 0.8 |
| GSC_0.22 | 30 | 3.0 | 2.6 | 1.8 | 1.5 | 1.3 | 1.1 | 0.7 | 0.5 | 0.6 | 0.3 | 0.5 | 0.3 |
| GSC_0.23 | 60 | 5.2 | 4.3 | 3.2 | 2.2 | 1.7 | 1.5 | 1.2 | 1.0 | 1.0 | 0.7 | 0.8 | 0.5 |
| GSC_0.24 | 100 | 7.1 | 6.3 | 4.6 | 3.4 | 2.2 | 1.7 | 1.0 | 1.0 | 0.9 | 1.0 | 0.9 | 0.8 |
| GSC_0.25 | 160 | 9.7 | 8.5 | 5.8 | 4.5 | 3.1 | 1.9 | 1.3 | 1.1 | 1.0 | 1.1 | 1.1 | 1.0 |
| GSC_0.26 | 220 | 11.1 | 9.8 | 6.9 | 5.4 | 3.9 | 2.2 | 1.5 | 1.3 | 1.2 | 1.1 | 1.2 | 1.0 |
| GSC_0.27 | 290 | 12.1 | 10.5 | 7.6 | 5.9 | 4.4 | 2.6 | 1.7 | 1.5 | 1.1 | 1.3 | 1.2 | 1.2 |
| GSC_0.28 | 360 | 13.0 | 10.9 | 8.1 | 6.5 | 4.8 | 2.9 | 1.8 | 1.5 | 1.4 | 1.2 | 1.2 | 1.0 |
| GSC_0.29 | 420 | 13.8 | 11.3 | 8.5 | 6.9 | 5.2 | 3.3 | 1.9 | 1.5 | 1.3 | 1.1 | 1.1 | 0.9 |
| GSC_0.30 | 490 | 14.4 | 11.5 | 8.7 | 7.1 | 5.4 | 3.4 | 1.9 | 1.6 | 1.3 | 1.0 | 1.0 | 0.8 |

| (1) | (2) | (3) | (4) | (5) | (6) | (7) | (8) | (9) | (10) | (11) | (12) | (13) | (14) |
|---|---|---|---|---|---|---|---|---|---|---|---|---|---|
| GSC_0.31 | 560 | 14.6 | 11.6 | 8.8 | 7.1 | 5.4 | 3.2 | 2.0 | 1.6 | 1.3 | 1.0 | 1.0 | 0.8 |
| GSC_0.32 | 15 | 1.8 | 1.5 | 1.0 | 0.7 | 0.6 | 0.7 | 0.8 | 0.7 | 0.6 | 0.5 | 0.3 | 0.3 |
| GSC_0.33 | 30 | 3.3 | 2.4 | 1.7 | 1.2 | 0.9 | 0.7 | 0.6 | 0.7 | 0.6 | 0.5 | 0.5 | 0.4 |
| GSC_0.34 | 60 | 4.7 | 3.6 | 2.7 | 1.8 | 1.2 | 0.9 | 0.7 | 0.8 | 0.7 | 0.7 | 0.5 | 0.5 |
| GSC_0.35 | 110 | 6.7 | 5.1 | 3.8 | 2.6 | 1.7 | 1.3 | 0.9 | 1.0 | 0.8 | 0.7 | 0.6 | 0.5 |
| GSC_0.36 | 160 | 8.1 | 6.1 | 4.5 | 3.2 | 2.2 | 1.5 | 1.1 | 1.1 | 0.8 | 0.7 | 0.6 | 0.6 |
| GSC_0.37 | 230 | 9.4 | 7.2 | 5.4 | 3.9 | 2.8 | 1.9 | 1.3 | 1.2 | 1.0 | 0.9 | 0.7 | 0.6 |
| GSC_0.38 | 300 | 10.7 | 8.3 | 6.2 | 5.0 | 3.6 | 2.2 | 1.2 | 1.3 | 1.0 | 0.8 | 0.7 | 0.7 |
| GSC_0.39 | 370 | 11.6 | 9.0 | 6.8 | 5.6 | 4.1 | 2.5 | 1.4 | 1.1 | 0.8 | 0.8 | 0.7 | 0.6 |
| GSC_0.40 | 430 | 12.2 | 9.5 | 7.2 | 6.1 | 4.5 | 2.8 | 1.6 | 1.2 | 0.8 | 0.7 | 0.6 | 0.6 |
| GSC_0.41 | 490 | 12.4 | 9.7 | 7.2 | 6.2 | 4.5 | 2.7 | 1.5 | 1.1 | 0.7 | 0.7 | 0.7 | 0.6 |
| GSC_0.42 | 540 | 12.5 | 9.7 | 7.2 | 6.3 | 4.4 | 2.7 | 1.5 | 1.0 | 0.7 | 0.7 | 0.6 | 0.6 |
| GSSC_1.1 | 10 | 2.8 | 2.1 | 1.5 | 1.4 | 1.2 | 1.3 | 1.0 | 0.9 | 0.7 | 0.5 | 0.5 | 0.4 |
| GSSC_1.2 | 20 | 3.7 | 2.8 | 1.6 | 1.5 | 1.4 | 1.2 | 1.3 | 1.2 | 0.9 | 0.8 | 0.6 | 0.6 |
| GSSC_1.3 | 30 | 4.7 | 3.4 | 2.1 | 1.7 | 1.4 | 1.3 | 1.0 | 1.0 | 0.9 | 0.9 | 0.7 | 0.6 |
| GSSC_1.4 | 45 | 5.6 | 4.4 | 2.4 | 1.8 | 1.5 | 1.2 | 1.1 | 0.9 | 1.0 | 0.8 | 0.8 | 0.7 |
| GSSC_1.5 | 75 | 6.5 | 4.9 | 2.8 | 2.0 | 1.9 | 1.3 | 1.0 | 1.0 | 0.9 | 0.9 | 0.8 | 0.7 |
| GSSC_1.6 | 105 | 7.5 | 5.2 | 3.1 | 2.3 | 2.1 | 1.5 | 1.1 | 0.9 | 0.9 | 0.8 | 0.9 | 0.8 |
| GSSC_1.7 | 135 | 8.6 | 5.5 | 3.4 | 2.5 | 2.3 | 1.4 | 1.0 | 1.0 | 0.9 | 0.9 | 0.9 | 0.8 |
| GSSC_1.8 | 165 | 9.3 | 6.6 | 3.9 | 2.6 | 2.4 | 1.5 | 1.2 | 1.1 | 1.1 | 1.0 | 0.9 | 0.9 |
| GSSC_1.9 | 205 | 9.8 | 7.3 | 4.2 | 2.7 | 2.5 | 1.7 | 1.2 | 0.9 | 1.0 | 1.0 | 0.9 | 1.0 |
| GSSC_1.10 | 235 | 10.1 | 7.6 | 4.4 | 2.9 | 2.6 | 1.7 | 1.4 | 1.1 | 1.0 | 1.0 | 0.9 | 1.0 |
| GSSC_1.11 | 265 | 10.6 | 8.1 | 4.7 | 3.0 | 2.7 | 1.9 | 1.4 | 1.2 | 1.1 | 1.1 | 1.0 | 1.0 |
| GSSC_1.12 | 295 | 11.3 | 8.9 | 4.9 | 3.3 | 2.8 | 2.0 | 1.3 | 1.2 | 1.2 | 1.1 | 1.0 | 0.9 |
| GSSC_1.13 | 325 | 11.6 | 9.4 | 5.1 | 3.6 | 2.9 | 2.2 | 1.4 | 1.2 | 1.3 | 1.2 | 1.1 | 1.1 |
| GSSC_1.14 | 355 | 11.9 | 9.8 | 5.5 | 3.8 | 3.1 | 2.5 | 1.6 | 1.3 | 1.3 | 1.2 | 1.0 | 0.9 |
| GSSC_1.15 | 385 | 12.1 | 10.0 | 5.8 | 4.0 | 3.1 | 2.3 | 1.2 | 1.4 | 1.4 | 1.2 | 1.0 | 0.8 |
| GSSC_1.16 | 415 | 12.3 | 10.2 | 6.2 | 4.2 | 3.2 | 2.2 | 1.1 | 0.9 | 0.9 | 1.0 | 0.8 | 0.9 |
| GSSC_1.17 | 445 | 12.6 | 10.8 | 6.5 | 4.2 | 3.2 | 2.6 | 1.2 | 1.0 | 0.8 | 0.9 | 1.0 | 0.9 |

| (1) | (2) | (3) | (4) | (5) | (6) | (7) | (8) | (9) | (10) | (11) | (12) | (13) | (14) |
|---|---|---|---|---|---|---|---|---|---|---|---|---|---|
| GSSC_1.18 | 475 | 12.9 | 11.0 | 6.9 | 4.3 | 3.4 | 3.0 | 2.4 | 1.3 | 1.1 | 0.8 | 1.0 | 0.9 |
| GSSC_1.19 | 505 | 13.0 | 11.2 | 7.3 | 4.4 | 3.5 | 3.3 | 2.4 | 1.3 | 1.0 | 0.7 | 0.7 | 0.6 |
| GSSC_1.20 | 535 | 13.2 | 11.5 | 7.6 | 4.6 | 3.6 | 3.3 | 2.2 | 1.3 | 1.1 | 0.8 | 0.6 | 0.6 |
| GSSC_1.21 | 565 | 13.4 | 11.8 | 7.7 | 4.9 | 3.7 | 3.3 | 2.2 | 1.2 | 1.0 | 0.8 | 0.6 | 0.7 |
| GSSC_1.22 | 595 | 13.5 | 12.0 | 8.0 | 5.1 | 3.7 | 3.3 | 2.1 | 1.4 | 1.1 | 0.8 | 0.7 | 0.7 |
| GSSC_1.23 | 625 | 13.5 | 12.1 | 8.1 | 5.2 | 3.7 | 3.2 | 2.0 | 1.5 | 1.2 | 0.9 | 0.7 | 0.8 |
| GSSC_1.24 | 655 | 13.6 | 12.1 | 8.2 | 5.2 | 3.8 | 3.2 | 2.0 | 1.5 | 1.2 | 0.9 | 0.8 | 0.8 |
| GSSC_1.25 | 685 | 13.6 | 12.2 | 8.2 | 5.3 | 3.8 | 3.3 | 2.0 | 1.4 | 1.1 | 0.9 | 0.7 | 0.8 |
| GSSC_1.26 | 10 | 3.4 | 2.6 | 1.8 | 1.5 | 1.4 | 1.4 | 1.2 | 1.1 | 1.0 | 0.9 | 0.7 | 0.7 |
| GSSC_1.27 | 25 | 5.8 | 3.9 | 2.6 | 2.0 | 1.7 | 1.6 | 1.3 | 1.2 | 1.2 | 1.0 | 0.8 | 0.7 |
| GSSC_1.28 | 40 | 7.6 | 5.1 | 3.2 | 2.2 | 1.6 | 1.4 | 1.4 | 1.3 | 1.1 | 1.0 | 0.8 | 0.8 |
| GSSC_1.29 | 55 | 8.9 | 6.0 | 3.9 | 3.1 | 2.2 | 1.9 | 1.7 | 1.4 | 1.1 | 1.0 | 0.9 | 0.8 |
| GSSC_1.30 | 70 | 9.8 | 6.7 | 4.6 | 3.3 | 2.6 | 2.0 | 1.4 | 1.2 | 1.1 | 1.0 | 0.9 | 0.8 |
| GSSC_1.31 | 85 | 10.5 | 7.4 | 5.3 | 3.6 | 2.9 | 2.1 | 1.5 | 1.3 | 1.2 | 0.9 | 0.9 | 0.8 |
| GSSC_1.32 | 100 | 11.3 | 8.4 | 5.9 | 4.5 | 3.1 | 2.3 | 1.9 | 1.4 | 1.1 | 1.1 | 1.0 | 0.8 |
| GSSC_1.33 | 130 | 11.6 | 9.2 | 6.6 | 4.8 | 3.4 | 2.4 | 1.7 | 1.5 | 1.2 | 1.0 | 0.9 | 0.9 |
| GSSC_1.34 | 160 | 11.9 | 10.1 | 7.3 | 5.1 | 3.7 | 2.5 | 2.0 | 1.3 | 1.0 | 0.9 | 0.8 | 0.7 |
| GSSC_1.35 | 190 | 12.1 | 10.5 | 7.7 | 5.3 | 3.8 | 3.0 | 2.2 | 1.5 | 1.0 | 0.8 | 0.8 | 0.6 |
| GSSC_1.36 | 220 | 12.5 | 11.4 | 8.1 | 5.4 | 4.1 | 3.2 | 1.7 | 1.6 | 0.9 | 0.7 | 0.6 | 0.5 |
| GSSC_1.37 | 265 | 12.8 | 11.8 | 8.7 | 5.7 | 4.6 | 2.1 | 1.8 | 1.7 | 0.9 | 0.6 | 0.6 | 0.6 |
| GSSC_1.38 | 295 | 13.0 | 12.1 | 9.1 | 6.1 | 5.0 | 3.5 | 1.9 | 1.5 | 0.8 | 0.7 | 0.7 | 0.5 |
| GSSC_1.39 | 340 | 13.4 | 12.3 | 9.5 | 6.4 | 5.3 | 3.9 | 2.1 | 1.7 | 0.9 | 0.9 | 0.7 | 0.6 |
| GSSC_1.40 | 415 | 13.7 | 12.5 | 10.0 | 6.7 | 5.7 | 4.2 | 2.4 | 1.7 | 1.0 | 0.8 | 0.7 | 0.6 |
| GSSC_1.41 | 445 | 13.9 | 12.6 | 10.2 | 6.8 | 5.8 | 4.7 | 2.6 | 2.0 | 1.1 | 1.0 | 0.8 | 0.8 |
| GSSC_1.42 | 505 | 14.0 | 12.6 | 10.2 | 6.9 | 5.7 | 4.7 | 2.8 | 2.0 | 1.3 | 1.0 | 0.8 | 0.7 |
| GSSC_1.43 | 565 | 14.0 | 12.6 | 10.3 | 6.9 | 5.8 | 4.8 | 2.8 | 2.0 | 1.3 | 1.0 | 0.8 | 0.7 |
| GSSC_1.44 | 640 | 14.0 | 12.7 | 10.3 | 6.9 | 5.8 | 4.7 | 2.9 | 2.0 | 1.4 | 1.1 | 0.8 | 0.7 |
| GSSC_1.45 | 10 | 6.7 | 3.5 | 2.3 | 1.9 | 1.6 | 1.4 | 1.3 | 1.1 | 1.0 | 0.8 | 0.6 | 0.6 |
| GSSC_1.46 | 25 | 8.7 | 4.6 | 2.7 | 2.2 | 2.0 | 1.7 | 1.5 | 1.2 | 1.0 | 0.8 | 0.7 | 0.6 |

| (1) | (2) | (3) | (4) | (5) | (6) | (7) | (8) | (9) | (10) | (11) | (12) | (13) | (14) |
|---|---|---|---|---|---|---|---|---|---|---|---|---|---|
| GSSC_1.47 | 45 | 9.6 | 6.1 | 3.5 | 2.6 | 2.3 | 2.0 | 1.7 | 1.4 | 1.1 | 0.9 | 0.8 | 0.6 |
| GSSC_1.48 | 65 | 10.5 | 7.4 | 4.8 | 3.0 | 2.7 | 2.4 | 2.0 | 1.6 | 1.2 | 0.9 | 0.8 | 0.7 |
| GSSC_1.49 | 85 | 11.1 | 8.2 | 5.8 | 3.5 | 3.0 | 2.7 | 2.2 | 1.7 | 1.3 | 1.0 | 0.8 | 0.7 |
| GSSC_1.50 | 115 | 11.4 | 8.9 | 6.1 | 4.0 | 3.3 | 2.8 | 2.6 | 2.0 | 1.5 | 1.1 | 0.9 | 0.7 |
| GSSC_1.51 | 145 | 11.8 | 9.6 | 6.5 | 4.5 | 3.6 | 3.4 | 3.1 | 2.3 | 1.7 | 1.0 | 0.9 | 0.7 |
| GSSC_1.52 | 175 | 12.1 | 10.4 | 7.7 | 4.4 | 3.9 | 3.7 | 3.2 | 2.5 | 2.1 | 1.3 | 0.9 | 0.8 |
| GSSC_1.53 | 205 | 12.4 | 11.1 | 8.3 | 4.7 | 4.1 | 4.0 | 3.5 | 2.4 | 2.2 | 1.2 | 1.1 | 0.9 |
| GSSC_1.54 | 235 | 12.9 | 11.6 | 8.7 | 5.1 | 4.2 | 3.9 | 3.3 | 2.2 | 2.0 | 1.1 | 1.1 | 1.0 |
| GSSC_1.55 | 265 | 13.2 | 12.4 | 9.5 | 5.6 | 4.4 | 3.9 | 3.5 | 2.0 | 1.8 | 1.3 | 1.2 | 1.0 |
| GSSC_1.56 | 295 | 13.5 | 13.0 | 9.7 | 5.4 | 4.5 | 3.7 | 3.4 | 1.6 | 1.7 | 1.7 | 1.2 | 0.9 |
| GSSC_1.57 | 325 | 14.1 | 13.2 | 9.9 | 6.0 | 4.7 | 3.9 | 3.1 | 1.8 | 1.6 | 1.3 | 1.2 | 1.0 |
| GSSC_1.58 | 355 | 14.4 | 13.2 | 10.3 | 6.4 | 4.9 | 4.0 | 3.0 | 1.8 | 1.6 | 1.2 | 1.1 | 1.0 |
| GSSC_1.59 | 415 | 14.8 | 13.4 | 10.6 | 7.1 | 5.1 | 4.0 | 2.9 | 1.9 | 1.6 | 1.2 | 1.1 | 0.9 |
| GSSC_1.60 | 475 | 15.1 | 13.5 | 10.6 | 7.5 | 5.2 | 4.2 | 3.0 | 1.9 | 1.5 | 1.1 | 1.0 | 0.9 |
| GSSC_1.61 | 535 | 15.1 | 13.6 | 10.7 | 7.8 | 5.2 | 4.3 | 3.0 | 2.0 | 1.5 | 1.2 | 1.0 | 0.8 |
| GSSC_1.62 | 595 | 15.1 | 13.6 | 10.7 | 7.9 | 5.2 | 4.3 | 3.1 | 2.0 | 1.5 | 1.2 | 1.0 | 0.8 |
| GSSC_1.63 | 15 | 4.6 | 2.9 | 2.1 | 1.7 | 1.5 | 1.4 | 1.2 | 1.1 | 1.1 | 1.1 | 1.2 | 1.0 |
| GSSC_1.64 | 30 | 6.1 | 4.0 | 2.9 | 2.1 | 1.8 | 1.6 | 1.3 | 1.2 | 1.2 | 1.1 | 1.1 | 1.0 |
| GSSC_1.65 | 45 | 7.1 | 4.8 | 3.4 | 2.9 | 2.1 | 1.8 | 1.4 | 1.3 | 1.2 | 1.2 | 1.2 | 1.1 |
| GSSC_1.66 | 60 | 7.9 | 5.8 | 4.3 | 3.4 | 2.5 | 2.2 | 1.6 | 1.3 | 1.2 | 1.1 | 1.1 | 1.0 |
| GSSC_1.67 | 75 | 8.8 | 7.0 | 5.1 | 3.9 | 2.9 | 2.8 | 2.1 | 1.8 | 1.4 | 1.2 | 1.2 | 1.1 |
| GSSC_1.68 | 90 | 9.2 | 7.5 | 5.8 | 4.5 | 3.4 | 3.2 | 2.5 | 2.0 | 1.5 | 1.3 | 1.2 | 1.1 |
| GSSC_1.69 | 105 | 9.4 | 8.1 | 6.4 | 4.8 | 3.8 | 3.5 | 2.9 | 2.4 | 1.7 | 1.4 | 1.3 | 1.2 |
| GSSC_1.70 | 135 | 10.0 | 8.6 | 7.0 | 5.1 | 4.2 | 3.7 | 3.1 | 2.2 | 1.7 | 1.5 | 1.3 | 1.2 |
| GSSC_1.71 | 165 | 10.4 | 9.1 | 6.6 | 5.5 | 4.5 | 4.1 | 3.2 | 2.3 | 1.6 | 1.5 | 1.4 | 1.1 |
| GSSC_1.72 | 195 | 10.9 | 9.6 | 7.1 | 5.8 | 4.7 | 4.3 | 3.4 | 2.4 | 1.7 | 1.5 | 1.3 | 1.2 |
| GSSC_1.73 | 225 | 11.2 | 10.3 | 7.8 | 6.0 | 5.1 | 4.6 | 3.4 | 2.4 | 2.0 | 1.7 | 1.4 | 1.1 |
| GSSC_1.74 | 255 | 11.6 | 11.0 | 8.2 | 6.2 | 5.2 | 4.8 | 3.2 | 2.6 | 2.3 | 1.6 | 1.2 | 1.4 |
| GSSC_1.75 | 285 | 12.2 | 11.6 | 9.0 | 6.5 | 5.4 | 5.0 | 3.4 | 2.7 | 2.1 | 1.6 | 1.1 | 1.5 |

| (1) | (2) | (3) | (4) | (5) | (6) | (7) | (8) | (9) | (10) | (11) | (12) | (13) | (14) |
|---|---|---|---|---|---|---|---|---|---|---|---|---|---|
| GSSC_1.76 | 315 | 12.6 | 12.1 | 9.4 | 6.7 | 5.6 | 5.1 | 3.5 | 2.7 | 1.9 | 1.5 | 1.0 | 1.3 |
| GSSC_1.77 | 360 | 13.2 | 12.4 | 10.0 | 6.9 | 5.7 | 4.9 | 3.6 | 2.6 | 2.0 | 1.5 | 0.9 | 1.0 |
| GSSC_1.78 | 420 | 14.2 | 12.7 | 10.4 | 7.1 | 5.8 | 4.8 | 3.6 | 2.7 | 2.1 | 1.6 | 0.8 | 0.6 |
| GSSC_1.79 | 480 | 14.4 | 12.8 | 10.5 | 7.2 | 5.8 | 4.9 | 3.7 | 2.8 | 2.0 | 1.5 | 0.9 | 0.7 |
| GSSC_1.80 | 560 | 14.4 | 13.0 | 10.6 | 7.4 | 5.8 | 4.9 | 3.6 | 3.0 | 2.0 | 1.5 | 0.9 | 0.8 |
| GSSC_1.81 | 650 | 14.4 | 13.0 | 10.6 | 7.3 | 5.9 | 4.9 | 3.6 | 3.0 | 2.1 | 1.5 | 0.9 | 0.8 |
| GSSC_2.1 | 15 | 3.6 | 2.5 | 1.7 | 1.4 | 1.1 | 0.7 | 0.6 | 0.6 | 0.7 | 0.6 | 0.6 | 0.6 |
| GSSC_2.2 | 30 | 4.9 | 3.6 | 2.1 | 1.9 | 1.3 | 0.9 | 0.5 | 0.7 | 0.8 | 0.6 | 0.8 | 0.7 |
| GSSC_2.3 | 50 | 5.8 | 4.5 | 2.5 | 2.4 | 1.7 | 1.4 | 0.7 | 0.7 | 0.6 | 0.7 | 0.7 | 0.7 |
| GSSC_2.4 | 65 | 6.6 | 5.3 | 2.9 | 2.8 | 2.0 | 1.8 | 1.3 | 0.9 | 0.7 | 0.8 | 0.8 | 0.8 |
| GSSC_2.5 | 80 | 7.1 | 6.0 | 3.4 | 3.2 | 2.2 | 1.9 | 1.6 | 1.1 | 0.9 | 0.9 | 0.8 | 0.8 |
| GSSC_2.6 | 100 | 8.0 | 6.9 | 4.1 | 3.6 | 2.6 | 2.1 | 1.8 | 1.3 | 1.1 | 1.0 | 0.9 | 1.0 |
| GSSC_2.7 | 110 | 8.5 | 7.2 | 4.4 | 3.7 | 2.4 | 2.1 | 1.8 | 1.2 | 1.0 | 1.0 | 0.9 | 0.9 |
| GSSC_2.8 | 145 | 9.4 | 7.6 | 5.0 | 4.1 | 2.8 | 2.3 | 2.0 | 1.5 | 1.2 | 1.2 | 1.0 | 0.9 |
| GSSC_2.9 | 155 | 9.8 | 7.8 | 5.1 | 4.1 | 3.5 | 2.3 | 2.1 | 1.4 | 1.1 | 1.3 | 1.0 | 0.9 |
| GSSC_2.10 | 190 | 10.3 | 8.2 | 5.5 | 4.4 | 3.8 | 2.3 | 1.9 | 1.6 | 1.3 | 1.4 | 1.1 | 0.8 |
| GSSC_2.11 | 215 | 10.6 | 8.5 | 6.0 | 4.8 | 4.3 | 2.4 | 2.1 | 1.7 | 1.4 | 1.5 | 1.2 | 0.9 |
| GSSC_2.12 | 250 | 11.1 | 9.0 | 6.3 | 5.1 | 4.2 | 2.5 | 2.3 | 1.6 | 1.3 | 1.5 | 1.2 | 1.0 |
| GSSC_2.13 | 275 | 11.7 | 9.4 | 6.6 | 5.4 | 4.6 | 2.9 | 2.6 | 1.6 | 1.2 | 1.4 | 1.2 | 0.8 |
| GSSC_2.14 | 320 | 12.1 | 10.1 | 7.1 | 5.7 | 4.8 | 3.1 | 2.4 | 1.6 | 1.1 | 1.2 | 1.0 | 0.7 |
| GSSC_2.15 | 380 | 12.5 | 10.5 | 7.4 | 5.9 | 4.8 | 3.4 | 2.5 | 1.7 | 1.3 | 1.2 | 0.9 | 0.6 |
| GSSC_2.16 | 455 | 12.6 | 10.7 | 7.6 | 6.0 | 4.9 | 3.6 | 2.5 | 1.7 | 1.4 | 1.3 | 1.0 | 0.7 |
| GSSC_2.17 | 545 | 12.7 | 10.8 | 7.5 | 6.0 | 5.1 | 3.7 | 2.4 | 1.8 | 1.4 | 1.3 | 1.0 | 0.7 |
| GSSC_2.18 | 680 | 12.7 | 10.8 | 7.5 | 6.0 | 5.1 | 3.7 | 2.4 | 1.8 | 1.4 | 1.2 | 0.9 | 0.7 |
| GSSC_2.19 | 10 | 2.1 | 1.5 | 1.1 | 0.8 | 0.6 | 0.4 | 0.4 | 0.5 | 0.3 | 0.3 | 0.4 | 0.4 |
| GSSC_2.20 | 25 | 3.4 | 2.5 | 1.9 | 1.1 | 0.7 | 0.6 | 0.4 | 0.8 | 0.5 | 0.3 | 0.4 | 0.4 |
| GSSC_2.21 | 40 | 4.4 | 3.5 | 2.5 | 1.5 | 1.0 | 0.7 | 0.5 | 0.8 | 0.5 | 0.4 | 0.4 | 0.3 |
| GSSC_2.22 | 55 | 5.2 | 4.3 | 3.1 | 1.7 | 1.3 | 0.8 | 0.7 | 0.9 | 0.7 | 0.5 | 0.4 | 0.4 |
| GSSC_2.23 | 70 | 5.9 | 4.9 | 3.6 | 1.6 | 1.4 | 1.0 | 0.9 | 0.9 | 0.7 | 0.5 | 0.5 | 0.4 |

| (1) | (2) | (3) | (4) | (5) | (6) | (7) | (8) | (9) | (10) | (11) | (12) | (13) | (14) |
|---|---|---|---|---|---|---|---|---|---|---|---|---|---|
| GSSC_2.24 | 85 | 6.7 | 5.6 | 4.1 | 1.7 | 1.7 | 1.1 | 1.0 | 1.0 | 0.6 | 0.5 | 0.5 | 0.4 |
| GSSC_2.25 | 105 | 7.4 | 6.3 | 4.4 | 2.0 | 1.7 | 1.2 | 1.2 | 1.0 | 0.8 | 0.6 | 0.5 | 0.4 |
| GSSC_2.26 | 135 | 8.1 | 7.1 | 4.8 | 2.3 | 2.0 | 1.5 | 1.2 | 1.1 | 0.8 | 0.5 | 0.5 | 0.5 |
| GSSC_2.27 | 170 | 9.0 | 7.8 | 5.1 | 2.6 | 2.1 | 1.6 | 1.3 | 1.0 | 0.8 | 0.6 | 0.5 | 0.4 |
| GSSC_2.28 | 210 | 9.9 | 8.5 | 5.4 | 2.8 | 2.4 | 1.9 | 1.3 | 1.2 | 0.9 | 0.6 | 0.5 | 0.5 |
| GSSC_2.29 | 250 | 10.7 | 9.2 | 5.8 | 3.1 | 2.7 | 2.1 | 1.5 | 1.1 | 0.9 | 0.7 | 0.6 | 0.5 |
| GSSC_2.30 | 320 | 11.4 | 9.9 | 6.1 | 3.0 | 2.8 | 2.2 | 1.6 | 1.0 | 0.9 | 0.7 | 0.6 | 0.5 |
| GSSC_2.31 | 380 | 11.7 | 10.4 | 6.5 | 3.4 | 2.9 | 2.4 | 1.7 | 1.1 | 0.8 | 0.7 | 0.7 | 0.5 |
| GSSC_2.32 | 470 | 11.9 | 10.5 | 6.7 | 3.7 | 2.7 | 2.1 | 1.7 | 1.2 | 0.8 | 0.8 | 0.7 | 0.6 |
| GSSC_2.33 | 560 | 11.8 | 10.6 | 6.8 | 4.0 | 2.8 | 2.2 | 1.6 | 1.3 | 0.9 | 0.8 | 0.7 | 0.6 |
| GSSC_2.34 | 660 | 11.9 | 10.6 | 6.9 | 4.0 | 2.9 | 2.2 | 1.7 | 1.2 | 0.9 | 0.8 | 0.8 | 0.6 |
| GSSC_2.35 | 760 | 11.9 | 10.6 | 6.8 | 4.1 | 2.9 | 2.3 | 1.8 | 1.2 | 0.9 | 0.8 | 0.7 | 0.7 |
| GSSC_2.36 | 10 | 2.6 | 2.1 | 1.5 | 1.2 | 1.0 | 0.8 | 0.8 | 0.7 | 0.5 | 0.6 | 0.6 | 0.5 |
| GSSC_2.37 | 25 | 3.4 | 2.8 | 2.0 | 1.5 | 1.4 | 1.0 | 0.8 | 0.7 | 0.6 | 0.5 | 0.7 | 0.5 |
| GSSC_2.38 | 35 | 4.3 | 3.6 | 2.5 | 1.9 | 1.7 | 1.2 | 0.9 | 0.8 | 0.6 | 0.6 | 0.5 | 0.6 |
| GSSC_2.39 | 55 | 5.2 | 4.1 | 3.1 | 2.2 | 1.9 | 1.4 | 1.1 | 0.9 | 0.7 | 0.6 | 0.6 | 0.6 |
| GSSC_2.40 | 75 | 6.1 | 4.5 | 3.5 | 2.5 | 2.2 | 1.6 | 1.3 | 0.9 | 0.8 | 0.7 | 0.7 | 0.6 |
| GSSC_2.41 | 95 | 6.9 | 5.0 | 3.9 | 2.8 | 2.4 | 1.9 | 1.5 | 0.8 | 0.9 | 0.7 | 0.8 | 0.7 |
| GSSC_2.42 | 125 | 7.9 | 5.6 | 4.4 | 3.0 | 2.6 | 2.1 | 1.7 | 1.0 | 1.1 | 0.8 | 0.7 | 0.6 |
| GSSC_2.43 | 155 | 9.0 | 6.4 | 4.8 | 3.2 | 2.9 | 2.2 | 1.7 | 1.0 | 1.2 | 0.8 | 0.8 | 0.8 |
| GSSC_2.44 | 185 | 9.9 | 7.4 | 5.1 | 3.5 | 3.1 | 2.5 | 1.9 | 1.1 | 1.3 | 1.0 | 0.8 | 0.7 |
| GSSC_2.45 | 230 | 10.4 | 8.2 | 5.4 | 3.8 | 3.5 | 2.7 | 2.1 | 1.2 | 1.4 | 1.0 | 0.9 | 0.8 |
| GSSC_2.46 | 280 | 11.0 | 9.1 | 5.7 | 4.2 | 3.8 | 3.0 | 2.2 | 1.0 | 1.2 | 0.9 | 0.9 | 0.9 |
| GSSC_2.47 | 320 | 11.4 | 9.7 | 6.1 | 4.5 | 4.0 | 3.3 | 2.2 | 0.8 | 1.0 | 1.1 | 1.0 | 0.9 |
| GSSC_2.48 | 365 | 11.7 | 10.3 | 6.3 | 4.7 | 4.1 | 3.6 | 2.0 | 0.9 | 1.1 | 1.1 | 0.9 | 0.9 |
| GSSC_2.49 | 425 | 12.0 | 10.8 | 6.8 | 4.9 | 4.1 | 3.5 | 2.2 | 1.1 | 1.1 | 1.0 | 1.0 | 1.0 |
| GSSC_2.50 | 500 | 12.1 | 10.9 | 7.2 | 5.1 | 4.2 | 3.3 | 2.4 | 1.3 | 1.0 | 1.1 | 1.1 | 1.0 |
| GSSC_2.51 | 600 | 12.2 | 11.0 | 7.3 | 5.1 | 4.1 | 3.4 | 2.5 | 1.2 | 1.1 | 1.0 | 1.0 | 1.0 |
| GSSC_2.52 | 725 | 12.2 | 11.0 | 7.4 | 5.2 | 4.2 | 3.4 | 2.5 | 1.3 | 1.0 | 0.9 | 1.0 | 1.0 |

| (1) | (2) | (3) | (4) | (5) | (6) | (7) | (8) | (9) | (10) | (11) | (12) | (13) | (14) |
|---|---|---|---|---|---|---|---|---|---|---|---|---|---|
| GSSC_2.53 | 10 | 5.4 | 2.9 | 2.1 | 1.6 | 1.3 | 1.1 | 1.0 | 0.8 | 0.6 | 0.5 | 0.6 | 0.5 |
| GSSC_2.54 | 20 | 7.1 | 4.4 | 2.9 | 2.1 | 1.8 | 1.3 | 1.0 | 1.0 | 0.8 | 0.7 | 0.7 | 0.6 |
| GSSC_2.55 | 35 | 8.2 | 5.4 | 3.6 | 2.7 | 2.2 | 1.6 | 1.2 | 1.0 | 0.8 | 0.7 | 0.7 | 0.6 |
| GSSC_2.56 | 50 | 9.1 | 6.3 | 4.2 | 3.2 | 2.4 | 2.0 | 1.4 | 1.2 | 0.9 | 0.7 | 0.7 | 0.8 |
| GSSC_2.57 | 80 | 9.9 | 7.1 | 4.9 | 3.8 | 2.9 | 2.4 | 1.6 | 1.3 | 1.0 | 0.9 | 0.8 | 0.7 |
| GSSC_2.58 | 100 | 10.3 | 7.9 | 5.3 | 4.2 | 3.2 | 2.6 | 1.7 | 1.3 | 1.0 | 0.9 | 1.0 | 0.8 |
| GSSC_2.59 | 120 | 10.7 | 8.6 | 5.7 | 4.5 | 3.4 | 2.8 | 1.8 | 1.4 | 1.1 | 1.0 | 0.9 | 0.8 |
| GSSC_2.60 | 140 | 11.0 | 9.2 | 6.1 | 4.8 | 3.7 | 3.0 | 2.1 | 1.5 | 1.1 | 0.9 | 0.8 | 0.8 |
| GSSC_2.61 | 170 | 11.2 | 9.8 | 6.4 | 5.0 | 4.0 | 3.2 | 2.2 | 1.6 | 1.2 | 1.0 | 0.9 | 0.8 |
| GSSC_2.62 | 200 | 11.5 | 10.4 | 6.7 | 5.3 | 4.2 | 3.4 | 2.3 | 1.6 | 1.3 | 1.0 | 0.9 | 0.9 |
| GSSC_2.63 | 250 | 11.8 | 11.1 | 7.1 | 5.6 | 4.5 | 3.6 | 2.5 | 1.7 | 1.3 | 1.1 | 1.0 | 0.9 |
| GSSC_2.64 | 290 | 12.1 | 11.6 | 7.6 | 6.0 | 4.9 | 3.9 | 3.0 | 1.9 | 1.4 | 1.2 | 1.0 | 0.9 |
| GSSC_2.65 | 335 | 12.4 | 11.9 | 8.0 | 6.2 | 5.1 | 4.1 | 3.2 | 2.0 | 1.4 | 1.1 | 1.1 | 1.0 |
| GSSC_2.66 | 380 | 12.7 | 11.9 | 8.2 | 6.3 | 5.2 | 4.3 | 3.2 | 2.2 | 1.4 | 1.0 | 1.0 | 1.0 |
| GSSC_2.67 | 470 | 12.9 | 12.0 | 8.3 | 6.3 | 5.3 | 4.4 | 3.4 | 2.2 | 1.4 | 1.0 | 1.0 | 1.1 |
| GSSC_2.68 | 570 | 13.1 | 12.1 | 8.3 | 6.3 | 5.3 | 4.3 | 3.4 | 2.4 | 1.5 | 0.9 | 0.9 | 1.0 |
| GSSC_2.69 | 660 | 13.2 | 12.1 | 8.3 | 6.4 | 5.3 | 4.3 | 3.3 | 2.4 | 1.5 | 1.0 | 0.9 | 0.9 |
| GSSC_3.1 | 10 | 2.2 | 1.6 | 1.2 | 1.0 | 0.9 | 0.7 | 0.6 | 0.6 | 0.4 | 0.4 | 0.4 | 0.3 |
| GSSC_3.2 | 30 | 3.4 | 2.6 | 2.0 | 1.4 | 1.2 | 0.8 | 0.6 | 0.6 | 0.5 | 0.4 | 0.3 | 0.3 |
| GSSC_3.3 | 50 | 4.1 | 3.0 | 2.2 | 1.6 | 1.3 | 0.9 | 0.7 | 0.6 | 0.6 | 0.5 | 0.4 | 0.3 |
| GSSC_3.4 | 70 | 5.0 | 3.8 | 2.3 | 1.9 | 1.4 | 1.1 | 1.0 | 0.7 | 0.5 | 0.5 | 0.4 | 0.4 |
| GSSC_3.5 | 90 | 5.8 | 4.1 | 2.6 | 1.9 | 1.3 | 1.0 | 0.9 | 0.7 | 0.5 | 0.4 | 0.4 | 0.5 |
| GSSC_3.6 | 110 | 6.1 | 4.4 | 2.8 | 2.0 | 1.5 | 1.1 | 1.0 | 0.8 | 0.6 | 0.4 | 0.5 | 0.5 |
| GSSC_3.7 | 130 | 6.4 | 4.7 | 3.0 | 2.1 | 1.7 | 1.2 | 1.0 | 0.8 | 0.7 | 0.5 | 0.4 | 0.5 |
| GSSC_3.8 | 160 | 6.7 | 5.1 | 3.1 | 2.1 | 1.6 | 1.1 | 1.1 | 0.8 | 0.6 | 0.6 | 0.5 | 0.5 |
| GSSC_3.9 | 190 | 7.3 | 5.7 | 3.4 | 2.2 | 1.6 | 1.2 | 1.0 | 0.9 | 0.7 | 0.6 | 0.5 | 0.4 |
| GSSC_3.10 | 235 | 7.9 | 6.1 | 3.7 | 2.7 | 1.7 | 1.4 | 1.0 | 0.8 | 0.7 | 0.7 | 0.5 | 0.5 |
| GSSC_3.11 | 280 | 8.4 | 6.8 | 4.0 | 2.9 | 1.8 | 1.6 | 1.1 | 0.7 | 0.9 | 0.7 | 0.6 | 0.5 |
| GSSC_3.12 | 325 | 8.8 | 7.5 | 4.2 | 2.8 | 1.9 | 1.6 | 1.2 | 0.6 | 0.7 | 0.8 | 0.6 | 0.5 |

| (1) | (2) | (3) | (4) | (5) | (6) | (7) | (8) | (9) | (10) | (11) | (12) | (13) | (14) |
|---|---|---|---|---|---|---|---|---|---|---|---|---|---|
| GSSC_3.13 | 370 | 9.3 | 7.9 | 4.5 | 2.9 | 2.1 | 1.9 | 1.2 | 0.8 | 0.8 | 0.9 | 0.8 | 0.6 |
| GSSC_3.14 | 430 | 9.7 | 8.4 | 4.6 | 2.7 | 2.2 | 1.9 | 1.1 | 0.8 | 0.8 | 0.9 | 0.8 | 0.7 |
| GSSC_3.15 | 520 | 10.0 | 8.7 | 4.8 | 2.8 | 2.2 | 1.9 | 1.2 | 0.9 | 0.8 | 0.8 | 0.8 | 0.8 |
| GSSC_3.16 | 640 | 10.2 | 8.8 | 5.1 | 2.8 | 2.3 | 1.9 | 1.3 | 0.9 | 0.8 | 0.9 | 0.8 | 0.8 |
| GSSC_3.17 | 760 | 10.3 | 8.8 | 5.1 | 2.9 | 2.3 | 1.9 | 1.2 | 0.9 | 0.8 | 0.8 | 0.9 | 0.8 |
| GSSC_3.18 | 10 | 4.1 | 2.0 | 1.4 | 1.1 | 1.2 | 1.1 | 0.8 | 0.7 | 0.6 | 0.5 | 0.4 | 0.4 |
| GSSC_3.19 | 20 | 4.9 | 3.1 | 2.2 | 1.5 | 1.3 | 1.1 | 0.8 | 0.5 | 0.8 | 0.6 | 0.5 | 0.5 |
| GSSC_3.20 | 35 | 5.8 | 3.9 | 2.6 | 2.0 | 1.8 | 1.3 | 0.9 | 0.7 | 0.6 | 0.5 | 0.7 | 0.5 |
| GSSC_3.21 | 50 | 6.4 | 4.6 | 2.8 | 2.2 | 1.9 | 1.5 | 1.1 | 0.8 | 0.6 | 0.6 | 0.5 | 0.5 |
| GSSC_3.22 | 65 | 6.8 | 5.1 | 3.1 | 2.2 | 1.9 | 1.6 | 1.3 | 0.9 | 0.7 | 0.6 | 0.6 | 0.5 |
| GSSC_3.23 | 85 | 7.2 | 5.6 | 3.3 | 2.4 | 2.0 | 1.6 | 1.2 | 1.0 | 0.7 | 0.7 | 0.6 | 0.6 |
| GSSC_3.24 | 115 | 7.8 | 6.6 | 3.7 | 2.6 | 2.1 | 1.7 | 1.3 | 1.2 | 0.8 | 0.6 | 0.7 | 0.6 |
| GSSC_3.25 | 145 | 8.1 | 7.5 | 4.1 | 1.9 | 1.7 | 1.7 | 1.2 | 1.0 | 0.8 | 0.7 | 0.7 | 0.6 |
| GSSC_3.26 | 190 | 8.5 | 8.1 | 4.5 | 2.0 | 1.8 | 1.6 | 1.3 | 1.0 | 0.8 | 0.7 | 0.6 | 0.6 |
| GSSC_3.27 | 235 | 8.9 | 8.8 | 4.6 | 2.2 | 1.9 | 1.6 | 1.2 | 0.9 | 0.8 | 0.7 | 0.7 | 0.7 |
| GSSC_3.28 | 275 | 9.2 | 9.5 | 4.7 | 2.3 | 2.0 | 1.6 | 1.3 | 0.9 | 0.7 | 0.6 | 0.7 | 0.6 |
| GSSC_3.29 | 320 | 9.5 | 10.1 | 4.8 | 2.4 | 2.2 | 1.7 | 1.2 | 0.9 | 0.7 | 0.7 | 0.6 | 0.6 |
| GSSC_3.30 | 365 | 9.8 | 10.6 | 5.0 | 2.5 | 2.0 | 1.8 | 1.2 | 1.0 | 0.8 | 0.7 | 0.6 | 0.5 |
| GSSC_3.31 | 405 | 10.1 | 11.1 | 5.4 | 2.9 | 2.1 | 1.9 | 1.3 | 1.0 | 0.7 | 0.7 | 0.7 | 0.5 |
| GSSC_3.32 | 465 | 10.4 | 11.6 | 6.0 | 3.2 | 2.3 | 2.2 | 1.4 | 1.1 | 0.8 | 0.7 | 0.7 | 0.6 |
| GSSC_3.33 | 565 | 10.6 | 11.6 | 6.1 | 3.3 | 2.3 | 2.2 | 1.6 | 1.2 | 0.8 | 0.8 | 0.7 | 0.6 |
| GSSC_3.34 | 705 | 10.8 | 11.7 | 6.1 | 3.3 | 2.3 | 2.1 | 1.7 | 1.2 | 0.8 | 0.7 | 0.6 | 0.6 |
| GSSC_3.35 | 30 | 3.1 | 2.1 | 1.5 | 1.2 | 0.9 | 0.7 | 0.6 | 0.5 | 0.5 | 0.4 | 0.6 | 0.5 |
| GSSC_3.36 | 60 | 4.3 | 3.1 | 2.4 | 1.6 | 1.2 | 0.8 | 0.6 | 0.5 | 0.4 | 0.5 | 0.5 | 0.6 |
| GSSC_3.37 | 90 | 5.1 | 3.8 | 3.0 | 1.8 | 1.3 | 0.8 | 0.5 | 0.5 | 0.5 | 0.5 | 0.6 | 0.6 |
| GSSC_3.38 | 120 | 6.0 | 4.5 | 3.5 | 2.1 | 1.5 | 1.0 | 0.6 | 0.5 | 0.5 | 0.6 | 0.5 | 0.6 |
| GSSC_3.39 | 165 | 6.7 | 5.2 | 3.9 | 2.2 | 1.7 | 1.1 | 0.6 | 0.6 | 0.5 | 0.7 | 0.6 | 0.6 |
| GSSC_3.40 | 210 | 7.5 | 6.2 | 4.5 | 2.4 | 1.8 | 1.0 | 0.7 | 0.5 | 0.7 | 0.6 | 0.7 | 0.8 |
| GSSC_3.41 | 255 | 8.3 | 7.1 | 4.7 | 2.9 | 2.2 | 1.4 | 0.7 | 0.6 | 0.7 | 0.7 | 0.8 | 0.8 |

| (1) | (2) | (3) | (4) | (5) | (6) | (7) | (8) | (9) | (10) | (11) | (12) | (13) | (14) |
|---|---|---|---|---|---|---|---|---|---|---|---|---|---|
| GSSC_3.42 | 330 | 8.9 | 7.8 | 5.2 | 3.4 | 2.4 | 1.9 | 1.1 | 0.8 | 0.7 | 0.8 | 0.6 | 0.8 |
| GSSC_3.43 | 375 | 9.1 | 8.3 | 5.1 | 3.8 | 2.7 | 2.1 | 1.2 | 0.9 | 0.6 | 0.6 | 0.7 | 0.8 |
| GSSC_3.44 | 420 | 9.4 | 8.7 | 5.4 | 3.7 | 2.6 | 2.1 | 1.1 | 0.9 | 0.7 | 0.6 | 0.8 | 0.7 |
| GSSC_3.45 | 465 | 9.8 | 9.1 | 5.5 | 3.9 | 2.7 | 2.0 | 1.1 | 0.9 | 0.7 | 0.8 | 0.8 | 0.8 |
| GSSC_3.46 | 510 | 10.1 | 9.5 | 5.8 | 4.0 | 2.9 | 2.0 | 1.0 | 1.0 | 0.8 | 0.8 | 0.8 | 0.7 |
| GSSC_3.47 | 555 | 10.3 | 9.7 | 5.9 | 4.1 | 3.1 | 2.2 | 1.2 | 1.0 | 0.8 | 0.8 | 0.6 | 0.7 |
| GSSC_3.48 | 615 | 10.5 | 9.8 | 5.7 | 4.1 | 3.0 | 2.3 | 1.2 | 1.0 | 0.8 | 0.7 | 0.6 | 0.6 |
| GSSC_3.49 | 735 | 10.6 | 9.7 | 5.6 | 4.1 | 3.0 | 2.4 | 1.2 | 1.0 | 0.8 | 0.7 | 0.6 | 0.6 |
| GSSC_3.50 | 15 | 1.6 | 1.1 | 0.9 | 0.6 | 0.8 | 0.5 | 0.5 | 0.4 | 0.4 | 0.6 | 0.4 | 0.5 |
| GSSC_3.51 | 35 | 2.0 | 1.6 | 1.2 | 0.8 | 0.7 | 0.7 | 0.7 | 0.6 | 0.6 | 0.5 | 0.5 | 0.7 |
| GSSC_3.52 | 50 | 2.5 | 1.8 | 1.5 | 1.0 | 0.8 | 0.7 | 0.6 | 0.6 | 0.7 | 0.7 | 0.6 | 0.6 |
| GSSC_3.53 | 70 | 2.9 | 2.2 | 1.9 | 1.2 | 0.9 | 0.7 | 0.7 | 0.6 | 0.6 | 0.5 | 0.4 | 0.5 |
| GSSC_3.54 | 100 | 3.3 | 2.5 | 2.1 | 1.4 | 1.1 | 0.8 | 0.7 | 0.7 | 0.5 | 0.4 | 0.6 | 0.6 |
| GSSC_3.55 | 130 | 4.1 | 3.0 | 2.4 | 1.5 | 1.0 | 0.6 | 0.7 | 0.6 | 0.6 | 0.8 | 0.7 | 0.7 |
| GSSC_3.56 | 160 | 4.8 | 3.5 | 2.9 | 1.4 | 0.9 | 0.7 | 0.6 | 0.6 | 0.7 | 0.7 | 0.8 | 0.6 |
| GSSC_3.57 | 190 | 5.5 | 3.9 | 2.8 | 1.5 | 1.0 | 1.2 | 0.9 | 0.7 | 0.6 | 0.8 | 0.7 | 0.5 |
| GSSC_3.58 | 240 | 6.5 | 4.8 | 3.2 | 1.6 | 1.1 | 0.9 | 0.7 | 0.7 | 0.7 | 0.6 | 0.6 | 0.5 |
| GSSC_3.59 | 300 | 7.4 | 5.6 | 3.7 | 1.8 | 1.0 | 0.8 | 0.7 | 0.7 | 0.6 | 0.6 | 0.5 | 0.5 |
| GSSC_3.60 | 360 | 8.1 | 6.4 | 3.4 | 1.6 | 1.0 | 1.0 | 1.0 | 0.7 | 0.7 | 0.6 | 0.6 | 0.5 |
| GSSC_3.61 | 420 | 8.6 | 7.2 | 3.7 | 1.7 | 1.1 | 1.0 | 1.0 | 0.9 | 0.7 | 0.6 | 0.7 | 0.6 |
| GSSC_3.62 | 480 | 9.0 | 7.7 | 3.6 | 1.8 | 1.4 | 1.2 | 0.9 | 1.0 | 0.7 | 0.6 | 0.7 | 0.7 |
| GSSC_3.63 | 540 | 9.4 | 8.0 | 4.0 | 2.1 | 1.7 | 1.3 | 1.0 | 0.9 | 0.6 | 0.6 | 0.6 | 0.8 |
| GSSC_3.64 | 600 | 9.8 | 8.3 | 4.2 | 2.2 | 1.8 | 1.5 | 1.1 | 0.8 | 0.7 | 0.6 | 0.6 | 0.7 |
| GSSC_3.65 | 660 | 10.0 | 8.4 | 4.4 | 2.4 | 2.0 | 1.6 | 1.5 | 1.0 | 0.8 | 0.7 | 0.7 | 0.6 |
| GSSC_3.66 | 720 | 10.1 | 8.4 | 4.3 | 2.4 | 2.0 | 1.6 | 1.4 | 1.0 | 0.9 | 0.8 | 0.7 | 0.7 |
| GSSC_3.67 | 780 | 10.1 | 8.3 | 4.4 | 2.4 | 2.1 | 1.6 | 1.3 | 1.0 | 0.9 | 0.8 | 0.8 | 0.7 |
| GSSC_4.1 | 10 | 1.5 | 1.1 | 0.8 | 0.5 | 0.6 | 0.8 | 0.6 | 0.4 | 0.5 | 0.6 | 0.5 | 0.4 |
| GSSC_4.2 | 30 | 2.4 | 2.1 | 1.6 | 0.7 | 0.6 | 0.5 | 0.6 | 0.5 | 0.4 | 0.4 | 0.5 | 0.5 |
| GSSC_4.3 | 40 | 3.3 | 3.0 | 2.1 | 1.1 | 0.7 | 0.6 | 0.5 | 0.5 | 0.6 | 0.5 | 0.4 | 0.5 |

| (1) | (2) | (3) | (4) | (5) | (6) | (7) | (8) | (9) | (10) | (11) | (12) | (13) | (14) |
|---|---|---|---|---|---|---|---|---|---|---|---|---|---|
| GSSC_4.4 | 60 | 3.9 | 3.7 | 2.6 | 1.5 | 0.7 | 0.8 | 0.5 | 0.5 | 0.5 | 0.4 | 0.5 | 0.5 |
| GSSC_4.5 | 80 | 4.8 | 4.3 | 3.3 | 2.1 | 0.9 | 0.7 | 0.6 | 0.6 | 0.5 | 0.5 | 0.5 | 0.4 |
| GSSC_4.6 | 100 | 5.6 | 4.8 | 3.7 | 2.5 | 1.0 | 0.9 | 0.7 | 0.6 | 0.5 | 0.5 | 0.6 | 0.6 |
| GSSC_4.7 | 130 | 6.4 | 5.5 | 4.3 | 2.8 | 1.3 | 1.0 | 0.6 | 0.6 | 0.5 | 0.6 | 0.6 | 0.6 |
| GSSC_4.8 | 160 | 7.0 | 6.0 | 4.9 | 3.3 | 1.7 | 1.2 | 0.6 | 0.5 | 0.5 | 0.7 | 0.6 | 0.7 |
| GSSC_4.9 | 210 | 7.5 | 6.6 | 5.6 | 3.9 | 2.1 | 1.1 | 0.7 | 0.6 | 0.6 | 0.7 | 0.7 | 0.7 |
| GSSC_4.10 | 270 | 7.8 | 7.2 | 6.1 | 4.3 | 2.6 | 1.4 | 1.1 | 0.7 | 0.6 | 0.6 | 0.7 | 0.8 |
| GSSC_4.11 | 310 | 8.0 | 7.5 | 6.4 | 4.6 | 3.3 | 1.7 | 1.4 | 0.6 | 0.7 | 0.7 | 0.6 | 0.7 |
| GSSC_4.12 | 370 | 8.1 | 7.8 | 6.7 | 5.0 | 3.7 | 2.3 | 1.7 | 0.7 | 0.7 | 0.6 | 0.7 | 0.7 |
| GSSC_4.13 | 430 | 8.2 | 8.0 | 6.9 | 5.3 | 3.9 | 2.7 | 2.0 | 0.7 | 0.7 | 0.8 | 0.7 | 0.8 |
| GSSC_4.14 | 545 | 8.4 | 7.9 | 7.1 | 5.5 | 4.1 | 2.6 | 1.9 | 0.8 | 0.7 | 0.7 | 0.8 | 0.8 |
| GSSC_4.15 | 665 | 8.5 | 8.0 | 7.0 | 5.7 | 4.2 | 2.7 | 1.8 | 1.0 | 0.9 | 0.9 | 1.0 | 0.8 |
| GSSC_4.16 | 785 | 8.5 | 8.1 | 7.1 | 5.6 | 4.1 | 2.7 | 2.0 | 1.1 | 0.9 | 1.0 | 0.9 | 0.9 |
| GSSC_4.17 | 15 | 2.3 | 1.6 | 1.0 | 0.7 | 0.7 | 0.7 | 0.6 | 0.7 | 0.6 | 0.4 | 0.4 | 0.3 |
| GSSC_4.18 | 30 | 2.8 | 2.3 | 1.3 | 1.0 | 0.8 | 0.7 | 0.7 | 0.7 | 0.6 | 0.5 | 0.4 | 0.3 |
| GSSC_4.19 | 38 | 3.4 | 2.8 | 1.8 | 1.3 | 1.1 | 0.8 | 0.7 | 0.7 | 0.6 | 0.5 | 0.4 | 0.4 |
| GSSC_4.20 | 50 | 3.8 | 2.7 | 2.4 | 1.7 | 1.2 | 0.9 | 0.7 | 0.6 | 0.5 | 0.5 | 0.5 | 0.4 |
| GSSC_4.21 | 70 | 4.6 | 3.3 | 3.0 | 1.8 | 1.3 | 0.9 | 0.8 | 0.7 | 0.5 | 0.5 | 0.6 | 0.5 |
| GSSC_4.22 | 95 | 5.6 | 3.9 | 3.5 | 2.2 | 1.6 | 1.2 | 0.9 | 0.8 | 0.6 | 0.6 | 0.6 | 0.5 |
| GSSC_4.23 | 120 | 6.3 | 4.4 | 4.1 | 2.4 | 2.2 | 1.7 | 1.1 | 0.8 | 0.7 | 0.6 | 0.6 | 0.6 |
| GSSC_4.24 | 150 | 6.6 | 4.8 | 4.5 | 2.8 | 2.6 | 2.0 | 1.2 | 1.0 | 0.7 | 0.7 | 0.6 | 0.7 |
| GSSC_4.25 | 180 | 7.1 | 5.3 | 4.9 | 3.2 | 2.6 | 2.2 | 1.2 | 1.1 | 0.9 | 0.7 | 0.7 | 0.6 |
| GSSC_4.26 | 210 | 7.4 | 5.8 | 5.4 | 3.6 | 2.9 | 2.4 | 1.5 | 1.4 | 0.8 | 0.7 | 0.7 | 0.8 |
| GSSC_4.27 | 250 | 7.7 | 6.2 | 5.8 | 3.9 | 3.2 | 2.6 | 1.8 | 1.6 | 1.0 | 0.8 | 0.7 | 0.7 |
| GSSC_4.28 | 310 | 8.7 | 6.7 | 6.0 | 4.3 | 3.5 | 2.9 | 2.2 | 1.8 | 0.9 | 0.8 | 0.8 | 0.7 |
| GSSC_4.29 | 350 | 9.1 | 7.1 | 6.3 | 4.6 | 3.5 | 3.1 | 2.3 | 1.9 | 1.0 | 0.9 | 0.8 | 0.8 |
| GSSC_4.30 | 390 | 9.6 | 7.3 | 6.4 | 4.8 | 3.8 | 3.2 | 2.5 | 2.0 | 1.0 | 0.8 | 0.9 | 0.8 |
| GSSC_4.31 | 450 | 9.8 | 7.6 | 6.5 | 5.0 | 3.9 | 3.2 | 2.6 | 2.0 | 1.0 | 0.9 | 0.9 | 0.9 |
| GSSC_4.32 | 525 | 9.7 | 7.8 | 6.5 | 5.1 | 3.9 | 3.3 | 2.5 | 2.1 | 1.0 | 1.0 | 0.8 | 0.8 |

| (1) | (2) | (3) | (4) | (5) | (6) | (7) | (8) | (9) | (10) | (11) | (12) | (13) | (14) |
|---|---|---|---|---|---|---|---|---|---|---|---|---|---|
| GSSC_4.33 | 615 | 9.8 | 7.8 | 6.6 | 5.3 | 3.9 | 3.3 | 2.6 | 2.2 | 1.1 | 1.0 | 0.9 | 0.8 |
| GSSC_4.34 | 715 | 9.7 | 7.8 | 6.7 | 5.3 | 4.1 | 3.3 | 2.5 | 2.1 | 1.1 | 1.0 | 0.9 | 0.9 |
| GSSC_4.35 | 15 | 3.1 | 1.8 | 1.4 | 1.0 | 0.8 | 0.7 | 0.7 | 0.6 | 0.5 | 0.5 | 0.4 | 0.4 |
| GSSC_4.36 | 30 | 4.2 | 2.5 | 2.0 | 1.5 | 0.6 | 0.8 | 0.7 | 0.7 | 0.6 | 0.5 | 0.5 | 0.4 |
| GSSC_4.37 | 45 | 4.9 | 3.4 | 2.6 | 2.1 | 0.8 | 1.0 | 0.6 | 0.7 | 0.6 | 0.6 | 0.5 | 0.5 |
| GSSC_4.38 | 75 | 5.5 | 4.1 | 3.0 | 2.6 | 1.3 | 1.2 | 0.5 | 0.8 | 0.7 | 0.6 | 0.6 | 0.5 |
| GSSC_4.39 | 105 | 6.1 | 4.9 | 3.6 | 3.2 | 1.9 | 1.4 | 0.9 | 1.0 | 0.7 | 0.7 | 0.6 | 0.6 |
| GSSC_4.40 | 135 | 6.6 | 5.5 | 4.1 | 3.7 | 2.4 | 1.7 | 1.1 | 1.2 | 0.9 | 0.8 | 0.6 | 0.7 |
| GSSC_4.41 | 165 | 7.1 | 6.1 | 4.8 | 4.1 | 2.8 | 1.8 | 1.1 | 1.4 | 1.0 | 0.9 | 0.7 | 0.7 |
| GSSC_4.42 | 195 | 7.6 | 6.6 | 5.3 | 4.5 | 3.3 | 2.0 | 1.4 | 1.6 | 0.9 | 0.8 | 0.8 | 0.7 |
| GSSC_4.43 | 250 | 8.3 | 7.4 | 6.1 | 5.1 | 3.9 | 2.5 | 1.7 | 1.7 | 1.1 | 0.9 | 1.0 | 0.8 |
| GSSC_4.44 | 280 | 8.8 | 7.9 | 6.6 | 5.5 | 4.3 | 2.7 | 1.6 | 1.6 | 1.1 | 1.0 | 1.0 | 0.9 |
| GSSC_4.45 | 325 | 9.3 | 8.4 | 7.0 | 5.9 | 4.6 | 3.0 | 1.9 | 1.7 | 1.2 | 1.1 | 1.0 | 1.0 |
| GSSC_4.46 | 400 | 9.7 | 8.7 | 7.3 | 6.2 | 4.9 | 3.4 | 2.3 | 1.9 | 1.4 | 1.1 | 1.1 | 1.0 |
| GSSC_4.47 | 430 | 9.6 | 8.6 | 7.3 | 6.5 | 5.1 | 3.8 | 2.7 | 2.1 | 1.2 | 1.0 | 0.9 | 0.9 |
| GSSC_4.48 | 460 | 9.9 | 8.8 | 7.5 | 6.7 | 5.3 | 4.0 | 2.9 | 2.2 | 1.2 | 0.9 | 1.0 | 0.9 |
| GSSC_4.49 | 500 | 10.1 | 8.9 | 7.7 | 6.9 | 5.5 | 4.3 | 3.3 | 2.3 | 1.4 | 0.9 | 0.9 | 1.0 |
| GSSC_4.50 | 530 | 10.1 | 8.9 | 7.6 | 6.8 | 5.6 | 4.6 | 3.5 | 2.4 | 1.6 | 1.0 | 1.0 | 0.9 |
| GSSC_4.51 | 565 | 10.3 | 9.1 | 7.6 | 7.0 | 5.6 | 4.8 | 3.4 | 2.4 | 1.7 | 1.0 | 1.0 | 1.0 |
| GSSC_4.52 | 625 | 10.4 | 9.2 | 7.7 | 7.0 | 5.7 | 5.0 | 3.5 | 2.4 | 1.8 | 1.1 | 1.0 | 1.0 |
| GSSC_4.53 | 710 | 10.4 | 9.2 | 7.9 | 7.0 | 5.8 | 4.9 | 3.6 | 2.4 | 1.7 | 1.1 | 0.9 | 0.9 |
| GSSC_4.54 | 15 | 1.7 | 1.6 | 1.0 | 0.7 | 0.6 | 0.6 | 0.7 | 0.7 | 0.5 | 0.8 | 0.6 | 0.6 |
| GSSC_4.55 | 35 | 2.6 | 2.2 | 1.4 | 0.9 | 0.7 | 0.7 | 0.5 | 0.5 | 0.6 | 0.5 | 0.6 | 0.5 |
| GSSC_4.56 | 50 | 3.3 | 3.0 | 2.0 | 1.3 | 0.9 | 0.8 | 0.7 | 0.5 | 0.7 | 0.8 | 0.7 | 0.6 |
| GSSC_4.57 | 70 | 4.0 | 3.7 | 2.2 | 1.6 | 1.2 | 0.8 | 0.8 | 0.7 | 0.8 | 0.8 | 0.7 | 0.6 |
| GSSC_4.58 | 85 | 4.5 | 4.3 | 2.5 | 1.9 | 1.4 | 0.9 | 0.9 | 0.8 | 0.8 | 0.8 | 0.7 | 0.7 |
| GSSC_4.59 | 100 | 4.9 | 4.8 | 2.9 | 2.1 | 1.5 | 1.1 | 0.9 | 0.9 | 0.8 | 0.9 | 0.8 | 0.7 |
| GSSC_4.60 | 130 | 5.3 | 5.1 | 3.1 | 2.3 | 1.8 | 1.2 | 1.0 | 0.8 | 0.8 | 0.8 | 0.8 | 0.7 |
| GSSC_4.61 | 150 | 5.7 | 5.5 | 3.4 | 2.5 | 2.0 | 1.2 | 1.1 | 0.9 | 0.8 | 0.9 | 0.8 | 0.8 |

| (1) | (2) | (3) | (4) | (5) | (6) | (7) | (8) | (9) | (10) | (11) | (12) | (13) | (14) |
|---|---|---|---|---|---|---|---|---|---|---|---|---|---|
| GSSC_4.62 | 180 | 6.2 | 5.8 | 4.1 | 2.7 | 1.9 | 1.5 | 1.2 | 0.8 | 0.9 | 0.8 | 1.0 | 0.9 |
| GSSC_4.63 | 210 | 6.4 | 6.3 | 4.7 | 3.0 | 2.1 | 1.5 | 1.1 | 0.9 | 0.9 | 0.8 | 0.9 | 0.8 |
| GSSC_4.64 | 270 | 6.8 | 6.5 | 5.3 | 3.4 | 2.5 | 1.5 | 1.2 | 0.9 | 0.9 | 1.0 | 1.0 | 0.9 |
| GSSC_4.65 | 330 | 7.1 | 6.2 | 5.8 | 3.8 | 3.1 | 1.6 | 1.2 | 0.9 | 0.9 | 0.8 | 0.9 | 1.0 |
| GSSC_4.66 | 390 | 7.4 | 6.4 | 6.1 | 4.1 | 3.5 | 1.9 | 1.3 | 1.0 | 0.8 | 0.9 | 1.0 | 1.0 |
| GSSC_4.67 | 460 | 7.6 | 6.6 | 6.3 | 4.3 | 3.8 | 2.2 | 1.4 | 1.1 | 1.0 | 1.1 | 1.2 | 1.0 |
| GSSC_4.68 | 550 | 7.6 | 6.8 | 6.2 | 4.5 | 3.8 | 2.4 | 1.3 | 1.1 | 1.1 | 1.2 | 1.2 | 1.3 |
| GSSC_4.69 | 650 | 7.7 | 6.8 | 6.4 | 4.6 | 3.9 | 2.6 | 1.3 | 1.1 | 1.1 | 1.1 | 1.2 | 1.3 |
| GSSC_4.70 | 770 | 7.7 | 6.8 | 6.4 | 4.6 | 3.9 | 2.6 | 1.3 | 0.9 | 1.1 | 1.2 | 1.2 | 1.3 |
| GSSC_5.1 | 15 | 1.3 | 1.1 | 0.9 | 0.9 | 0.7 | 0.6 | 0.6 | 0.5 | 0.6 | 0.4 | 0.5 | 0.5 |
| GSSC_5.2 | 30 | 1.7 | 1.5 | 1.2 | 0.8 | 0.7 | 0.9 | 0.7 | 0.6 | 0.5 | 0.5 | 0.4 | 0.6 |
| GSSC_5.3 | 50 | 2.0 | 1.8 | 1.5 | 1.3 | 0.9 | 0.7 | 0.7 | 0.6 | 0.7 | 0.5 | 0.6 | 0.5 |
| GSSC_5.4 | 70 | 2.3 | 2.0 | 2.0 | 1.9 | 1.3 | 0.9 | 0.8 | 0.8 | 0.7 | 0.6 | 0.7 | 0.5 |
| GSSC_5.5 | 100 | 2.6 | 2.3 | 2.5 | 2.3 | 1.6 | 0.9 | 0.8 | 1.1 | 0.9 | 0.6 | 0.7 | 0.6 |
| GSSC_5.6 | 130 | 3.1 | 2.8 | 3.0 | 2.7 | 1.9 | 1.0 | 0.8 | 0.9 | 0.8 | 0.7 | 0.8 | 0.7 |
| GSSC_5.7 | 175 | 3.5 | 3.2 | 3.4 | 3.1 | 2.2 | 0.9 | 0.9 | 0.7 | 0.7 | 0.8 | 0.9 | 0.7 |
| GSSC_5.8 | 235 | 3.8 | 3.7 | 3.9 | 3.3 | 2.4 | 1.0 | 0.9 | 0.8 | 0.8 | 0.7 | 0.9 | 0.8 |
| GSSC_5.9 | 295 | 4.2 | 4.1 | 4.1 | 3.5 | 2.5 | 1.2 | 0.9 | 0.8 | 1.0 | 0.8 | 0.9 | 0.9 |
| GSSC_5.10 | 355 | 4.5 | 4.6 | 4.4 | 3.7 | 2.4 | 1.4 | 1.1 | 0.8 | 1.0 | 0.9 | 0.9 | 1.0 |
| GSSC_5.11 | 415 | 4.7 | 5.0 | 4.6 | 3.7 | 2.5 | 1.6 | 1.1 | 0.9 | 0.9 | 1.0 | 1.1 | 1.0 |
| GSSC_5.12 | 475 | 4.9 | 5.3 | 4.7 | 3.9 | 2.7 | 1.6 | 1.0 | 0.7 | 1.0 | 1.0 | 1.1 | 0.8 |
| GSSC_5.13 | 535 | 5.1 | 5.5 | 4.9 | 3.8 | 2.8 | 1.7 | 0.9 | 0.8 | 0.9 | 0.9 | 1.1 | 0.8 |
| GSSC_5.14 | 595 | 5.2 | 5.6 | 5.1 | 3.9 | 2.8 | 1.8 | 1.1 | 0.8 | 0.8 | 1.0 | 0.9 | 0.9 |
| GSSC_5.15 | 655 | 5.2 | 5.8 | 5.0 | 4.0 | 3.0 | 2.0 | 1.2 | 0.9 | 0.9 | 1.0 | 0.9 | 1.0 |
| GSSC_5.16 | 715 | 5.3 | 5.7 | 5.2 | 4.0 | 3.0 | 1.9 | 1.2 | 0.9 | 0.9 | 0.9 | 0.9 | 0.9 |
| GSSC_5.17 | 790 | 5.3 | 5.7 | 5.1 | 4.1 | 2.9 | 1.9 | 1.2 | 0.9 | 0.9 | 0.9 | 0.8 | 0.9 |
| GSSC_5.18 | 15 | 1.0 | 1.1 | 0.9 | 0.8 | 0.8 | 0.7 | 0.7 | 0.6 | 0.5 | 0.4 | 0.4 | 0.3 |
| GSSC_5.19 | 25 | 1.3 | 1.9 | 1.4 | 1.1 | 1.0 | 0.8 | 0.7 | 0.6 | 0.6 | 0.5 | 0.4 | 0.4 |
| GSSC_5.20 | 40 | 1.5 | 2.5 | 1.8 | 1.4 | 1.2 | 0.9 | 0.8 | 0.7 | 0.6 | 0.6 | 0.5 | 0.6 |

| (1) | (2) | (3) | (4) | (5) | (6) | (7) | (8) | (9) | (10) | (11) | (12) | (13) | (14) |
|---|---|---|---|---|---|---|---|---|---|---|---|---|---|
| GSSC_5.21 | 65 | 1.7 | 3.1 | 2.1 | 1.5 | 1.4 | 1.1 | 0.9 | 0.7 | 0.7 | 0.7 | 0.6 | 0.6 |
| GSSC_5.22 | 95 | 2.0 | 3.8 | 2.5 | 1.7 | 1.4 | 1.3 | 0.9 | 0.8 | 0.7 | 0.8 | 0.7 | 0.7 |
| GSSC_5.23 | 125 | 2.4 | 4.4 | 3.0 | 2.0 | 1.3 | 1.2 | 1.1 | 0.9 | 0.8 | 0.8 | 0.7 | 0.8 |
| GSSC_5.24 | 155 | 2.8 | 4.8 | 3.4 | 2.3 | 1.5 | 1.1 | 1.1 | 0.8 | 0.9 | 0.9 | 0.8 | 0.8 |
| GSSC_5.25 | 185 | 3.3 | 5.0 | 3.7 | 2.2 | 1.8 | 1.2 | 1.0 | 1.0 | 0.9 | 0.9 | 0.9 | 0.8 |
| GSSC_5.26 | 215 | 3.7 | 5.4 | 4.1 | 2.5 | 1.7 | 1.4 | 1.2 | 0.9 | 1.0 | 1.0 | 1.0 | 0.8 |
| GSSC_5.27 | 255 | 4.1 | 5.8 | 4.4 | 2.8 | 2.0 | 1.6 | 1.2 | 1.0 | 1.1 | 1.0 | 0.9 | 0.8 |
| GSSC_5.28 | 295 | 4.4 | 6.1 | 4.7 | 3.2 | 2.4 | 1.9 | 1.3 | 1.1 | 1.0 | 1.2 | 0.9 | 1.0 |
| GSSC_5.29 | 375 | 5.2 | 6.4 | 5.1 | 3.6 | 2.7 | 2.1 | 1.4 | 1.2 | 1.1 | 1.1 | 1.0 | 0.9 |
| GSSC_5.30 | 435 | 5.9 | 6.6 | 5.5 | 4.0 | 2.9 | 2.3 | 1.5 | 1.2 | 1.2 | 1.1 | 1.1 | 1.0 |
| GSSC_5.31 | 510 | 6.3 | 6.9 | 5.6 | 4.3 | 3.0 | 2.4 | 1.4 | 1.1 | 1.0 | 1.2 | 1.0 | 0.9 |
| GSSC_5.32 | 585 | 6.5 | 7.0 | 5.7 | 4.4 | 3.1 | 2.3 | 1.4 | 1.0 | 0.9 | 0.9 | 1.0 | 0.8 |
| GSSC_5.33 | 705 | 6.6 | 7.1 | 5.7 | 4.4 | 3.1 | 2.3 | 1.3 | 1.0 | 1.0 | 1.0 | 0.9 | 0.9 |
| GSSC_5.34 | 780 | 6.5 | 7.1 | 5.7 | 4.4 | 3.1 | 2.3 | 1.4 | 1.0 | 1.0 | 0.8 | 0.8 | 0.7 |
| GSSC_5.35 | 15 | 1.1 | 0.9 | 1.2 | 1.0 | 0.8 | 0.7 | 0.5 | 0.6 | 0.6 | 0.3 | 0.5 | 0.4 |
| GSSC_5.36 | 30 | 1.9 | 1.4 | 2.0 | 1.7 | 1.1 | 0.9 | 0.7 | 0.7 | 0.7 | 0.5 | 0.6 | 0.5 |
| GSSC_5.37 | 60 | 2.7 | 2.1 | 2.6 | 2.4 | 0.9 | 0.8 | 0.8 | 0.9 | 0.7 | 0.5 | 0.6 | 0.6 |
| GSSC_5.38 | 90 | 3.5 | 2.9 | 3.0 | 2.9 | 1.4 | 1.1 | 0.9 | 0.8 | 0.8 | 0.7 | 0.7 | 0.6 |
| GSSC_5.39 | 135 | 4.2 | 3.8 | 3.5 | 3.5 | 1.9 | 1.0 | 1.0 | 1.1 | 0.9 | 0.8 | 0.7 | 0.7 |
| GSSC_5.40 | 170 | 4.8 | 4.6 | 4.0 | 4.2 | 2.3 | 1.4 | 0.9 | 1.2 | 0.8 | 0.8 | 0.7 | 0.8 |
| GSSC_5.41 | 255 | 6.0 | 5.6 | 4.6 | 4.7 | 2.8 | 1.9 | 1.2 | 1.1 | 0.7 | 0.8 | 0.8 | 0.7 |
| GSSC_5.42 | 305 | 6.4 | 6.4 | 5.1 | 5.3 | 3.4 | 2.4 | 1.4 | 1.1 | 0.8 | 0.7 | 0.8 | 0.8 |
| GSSC_5.43 | 400 | 7.0 | 6.9 | 5.8 | 5.7 | 3.7 | 2.8 | 1.5 | 1.0 | 0.9 | 0.9 | 0.8 | 0.9 |
| GSSC_5.44 | 450 | 7.3 | 7.1 | 6.2 | 5.8 | 4.0 | 3.2 | 1.7 | 1.2 | 1.1 | 1.0 | 0.9 | 0.9 |
| GSSC_5.45 | 530 | 7.5 | 7.4 | 6.5 | 5.9 | 4.2 | 3.4 | 2.0 | 1.5 | 1.0 | 0.9 | 1.0 | 0.9 |
| GSSC_5.46 | 650 | 7.7 | 7.5 | 6.7 | 5.8 | 4.4 | 3.6 | 2.2 | 1.7 | 0.9 | 0.9 | 1.0 | 1.0 |
| GSSC_5.47 | 740 | 7.8 | 7.7 | 6.7 | 6.0 | 4.4 | 3.7 | 2.2 | 1.6 | 1.1 | 1.0 | 1.0 | 1.0 |
| GSSC_5.48 | 800 | 7.8 | 7.7 | 6.8 | 5.9 | 4.5 | 3.6 | 2.3 | 1.6 | 1.2 | 1.0 | 0.9 | 1.0 |
| GSSC_5.49 | 10 | 1.3 | 1.1 | 1.2 | 1.1 | 0.9 | 1.0 | 0.8 | 0.6 | 0.5 | 0.5 | 0.5 | 0.4 |

| (1) | (2) | (3) | (4) | (5) | (6) | (7) | (8) | (9) | (10) | (11) | (12) | (13) | (14) |
|---|---|---|---|---|---|---|---|---|---|---|---|---|---|
| GSSC_5.50 | 25 | 2.4 | 1.8 | 1.5 | 1.2 | 1.2 | 1.0 | 0.9 | 0.7 | 0.6 | 0.6 | 0.5 | 0.4 |
| GSSC_5.51 | 50 | 3.4 | 2.5 | 2.1 | 1.6 | 1.4 | 0.9 | 0.9 | 0.7 | 0.6 | 0.6 | 0.6 | 0.5 |
| GSSC_5.52 | 85 | 4.5 | 3.3 | 2.8 | 2.2 | 1.7 | 1.1 | 1.0 | 0.9 | 0.7 | 0.8 | 0.7 | 0.5 |
| GSSC_5.53 | 125 | 5.5 | 4.3 | 3.3 | 2.8 | 2.0 | 1.3 | 1.2 | 1.0 | 0.7 | 0.9 | 0.6 | 0.6 |
| GSSC_5.54 | 155 | 6.3 | 5.2 | 3.9 | 3.3 | 2.3 | 1.4 | 1.4 | 1.1 | 0.9 | 1.0 | 0.7 | 0.8 |
| GSSC_5.55 | 240 | 7.2 | 6.2 | 4.9 | 3.8 | 2.8 | 1.7 | 1.5 | 1.3 | 1.0 | 1.1 | 0.9 | 0.9 |
| GSSC_5.56 | 300 | 7.8 | 6.9 | 5.6 | 4.6 | 3.3 | 1.9 | 1.6 | 1.2 | 1.1 | 1.4 | 1.0 | 0.8 |
| GSSC_5.57 | 350 | 8.4 | 7.6 | 6.0 | 5.2 | 3.6 | 2.2 | 1.2 | 1.1 | 1.1 | 1.2 | 1.0 | 0.8 |
| GSSC_5.58 | 420 | 8.9 | 8.0 | 6.5 | 5.5 | 4.0 | 2.1 | 1.5 | 1.1 | 1.0 | 0.7 | 1.0 | 0.9 |
| GSSC_5.59 | 455 | 9.1 | 8.2 | 6.8 | 5.7 | 4.2 | 2.2 | 1.6 | 1.2 | 1.0 | 0.8 | 0.9 | 0.8 |
| GSSC_5.60 | 515 | 9.3 | 8.3 | 7.0 | 5.9 | 4.1 | 2.4 | 1.5 | 1.1 | 0.8 | 0.8 | 0.9 | 0.9 |
| GSSC_5.61 | 590 | 9.4 | 8.2 | 7.3 | 6.1 | 4.2 | 2.6 | 1.6 | 1.2 | 0.9 | 0.9 | 0.8 | 0.9 |
| GSSC_5.62 | 670 | 9.5 | 8.4 | 7.2 | 6.2 | 4.2 | 2.7 | 1.7 | 1.2 | 0.9 | 0.9 | 0.8 | 0.8 |
| GSSC_5.63 | 760 | 9.4 | 8.4 | 7.2 | 6.3 | 4.1 | 2.8 | 1.6 | 1.2 | 1.0 | 0.8 | 0.8 | 0.8 |
| GSSC_0.1 | 20 | 4.0 | 2.9 | 1.5 | 1.4 | 1.3 | 1.1 | 0.9 | 0.9 | 0.7 | 0.7 | 1.0 | 0.9 |
| GSSC_0.2 | 40 | 6.4 | 3.7 | 2.2 | 1.9 | 1.4 | 1.2 | 1.1 | 1.2 | 1.0 | 1.0 | 1.1 | 1.2 |
| GSSC_0.3 | 60 | 7.5 | 4.3 | 2.8 | 2.2 | 1.7 | 1.5 | 1.3 | 1.4 | 1.1 | 1.2 | 1.2 | 1.1 |
| GSSC_0.4 | 90 | 8.3 | 5.0 | 3.5 | 2.6 | 1.8 | 1.7 | 1.4 | 1.3 | 1.1 | 1.3 | 1.2 | 1.1 |
| GSSC_0.5 | 135 | 9.1 | 5.8 | 4.3 | 3.2 | 2.3 | 1.8 | 1.5 | 1.4 | 1.3 | 1.2 | 1.1 | 1.1 |
| GSSC_0.6 | 210 | 10.1 | 6.6 | 5.0 | 3.9 | 2.8 | 1.9 | 1.5 | 1.5 | 1.4 | 1.3 | 1.1 | 1.1 |
| GSSC_0.7 | 270 | 10.8 | 7.3 | 5.7 | 4.6 | 3.3 | 2.2 | 1.6 | 1.6 | 1.5 | 1.2 | 1.0 | 1.0 |
| GSSC_0.8 | 350 | 11.7 | 7.9 | 6.2 | 5.1 | 3.6 | 2.4 | 1.6 | 1.8 | 1.4 | 1.4 | 1.2 | 1.0 |
| GSSC_0.9 | 390 | 12.1 | 8.4 | 6.6 | 5.4 | 3.8 | 2.5 | 1.7 | 1.7 | 1.3 | 1.4 | 1.3 | 0.9 |
| GSSC_0.10 | 470 | 12.4 | 8.8 | 6.9 | 5.6 | 3.9 | 2.4 | 1.6 | 1.6 | 1.3 | 1.3 | 1.3 | 1.0 |
| GSSC_0.11 | 540 | 12.6 | 8.9 | 7.1 | 5.8 | 4.2 | 2.5 | 1.7 | 1.5 | 1.3 | 1.3 | 1.2 | 1.0 |
| GSSC_0.12 | 660 | 12.8 | 9.1 | 7.2 | 5.9 | 4.1 | 2.3 | 1.5 | 1.6 | 1.5 | 1.2 | 1.1 | 1.0 |
| GSSC_0.13 | 830 | 12.9 | 9.1 | 7.3 | 5.9 | 4.1 | 2.3 | 1.5 | 1.5 | 1.4 | 1.2 | 1.1 | 0.9 |
| GSSC_0.14 | 25 | 6.4 | 4.9 | 2.4 | 1.8 | 1.5 | 1.1 | 0.7 | 0.5 | 0.5 | 0.6 | 0.8 | 0.5 |
| GSSC_0.15 | 40 | 9.2 | 6.3 | 3.4 | 2.3 | 1.7 | 1.3 | 1.0 | 0.9 | 0.9 | 0.8 | 0.9 | 0.8 |

| (1) | (2) | (3) | (4) | (5) | (6) | (7) | (8) | (9) | (10) | (11) | (12) | (13) | (14) |
|---|---|---|---|---|---|---|---|---|---|---|---|---|---|
| GSSC_0.16 | 60 | 11.1 | 8.2 | 4.6 | 2.7 | 1.9 | 1.5 | 1.2 | 1.2 | 1.3 | 1.0 | 1.1 | 1.0 |
| GSSC_0.17 | 83 | 12.2 | 10.1 | 5.7 | 3.4 | 2.3 | 1.7 | 1.4 | 1.4 | 1.6 | 1.7 | 1.2 | 1.1 |
| GSSC_0.18 | 123 | 13.4 | 11.3 | 6.9 | 3.8 | 2.5 | 1.9 | 1.6 | 1.7 | 1.5 | 1.6 | 1.2 | 1.0 |
| GSSC_0.19 | 143 | 14.0 | 12.4 | 7.7 | 4.0 | 2.6 | 2.1 | 1.7 | 2.0 | 1.6 | 1.4 | 1.2 | 1.2 |
| GSSC_0.20 | 183 | 14.3 | 13.1 | 7.7 | 4.1 | 2.6 | 2.0 | 1.7 | 2.0 | 1.6 | 1.5 | 1.4 | 1.4 |
| GSSC_0.21 | 228 | 14.6 | 13.5 | 7.9 | 4.6 | 2.8 | 2.0 | 1.7 | 1.9 | 1.7 | 1.7 | 1.4 | 1.4 |
| GSSC_0.22 | 283 | 14.7 | 13.7 | 8.1 | 4.8 | 2.9 | 2.1 | 1.8 | 1.8 | 1.7 | 1.9 | 1.3 | 1.3 |
| GSSC_0.23 | 328 | 14.6 | 13.7 | 8.1 | 4.9 | 3.0 | 2.3 | 1.9 | 1.8 | 1.6 | 1.8 | 1.3 | 1.2 |
| GSSC_0.24 | 15 | 5.3 | 3.2 | 2.1 | 1.0 | 0.8 | 0.8 | 0.6 | 0.5 | 0.4 | 0.3 | 0.3 | 0.2 |
| GSSC_0.25 | 33 | 7.6 | 5.0 | 2.5 | 1.5 | 1.2 | 1.0 | 0.7 | 0.6 | 0.7 | 0.6 | 0.5 | 0.6 |
| GSSC_0.26 | 59 | 10.0 | 7.9 | 3.7 | 1.9 | 1.6 | 1.4 | 1.0 | 0.8 | 1.0 | 0.7 | 0.7 | 0.9 |
| GSSC_0.27 | 87 | 11.8 | 10.2 | 4.5 | 2.3 | 1.6 | 1.6 | 1.3 | 1.1 | 1.2 | 0.8 | 0.8 | 1.1 |
| GSSC_0.28 | 143 | 12.4 | 11.0 | 5.3 | 2.5 | 1.8 | 1.7 | 1.5 | 1.2 | 1.3 | 0.8 | 0.8 | 1.2 |
| GSSC_0.29 | 192 | 12.7 | 11.7 | 6.1 | 2.9 | 1.9 | 1.8 | 1.7 | 1.4 | 1.3 | 0.9 | 0.8 | 1.3 |
| GSSC_0.30 | 272 | 12.9 | 12.0 | 7.2 | 3.3 | 2.1 | 1.9 | 1.8 | 1.4 | 1.4 | 1.1 | 0.9 | 1.1 |
| GSSC_0.31 | 325 | 13.1 | 12.1 | 7.7 | 3.4 | 2.2 | 2.0 | 1.9 | 1.5 | 1.4 | 1.1 | 0.9 | 1.2 |
| GSSC_0.32 | 380 | 13.1 | 12.0 | 7.9 | 3.4 | 2.3 | 2.1 | 1.9 | 1.5 | 1.4 | 1.1 | 1.0 | 1.1 |
| GSSC_0.33 | 14 | 6.9 | 5.2 | 2.7 | 2.1 | 1.3 | 1.0 | 0.6 | 0.5 | 0.6 | 0.4 | 0.5 | 0.3 |
| GSSC_0.34 | 30 | 8.9 | 7.7 | 3.5 | 2.6 | 1.6 | 0.9 | 0.7 | 0.8 | 0.7 | 1.0 | 0.6 | 0.5 |
| GSSC_0.35 | 49 | 10.6 | 9.9 | 4.4 | 3.2 | 1.9 | 1.2 | 0.8 | 0.9 | 1.2 | 0.8 | 0.4 | 0.4 |
| GSSC_0.36 | 69 | 11.8 | 11.1 | 6.0 | 3.8 | 2.3 | 1.5 | 1.1 | 1.3 | 1.5 | 1.1 | 0.7 | 0.6 |
| GSSC_0.37 | 89 | 12.5 | 12.1 | 7.3 | 4.4 | 2.5 | 1.8 | 1.2 | 1.6 | 1.7 | 1.3 | 1.0 | 0.9 |
| GSSC_0.38 | 113 | 13.2 | 12.9 | 8.9 | 4.7 | 2.6 | 2.1 | 1.4 | 1.6 | 1.6 | 1.3 | 0.7 | 0.6 |
| GSSC_0.39 | 141 | 13.9 | 13.6 | 10.3 | 5.1 | 2.8 | 2.2 | 1.6 | 1.5 | 1.4 | 1.4 | 0.8 | 0.9 |
| GSSC_0.40 | 170 | 14.3 | 14.3 | 10.5 | 5.2 | 3.0 | 2.2 | 1.6 | 1.4 | 1.4 | 1.3 | 0.7 | 0.8 |
| GSSC_0.41 | 194 | 14.5 | 14.4 | 10.4 | 5.3 | 3.1 | 2.2 | 1.6 | 1.5 | 1.4 | 1.2 | 0.8 | 0.8 |
| SSC_1.1 | 10 | 3.3 | 3.1 | 2.5 | 2.1 | 1.5 | 1.4 | 1.0 | 0.6 | 0.8 | 0.7 | 0.5 | 0.7 |
| SSC_1.2 | 20 | 4.4 | 4.0 | 3.6 | 3.0 | 2.4 | 1.7 | 1.3 | 1.1 | 1.1 | 0.8 | 0.6 | 0.7 |
| SSC_1.3 | 30 | 5.3 | 4.9 | 4.2 | 3.3 | 2.7 | 2.0 | 1.3 | 1.4 | 1.3 | 0.9 | 0.8 | 0.8 |

| (1) | (2) | (3) | (4) | (5) | (6) | (7) | (8) | (9) | (10) | (11) | (12) | (13) | (14) |
|---|---|---|---|---|---|---|---|---|---|---|---|---|---|
| SSC_1.4 | 40 | 6.1 | 5.6 | 5.0 | 3.7 | 2.8 | 2.3 | 1.5 | 1.6 | 1.5 | 1.2 | 1.0 | 0.9 |
| SSC_1.5 | 50 | 6.8 | 6.3 | 5.6 | 4.1 | 3.1 | 2.1 | 1.6 | 1.8 | 1.7 | 1.5 | 1.3 | 1.1 |
| SSC_1.6 | 65 | 7.3 | 6.8 | 6.3 | 4.7 | 3.3 | 2.5 | 1.7 | 1.6 | 1.9 | 1.6 | 1.5 | 1.4 |
| SSC_1.7 | 80 | 7.8 | 7.2 | 6.7 | 5.1 | 3.7 | 2.8 | 2.0 | 2.0 | 2.1 | 1.9 | 1.8 | 1.6 |
| SSC_1.8 | 115 | 8.3 | 7.7 | 7.1 | 6.1 | 4.4 | 3.1 | 2.3 | 2.3 | 2.3 | 2.1 | 1.9 | 1.8 |
| SSC_1.9 | 145 | 9.0 | 8.1 | 7.7 | 6.6 | 5.1 | 3.5 | 2.5 | 2.3 | 2.4 | 2.3 | 2.1 | 2.1 |
| SSC_1.10 | 190 | 10.1 | 8.8 | 8.2 | 7.1 | 6.0 | 4.3 | 3.0 | 3.0 | 2.6 | 2.6 | 2.3 | 2.4 |
| SSC_1.11 | 230 | 10.9 | 9.4 | 8.8 | 7.5 | 6.4 | 5.1 | 3.4 | 3.2 | 2.9 | 2.8 | 2.7 | 2.5 |
| SSC_1.12 | 265 | 11.6 | 10.0 | 9.3 | 7.8 | 6.8 | 5.6 | 3.9 | 3.4 | 3.0 | 2.9 | 2.8 | 2.6 |
| SSC_1.13 | 320 | 12.3 | 10.5 | 9.6 | 8.2 | 7.1 | 5.9 | 4.3 | 3.6 | 3.3 | 3.1 | 3.0 | 2.9 |
| SSC_1.14 | 385 | 12.6 | 10.7 | 9.8 | 8.5 | 7.3 | 6.2 | 4.4 | 3.8 | 3.4 | 3.2 | 3.2 | 2.9 |
| SSC_1.15 | 445 | 12.7 | 10.9 | 10.0 | 8.6 | 7.5 | 6.5 | 4.6 | 4.0 | 3.6 | 3.4 | 3.3 | 3.0 |
| SSC_1.16 | 505 | 12.7 | 11.0 | 10.2 | 8.7 | 7.7 | 6.6 | 4.6 | 3.9 | 3.5 | 3.4 | 3.3 | 3.1 |
| SSC_1.17 | 565 | 12.8 | 11.1 | 10.2 | 8.9 | 7.8 | 6.7 | 4.6 | 4.0 | 3.4 | 3.3 | 3.3 | 3.2 |
| SSC_1.18 | 625 | 12.8 | 11.1 | 10.2 | 9.0 | 7.8 | 6.6 | 4.7 | 3.9 | 3.4 | 3.3 | 3.2 | 3.2 |
| SSC_1.19 | 15 | 2.2 | 1.8 | 1.5 | 1.1 | 0.8 | 0.7 | 0.7 | 0.6 | 0.6 | 0.5 | 0.5 | 0.8 |
| SSC_1.20 | 30 | 3.1 | 2.6 | 2.3 | 1.4 | 1.2 | 1.0 | 0.8 | 0.7 | 0.6 | 0.6 | 0.5 | 0.6 |
| SSC_1.21 | 45 | 4.0 | 3.4 | 2.7 | 1.9 | 1.6 | 1.3 | 1.0 | 0.9 | 0.7 | 0.7 | 0.6 | 0.7 |
| SSC_1.22 | 65 | 4.8 | 4.1 | 3.3 | 2.3 | 2.1 | 1.5 | 1.2 | 0.9 | 0.8 | 0.7 | 0.7 | 0.7 |
| SSC_1.23 | 95 | 5.4 | 4.6 | 3.8 | 2.7 | 2.3 | 1.7 | 1.4 | 1.2 | 0.9 | 0.7 | 0.8 | 0.8 |
| SSC_1.24 | 125 | 5.8 | 5.1 | 4.2 | 3.1 | 2.5 | 1.9 | 1.5 | 1.2 | 0.9 | 0.9 | 0.8 | 0.9 |
| SSC_1.25 | 170 | 6.5 | 5.7 | 4.8 | 3.4 | 2.9 | 2.3 | 1.7 | 1.4 | 1.0 | 0.9 | 0.9 | 0.8 |
| SSC_1.26 | 200 | 6.9 | 6.1 | 5.2 | 3.7 | 3.3 | 2.6 | 1.9 | 1.6 | 1.1 | 0.9 | 1.0 | 0.9 |
| SSC_1.27 | 235 | 7.5 | 6.6 | 5.6 | 4.0 | 3.6 | 2.9 | 2.1 | 1.7 | 1.2 | 1.0 | 1.0 | 1.0 |
| SSC_1.28 | 275 | 8.1 | 7.1 | 6.0 | 4.3 | 4.0 | 3.2 | 2.3 | 2.0 | 1.5 | 1.1 | 1.0 | 1.1 |
| SSC_1.29 | 315 | 8.6 | 7.5 | 6.4 | 4.6 | 4.3 | 3.4 | 2.4 | 2.1 | 1.7 | 1.4 | 1.2 | 1.0 |
| SSC_1.30 | 340 | 9.1 | 8.0 | 6.8 | 5.0 | 4.6 | 3.8 | 2.6 | 2.2 | 1.8 | 1.5 | 1.3 | 1.2 |
| SSC_1.31 | 400 | 9.7 | 8.4 | 7.3 | 5.4 | 5.0 | 4.0 | 2.8 | 2.5 | 2.0 | 1.7 | 1.4 | 1.4 |
| SSC_1.32 | 460 | 10.3 | 8.7 | 7.5 | 5.7 | 5.3 | 4.2 | 3.2 | 2.6 | 2.2 | 1.9 | 1.5 | 1.4 |

| (1) | (2) | (3) | (4) | (5) | (6) | (7) | (8) | (9) | (10) | (11) | (12) | (13) | (14) |
|---|---|---|---|---|---|---|---|---|---|---|---|---|---|
| SSC_1.33 | 520 | 10.7 | 8.8 | 7.7 | 5.9 | 5.4 | 4.4 | 3.3 | 2.6 | 2.2 | 1.8 | 1.6 | 1.4 |
| SSC_1.34 | 610 | 10.9 | 8.8 | 7.8 | 5.9 | 5.5 | 4.5 | 3.2 | 2.7 | 2.2 | 1.9 | 1.6 | 1.3 |
| SSC_1.35 | 670 | 10.9 | 8.9 | 7.8 | 5.9 | 5.4 | 4.5 | 3.4 | 2.7 | 2.3 | 1.8 | 1.5 | 1.3 |
| SSC_1.36 | 10 | 1.7 | 1.3 | 1.1 | 0.8 | 0.8 | 0.7 | 0.6 | 0.6 | 0.5 | 0.6 | 0.6 | 0.7 |
| SSC_1.37 | 30 | 2.5 | 2.0 | 1.6 | 1.2 | 1.0 | 1.0 | 0.9 | 0.7 | 0.6 | 0.6 | 0.7 | 0.7 |
| SSC_1.38 | 40 | 3.1 | 2.7 | 2.2 | 1.6 | 1.3 | 1.1 | 0.9 | 0.7 | 0.7 | 0.7 | 0.8 | 0.8 |
| SSC_1.39 | 55 | 4.1 | 3.4 | 3.0 | 2.2 | 1.2 | 1.5 | 1.3 | 1.1 | 0.8 | 0.8 | 0.8 | 0.9 |
| SSC_1.40 | 100 | 5.2 | 4.2 | 3.5 | 2.8 | 1.6 | 1.3 | 1.2 | 1.1 | 1.0 | 0.8 | 0.9 | 0.9 |
| SSC_1.41 | 150 | 5.9 | 4.8 | 4.0 | 3.1 | 2.0 | 1.5 | 1.3 | 1.2 | 1.0 | 0.9 | 0.9 | 0.8 |
| SSC_1.42 | 220 | 6.6 | 5.4 | 4.5 | 3.5 | 2.8 | 2.0 | 1.5 | 1.3 | 1.0 | 1.1 | 1.1 | 1.0 |
| SSC_1.43 | 270 | 7.2 | 6.0 | 5.0 | 4.0 | 3.2 | 2.2 | 1.8 | 1.5 | 1.2 | 1.2 | 1.3 | 1.2 |
| SSC_1.44 | 330 | 7.8 | 6.5 | 5.4 | 4.3 | 3.5 | 2.5 | 2.0 | 1.6 | 1.4 | 1.3 | 1.2 | 1.3 |
| SSC_1.45 | 390 | 8.4 | 7.1 | 5.9 | 4.7 | 3.9 | 3.0 | 2.3 | 1.9 | 1.5 | 1.5 | 1.3 | 1.4 |
| SSC_1.46 | 450 | 9.0 | 7.8 | 6.5 | 5.2 | 4.2 | 3.3 | 2.6 | 2.2 | 1.8 | 1.6 | 1.4 | 1.4 |
| SSC_1.47 | 510 | 9.6 | 8.2 | 6.9 | 5.7 | 4.6 | 3.6 | 2.9 | 2.4 | 2.1 | 1.8 | 1.6 | 1.5 |
| SSC_1.48 | 570 | 9.8 | 8.4 | 6.9 | 5.8 | 4.7 | 3.6 | 2.8 | 2.2 | 2.0 | 1.8 | 1.6 | 1.6 |
| SSC_1.49 | 660 | 9.9 | 8.4 | 7.0 | 5.7 | 4.7 | 3.6 | 2.7 | 2.1 | 2.0 | 1.7 | 1.7 | 1.6 |
| SSC_1.50 | 10 | 2.6 | 2.1 | 1.3 | 1.0 | 0.8 | 0.9 | 0.6 | 0.6 | 0.7 | 0.6 | 0.5 | 0.7 |
| SSC_1.51 | 25 | 3.7 | 3.0 | 1.8 | 1.5 | 1.3 | 1.1 | 0.7 | 0.7 | 0.6 | 0.6 | 0.5 | 0.6 |
| SSC_1.52 | 35 | 4.6 | 3.8 | 2.4 | 1.8 | 1.5 | 1.4 | 1.0 | 0.9 | 0.9 | 0.7 | 0.6 | 0.7 |
| SSC_1.53 | 45 | 5.1 | 4.2 | 2.9 | 2.2 | 1.8 | 1.5 | 1.2 | 1.0 | 0.9 | 0.7 | 0.8 | 0.8 |
| SSC_1.54 | 55 | 5.5 | 4.5 | 3.3 | 2.6 | 2.1 | 1.7 | 1.3 | 1.1 | 1.0 | 0.8 | 0.8 | 0.9 |
| SSC_1.55 | 70 | 6.0 | 4.9 | 3.7 | 2.9 | 2.4 | 2.0 | 1.5 | 1.2 | 1.0 | 0.9 | 0.8 | 1.0 |
| SSC_1.56 | 90 | 6.6 | 5.4 | 4.4 | 2.7 | 2.5 | 2.2 | 1.8 | 1.5 | 1.3 | 1.0 | 0.9 | 0.9 |
| SSC_1.57 | 115 | 7.3 | 6.2 | 5.1 | 3.3 | 3.0 | 2.5 | 2.1 | 1.6 | 1.2 | 1.0 | 0.9 | 1.0 |
| SSC_1.58 | 150 | 8.0 | 6.9 | 5.7 | 3.8 | 3.3 | 2.8 | 2.4 | 1.7 | 1.4 | 1.2 | 1.2 | 1.1 |
| SSC_1.59 | 185 | 8.7 | 7.5 | 6.1 | 4.2 | 3.6 | 3.1 | 2.7 | 1.9 | 1.6 | 1.5 | 1.4 | 1.2 |
| SSC_1.60 | 230 | 9.3 | 8.1 | 6.6 | 4.6 | 3.9 | 3.3 | 2.9 | 2.2 | 1.8 | 1.7 | 1.5 | 1.3 |
| SSC_1.61 | 275 | 10.0 | 8.7 | 7.2 | 5.1 | 4.4 | 3.4 | 2.8 | 2.4 | 1.9 | 1.8 | 1.6 | 1.3 |

| (1) | (2) | (3) | (4) | (5) | (6) | (7) | (8) | (9) | (10) | (11) | (12) | (13) | (14) |
|---|---|---|---|---|---|---|---|---|---|---|---|---|---|
| SSC_1.62 | 330 | 10.7 | 9.3 | 7.7 | 5.5 | 4.8 | 3.7 | 3.0 | 2.6 | 2.0 | 2.0 | 1.7 | 1.5 |
| SSC_1.63 | 405 | 11.3 | 9.6 | 7.9 | 5.8 | 5.0 | 3.8 | 3.2 | 2.9 | 2.2 | 2.1 | 1.8 | 1.6 |
| SSC_1.64 | 485 | 11.5 | 9.6 | 8.1 | 5.9 | 5.0 | 3.9 | 3.4 | 2.9 | 2.3 | 2.0 | 1.8 | 1.7 |
| SSC_1.65 | 555 | 11.5 | 9.7 | 8.1 | 6.1 | 5.1 | 4.0 | 3.5 | 2.8 | 2.4 | 1.9 | 1.8 | 1.7 |
| SSC_1.66 | 630 | 11.6 | 9.6 | 8.2 | 6.1 | 5.2 | 4.1 | 3.4 | 2.8 | 2.3 | 1.8 | 1.7 | 1.7 |
| SSC_2.1 | 15 | 2.6 | 2.1 | 1.4 | 1.1 | 0.7 | 0.6 | 0.8 | 0.6 | 0.5 | 0.4 | 0.3 | 0.4 |
| SSC_2.2 | 35 | 3.8 | 3.2 | 2.0 | 1.6 | 1.1 | 0.9 | 0.7 | 0.5 | 0.5 | 0.6 | 0.4 | 0.5 |
| SSC_2.3 | 60 | 4.4 | 3.6 | 2.4 | 1.9 | 1.4 | 1.2 | 0.9 | 0.7 | 0.6 | 0.5 | 0.5 | 0.5 |
| SSC_2.4 | 95 | 5.0 | 4.1 | 2.9 | 2.3 | 1.6 | 1.4 | 1.2 | 0.8 | 0.6 | 0.5 | 0.6 | 0.6 |
| SSC_2.5 | 120 | 5.4 | 4.5 | 3.3 | 2.6 | 2.1 | 1.7 | 1.4 | 1.0 | 0.7 | 0.6 | 0.6 | 0.7 |
| SSC_2.6 | 145 | 5.9 | 5.0 | 3.6 | 2.8 | 2.3 | 1.7 | 1.5 | 1.1 | 0.9 | 0.7 | 0.7 | 0.6 |
| SSC_2.7 | 210 | 6.7 | 5.7 | 4.1 | 3.2 | 2.7 | 2.0 | 1.7 | 1.2 | 0.9 | 0.8 | 0.7 | 0.7 |
| SSC_2.8 | 265 | 7.4 | 6.3 | 5.1 | 3.9 | 3.2 | 2.3 | 1.8 | 1.3 | 0.9 | 0.8 | 0.8 | 0.8 |
| SSC_2.9 | 330 | 8.2 | 7.0 | 5.8 | 4.3 | 3.5 | 2.4 | 1.9 | 1.5 | 1.1 | 1.0 | 0.9 | 0.9 |
| SSC_2.10 | 385 | 8.9 | 7.7 | 6.3 | 4.8 | 3.8 | 2.6 | 2.0 | 1.6 | 1.2 | 1.0 | 1.0 | 0.9 |
| SSC_2.11 | 445 | 9.8 | 8.1 | 6.9 | 5.2 | 4.1 | 2.8 | 2.2 | 1.7 | 1.3 | 1.1 | 1.0 | 1.0 |
| SSC_2.12 | 515 | 10.3 | 8.4 | 7.1 | 5.2 | 4.2 | 3.0 | 2.2 | 1.7 | 1.4 | 1.2 | 1.0 | 1.1 |
| SSC_2.13 | 585 | 10.4 | 8.5 | 7.1 | 5.2 | 4.2 | 3.1 | 2.1 | 1.6 | 1.3 | 1.2 | 1.1 | 1.1 |
| SSC_2.14 | 680 | 10.4 | 8.5 | 7.2 | 5.2 | 4.2 | 3.0 | 2.1 | 1.6 | 1.2 | 1.1 | 1.1 | 1.0 |
| SSC_2.15 | 35 | 1.7 | 1.3 | 1.1 | 0.9 | 0.6 | 0.5 | 0.4 | 0.5 | 0.5 | 0.4 | 0.3 | 0.5 |
| SSC_2.16 | 70 | 2.4 | 1.9 | 1.7 | 1.4 | 1.0 | 0.8 | 0.6 | 0.5 | 0.7 | 0.6 | 0.5 | 0.6 |
| SSC_2.17 | 90 | 2.8 | 2.2 | 2.1 | 1.6 | 1.3 | 1.0 | 0.9 | 0.7 | 0.6 | 0.7 | 0.7 | 0.6 |
| SSC_2.18 | 130 | 3.5 | 2.6 | 2.3 | 1.9 | 1.6 | 1.2 | 1.0 | 0.8 | 0.7 | 0.8 | 0.7 | 0.7 |
| SSC_2.19 | 180 | 4.3 | 3.2 | 2.8 | 2.3 | 2.1 | 1.5 | 1.2 | 0.9 | 0.9 | 1.0 | 0.9 | 1.0 |
| SSC_2.20 | 240 | 5.1 | 3.8 | 3.2 | 2.7 | 2.4 | 1.7 | 1.3 | 1.1 | 0.9 | 0.9 | 1.0 | 1.1 |
| SSC_2.21 | 305 | 6.0 | 4.4 | 3.5 | 3.1 | 2.7 | 1.9 | 1.6 | 1.2 | 0.9 | 0.8 | 0.9 | 1.2 |
| SSC_2.22 | 370 | 6.8 | 5.2 | 3.9 | 3.4 | 3.0 | 2.2 | 1.9 | 1.4 | 1.1 | 0.9 | 1.0 | 1.1 |
| SSC_2.23 | 430 | 7.5 | 5.6 | 4.4 | 3.7 | 3.3 | 2.4 | 2.1 | 1.6 | 1.2 | 1.0 | 1.1 | 1.2 |
| SSC_2.24 | 495 | 8.3 | 6.0 | 4.6 | 4.0 | 3.4 | 2.6 | 2.2 | 1.8 | 1.3 | 1.1 | 1.0 | 1.1 |

| (1) | (2) | (3) | (4) | (5) | (6) | (7) | (8) | (9) | (10) | (11) | (12) | (13) | (14) |
|---|---|---|---|---|---|---|---|---|---|---|---|---|---|
| SSC_2.25 | 610 | 9.0 | 6.3 | 4.7 | 4.2 | 3.5 | 2.5 | 2.1 | 1.8 | 1.4 | 1.1 | 1.0 | 1.0 |
| SSC_2.26 | 700 | 9.3 | 6.5 | 4.8 | 4.2 | 3.4 | 2.5 | 2.0 | 1.7 | 1.3 | 1.0 | 1.1 | 1.0 |
| SSC_2.27 | 15 | 2.9 | 2.5 | 2.0 | 1.3 | 1.1 | 0.8 | 0.7 | 0.6 | 0.7 | 0.6 | 0.4 | 0.5 |
| SSC_2.28 | 30 | 3.6 | 3.0 | 2.6 | 1.9 | 1.4 | 1.0 | 0.6 | 0.6 | 0.6 | 0.6 | 0.5 | 0.3 |
| SSC_2.29 | 45 | 4.4 | 3.7 | 3.2 | 2.4 | 1.7 | 1.2 | 0.8 | 0.7 | 0.9 | 0.8 | 0.7 | 0.5 |
| SSC_2.30 | 60 | 5.1 | 4.3 | 3.9 | 3.0 | 2.1 | 1.5 | 1.0 | 0.8 | 0.9 | 1.0 | 0.8 | 0.7 |
| SSC_2.31 | 75 | 5.8 | 4.8 | 4.2 | 3.4 | 2.6 | 1.9 | 1.3 | 1.1 | 1.2 | 1.1 | 0.9 | 0.8 |
| SSC_2.32 | 95 | 6.4 | 5.3 | 4.8 | 3.7 | 2.8 | 2.2 | 1.5 | 1.2 | 1.3 | 1.2 | 1.1 | 0.9 |
| SSC_2.33 | 115 | 6.8 | 5.9 | 5.2 | 4.1 | 3.1 | 2.5 | 1.7 | 1.2 | 1.4 | 1.3 | 1.2 | 1.1 |
| SSC_2.34 | 140 | 7.2 | 6.2 | 5.6 | 4.4 | 3.6 | 2.8 | 1.9 | 1.5 | 1.5 | 1.5 | 1.4 | 1.2 |
| SSC_2.35 | 160 | 7.5 | 6.7 | 6.0 | 4.7 | 4.0 | 3.1 | 2.1 | 1.6 | 1.5 | 1.6 | 1.5 | 1.4 |
| SSC_2.36 | 190 | 8.1 | 7.2 | 6.4 | 5.1 | 4.3 | 3.4 | 2.3 | 1.7 | 1.6 | 1.6 | 1.6 | 1.5 |
| SSC_2.37 | 220 | 8.7 | 7.8 | 6.8 | 5.5 | 4.6 | 3.8 | 2.6 | 1.9 | 1.7 | 1.6 | 1.8 | 1.7 |
| SSC_2.38 | 250 | 9.1 | 8.2 | 7.2 | 5.9 | 4.9 | 4.2 | 3.0 | 2.1 | 1.9 | 1.9 | 2.0 | 1.8 |
| SSC_2.39 | 285 | 9.7 | 8.9 | 7.7 | 6.2 | 5.1 | 4.5 | 3.4 | 2.3 | 2.1 | 2.0 | 2.1 | 1.8 |
| SSC_2.40 | 325 | 10.3 | 9.3 | 8.1 | 6.6 | 5.5 | 4.8 | 3.7 | 2.5 | 2.2 | 2.2 | 2.3 | 2.0 |
| SSC_2.41 | 385 | 11.0 | 9.8 | 8.5 | 6.9 | 5.8 | 5.0 | 4.0 | 2.7 | 2.3 | 2.2 | 2.3 | 2.1 |
| SSC_2.42 | 430 | 11.4 | 10.1 | 8.8 | 7.1 | 5.9 | 5.2 | 4.2 | 2.8 | 2.4 | 2.3 | 2.2 | 2.1 |
| SSC_2.43 | 490 | 11.6 | 10.2 | 9.0 | 7.3 | 6.1 | 5.2 | 4.2 | 3.0 | 2.5 | 2.2 | 2.2 | 2.2 |
| SSC_2.44 | 550 | 11.7 | 10.2 | 9.2 | 7.4 | 6.3 | 5.3 | 4.2 | 3.1 | 2.4 | 2.2 | 2.3 | 2.2 |
| SSC_2.45 | 640 | 11.6 | 10.3 | 9.2 | 7.4 | 6.4 | 5.3 | 4.1 | 3.1 | 2.3 | 2.2 | 2.2 | 2.1 |
| SSC_2.46 | 15 | 2.1 | 1.6 | 1.2 | 0.9 | 0.8 | 0.6 | 0.6 | 0.7 | 0.5 | 0.6 | 0.3 | 0.4 |
| SSC_2.47 | 30 | 3.0 | 2.3 | 1.7 | 1.3 | 1.0 | 0.8 | 0.8 | 0.6 | 0.7 | 0.7 | 0.5 | 0.5 |
| SSC_2.48 | 45 | 3.6 | 2.7 | 2.1 | 1.6 | 1.3 | 1.1 | 1.0 | 0.9 | 0.7 | 0.8 | 0.6 | 0.5 |
| SSC_2.49 | 60 | 4.1 | 3.1 | 2.4 | 1.9 | 1.5 | 1.2 | 1.0 | 0.8 | 0.9 | 0.9 | 0.8 | 0.6 |
| SSC_2.50 | 80 | 4.6 | 3.5 | 2.8 | 2.2 | 1.8 | 1.4 | 1.2 | 1.1 | 1.0 | 1.0 | 1.1 | 0.8 |
| SSC_2.51 | 100 | 5.5 | 4.1 | 3.3 | 2.6 | 2.1 | 1.7 | 1.5 | 1.2 | 1.0 | 1.1 | 1.0 | 0.9 |
| SSC_2.52 | 130 | 6.1 | 4.6 | 3.8 | 3.0 | 2.4 | 1.9 | 1.6 | 1.4 | 1.2 | 1.3 | 1.2 | 1.1 |
| SSC_2.53 | 180 | 6.8 | 5.2 | 4.4 | 3.5 | 2.8 | 2.2 | 1.7 | 1.3 | 1.2 | 1.1 | 1.4 | 1.3 |

| (1) | (2) | (3) | (4) | (5) | (6) | (7) | (8) | (9) | (10) | (11) | (12) | (13) | (14) |
|---|---|---|---|---|---|---|---|---|---|---|---|---|---|
| SSC_2.54 | 220 | 7.3 | 5.9 | 5.0 | 4.1 | 3.2 | 2.5 | 2.0 | 1.5 | 1.6 | 1.4 | 1.5 | 1.5 |
| SSC_2.55 | 280 | 8.1 | 6.6 | 5.6 | 4.5 | 3.6 | 2.8 | 2.3 | 1.9 | 1.7 | 1.6 | 1.5 | 1.6 |
| SSC_2.56 | 325 | 8.6 | 7.1 | 6.2 | 5.0 | 4.0 | 3.2 | 2.6 | 2.1 | 1.9 | 1.9 | 1.7 | 1.8 |
| SSC_2.57 | 370 | 9.1 | 7.6 | 6.6 | 5.4 | 4.5 | 3.5 | 3.0 | 2.3 | 2.1 | 1.9 | 1.8 | 1.9 |
| SSC_2.58 | 430 | 9.5 | 8.1 | 7.0 | 5.8 | 4.8 | 3.9 | 3.2 | 2.5 | 2.2 | 2.0 | 1.9 | 1.9 |
| SSC_2.59 | 490 | 9.7 | 8.4 | 7.3 | 6.0 | 5.1 | 4.1 | 3.2 | 2.6 | 2.1 | 2.2 | 1.9 | 2.0 |
| SSC_2.60 | 550 | 9.8 | 8.6 | 7.4 | 6.1 | 5.1 | 4.2 | 3.2 | 2.7 | 2.2 | 2.2 | 2.0 | 2.0 |
| SSC_2.61 | 610 | 9.9 | 8.6 | 7.4 | 6.2 | 5.2 | 4.1 | 3.2 | 2.6 | 2.2 | 2.1 | 2.1 | 2.1 |
| SSC_2.62 | 670 | 9.9 | 8.6 | 7.4 | 6.2 | 5.3 | 4.2 | 3.0 | 2.7 | 2.1 | 2.1 | 2.1 | 2.1 |
| SSC_3.1 | 10 | 1.7 | 1.5 | 1.1 | 1.0 | 0.6 | 0.4 | 0.5 | 0.4 | 0.4 | 0.5 | 0.3 | 0.4 |
| SSC_3.2 | 30 | 2.4 | 1.9 | 1.4 | 1.3 | 0.8 | 0.6 | 0.3 | 0.4 | 0.3 | 0.3 | 0.3 | 0.4 |
| SSC_3.3 | 40 | 2.7 | 2.1 | 1.7 | 1.5 | 1.1 | 0.8 | 0.6 | 0.4 | 0.3 | 0.4 | 0.4 | 0.5 |
| SSC_3.4 | 50 | 3.0 | 2.4 | 2.1 | 1.8 | 1.5 | 1.0 | 0.8 | 0.5 | 0.4 | 0.4 | 0.5 | 0.5 |
| SSC_3.5 | 70 | 3.4 | 2.7 | 2.5 | 2.1 | 1.7 | 1.3 | 1.0 | 0.7 | 0.5 | 0.5 | 0.5 | 0.6 |
| SSC_3.6 | 95 | 3.8 | 3.1 | 3.0 | 2.5 | 1.9 | 1.6 | 1.2 | 0.9 | 0.6 | 0.7 | 0.6 | 0.7 |
| SSC_3.7 | 125 | 4.2 | 3.6 | 3.6 | 2.9 | 2.1 | 1.9 | 1.6 | 1.2 | 0.8 | 0.8 | 0.7 | 0.8 |
| SSC_3.8 | 160 | 4.7 | 4.1 | 4.0 | 3.3 | 2.7 | 2.3 | 2.0 | 1.5 | 1.1 | 0.9 | 0.8 | 0.8 |
| SSC_3.9 | 200 | 5.1 | 4.5 | 4.4 | 3.7 | 2.8 | 2.5 | 2.1 | 1.8 | 1.3 | 1.1 | 0.9 | 0.9 |
| SSC_3.10 | 240 | 5.5 | 4.9 | 4.8 | 4.1 | 3.1 | 2.7 | 2.2 | 1.9 | 1.5 | 1.2 | 0.9 | 1.0 |
| SSC_3.11 | 300 | 6.1 | 5.5 | 5.3 | 4.5 | 3.4 | 2.9 | 2.4 | 2.1 | 1.6 | 1.3 | 1.0 | 1.1 |
| SSC_3.12 | 350 | 6.7 | 5.9 | 5.7 | 4.9 | 3.6 | 3.1 | 2.7 | 2.2 | 1.7 | 1.2 | 1.1 | 1.1 |
| SSC_3.13 | 405 | 7.1 | 6.3 | 6.1 | 5.3 | 3.9 | 3.3 | 2.8 | 2.2 | 1.8 | 1.3 | 1.2 | 1.1 |
| SSC_3.14 | 455 | 7.9 | 6.7 | 6.4 | 5.7 | 4.2 | 3.5 | 3.1 | 2.4 | 1.8 | 1.2 | 1.4 | 1.3 |
| SSC_3.15 | 515 | 8.2 | 6.9 | 6.6 | 5.8 | 4.4 | 3.6 | 3.2 | 2.3 | 1.9 | 1.1 | 1.2 | 1.2 |
| SSC_3.16 | 575 | 8.4 | 7.0 | 6.7 | 5.8 | 4.6 | 3.6 | 3.2 | 2.2 | 1.9 | 1.2 | 1.4 | 1.3 |
| SSC_3.17 | 675 | 8.6 | 7.3 | 6.9 | 6.0 | 4.7 | 3.7 | 3.2 | 2.3 | 1.9 | 1.3 | 1.3 | 1.2 |
| SSC_3.18 | 745 | 8.6 | 7.3 | 7.0 | 6.0 | 4.7 | 3.7 | 3.2 | 2.2 | 1.8 | 1.2 | 1.3 | 1.2 |
| SSC_3.19 | 10 | 2.1 | 1.5 | 1.1 | 0.7 | 0.8 | 0.7 | 0.6 | 0.4 | 0.5 | 0.3 | 0.4 | 0.5 |
| SSC_3.20 | 25 | 2.9 | 2.1 | 1.4 | 1.0 | 0.8 | 0.7 | 0.8 | 0.6 | 0.7 | 0.4 | 0.5 | 0.5 |

| (1) | (2) | (3) | (4) | (5) | (6) | (7) | (8) | (9) | (10) | (11) | (12) | (13) | (14) |
|---|---|---|---|---|---|---|---|---|---|---|---|---|---|
| SSC_3.21 | 40 | 3.5 | 2.5 | 1.8 | 1.4 | 1.1 | 0.9 | 1.0 | 0.7 | 0.9 | 0.7 | 0.7 | 0.8 |
| SSC_3.22 | 55 | 3.9 | 3.0 | 2.1 | 1.8 | 1.4 | 1.1 | 1.1 | 0.9 | 0.9 | 0.9 | 0.8 | 0.9 |
| SSC_3.23 | 75 | 4.3 | 3.3 | 2.5 | 2.0 | 1.7 | 1.3 | 1.1 | 1.0 | 1.1 | 1.0 | 1.0 | 1.1 |
| SSC_3.24 | 105 | 4.8 | 3.7 | 2.8 | 2.3 | 2.0 | 1.6 | 1.2 | 1.1 | 1.3 | 1.2 | 1.3 | 1.2 |
| SSC_3.25 | 135 | 5.3 | 4.1 | 3.1 | 2.7 | 2.2 | 1.9 | 1.4 | 1.2 | 1.4 | 1.3 | 1.5 | 1.4 |
| SSC_3.26 | 175 | 5.9 | 4.5 | 3.5 | 3.1 | 2.5 | 2.1 | 1.6 | 1.3 | 1.3 | 1.5 | 1.4 | 1.4 |
| SSC_3.27 | 215 | 6.6 | 4.9 | 3.8 | 3.4 | 2.8 | 2.2 | 1.7 | 1.4 | 1.2 | 1.3 | 1.3 | 1.5 |
| SSC_3.28 | 260 | 7.1 | 5.3 | 4.2 | 3.6 | 3.1 | 2.5 | 1.9 | 1.5 | 1.3 | 1.2 | 1.4 | 1.3 |
| SSC_3.29 | 305 | 7.7 | 5.7 | 4.6 | 3.9 | 3.3 | 2.7 | 2.1 | 1.8 | 1.4 | 1.3 | 1.4 | 1.4 |
| SSC_3.30 | 365 | 8.3 | 6.1 | 5.1 | 4.2 | 3.6 | 3.0 | 2.2 | 1.9 | 1.5 | 1.4 | 1.4 | 1.5 |
| SSC_3.31 | 425 | 8.8 | 6.5 | 5.4 | 4.5 | 3.9 | 3.2 | 2.4 | 2.1 | 1.7 | 1.5 | 1.5 | 1.6 |
| SSC_3.32 | 495 | 9.1 | 6.7 | 5.6 | 4.8 | 4.1 | 3.3 | 2.4 | 2.2 | 1.9 | 1.6 | 1.6 | 1.5 |
| SSC_3.33 | 585 | 9.3 | 6.8 | 5.7 | 4.8 | 4.1 | 3.2 | 2.3 | 2.2 | 1.9 | 1.6 | 1.5 | 1.5 |
| SSC_3.34 | 690 | 9.4 | 6.8 | 5.8 | 4.7 | 4.1 | 3.2 | 2.2 | 2.1 | 1.9 | 1.6 | 1.5 | 1.4 |
| SSC_3.35 | 20 | 1.6 | 1.3 | 1.1 | 1.0 | 0.8 | 0.7 | 0.5 | 0.6 | 0.4 | 0.5 | 0.6 | 0.6 |
| SSC_3.36 | 45 | 2.1 | 1.8 | 1.4 | 1.1 | 1.0 | 0.8 | 0.6 | 0.5 | 0.5 | 0.7 | 0.8 | 0.7 |
| SSC_3.37 | 70 | 2.5 | 2.1 | 1.7 | 1.4 | 1.2 | 0.9 | 0.7 | 0.6 | 0.7 | 0.8 | 0.9 | 0.9 |
| SSC_3.38 | 90 | 2.9 | 2.4 | 2.1 | 1.6 | 1.4 | 1.0 | 0.8 | 0.6 | 0.6 | 0.7 | 0.9 | 1.0 |
| SSC_3.39 | 115 | 3.2 | 2.8 | 2.4 | 1.8 | 1.6 | 1.2 | 0.9 | 0.7 | 0.8 | 0.8 | 0.9 | 1.0 |
| SSC_3.40 | 140 | 3.5 | 3.1 | 2.8 | 2.0 | 1.5 | 1.1 | 0.8 | 0.9 | 0.8 | 0.9 | 1.0 | 1.0 |
| SSC_3.41 | 170 | 4.0 | 3.3 | 3.1 | 2.1 | 1.7 | 1.2 | 1.0 | 0.9 | 0.9 | 1.0 | 1.1 | 1.0 |
| SSC_3.42 | 220 | 4.5 | 3.6 | 3.4 | 2.5 | 1.9 | 1.5 | 1.1 | 1.0 | 0.9 | 1.1 | 1.1 | 1.1 |
| SSC_3.43 | 280 | 5.3 | 4.1 | 3.7 | 2.7 | 2.1 | 1.7 | 1.2 | 1.0 | 1.0 | 1.1 | 1.2 | 1.1 |
| SSC_3.44 | 325 | 5.9 | 4.5 | 4.1 | 3.0 | 2.3 | 1.9 | 1.4 | 1.1 | 1.2 | 1.1 | 1.1 | 1.2 |
| SSC_3.45 | 380 | 6.6 | 4.9 | 4.3 | 3.2 | 2.6 | 2.1 | 1.5 | 1.3 | 1.2 | 1.2 | 1.0 | 1.1 |
| SSC_3.46 | 430 | 7.1 | 5.2 | 4.7 | 3.5 | 2.7 | 2.2 | 1.6 | 1.2 | 1.3 | 1.2 | 1.1 | 1.0 |
| SSC_3.47 | 490 | 7.7 | 5.6 | 5.1 | 3.7 | 3.0 | 2.5 | 1.7 | 1.3 | 1.4 | 1.3 | 1.2 | 1.1 |
| SSC_3.48 | 550 | 8.1 | 6.1 | 5.4 | 3.9 | 3.1 | 2.5 | 1.8 | 1.4 | 1.2 | 1.1 | 1.1 | 1.0 |
| SSC_3.49 | 630 | 8.3 | 6.2 | 5.4 | 4.1 | 3.1 | 2.6 | 1.7 | 1.4 | 1.3 | 1.2 | 1.0 | 1.0 |

| (1) | (2) | (3) | (4) | (5) | (6) | (7) | (8) | (9) | (10) | (11) | (12) | (13) | (14) |
|---|---|---|---|---|---|---|---|---|---|---|---|---|---|
| SSC_3.50 | 710 | 8.4 | 6.2 | 5.3 | 4.1 | 3.2 | 2.6 | 1.6 | 1.4 | 1.3 | 1.1 | 1.0 | 1.0 |
| SSC_3.51 | 25 | 1.5 | 1.3 | 1.0 | 0.8 | 0.7 | 0.5 | 0.6 | 0.4 | 0.3 | 0.3 | 0.4 | 0.5 |
| SSC_3.52 | 55 | 2.0 | 1.7 | 1.2 | 1.1 | 0.9 | 0.7 | 0.7 | 0.5 | 0.5 | 0.4 | 0.5 | 0.4 |
| SSC_3.53 | 75 | 2.4 | 2.1 | 1.5 | 1.3 | 1.0 | 0.9 | 0.7 | 0.6 | 0.6 | 0.5 | 0.5 | 0.6 |
| SSC_3.54 | 115 | 3.1 | 2.5 | 1.9 | 1.6 | 1.4 | 1.2 | 0.8 | 0.7 | 0.6 | 0.6 | 0.7 | 0.7 |
| SSC_3.55 | 150 | 3.6 | 2.6 | 2.3 | 2.1 | 1.8 | 1.4 | 1.0 | 0.9 | 0.7 | 0.8 | 0.8 | 0.7 |
| SSC_3.56 | 205 | 4.3 | 2.9 | 2.7 | 2.5 | 2.1 | 1.6 | 1.1 | 0.9 | 0.8 | 0.8 | 0.9 | 0.8 |
| SSC_3.57 | 265 | 5.0 | 3.3 | 3.0 | 2.8 | 2.3 | 1.7 | 1.3 | 1.0 | 0.9 | 0.8 | 0.8 | 0.9 |
| SSC_3.58 | 325 | 5.7 | 3.6 | 3.3 | 3.1 | 2.5 | 2.0 | 1.6 | 1.2 | 1.1 | 0.9 | 0.9 | 1.1 |
| SSC_3.59 | 365 | 6.3 | 4.0 | 3.7 | 3.3 | 2.8 | 2.2 | 1.7 | 1.4 | 1.2 | 1.0 | 1.0 | 1.1 |
| SSC_3.60 | 425 | 6.9 | 4.5 | 3.9 | 3.5 | 3.1 | 2.5 | 1.9 | 1.6 | 1.3 | 1.1 | 1.2 | 1.2 |
| SSC_3.61 | 505 | 7.3 | 5.0 | 4.3 | 3.7 | 3.4 | 2.7 | 2.2 | 2.0 | 1.5 | 1.4 | 1.3 | 1.2 |
| SSC_3.62 | 610 | 7.6 | 5.5 | 4.8 | 4.0 | 3.6 | 3.0 | 2.3 | 2.2 | 2.1 | 1.6 | 1.5 | 1.4 |
| SSC_3.63 | 705 | 8.1 | 5.9 | 5.0 | 4.1 | 3.8 | 3.1 | 2.4 | 2.2 | 2.0 | 1.7 | 1.5 | 1.4 |
| SSC_3.64 | 740 | 8.1 | 6.0 | 5.1 | 4.0 | 3.6 | 3.2 | 2.5 | 2.2 | 1.9 | 1.7 | 1.4 | 1.4 |
| SSC_4.1 | 10 | 2.1 | 1.4 | 1.1 | 0.8 | 0.9 | 0.8 | 0.6 | 0.5 | 0.6 | 0.5 | 0.4 | 0.6 |
| SSC_4.2 | 25 | 2.4 | 1.8 | 1.4 | 1.0 | 1.1 | 1.1 | 0.9 | 0.9 | 0.7 | 0.7 | 0.6 | 0.7 |
| SSC_4.3 | 35 | 2.7 | 2.2 | 1.6 | 1.3 | 1.2 | 1.3 | 0.9 | 1.0 | 1.0 | 0.8 | 0.8 | 0.8 |
| SSC_4.4 | 50 | 3.1 | 2.6 | 1.9 | 1.7 | 1.4 | 1.2 | 1.0 | 0.9 | 0.9 | 0.8 | 0.9 | 0.9 |
| SSC_4.5 | 60 | 3.4 | 2.9 | 2.2 | 1.9 | 1.6 | 1.4 | 1.1 | 1.2 | 1.3 | 1.0 | 1.0 | 1.1 |
| SSC_4.6 | 90 | 3.8 | 3.4 | 2.6 | 2.1 | 1.8 | 1.5 | 1.2 | 1.1 | 1.1 | 1.1 | 1.2 | 1.2 |
| SSC_4.7 | 105 | 4.0 | 3.7 | 3.0 | 2.4 | 2.0 | 1.7 | 1.3 | 1.2 | 1.1 | 1.2 | 1.3 | 1.4 |
| SSC_4.8 | 130 | 4.4 | 4.1 | 3.3 | 2.7 | 2.2 | 1.8 | 1.5 | 1.3 | 1.2 | 1.3 | 1.4 | 1.4 |
| SSC_4.9 | 170 | 4.7 | 4.5 | 3.7 | 3.1 | 2.6 | 2.0 | 1.6 | 1.4 | 1.3 | 1.4 | 1.6 | 1.5 |
| SSC_4.10 | 205 | 5.1 | 5.0 | 3.9 | 3.4 | 2.9 | 2.2 | 1.8 | 1.5 | 1.4 | 1.3 | 1.4 | 1.5 |
| SSC_4.11 | 250 | 5.6 | 5.6 | 4.3 | 3.6 | 3.1 | 2.5 | 2.0 | 1.7 | 1.5 | 1.5 | 1.5 | 1.4 |
| SSC_4.12 | 290 | 6.1 | 6.2 | 4.7 | 3.8 | 3.3 | 2.7 | 2.1 | 1.9 | 1.8 | 1.6 | 1.5 | 1.6 |
| SSC_4.13 | 355 | 6.7 | 6.7 | 5.1 | 4.0 | 3.5 | 3.1 | 2.3 | 2.1 | 2.0 | 1.8 | 1.6 | 1.6 |
| SSC_4.14 | 390 | 7.1 | 7.2 | 5.4 | 4.2 | 3.6 | 3.3 | 2.5 | 2.4 | 2.1 | 1.9 | 1.7 | 1.6 |

| (1) | (2) | (3) | (4) | (5) | (6) | (7) | (8) | (9) | (10) | (11) | (12) | (13) | (14) |
|---|---|---|---|---|---|---|---|---|---|---|---|---|---|
| SSC_4.15 | 450 | 7.5 | 7.5 | 5.8 | 4.5 | 3.6 | 3.3 | 2.6 | 2.3 | 2.1 | 1.9 | 1.8 | 1.7 |
| SSC_4.16 | 510 | 7.8 | 7.9 | 6.1 | 4.8 | 3.7 | 3.5 | 2.9 | 2.4 | 2.2 | 1.9 | 1.7 | 1.7 |
| SSC_4.17 | 570 | 8.0 | 8.3 | 6.3 | 5.1 | 3.9 | 3.5 | 3.0 | 2.3 | 2.1 | 1.8 | 1.7 | 1.6 |
| SSC_4.18 | 630 | 8.1 | 8.5 | 6.4 | 5.2 | 3.9 | 3.4 | 3.1 | 2.2 | 2.0 | 1.8 | 1.6 | 1.6 |
| SSC_4.19 | 700 | 8.1 | 8.6 | 6.4 | 5.3 | 4.0 | 3.3 | 3.2 | 2.2 | 1.9 | 1.8 | 1.6 | 1.6 |
| SSC_4.20 | 10 | 1.6 | 1.5 | 1.1 | 0.6 | 0.5 | 0.6 | 0.7 | 0.5 | 0.4 | 0.5 | 0.5 | 0.6 |
| SSC_4.21 | 25 | 2.1 | 1.9 | 1.4 | 0.9 | 0.5 | 0.6 | 0.6 | 0.4 | 0.5 | 0.3 | 0.5 | 0.5 |
| SSC_4.22 | 40 | 2.6 | 2.2 | 1.8 | 1.1 | 0.7 | 0.7 | 0.5 | 0.6 | 0.4 | 0.4 | 0.6 | 0.5 |
| SSC_4.23 | 60 | 3.2 | 2.6 | 2.3 | 1.4 | 1.1 | 0.8 | 0.6 | 0.7 | 0.6 | 0.5 | 0.6 | 0.6 |
| SSC_4.24 | 90 | 3.7 | 2.9 | 2.6 | 1.6 | 1.2 | 1.0 | 0.8 | 0.7 | 0.7 | 0.6 | 0.7 | 0.7 |
| SSC_4.25 | 115 | 4.1 | 3.3 | 3.0 | 1.9 | 1.4 | 1.1 | 1.0 | 0.8 | 0.7 | 0.8 | 0.8 | 0.7 |
| SSC_4.26 | 145 | 4.5 | 3.7 | 3.4 | 2.1 | 1.6 | 1.2 | 0.9 | 0.9 | 0.8 | 0.9 | 0.9 | 0.9 |
| SSC_4.27 | 195 | 4.8 | 4.1 | 3.3 | 2.5 | 2.0 | 1.7 | 1.2 | 1.1 | 0.9 | 1.0 | 1.1 | 1.0 |
| SSC_4.28 | 240 | 5.2 | 4.6 | 3.5 | 3.0 | 2.3 | 1.9 | 1.6 | 1.3 | 1.2 | 1.1 | 1.2 | 1.2 |
| SSC_4.29 | 285 | 5.6 | 5.1 | 4.0 | 3.3 | 2.6 | 2.1 | 1.7 | 1.6 | 1.4 | 1.3 | 1.2 | 1.1 |
| SSC_4.30 | 335 | 6.1 | 5.3 | 4.2 | 3.3 | 3.0 | 2.4 | 1.9 | 1.8 | 1.4 | 1.5 | 1.3 | 1.2 |
| SSC_4.31 | 390 | 6.6 | 5.6 | 4.4 | 3.4 | 3.4 | 2.1 | 2.1 | 1.8 | 1.6 | 1.5 | 1.5 | 1.4 |
| SSC_4.32 | 440 | 7.1 | 5.9 | 4.5 | 3.4 | 3.6 | 2.4 | 2.5 | 2.3 | 1.9 | 1.7 | 1.6 | 1.6 |
| SSC_4.33 | 515 | 7.6 | 6.0 | 4.6 | 3.5 | 3.6 | 2.6 | 2.8 | 2.3 | 2.1 | 1.9 | 1.7 | 1.6 |
| SSC_4.34 | 580 | 7.9 | 6.2 | 4.7 | 3.5 | 3.7 | 2.9 | 3.0 | 2.3 | 1.9 | 1.9 | 1.6 | 1.6 |
| SSC_4.35 | 710 | 8.0 | 6.4 | 4.7 | 3.6 | 3.7 | 3.0 | 2.9 | 2.2 | 1.9 | 1.9 | 1.7 | 1.6 |
| SSC_4.36 | 30 | 1.3 | 1.1 | 0.8 | 0.6 | 0.5 | 0.5 | 0.4 | 0.5 | 0.3 | 0.3 | 0.5 | 0.4 |
| SSC_4.37 | 45 | 1.6 | 1.5 | 1.3 | 1.0 | 0.9 | 0.8 | 0.8 | 0.7 | 0.6 | 0.5 | 0.5 | 0.6 |
| SSC_4.38 | 60 | 2.1 | 1.9 | 1.6 | 1.3 | 1.0 | 0.9 | 0.8 | 0.8 | 0.6 | 0.6 | 0.5 | 0.7 |
| SSC_4.39 | 75 | 2.4 | 2.2 | 2.0 | 1.6 | 1.2 | 1.1 | 0.9 | 1.0 | 0.8 | 0.7 | 0.6 | 0.6 |
| SSC_4.40 | 100 | 2.8 | 2.5 | 2.3 | 2.0 | 1.5 | 1.2 | 1.0 | 1.0 | 0.9 | 0.8 | 0.7 | 0.6 |
| SSC_4.41 | 120 | 3.2 | 2.8 | 2.6 | 2.2 | 1.7 | 1.3 | 1.0 | 1.1 | 0.9 | 0.9 | 0.7 | 0.7 |
| SSC_4.42 | 150 | 3.6 | 3.2 | 3.0 | 2.5 | 1.9 | 1.5 | 1.3 | 1.2 | 1.0 | 0.9 | 0.8 | 0.8 |
| SSC_4.43 | 205 | 4.3 | 3.5 | 3.3 | 2.8 | 2.1 | 1.6 | 1.3 | 1.1 | 1.1 | 1.0 | 1.0 | 0.9 |

| (1) | (2) | (3) | (4) | (5) | (6) | (7) | (8) | (9) | (10) | (11) | (12) | (13) | (14) |
|---|---|---|---|---|---|---|---|---|---|---|---|---|---|
| SSC_4.44 | 260 | 4.9 | 3.7 | 3.6 | 3.0 | 2.4 | 1.9 | 1.4 | 1.3 | 1.2 | 1.1 | 1.1 | 1.1 |
| SSC_4.45 | 295 | 5.2 | 4.1 | 4.0 | 3.3 | 2.6 | 2.2 | 1.7 | 1.5 | 1.3 | 1.2 | 1.1 | 1.2 |
| SSC_4.46 | 335 | 5.7 | 4.5 | 4.3 | 3.5 | 2.7 | 2.4 | 2.0 | 1.7 | 1.6 | 1.4 | 1.3 | 1.2 |
| SSC_4.47 | 385 | 6.1 | 4.8 | 4.6 | 3.6 | 2.7 | 2.6 | 2.3 | 2.1 | 1.9 | 1.5 | 1.4 | 1.3 |
| SSC_4.48 | 445 | 6.6 | 5.1 | 5.1 | 4.0 | 2.8 | 2.5 | 2.4 | 2.2 | 2.0 | 1.7 | 1.5 | 1.5 |
| SSC_4.49 | 535 | 7.1 | 5.6 | 5.4 | 4.2 | 3.1 | 2.8 | 2.5 | 2.2 | 1.9 | 1.7 | 1.6 | 1.5 |
| SSC_4.50 | 625 | 7.2 | 5.7 | 5.6 | 4.4 | 3.3 | 2.8 | 2.5 | 2.1 | 1.9 | 1.7 | 1.5 | 1.5 |
| SSC_4.51 | 730 | 7.3 | 5.7 | 5.6 | 4.4 | 3.2 | 2.8 | 2.5 | 2.2 | 1.9 | 1.7 | 1.5 | 1.5 |
| SSC_4.52 | 50 | 1.4 | 1.1 | 0.8 | 0.5 | 0.5 | 0.6 | 0.4 | 0.4 | 0.3 | 0.4 | 0.4 | 0.3 |
| SSC_4.53 | 80 | 2.0 | 1.7 | 1.2 | 0.9 | 0.8 | 0.8 | 0.6 | 0.7 | 0.5 | 0.5 | 0.6 | 0.5 |
| SSC_4.54 | 115 | 2.5 | 2.3 | 1.3 | 1.4 | 1.0 | 0.9 | 0.8 | 0.6 | 0.6 | 0.6 | 0.5 | 0.5 |
| SSC_4.55 | 150 | 2.9 | 2.6 | 1.5 | 1.2 | 1.2 | 1.1 | 0.9 | 0.8 | 0.8 | 0.7 | 0.8 | 0.7 |
| SSC_4.56 | 180 | 3.5 | 3.0 | 1.4 | 1.7 | 1.5 | 1.2 | 1.0 | 0.9 | 0.9 | 0.9 | 0.8 | 0.8 |
| SSC_4.57 | 240 | 4.1 | 3.4 | 1.8 | 1.9 | 1.7 | 1.5 | 1.3 | 1.1 | 1.0 | 1.1 | 1.0 | 0.9 |
| SSC_4.58 | 330 | 4.5 | 3.6 | 2.1 | 2.2 | 2.0 | 1.8 | 1.5 | 1.4 | 1.2 | 1.1 | 1.0 | 1.0 |
| SSC_4.59 | 410 | 4.9 | 3.7 | 2.4 | 2.3 | 2.2 | 1.9 | 1.6 | 1.5 | 1.4 | 1.3 | 1.1 | 1.0 |
| SSC_4.60 | 480 | 5.2 | 4.1 | 2.5 | 2.6 | 2.3 | 2.0 | 1.6 | 1.5 | 1.4 | 1.3 | 1.1 | 1.1 |
| SSC_4.61 | 540 | 5.6 | 4.3 | 2.8 | 2.9 | 2.3 | 1.9 | 1.7 | 1.5 | 1.5 | 1.3 | 1.2 | 1.1 |
| SSC_4.62 | 600 | 5.8 | 4.4 | 2.9 | 2.8 | 2.4 | 2.0 | 1.7 | 1.5 | 1.4 | 1.4 | 1.1 | 1.0 |
| SSC_4.63 | 720 | 5.9 | 4.4 | 2.9 | 2.8 | 2.5 | 2.0 | 1.6 | 1.5 | 1.4 | 1.3 | 1.1 | 1.0 |
| SSC_5.13 | 15 | 2.0 | 1.4 | 1.1 | 0.8 | 0.6 | 0.6 | 0.7 | 0.5 | 0.4 | 0.5 | 0.3 | 0.4 |
| SSC_5.14 | 35 | 2.6 | 1.8 | 1.5 | 1.0 | 0.7 | 0.8 | 0.6 | 0.5 | 0.5 | 0.4 | 0.4 | 0.5 |
| SSC_5.15 | 50 | 3.1 | 2.1 | 1.8 | 1.2 | 0.9 | 0.8 | 0.7 | 0.6 | 0.5 | 0.4 | 0.5 | 0.5 |
| SSC_5.16 | 60 | 3.4 | 2.5 | 2.1 | 1.4 | 1.0 | 0.9 | 0.9 | 0.7 | 0.6 | 0.6 | 0.6 | 0.5 |
| SSC_5.17 | 80 | 3.8 | 2.8 | 2.4 | 1.6 | 1.1 | 1.0 | 1.1 | 0.8 | 0.7 | 0.7 | 0.6 | 0.5 |
| SSC_5.18 | 95 | 4.1 | 3.0 | 2.6 | 1.9 | 1.4 | 1.1 | 1.0 | 1.0 | 0.9 | 0.8 | 0.7 | 0.6 |
| SSC_5.19 | 115 | 4.4 | 3.4 | 2.7 | 2.1 | 1.6 | 1.4 | 1.1 | 0.9 | 0.9 | 0.9 | 0.7 | 0.7 |
| SSC_5.20 | 140 | 4.8 | 3.8 | 2.9 | 2.4 | 1.8 | 1.6 | 1.3 | 1.0 | 1.0 | 0.9 | 0.8 | 0.9 |
| SSC_5.21 | 170 | 5.2 | 4.3 | 3.2 | 2.5 | 2.1 | 1.7 | 1.4 | 1.1 | 1.1 | 0.9 | 0.9 | 0.8 |

| (1) | (2) | (3) | (4) | (5) | (6) | (7) | (8) | (9) | (10) | (11) | (12) | (13) | (14) |
|---|---|---|---|---|---|---|---|---|---|---|---|---|---|
| SSC_5.22 | 200 | 5.7 | 4.7 | 3.6 | 2.7 | 2.3 | 1.9 | 1.5 | 1.3 | 1.3 | 1.0 | 1.0 | 0.9 |
| SSC_5.23 | 245 | 6.1 | 5.2 | 4.0 | 3.1 | 2.5 | 2.1 | 1.8 | 1.4 | 1.2 | 1.0 | 0.9 | 0.8 |
| SSC_5.24 | 285 | 6.7 | 5.7 | 4.4 | 3.5 | 2.4 | 2.0 | 1.5 | 1.4 | 1.2 | 1.1 | 1.0 | 0.9 |
| SSC_5.25 | 340 | 7.1 | 6.2 | 4.8 | 3.8 | 2.6 | 2.1 | 1.7 | 1.4 | 1.1 | 1.1 | 1.1 | 1.0 |
| SSC_5.26 | 390 | 7.5 | 6.7 | 5.1 | 4.0 | 2.7 | 2.3 | 1.8 | 1.5 | 1.3 | 1.2 | 1.1 | 1.1 |
| SSC_5.27 | 450 | 7.8 | 7.0 | 5.2 | 4.1 | 3.0 | 2.5 | 1.9 | 1.6 | 1.4 | 1.3 | 1.2 | 1.1 |
| SSC_5.28 | 480 | 7.9 | 7.1 | 5.2 | 4.2 | 3.2 | 2.6 | 2.1 | 1.6 | 1.4 | 1.3 | 1.2 | 1.2 |
| SSC_5.29 | 560 | 7.9 | 7.2 | 5.4 | 4.3 | 3.4 | 2.7 | 2.1 | 1.8 | 1.4 | 1.4 | 1.3 | 1.2 |
| SSC_5.30 | 640 | 8.0 | 7.2 | 5.4 | 4.4 | 3.3 | 2.7 | 2.1 | 1.8 | 1.6 | 1.5 | 1.3 | 1.3 |
| SSC_5.31 | 720 | 8.0 | 7.2 | 5.4 | 4.4 | 3.3 | 2.8 | 2.1 | 1.7 | 1.6 | 1.5 | 1.3 | 1.2 |
| SSC_5.32 | 10 | 1.4 | 1.0 | 0.8 | 0.6 | 0.7 | 0.5 | 0.7 | 0.4 | 0.4 | 0.3 | 0.4 | 0.5 |
| SSC_5.33 | 20 | 1.8 | 1.4 | 1.1 | 1.0 | 0.8 | 0.7 | 0.7 | 0.5 | 0.4 | 0.5 | 0.5 | 0.6 |
| SSC_5.34 | 35 | 2.3 | 1.8 | 1.4 | 1.2 | 1.1 | 0.9 | 1.0 | 0.9 | 0.7 | 0.5 | 0.6 | 0.6 |
| SSC_5.35 | 50 | 2.1 | 2.1 | 1.8 | 1.6 | 1.3 | 1.1 | 0.9 | 1.0 | 0.9 | 0.7 | 0.6 | 0.7 |
| SSC_5.36 | 85 | 2.5 | 2.6 | 2.2 | 1.9 | 1.5 | 1.3 | 1.0 | 1.1 | 1.1 | 0.9 | 0.7 | 0.7 |
| SSC_5.37 | 115 | 2.9 | 2.9 | 2.5 | 2.1 | 1.8 | 1.5 | 1.3 | 1.1 | 1.0 | 1.0 | 0.8 | 0.7 |
| SSC_5.38 | 155 | 3.4 | 3.3 | 2.9 | 2.4 | 2.0 | 1.7 | 1.5 | 1.2 | 1.1 | 0.9 | 0.9 | 0.8 |
| SSC_5.39 | 195 | 3.7 | 3.6 | 3.3 | 2.7 | 2.3 | 1.9 | 1.6 | 1.4 | 1.2 | 1.0 | 1.0 | 0.9 |
| SSC_5.40 | 240 | 4.1 | 3.9 | 3.7 | 3.1 | 2.5 | 1.9 | 1.8 | 1.5 | 1.4 | 1.2 | 1.0 | 1.0 |
| SSC_5.41 | 295 | 4.6 | 4.3 | 4.1 | 3.4 | 2.6 | 2.1 | 1.9 | 1.5 | 1.3 | 1.2 | 0.9 | 1.0 |
| SSC_5.42 | 355 | 5.3 | 4.8 | 4.5 | 3.7 | 2.8 | 2.3 | 2.0 | 1.7 | 1.4 | 1.3 | 1.0 | 1.1 |
| SSC_5.43 | 445 | 5.8 | 5.1 | 4.8 | 4.1 | 3.0 | 2.5 | 2.1 | 2.0 | 1.5 | 1.4 | 1.2 | 1.1 |
| SSC_5.44 | 535 | 6.1 | 5.5 | 5.1 | 4.3 | 3.1 | 2.7 | 2.2 | 2.0 | 1.6 | 1.4 | 1.3 | 1.1 |
| SSC_5.45 | 625 | 6.2 | 5.6 | 5.2 | 4.2 | 3.2 | 2.8 | 2.2 | 1.9 | 1.7 | 1.5 | 1.4 | 1.1 |
| SSC_5.46 | 740 | 6.3 | 5.6 | 5.2 | 4.2 | 3.3 | 2.7 | 2.1 | 1.9 | 1.7 | 1.5 | 1.3 | 1.1 |
| SSC_5.47 | 20 | 1.3 | 0.9 | 0.8 | 0.6 | 0.6 | 0.4 | 0.5 | 0.4 | 0.3 | 0.5 | 0.5 | 0.4 |
| SSC_5.48 | 60 | 1.8 | 1.3 | 1.1 | 0.8 | 0.6 | 0.7 | 0.7 | 0.6 | 0.5 | 0.6 | 0.6 | 0.6 |
| SSC_5.49 | 100 | 2.3 | 1.9 | 1.5 | 1.1 | 0.9 | 0.8 | 0.8 | 0.7 | 0.6 | 0.6 | 0.7 | 0.7 |
| SSC_5.50 | 140 | 2.9 | 2.3 | 1.8 | 1.4 | 1.2 | 1.0 | 0.9 | 0.7 | 0.7 | 0.7 | 0.7 | 0.8 |

| (1) | (2) | (3) | (4) | (5) | (6) | (7) | (8) | (9) | (10) | (11) | (12) | (13) | (14) |
|---|---|---|---|---|---|---|---|---|---|---|---|---|---|
| SSC_5.51 | 190 | 3.4 | 2.8 | 2.1 | 1.8 | 1.4 | 1.2 | 1.1 | 0.9 | 0.8 | 0.9 | 0.7 | 0.9 |
| SSC_5.52 | 250 | 4.0 | 3.1 | 2.6 | 2.2 | 1.7 | 1.3 | 1.0 | 0.9 | 0.9 | 0.9 | 0.8 | 1.0 |
| SSC_5.53 | 310 | 4.5 | 3.5 | 3.0 | 2.5 | 2.1 | 1.5 | 1.2 | 1.1 | 1.0 | 0.9 | 0.9 | 1.0 |
| SSC_5.54 | 370 | 5.0 | 4.1 | 3.3 | 2.8 | 2.5 | 1.7 | 1.4 | 1.3 | 1.1 | 1.0 | 0.9 | 0.9 |
| SSC_5.55 | 430 | 5.5 | 4.6 | 3.6 | 2.9 | 2.6 | 1.9 | 1.4 | 1.2 | 1.0 | 1.0 | 1.0 | 0.9 |
| SSC_5.56 | 505 | 5.8 | 4.9 | 3.7 | 3.1 | 2.8 | 2.1 | 1.6 | 1.3 | 1.1 | 1.0 | 1.1 | 1.0 |
| SSC_5.57 | 595 | 6.0 | 5.1 | 3.8 | 3.2 | 2.9 | 2.2 | 1.7 | 1.3 | 1.2 | 1.0 | 1.1 | 1.0 |
| SSC_5.58 | 735 | 6.0 | 5.1 | 3.7 | 3.3 | 2.9 | 2.3 | 1.7 | 1.2 | 1.1 | 1.1 | 1.0 | 1.0 |
| SSC_5.59 | 15 | 1.7 | 1.1 | 0.9 | 0.8 | 1.0 | 0.8 | 0.6 | 0.5 | 0.5 | 0.5 | 0.4 | 0.3 |
| SSC_5.60 | 30 | 2.1 | 1.4 | 1.1 | 1.2 | 1.0 | 0.9 | 0.9 | 0.7 | 0.6 | 0.6 | 0.5 | 0.4 |
| SSC_5.61 | 45 | 2.6 | 1.8 | 1.3 | 1.2 | 1.1 | 0.9 | 0.9 | 0.8 | 0.7 | 0.6 | 0.5 | 0.5 |
| SSC_5.62 | 65 | 2.8 | 1.9 | 1.5 | 1.3 | 1.1 | 0.9 | 0.8 | 0.8 | 0.7 | 0.6 | 0.6 | 0.5 |
| SSC_5.63 | 85 | 3.1 | 2.2 | 1.8 | 1.4 | 1.2 | 1.0 | 0.9 | 0.8 | 0.8 | 0.7 | 0.6 | 0.6 |
| SSC_5.64 | 105 | 3.5 | 2.5 | 2.1 | 1.6 | 1.3 | 1.1 | 1.0 | 0.9 | 0.8 | 0.8 | 0.7 | 0.6 |
| SSC_5.65 | 125 | 3.8 | 2.7 | 2.4 | 1.8 | 1.5 | 1.2 | 1.0 | 1.0 | 0.9 | 0.8 | 0.7 | 0.7 |
| SSC_5.66 | 155 | 4.2 | 3.1 | 2.6 | 2.1 | 1.6 | 1.3 | 1.1 | 1.2 | 1.0 | 0.8 | 0.8 | 0.7 |
| SSC_5.67 | 185 | 4.6 | 3.5 | 2.8 | 2.4 | 1.6 | 1.4 | 1.2 | 1.1 | 1.1 | 1.0 | 0.9 | 0.8 |
| SSC_5.68 | 215 | 5.1 | 3.9 | 3.1 | 2.8 | 1.7 | 1.6 | 1.3 | 1.2 | 1.1 | 0.9 | 0.9 | 0.8 |
| SSC_5.69 | 260 | 5.7 | 4.3 | 3.4 | 3.1 | 2.0 | 1.7 | 1.4 | 1.3 | 1.2 | 1.1 | 1.0 | 1.0 |
| SSC_5.70 | 305 | 6.3 | 4.7 | 3.6 | 3.3 | 2.3 | 1.9 | 1.6 | 1.4 | 1.2 | 1.0 | 1.0 | 1.1 |
| SSC_5.71 | 350 | 6.6 | 5.1 | 3.8 | 3.5 | 2.6 | 2.1 | 1.8 | 1.5 | 1.4 | 1.2 | 1.1 | 1.1 |
| SSC_5.72 | 410 | 6.9 | 5.6 | 4.1 | 3.7 | 2.8 | 2.3 | 1.9 | 1.6 | 1.4 | 1.3 | 1.2 | 1.2 |
| SSC_5.73 | 470 | 7.1 | 5.7 | 4.5 | 4.1 | 3.1 | 2.6 | 2.0 | 1.7 | 1.5 | 1.3 | 1.2 | 1.1 |
| SSC_5.74 | 530 | 7.2 | 5.9 | 4.8 | 4.5 | 3.3 | 2.8 | 2.1 | 1.8 | 1.5 | 1.4 | 1.2 | 1.2 |
| SSC_5.75 | 590 | 7.1 | 6.0 | 4.8 | 4.8 | 3.5 | 2.9 | 2.2 | 1.8 | 1.5 | 1.3 | 1.1 | 1.1 |
| SSC_5.76 | 650 | 7.1 | 6.1 | 5.3 | 5.0 | 3.6 | 3.0 | 2.1 | 1.7 | 1.5 | 1.2 | 1.1 | 1.0 |
| SSC_5.77 | 710 | 7.1 | 6.1 | 5.4 | 5.0 | 3.7 | 3.0 | 2.1 | 1.7 | 1.4 | 1.1 | 1.1 | 1.0 |
| SSC_0.1 | 30 | 2.2 | 1.8 | 1.4 | 1.0 | 0.7 | 0.6 | 0.7 | 0.6 | 0.5 | 0.5 | 0.6 | 0.6 |
| SSC_0.2 | 45 | 3.1 | 2.5 | 1.8 | 1.2 | 0.7 | 0.6 | 0.7 | 0.6 | 0.5 | 0.6 | 0.7 | 0.7 |

| (1) | (2) | (3) | (4) | (5) | (6) | (7) | (8) | (9) | (10) | (11) | (12) | (13) | (14) |
|---|---|---|---|---|---|---|---|---|---|---|---|---|---|
| SSC_0.3 | 75 | 4.3 | 3.4 | 2.6 | 1.6 | 1.1 | 0.8 | 0.4 | 0.6 | 0.6 | 0.7 | 0.7 | 0.8 |
| SSC_0.4 | 110 | 5.2 | 4.1 | 3.3 | 2.2 | 1.5 | 1.1 | 0.6 | 0.6 | 0.4 | 0.6 | 0.7 | 0.8 |
| SSC_0.5 | 185 | 6.7 | 5.1 | 4.2 | 2.9 | 2.0 | 1.5 | 1.1 | 1.0 | 0.7 | 0.7 | 0.6 | 0.8 |
| SSC_0.6 | 220 | 7.5 | 6.2 | 5.1 | 3.6 | 2.5 | 1.8 | 1.3 | 1.2 | 0.8 | 0.8 | 0.7 | 0.7 |
| SSC_0.7 | 305 | 8.6 | 7.2 | 6.0 | 4.3 | 3.2 | 2.2 | 1.5 | 1.4 | 1.1 | 1.0 | 0.8 | 0.8 |
| SSC_0.8 | 365 | 9.2 | 7.9 | 6.7 | 5.1 | 3.8 | 2.7 | 1.8 | 1.5 | 1.2 | 1.0 | 0.8 | 0.9 |
| SSC_0.9 | 430 | 9.6 | 8.2 | 7.0 | 5.5 | 4.1 | 3.2 | 2.1 | 1.8 | 1.3 | 1.1 | 0.9 | 0.9 |
| SSC_0.10 | 465 | 9.8 | 8.5 | 7.3 | 5.7 | 4.4 | 3.3 | 2.3 | 1.9 | 1.6 | 1.2 | 1.0 | 1.0 |
| SSC_0.11 | 525 | 10.1 | 8.7 | 7.6 | 5.9 | 4.7 | 3.5 | 2.5 | 2.0 | 1.7 | 1.3 | 0.9 | 1.0 |
| SSC_0.12 | 630 | 10.5 | 9.0 | 7.8 | 6.3 | 4.9 | 3.8 | 2.7 | 2.1 | 1.8 | 1.5 | 1.1 | 1.0 |
| SSC_0.13 | 755 | 10.7 | 9.1 | 7.9 | 6.3 | 4.9 | 3.9 | 2.8 | 2.1 | 1.8 | 1.5 | 1.1 | 1.1 |
| SSC_0.14 | 870 | 10.7 | 9.1 | 7.9 | 6.4 | 4.9 | 3.8 | 2.8 | 2.2 | 1.8 | 1.5 | 1.1 | 1.1 |
| SSC_0.15 | 15 | 2.8 | 2.2 | 1.3 | 1.1 | 0.9 | 0.9 | 0.7 | 0.5 | 0.6 | 0.7 | 0.6 | 0.6 |
| SSC_0.16 | 35 | 4.1 | 3.5 | 2.3 | 1.7 | 1.2 | 1.0 | 0.8 | 0.6 | 0.6 | 0.7 | 0.7 | 0.6 |
| SSC_0.17 | 55 | 5.0 | 4.2 | 3.1 | 2.4 | 1.5 | 1.1 | 0.8 | 0.7 | 0.6 | 0.8 | 0.8 | 0.8 |
| SSC_0.18 | 90 | 5.9 | 4.7 | 3.8 | 2.9 | 2.1 | 1.3 | 1.1 | 0.9 | 0.8 | 0.9 | 0.9 | 1.0 |
| SSC_0.19 | 145 | 6.9 | 5.6 | 4.7 | 3.5 | 2.6 | 1.7 | 1.5 | 1.2 | 1.0 | 1.1 | 1.0 | 1.0 |
| SSC_0.20 | 175 | 7.3 | 5.9 | 5.0 | 3.8 | 3.1 | 1.7 | 1.4 | 1.2 | 1.1 | 1.2 | 1.1 | 1.0 |
| SSC_0.21 | 275 | 8.4 | 6.6 | 5.7 | 4.8 | 3.5 | 2.1 | 1.7 | 1.5 | 1.3 | 1.2 | 1.2 | 1.1 |
| SSC_0.22 | 335 | 9.1 | 7.2 | 6.2 | 5.3 | 4.0 | 2.0 | 1.6 | 1.6 | 1.4 | 1.3 | 1.1 | 1.2 |
| SSC_0.23 | 395 | 10.0 | 7.8 | 6.7 | 5.9 | 4.2 | 2.2 | 1.9 | 1.7 | 1.5 | 1.3 | 1.2 | 1.1 |
| SSC_0.24 | 440 | 11.3 | 8.7 | 7.5 | 6.5 | 4.4 | 2.5 | 2.1 | 1.8 | 1.7 | 1.4 | 1.3 | 1.2 |
| SSC_0.25 | 570 | 12.3 | 9.5 | 8.2 | 7.1 | 4.8 | 2.6 | 2.3 | 1.9 | 1.7 | 1.4 | 1.2 | 1.1 |
| SSC_0.26 | 710 | 12.6 | 9.8 | 8.4 | 7.3 | 5.1 | 2.8 | 2.4 | 1.9 | 1.7 | 1.4 | 1.1 | 1.1 |
| SSC_0.27 | 815 | 12.7 | 9.9 | 8.4 | 7.4 | 5.1 | 2.8 | 2.4 | 1.9 | 1.7 | 1.4 | 1.1 | 1.1 |
| SSC_0.28 | 15 | 3.1 | 2.6 | 2.3 | 2.0 | 1.7 | 1.3 | 1.1 | 0.9 | 0.8 | 0.8 | 0.6 | 0.6 |
| SSC_0.29 | 30 | 4.6 | 3.8 | 3.3 | 2.7 | 2.1 | 1.4 | 1.1 | 1.3 | 1.1 | 0.9 | 0.8 | 0.8 |
| SSC_0.30 | 60 | 5.7 | 4.7 | 3.9 | 3.3 | 2.4 | 1.6 | 1.3 | 1.6 | 1.3 | 1.1 | 0.9 | 0.9 |
| SSC_0.31 | 90 | 6.4 | 5.2 | 4.4 | 3.7 | 2.8 | 2.1 | 1.6 | 1.5 | 1.4 | 1.3 | 1.2 | 1.1 |

| (1) | (2) | (3) | (4) | (5) | (6) | (7) | (8) | (9) | (10) | (11) | (12) | (13) | (14) |
|---|---|---|---|---|---|---|---|---|---|---|---|---|---|
| SSC_0.32 | 135 | 7.4 | 6.1 | 5.2 | 4.4 | 3.3 | 2.6 | 2.0 | 1.6 | 1.6 | 1.5 | 1.5 | 1.3 |
| SSC_0.33 | 195 | 8.3 | 6.7 | 5.8 | 4.9 | 3.7 | 3.1 | 2.3 | 1.9 | 1.6 | 1.5 | 1.7 | 1.4 |
| SSC_0.34 | 275 | 9.3 | 7.5 | 6.4 | 5.8 | 4.4 | 3.8 | 2.7 | 2.2 | 1.8 | 1.8 | 1.7 | 1.6 |
| SSC_0.35 | 355 | 10.2 | 8.3 | 7.1 | 6.3 | 4.9 | 4.2 | 3.1 | 2.3 | 2.0 | 1.9 | 1.7 | 1.5 |
| SSC_0.36 | 435 | 11.0 | 9.1 | 7.7 | 6.8 | 5.4 | 4.5 | 3.3 | 2.6 | 2.3 | 2.2 | 1.6 | 1.6 |
| SSC_0.37 | 495 | 11.7 | 9.6 | 8.2 | 7.1 | 5.8 | 4.8 | 3.6 | 2.7 | 2.1 | 2.2 | 1.8 | 1.7 |
| SSC_0.38 | 585 | 12.6 | 10.1 | 8.8 | 7.5 | 6.2 | 5.2 | 3.9 | 3.0 | 2.2 | 2.3 | 1.9 | 1.7 |
| SSC_0.39 | 675 | 13.1 | 10.3 | 9.1 | 7.7 | 6.4 | 5.3 | 4.1 | 3.0 | 2.3 | 2.2 | 2.0 | 1.8 |
| SSC_0.40 | 795 | 13.3 | 10.3 | 9.2 | 7.7 | 6.4 | 5.3 | 4.1 | 3.1 | 2.3 | 2.2 | 2.0 | 1.8 |
| SSC_0.41 | 30 | 2.4 | 2.1 | 1.7 | 1.5 | 1.1 | 1.0 | 0.7 | 0.5 | 0.6 | 0.4 | 0.5 | 0.6 |
| SSC_0.42 | 45 | 3.1 | 2.7 | 2.4 | 2.1 | 1.4 | 1.1 | 0.7 | 0.6 | 0.4 | 0.5 | 0.6 | 0.5 |
| SSC_0.43 | 75 | 4.2 | 3.5 | 3.1 | 2.7 | 1.8 | 1.3 | 1.1 | 0.7 | 0.6 | 0.6 | 0.7 | 0.6 |
| SSC_0.44 | 110 | 5.0 | 4.2 | 3.7 | 3.3 | 2.2 | 1.7 | 1.3 | 1.1 | 0.9 | 1.0 | 0.8 | 0.6 |
| SSC_0.45 | 155 | 5.8 | 4.9 | 4.4 | 3.7 | 2.6 | 2.1 | 1.5 | 1.4 | 1.1 | 1.1 | 1.0 | 0.8 |
| SSC_0.46 | 215 | 6.5 | 5.6 | 4.9 | 4.2 | 2.9 | 2.3 | 1.8 | 1.7 | 1.3 | 1.3 | 1.1 | 1.0 |
| SSC_0.47 | 295 | 7.3 | 6.4 | 5.5 | 4.7 | 3.3 | 2.5 | 2.1 | 2.0 | 1.5 | 1.5 | 1.2 | 1.0 |
| SSC_0.48 | 370 | 8.1 | 6.9 | 6.1 | 5.2 | 3.8 | 2.9 | 2.3 | 2.1 | 1.8 | 1.6 | 1.3 | 1.1 |
| SSC_0.49 | 445 | 9.0 | 7.6 | 6.7 | 5.6 | 4.3 | 3.3 | 2.7 | 2.2 | 1.8 | 1.6 | 1.5 | 1.4 |
| SSC_0.50 | 485 | 9.6 | 8.1 | 7.2 | 5.9 | 4.7 | 3.6 | 2.9 | 1.9 | 1.6 | 1.5 | 1.4 | 1.2 |
| SSC_0.51 | 545 | 10.5 | 8.8 | 7.9 | 6.5 | 5.2 | 3.9 | 3.2 | 2.2 | 1.5 | 1.4 | 1.3 | 1.2 |
| SSC_0.52 | 620 | 11.3 | 9.5 | 8.4 | 6.9 | 5.4 | 4.2 | 3.3 | 2.2 | 1.7 | 1.5 | 1.4 | 1.3 |
| SSC_0.53 | 720 | 11.6 | 9.8 | 8.7 | 7.1 | 5.5 | 4.3 | 3.3 | 2.4 | 1.9 | 1.9 | 1.7 | 1.5 |
| SSC_0.54 | 840 | 11.8 | 9.9 | 8.7 | 7.1 | 5.6 | 4.3 | 3.2 | 2.4 | 2.0 | 1.9 | 1.6 | 1.5 |